

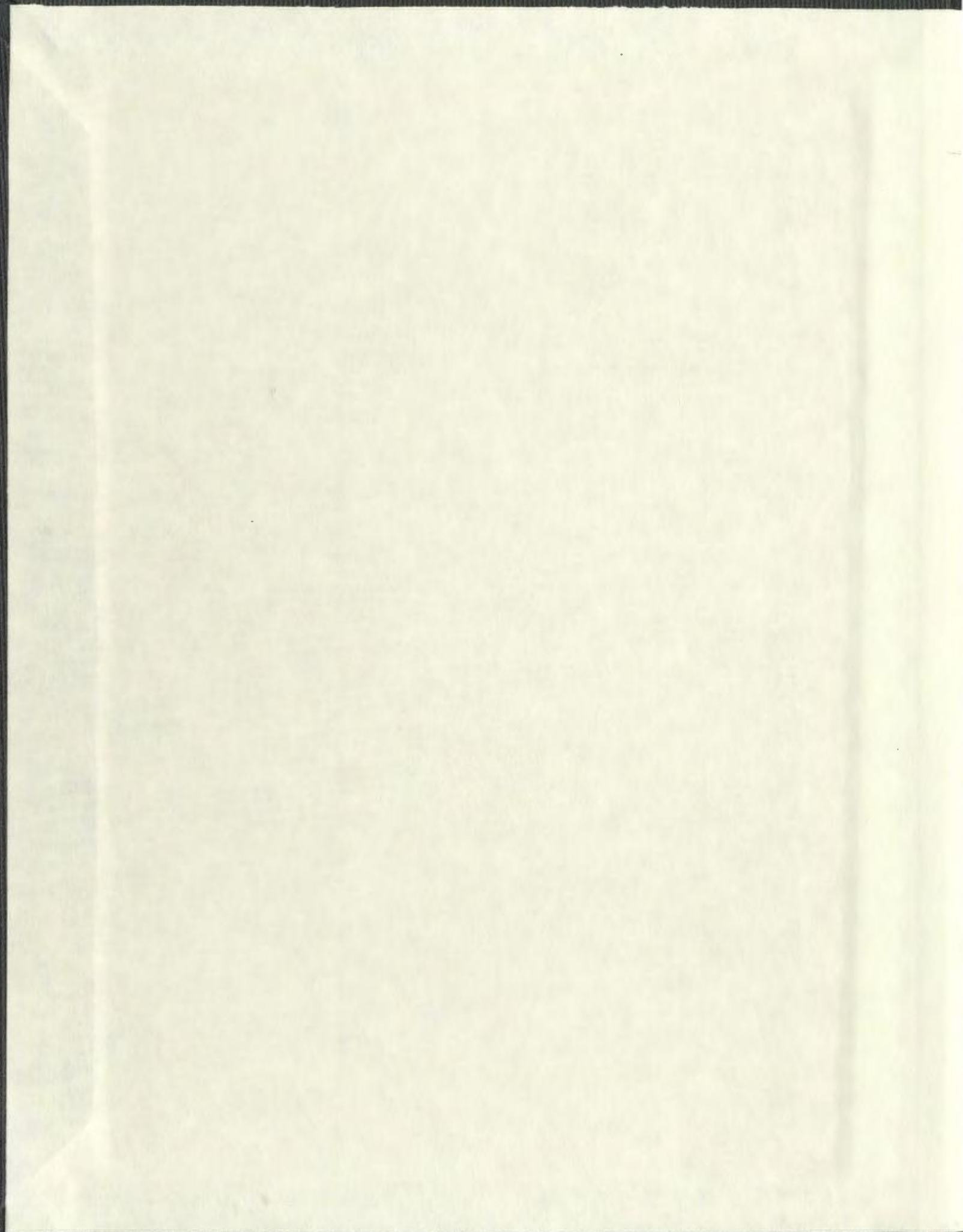
ORIGIN AND DIAGENESIS OF FINE-
GRAINED SLOPE SEDIMENTS: COW
HEAD GROUP (CAMBRO-ORDOVICIAN),
WESTERN NEWFOUNDLAND VOLUME 1

CENTRE FOR NEWFOUNDLAND STUDIES

**TOTAL OF 10 PAGES ONLY
MAY BE XEROXED**

(Without Author's Permission)

MARIO CONIGLIO





National Library
of Canada

Bibliothèque nationale
du Canada

Canadian Theses Service

Services des thèses canadiennes

Ottawa, Canada
K1A 0N4

CANADIAN THESES

THÈSES CANADIENNES

NOTICE

The quality of this microfiche is heavily dependent upon the quality of the original thesis submitted for microfilming. Every effort has been made to ensure the highest quality of reproduction possible.

If pages are missing, contact the university which granted the degree.

Some pages may have indistinct print especially if the original pages were typed with a poor typewriter ribbon or if the university sent us an inferior photocopy.

Previously copyrighted materials (journal articles, published tests, etc.) are not filmed.

Reproduction in full or in part of this film is governed by the Canadian Copyright Act, R.S.C. 1970, c. C-30.

**THIS DISSERTATION
HAS BEEN MICROFILMED
EXACTLY AS RECEIVED**

AVIS

La qualité de cette microfiche dépend grandement de la qualité de la thèse soumise au microfilmage. Nous avons tout fait pour assurer une qualité supérieure de reproduction.

S'il manque des pages, veuillez communiquer avec l'université qui a conféré le grade.

La qualité d'impression de certaines pages peut laisser à désirer, surtout si les pages originales ont été dactylographiées à l'aide d'un ruban usé ou si l'université nous a fait parvenir une photocopie de qualité inférieure.

Les documents qui font déjà l'objet d'un droit d'auteur (articles de revue, examens publiés, etc.) ne sont pas microfilmés.

La reproduction, même partielle, de ce microfilm est soumise à la Loi canadienne sur le droit d'auteur, SRC 1970, c. C-30.

**LA THÈSE A ÉTÉ
MICROFILMÉE TELLE QUE
NOUS L'AVONS REÇUE**

ORIGIN AND DIAGENESIS OF FINE-GRAINED SLOPE SEDIMENTS:
COW HEAD GROUP (CAMBRO-ORDOVICIAN), WESTERN NEWFOUNDLAND

VOLUME I

by

© Mario Coniglio, M.Sc.

A thesis submitted to the School of Graduate
Studies in partial fulfillment of the
requirements for the degree of
Doctor of Philosophy

Department of Earth Sciences
Memorial University of Newfoundland

January 1985

St. John's

Newfoundland

Permission has been granted to the National Library of Canada to microfilm this thesis and to lend or sell copies of the film.

The author (copyright owner) has reserved other publication rights, and neither the thesis nor extensive extracts from it may be printed or otherwise reproduced without his/her written permission.

L'autorisation a été accordée à la Bibliothèque nationale du Canada de microfilmer cette thèse et de prêter ou de vendre des exemplaires du film.

L'auteur (titulaire du droit d'auteur) se réserve les autres droits de publication; ni la thèse ni de longs extraits de celle-ci, ne doivent être imprimés ou autrement reproduits sans son autorisation écrite.

ISBN 0-315-31014-6

ABSTRACT

The Cow Head Group is a base-of-slope apron deposit composed of 5 lithofacies: (1) conglomerate, (2) calcarenite, (3) siltstone, (4) shale, and (5) lime mudstone. Conglomerates were deposited by debris flows and the calcarenite grainstones by high-density turbidity currents. Siltstones and shales represent interbedded fine-grained turbidites and terrigenous hemipelagites. Rhythmically-bedded parted, ribbon, and nodular lime mudstones, composed mostly of microspar and pseudospar, resulted from the interplay of climatically-controlled carbonate-abundance cycles and event deposits. Peloids and intraclasts, derived mainly from the breakdown of the calcified algae Girvanella and Epiphyton, are the most important allochems in the fine-grained sediments.

Burial compaction occurred mainly in argillaceous sediments. Limestones are uncompacted and demonstrate only minor pressure solution effects. Intrastratal deformation was due to submarine failure and layer-parallel compression during Taconic orogenesis. Subtly-expressed synsedimentary deformation fabrics indicate that slope failure was more common than is apparent based solely on the presence of intraformational truncation surfaces and slide masses.

In conglomerates, clasts with diagenetic microfabrics identical to those of the thinly-bedded, fine-grained sediments indicate that lithification (calcite authigenesis, early dolomitization, and some silicification) occurred within several metres of the sediment-water interface. Carbon isotope analyses suggest that carbonate precipitation was driven by

bacterial sulphate reduction and methane generation. Trace element (Mg, Fe, Mn, and Sr) and cathode luminescence patterns record calcite precipitation from progressively more reduced pore-waters. These patterns are indistinguishable from those generated during meteoric-water diagenesis.

Cathode luminescence microfabrics of radial fibrous calcite from shallow-water boulders in conglomerates and in situ displacive fibrous calcite indicate that these crystals are composite and grew both as spherocrystals and unit crystals. Aggrading neospar on the margins of mudstone beds and nodules resulted from decreased nucleation density and precipitation of progressively younger calcite, commonly as asymmetrical, irregular increments.

Three types of dolomite are differentiated: (1) detrital, (2) early diagenetic, and (3) late diagenetic. Silt-size particles of detrital dolomite were derived from weathering of older carbonates or penecontemporaneous dolomite from the adjacent, shallow-water platform.

Diagenetic dolomite occurs both as a replacement and a pore-filling phase. Early dolomitization was synchronous with or postdated the main phase of calcite authigenesis. Late dolomitization is related to tectonic faults and joints. Silicification also has a protracted diagenetic history, but its distribution is controlled primarily by the abundance of radiolaria and siliceous sponge spicules.

ACKNOWLEDGEMENTS

I am indebted to my thesis supervisor, N. P. James, for suggesting this project and his interest, advice, encouragement, and manuscript editing. I am also grateful for opportunities presented to me during my graduate programme for field experience in Oman, Egypt, southwest USA, and Gaspé, Quebec. My thesis committee members, R. N. Hiscott and R. K. Stevens, also provided helpful advice and encouragement.

Special thanks are extended to P. W. Choquette and Marathon Oil Company (Littleton, Colorado) for their interest in this study and for providing stable isotope analyses.

This project was financed primarily by Petro-Canada (Calgary, Alberta) and Natural Sciences and Engineering Research Council funding to N. P. James. Thesis preparation costs were partially offset by an American Association of Petroleum Geologists Grants-in-Aid award. My personal support was provided by a Natural Sciences and Engineering Research Council postgraduate scholarship. Parks Canada permitted sampling in Gros Morne National Park.

I would also like to thank the following individuals for their contributions to this study: G. Andrews for atomic absorption spectrophotometry and advice on preparatory procedures; T. J. Calon for discussion of problems relating to differentiation of soft-sediment from tectonic deformation, and also for constructive criticism of Chapter 4; N. Chow for constructive criticism of ideas in Chapters 3 and 6; F. Follett for printing the plates; D. Haywick for providing samples of dololaminites and discussion of dolomitization in western Newfoundland;

- v -

A. C. Kendall for providing a preprint of his manuscript on radialial fibrous calcite; F. Kerri for preparation of shale samples for X-ray diffraction; B. King for powdering samples for AAS analyses and assistance with the use of the SPSS statistics programme; H. Longrich for assistance with microprobe analyses and data interpretation; W. Marsh for photographic services, darkroom facilities, and technical advice; B. R. Pratt for his helpful advice and criticism of Chapter 6; A. Pye for photoreduction work and drafting of numerous diagrams; F. Thornhill, L. Warford, G. Ford, and R. Soper for making most of the thin sections and for providing facilities and supplies for slabbing and polishing; H. R. Wanless for sharing field observations and insight; H. Wood for assistance with X-ray diffraction and sample preparation; Leda, Scylla, and Medusa for their generously-given company during numerous late nights and early mornings of word processing.

I also thank my parents for their constant encouragement.

Finally, I thank my wife, Leanne, for her assistance during field work, sample preparation and organization, and manuscript editing and proofreading. Her interest, support, and patience, especially during the last 6 months of this project, are sincerely appreciated.

TABLE OF CONTENTS

VOLUME I

	PAGE
ABSTRACT.....	vii
ACKNOWLEDGEMENTS.....	iv
LIST OF FIGURES.....	xvii
LIST OF TABLES.....	xix
LIST OF PLATES.....	xx
 Chapter 1: INTRODUCTION	
1.1 INTRODUCTORY REMARKS.....	1
1.2 PREVIOUS SEDIMENTOLOGICAL STUDIES.....	2
1.3 GEOLOGIC SETTING OF THE COW HEAD GROUP.....	15
1.4 STRUCTURAL GEOLOGY.....	17
1.4.1 Regional.....	17
1.4.2 Humber Arm Allochthon and Cow Head Group Structure.....	18
1.5 PALEOGEOGRAPHY AND DEPOSITIONAL SETTING.....	19
1.5.1 Hypothesis of Hubert <i>et al.</i> (1977).....	19
1.5.2 A Revised Paleogeography.....	21
1.6 APPROACH TO STUDY.....	24
1.6.1 Database.....	24
1.6.2 Organization.....	25
 PART A: SEDIMENTOLOGY.....	
	26
 Chapter 2: LITHOFACIES OF THE COW HEAD GROUP	
2.1 INTRODUCTION.....	28
2.2 CLASSIFICATION AND TERMINOLOGY.....	29
2.2.1 Basic Definitions.....	29
2.2.2 Classification of Bedding.....	30
2.2.3 Clarification of the Term "Mudstone".....	35
2.3 CONGLOMERATE LITHOFACIES: DESCRIPTION.....	36
2.3.1 Introduction.....	36
2.3.2 General Description.....	37
2.3.3 Clasts.....	38
2.3.4 Matrix.....	41
2.3.5 Grading, Internal Structure, and Packing.....	42
2.3.6 Isolated Boulders.....	45
2.4 CONGLOMERATE LITHOFACIES: INTERPRETATION.....	45

TABLE OF CONTENTS (continued)

	PAGE
2.5 CALCARENITE LITHOFACIES: DESCRIPTION.....	49
2.5.1 General Description.....	49
2.5.2 Grading and Stratification.....	49
2.5.3 Other Calcarenites.....	50
2.6 CALCARENITE LITHOFACIES: INTERPRETATION.....	51
2.6.1 Interpretation of Calcarenite Lithofacies.....	51
2.6.2 Interpretation of Other Calcarenites.....	53
2.7 SILTSTONE LITHOFACIES AND SHALE LITHOFACIES: DESCRIPTION.....	54
2.7.1 Introduction.....	54
2.7.2 Colour.....	55
2.7.3 Bedding Characteristics.....	57
2.7.4 Internal Structures.....	58
2.7.5 Graded Laminations.....	58
2.7.6 Shale Microfabric.....	59
2.7.7 Trace Fossils.....	61
2.8 SILTSTONE LITHOFACIES AND SHALE LITHOFACIES: INTERPRETATION.....	62
2.8.1 Sequence of Sedimentary Structures.....	62
2.8.2 Interpretation as Fine-Grained Turbidites.....	66
2.8.3 Shale Microfabrics, Colours, and Cyclicity.....	71
2.8.4 Origin of Cracks in Shale.....	74
2.8.5 Fine-Grained Turbidites and Muddy Contourites.....	74
2.9 MUDSTONE LITHOFACIES: DESCRIPTION.....	76
2.9.1 Introduction.....	76
2.9.2 Bedding Characteristics.....	77
2.9.3 Mudstone Microfacies.....	78
2.9.4 Clastic Dikes.....	80
2.9.5 Transition to Argillaceous Matrix.....	80
2.9.6 Trace Fossils.....	81
2.9.7 Nodular Limestones: Details.....	82
2.9.7.1 Distribution, Shape, and Size of Nodules.....	82
2.9.7.2 Types of Nodules.....	83
2.10 MUDSTONE LITHOFACIES: INTERPRETATION.....	88
2.10.1 Introduction.....	88
2.10.2 Depositional Mechanisms for Parted and Ribbon Mudstones.....	90
2.10.2.1 Dilute Turbidity Current Hypothesis.....	92
2.10.2.2 Hemipelagic Settling Hypothesis.....	93
2.10.2.3 Contourite Hypothesis.....	94
2.10.3 Interpretation of Nodular Limestones.....	94
2.11 SUMMARY OF LITHOFACIES INTERPRETATIONS.....	96
2.12 DISCUSSION: CARBONATE APRONS.....	98

TABLE OF CONTENTS (continued)

	PAGE
Chapter 3: SUBMARINE SLIDING: EVIDENCE FOR DEPOSITION ON A SLOPING SURFACE	
3.1 INTRODUCTION.....	100
3.2 TERMINOLOGY.....	101
3.3 FIELD DESCRIPTIONS.....	102
3.3.1 Intraformational Truncation Surfaces.....	103
3.3.1.1 Lower Head.....	103
3.3.1.2 Green Point.....	106
3.3.1.3 Interpretation.....	107
3.3.2 Slides.....	108
3.3.2.1 Green Point.....	108
3.3.2.2 Cow Head South.....	108
3.3.2.3 Interpretation.....	109
3.3.3 Possible Internal Shear Zones.....	110
3.3.3.1 Green Point.....	111
3.3.3.2 Cow Head North.....	111
3.3.3.3 Interpretation.....	112
3.4 DISCUSSION.....	113
3.4.1 Model for Sediment Failure.....	113
3.4.2 Dimensions of Truncation Surfaces and Slide Masses.....	117
3.4.3 Causes of Sediment Failure in the CHG.....	119
3.5 CONCLUSIONS.....	119
Chapter 4: ORIGIN OF CONTORTED LIMESTONES	
4.1 INTRODUCTION.....	123
4.2 FIELD DESCRIPTION.....	124
4.3 VOIDS IN CONTORTED LIMESTONES.....	128
4.4 DISCUSSION.....	129
4.4.1 Other Occurrences.....	129
4.4.2 Hypotheses of Formation.....	130
4.4.2.1 Expansive Diagenesis.....	133
4.4.2.2 Submarine Sliding at the Sediment - Seawater Interface.....	133
4.4.2.3 Synsedimentary Shear Zone Versus Tectonic Origin.....	136
4.5 CONCLUSIONS.....	140
Chapter 5: COMPACTION IN THE COW HEAD GROUP	
5.1 INTRODUCTION.....	141
5.2 BURIAL COMPACTION.....	142
5.2.1 Field Observations and Measurements.....	142
5.2.2 Slab Study and Microscopy.....	143
5.2.3 Interpretation and Discussion.....	144
5.3 TECTONIC COMPACTION.....	146
5.3.1 Description of Pressure Solution Effects.....	146
5.3.2 Local Structures.....	147

TABLE OF CONTENTS (continued)

	PAGE
5.3.3 Interpretation and Discussion.....	147
5.3.4 Relative Timing of Burial and Tectonic Pressure Solution.....	151
5.4 SUMMARY AND CONCLUSIONS.....	151
Chapter 6: SEDIMENTARY PARTICLES AND THE ROLE OF CALCIFIED ALGAE AS SEDIMENT PRODUCERS IN THE COW HEAD GROUP	
6.1 INTRODUCTION.....	153
6.2 GENERAL DESCRIPTION OF SEDIMENTS.....	154
6.3 PELOIDS, MICRITIC INTRACLASTS, AND PELOIDAL INTRACLASTS.....	158
6.4 PARTICLES OF CALCIFIED ALGAE.....	162
6.4.1 <u>Girvanella</u>	162
6.4.1.1 <u>Single Girvanella Tubules</u>	163
6.4.1.2 <u>Girvanella Rafts</u>	164
6.4.1.3 <u>Girvanella Oncolites</u>	164
6.4.1.4 <u>Girvanella Intracasts</u>	164
6.4.2 <u>Epiphyton</u>	165
6.4.3 <u>Nuia</u>	166
6.4.4 <u>Summary</u>	166
6.5 ALGAL SEDIMENTS FROM THE PLATFORM MARGIN AND INTERIOR.....	167
6.5.1 Petrography of Platform Margin Boulders.....	167
6.5.2 Algae of the Platform Interior.....	169
6.5.3 <u>Summary</u>	169
6.6 DISCUSSION.....	172
6.6.1 <u>Girvanella</u>	172
6.6.2 <u>Epiphyton</u>	175
6.6.3 <u>Comparison with Modern Calcified Algae</u>	176
6.7 CONCLUSIONS.....	178

PART B: DIAGENESIS

INTRODUCTION.....	180
TYPES OF CALCITE.....	181
OTHER DIAGENETIC MINERALS.....	184
Chapter 7: RADIAL FIBROUS CALCITE	
7.1 INTRODUCTION.....	185
7.2 FIELD RELATIONSHIPS.....	187
7.3 PETROGRAPHY.....	189
7.3.1 General Description.....	189
7.3.2 Inclusion Patterns.....	190
7.3.3 Microdolomite.....	190

- x -

TABLE OF CONTENTS (continued)

	PAGE
7.4 CATHODE LUMINESCENCE.....	191
7.5 INTERPRETATION.....	192
7.5.1 Inclusion Patterns.....	192
7.5.2 Cathode Luminescence.....	193
7.5.2.1 Interpretation as Composite Crystals.....	193
7.5.2.2 Controls of Growth Surface Morphology.....	195
7.5.2.3 Uncertainties.....	196
7.5.2.4 Crystal Boundaries and Subcrystals.....	197
7.5.3 Optic Axes Convergence: Kendall's Hypothesis.....	198
7.5.4 A Modification to Kendall's Hypothesis.....	202
7.5.5 Explanation of Fascicular Optic Calcite.....	204
7.6 SUMMARY AND CONCLUSIONS.....	206
Chapter 8: AUTHIGENIC CALCITE CEMENT AND NEOSPAR	
8.1 GENERAL INTRODUCTION.....	209
8.2 EQUANT CEMENT AND NEOSPAR.....	210
8.2.1 Equant Cement.....	210
8.2.2 Neospar.....	212
8.2.3 Timing: Evidence for Early Lithification.....	214
8.2.4 Marginal Aggradation in Mudstones.....	215
8.2.5 Discussion: Implications for Aggrading Neomorphism.....	216
8.2.5.1 Introduction.....	216
8.2.5.2 Cathode Luminescence; Growth of Neospar.....	218
8.2.5.3 Other Ancient Examples of Aggrading Neomorphism.....	219
8.2.6 Conclusions.....	222
8.3 FRACTURE CALCITE.....	223
8.3.1 Introduction.....	223
8.3.2 Early Fracture Calcite.....	224
8.3.3 Late Fracture Calcite.....	224
8.3.4 Origin of Early Fractures.....	225
8.3.4.1 Septarian Cracks.....	225
8.3.4.2 Ladder Cracks.....	226
8.3.4.3 V-Shaped Marginal Fractures.....	228
8.3.5 Conclusions.....	228
8.4 CONGLOMERATE FIBROUS CALCITE.....	229
8.4.1 Introduction.....	229
8.4.2 Petrography.....	230
8.4.2.1 Cement.....	230
8.4.2.2 Internal Sediments.....	231
8.4.3 Matrix Organization.....	232
8.4.4 Interpretation and Discussion.....	232
8.4.5 Origin of "Scheck"-Type Conglomerates.....	234
8.4.6 Conclusions.....	234

TABLE OF CONTENTS (continued)

	PAGE
8.5 CATHODE LUMINESCENCE OF CALCITE.....	235
8.5.1 Luminescence Stages.....	235
8.5.2 Cathode Luminescence and Trace Element Composition.....	239
8.5.3 Discussion of Cathode Luminescence Trends.....	240
8.5.4 Conclusions.....	246
 Chapter 9: DISPLACIVE FIBROUS CALCITE	
9.1 INTRODUCTION.....	247
9.2 FIELD RELATIONSHIPS.....	250
9.3 PETROGRAPHY.....	254
9.3.1 Types of Displacive Fibrous Calcite.....	254
9.3.2 General Characteristics.....	255
9.3.3 Inclusions.....	257
9.4 CATHODE LUMINESCENCE.....	259
9.5 FRINGE ORGANIZATION.....	261
9.6 TRANSITION FROM SUBSTRATE TO FRINGE.....	262
9.7 NATURE OF ASSOCIATED SHALE.....	263
9.8 DISPLACIVE ORIGIN OF FRINGES.....	264
9.9 EARLY ORIGIN OF DFC FRINGES: FIELD EVIDENCE.....	265
9.9.1 Fibrous Calcite Clasts.....	265
9.9.2 Curved Crystals.....	265
9.9.3 Truncation Surface Deformation.....	267
9.10 MICRO-FRINGES OF DISPLACIVE FIBROUS CALCITE.....	268
9.10.1 Introduction.....	268
9.10.2 Petrography.....	269
9.10.3 Iron content and Cathode Luminescence.....	269
9.11 INTERPRETATION AND DISCUSSION.....	270
9.11.1 Interpretation of Microfabrics.....	270
9.11.2 Controls on Growth Surface Morphology and DFC Type....	272
9.11.3 Implications for Neospar as Composite Crystals.....	274
9.11.4 Origin of DFC and Cone-in-Cone Structure.....	276
9.12 SUMMARY AND CONCLUSIONS.....	279
 Chapter 10: CALCITE TRACE ELEMENT GEOCHEMISTRY	
10.1 INTRODUCTION.....	281
10.2 MAGNESIUM.....	282
10.3 IRON.....	289
10.4 MANGANESE.....	292
10.5 STRONTIUM.....	293
10.6 INTERPRETATION AND DISCUSSION.....	296
10.6.1 Magnesium and Strontium.....	299
10.6.2 Iron and Manganese.....	303
10.7 SUMMARY AND CONCLUSIONS.....	304

TABLE OF CONTENTS (continued)

	PAGE
Chapter 11: CALCITE STABLE ISOTOPE GEOCHEMISTRY	
11.1 INTRODUCTION.....	306
11.2 BACKGROUND: FUNDAMENTALS OF ORGANIC MATTER OXIDATION.....	307
11.2.1 Oxidizing Reactions.....	307
11.2.2 Isotopic Signatures.....	312
11.3 CALCITE STABLE ISOTOPES.....	313
11.4 RADIAL FIBROUS CALCITE.....	314
11.4.1 Samples and Data.....	314
11.4.2 Interpretation.....	314
11.5 <u>IN SITU</u> AUTHIGENIC CALCITE: SAMPLES AND DATA.....	317
11.5.1 Conglomerate Fibrous Calcite.....	317
11.5.2 Equant Calcite Cements.....	318
11.5.3 Grainstones.....	318
11.5.4 Microspar.....	318
11.5.5 Pseudospar and Related Cement.....	321
11.5.6 Displacive Fibrous Calcites and Associated Neospar....	325
11.6 INTERPRETATION OF CALCITE STABLE ISOTOPES.....	328
11.6.1 Introduction.....	328
11.6.2 Cements: CFC, Equant Calcites, and Grainstones.....	331
11.6.3 Microspar and Pseudospar (Omitting Groups C and I)....	332
11.6.4 Displacive Fibrous Calcite and Associated Neospar....	334
11.7 DISCUSSION: COMPARISON WITH OTHER STUDIES.....	335
11.8 SUMMARY AND CONCLUSIONS.....	336c
Chapter 12: DOLOMITIZATION IN THE COW HEAD GROUP	
12.1 INTRODUCTION.....	337
12.2 EARLY DOLOMITES.....	338
12.2.1 Distribution.....	338
12.2.2 Petrography.....	339
12.2.3 Cathode Luminescence and Trace Elements.....	341
12.2.3.1 Cores.....	341
12.2.3.2 Rims.....	342
12.2.4 Corrosion.....	346
12.2.4.1 Corrosion Followed by More Dolomite Precipitation.....	346
12.2.4.2 Corrosion Followed by Calcite.....	346
12.2.4.3 Corrosion Followed by Chert.....	347
12.2.5 Stable Isotopes.....	347
12.2.6 Timing.....	350
12.3 INTERPRETATION OF EARLY DOLOMITES.....	354
12.3.1 Cores.....	354
12.3.1.1 Source.....	357
12.3.2 Cathode Luminescence and Trace Elements.....	358
12.3.3 Interpretation of Stable Isotopes.....	358
12.4 DISCUSSION.....	363

TABLE OF CONTENTS (continued)

	PAGE
12.5 LATE DOLOMITE.....	370
12.5.1 Introduction.....	370
12.5.2 Petrography.....	371
12.5.3 Cathode Luminescence and Trace Elements.....	373
12.5.4 Stable Isotopes.....	374
12.6 INTERPRETATION.....	374
12.6.1 Field Relationships and Petrography.....	374
12.6.2 Stable Isotopes.....	375
12.7 CONCLUSIONS.....	375
12.7.1 Early Dolomites.....	375
12.7.2 Late Dolomites.....	377
 Chapter 13: SILICIFICATION AND MINOR AUTHIGENIC PHASES	
13.1 GENERAL INTRODUCTION.....	378
13.2 SILICIFICATION.....	378
13.2.1 Introduction.....	378
13.2.2 Field Description.....	379
13.2.2.1 Conglomerate Crusts.....	379
13.2.2.2 Marginal Crusts.....	379
13.2.2.3 Completely Silicified Shale and Limestone...	380
13.2.2.4 Nodules.....	380
13.2.2.5 Allochthonous(?) Chert.....	381
13.2.3 Petrography.....	381
13.2.3.1 Components of Chert.....	381
13.2.3.2 Replacive Chert.....	381
13.2.3.3 Pore-Filling Chert.....	382
13.2.4 Diagenesis of Siliceous Bioclasts.....	383
13.2.4.1 Introduction.....	383
13.2.4.2 Petrography of Radiolaria and Spicules.....	383
13.2.4.3 Group 1: Limestone Microfacies.....	384
13.2.4.4 Group 2: Shale Microfacies.....	385
13.2.4.5 Evidence for Vanished Radiolaria.....	386
13.2.5 Interpretation.....	388
13.2.5.1 Origin of Replacement Minerals.....	388
13.2.5.2 Timing of Silicification: Relative and Absolute.....	389
13.2.6 Discussion.....	391
13.2.7 Summary and Conclusions.....	392
13.3 BARITE.....	393
13.3.1 Occurrences and Petrography.....	393
13.3.2 Interpretation and Discussion.....	395
13.4 PYRITE.....	397
13.4.1 Occurrences and Petrography.....	397
13.4.2 Interpretation and Discussion.....	398

TABLE OF CONTENTS (continued)

VOLUME II

PART C

	PAGE
Chapter 14: ORIGIN OF PARTED, RIBBON, AND MODULAR LIMESTONES	
14.1 INTRODUCTION.....	400
14.2 DIAGENETIC MODELS FOR PERIODITES.....	401
14.2.1 Rhythmic Unmixing Model.....	402
14.2.2 Pressure Solution Model.....	402
14.2.3 Early Diagenetic Overprint Model.....	404
14.3 PHYSICAL MODEL.....	405
14.3.1 Introduction.....	405
14.3.2 Details.....	406
14.3.3 Origin of Continuous Mudstone Beds.....	410
14.3.4 Source of Calcium Carbonate.....	412
14.3.5 Origin of Mudstone Envelopes and Composite Bedding....	413
14.3.6 Origin of Fitted Fabrics.....	414
14.3.7 Origin of CFC and DFC.....	414
14.3.8 Original Mineralogy and Other Considerations.....	415
14.4 CHEMICAL MODEL.....	416
14.4.1 Introduction.....	416
14.4.2 Features of the $\delta^{13}\text{C}$ Model.....	417
14.4.3 Application of the Model: Implications for the Lithification of "Ordinary" CHG Mudstones.....	421
14.5 OTHER DIAGENETIC COMPONENTS.....	424
14.5.1 Early Dolomite.....	424
14.5.1.1 Pervasive Dolomitic Siltstones.....	424
14.5.1.2 Conglomerate Matrix Dolomite.....	425
14.5.1.3 Matrix Dolomite.....	426
14.5.1.4 Limestone-Hosted Dolomite.....	426
14.5.1.5 Dolomite and the Chemical Model.....	427
14.5.2 Silicification.....	427
14.5.3 Barite Authigenesis.....	428
14.5.4 Pyrite Authigenesis.....	429
14.6 MUDSTONE LITHOFACIES AND TIME.....	429
Chapter 15: CONCLUSIONS	
15.1 SEDIMENTATION.....	431
15.2 INTRASTRATAL DEFORMATION.....	434
15.3 MECHANICAL AND CHEMICAL COMPACTION.....	435
15.4 ORIGIN OF PELOIDS AND INTRACLASTS.....	436

TABLE OF CONTENTS (continued)

	PAGE
15.5 DIAGENETIC CALCITES.....	437
15.5.1 Field Data, Petrography, and Cathode Luminescence.....	437
15.5.2 Geochemistry of Calcite.....	439
15.6 MODEL FOR GENERATION OF PARTED, RIBBON, AND NODULAR LIMESTONES..	440
15.7 DOLOMITIZATION.....	442
15.8 SILICIFICATION.....	443
15.9 CALCITE MICROFABRICS.....	443
15.9.1 Radial Fibrous Calcite.....	443
15.9.2 Neospar.....	444
15.9.3 Displacive Fibrous Calcite.....	444
REFERENCES CITED.....	446
PLATES.....	493
Appendix A: OUTCROP LISTS AND DESCRIPTIONS OF LITHOFACIES.....	605
A.1 CALCARENITE AND SILTSTONE LITHOFACIES.....	605
A.2 MUDSTONE LITHOFACIES: OUTCROP DESCRIPTIONS.....	606
Appendix B: CLAY MINERALOGY OF SHALES.....	611
B.1 INTRODUCTION.....	611
B.2 SAMPLE PREPARATION.....	611
B.3 OBSERVATIONS.....	612
B.4 INTERPRETATION.....	614
B.5 COMPARISON WITH SUCHECKI <u>ET AL.</u> (1977).....	615
Appendix C: CAUSES OF SUBMARINE SEDIMENT FAILURE: AN OVERVIEW.....	621
C.1 INTRODUCTION.....	621
C.2 TECTONIC AND OCEANOGRAPHIC CAUSES.....	622
Appendix D: CONTORTED LIMESTONE DATA.....	627
Appendix E: COMPACTION ESTIMATION DATA.....	628
Appendix F: PETROGRAPHY OF OIDS AND SILICICLASTICS.....	631
F.1 OIDS.....	631
F.2 QUARTZ SAND.....	631
F.3 FELDSPAR SILT AND SAND.....	633
Appendix G: <u>STRUCTURE GRUMELEUSE</u> AND CALCIFIED ALGAE.....	636
G.1 INTRODUCTION.....	636
G.2 ALTERATION OF <u>GIRVANELLA</u> SHEETS.....	637
G.3 SUMMARY.....	638

TABLE OF CONTENTS (continued)

	PAGE
Appendix H: CEMENTATION AND NEOMORPHISM.....	640
H.1 TERMINOLOGY.....	640
H.2 AGGRADING NEOMORPHISM ACCORDING TO FOLK (1965).....	641
H.3 CEMENT AND NEOSPAR CRITERIA.....	643
Appendix I: GEOCHEMICAL ANALYSES: METHODOLOGY, INSTRUMENTATION, AND DATA.....	646
I.1 ATOMIC ABSORPTION SPECTROPHOTOMETRY.....	646
I.2 STABLE ISOTOPE ANALYSES.....	647
I.3 MICROPROBE ANALYSES.....	648
I.4 CATHODE LUMINESCENCE.....	649
Appendix J: SAMPLE DESCRIPTIONS.....	659
J.1 INTRODUCTION.....	659
J.2 CALCITE SAMPLES.....	659
J.3 DOLOMITE SAMPLES.....	661
Appendix K: TRACE ELEMENTS AND WATER-ROCK RATIOS: BACKGROUND.....	666
Appendix L: MINOR AUTHIGENIC MINERALS.....	670
L.1 SPHALERITE.....	670
L.2 FLOURITE.....	671
L.3 CHLORITE.....	671
Appendix M: SYNSEDIMENTARY BOUDINS.....	673
M.1 INTRODUCTION.....	673
M.2 FIELD TEST.....	674
Appendix N: EVIDENCE FOR SUBMARINE EXPOSURE OF NODULAR MUDSTONES.....	677
N.1 INTRODUCTION.....	677
N.2 EXAMPLE 1: NODULE FROM COW HEAD NORTH.....	677
N.3 EXAMPLE 2: NODULE FROM ST. PAUL'S QUARRY.....	678
N.4 CONCLUSION.....	680
Appendix O: MINERALOGY OF CONCRETIONS AND HARDGROUNDS.....	681
O.1 INTRODUCTION.....	681
O.2 DISCUSSION.....	681

LIST OF FIGURES

	PAGE
1.1 Geologic setting of the Cow Head Group.....	3
1.2 Outcrop localities.....	5
1.3 Composite stratigraphic section of the Cow Head Group.....	9
1.4 Depositional setting of the Cow Head Group.....	22
2.1 Terminology for the description of bedding.....	31
2.2 Variations in clast-matrix and clast-clast relationships in the conglomerate lithofacies.....	43
2.3 Schematic composite sequence of sedimentary structures in siltstone-shale cycles.....	63
2.4 Correlation of divisions in sand and silt turbidites.....	68
2.5 Schematic summary of the various types of nodular limestones.....	84
3.1 Measured outcrops of truncation surfaces at Lower Head and Green Point.....	104
3.2 Schematic diagram of shear zones.....	115
4.1 Schematic diagram of contorted limestone.....	125
4.2 Schematic summary of possible origins for contorted limestones...	131
5.1 Orientation of vertical stylolites.....	148
6.1 Point-count histograms for representative grainstones.....	156
6.2 Schematic diagram illustrating the relationship between peloids, micritic intraclasts, and peloidal intraclasts.....	159
6.3 Schematic reconstruction of the distribution of Lower Paleozoic calcified and non-calcifying algae from western Newfoundland.....	170
6.4 Summary diagram of break-down of calcified algae.....	173
6.5 Radial fibrous calcite (a) schematic depiction of asymmetric split-growth, (b) schematic explanation of distal convergence of optic axes.....	200
8.1 Schematic diagram of aggrading neomorphism.....	220
8.2 Summary diagram of CL characteristics of various calcites.....	237
8.3 Summary of luminescence data for dolomite and calcite from literature survey.....	241
8.4 Luminescence fields for calcite cement, neospar, and minor DFC...	243
9.1 Schematic summary of the various relationships observed between fringes of DFC and substrat�.....	252
10.1 Microprobe step-traverses of selected calcites.....	283
10.2 FeO, MnO, and Sr trends in serial samples of microspar pseudospar, and displacive fibrous calcite.....	290
10.3 Sr distribution in various diagenetic calcites.....	294
10.4 (a) Simplified model of trace element distribution in open and closed diagenetic systems; (b) schematic distribution Mg, Sr, Fe, and Mn in authigenic calcites.....	297

LIST OF FIGURES (continued)

	PAGE
11.1 $\delta^{13}\text{C}$ versus $\delta^{18}\text{O}$ of RFC, CFC, and miscellaneous calcite cements.....	315
11.2 $\delta^{13}\text{C}$ versus $\delta^{18}\text{O}$ of various microspars, grainstones, and a wackestone nodule.....	319
11.3 $\delta^{13}\text{C}$ versus $\delta^{18}\text{O}$ of various pseudospars, associated microspars, and a calcite cement filling a septarian crack.....	322
11.4 $\delta^{13}\text{C}$ versus $\delta^{18}\text{O}$ of serial samples of microspar, pseudospar, and DFC.....	326
12.1 Microprobe step traverses across dolomite crystals.....	344
12.2 $\delta^{13}\text{C}$ versus $\delta^{18}\text{O}$ plot for various types of dolomite.....	348
12.3 Schematic summary of dolomitization in the Cow Head Group.....	351
12.4 Plot of Early dolomite $\delta^{13}\text{C}$ versus bulk FeO concentration.....	361
12.5 $\delta^{13}\text{C}$ versus $\delta^{18}\text{O}$ of "methanogenic" dolomites from other studies and Early dolomites of this study.....	367
14.1 Schematic physical model for generation of parted and ribbon limestones.....	408
14.2 Chemical (isotopic) model for the evolution of parted and ribbon limestones.....	418

LIST OF TABLES

	PAGE
2.1 Types of conglomerate clasts.....	39
10.2 Pore-water calculations.....	301
11.1 Various bacterial reactions.....	310
12.1 Selected studies of organically-related concretionary dolomites.....	366
A.1 Calcarenite lithofacies outcrops.....	605
A.2 Siltstone lithofacies outcrops.....	605
B.1 Clay mineralogy.....	618
B.2 Chemical analyses of a potassium-metasomatized shale.....	620
C.1 Causes of sediment failure.....	624
C.2 Shear zone and truncation surface localities.....	626
D.1 Contorted limestone and bedding overlap outcrop localities.....	627
D.2 Orientation of dome-and-basin elongation.....	627
E.1 Compaction estimation data.....	628
E.2 Vertical stylolite data.....	629
F.1 Point-count data of selected grainstones.....	634
F.2 Feldspar silt microprobe analyses.....	635
F.3 Phosphate AAS analysis.....	635
I.1 Calcite AAS analyses.....	650
I.2 Replicate calcite AAS analyses.....	652
I.3 Dolomite AAS analyses.....	653
I.4 Replicate dolomite AAS analyses.....	655
I.5 Calcite stable isotope analyses (serial samples).....	656
I.6 Calcite stable isotope analyses (single samples).....	657
I.7 Dolomite stable isotope analyses.....	658a
I.8 Precision of microprobe analyses.....	658b
L.1 Sphalerite microprobe analysis.....	672
M.1 Nodule Measurements.....	676

LIST OF PLATES

	PAGE
1. Conglomerate lithofacies.....	494
2. Conglomerate lithofacies.....	496
3. Calcarene lithofacies.....	498
4. Calcarene lithofacies.....	500
5. Siltstone lithofacies - shale lithofacies.....	502
6. Siltstone lithofacies - shale lithofacies.....	504
7. Siltstone lithofacies - shale lithofacies.....	506
8. Siltstone lithofacies - shale lithofacies.....	508
9. Mudstone lithofacies.....	510
10. Mudstone lithofacies.....	512
11. Trace fossils in mudstone lithofacies.....	514
12. Nodules in mudstone lithofacies.....	516
13. Nodules in mudstone lithofacies.....	518
14. Lower Head truncation surface.....	521
15. Truncation surfaces.....	523
16. Slide masses and related deformation.....	525
17. Subsurficial shear zones.....	527
18. Contorted limestones.....	529
19. Contorted limestones.....	531
20. Voids in fold noses.....	533
21. Compaction.....	535
22. Peloids and intraclasts.....	537
23. <u>Girvanella</u> clasts.....	539
24. <u>Girvanella</u> intraclasts.....	541
25. <u>Epiphyton</u>	543
26. Boundstone boulders.....	545
27. Radial fibrous calcite: field relationships.....	547
28. Radial fibrous calcite: petrography.....	549
29. Radial fibrous calcite: cathode luminescence.....	551
30. Radial fibrous calcite: cathode luminescence.....	553
31. Radial fibrous calcite: cathode luminescence.....	555
32. Conglomerate fibrous calcite.....	557
33. Conglomerate fibrous calcite.....	559
34. Cement and neospar.....	561
35. Cement and neospar: cathode luminescence.....	563
36. Displacive fibrous calcite.....	565
37. Displacive fibrous calcite.....	567
38. Displacive fibrous calcite.....	569
39. Displacive fibrous calcite.....	572
40. Displacive fibrous calcite.....	574
41. Displacive fibrous calcite.....	576
42. Displacive fibrous calcite.....	578
43. DFC and associated pseudospar.....	580
44. Equant pseudospar.....	582
45. DFC: evidence for early origin.....	584

LIST OF PLATES (continued)

	PAGE
46. Cathode luminescence and microprobe traverses.....	586
47. Dolomitization: field relationships.....	589
48. Dolomitization: petrography.....	591
49. Dolomitization: cathode luminescence.....	593
50. Siliceous sediments.....	596
51. Pseudo-wackestones: cathode luminescence.....	599
52. Barite.....	601
53. Nodule-matrix relationships.....	603

Chapter 1

INTRODUCTION

1.1 INTRODUCTORY REMARKS

Paleozoic deep-water carbonates are poorly understood rocks. They are not as widely exposed as their Mesozoic and younger counterparts nor are they as extensive and well-studied as shallow-water carbonates in general. Commonly deposited at continental margins, ancient deep-water successions are characteristically tectonized and consequently unsuitable for detailed analysis. Holocene analogues are not easily examined although physical processes and facies in deep-water carbonate slope environments are gradually becoming better-known based on study of Holocene slopes by dredging, coring, submersible observation, and remote detection. As Paleozoic deep-water carbonates formed at a time preceeding the explosion of calcareous plankton in the Mesozoic, direct comparison with post-Paleozoic deep-water carbonate sediments is not possible. The above, in conjunction with the paucity of exploitable hydrocarbon resources hosted within deep-water carbonates, has resulted in relatively few studies of these sediments.

Yet, deep-water slope carbonates are an extremely important element of the carbonate facies spectrum. In addition to the evidence they contain

of vanished platform margins, slope successions yield important information regarding slope processes and products, and some aspects of paleoceanography. Furthermore, slope carbonates may be potential reservoirs for hydrocarbons or the conduits through which basin-generated hydrocarbon migrates upslope to platformal reservoirs:

The Lower Paleozoic Cow Head Group is a relatively undeformed sequence of deep-water carbonates exposed in central western Newfoundland, mostly within the northwestern portion of Gros Morne National Park and the immediately surrounding area (Figures 1.1, 1.2). The Cow Head Group outcrops mainly as extensive coastal exposures, and to a lesser extent along the shorelines of ponds and inlets and in roadcuts and quarries. This study is an analysis of the sedimentology and diagenesis of the fine-grained sediments in this sequence.

1.2 PREVIOUS SEDIMENTOLOGICAL STUDIES

Schuchert and Dunbar (1934) conducted the first comprehensive regional study of western Newfoundland stratigraphy and considered the "Cow Head Limestone Breccia" as the "most striking and puzzling formation of western Newfoundland" (p. 73). Within this sequence, they included younger sediments now recognized to be autochthonous and indicated an age ranging from Upper Cambrian to Chazyan. Some of the finer grained sediments were included in a lowermost Ordovician "Green Point Series". They considered the breccias to have been shed from the noses of thrust sheets during Taconic Orogeny.

Figure 1.1: Geologic setting of the Cow Head Group, western Newfoundland (modified from Stevens, 1970).

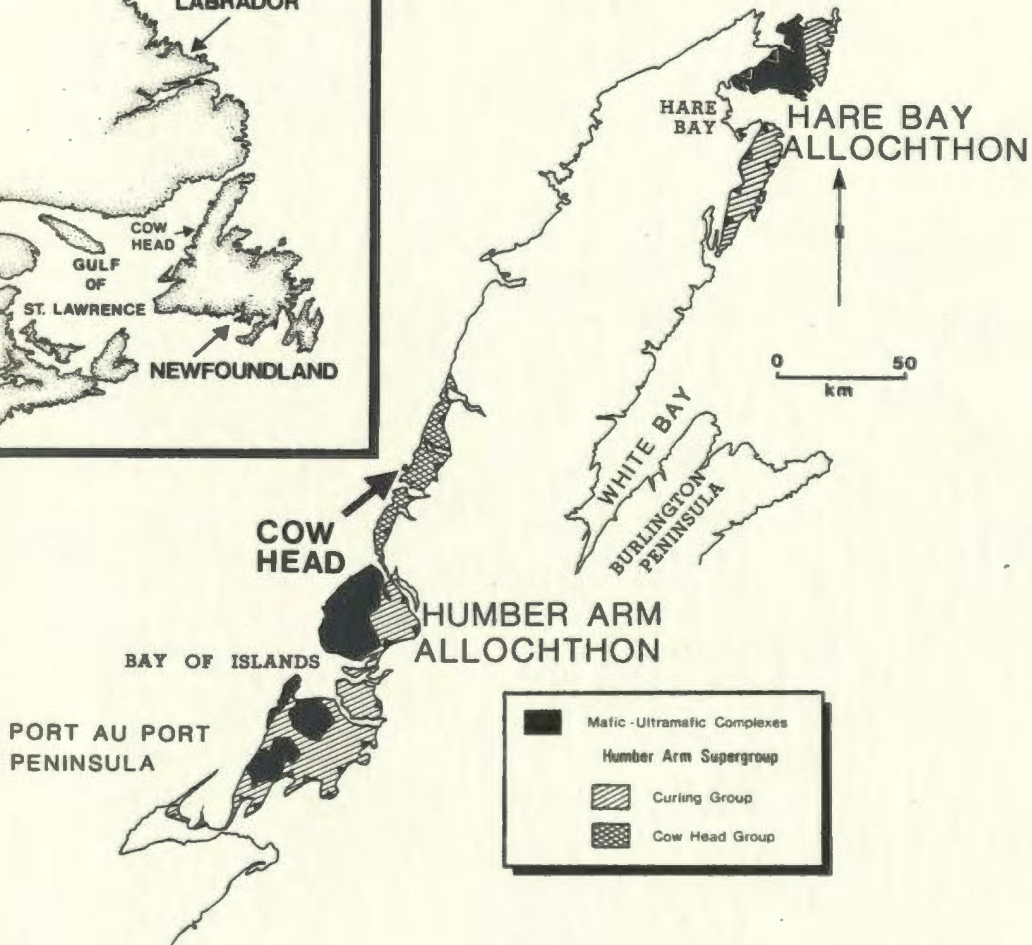
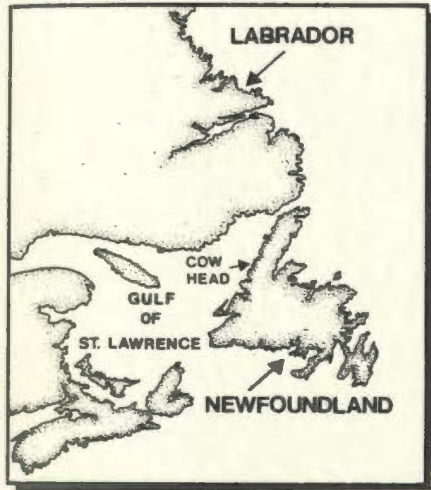
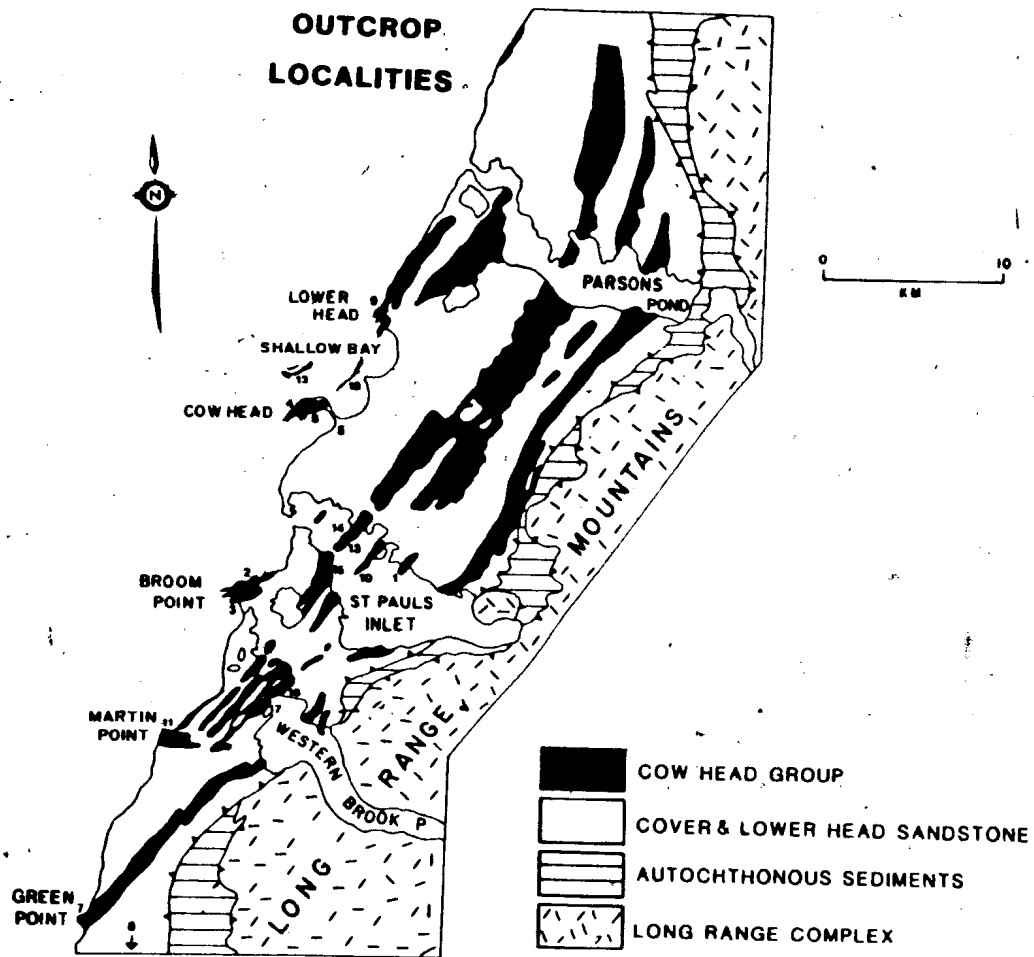


Figure 1.2: Outcrop localities (modified from James and Stevens, in prep.). Important locations and their abbreviated names as used in sample numbering and outcrop locations are listed below: (1) BB-Black Brook; (2) BPN-Broom Point North; (3) BPS-Broom Point South; (4) CHN-Cow Head North; (5) CHQ-Cow Head Quarry; (6) CHS-Cow Head South; (7) GP-Green Point; (8) LC-Lobster Cove; (9) LH-Lower Head; (10) LP-Long Point; (11) MP-Martin Point; (12) SI-Steering Islands; (13) SPN-St. Paul's North; (14) SPQ-St. Paul's Quarry; (15) SPS-St. Paul's South; (16) WBPN-Western Brook Pond North; (17) WBPS-Western Brook Pond South; (18) WI-White Rock Islets. All references to Bed and unit numbers are those of James and Stevens (in prep.).



Johnson (1941) noted faulting in the Parson's Pond, St. Paul's, and Western Brook Pond areas which he interpreted as high-angle thrusts (Figure 1.2). An exceptional low-angle thrust was observed along the southeastern shore in St. Paul's Inlet where crystalline basement is thrust over Ordovician limestone.

Oxley (1953) mapped the Cow Head area and suggested that regional structures indicated compression from the southeast. He also agreed with Schuchert and Dunbar (1934) as to the stratigraphic location of the sequence but noted the difficulty in correlating breccias over long distances.

Nelson (1955) examined the sequence in the Portland Creek area (north of study area shown in Figure 1.2) and noted the limited range of lithologies within any one breccia unit. He suggested that breccia formation may have been due to earthquakes affecting semi-consolidated muds. Because Schuchert and Dunbar (1934) had, however, examined more exposures, Nelson (1955, p. 45) stated that their origin hypothesis "is probably the best so far presented."

Kindle and Whittington (1958) elevated the sequence to "group" status and included both Schuchert and Dunbar's (1934) Green Point Series and older rocks near the type exposure on the Cow Head Peninsula (Figure 1.2). They compiled extensive faunal lists and noted that trilobites contained within fossiliferous clasts of the breccia units were approximately the same age as graptolites in immediately underlying shales. The Cow Head Group was found to range in age from late Middle Cambrian (Bathyuriscus - Elrathina zone) to earliest Middle Ordovician

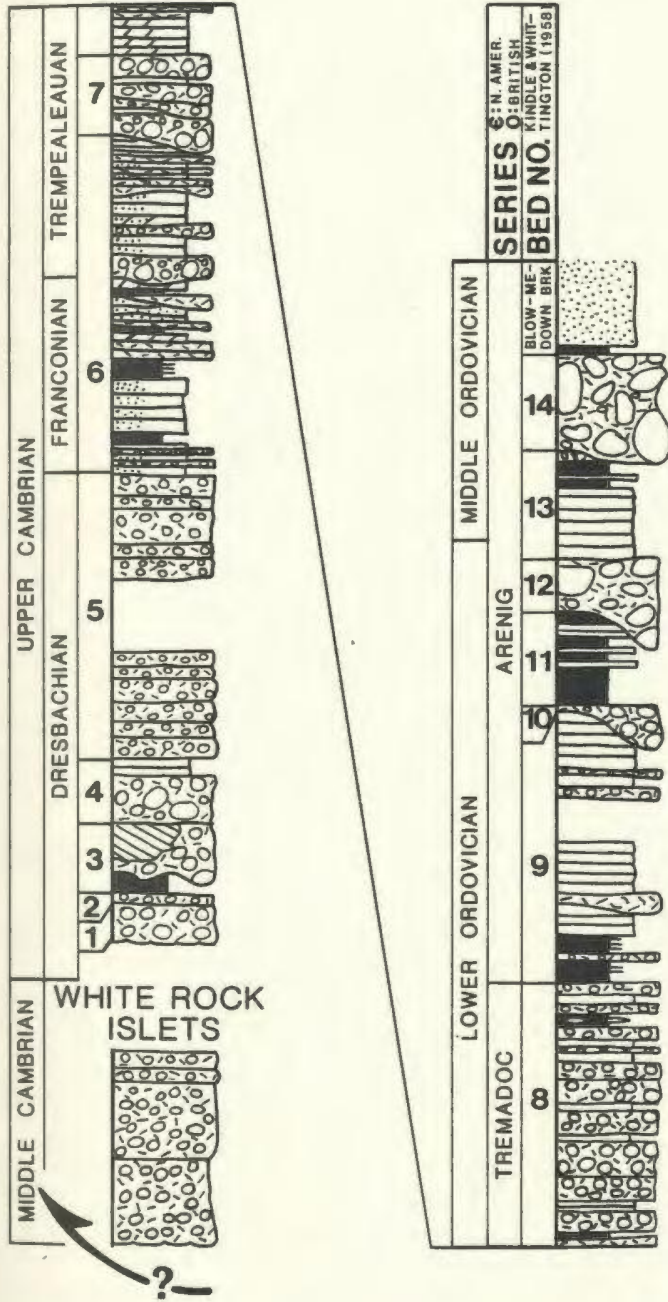
(James et al., 1980), a time span of approximately 70 million years. At the type locality the sequence was informally divided, based on lithology and faunal content, into 14 beds (Figure 1.3). Kindle and Whittington (1958) suggested that the breccia clasts slid down a submarine slope. They deduced the necessity of a raised source area for the production of larger (exotic) clasts, and the flat clasts were thought to have been produced by simple slumping. The limited age range of the clasts was interpreted to reflect derivation from a low-relief, submarine fault scarp, which initiated the slides. The entire Cow Head Group was considered as a flysch sequence based on comparison with flysch sequences known at that time.

Baird (1960) conducted the first detailed sedimentological study of the Cow Head Group. He recognized four types of breccias: (1) chaotic megabreccia, which was composed of an unbedded "wild jumble" of large "chunks" of various limestones; (2) shingle breccia, which was composed of flat, micritic, limestone clasts; (3) erratic boulder breccia, which was characterized by the presence of erratic boulders apparently "dropped into a mass of normally accumulating sedimentary material" (Baird, 1960, p. 3); and (4) common limestone breccia, which by his description, appears to be an indistinct hybrid of the above-listed sediments. Baird (1960) envisaged the sediments of the Cow Head Group as originating in a re-entrant in a northeast-trending shoreline. Earthquake shocks, faulting, or oversteepening of some uplifted area may have all acted as triggers for the sliding, slumping, and turbidity currents. Locally, where the basin was sufficiently shallow, waves and shore currents produced intraformational conglomerates.

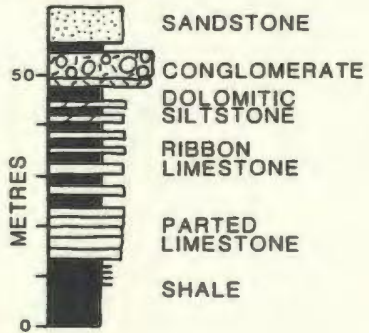
Figure 1.3: Composite stratigraphic section of the Cow Head Group type section from the Cow Head Peninsula (Upper Cambrian to Middle Ordovician) and White Rock Islets (Late Middle Cambrian), western Newfoundland (adapted from James and Stevens, in prep.). The Middle Ordovician Blow-Me-Down-Brook Sandstone has been renamed the Lower Head Sandstone (Williams et al., 1984).

COW HEAD GROUP TYPE SECTION

(COMPOSITE)



LEGEND



Rodgers and Neale (1963) recognized that shallow-water, platformal sediments surrounded on all three sides and probably underlay the deep-water sediments in western Newfoundland. The Cow Head terrane was noted to be similar to the Taconic Sequence and likewise was interpreted to be transported by westward gravity sliding to overlie the platformal sequence. The deep-water sediments were considered to be the result of "slow" mud deposition and turbidity current sedimentation. They also suggested that exotic clasts were derived from a shallow-water carbonate sequence to the west, but a mechanism for breccia formation was not specified.

Stevens (1970) recognized and described the Humber Arm and Hare Bay allochthons and interpreted the Cow Head Group as a flysch sequence deposited in a continental terrace - rise prism. He further indicated that the Cow Head Group was an example of an Atlantic-type proximal flysch and interpreted many of the thinly-bedded limestones as turbidites. The source of these sediments was considered to be the "over-steepened" oceanward edge of a carbonate bank, that provided detritus from Middle Cambrian to Middle Ordovician time." (Stevens, 1970, p. 167).

Fahraeus et al. (1974) described "pseudopellets" [1] from the Cow Head Group and considered them to be strongly cohesive micritic intraclasts scoured from the sea bottom. Their hydraulic equivalence with quartz sand grains within the same sediment was also established.

1. These particles are reexamined in Chapter 6.

Jansa (1974) examined the U-shaped burrows which occur in some of the bedded limestones and concluded that the trace fossil was Arenicolites, the result of a suspension-feeding polychaete [2]. The supposedly inclined burrow shafts were also interpreted as indicative of a southward-dipping depositional slope. Water depth was estimated at greater than 200 m and deposition was slow.

Nowlan (1974) briefly described lithologies at the type section in a study focussed mainly on conodont biostratigraphy. Breccias were suggested to have originated on the continental shelf and upper slope and to have been deposited on the lower continental slope. The detachment of breccia clasts was interpreted to be the result of earthquakes or increased sediment pore pressures in conjunction with an unspecified stimulus. Mass gravity flows with minor turbidity currents were considered to be the most significant transport mechanisms. Some "ungraded, well-sorted" micritic limestones and non-calcareous shales were thought to be pelagic and hemi-pelagic sediments. The lower continental slope depositional environment was based on the continuous bedding of some of the thinly-bedded sediments and some breccias, in contrast with the more channel-like deposits expected on the upper slope.

Callahan (1974) and Suchecki (1975) examined most of the major stratigraphic sections of the Cow Head Group, describing the sediments and conducting numerous measurements of paleocurrents, breccia fabrics,

2. These burrows are presently considered to be Diplocraterion by Narbonne and James (1984).

and various paleoslope indicators. Their data were integrated into the more regional synthesis of Hubert et al. (1977) who proposed a complex paleogeographic setting for the Cow Head Group with two narrow northwest-southeast trending carbonate platforms that were positioned on a regional, northeast-dipping slope. Breccias were interpreted as debris flows. Paleocurrents in thinly-bedded limestones beds were found to flow parallel to interpreted paleoslope contours and thus thought to be contour currents. In addition to previously listed causes, debris flows were hypothesized to have been triggered by platform collapse due to patchy distribution of early sediments increasing the sediment mass (cf. Hopkins, 1977) or to tsunamis.

Suchecki (1975) conducted a structural analysis of deformation at Broom Point (Figure 1.2) and suggested that all structures indicate northwest-directed compression, confirming Oxley's (1953) conclusions. Suchecki (1975) also studied the mineralogy and chemistry of clays in the Cow Head Group and later published his significantly revised results in Suchecki et al. (1977). This study is considered further in Appendix B.

James (1981) documented the common white limestone clasts that occur scattered throughout breccias in the sequence and found that they were remnants of algal mounds or bioherms. Their principal components are the calcified algae Girvanella and Epiphyton, with Renalcis and minor stromatolitic algae. These bioherms were interpreted to be a margin facies common to the platform edge of North America during the Lower Paleozoic.

The monograph of James and Stevens (in prep.) presents detailed lithostratigraphic and biostratigraphic data and analyses on all major exposures of the Cow Head Group. In this work, much new data is added to and modifies the existing biostratigraphic framework. They reject Hubert et al.'s (1977) previous assessment of paleogeography and propose a simpler reconstruction which is both internally consistent and congruous with regional considerations. This is discussed in more detail in a later section. The numerous graphic logs of measured sections in their study form the foundation upon which sampling and field observations of the present study are based.

Hiscott and James (in press) recently examined rheological aspects of the debris flows and concluded that paleoslopes were on the order of few degrees and that excess pore fluid pressures were important in permitting movement on such shallow slopes. Based on the thickest debris flows and largest clasts being Ordovician in age, Hiscott and James (in prep.) suggested that the shallow-water, platform margin progressively steepened through time. Their measurements of clast orientation fabrics provide a further basis for rejection of Hubert et al.'s paleoslope interpretation.

Other studies of the Cow Head Group are mainly taxonomic and biostratigraphic and of peripheral importance to the present study. Published studies not mentioned above include Fahraeus (1970); Fahraeus and Nowlan (1978); Fortey and Skevington (1980); and Kindle (1982). These studies are considered further in James and Stevens (in prep.). Other studies include graduate theses and various other projects in progress, and numerous abstracts.

1.3 GEOLOGIC SETTING OF THE COW HEAD GROUP

The Cow Head Group is 300-500 m in thickness and is interpreted as a base-of-slope carbonate apron deposited on the western flank of the Late Precambrian-Lower Paleozoic Iapetus Ocean (Stevens, 1970; James and Steven, in prep.). This succession occurs in a series of southeastward-dipping thrust slices (Oxley, 1953; Williams, 1975; James and Stevens, in prep.). Sediments vary considerably in composition and include coarse conglomerates, calcarenites, lime and dolomitic siltstones, ribbon, parted, and nodular limestones, shales, cherts, and minor quartz-rich calcarenites (Figure 1.3).

Partly coeval and lithologically similar strata of the Curling Group are exposed south of the Cow Head region and to the north surrounding Hare Bay (Figure 1.1; Stevens, 1970). Both the Cow Head and Curling Groups occur within the lowermost structural slices of the Humber Arm allochthon, although only the Curling Group is recognized in the Hare Bay allochthon. These allochthons are major components of the tectonostratigraphic Humber Zone which records the generation and destruction of the western margin of Iapetus (Stevens, 1970; Williams, 1979).

The Cow Head and Curling Groups are interpreted to have developed as part of the continental slope-rise complex (Stevens, 1970) which, based on palinspastic restoration of thrust slices, is suggested to have been approximately 200 km wide (Williams, 1980). The Cow Head and Curling

Groups along with minor interbedded volcanics and other transported sedimentary rocks constitute the Humber Arm Supergroup. This succession is structurally overlain by the Bay of Islands and Hare Bay ophiolite suites (Stevens, 1970). Possible metamorphosed equivalents of the Cow Head or Curling Groups occur in the Fleur de Lys succession of the Burlington Peninsula (Stevens, 1970; Bursnall and de Witt, 1975) and on the western side of White Bay (Lock, 1972).

Adjacent to and possibly underlying the allochthon is a 2 km-thick sequence of shallow-water, platform carbonates and siliciclastics which range in age from Lower Cambrian to Middle Ordovician (James, 1981). This sequence rests directly upon Grenville crystalline basement and is generally considered to be autochthonous (Figure 1.3). The shallow-water, platform-edge equivalents of the Middle to Upper Cambrian Port au Port Group [3] (James *et al.*, in prep.) and the Lower Ordovician St. George Group (Pratt, 1979) both presumably were important contributors of detrital carbonate to the slope environment, but these platform-edge sediments are not exposed.

The Taconic orogeny reflects the partial to complete closing of the Iapetus Ocean (Rodgers and Neale, 1963; Stevens, 1970). During Early and Middle Ordovician time, eastward-imblicated slices of ophiolite travelled toward the western flank of the ocean. The upward-deepening facies of the autochthonous, Middle Ordovician Table Head Group are interpreted to reflect this eastward tectonic loading (Klappa *et al.*,

3. Correlation of the Cow Head Group with time-equivalent, shallow-water, platform sediments is found in James and Stevens (in prep.).

1980). This Middle Ordovician platformal succession eventually foundered and an easterly-derived, diachronous flysch capped both the platformal succession (Mainland Sandstone) and slope-rise complex (Lower Head Sandstone; Williams et al., 1984). The slope-rise sediments were subsequently overthrust by the stacked allochthons, incorporated into their bases, transported westward and finally emplaced over the shallow-water, platformal succession (Stevens, 1970; Williams, 1979). Time of emplacement of the Humber Arm allochthon is estimated to be Llandeilian or early Caradocian whereas the Hare Bay Allochthon may have been emplaced slightly earlier (Stevens, 1970).

1.4 STRUCTURAL GEOLOGY

1.4.1 Regional

Three tectonic events, spanning a large portion of the Paleozoic, affected rocks in the northern Appalachians, although not all areas were equally deformed. The Middle Ordovician Taconic orogeny was followed by Middle Devonian Acadian orogeny, and lastly the Permo-Carboniferous Alleghanian orogeny. All three involved compression and shortening along a sub-parallel, northeast-southwest structural trend (Williams et al., 1972; Williams, 1980; Kennedy, 1982). Based on regional syntheses, the deformation styles of these orogenies are known in a general way (Williams, 1979; Colman-Sadd, 1982). Recent detailed analyses suggest that the deformation history is complex and individual orogenies may consist of more than one deformation event (Kennedy, 1982; T.J. Calon, pers. comm., 1983).

Taconic deformation is generally characterized by west-facing recumbent

structures and westward transport of allochthonous terranes. This orogeny is explained by a plate tectonic model in which the Iapetus-closing episode terminated with attempted eastward subduction of continental crust under oceanic crust (Dunnage Zone). Acadian deformation is more widespread than Taconic deformation and is most intensely developed in central Newfoundland where it is characterized by tight, upright folds, commonly northeast-plunging, and a steep cleavage. The plate tectonic cause of this orogeny is uncertain although it is generally assumed to be a major continental collision east of the Avalon Zone (Williams, 1979; Kennedy, 1982). According to Williams (1980) the effects of Alleghanian orogeny at the northern end of the Appalachians are minimal relative to effects found in the rest of the Appalachians (i.e. mainland Canada and the southern orogen), although deformation may be localized to fault zones of unknown displacement (Kennedy, 1982). The causes of this orogeny are uncertain.

1.4.2 Humber Arm Allochthon and Cow Head Group Structure

Taconic and Acadian orogenies are the most important deformation events to have affected the rocks of the Humber Arm allochthon although the most widespread deformation is generally regarded as Acadian (Williams, 1979). In contrast, recent unpublished work suggests that Taconic orogeny resulted in the most important deformation and Acadian orogeny only modified to a minor extent an already deformed terrane (T.J. Calon, pers. comm., 1983).

Oxley's (1953) geological map of the Cow Head area demonstrates that northeast-southwest striking faults with dips of 30-85 degrees SE are

the most salient aspect of the structure. Since this early work, there have been no specific studies of Cow Head Group structure except by Suchecki (1975) at Broom Point whose study of smaller scale structures such as small folds and vein patterns was in agreement with Oxley's (1953) major findings as well as more regional analyses (Williams et al., 1972).

There is no available published data on the recognition of Taconic (emplacement) structures from those of later Acadian and possibly Alleghanian orogenies in the Cow Head Group. Possible emplacement structures include folding at Lower Head, Broom Point North, and Martin Point (R. K. Stevens, pers. comm., 1983) and vertical-to-bedding pressure solution interfaces (discussed in Chapter 5).

1.5 PALEOGEOGRAPHY AND DEPOSITIONAL SETTING

1.5.1 Hypothesis of Hubert et al. (1977)

The paleogeographic reconstruction of the Cow Head Group (henceforth abbreviated "CHG") proposed by Hubert et al. (1977) was based on the relationship between deduced paleoslope orientation and measured paleocurrents. The orientation of the paleoslope was derived indirectly from measurements of synsedimentary boudins (discussed in Chapter 14 and Appendix M), "elongate load casts" or "load axes", and fold axes in in situ sediments (discussed in Chapters 3 and 4) as well as in deformed clasts within conglomerates (Callahan, 1974; Suchecki, 1975; Hubert et al., 1977). Their treatment of these data led them to conclude that

paleoslopes dipped mostly to the southwest and to a lesser degree, to the northeast. Furthermore, there were at least two northwest-southeast trending carbonate platforms; one located between Cow Head and Lower Head and the other near Martin Point and Gulls Marsh. An additional platformal source southwest of Green Point was also hypothesized. These platforms were located on a regional northeast-dipping slope whose orientation was, "in part inferred from thirty Ordovician sections" (Hubert et al., 1977, p. 139).

Based on more than 1200 measurements of cross-laminations (mega-ripple and ripple), flutes, grooves, and grain lineations, they found paleocurrents to be dominantly southeastward flowing [4]. Their averages for Cambrian and Ordovician strata are 150 and 130 degrees SE, respectively. There is considerable data scatter, however, and currents directed anywhere between east and south are common. The postulated paleogeography necessitated that these paleocurrents be interpreted as contour currents which flowed parallel to paleoslope contours. In addition, these currents were presumably accelerated between the platforms and thus deposited graded, ungraded, planar, and cross-bedded limestones. Flutes, grooves, and grain lineations were also formed by these currents.

4. Their results have been confirmed by this study as well as that of James and Stevens (in prep.) and Hiscott and James (in press).

1.5.2 A Revised Paleogeography

In light of regional, biostratigraphic, and lithostratigraphic considerations, the above paleogeographic model has been revised by James and Stevens (in prep.) who instead propose a simpler, interpretation without the complex elements of Hubert et al.'s (1977) model. The revised paleogeography is also supported by Hiscott and James (in prep.) and this study. The salient aspects of the preliminary model of James and Stevens (in prep.) are the following (Figure 1.4):

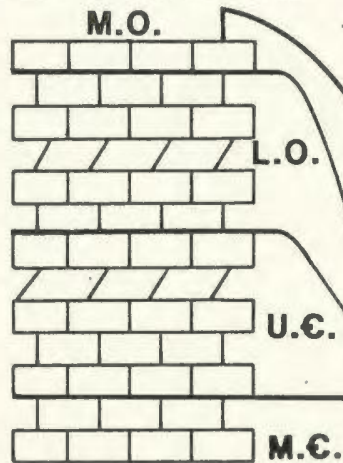
(1) Based on palinspastic reconstruction, there is a northwest-southeast change in the dominant lithofacies from proximal (area around Cow Head and Lower Head) to distal (Green Point). In the area of Cow Head and Lower Head, sediments are mainly conglomeratic whereas thinly-bedded limestones and shales become more prominent southeastward. Accompanying this change is a decrease in the maximum clast size in conglomerates. A sharp change in the lithofacies transition occurs between Cow Head and St. Paul's/ Broom Point which is interpreted by James and Stevens (in prep.) to represent a break in slope (see Figure 1.4).

(2) The southeastward-oriented paleocurrents are not parallel to the presumed paleoslope contours as suggested by Hubert et al. (1977) but instead are normal to the southeastward-dipping paleoslope as determined from regional considerations. These sediments were derived from a carbonate platform which was oriented approximately northeast-southwest, normal to the observed facies trends.

FIGURE 1.4: Depositional setting of the Cow Head Group (allochthon) relative to hypothesized shelf break and autochthonous platformal succession. Generalized lithofacies distribution in the Cow Head Group is also shown. Outcrop localities are shown in Figure 1.3 (modified from James and Stevens, in prep.).

DEPOSITIONAL SETTING

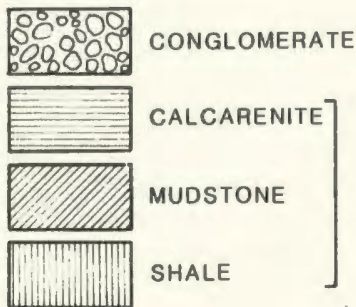
AUTOCHTHON



**SHELF BREAK
(NOT PRESENT)**

ALLOCHTHON

LITHOFACIES



includes
SILTSTONE

STEARING ISLANDS

COW HEAD

BROOM POINT

ST. PAUL'S

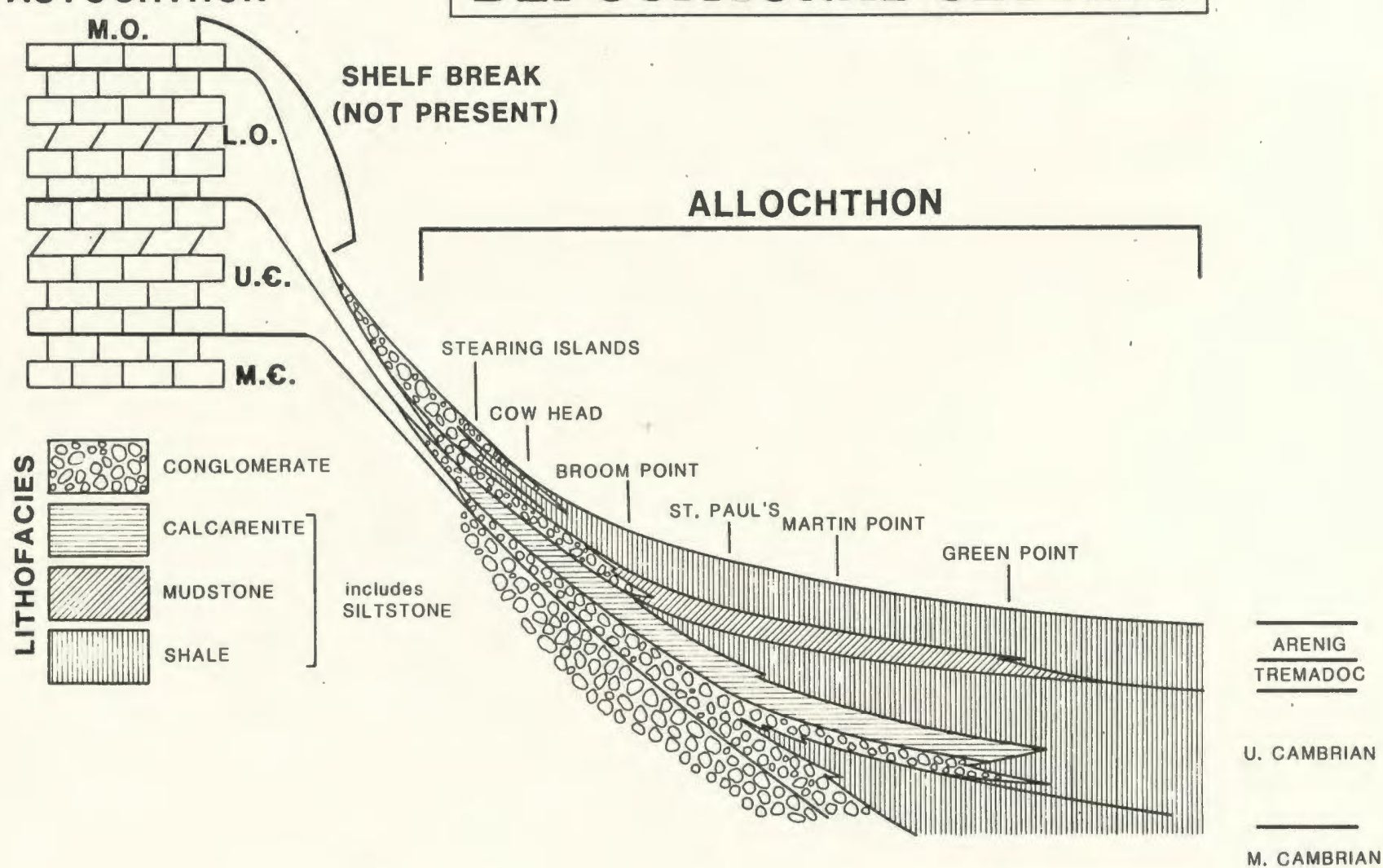
MARTIN POINT

GREEN POINT

ARENIG
TREMADOC

U. CAMBRIAN

M. CAMBRIAN



The Middle Ordovician Lower Head Sandstone which overlies the CHG is interpreted by James and Stevens (in prep.) to have been derived from the north and deposited into an elongate trough with a relatively flat floor. This, in conjunction with evidence in the CHG for slope failure even in the most distal outcrops (see Chapter 3), led James and Stevens (in prep.) to suggest a base-of-slope setting for the CHG. Sediments were deposited as a base-of-slope apron at the transition from the continental slope to rise (see Cook, 1983b for discussion of ancient slope deposits).

1.6 APPROACH TO STUDY

1.6.1 Database

This study is based on integration of field relationships and petrography, supported by cathode luminescence, X-ray diffraction, scanning electron microscopy, and geochemical analyses (microprobe, atomic absorption spectrophotometry, stable isotopes). Field work was carried out over the course of two summers in 1981 and 1982. A total of 825 hand specimens were collected and slabbed. Thin sections were routinely stained with standard solutions of Alizarin Red S and potassium ferricyanide, and then coated with a spray-on cover slip. 750 stained thin sections were examined during the course of this study from specimens collected by the author. An additional 400 thin sections were examined from the collection of N.P. James. Approximately 150 polished thin sections were studied with cathode luminescence; 60

thin sections were analysed by microprobe. Samples used for atomic absorption spectrophotometry, stable isotope analysis, and X-ray diffraction (shales) are described in Appendices B, I, and J. Technical procedures and instrumentation are described in Appendices B and I.

1.6.2 Organization

This thesis is divided into 3 parts - A (Chapters 2-6), B (Chapters 7-13), and C (Chapter 14). Part A deals with various aspects of the sedimentology, including: primary sedimentation, especially of the fine-grained (non-conglomeratic) lithofacies; synsedimentary deformation related to slope failure and other intrastratal deformation related to tectonic compression; effects of mechanical compaction and pressure solution; and the composition of the fine-grained (i.e. non-conglomeratic) sediments. In Part B the emphasis is on diagenesis, focussing primarily on the fine-grained sediments, but also incorporating information from select conglomerates. Calcite authigenesis, dolomitization, silicification, replacement of siliceous components, and barite and pyrite precipitation are all discussed. Part C synthesizes previously examined field, petrographic, cathode luminescence, and geochemical relationships and interpretations and proposes physical and chemical models to explain the genesis of parted, ribbon, and nodular carbonate mudstones.

PART A: SEDIMENTOLOGY

This section is a documentation of the physical aspects of the CHG, including depositional mechanisms, submarine sliding, compaction, and sedimentary components.

The lithofacies spectrum is described in Chapter 2, emphasizing the fine-grained (non-conglomerate) sediments. Five lithofacies are recognized: (1) conglomerate, (2) calcarenite, (3) siltstone, (4) shale, and (5) mudstone. The mudstone lithofacies, which includes parted, ribbon, and nodular limestones, is characteristic of many Paleozoic and Mesozoic deep-water carbonate successions. Some features of this lithofacies cannot be explained on the basis of physical sedimentation alone, and these sediments are further analysed in Part B of this thesis.

The evidence that the CHG was deposited on a slope is outlined in Chapter 3 and includes discussion of syndimentary deformation fabrics and a sediment failure model.

In Chapter 4 enigmatic contorted limestones which commonly form dome-and-basin structures are examined in light of hypotheses suggesting: (1) syndimentary deformation due to submarine sliding; (2) expansive crystallization; and (3) horizontal tectonic compression.

The relative importance of mechanical compaction and pressure solution during burial diagenesis is examined in Chapter 5. In addition, pressure

solution related to tectonically-produced horizontal compression is discussed.

CHG limestones, as with many other Paleozoic shallow- and deep-water limestones, are characterized by abundant peloids. Microfabrics of exceptionally well-preserved peloids are examined in Chapter 6 and it is proposed that many are algal in origin.

Chapter 2

LITHOFACIES OF THE COW HEAD GROUP

2.1 INTRODUCTION

Conglomerates in the CHG have been the focus of virtually all previous sedimentological studies (e.g. Schuchert and Dunbar, 1934; Baird, 1960; Hubert et al., 1977; James, 1981; Hiscott and James, in press). In contrast, the relatively thinly-bedded, fine-grained (i.e. non-conglomeratic) sediments have been little studied. "First-order" appraisals of the fine-grained sediments include those of Kindle and Whittington (1958), Rodgers and Neale (1963), Stevens (1970), Callahan (1974), Fahraeus et al. (1974), Nowlan (1974), Suchecki (1975), Hubert et al. (1977), and James and Stevens (in prep.). Although the temporal and spatial distribution of the fine-grained sediments are well known (see James and Stevens, in prep), there are no detailed studies of these sediments.

Sediments of the CHG are divisible into 5 principle lithofacies: (1) conglomerate, (2) calcarenite, (3) siltstone, (4) shale, and (5) mudstone. The siltstone and shale lithofacies are considered together in the same discussion for reasons that will be apparent later on. Although the primary focus of this chapter is the fine-grained

sediments, conglomerates are also examined in order to complete the sedimentological framework. Primary sedimentary processes responsible for deposition of the CHG can thus be compared to processes known to occur on modern slopes (e.g. Mullins, 1983; Cook and Mullins, 1983) as well as on other ancient slopes (e.g. Cook and Enos, 1977; Cook, 1983b; McIlreath and James, 1984). The primary sedimentary framework also provides the critical foundation upon which all subsequent aspects of this thesis are based.

2.2 CLASSIFICATION AND TERMINOLOGY

2.2.1 Basic Definitions

Some of the terminology used in this thesis is defined in the following section. Deviation from these definitions are either explained where they occur or are left unexplained where their meaning is obvious from their usage in context. The following definitions, except for "composite bedding", are discussed further in Pettijohn (1975); Fairbridge and Bourgeois (1978); and Potter et al. (1980).

Beds are relatively homogeneous lithologic units separated from their neighbours by bedding planes or by changes in mineralogy, texture, colour, or other physical attributes. These changes may be primary depositional or diagenetic. Beds are differentiated from laminations by size; laminations are 1 cm thick or less whereas beds are greater than 1 cm in thickness. The different parts of the Bouma (1962) sequence are referred to as divisions. Composite bed, as defined in this thesis,

refers to a rock unit bounded above and below by partings and which internally consists of two or more beds.

2.2.2 Classification of Bedding

An uncomplicated, easily-applicable classification for the qualitative field description of bedding is used to describe depositional as well as diagenetic bedding characteristics, independent of origin. Two basic characteristics are important: (1) the proportion of carbonate beds relative to shale or marl beds, and (2) the geometry of the carbonate beds (Figure 2.1).

Carbonate beds consist of limestone and/or dolostone. Limestone textures range from mudstone through grainstone (sensu Dunham, 1962).

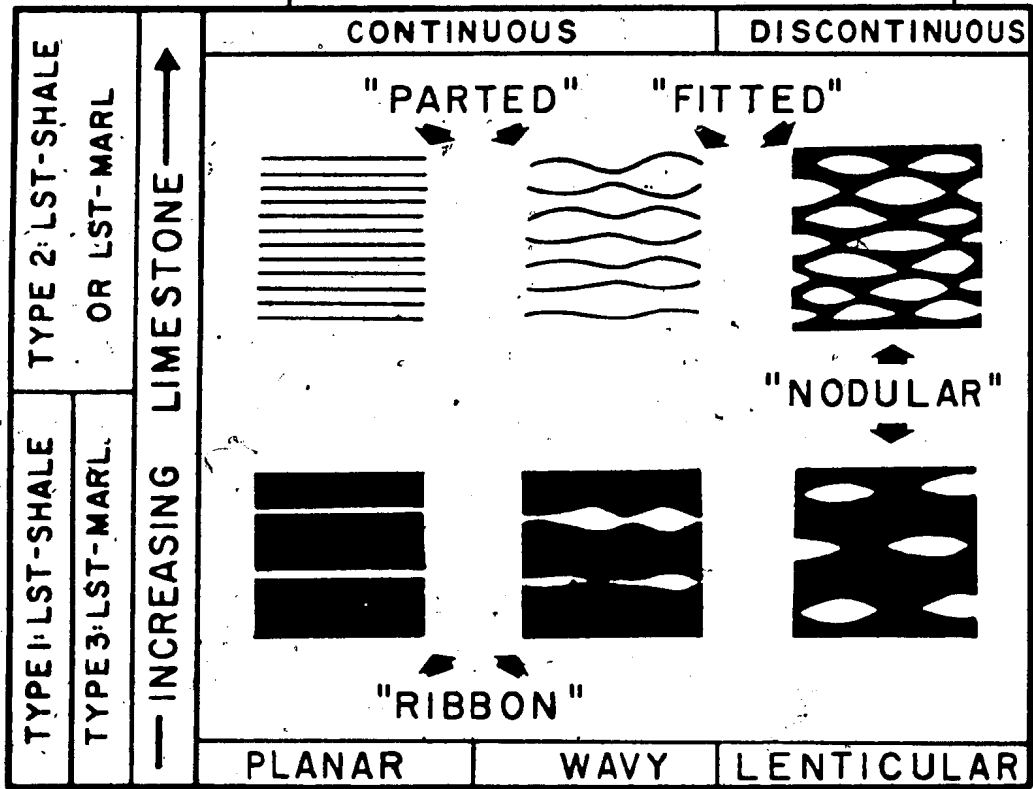
All muds and mudstones referred to in this thesis are calcareous; siliciclastic muds are referred to as terrigenous muds and their lithified equivalents are shales. Shales contain little or no carbonate. Marl refers to sediment composed of clays and carbonate. It includes argillaceous carbonates through to carbonate-rich shales (see Pettijohn, 1975).

Carbonate beds are separated from one another by shales or marls. In this study parted [1] refers to a carbonate sequence (usually limestone) in which the beds are separated by argillaceous layers (shale, marl, or silicified equivalents) up to 1 cm thick (Type 2 bedding in Figure 2.1).

1. The term "parted" was originally used to designate interbedded pure carbonates and argillaceous, siliceous, or silty carbonates whose weathering produces a "flaggy character to the outcrops" (see Aitken, 1966, p. 411).

Figure 2.1: Terminology for the description of bedding in the Cow Head Group sediments. See text for discussion.

BEDDING TERMINOLOGY



Ribbon carbonates are differentiated from parted carbonates when the thickness of the argillaceous interbed is more than 1 cm (Types 1 and 3 bedding in Figure 2.1). Type 1 ribbon carbonates are separated by relatively carbonate-free shales. Type 3 ribbon carbonates, on the other hand, are interbedded with calcareous or dolomitic marls. These bedding types are intergradational.

Description of bed geometry considers two additional variables - bed continuity and thickness variation. Beds which are laterally continuous and have constant thickness are planar. Variations in thickness occur as symmetrical or asymmetrical pinch-and-swell or wavy bedding.

Discontinuous bedding is lenticular or nodular. Where interbedded marl or shale is minor (less than 1 cm in thickness), wavy and lenticular beds commonly demonstrate a fitted 2} fabric where thicks fit into thins of adjacent carbonate beds.

The terms "lenticular" or "nodular" are strictly non-genetic descriptors. "Concretion", on the other hand is genetic and refers to carbonate of accretionary origin, i.e. carbonate beds or nodules growing from progressive, centrifugal precipitation of carbonate or other mineral phases. This process is commonly an early, pre-burial-compaction phenomenon. This is synonymous with "diagenetic segregations" as used in Pettijohn (1975). The above conforms with usage in most other, recent studies. Early-cemented grainstones may also be considered as concretions.

2. Wanless (1979) also used this term to describe a similar fabric in strata modified by pressure solution.

This bedding geometry nomenclature is similar to that of Reineck and Wunderlich (1968). Fitted fabrics of this study resemble the effect of mud flasers draping ripples. Wavy and lenticular beds in the CHG also demonstrate similar geometric, though not necessarily genetic, relationships as those of Reineck and Wunderlich (1968).

A number of complexities are ignored in applying the above classification. These include the following:

- (1) The carbonate-shale or carbonate-marl boundary is not always sharp and the limiting "parting" thickness of 1 cm, in addition to being arbitrary, is also subjective.
- (2) Shale or marl thickness varies in wavy and lenticular beds.
- (3) Thick shale or marl interbeds often contain thin (few millimetres or less) pure carbonate laminations.
- (4) Silicification and dolomitization obliterate or alter primary sedimentary characteristics thus reducing distinction between carbonate and originally more argillaceous interbeds.
- (5) The field HCl test does not readily differentiate mixed carbonate content (i.e. calcite and dolomite) in marls. A sediment whose carbonate fraction contains 20% calcite and 80% dolomite, for example, is only mildly effervescent.
- (6) Proper recognition of wavy and lenticular bedding ideally necessitates mutually perpendicular views of bedding (Reineck and Wunderlich, 1968). This is a condition not commonly encountered in the

CHG sediments.

2.2.3 Clarification of the Term "Mudstone"

Before proceeding to description, some discussion of the term "mudstone" as used in this thesis is necessary. In his limestone classification, Dunham (1962) used the term to describe rocks of detrital carbonate mud origin containing less than 10% allochems. In many carbonates, however, the occurrence of microspar or pseudospar often renders the presence of a carbonate mud precursor to be inferred from textural relationships. The term "crystalline carbonate" was used by Dunham (1962) for limestone or dolostone which retained insufficient fabric relics necessary to successfully classify them according to depositional texture. This category could easily be expanded to include purely secondary carbonates, for example concretions, which are not necessarily neomorphosed primary muddy sediments.

Field and laboratory examination of parted and ribbon limestones demonstrates that they are what most sedimentologists would unhesitatingly classify as microspar or pseudospar [3] "mudstones". It will be shown later that these mudstones are, in many instances, petrographically and geochemically identical to associated "crystalline limestone" nodules of probable concretionary origin. To avoid potential nomenclatural entanglements, the term "mudstone" is used in this thesis not as Dunham (1962) originally intended, but instead to refer to limestones composed of micrite, microspar, or pseudospar containing less

3. Definitions of these terms are provided in Appendix H.

than 10% detrital particles, irrespective of origin. These mudstones may be (1) entirely diagenetic in origin, (2) neomorphosed "primary" mudstones, or (3) a combination of 1 and 2 above.

2.3 CONGLOMERATE LITHOFACIES: DESCRIPTION

2.3.1 Introduction

Conglomerates typically occur as resistant-weathering, extensive outcrops characterized by light to medium grey-weathering carbonate clasts set in a darker-coloured matrix. Traditionally inaccurately labelled as "breccia" (e.g. Schuchert and Dunbar, 1934; Hubert *et al.*, 1977), these sediments range from monomictic to polymictic and have variable internal structure, clast-packing fabrics, and matrices. Their lateral continuity is remarkable in some instances and correlations over distances of 20 km are possible (James and Steven, in prep.). Baird (1960) attempted the first detailed sedimentological study of this lithofacies and provided a template for the recent study by Hiscott and James (in press) who recognized 5 different conglomerate sublithofacies types based on sedimentary structures, grading, matrix composition, sorting, and clast types. The following section is based upon my own observations, supported and expanded where appropriate, by data from the above-listed and other studies. Conglomerates similar to those of the CHG are common throughout the geologic record. Other Appalachian examples have been described from the Taconic allochthon (Keith and Friedman, 1977) and the southern Appalachians (Pfeil and Read, 1980).

2.3.2 General Description

The most important variations in the conglomerates are a function of their relative geographic locations. In the northern part of the study area, such as Lower Head or Cow Head North (Figure 1.2), outcrops are characterized by the most and thickest conglomerates, largest size and variety of clasts, poorest sorting, and greatest amount of basal scour (Plate 1a). Toward the south, for example at Martin Point or Green Point, conglomerates constitute a minor portion of the sequence, are reduced in thickness, and contain smaller, less variable clasts.

Beds vary from 10 cm to greater than 10 m in northern outcrops. At Cow Head North, a northern outcrop, conglomerates reach 25 m thickness and comprise 55% of the exposed sequence (Hiscott and James, in press). Bed geometry is gently wavy or lenticular with abrupt or gradual, tapered margins (Plate 1b). Basal scour is generally absent or minor, although some thicker conglomerates erode 10 metres or more of the underlying thinly bedded limestones and shales. Sole marks are infrequent and dominated by broad, elongate casts which are either flutes or loads. "Mega-flames" (injection structures) of ribbon limestone, up to 8 m in length, occur at the base of conglomerates at Cow Head North and Lower Head and are characterized by relatively coherent or fragmented bedding. Several isolated boulders also appear to have sunk out of the conglomerate into the underlying ribbon limestones at Cow Head North (see Hiscott and James, in press).

Conglomerate beds are both single and composite, the latter consisting

of two or more amalgamated ("welded") conglomerates. Recognition of composite beds is based on: (1) abrupt vertical change in dominant clast size, relative abundance of various clasts types, or characteristics of matrix, or (2) in situ relics of beds which capped a conglomerate (now lower part of amalgamated unit) but were not completely eroded prior to or during emplacement of overlying conglomerate.

2.3.3 Clasts

Maximum clast size and bed thickness are commonly positively correlated. In northern outcrops (e.g. Lower Head and Cow Head North), thick conglomerates of Bed 14 (Figure 1.3) contain several house-size and larger boulders, the largest being the "Lower Head Boulder", which, in plan view, measures approximately 200 X 50 m in size (Kindle and Whittington, 1958). Maximum clast size is usually considerably smaller, commonly within the cobble-size range or below, especially in more southern outcrops.

Clasts are classified as "endemic" or "exotic", based on whether they were derived from the slope or from the shallow-water carbonate platform, respectively (Table 2.1). Based on qualitative estimates, the proportion of exotic to endemic clasts may be as high as 1:1 in northern exposures. With decreasing bed thickness, there is a decrease in relative proportion and size of exotic clasts.

Exotic Clasts: Exotic clasts span a wide variety of lithologies and commonly contain sedimentologic or faunal evidence of shallow-water, photic-zone derivation, for example, blocks containing calcified algae

TABLE 2.1: TYPES OF CONGLOMERATE CLASTS

EXOTIC BOULDERS

Shallow-water derivation. Lithologically variable, clasts are represented in the autochthonous succession of western Newfoundland with some exceptions (e.g. calcified algal mounds). Fractures in clasts often contain abundant radiaxial fibrous calcite. Fossils include trilobites, brachiopods, pelmatozoans, sponges, calcified algae, cephalopods, gastropods, ostracods, bryozoans, and stromatoporoids(?). Maximum size is 500 m (Lower Head). Up to 10-20 m size is common in proximal exposures. Most clasts are in the boulder-size range and smaller.

FLAT CLASTS

Slope derivation, dominated by mudstones and minor grainstones. Clasts may be massive, parallel-laminated, or more rarely, rippled. Dolomitic and chert clasts are also locally important. Maximum size is 1 m length and 15 cm thick.

RAFTS

Slope derivation. Consists of interbedded limestone and shale/marl. Limestone lithology is same as for flat pebbles. Nodular rafts are rare. Clasts contain abundant evidence of soft-sediment deformation. Fragmentation of rafts produces flat pebbles and argillaceous conglomerate matrix. Maximum size is 20 m.

MISCELLANEOUS

Rare isolated fossils include cephalopods, planispiral gastropods. Other, presumably slope-derived clasts include dolomitic armoured mudballs, resedimented conglomerate fragments, shale clasts, phosphatic pebbles, pyrite concretions, septarian and other calcite concretions, displacive fibrous calcite clasts.

(Plate 1a; James, 1981). Their shape is usually equant to elongate and they are rounded to angular with no evidence of plastic, synsedimentary deformation. This implies they were incorporated into the conglomerates as well-lithified limestone.

Flat Clasts: Most flat clasts are inferred to be the product of resedimentation of slope-derived material, although, in most instances, this is difficult to prove directly in the field or petrographically. These endemic clasts are typically tabular, less than 30 cm long and 2-5 cm thick, have rounded to irregular polygonal outlines, and are commonly bent and fractured. The tabular aspect diminishes with decreasing clast size (Plate 1c). They dominantly consist of massive or parallel-laminated mudstone with subordinate grainstone and packstone.

Rafts: An important exception to the above size limitation of endemic clasts are large "rafts", up to 25 m in length, of coherently-bedded parted and, to a much lesser extent, ribbon and nodular limestones. Rafts are most abundant in the Late Cambrian strata at Cow Head North and Middle Ordovician strata at Lower Head and Cow Head North and South. Lithologically they are identical to (and likely the source of) the flat pebbles. The paucity of ribbon and nodular limestone rafts is probably the result of their disaggregation to flat pebble clasts during transport, a function of their relatively lower content of limestone.

"Soft sediment" folding, faulting, fracture cleavage formation, and brecciation are common in large rafts and lucidly demonstrate the high degree of limestone lithification relative to plastically-deformed argillaceous interbeds. Competent limestone beds are of constant

thickness and control folding in the rafts (Plate 1d). In contrast, argillaceous interbeds are characterized by similar folding where thickening occurs in fold hinge zones and thinning occurs in the limbs. Limestone beds which develop a pronounced fracture cleavage may also have the resultant microlithons (i.e. unit of rock bounded by cleavages and bedding) slightly rotated due to interlayer shear generated during folding (Plate 1d). Faulting and brecciation within the rafts produce angular, commonly rectangular, limestone fragments enclosed within an argillaceous matrix (Plate 1e,f). The shape of these fragments reflects the influence of an early fracture cleavage oriented perpendicular to bedding.

These deformation characteristics are very similar to those expected during "hard rock" tectonic deformation. Such an origin can be safely discounted based on: (1) lack of associated veining, (2) lack of consistent orientation of folds or fracture cleavages, and most importantly, (3) the invariable restriction of this style of deformation to rafts.

2.3.4 Matrix

Conglomerate matrix may be muddy (shale, marl, or lime mudstone), grainy, or any mixture of these. Less commonly, infiltrated lithic sands (Hiscott and James, in press), and bladed calcite cement and associated internal sediment (discussed in Part II) are found in the uppermost metre of some conglomerates. Grainy matrices are typically poorly-sorted peloid and intraclast grainstones and packstones. The boundary between conglomerate clast and matrix clast in these poorly

sorted sediments is arbitrarily assigned at 1 mm (cf. Naylor, 1980). The nature of the original matrix is uncertain in some conglomerates due to significant diagenetic overprinting.

2.3.5 Grading, Internal Structure, and Packing

Most conglomerates demonstrate a massive (i.e. structureless), chaotic clast fabric, regardless of matrix composition (A in Figure 2.2). Crude, normal grading of pebble-size clasts through to sand-size grainstone (C in Figure 2.2; Plate 1c) and graded matrices are comparatively rare, found only in conglomerates which grade upward into pebbly calcarenites (discussed in next section). Many conglomerates are capped by parallel- and ripple-laminated grainstone layers up to 15 cm in thickness, a situation similar to the "two layer" deposits described by Krause and Oldershaw (1979).

Wave-forms such as those described by Hubert et al. (1977) are only locally developed and are neither as extensive nor as obvious as their descriptions suggest (Plate 2a; also see Hiscott and James, in press). Cross-bedding in conglomerates is rare, and is delineated by flat clast alignment defining coarse foresets (Plate 2b). Other conglomerates are characterized by local clast imbrication and "swirled" domains (B in Figure 2.2), the latter displaying a gradual change in flat clast orientation.

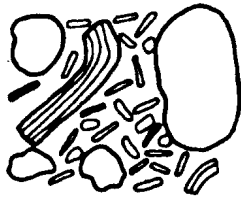
Clast packing varies between and within flows (Plates 1d, 2c; Figure 2.2). Floating ("particulate rubble floatbreccia" - Morrow, 1982c) and clast-supported ("particulate rubble packbreccia") fabrics occur in

Figure 2.2: Variations in clast-matrix and clast-clast relationships in the conglomerate lithofacies.

CONGLOMERATE FABRICS

CLAST-CLAST

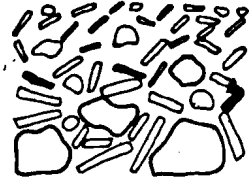
A MASSIVE



B IMBRICATED, SWIRLED

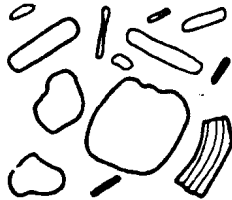


C GRADED



CLAST-MATRIX

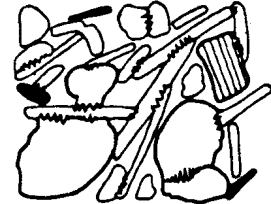
D MATRIX-SUPPORTED



E CLAST-SUPPORTED



F CONDENSED



conglomerates with shale, mudstone, and grainy matrices.

Interpenetrating or condensed clast fabrics are the result of pressure solution (discussed further in Chapter 5).

2.3.6 Isolated Boulders

The presence of isolated, white limestone boulders in Bed 6 at Cow Head North was originally noted by Kindle and Whittington (1958; Plate 2d, Figure 1.3). These boulders occur in a parted sequence of mudstones, grainstones, and marls. Some beds abruptly terminate at the boulders, whereas others drape under and over them. Pebbles, which appear to have been trapped, are found below the boulder shown in Plate 2d.

2.4 CONGLOMERATE LITHOFACIES: INTERPRETATION

Studies as early as that of Kindle and Whittington (1958) suggested that "slumping" (sliding) formed these conglomerates, but it was not until the compilation of Hubert et al. (1977) that a debris flow [4] mechanism was proposed. Recently, Hill et al. (1982) and Hiscott and James (in press) have examined rheological aspects of these flows. Hiscott and James (in press) concluded that CHG debris flows had strengths similar to those of modern subaerial debris flows.

4. The term "debris flow", is strictly a petrogenetic term, but it is also often used to describe the deposits of debris flows (synonymous with "olistostrome" as used by other authors, e.g. Naylor, 1981). Debris flows are characterized by a clay and water matrix which has a finite yield strength (cohesion), which, in concert with buoyancy, provides the required particle support (Middleton and Hampton, 1976).

A debris flow origin for most CHG conglomerates is suggested by the following: (1) lack of or poor normal grading; (2) irregular tops with projecting boulders; (3) abrupt thinning at margins; (4) lack of stratification; (5) broad basal scours and sharp relatively planar bases; and (6) incorporation of penecontemporaneously-deformed material (Cook et al., 1972; Middleton and Hampton, 1976; Surlyk, 1978; Kepper, 1981; Hiscott and James, in press).

The paucity of mud matrix in many conglomerates interpreted as debris flows in the CHG as well as in other successions indicates that other factors, such as dispersive pressure and possibly turbulence, besides yield strength and buoyancy, must be involved in particle support (Middleton and Hampton, 1976; Pierson, 1980). Water incorporated at the base or top of a flow, for example, may diminish effective viscosity thus allowing clast collisions (dispersion) to assume a greater role in particle support (Middleton and Hampton, 1976; Surlyk, 1978). On the other hand, in low velocity debris flows, a grain-support framework may be an important support mechanism (Pierson, 1980).

Coarse foresets in some CHG conglomerates were previously interpreted as pseudo-cross-beds generated by flat clasts sliding down the front margin of the debris flow, producing down-slope imbrication (Suchecki, 1975). These coarse foreset laminations and rare normal grading are presently interpreted to result from more evolved flows in which particle interaction and segregation are possible (cf. Surlyk, 1978). Grading could also be an expression of the gradual downward migration of the rigid plug boundary in a debris flow (Nemec et al., 1980).

Conglomerates with both particle and matrix support suggest variability of flow mechanism within a single flow. Certain domains within the flow may be true debris flow (i.e. particles supported by matrix strength and buoyancy) whereas others could be density-modified grain flows (cf. Surlyk, 1980). This latter possibility can also explain the local clast imbrication. Internal differential shear could also produce local imbrication of flat clasts and possibly reflect formation of a rigid plug (Walker, 1975).

Parallel- and ripple-laminated grainstone caps on CHG conglomerates have been previously attributed to contour current deposition (Callahan, 1974; Suchecki, 1975; Hubert et al., 1977). Comparison with similar occurrences elsewhere suggests that these caps are turbidites which are genetically related to the underlying debris flows (Cook et al., 1972; Krause and Oldershaw, 1979; Crevello and Schlager, 1980).

Smaller clasts trapped below the isolated boulder shown in Plate 2d suggest that it was once part of a more continuous debris flow. This situation may have occurred in several ways. These boulders may be the larger, heavier, stranded freight of a debris flow whose competence was reduced through dilution and the flow was no longer able to carry heavy clasts either suspended or by traction. Another possible explanation is that this situation arose from surges in the debris flow (cf. Hill et al., 1982). The debris flow may have been scoured away by bottom or turbidity currents leaving behind the boulders as a lag deposit. Evidence for scour is, however, lacking. A final possibility is that the boulders outran the debris flow which originally transported them, similar to the situation depicted by Conaghan et al. (1976) for the

isolated boulders in New South Wales. Smoothly lenticular, isolated boulders form "detrital nodules" but these may be easily mistaken for concretions (discussed later in this chapter).

Using Walker and Mutti's (1973) "turbidite" facies classification, some of CHG conglomerates are comparable to the disorganized conglomerates (Facies A1), characterized by sandy matrix, low mud content, and lack of internal structures. Conglomerates with shale, marl, or mudstone matrices are placed in the chaotic deposits (Facies F) which is a heterogeneous suite of lithofacies which also includes muddy matrix debris flows. These conglomerates may also be considered as disorganized conglomerates but with a muddy matrix. Conglomerates with a sandy matrix and internal sedimentary structures (normal grading, clast imbrication, and preferred clasts orientation) are similar to Walker and Mutti's (1973) organized conglomerates (Facies A2). Conglomerates with internal structures and shale, marl, or mudstone matrices could also be included here.

The north to south (or palinspastically-restored northwest to southeast) decrease in the size of the conglomerates and their clasts is interpreted by Hiscott and James (in press) and James and Stevens (in prep.) to indicate a southeast-dipping paleoslope. This is consistent with the south- to east-directed paleocurrents (refer to Chapter 1) interpreted as turbidity flows (discussed in following sections). Outcrops in the northern portion of the study area (e.g. Cow Head North) are therefore interpreted to be proximal to the shelf break. Toward the south, exposures are more distal (e.g. Green Point).

2.5 CALCARENITE LITHOFACIES: DESCRIPTION

2.5.1 General Description

A calcarenite-dominated lithofacies is locally important in Upper Cambrian strata of the CHG (Figure 1.4; outcrops listed in Appendix A). Bedding is usually wavy or lenticular, often reflecting ripple and less commonly megaripple forms, and some outcrops demonstrate lateral transition of wavy to lenticular beds. Bed thickness typically ranges from 5-100 cm. Solitary lenses of calcarenite may reach 15-20 m in length and 1 m in thickness, but most are less than 5 m long and proportionately thinner. Recessive-weathering interbedded shales and siltstones are a few millimetres to 50 cm thick (Plate 3a). The lithofacies usually extends for 1-3 m in thickness, rarely reaching 10 m or more (e.g. Cow Head North Bed 6). Sediments are dominated by peloids and intraclasts, mostly as grainstones (discussed in Chapter 6). This lithofacies is spatially associated with and often grades upward from conglomerates with grainy matrices.

2.5.2 Grading and Stratification

Most beds are massive (structureless); graded and trough cross-laminated beds are comparatively rare. Normally-graded beds may have flat mudstone pebbles concentrated and locally imbricated at their bases (Plate 3b). In some beds, size and compositional grading is delineated by resistant-weathering siliciclastic sand and silt (Plate 3c). Such

grading, however, occurs only within the uppermost few centimetres of the bed.

Trough cross-lamination foresets reach 30 cm in height (Plates 3d; 4a,b). Individual foreset laminations are rarely normally graded from medium to fine sand-size. Both parallel and cross laminations may be enhanced by concentrations of siliciclastic sand or silt, shale intraclasts, or by stylolites (Plates 3c; 4a).

Upper and lower bedding contacts with interbedded siltstones, marls, and shales are typically abrupt and centimetre-scale basal scour and loading into the underlying sediments is ubiquitous. Large-scale scour suggestive of channeling is rare (Plate 4c).

Lenticular grainstone beds, 2-4 m long with form-concordant laminations, are found in Bed 6 at the type section (Plate 4d). These lenses grade upward into rippled, silt-size grainstone which is locally scoured from the lens margins. The sequence suggests parasitic ripples developed on isolated mega-ripples.

2.5.3 Other Calcarenites

Single beds of calcarenite are also dispersed within the siltstone, shale, and mudstone lithofacies. These calcarenites are usually less than 10 cm in thickness; may be normally graded or ungraded; massive, parallel-, or ripple-laminated; and occasionally demonstrate T_{bc} sequences. Their common wavy or lenticular bedding reflects both ripple forms as well as basal loading and scour. Some bedding surfaces are characterized by trains of sinuously-crested ripples with wavelengths of 15-30 cm (Plate 10c, d). The few ripple crest

orientations measured indicate paleocurrents to the south and southeast, confirming the paleocurrent measurements of Hubert et al. (1977).

2.6 CALCARENITE LITHOFACIES: INTERPRETATION

2.6.1 Interpretation of Calcarenite Lithofacies

The predominantly massive bedding with rare normal grading resembles the T_A division of the Bouma (1962) sequence. The lack of the "normal" or "classical" turbidite successions, however, and the occasional presence of large-scale cross-lamination suggests that the Bouma (1962) turbidite sequence is inadequate to model this lithofacies. In addition, the lack of inverse grading suggests these deposits are not grain flow deposits (see Cook, 1983b). The ubiquity of small-scale scours indicates fluid turbulence is important, but the lack of large scours suggests channels are rare or absent.

Mega-ripple cross-lamination in carbonate flysch has been reported from several localities (e.g. Lower Pennsylvanian Dimple Limestone of Texas - Thompson and Thomasson, 1969; Devonian Marble Cliff Beds of Cornwall - Tucker, 1969; Cambrian of the Taconic sequence in New York - Keith and Friedman, 1977). To explain such occurrences, Hubert (1966) and Hubert et al. (1977) suggested modification to the Bouma (1962) sequence where a dune (mega-ripple) phase is inserted between the T_B and T_C divisions.

Beds in the calcarenite lithofacies shares various elements of Walker and Mutti's (1973) A4 and B2 facies (organized pebbly sandstone and massive sandstone without dish structure facies, respectively).

Included are: coarse-tail grading (A4), local pebble imbrication (A4), basal scour (B2), and common lenticular bedding (B2). This lithofacies lacks, however, the common amalgamation which characterizes Walker and Mutti's (1973) B2 facies. The calcarenite lithofacies is also in part comparable to Walker and Mutti's (1973) C facies, the "classical" proximal turbidites which are characterized by numerous beds which begin with the T_A division. The continuity of the Facies C turbidites does not, however, characterize the calcarenite lithofacies.

Beds in the calcarenite lithofacies closely resemble proximal turbidites described by Lowe (1976), Surlyk (1978), Hiscott and Middleton (1979), and Hurst and Surlyk (1983). These turbidites were interpreted to be deposited from high density turbidity currents, thus explaining the difficulty in applying the Bouma (1962) sequence which is only applicable to the lower density, "classical" turbidity currents (Lowe, 1982).

Particle support in high density flows results from the interaction of turbulence, hindered settling, bouyancy, and dispersion. Deposition is thought to occur in three successive phases which reflect increasing flow unsteadiness (Lowe, 1982). These phases are:

(1) A traction sedimentation stage, which produces bedforms of classical turbidites along with dune-like features and erosion. This may account for the lenticularity of some beds and the occasional development of trough cross-lamination.

(2) A traction carpet, freezing stage which may result in the preservation of inverse grading (also see Hiscott and Middleton, 1980).

This is not observed in CHG calcarenites.

(3) A direct suspension sedimentation stage which leads to loosely packed sediments. This last stage of deposition is characterized by massive or normally graded bedding and is the T_A division. Most of the calcarenite lithofacies is interpreted to be an expression of this last phase of deposition from high density flows. Residual flows then give rise to finer grained turbidites with which they are commonly interbedded (discussed in next section).

The absence of dewatering structures in the calcarenite lithofacies is possibly explained by the lack of fine interstitial sediment. This may be the result of either original sorting (most probable) or diagenetic effects (cf. Hurst and Surlyk, 1983).

2.6.2 Interpretation of Other Calcarenites

Calcarenites dispersed in the siltstone, mudstone, and shale lithofacies are interpreted as turbidites based on their ungraded to normally-graded beds; massive internal fabric, or parallel and ripple laminations, often following sequentially; and basal loading or scour. Many of the above characteristics have also been noted in other carbonate sequences, interpreted as turbiditic, throughout the geologic column from Precambrian to Quaternary (e.g. Meischner, 1964; Thomson and Thomasson, 1969; Tucker, 1969; Marcinowski, 1970; Eder, 1971; various papers in Cook and Enos, 1977; Scholle, 1977; Cook, 1979; Crevello and Schlager, 1980; Cook and Mullins, 1983). Massive and graded beds are interpreted to be the T_A division whereas the parallel- and ripple-laminated beds are the T_B and T_C divisions, respectively, commonly forming the classical T_{BC} turbidite sequence (Walker and Mutti, 1973).

2.7 SILTSTONE LITHOFACIES AND SHALE LITHOFACIES: DESCRIPTION

2.7.1 Introduction

Siltstones and shales are volumetrically important in most exposures of the CHG. In the following discussion, these sediments are considered as a spectrum with a "siltstone lithofacies" as one end member and a "shale lithofacies" as the other.

In the siltstone lithofacies beds of siltstone and shale are of comparable thickness and occur in approximately equal proportions (Plate 5a,b). This lithofacies is 1-4 m in thickness and some of the more extensive intervals are listed in Appendix A. Many of these intervals are the "dolomitic siltstones" designated in the stratigraphic sections of James and Stevens (in prep.; also see Figure 1.2); these siltstones, however, may also comprise fine-grained peloidal grainstones, siliciclastic siltstones (relatively rare), or commonly mixtures of the above three components. Beds composed of very fine sand- or fine sand-size particles occur, but these are volumetrically minor relative to siltstones. Thinner intervals of interbedded siltstones and shales (10-100 cm thick) typically constitute the recessive units interbedded with calcarenites and conglomerates throughout the CHG.

As siltstone beds become thinner and the siltstone/shale ratio decreases, sediments progressively approach the other end member of the spectrum, the "shale lithofacies", which is characterized by

shale-dominated intervals 1-10 m or more in thickness (Plate 5c). Siltstones, though reduced in thickness and volumetric importance, are found as "stringers" in all shale sequences in the CHG. Important attributes of the shales include: (1) thickness of the intervals in which they occur, (2) variation and alternation of colour on a millimetre to metre scale, and (3) the abundance of red shales in the Arenig sequence. The clay mineralogy of these shales was initially studied by Suhecki et al. (1977) and subsequently re-examined during the course of this study. Based on this study, shales are dominated by chlorite and illite (also a conclusion of Suhecki et al., 1977), may contain traces of kaolinite, and the Ordovician shales also contain minor corrensite. These results differ slightly from those of Suhecki et al. (1977) and further discussion, including analytical methods, is provided in Appendix B. Scattered throughout most shales are varying quantities of fine to medium silt-size dolomite crystals, quartz and feldspar silt, pyrite crystals and aggregates, and microspar. Shales may also be largely dolomitized (dolomitic marls; see Chapter 12), silicified to form bedded cherts (Chapter 13), or rarely, potassium-metasomatized to potassium feldspar (Table B.2 in Appendix B).

2.7.2 Colour

Dolomitic and siliciclastic-rich siltstones typically weather dusk yellow (5 Y 6/4 [dry]; [5]), but fresh wet surfaces are light olive grey (5 Y 6/1) or brownish grey (5 YR 4/1). More calcareous siltstones

5. Colours are of wet specimens unless indicated otherwise and are based on the Geological Society of America rock colour chart.

weather numerous shades of grey.

Three dominant shale colours are recognized: black (N 1), green (5 Y 3/2, 5 Y 4/1), or red (5 GY 4/1). Black and green shales and green and red shales are commonly interbedded with one another. Interbedded black and red shales are never found. Purple shale (approximately 5 PB 3/2) is minor and is interbedded with either green or red shale.

Beds dominated by one shale colour commonly reach 1-2 m in thickness ("metre-cycles") and these in turn consist of numerous millimetre to centimetre-thick colour alternations ("millimetre cycles"). An excellent example of this is a Lower Ordovician shale interval (unit 29) exposed at Green Point (Plate 5c). The sequence consists of 10-30 cm-thick, interbedded black and green shales (metre-cycles). Each black and green band comprises numerous millimetre-size black and green laminations (millimetre-cycles), many of which are discontinuous in outcrop as well as thin section. Analogous relationships also occur in interbedded red and green shales.

Red shale is commonly locally reduced to pale green but this accounts for a negligible fraction of the green shale observed in the sequence. The most frequent occurrence is reduction of red shale immediately underlying and overlying siltstone stringers. Reduced bands are 1-5 mm thick and gradationally pass into surrounding red shale. In addition, red shales are reduced laterally within beds or along fractures and faults; reduction spheres or ellipsoids occur scattered along preferred horizons; and reduced rims surround rare red shale clasts within conglomerates.

2.7.3 Bedding Characteristics

Shales interbedded with dolomitic siltstones are commonly dolomitized (Plate 5d). Consequently, many resistant-weathering "beds" are actually composite beds, consisting of two or more siltstone beds with intervening, dolomitized shale. Because primary sedimentary structures are often faithfully preserved in these sediments, much of the information on the silt to shale transition, grading, and other internal fabrics is drawn from such dolomitized siltstone-shale couplets.

Siltstone beds in the siltstone lithofacies are 2-6 cm thick, but occasionally beds reach 25 cm in thickness. Stringers are considerably thinner, often only 5-10 mm in thickness, rarely attaining a thickness as great as 2 cm. Beds are typically planar and continuous but become less so with decreasing bed thickness. Beds with rippled tops have an undulating upper surface and isolated (starved) ripples define lenticular beds.

Basal scour, loading, and development of small flames are common and many of these are visible only in thin section. Inorganic sole markings are common and dominated by small grooves and flutes with occasional bounce marks. A varied trace fossil assemblage is locally abundant and may initialize current scour around them (Plate 5e). Parting lineations, when present, are only weakly developed. In contrast to their abrupt bases, siltstones typically demonstrate a gradual upper transition into overlying shales. In relatively undolomitized shale, this is seen as an increase in fissility and weathering recessiveness. Slab and thin

section study provides the important details (discussed below).

2.7.4 Internal Structures

Massive or normally graded beds (T_A of Bouma, 1962), some with basal accumulations of coarse sand- to granule-size clasts of quartz, shale, chert, and phosphate, are comparatively rare (Plate 6a). In contrast, parallel and cross laminations, commonly forming T_{BC} sequences, are ubiquitous (Plate 6c). Slabs and thin sections commonly demonstrate lateral transition from cross laminated silt to shale in the troughs - the "fading ripples" described in Stow and Shanmugam (1980; Plate 6b,e). These are equivalent to Type C ripple drift cross-lamination of Jopling and Walker (1968). Climbing ripples are rare.

Heights of ripples vary. In the thickest beds they are 1-2 cm high and have wavelengths of 10-20 cm. In thinner beds, especially stringers, ripples are less than 1 cm high and may be as small as 2 mm.

Wavelengths are correspondingly shorter, down to a minimum of 2 cm.

Convolute laminations follow undisturbed parallel laminations in some siltstones and are likely the result of dewatering or current drag effects on ripples (Plate 6c). Other convoluted laminations are found in isolated siltstone lenticles in shale and are due to loading of ripples.

2.7.5 Graded Laminations

Slabbed specimens of siltstone- shale couplets clearly demonstrate that the transition from siltstone to shale is always gradual and expressed

as: (1) graded laminations, (2) grain or crystal-size grading, (3) compositional grading, or (4) any combination of the above.

Graded laminations (sensu Piper, 1972); also termed graded rhythmites - see Reineck and Singh, 1980, p. 125) consist of continuous and discontinuous (on scale of slab or thin section) parallel silt laminations, which decrease in frequency, thickness, and grain size upward into overlying shale (Plate 6d, e). Individual laminations commonly range from 50-500 μm in thickness. Five to 15 silt laminations occur in a 1 cm interval although most graded-lamination divisions are 2-5 mm in thickness.

A division of graded laminations commonly follows cross-laminated siltstone and, in some samples, discontinuous graded laminations are preferentially developed over the positive relief of underlying ripples. Graded laminations can also occur immediately over shale, without the underlying siltstone (bottom cut-out - see later discussion).

2.7.6 Shale Microfabric

Graded laminations pass gradationally upward into shale in which the microfabric is either particle-foliated, massive, or some intermediate microfabric. The particle-foliated and massive microfabrics are end members of a textural spectrum and can be identified with certainty only in thin section.

Particle-foliated shale contains numerous opaque or yellow to brown translucent particles which are oriented parallel to bedding and thus

create a pronounced bedding-parallel foliation (Plate 7a). These particles are as large as 0.5-2 mm length and generally less than 10 μm in thickness and are especially prominent in many black shales in which they are judged to be largely responsible for the black colour. Based on prepared samples for a pending pyrobitumen study of thermal maturation of the CHG, these particles are probably largely undifferentiated organic materials. Occasionally, definitive remains of partially flattened graptolite fragments can be identified.

In contrast obvious particle foliation is absent in massive, homogeneous shales. Massive shales also tend to have fewer and smaller dispersed siliciclastic and dolomitic silt grains and are generally lighter coloured (grey or green) than the particle-foliated shale.

As is typical for shales in general, there is a preferred bedding-parallel alignment of clay platelets as indicated by the aggregate illumination (i.e. maximum light transmission) and extinction characteristics under crossed polarizers. The preferred orientation in the massive shales, however, appears to be greater than that of particle-foliated shales, based on more pronounced illumination.

Some shales consist of numerous alternations of millimetre-thick laminations of particle-foliated and massive shale; these are seen in outcrops and slabs as the millimetre-cycles referred to earlier. Upward gradation of particle-foliated to massive shale is more common than upward gradation of massive into particle-foliated shale (Plate 7b).

A relatively uncommon, third type of shale microfabric consists of resedimented and compacted intraclasts of particle-foliated or massive

shale (Plate 7c). These intraclasts are lenticular, up to 5 mm in length and 0.5 mm in width, and are fitted tightly together, being separated by darker argillaceous or carbonaceous seams and scattered siliciclastics and peloids.

In addition to the disruption of shale laminations due to submarine sliding (see Chapter 3) other secondary structures include tension cracks (Plate 7d). These vertically-oriented, sheet cracks have been observed in only one slab. They are clearly of pre-compaction origin. In cross-sectional view they are approximately 1 mm wide and filled with 60-200 μm -size, slightly ferroan calcite cement.

2.7.7 Trace Fossils

Trace fossils are common in many shale sequences, particularly on the soles of siltstones (Plate 5e). Traces are especially prolific in red shales and their siltstone stringers (Plates 6a, 8a). Burrows are distinguished from surrounding sediment by textural or compositional differences, usually dolomite crystal size or the amount of intercrystalline, argillaceous material. The latter produces the distinctive red to purple colour of the burrows in siltstones within red shale sequences.

Common traces include Skolithos, Paleophycus, and Planolites, and in red shale sequences, Syncoprulus (Plate 8b) and Cylindrichnus (Plate 8c ; Narbonne and James, 1984). Chondrites has also been identified (Plate 8a): Bioturbation is inferred in some sediments characterized by disrupted silt and shale laminations and lacking distinctive burrows

(Plate 8d).

The relationship of trace fossils to sediment is readily observed in red shales due to the abundance of burrows. In these sediments, traces are most common in the silty shale overlying a siltstone stringer and they become less numerous towards the siltstone stringer (Plates 6a, 8a).

Within siltstones, burrows rarely demonstrate obvious compaction although they are usually squashed in undolomitized shales. Burrows in dolomitized and silicified shales, however, are commonly uncompacted, indicating early lithification (Plate 8e; discussed in Chapters 12 and 13).

2.8 SILTSTONE LITHOFACIES AND SHALE LITHOFACIES: INTERPRETATION

2.8.1 Sequence of Sedimentary Structures

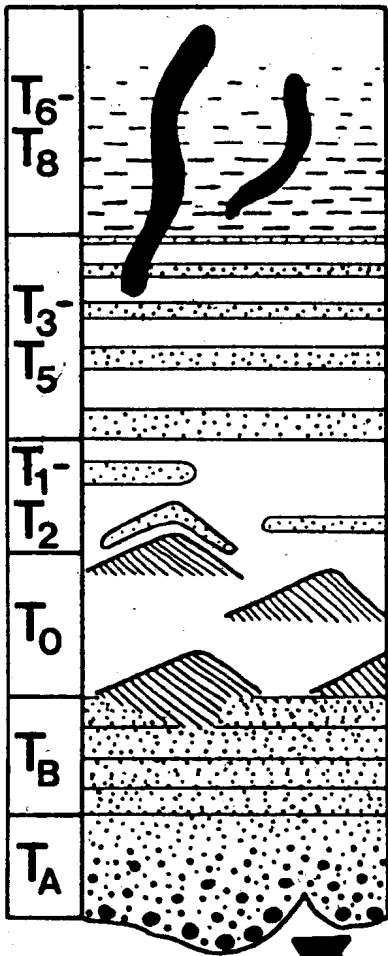
The sedimentary structures in the siltstone-shale couplets and siltstone stringers in shale provides the basis for construction of a composite siltstone-shale cycle (Figure 2.3). The lower part of this cycle is conveniently described with reference to the standard Bouma (1962) turbidite sequence whereas the upper part is discussed in terms of the model for terrigenous mud turbidites proposed by Stow and Shanmugam (1980; Figure 2.4).

Massive and normally graded siltstones (T_A) are rare and thus most cycles are bottom cut-out (i.e. the lower divisions are missing) with reference to the complete Bouma (1962) sequence. Instead, most

Figure 2.3: Schematic composite sequence of sedimentary structures in siltstone-shale cycles in the Cow Head Group. Absolute or relative scales are not implied.

STOW AND SHANMUGAM
(1980) SUBDIVISIONS

COMPOSITE SILTSTONE-SHALE - CYCLE



MASSIVE SHALE
(HEMPELAGITE)
PARTICLE-FOLIATED SHALE

MAY CONTAIN
RADIOLARIA, SPICULES
MAY BE DISRUPTED DUE
TO SLOPE FAILURE
OR SYNAERESIS

GRADED SILT LAMINATIONS

DISCONTINUOUS SILT LAMINATIONS

SMALL-SCALE X-LAMINATED SILT,
FADING RIPPLES, ISOLATED RIPPLES,
CONVOLUTED LAMINATIONS

PARALLEL LAMINATED SILT TO
VERY FINE SAND

MASSIVE OR NORMALLY GRADED,
LARGEST CLASTS MAY BE GRANULE-SIZE

SHARP BASE WITH SCOUR,
LOADING AND FLAMES

siltstones are parallel-laminated (T_B) or cross-laminated ($T_C = T_D$ in Figure 2.3) at their bases and beds composed of T_{BC} divisions are common. The siltstone-shale transition is characterized by parallel, graded laminations (T_{1-5}) which are considered to be equivalent to Bouma's (1962) T_D division (Piper, 1972). The graded lamination division is commonly followed by particle-foliated shale (T_E -TURBIDITE?) and finally, massive shale (T_E -HEMIPELAG?). In red shale sequences, burrowing is abundant in the shaly portion of the cycle and diminishes toward the underlying siltstone.

This systematic, predictable succession of sedimentary structures is accompanied by particle or crystal size grading, usually from coarse to medium silt-size. The normal grading of dolomite crystal size is more subdued than for peloids, this being largely a function of diagenetic enlargement of original detrital dolomite crystals as well as replacement of calcite allochems (see Chapter 12). In addition, compositional grading occurs where there is an increase in siliciclastic silt or argillaceous intercrystalline material upward.

As with the standard Bouma (1962) sequence, few cycles demonstrate the entire sequence of sedimentary structures seen in Figure 2.3. Inversions in the structural sequence are rare except in shales, where the relationship between particle-foliated and massive shale is neither as clear nor as consistent as for the other parts of the sequence.

The thickness of the silt to shale cycles in the siltstone lithofacies is typically 10 cm or less. As the quantity of shale increases and siltstone thickness and abundance decreases within an interval, cycles

become smaller, and expectedly, bottom cut-out is more pronounced.

Partial cycles may be only a few millimetres in thickness.

Silt laminations which are 40-600 μm in thickness, ungraded, continuous on the scale of the rock slab, and have planar and abrupt upper and lower surfaces do not fit well into the sequence of structures. Such laminations are rare, however, and when they occur they are in close proximity to laminations which do fit the sequence. Such anomalous laminations are interpreted as bottom and top cut-out relics.

2.8.2 Interpretation As Fine Grained Turbidites

Using criteria in Stow and Piper (in press), a turbidite origin for the silt to shale cycles is indicated by the following: (1) a systematic, predictable vertical sequence of structures is associated with normal grain size and compositional grading; (2) bioturbation is concentrated at the tops of beds; and (3) there is compositional, textural and other evidence to indicate that many grains are exotic to the depositional environment.

Points 1 and 2 have been discussed in the previous section.

Petrographic analysis of calcareous grains clearly indicates their shallow-water origin (point 3), especially grains which contain evidence of calcified algae (see Chapter 6). In addition, detrital dolomite, which is volumetrically significant in many siltstones, may have been derived from vast supratidal zones on the contemporaneous or older shallow-water carbonate platform (see Chapter 12). Criteria which would indicate rapid deposition, such as escape burrows and climbing ripples,

are generally lacking.

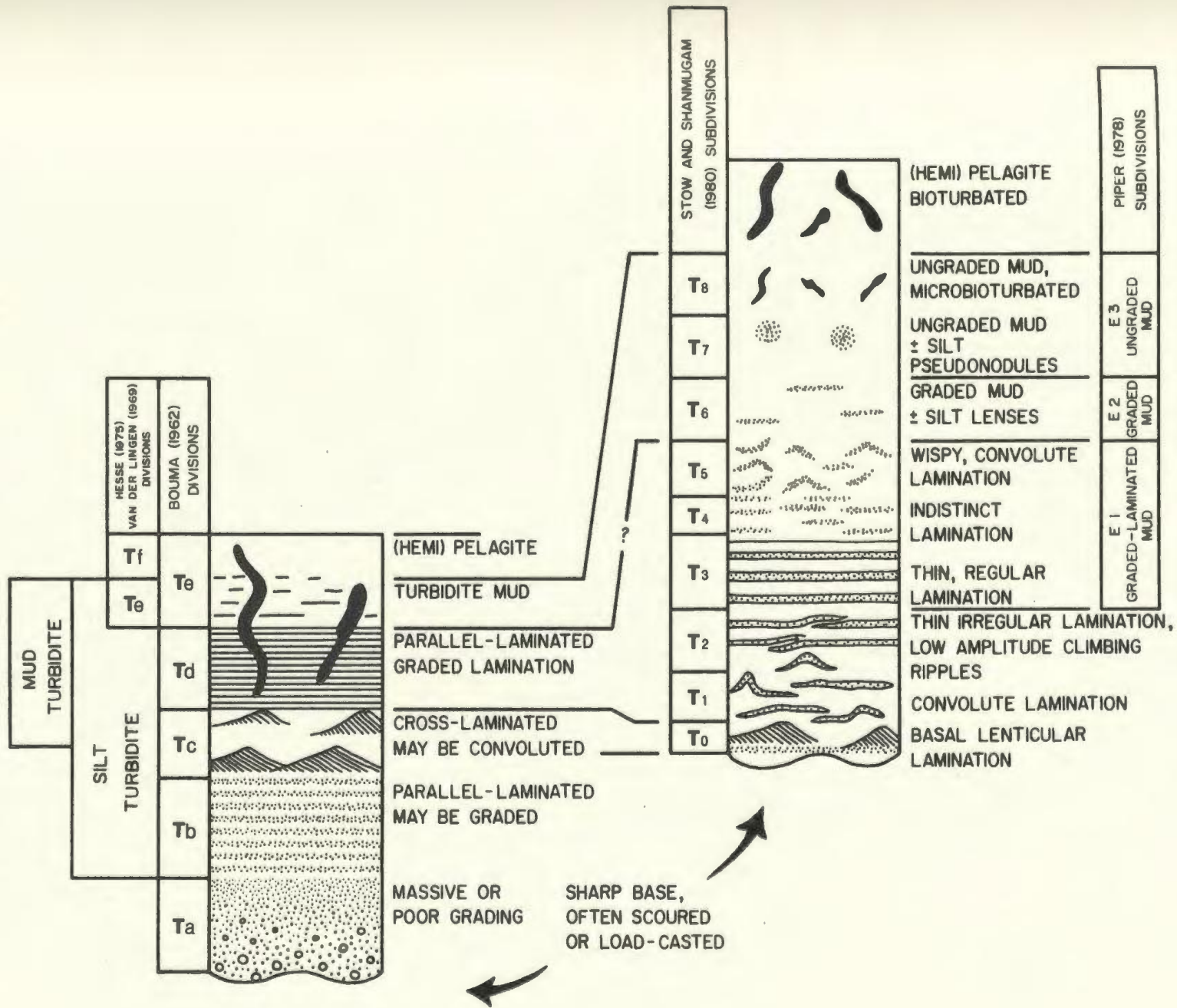
The sequence of sedimentary structures and the grain size and compositional grading are comparable with those of the idealized sequence described for fine grained turbidites from both modern and ancient slope, rise, basin plain, and submarine fan successions (Figure 2.4; Shanmugam and Walker, 1978; Stow and Shanmugam, 1980; Kelts and Arthur, 1981; Stow and Piper, in press).

Fine grained turbidites have greater than 50% of the grains smaller than 63 μm in size, i.e. they consist of silt- and clay-size particles.

Silt turbidites are differentiated from terrigenous mud turbidites based on the relative amount of silt and shale (Stow and Piper, in press) although the distinction is arbitrary in many cases because muddy turbidity currents can evolve from silty turbidity currents in time or space, a situation analogous to that in sandy turbidites where distal and proximal turbidites are distinguished (see Walker, 1967). The prominence of silt-size particles in the siltstone-shale cycles of the siltstone lithofacies indicates these to be silt turbidites. In contrast, the siltstone stringers and the finely interlaminated particle-foliated and massive shales in the shale lithofacies are terrigenous mud turbidites.

Silt turbidites exhibit the same sequence of structures (T_A through T_E divisions) as the Bouma (1962) sequence for sandy turbidites (Stow and Piper, in press). Their interpretation, consequently, is the conventional one of a progressively waning flow (Walker, 1967; Middleton and Hampton, 1976). Silt turbidites from the CHG which start at the T_B ,

Figure 2.4: Correlation of divisions in sand and silt turbidites (left side of diagram) and terrigenous mud turbidites (right side of diagram). Absolute or relative scales are not implied. This diagram is based mainly on information in Stow and Piper (in press).



T_C , or T_D divisions resemble the "classical" distal turbidites or Facies D of Walker and Mutti (1973).

As grain size diminishes and sediments become more argillaceous, the Bouma (1962) sequence becomes progressively less applicable and facies models for finer grained sediments must be considered (Stow, 1982). Stow and Shanmugam (1980) proposed a standard structural sequence for fine grained (terrigenous mud) turbidites which was based on data from both modern and ancient sediments (Quaternary deep-sea muds of the Nova Scotian slope and rise, Middle Ordovician Sevier Formation of the southern Appalachian Valley and Ridge Province, and the Cambro-Ordovician Halifax Slate of the Meguma Group in Nova Scotia).

Their idealized standard sequence consists of 9 subdivisions - T_0 through T_8 - and is shown in Figure 2.4. The standard sequence is about 7 cm thick and as with the Bouma (1962) sequence for sandy turbidites, beds which contain all the subdivisions are rare. This sequence is approximately equivalent to the T_{CDE} divisions of the Bouma (1962) model and is interpreted to represent progressive deposition from different stages of a waning, low density, thick turbid flow..

The similarity of the composite sequence for the CHG and that proposed by Stow and Shanmugam (1980) is striking and there is little doubt of their common origin. The cross-laminated division in the CHG sediments is considered to be the T_0 subdivision. The overlying discontinuous silt laminations are equivalent to the T_1 and T_2 subdivisions and the division of graded laminations is the T_3 , T_4 , and possibly T_5 subdivisions of Stow and Shanmugam (1980). The shales are equivalent to

the T₆ to T₈ subdivisions.

Alternation of silt and terrigenous mud laminations to form graded laminations is interpreted to be the result of depositional sorting of silt grains from clay floccs due to increased shear in the bottom boundary layer of a turbidity current (Stow and Bowen, 1978; 1980).

Fading ripples are interpreted to indicate a high proportion of clay-size material in the turbidity flow (Stow and Shanmugam, 1980).

2.8.3 Shale Microfabrics, Colours, and Cyclicity

The interpretation of particle-foliated and massive shale microfabrics with reference to the terrigenous mud turbidite model is less certain. The higher abundance and larger size of dispersed siliciclastic and dolomitic silt grains within particle-foliated shale relative to massive shale suggests that particle-foliated shale is genetically related to the underlying turbidite. In addition, the numerous organic flakes and the resultant darker colour which characterizes this microfabric indicate that entombment of organics occurred due to sufficiently rapid burial and escape from potential oxidation. The dark shale colours and presence of ichnofauna suggest dysaerobic bottom waters (dissolved oxygen between 0.1 and 1.0 ml/L); barren sequences indicate anaerobic bottom waters (dissolved oxygen less than 0.1 ml/L; Byers, 1977; Savrda et al., 1984).

The massive shale, in contrast, has more pronounced aggregate illumination (maximum transmission of light) under crossed polarizers indicating a higher degree of clay platelet orientation, and suggesting

slow deposition of dispersed, hemipelagic clays. This contrasts with suspension fall-out from turbidity currents which would be relatively rapid and the flocculated state of the clays as well as abundant dispersed silt-size grains would not allow such an ordered arrangement of clay platelets. This interpretation is supported by O'Brien et al.'s (1980) study of clay fabrics in terrigenous turbidite and hemipelagic muds. The interpretation of particle-foliated shale as turbidite and massive shale as hemipelagite is also consistent with the observation that upward gradation from particle-foliated to massive shale is more common than the other way around. In addition, the generally lighter colours of the massive shales may be due to the oxidation of any entrained organics either during settling through the water column, or while on the sea floor.

In siliceous shales, radiolaria and sponge spicules also suggest a hemipelagic origin for massive shale. The rare occurrence of normally-graded radiolaria-sponge spicule laminations indicates that biogenic turbidites, in this case probably reworked pelagites, are comparatively rare (cf. Kelts and Arthur, 1981).

Following from the above conclusions, millimetre-cycles of black and green shale are interpreted to reflect interlamination of organic-rich turbidites and organic-poor hemipelagites. A similar explanation for millimetre-cycles of green and red shale is proposed; only in this case, the overall abundance of organics is reduced and bottom waters are more oxidizing.

Superimposed on these fine-scale alternations in shale are

metre-cycles which may contain hundreds of millimetre-cycles. Rather than reflecting the preservation potential of organics in event (turbidite) and background (hemipelagite) sedimentation, these larger-scale alternations are interpreted to indicate periodic variations in the overall abundance of organics in the source region, as well as oxygen levels of bottom waters. The alternation of dominantly black and dominantly green shales throughout most of the CHG deposition indicates that organic material was plentiful in the source region of the shales (both turbidites and hemipelagites) and that bottom waters contained low oxygen levels and were probably either dysaerobic or anaerobic.

With time, the increasing importance of red shales in all but the most proximal outcrops of the CHG (James and Stevens, in prep.) indicates that oxygen levels of bottom waters were gradually increasing, exemplified especially clearly by the homogeneous, massive fabric of many red shales and the proliferation of trace fossils in the enclosed siltstones. Red shales, such as these, are indicative of deposition or diagenesis or both under oxidizing conditions (Hoffert, 1980). The relative paucity of millimetre-cycle laminations in red shales compared to black and green shales is interpreted to result from either diminishing importance of fine grained turbidites or obliteration due to intensive bioturbation or both.

Similar fine- and coarse-scale alternations were described in DSDP cores of Cretaceous and Miocene sediments from the continental margin off northwest Africa by Dean et al. (1977). Centimetre-thick cycles of black-green shale alternations were interpreted as turbidites of organic-rich, terrigenous muds (black shales) grading upward into

hemipelagic muds, which were often bioturbated and contained considerably less organic carbon (green shales). Sequences dominated by green and red shale alternations were also encountered sandwiched between those dominated by black and green shale alternations. These larger-scale packages were interpreted to reflect cyclical variations in the amount of organic material within the terrigenous sediments, a direct effect of climatic cycles. Times of higher organic matter production resulted in black-green shale alternations whereas reduced organic matter production resulted in the green-red shale sequences.

2.8.4 Origin Of Cracks In Shale

The tension cracks from St. Paul's Quarry are clearly pre-compaction. Lack of internal sediment within cracks and lack of confinement to specific beds or laminations suggest they formed substratally (cf. Plummer and Gostin, 1981). These cracks may be due to either synaeresis or tensional stress produced by down-slope creep (Potter *et al.*, 1980). The single occurrence of these cracks does not provide sufficient evidence to distinguish between these 2 alternatives.

2.8.5 Fine-Grained Turbidites and Muddy Contourites

From the preceding discussion, it is concluded that the siltstone and shale lithofacies consist of fine-grained (silt and terrigenous mud) turbidites interbedded with terrigenous hemipelagite. Studies of modern as well as other ancient deep-water sediments have also documented the importance of fine-grained turbidites. Hesse (1975) indicated that up to 86% of the fine-grained beds in Cretaceous flysch of the Eastern Alps

was deposited by turbidity currents. This estimate was based on evidence using carbonate content, colour, sequential analysis, and microfauna. Based on compositional and textural criteria, cored terrigenous muds from the Balearic Abyssal Plain (western Mediterranean) were suggested to contain more than 50% turbidite mud (Rupke, 1978). In Pliocene and Quaternary sediments from the Gulf of California up to 60-75% of the sediment was interpreted to be terrigenous, turbidite mud (Einsele and Kelts, 1982).

Quantitative estimates of the contribution of fine-grained turbidites are not available for the CHG. Qualitative field and petrographic evidence, however, suggest that fine-grained turbidites, as identified by the previously discussed criteria, comprise at least half of the sediment in the siltstone and shale lithofacies, an estimate which is consistent with those from the above-listed studies. The remaining portion is composed of hemipelagites.

Terrigenous, muddy contourites (Stow and Lovell, 1979) must also be considered as a possible origin for these fine-grained sediments. This origin, however, can be discounted based on the systematic, predictable sequence of sedimentary structures, many of which can be directly correlated with those of the Bouma sequence for sandy turbidites. In addition, the normal size and compositional grading also indicate a turbidite origin for these sediments. In contrast, contourites are characterized by a lack of a regular sedimentary sequence, occasional normal or reverse grading, and a lack of evidence for relatively rapid deposition (Rupke, 1978; Stow, 1979; Stow and Lovell, 1979; Lovell and Stow, 1981; Stow and Piper, in press).

2.9 MUDSTONE LITHOFACIES: DESCRIPTION

2.9.1 Introduction

The numerous parted, ribbon, and nodular sequences in the CHG are lumped together into a "mudstone lithofacies" in order to emphasize their most important common denominator - the high content of lime mudstone. This lithofacies is, to a greater degree than any other, a complex assemblage of diverse primary as well as diagenetic elements. Only those aspects related to primary sedimentation, as observed in the field or laboratory, are detailed in this chapter. As will be demonstrated in this and later chapters, the differentiation of primary from diagenetic is seldom clear, a relevant example being the interpretation of some lenticular or nodular limestones. Nodules are volumetrically important in this lithofacies but are also scattered throughout black and green shales as well as the calcarenite and siltstone lithofacies much in the same way as isolated ribbons of mudstone are. The spectrum of nodular limestones is considered here to complete the outcrop descriptions and to emphasize relationships and similarities with their surrounding planar- or wavy-bedded sediments.

The importance of this lithofacies is multi-faceted. Platy clasts as well as the mudstone, shale, or marl matrices of the numerous debris flows finds a ready, local source. This lithofacies also preserves unequivocal evidence for in situ sediment instability and, consequently, deposition of the CHG on a sloping surface (see Chapter 3). Finally, the

mudstone lithofacies is the locus of numerous complex diagenetic phenomena which include fibrous ("beef") and cone-in-cone calcite, septarian concretions, silicification, barite precipitation, and contorted limestones. These topics are considered in later chapters.

The following discussion is divided into three parts. The first is a distillate of information from numerous parted, ribbon, and nodular limestone sequences which were examined in detail. Some of the more informative outcrops are described individually in Appendix A. The second part is concerned with additional description of nodular limestones. The last part is an interpretation of the lithofacies based on the previously discussed evidence.

2.9.2 Bedding Characteristics

Intervals of ribbon, parted, and nodular limestones vary from 50 cm to greater than 30 m in thickness (Plate 9a-d). Individual limestone beds typically range from 2-10 cm in thickness but some beds may be as thick as 30 cm. Systematic changes in bed geometry and thickness are generally not present except in the transition to shale-dominated intervals where several exceptional outcrops demonstrate thinning of mudstone beds in conjunction with increasing lenticularity (Plate 9b). A similar change was also noted by Keith and Friedman (1977) in Cambrian deep-water limestones from New York State. Interbedded marls and shales are massive or parallel-laminated (Plate 10e) and vary from paper-thin partings to 30 cm in thickness.

Planar, wavy, and nodular beds occur in any proportion. Sequences

dominated by planar beds are mainly composed of mudstone and many are remarkable for their lateral continuity over hundreds of metres along strike, with little or no change in bed thickness (Plate 9d). In other sequences, wavy and lenticular bedding demonstrate fitted fabrics which preserve sediment package thickness (Plate 10a). Although mudstones are volumetrically the most significant sediment type - wackestones, packstones, and grainstones - often interbedded with one another - are also locally important as planar, wavy, and nodular beds (Plate 10b). In contrast to grainstones which commonly demonstrate parallel and ripple laminations (see previous discussion), wackestones and packstones are usually massive (structureless). Grains include silt- and sand-size peloids, bioclasts, limestone and shale intraclasts, dolomite, siliciclastics, and glauconite peloids. Accumulations of sponge spicules, trilobite and brachiopod (calcitic and phosphatic) shell fragments, and graptolites occur on some bedding planes.

As with the dolomitic siltstones described previously, many limestone beds, both continuous, wavy, and lenticular, are composite. These typically consist of mudstone underlying, overlying, or completely enveloping grainstone or packstone. There is no obvious control on the position of the mudstone bed relative to the grainstone or packstone.

2.9.3 Mudstone Microfacies

Mudstones consist of microspar and pseudospar (discussed in Chapter 8) with micrite occurring mainly in peloids and intraclasts. Siliciclastic and dolomitic silt, peloids, indeterminate shelly bioclasts, and radiolaria and sponge spicules also occur in most mudstones

in minor quantities. Two intergradational mudstone microfacies are recognized: (1) homogeneous mudstone and (2) marginally-aggraded mudstone.

Homogeneous Mudstone commonly consists of microspar mosaics with 10-25 μm -size crystals to coarser mosaics dominated by 100 μm -size pseudospar. Although usually massive (structureless) in outcrop, exceptionally well-polished outcrops suggest that subtle parallel laminations are more common than is usually apparent (Plate 10e). These laminations appear as subtle colour variations in outcrop but in thin section are seen to be caused by differences in crystal size or concentrations of peloids, siliciclastic silt, dolomitic silt, or intercrystalline argillaceous material (Plate 13a). In some cases, however, the reasons for colour differences are not recognizable texturally, either in outcrop, slab, or thin section.

Marginally-Aggraded Mudstone is common, but varies greatly in its appearance. It is characterized by an increase in the crystal size of microspar or pseudospar toward the bed or nodule margins. This increase may be subtly expressed, for example a barely noticeable change from a 5-10 μm mosaic at the centre of a bed to a mosaic of 10-15 μm crystals at the bed margins, or the change may be striking, in terms of crystal size, shape, intercrystalline paste content, and iron content as determined by staining with potassium ferricyanide. For example, 10-15 μm -size microspar at the bed centre may pass gradationally to 50-60 μm -size or larger pseudospar at the bed margin. The crystals also become more ferroan and further separated from one another by a prominent intercrystalline "paste" toward the margin. This change in

crystal size, when pronounced, can easily be detected in the field with a hand lens. Otherwise, petrographic analysis is necessary for the distinction of the two mudstone microfacies.

2.9.4 Clastic Dikes

Clastic dikes [6] are generally compacted and less than 1 m in length (unfolded), but an exceptional dike at Broom Point North was traced through 4 m of section. Intruded lithologies are ribbon mudstones and their associated shales and marls (Plate 21a). Sheeted dikes, consisting of two or three sub-parallel, variably distorted dikes, are comparatively rare. Sills extending from dikes are also rare and difficult to distinguish from lenticular, primary beds.

Dikes mostly consist of fine to medium sand-size grainstone, but larger dikes also contain flat mudstone pebbles up to 10 cm in length, often aligned sub-parallel to dike walls. Dike width varies from a few grain diameters to 15 cm. Some of the smaller millimetre-wide dikes are uncompact and encased in an envelope of mudstone (Plate 13e,f; discussed later).

2.9.5 Transition to Argillaceous Matrix

The transition from continuous mudstone beds or nodules to the adjacent argillaceous, often dolomitic, matrix may be abrupt, occurring within a millimetre or less, or gradational over a few millimetres. In

6. Compaction estimates calculated from clastic dikes are discussed in Chapter 5

marginally-aggraded mudstones, microspar or pseudospar becomes increasingly coarser and more dispersed and then abruptly disappears. Pressure solution features such as peaked stylolites, prominent argillaceous seams, microstylolite swarms and accumulations of other insolubles in the transition zone are rare (cf. Wanless, 1979, 1983).

Field and petrographic relationships demonstrate that near nodule margins, grainy laminations typically converge toward the horizontal axial plane of the nodule (Plate 13g). In addition, grainy laminations within nodules are commonly traceable into the adjacent internodular matrix until they disappear, usually within a distance of 2-5 cm from the nodule. The petrographic changes which occur in the transition zone are detailed in Plate 53a-d.

2.9.6 Trace Fossils

Most beds in this lithofacies are devoid of traces. They may be locally abundant, however, and observed in, on, or under planar through to lenticular beds. The irregular, lumpy bedding and pin-cushion-like surfaces of some mudstones can occasionally be correlated with the presence of burrows but many such beds have no apparent cause for the irregularities (Plate 10d).

The horizontal traces Planolites and Paleophycus are found on bottoms and, less commonly, tops of mudstone beds (Plate 11a; Narbonne and James, 1984). The most obvious traces are Skolithos burrows which range from 1-5 mm in diameter (Plate 11b-d). They are usually filled with calcite cement, grainstone (Plate 11b), or mudstone (Plate 11d).

Pervasive or selective pyritization of traces or their fills is also common. In a few beds the U-shaped spreite of Diplocraterion occurs (Narbonne and James, 1984). Burrows are never compacted in mudstone; but those in shales are usually squashed. Some mudstones have an irregularly-mottled appearance and are interpreted as the result of indeterminate bioturbation (Plate 11e).

2.9.7 Nodular Limestones; Details

2.9.7.1 Distribution, Shape and Size of Nodules

When they occur in ribbon limestone sequences, nodules tend to be lenticular in cross-section; evenly spaced, usually separated by distances ranging from 10 cm to greater than 1 m; and distributed along discrete horizons (Plates 12c-f; 13a). In parted limestones sequences, however, they are closely "fitted" together and vary considerably more in shape. Some beds consist of fitted lenses, invariably with the long dimension of the nodule parallel to bedding (Plate 13b). Other beds consist of irregularly-shaped nodules that resemble loosely-fitting pieces of a jigsaw puzzle (Plate 12a). Rare beds exhibit irregularly-shaped nodules which are elongated sub-vertical to vertical to bedding (Plate 13c,d).

Isolated nodules in ribbon limestone or shale sequences reach up to 1 m in length and 30 cm in thickness (Plate 12d). Most, however, are considerably smaller and typically range from 10-20 cm in length and 2-4 cm in thickness, more or less the same thickness as associated continuous beds (Plate 12f; 13f). In plan view, nodules are sub-circular in shape

with the longest dimension 30-40% longer than the shortest (Plate 12c; see Appendix M). Fitted nodules range from 1-10 cm in the longest dimension and 1-4 cm in thickness. Their shapes in plan view vary from sub-circular to irregular.

2.9.7.2 Types of Nodules

Five types of limestone nodules are differentiated based mainly on field criteria: (1) grainy, (2) chaotic, (3) detrital, (4) mudstone, and (5) cored. These are schematically illustrated in Figure 2.5.

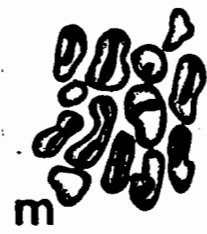
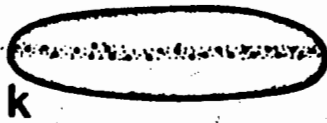
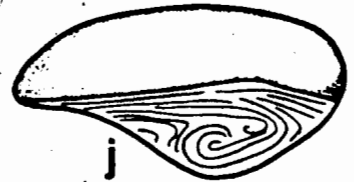
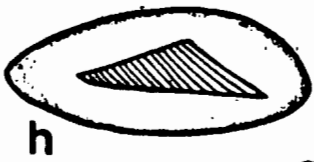
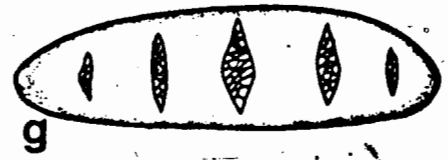
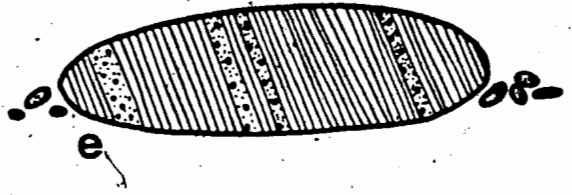
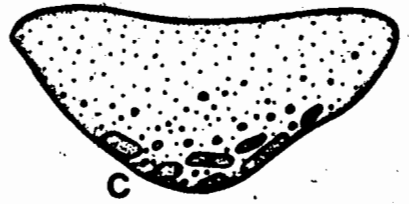
Grainy nodules are common and are simply primary, laterally discontinuous beds which consist of isolated, loaded, or convoluted ripples or scour-fills (Figure 2.5a-c; Plate 53f). Sediments are typically silt- and sand-size grainstone, but also may include lenses of pebble-size conglomerate. This type of nodule occurs isolated or in fitted patterns.

Chaotic nodules are commonly fitted and consist of grainstone, packstone, or wackestone (Figure 2.5d; Plate 12a). There is usually no obvious cause for this fabric which is often referred to in the literature as "mottled" limestone. While comparatively rare in the CHG, this fabric is extremely common in many shallow-water carbonate successions, for example the Table Point Limestone in western Newfoundland (see Klappa et al., 1980).

Detrital nodules reach 50 cm in length and are relatively rare (Figure 2.5e; Plate 12b). These nodules consist of silicified shale and are lithologically distinct from surrounding sediments. Evidence of their

Figure 2.5: Schematic summary of the various types of nodular limestones in the Cow Head Group. Labels "a" to "p" are referred to in text.

NODULAR LIMESTONES



detrital origin is based on (1) their lithology; (2) the high angle-to-bedding of internal laminations in some samples; and (3) occasional accumulations of centimetre-size pebbles and granule-size clasts at the nodule margins. These nodules are probably the heavier, larger freight from a debris flow which has been eroded away by later currents or simply passed over the area leaving behind the heaviest particles as flow competence decreased. In this respect these nodules are similar to the isolated boulders in Bed 6 at Cow Head North (discussed previously).

The last two types of nodules - mudstone and cored - are closely related and are the most important types of nodules in the CHG, both in terms of abundance as well as the critical petrographic and geochemical information they provide (Plate 12c). These are the only nodules that are considered further in this thesis. They may form nodular intervals (Plate 12f; 13b) or occur isolated in shales. These nodules also commonly occur in ribbon and parted sequences (Plate 12d).

Mudstone nodules are generally homogeneously crystalline or gradually coarsen toward their margins (Figure 2.5f) occasionally demonstrating concentric banding characterized by increasing crystal size, intercrystalline paste, and iron-content in successive bands. Some mudstone nodules contain spindle-shaped septarian cracks (Figure 2.5g; Plate 12e) filled with calcite or, less commonly, pyrite. The cracks are 2-4 cm in length and up to 1 cm in width and are arranged normal to bedding. Calcite within the cracks is ferroan, equant to slightly elongate, and up to 1 cm in size.

Cored nodules are similar to mudstone nodules except that they have an obvious core [7] (Figure 2.5h-p; Plate 12f; 13a-g). The cores most often consist of one or several, millimetre-thick peloidal silt laminations (Figure 2.5k) or isolated ripples and convolute laminations (Figure 2.5h-j; Plate 13a). These nodules occur either isolated or fitted together. Mudstone envelopes may be asymmetrically developed or incomplete.

Burrows and grainstone dikes may also be enveloped by mudstone.

Abundant burrows form beds of fitted nodules aligned parallel (Figure 2.5l; Plate 13b) or sub-vertical (Figure 2.5m; Plate 13c,d) to bedding, depending upon burrow orientation. Grainstone dikes tend to occur sporadically in ribbon or parted limestone sequences and are commonly only a millimetre or so in thickness and may be difficult to see within the nodule other than in thin section (Figure 2.5n; Plate 13e,f).

Compound nodules (Figure 2.5o, p; Plate 13g) result from the superposition and occasional merging of two or more simple, mudstone or cored nodules. Occasionally, compound nodules or two simple nodules separated by a thin shale seam develop V-shaped cracks near their margins (Plate 53e). These cracks are filled with calcite cement, squeezed in shale, or both.

7. Cathode luminescence demonstrates that the cores are lithified contemporaneously or earlier than their surrounding mudstone envelope.

2.10 MUDSTONE LITHOFACIES: INTERPRETATION

2.10.1 Introduction

Parted and ribbon limestones are a characteristic lithofacies of carbonate slope and, in some cases, basin sedimentation of all ages (Wilson, 1969; 1975) although they are not restricted to these environments. This type of sediment is also found, commonly being quite nodular and more fossiliferous, in shallow-water, subtidal shelf carbonates (e.g. Cambrian Whipple Cave Formation of Nevada - Cook and Taylor, 1977; Patterson Member of Cambrian Shady Dolomite of southwestern Virginia - Pfeil and Read, 1980). In general, the following characteristics, based on the CHG and compiled from the following sources, apply to parted and ribbon limestones: (Wilson, 1969; 1975; Marcinowski, 1970; Cook and Taylor, 1977; Evans and Kendall, 1977; Keith and Friedman, 1977; Hemleben and Reuther, 1980; Pfeil and Read, 1980; Read, 1980; Hurst, 1981; Bertrand-Sarfati and Moussine-Pouchkine, 1983; Hurst and Surlyk, 1983):

(1) Limestones are dominated by mudstone and to a lesser extent wackestone. These are interbedded with argillaceous sediments - either shales or marls, calcareous or dolomitic, and occasionally silicified - to form parted or ribbon limestones ("rhythmites" of Wilson, 1969) of remarkably constant thickness and spacing. These sediments are volumetrically important, and often dominate in slope successions. For example, 75% of the Cambrian Hales Limestone exposed in the Hot Creek

Range of Nevada consists of dark grey to black mudstone with minor wackestone and interbedded argillaceous sediments (Cook and Taylor, 1977). The vertical persistence of this lithofacies is also remarkable in many cases. This is most dramatically exemplified by the Late Proterozoic Dimamou Formation of West Africa where over 2000 m of ribbon limestones were measured (Bertrand-Sarfati and Moussine-Pouchkine, 1983).

(2) Beds are usually less than 10-20 cm in thickness and are planar, having abrupt upper and lower contacts. Exceptional mudstones are more than 1 m thick (e.g. 75-150 cm - Evans and Kendall, 1977; 5-300 cm - Hurst and Surlyk, 1983) but the thickest recorded in the CHG is 30 cm. Nodular beds may be locally important and randomly interspersed with continuous, planar beds and, in some cases, dominate the sequence.

(3) Mudstones are massive or very finely laminated on a millimetre-scale, usually lacking bioturbation or are only slightly bioturbated. Mudstones consist of micrite, microspar, or pseudospar, and contain variable amounts of silt-size peloids, siliciclastics, and shelly bioclasts. Pelagic fossils such as radiolaria and sponge spicules are locally abundant, occasionally dominating beds, and high concentrations of these components are spatially associated with silicification, in the form of nodules, stringers, and crusts within limestones and interbedded shales (see Chapter 13). Skeletons of indigenous, calcareous benthic invertebrates, such as trilobites and brachiopods, are also found. In Mesozoic and younger sediments, calcareous and aragonitic microplankton, notably coccoliths, foraminifera, and pteropods, are important.

(4) Interbedded shales are often dark, organic-rich, finely laminated, and variably dolomitic. In Lower and Middle Paleozoic sediments, shales are often graptolitic and may also contain radiolaria and sponge spicules either dispersed or concentrated in laminations.

(5) Sediments of this lithofacies lack evidence of shallow-water deposition. Associated coarser sediments are various types of gravity flows, most importantly turbidites and debris flows. This lithofacies also demonstrates evidence for deposition on a slope in the form of intraformational truncation surfaces and deformational fabrics associated with sediment failure.

2.10.2 Depositional Mechanisms for Parted and Ribbon Mudstones

From basic field relationships, early lithification of mudstones is certain. The origin of the rhythmite character of these sediments, however, is not straightforward and could be either primary, early diagenetic, late diagenetic, or all 3. For example, interbedded shales and marls could be interpreted as "stylocumulates" (Logan and Semeniuk, 1976) resulting from pervasive or "non-seam" pressure solution (Wanless, 1979, 1983) which are interbedded with more "resistant units" (Wanless, 1979; "idens" of Logan and Semeniuk, 1976) composed of relatively pure limestone. Most evidence, however, suggests that the "rhythmite" character is a primary or early diagenetic feature, which has been modified subsequently by preferential compaction of the argillaceous interbeds (see Chapter 5).

The strongest evidence for this is the contrasting rheologic behavior of argillaceous and mudstone beds within rafts. The observation that shales and marls deform plastically around fragments of limestone and flow into fold hinges demonstrates that the argillaceous sediments were not lithified early (Plate 1d,e). This implies that significant, fundamental differences in composition between the argillaceous and limestone beds were present at the outset.

Based upon (1) well-studied fine-grained siliciclastic muds from modern and ancient slope, rise, and basin systems, (e.g. Stanley, 1981; Stanley and Maldonado, 1981; Einsele and Kelts, 1982), (2) the carbonate slope and basinal sediments of the Bahama region (Mullins, 1983 and numerous references therein), and (3) ancient slope and basinal sediments (e.g. Cook, 1983b; Cook and Mullins, 1983; Scholle et al., 1983), several depositional mechanisms may account for the (1) dominance of mudstone, (2) lack of obvious structures attributable to traction sedimentation, (3) fine parallel laminations, (4) poor sorting of enclosed peloids and bioclasts, (5) lateral continuity of beds, and (6) rhythmicity of these sediments. These mechanisms include (1) dilute turbidity currents; (2) hemipelagic settling (or similar settling from nepheloid layers or from turbid flows spread out over pycnoclines); and (3) bottom (contour) currents. These depositional processes are not easily separable in time and space, especially in slope and rise environments where turbidites, contourites, and hemipelagites or pelagites are often interbedded with one another. Furthermore, a continuum may exist between dilute

turbidity flows, bottom currents, and hemipelagic or pelagic settling (Stow and Lovell, 1979) and different depositional mechanisms may interact or influence one another or their deposits. For example, tails of turbidity currents may be deflected by bottom currents; or, turbidity or contour currents may feed nepheloid layers (Piper, 1978).

2.10.2.1 Dilute Turbidity Current Hypothesis

Transportation and deposition of peri-platform muds [8] from dilute turbidity currents - either the tail ends of sandy or silty flows, or initially muddy flows - accounts for the above-listed characteristics, as well as the association of these sediments with coarser-grained turbidites and finely-laminated, interbedded turbiditic shales and marls. Dilute turbidity currents have also been suggested in other studies to account for the origin of parted and ribbon mudstones (e.g. Keith and Friedman, 1977; Pfeil and Read, 1980).

The mechanism, however, has several inadequacies. Unlike sediments in the siltstone and shale lithofacies, these mudstones do not show consistent grading relationships with overlying argillaceous sediments. Silty laminations within mudstones also do not demonstrate consistent grading relationships. The uniformly-thick, planar beds, the lack of basal loading and scour, and the paucity of horizontal traces is also quite unlike the fine-grained turbidites in the siltstone and shale lithofacies.

8. Schlager and James (1978) used this term to describe a mixture of shallow-water, platformal lime muds and bioclasts mixed with pelagic material and deposited on the adjacent slope or basin.

In addition, these mudstones do not immediately overlie coarser peloidal silt- and sand-size turbidites as might be expected if they had arisen from the same flows. In the CHG, mudstones are found under, over, or both under and over grainy sediments to form composite beds. Other mudstones are not associated with grainy sediments. This lack of a systematic relationship between mudstones and associated grainy sediments has also been noted in other studies (e.g. Bertrand-Sarfati and Moussine-Pouchkine, 1983). A mudstone "pre-phase" plastered to the base of Devonian carbonate turbidites in Germany was attributed to diagenetic migration of carbonate to these turbidites which were apparently favourable precipitation sites (Meischner, 1964; Eder, 1971). In contrast, carbonate turbidites from the Devonian of Cornwall are devoid of a mudstone "pelitic" division (Tucker, 1969). This was interpreted to be due either to the absence of mud in the source region of the turbidites or continued downslope transport and deposition of fines elsewhere. Keith and Friedman (1977), on the other hand, noted that mudstone beds were always associated with carbonate beds of other lithofacies.

2.10.2.2 Hemipelagic Settling Hypothesis

The characteristics of parted and ribbon limestones could also be interpreted as the result of suspension settling of peri-platform muds either from the entire water column, nepheloid layers, or from turbidity currents which have spread out over pycnoclines. Suspension settling has also been suggested as a mechanism for the deposition of parted and ribbon limestones in other studies (e.g. Wilson, 1969; Cook and Taylor,

1977; Keith and Friedman, 1977; Hurst and Surlyk, 1983). The argillaceous interbeds are interpreted to represent times of little or no carbonate input into the basin or slope environment and consequently, background sedimentation was more siliciclastic, consisting mainly of detrital clays.

2.10.2.3 Contourite Hypothesis

The evidence for a contourite [9] origin for mudstones and grainstones in the CHG as well as in other studies of ancient carbonates, is not compelling (e.g. Bein and Weiler, 1976; Cook and Taylor, 1977; Cook and Egbert, 1981; Cook, 1983; Bertrand-Sarfati and Moussine-Pouchkine, 1983). In part and ribbon sequences of the CHG, the intimate association of mudstones with sediments interpreted as turbidites based on sedimentary structures as well as paleocurrent measurements, suggests that mudstones are unlikely to be contourites.

2.10.3 Interpretation of Nodular Limestones

Nodular limestones, specifically the "mudstone" and "cored" types, are similar to those described from many other sequences (e.g. Jenkyns, 1974; Jones et al., 1979; Wanless, 1979). Considering only mudstone and cored nodules, these, along with continuously-bedded mudstones both exhibit the following characteristics:

9. Lovell and Stow (1981; p. 349) defined a contourite as "a bed deposited or significantly reworked by a current that is persistent in time and space and flows along slope in relatively deep water (certainly below wave base)".

- (1) identical microfacies,
- (2) association with "beef" and "cone-in-cone" fibrous calcite,
- (3) marginal aggradation of crystal size,
- (4) variable relationships with grainy sediments in cored nodules and composite beds. Mudstone may underlie, overlie, or surround grainy sediments.
- (5) Both nodules and continuously-bedded parted mudstones commonly demonstrate fitted fabrics.

Given the preceding it is difficult to accept any conclusion other than nodular and continuously-bedded mudstones are genetically-related. These sediments are commonly intergradational with successive beds becoming either more nodular or continuous. The similarity of nodular limestones with associated, more continuously-bedded limestones has also been stressed in other studies (e.g. Garrison and Fisher, 1969; Bjorlykke, 1973; Henningsmoen, 1974). Possible mechanisms to explain the relationship between nodular and continuously-bedded mudstones include: (1) synsedimentary boudinage (e.g. McCrossan, 1958), (2) subsolution (e.g. Holmann, 1962, 1964), (3) pressure solution (e.g. Logan and Semeniuk, 1976; Wanless, 1979), and (4) lateral coalescence of concretions (e.g. Henningsmoen, 1974; Jenkyns, 1974). Based on field evidence alone it is not possible to decide which is the most likely. A detailed evaluation of these mechanisms, based largely on slab study and petrography, is presented in Chapter 14.

2.11 SUMMARY OF LITHOFACIES INTERPRETATIONS

Conglomerate Lithofacies: Most characteristics of these deposits are consistent with a debris flow origin. Those conglomerates with sandy matrices, crude pebble imbrication, normal grading, or coarse foresets, however, suggest deposition from more evolved flows in which particle segregation was possible. In these flows, dispersion or turbulence may have been a complimentary particle support mechanism.

Calcarenite Lithofacies: The Bouma (1962) sequence is inadequate to model the sediments of this lithofacies. These sediments do, however, resemble proximal turbidites described from siliciclastic successions. The typical massive bedding (T_A) with less common normal grading are interpreted to result from a direct suspension settling from high density flows as they lost energy, evolving toward more dilute flows. Other grainstones scattered throughout the sequence are interpreted as turbidites deposited from such dilute flows.

Siltstone Lithofacies and Shale Lithofacies: These two lithofacies are defined by the relative abundance of silt and shale within a given interval. Both contain siltstone beds which commonly grade upward into shale in a predictable, regular fashion. Both lithofacies are interpreted to consist mainly of fine-grained turbidites (silt or terrigenous mud) which grade upward into terrigenous mud hemipelagites. Millimetre-cycles in shales are interpreted to reflect the different abundance as well as preservation potential of organic material in

terrigenous turbidites versus hemipelagites. Thicker metre-cycles in shales are interpreted to be the result of periodic variations in the amount of organic matter in the source regions for these shales as well as the oxygen levels of the bottom waters.

Mudstone Lithofacies: Mudstones may be either deposits of dilute turbidity currents or the result of settling of hemipelagic (peri-platform) fines. Based on available data, including comparison with similar deposits in the literature, it is not possible to state unequivocally which is the more probable origin. Nodular mudstones are genetically-related to the continuously-bedded mudstones but the fundamental nature of their relationship is not clear based on field observation.

The interpretation of the mudstone lithofacies according to the proposed depositional mechanisms is far from satisfactory. Aspects of these limestone sequences that are not adequately explained by turbidity current or hemipelagic settling mechanisms include: (1) fitted fabrics in both continuous and nodular beds; (2) composite beds and nodules with mudstone plastered under, over, or both under and over grainy sediments; and (3) marginal aggradation of crystal size or coarsening of calcite crystal size in certain bands within mudstones.

If mudstones and grainstones are contourites, as inferred from the hypothesis of Hubert et al. (1977), it is unlikely that they would be sufficiently distinct from turbidites to be recognized as such. In addition, the southeast paleocurrents are consistent with down-slope flow of turbidity currents, based on regional and lithostratigraphic

considerations (James and Stevens, in prep.) and therefore a contourite origin for these sediments is highly unlikely.

2.12 DISCUSSION: CARBONATE APRONS

From the preceding discussion and the measured sections of James and Stevens (in prep) it is obvious that the CHG is a disorganized, unpredictable array of lithofacies. Thickening-upward packages of sediments suggestive of a prograding submarine fan are not present, nor are other fan-like features such as thinning-upward sequences (as fan-channel fills) or extensive channeling (see Walker, 1984). The lack of fan characteristics is now generally regarded as typical for most carbonate slope deposits, modern and ancient (Cook and Mullins, 1983; Cook, 1983b; Mullins, 1983). This contrasts with siliciclastic systems in which sediments disgorge from a principle canyon ("point source"), to form a submarine fan. Siliciclastic fans are well-known from the modern as well as ancient record and their systematic spatial and temporal characteristics have led to the construction of a well-tested submarine fan model in which there is a systematic downcurrent (or downsection) development of inner, middle, and outer fan facies sequences (see overview in Walker, 1984). There are no documented submarine fans in modern carbonate environments and only a few have been recognized in the ancient record (Cook, 1983b). The most notable of these occur in the Upper Cambrian-Lower Ordovician of the Basin and Range Province (Cook and Taylor, 1977; Cook, 1979) and the Jurassic of southern Spain (Ruiz-Ortiz, 1983) and Portugal (Wright and Wilson, 1984). The lack of

fan characteristics has also been noted in numerous modern and ancient carbonate slope studies (see numerous references in Mullins, 1983; Cook and Mullins, 1983; Cook, 1983b; McIlreath and James, 1984).

The rarity of carbonate submarine fans is thought to be the result from dispersal of sediment along a semi-continuous line-source rather than from a major canyon as is the usual case for siliciclastic sediments (Schlager and Chermak, 1979). Carbonate sediments move down the slope by various types of unchannelled, sheet-like gravity flows (Cook, 1983b). In the Bahamas, turbidity currents and debris flows are the dominant mechanisms of downslope transport, accounting for 25-30% of the sediment (Mullins, 1983). Deposition of carbonate sediments in this manner builds a wedge-shaped apron of sediment. In a "slope apron" the sediments extend from the platform margin down to the basin whereas in a "base-of-slope" apron most of the sediments are deposited at the base of the slope and on the rise, but with some turbidites and debris flow conglomerates extending further basinward, away from the main accumulation (Cook, 1983a).

Chapter 3

SUBMARINE SLIDING: EVIDENCE FOR
DEPOSITION ON A SLOPING SURFACE

3.1 INTRODUCTION

Evidence for slope failure is common in the parted and ribbon limestones of the Cow Head Group. Much of this evidence, however, is subtly expressed, which probably accounts for it having remained unreported until now. By cataloguing the various synsedimentary deformation fabrics associated with rare, well-exposed truncation surfaces and allochthonous slide masses, it is possible to interpret many of the bedding disruptions in these evenly bedded limestones as being the expression of sediment failure. The recognition and proper interpretation of these synsedimentary deformation fabrics is especially important where outcrop is limited or there is a lack of sufficiently extensive strike exposure that would allow straightforward recognition of intraformational truncation surfaces or allochthonous slide masses. Such sediment failures are unequivocal evidence for deposition on a sloping surface.

3.2 TERMINOLOGY

Reviews of processes and terminology currently used in the interpretation of sediment failure and gravity flow have been compiled by numerous workers (e.g. Carter, 1975; Nardin et al., 1979a; Cook and Mullins, 1983). Following the definitions provided in Nardin et al. (1979a) a slide is defined as the movement of a rigid, internally undeformed mass along a discrete shear surface. Slides can be subdivided into slumps where rotational motion is apparent, and glides where the mass has translated along a planar surface. Differentiation of slumps from glides in ancient sequences is usually not possible because of insufficient exposure, therefore, only the general term slide is used (also see Cook and Mullins, 1983).

Sliding gives rise to an allochthonous slide mass which is laterally displaced relative to underlying, assumed in situ sediments. The original position of a slide mass is demarcated by an intraformational truncation surface where beds intersect the surface with angular disconformity. The truncation surface is exposed on the sea floor and is subject to burial from subsequent deposition (cf. "major cut-and-fill structure" of Wilson, 1969). Analogous truncation surfaces are recognized on present-day continental slopes and other slopes as trough or scallop-shaped depressions commonly referred to as slide scars or slump scars (e.g. Cook and Mullins, 1983; Enos and Moore, 1983).

The surface along which failure has taken place may be a true two-dimensional surface. It is, however, commonly more appropriately described as a shear zone which lacks an obvious basal shear plane. In

this zone, plastic and elastic deformation disrupts, and in some cases, homogenizes original sedimentary fabrics. A shear zone may develop immediately below a truncation surface or where an overlying sediment mass moved a short distance downslope but did not detach from underlying sediments. Similarly, the leading edges, the base, and in some cases the entire slide mass are also subject to deformation. Tank experiments (Schwarz, 1982), high resolution seismic observations and cores of modern slide masses (e.g. Nardin et al. 1979b), and observations from the CHG demonstrate that internal deformation in slide masses is common. The transition from slide movement to debris flow (e.g. Cook, 1979; Cook and Mullins, 1983) and ultimately to various gravity flows (e.g. turbidity currents, grain flows) is readily attained in the submarine environment by addition of water and mixing (Middleton and Hampton, 1976; Nardin et al., 1979a).



3.3 FIELD DESCRIPTIONS

The following section examines the field relationships between two well-exposed intraformational truncation surfaces and the deformation fabrics in the shear zones which immediately underlie them. Following this, two allochthonous slide masses are also described. Relationships established from these observations are subsequently used to interpret two other outcrops where the origin of deformation is less certain. A listing of outcrops which contain evidence of sediment failure is provided in Table C.2 of Appendix C.

3.3.1 Intraformational Truncation Surfaces

3.3.1.1 Lower Head

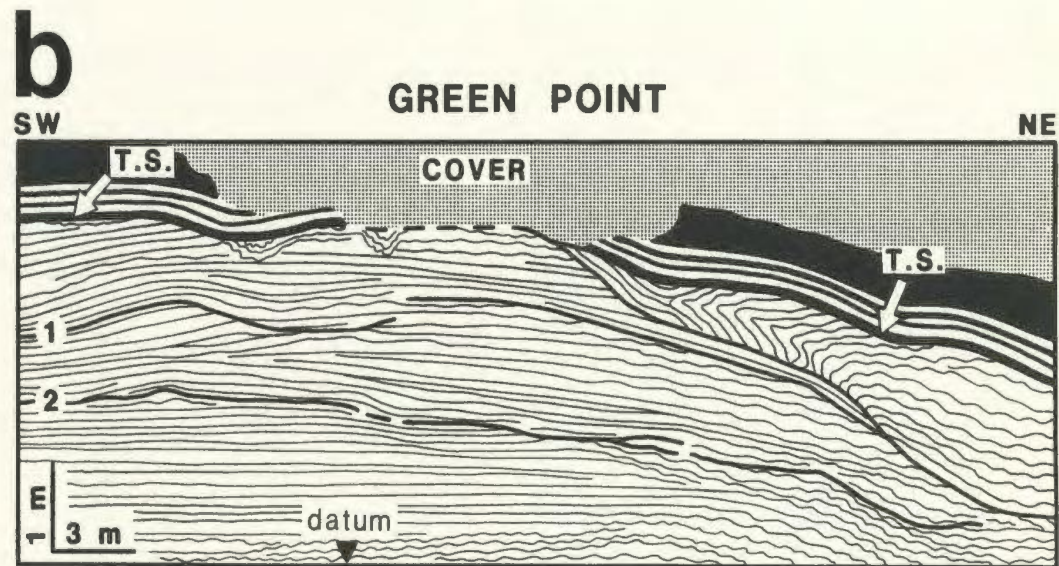
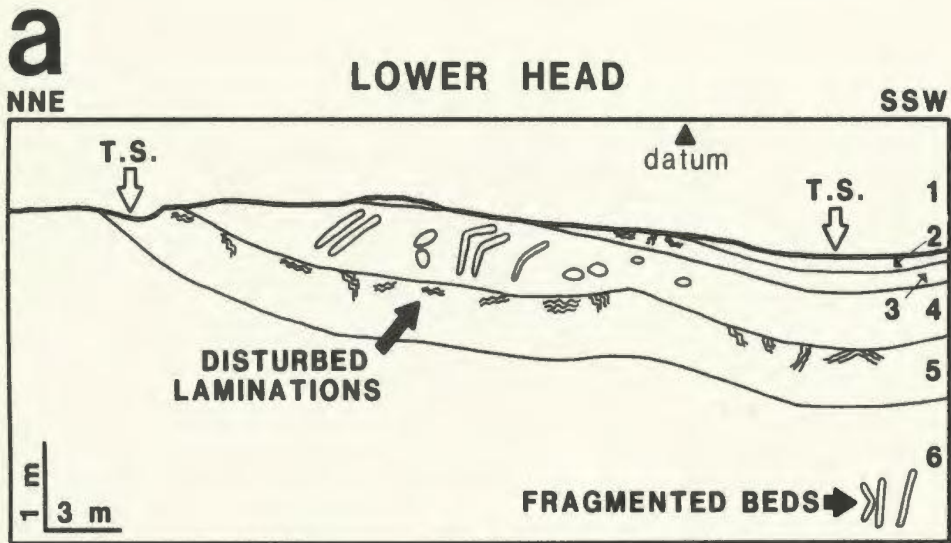
A prominent truncation surface is found within the Arenig sequence beneath the massive boulder conglomerate of Bed 14 at Lower Head (Figure 3.1). Approximately 2.5 m of demonstrable erosion occurs in the measured area with an additional 3-4 m further along strike. The truncation surface depression is filled with thinly-bedded parted limestones (grainstones and mudstones; bed 1 [1] in Figure 3.1; Plate 14a). In contrast, sediments below the truncation surface consist of black shales (bed 2), finely-laminated marls (beds 3 and 5), and ribbon limestones (beds 4 and 6).

The effects of shear are seen both at and below the truncation surface. Ribbon limestones in beds 4 and 6 are fragmented and rotated (Plate 14b,c). Although most of these fragments are irregularly shaped and randomly distributed, tabular clasts in bed 4 have a sub-parallel alignment and suggest a minimal amount of rotation of these slabs (Plate 14b). In bed 6, some 3 m below the truncation surface, ribbon limestones have been rotated so that they are now oriented perpendicular to bedding and localized pods of intraformational conglomerate are developed by piling-up of mudstone beds (Plate 14d,e). The draping of mudstone beds and laminated marls over the perpendicular slabs of ribbon limestone confirm that disruption occurred prior to significant compaction.

1. These bed numbers refer to those in Figure 3.1 only.

Figure 3.1: (a) Measured outcrop of Lower Head truncation surface. Details of lithologies and deformation fabrics are provided in text. The datum used for measurement is a continuous grainstone bed in the sediments above the truncation surface. Rotated mudstone slabs and re-oriented and homogenized laminations in marls are shown in their approximate positions. "T.S." is truncation surface.

(b) Measured outcrop of Green Point truncation surface. The succession is overturned but is turned right way up in this sketch. Details of lithologies and fabrics are provided in text. "T.S." is truncation surface. Heavy lines "1" and "2" are small displacement synsedimentary faults which are traceable over most of the outcrop. Wavy lines indicate the distribution of disturbed bedding as illustrated in Plate 15c. Position of drag folds are shown in exact positions immediately underlying truncation surface.



Evidence for disruption is also found in the finely-laminated marls of beds 2 and 5. In most places the millimetre-size lamination is undisturbed and continuous. In some areas, however, especially in the upper 15-20 cm of bed 5, decimetre-size domains are defined by disturbed laminations which are variably re-oriented, often at high angle or perpendicular to bedding (Plate 14f). Other domains in these beds are devoid of lamination and the sediment appears massive, although this could be the effect of looking at a surface parallel to the laminations. Small displacement microfaults and isoclinally-folded laminations are also observable in outcrop as well as thin section.

3.3.1.2 Green Point

Another truncation surface and its underlying shear zone is found in the Tremadoc section at Green Point (unit 28 of James and Stevens, in prep.; Figure 3.1). Approximately 2 m of erosion occurs in the measured area and the truncation surface can be followed sporadically for over 20 m outside the measured area where it continues to gradually down-cut until it is lost due to tectonic faulting. The depression formed by the truncation surface is filled with sediments similar to those which lie above the Lower Head truncation surface (Plate 15a). The parting to ribbon limestones below the truncation surface consist of planar, thinly-bedded, massive to parallel-laminated mudstones interbedded with dolomitic marls.

The style of deformation in the shear zone is significantly different from that described from Lower Head. Here, the sediments are locally drag-folded just below the truncation surface (Figure 3.1, Plate 15b).

In addition, 2 small synsedimentary faults are traceable throughout most of the measured outcrop and show discordance with both underlying as well as overlying beds (Figure 3.1). A large portion of the measured outcrop demonstrates irregular, wavy bedding which can be followed laterally and vertically into relatively undisturbed planar-bedded sediments (Plate 15c). The disturbed bedding is most prominently developed immediately below the large drag-fold.

3.3.1.3 Interpretation

The truncation surfaces at Lower Head and Green Point are not traceable to their displaced sediment masses, a situation typical for ancient sequences in general (see Davies, 1977). These outcrops are interpreted as truncation surfaces (slide scars) rather than channels or current scours based on criteria, used collectively, to suggest a truncation surface origin. Channels and scours are also common in ancient as well as modern slopes (e.g. Walker, 1975; Cook, 1979; McGregor et al., 1982) and some are extremely large, for example, the current scours up to 500 m wide and 20 m deep which have been described from the Navy submarine fan off the California borderland (Normark et al., 1979).

Criteria from Davies (1977) and Clari and Ghuibaudo (1979) which are applicable to interpretation of truncation surfaces at Lower Head and Green Point are (1) the absence of smaller scours or channels in the "footwall" beds, and (2) the absence of obvious lag deposits suggestive of channels. In addition, the association with the underlying disrupted sediments (shear zones) would be difficult to explain by current action or channel cutting whereas the stresses generated during failure could

readily account for the observed deformation. Many other truncation surfaces, however, appear to lack obvious shear zone deformation (Figure 15d) and may be scour-related (e.g. Yurewicz, 1977).

3.3.2 Slides

3.3.2.1 Green Point

A slide mass separate from the truncation surface described above and which locally reaches 4 m thickness is traceable for approximately 180 m along strike in Tremadoc ribbon mudstone and shale sequence at Green Point (unit 27 of James and Stevens, in prep.). The only lateral margin visible is markedly lenticular and approximately 1 m of basal erosion is seen (Plate 16a).

The transported sediments consist of thinly-bedded, locally burrowed parted mudstones. The greatest amount of internal bedding disruption and homogenization is found near the lateral margin; elsewhere, bedding is only slightly disturbed. Throughout most of this outcrop, there is no discernible basal shear zone and the contact of the slide mass with underlying sediments is without detectable erosion or deformation.

3.3.2.2 Cow Head South

A slide mass of thinly-bedded parted grainstones disconformably overlies similar sediments in Arenig sediments at Cow Head South (Bed 13s.4 of James and Stevens, in prep.). The slide is approximately 1 m thick and is overlain by 1.5 m of graded conglomerate (Plate 16b; 1c). This

disconformity truncates beds below it and is probably a truncation surface.

Bedding in this slide is locally disrupted near its base occurring as an anastomosing web of millimetre-thick partings defining phacoidal or fitted lenticular bedding (Plate 16 c,d). Away from the base, intensity of bedding disruption diminishes and bedding is more regular.

3.3.2.3 Interpretation

The slide mass at Green Point is lithologically distinct from the sediments into which it has moved. This, in concert with chaotic, locally homogenized bedding and erosion of underlying sediment at the margin permits identification as a slide to be straightforward. For most of its exposure, however, the lack of a basal shear zone and basal erosion implies that such a slide mass could readily be mistaken to be undisturbed, in situ sediment. This underscores the importance of carefully recording the most minute bedding irregularities and, if possible, tracing questionable beds laterally for exposures of either basal erosion or lateral pinching-out. If "host" sediments are not distinct, as is the case at Cow Head South, the locally chaotic, homogenized, or phacoidal bedding in the basal region of the slide mass could serve as an important signal of sediment failure.

The contacts of the slides with overlying sediments do not contain evidence of their allochthonous nature, except at the lateral margin of the Green Point slide where chaotic bedding is apparent at the top of the slide. It is conceivable, however, that surfaces of slide masses

could be subjected to preferential erosion and smoothing due to their positive relief and a slope or base of slope position favourable to eroding currents (Schwarz, 1982).

3.3.3 Possible Internal Shear Zones

In the previous examples, there is clear evidence for the existence of both truncation surfaces as well as allochthonous slide masses. Their shear zones, where developed, are located precisely where expected - just below the truncation surface where some deformation would occur as the slide mass moved away, and in the case of the slide masses, at their bases due to stresses generated during initial movement or later downslope translation.

There are numerous outcrops, however, where sediments are noticeably disrupted, but evidence of a truncation surface or allochthonous slide mass is missing (Table C.2 in Appendix C). Although in some of these it is possible that the critical relationships discussed above are not exposed, the possibility that these are internal shear zones must also be considered. Deformation in these shear zones would reflect minor downslope translation of an upper "package" of sediments relative to a presumably, though not necessarily, in situ lower package of sediments.

Such internal shear zones could be regarded as approximately bedding-parallel, synsedimentary faults. In order to emphasize their probable relationship to previously discussed sediment failures, however, these are considered as one variation in the spectrum of shear zones generated by sediment failure on a sloping surface.

3.3.3.1 Green Point

Approximately 500 m south along strike from the previously described truncation surface at Green Point, there is an approximately 2 m thick interval in these ribbon and parted limestones in which several laterally extensive zones of disrupted sediments are found. The disrupted zones vary from 20-30 cm in thickness and consist of distorted, folded, and fragmented mudstones in a marl matrix (Plate 17a). One disrupted zone locally attains 1 m thickness but vanishes 200 m northeastward along strike into regularly-bedded sediment. The sole of another zone is characterized by "mullion" structures which result from the sub-parallel alignment of intrafolial fold hinges. No obvious sense of overturning is apparent, but based on relative limb lengths, they suggest downslope translation of the overlying sediments towards the southeast [2]. Caution, however, is suggested in attempting to distill paleoslope information from a single outcrop (see additional discussion in Hiscott and James, in press).

3.3.3.2 Cow Head North

Several disrupted zones also occur in the extensive Late Cambrian sequence of parted mudstones and grainstones at Cow Head North (units 6.37-6.44). The most conspicuous disrupted zone varies from several centimetres to 1 m in thickness and can be traced laterally along strike

2. Sixteen measurements of fold axes provide an average azimuth of 40 degrees to the northeast.

for 100 m after which it is no longer safely accessible. Bedding disruption is most apparent in the thicker portions of this zone where a chaotic array of folded and fragmented beds occur isolated or clustered together in a marl matrix (Plate 17b). Elsewhere, disruption in this zone and in the other, thinner zones is characterized by discordance with underlying and overlying beds where deformation fabrics are apparently absent. In addition, intrafolial drag folds may be developed in an otherwise apparently undisturbed sequence of sediments (Plate 17c).

3.3.3.3 Interpretation

The disrupted zones exemplified by the outcrops at Green Point, Cow Head North, and other locations (e.g Plate 17d) have received little attention by other workers. These were interpreted as "slump sheets" which slid at the sediment-water interface by Hubert *et al.* (1977, see their figure 3B; also Suchecki, 1975, his figure 11A). In addition, these were reported to be commonly eroded prior to subsequent deposition.

If the above interpretation of Hubert *et al.* (1977) is correct, then other evidence which would enhance this interpretation might include: (1) ponding of sediment in depressions formed by the small scale relief of folded and fragmented beds, (2) reworking of fragmented bedding, (3) lateral transformation of "slump sheet" into flat pebble conglomerate, and (4) absence of discordance with overlying beds.

Field observations indicate that none of the above criteria are

present. Instead, field evidence suggests that these bedding disruptions are shear zones which occurred in the shallow subsurface due to sliding while sediments were still sufficiently unlithified to be folded and fragmented. In addition, overlying beds are occasionally drawn into the folding and fragmentation of the shear zone suggesting that disturbance was subsequent to deposition of overlying strata.

The relationship between the truncation surface and the shear zone at Green Point is uncertain. At the southwestern end the unit is approximately 8 m thick. In contrast, 500 m to the northeast in the vicinity of the truncation surface it diminishes to 2 m in thickness. Due to structural complications, it is not possible to follow the truncation surface for more than 60 m and the subsurficial shear zones, due to their lateral variations in size and degree of sediment disruption, are also not traceable across the outcrop. Other sequences of similar ribbon limestones are remarkable for their continuity as well as constant thickness and it is therefore reasonable to assume that this variation in thickness from one end of the Green Point outcrop to the other is the product of sediment failure. The truncation surface and the shear zone may be responses to the same or separate events.

3.4 DISCUSSION

3.4.1 Model for Sediment Failure

Using the previously discussed examples of sediment failure, a general model is outlined which relates displaced sediment to its slide surface

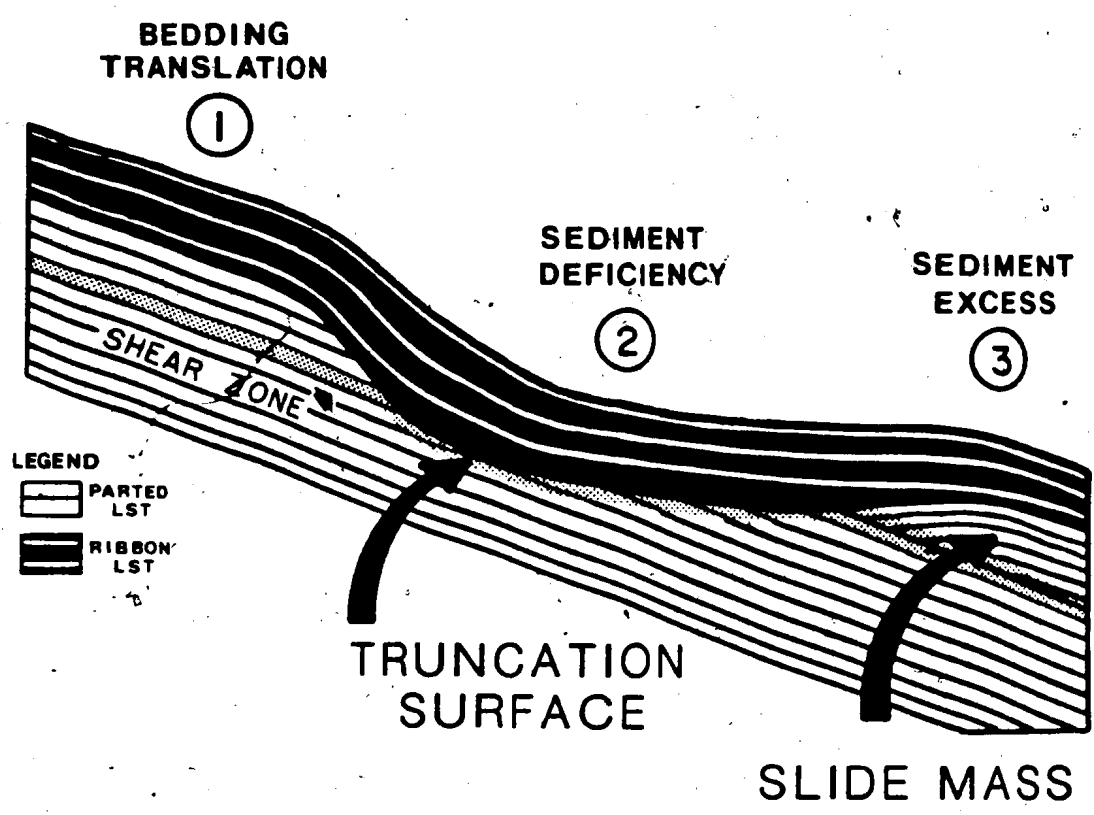
or shear zone. Three end member cases or conditions are envisaged (Figure 3.2). The first case is a bedding-parallel translation ("bedding translation") of sediments in which the vertical succession remains unaffected as there is neither removal nor accumulation of sediment. The shear zones at Green Point and Cow Head North are probable examples of bedding translations.

The second case is the formation of a truncation surface (slide scar) by sliding away of sediment with the resultant depression subsequently filled by younger sediments. The displaced sediments are missing from the local stratigraphy and thus a "sediment deficiency" (Fairbridge, 1946) occurs. The truncation surfaces at Lower Head and Green Point are examples of sediment deficiencies.

In the third case, a sediment package is moved downslope to rest on top of equivalent age sediments, though the sediments may not be of identical lithology. A local repetition of the stratigraphy or a "sediment excess" (Fairbridge, 1946) results. The slides at Green Point and Cow Head South are examples of sediment excesses.

Associated with each of the above types of sediment failure may be shear zones characterized by a suite of disturbed bedding fabrics. For bedding translations, the shear zone occurs in the shallow subsurface and separates an overlying downslope-translated sediment mass from a relatively in situ mass. For sediment deficiencies and excesses, a shear zone occurs immediately below the truncation surface, or along the sole of the slide mass or the surface of the overridden sediments, respectively.

Figure 3.2: Schematic diagram illustrates shear zones and their relationship to bedding-parallel movements, truncation surfaces, and slide masses. Refer to text for discussion.



Distinguishing among the three cases is not always straightforward and may not be possible, especially where strike exposure is limited, such as in the CHG. If the slide mass is identical to enveloping sediments or if the slide mass is too large and its boundaries cannot be defined, then bedding translations and sediment excesses may not be differentiable. Other criteria, such as repetitive biostratigraphic intervals (e.g. Embley and Jacobi, 1978) must be relied upon, if applicable. Obviously this would be inapplicable in many ancient, especially Paleozoic, sediments where biostratigraphic zonation is likely to be much coarser than the thickness of sediments involved in the failures. On the other hand, the high resolution afforded by Cenozoic marine biostratigraphy could easily be repeated by sediment failures the size of those in the CHG.

Both bedding translations and slide masses may be discordant with underlying as well as overlying bedding depending on the geometry of the shear zone or basal erosion. In contrast, truncation surfaces are characterized only by discordance with underlying bedding. In general, mudstones which fill the depression are continuously bedded in contrast to grainy sediments which are often discontinuously bedded and drape the truncation surface. Drape of beds infilling a depression could be misinterpreted for discordance with overlying bedding.

3.4.2 Dimensions of Truncation Surfaces and Slide Masses

The largest truncation surfaces in terms of cut-out sediment occur at Green Point and Lower Head where up to 7 m of erosion is demonstrable. Most other CHG truncation surfaces show less than 1 m of erosion. This

contrasts to 15-25 m cut into Miocene slope sediments in the Piedmont Basin of Northern Italy (Clari and Ghuibaudo, 1979) or 100-150 m of erosion in Upper Paleozoic carbonates of the Sverdrup Basin (Davies, 1977b). There is clearly insufficient exposure of the CHG to appreciate if structures of this scale are present. Such large truncation surfaces as those reported from the Piedmont and Sverdrup Basins are exceptionally large for ancient rocks. Even these, however, are small relative to the largest slides recognized in present-day oceans (e.g. Embley, 1982). Further discussion of size discrepancy between ancient slides and those recognizable in the modern ocean is found in Woodcock (1979).

The largest shear zone examined in the CHG is approximately 3 m thick, occurring below the truncation surface at Lower Head. At this depth, however, bedding disruption is minor. Shear zones are generally 1 m thick or less and thickness varies over short distances. In general, shear zone thicknesses in the CHG are similar to those observed in the Hales Limestone (Late Cambrian - Lower Ordovician) of the Great Basin in Nevada where slide masses vary from 2-10 m in thickness (Cook, 1979). If there is a correlation in the thickness of shear zone and slide mass, then CHG shear zones suggest slide masses on the order of 10 m thickness or less. This is supported by the 1 and 4 m thick (maximum) slide masses described from Cow Head South and Green Point which are the only examples available where thickness is measureable. Disruption in their basal shear zones is limited to a few tens of centimetres or less and in general, bedding disruption is minimal.

3.4.3 Causes of Sediment Failure in the CHG

The causes of sediment failure are diverse (see volume edited by Saxov and Nieuwenhuis, 1982; Schwarz, 1982) and a brief overview of the topic is provided in Appendix C. Two major controls of sediment failure are recognized: tectonic and oceanographic. Of the tectonic controls, earthquakes have long been cited as triggering mechanisms of failures on both passive and active margins, in both ancient and modern oceans. Oceanographic controls involve elements of the hydrosphere, such as sediment transport and sea level changes.

The causes of sediment failure in the CHG are uncertain and both tectonic (e.g. earthquakes) and oceanographic (e.g. changes in sediment pore pressures) controls must be considered. The largest conglomerates of the CHG, and also the Curling (Lower Cambrian to Lower Ordovician), and Table Head (Middle Ordovician Groups in western Newfoundland may be correlative with regressive events or changes in shelf sedimentation (James et al., 1979).

3.5 CONCLUSIONS

Prior to recognition of truncation surfaces, slide masses, and shear zones in the CHG, the only evidence of sediment failure was debris flows and possibly related turbidity currents. Detailed examination of several well-exposed outcrops exhibiting various types of evidence for sediment failure within parted and ribbon limestone sequences guides the interpretation of the numerous minor bedding disruptions in these

sediments and implies that sediment failure is a common and important part of the sediment's history.

A simple model for slope failure is based on the position of the detached mass and discordant bedding relationships. Sediment deficiencies occur with the formation of truncation surfaces and removal of the overlying sediments. Sediment excesses result from the emplacement of allochthonous slide mass onto sediments of equivalent age. Bedding translations are the most difficult to identify relying heavily on negative evidence for either truncation surfaces or slide masses.

Shear zones are generated during sediment failure. They occur (1) in the shallow subsurface of bedding translations, (2) below truncation surfaces, and (3) on the soles of slide masses or near the surfaces of overridden, relatively in situ strata. Shear zones are variable in size although usually a metre or less in thickness. The distilled model for the location of these shear zones is admittedly simplistic; for example differential movement within a slide mass may produce internal zones of longitudinal shear parallel to the slide axis, in addition to basal shear (e.g. Prior et al., 1982).

A suite of often subtly expressed deformation fabrics characterizes these shear zones. These include: (1) intrafolial folding, (2) brecciation, and (3) rotation of slabs of limestone. Phacoidal bedding (4) may be produced in some mudstones and grainstones by the development of irregular, anastomosing, argillaceous seams. In addition, finely laminated shales and marls contain domains where laminations are (5)

reoriented or (6) homogenized. Small-scale (7) isoclinal folding and (8) microfaulting are also locally developed.

The recognition of truncation surfaces and slide masses usually requires extensive strike exposure. In areas of limited outcrop, however, the various shear zone deformation fabrics may be the only clues to indicate the depositional environment was a sloping surface with sediments subject to periodic failure. Using the CHG as an example, intensive examination of outcrops which showed some bedding disturbances usually led to the discovery of other, related deformation fabrics:

"In the mapping of major geological structures, the field geologist often finds unaccountable little disturbances which appear to have nothing to do with the main issue."
(Fairbridge, 1946, p. 84.)

In the CHG, the "little disturbances" are interpreted to be the result of sediment failure, an indication of instability in a stratigraphic sequence, which, for various reasons, may otherwise go undetected.

In addition to their paleoenvironmental and paleogeographical implications, recognition and proper interpretation of sediment failure may help explain missing or repeated lithologies or biostratigraphic intervals. Finally, detection of sediment failure in ancient sequences may be important economically, for example, where a porous carbonate sand sequence has slid into a shale basin and subsequently acted as a trap for hydrocarbons (Fairbridge, 1946; Schwarz, 1982).

It is suggested that these subtle shear zone fabrics are more common than would be gathered from literature on ancient slope sediments. If this is so, sediment failures are probably more abundant than previously

thought. This places the common sediment disruptions encountered in piston and box cores from present-day slopes (e.g. Nardin et al., 1979b) in a more realistic perspective relative to their ancient counterparts.

Chapter 4

ORIGIN OF CONTORTED LIMESTONES

4.1 INTRODUCTION

Many parted and ribbon limestone sequences in the CHG are characterized by "contorted" ("wrinkled" or buckle-folded) limestones. Important outcrops are listed in Appendix D. These enigmatic folds were described in passing by Kindle and Whittington (1958) and Baird (1960) and a submarine sliding origin was proposed. Although there is abundant evidence for submarine sliding in the CHG (see Chapter-3), structural and diagenetic origins for the contorted limestones must also be considered. As will be shown from evidence presented in this chapter, arguments for a submarine sliding origin are difficult to substantiate using field or petrographic data. Contorted limestones have also been described from other localities in the Appalachian orogen (discussed later) and, therefore, conclusions derived for the CHG may have applicability.

4.2 FIELD DESCRIPTION

Contorted limestones are usually mudstones and lithologically identical to surrounding, unfolded limestones. Contorted grainstones are rare. Beds typically vary from 2-10 cm in thickness and most are planar and continuous. Discontinuous and lenticular beds may also be contorted but these appear to follow the distortion in the associated continuous beds. Within a parted or ribbon limestone sequence, the number of beds involved in the intrafolial folding is variable. In some sequences, only a single bed may be folded with underlying and overlying beds unaffected. In other cases several beds may be contorted, either harmonically or disharmonically (Plate 18a, b).

In two dimensions, fold profiles are usually symmetrical, open, and rounded (Figure 4.1). Fold wavelength varies from 20-100 cm with amplitudes generally less than 15 cm. Layer-parallel shortening is estimated at 20% or less, assuming constant volume deformation, an assumption that may not be valid particularly where the development of numerous vertical stylolites has occurred (see Chapter 5). Rare three dimensional outcrops illustrate an elongate dome-and-basin (periclinal) configuration, some of which demonstrate a predominant shortening direction (Figure 4.1; Plate 18c, d). Based on 7 three-dimensional exposures, the average elongation trend of the fold pattern is 71 degrees to the northeast (measurements in Appendix D).

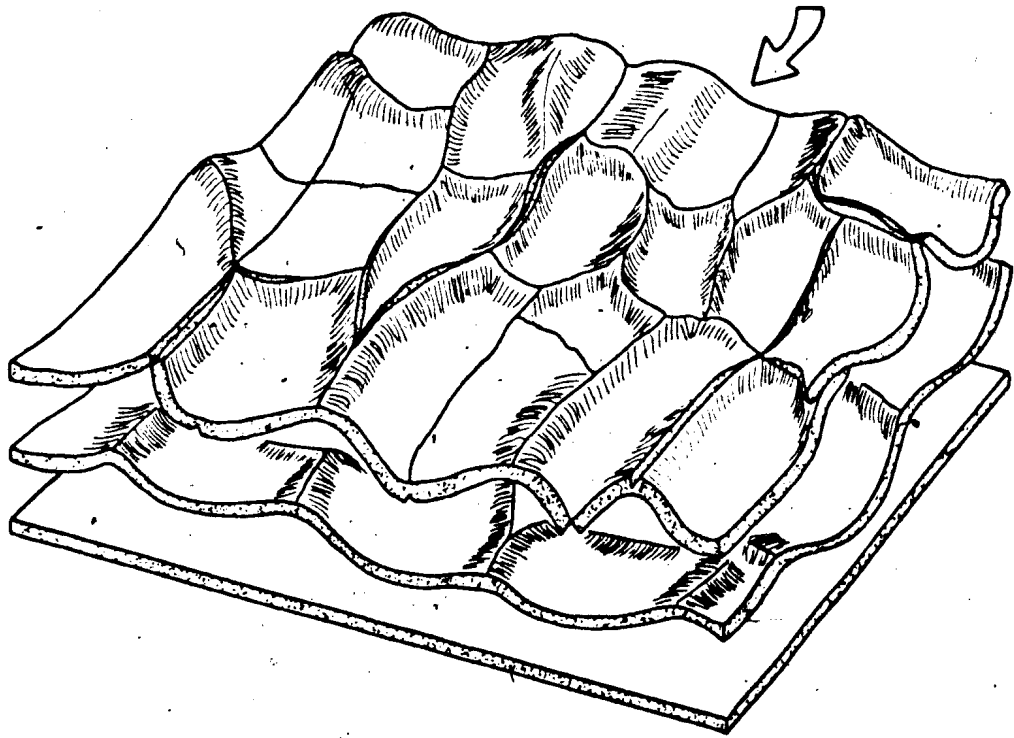
Some beds have the outer arc of the folds fractured, with cracks

Figure 4.1: Schematic diagram of a contorted limestone illustrates the dome-and-basin folding and the irregular geometry of polygons formed by fracturing along fold hinges. Bedding overlap is also shown. This diagram is based largely on the contorted limestone in the Upper Cambrian strata at Green Point (Plate 18c,d).

3



CONTORTED LIMESTONE



partially or completely penetrating the bed. V-shaped cracks may grade into stylolites towards the inner arc of the folds and illustrate the presence of extensional and shortening domains separated by a neutral surface within the folded bed. Extensional fracturing occurs on the outer arc of the fold under tensional stress whereas pressure solution occurs on the inner arc of the fold under compressive stress (see Ramsay, 1967). Fractures may occur preferentially either in the antiformal or synformal portions of the bed or both. Whereas the profiles of most contorted limestones are gently undulating, other beds are flat and only folded and fractured locally (Plate 18 a; 19a).

The best three dimensional outcrop of contorted limestones is found in Upper Cambrian strata at Green Point (Plate 18c, d). This 25 cm-thick interval consists of 4 few-centimetre-thick mudstones which are both continuously- and lenticularly-bedded and can be traced for over 200 m from the beach cliffs across the wave-cut platform. The cliff exposure demonstrates an elongate dome-and-basin morphology where preferential fracturing of the synclinal fold hinge areas in the lowermost, continuous bed has resulted in the production of numerous, irregular, 30-40 cm-size polygons:

Two other occurrences of contorted limestone merit separate mention: (1) at Martin Point (unit 8) where a contorted, fractured mudstone is locally infolded into an overlying conglomerate (Plate 19b); and (2) At Green Point (unit 18) where several lenses of sediment are found in the synclinal depression of a contorted bed (Plate 19c). A thin shale seam separates the contorted mudstone from this apparently "ponded" sediment.

Bedding "overlaps" are associated with some contorted limestones (Figure 4.1). The amount of overlap is generally less than 15 cm although an exceptional occurrence with 3 m of overlap has been recorded from Green Point (unit 34). As overlaps are only seen in two dimensions and therefore direction of the displacement vector is unknown, estimates of shortening are minimal.

Other intrafolial folds developed in parted and ribbon sequences demonstrate chevron and box-like styles with beds folded harmonically over thicknesses of 1 m or more (Plate 19d). Axial plane crenulation cleavage, formed by a high-angle intersection of cleavage and primary sedimentary laminations, is only rarely developed in the interbedded shales. Several of these folds which occur in otherwise monotonous, evenly bedded mudstones suggest nucleation on bedding heterogeneities such as grainstone lenses or sedimentary dikes.

4.3 VOIDS IN CONTORTED LIMESTONES

Several occurrences of contorted limestones have voids associated with their fold hinge areas (Plate 18b; 20a, b). These cavities are filled by coarse, sparry calcite with minor amounts of barite, quartz, and pyrite. Mudstone intraclasts and peloids are also found.

Calcite may be ferroan or non-ferroan, or zoned based on thin section staining for iron. The mosaics generally consist of 0.2-1 mm-sized, anhedral to subhedral (rarely bladed) crystals which are often intensely

twinned, turbid, and have undulose extinction. Barite crystals up to 1 cm in size are found in anhedral mosaics, either with calcite or by itself. Megaquartz is rare and in the the one occurrence discovered, it was precipitated after calcite. Pyrite commonly occurs as cubes, rods, or irregular aggregates of variable size. Several samples also contain minor authigenic sphalerite. Veinlets in the cavity areas may also contain similar calcite and barite to that which occurs in the cavities.

In addition to the authigenic components, some cavities also contain sand- to pebble-size, angular to sub-angular mudstone intraclasts and silt-size (25-50 μ m) peloids. The intraclasts consist of microspar [1] identical to that of the enclosing contorted limestones. Peloids are not present in every sample containing the larger intraclasts, but when they do occur, they are geopetal. Some fold hinges also contain shale which was plastically deformed and squeezed into the cavity in addition to or in place of peloids and intraclasts.

4.4 DISCUSSION

4.4.1 Other Occurrences

Contorted limestones have been found elsewhere besides western Newfoundland. Vanuxem (1842, p. 53) wrote that the Trenton Limestone at Trenton Falls, New York "exhibits extraordinary contortions for one

1. Terminology for neomorphic calcites is discussed in Appendix H.

whose layers are so regularly disposed, forming almost semicircular curvatures, and not unlike the writhings of a huge serpent". White (1896, p.89-90) further noted that the "semi-circular plications" at Trenton Falls were not accompanied by metamorphism.

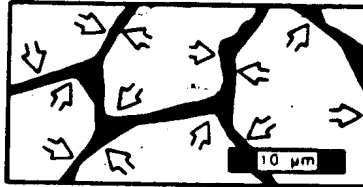
Other contorted limestones also occur in the ribbon limestones of the Dolgeville Formation exposed in the central Mohawk Valley of New York State (Fisher, 1979). In this sequence, a 2 m-thick zone of deformed strata lies between undeformed bedding. As with the Cow Head Group, deformation is characterized by broken fold hinges, bedding overlaps up to 15 cm, and a variability in fold wavelength and amplitude. Fisher (1979, p.457) also indicated that "in a few cases, a sharp broken fold is overlain by unfolded or gently folded limestone".

4.4.2 Hypotheses of Formation

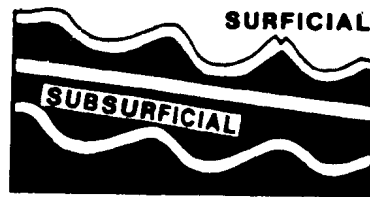
There are 4 hypotheses which may explain intrafolial folding in the CHG as well as at the New York State localities. These are: (1) expansive diagenesis, (2) formation at the sediment-sea water interface by submarine sliding, (3) formation in the shallow subsurface within a shear zone associated with submarine sliding, and (4) tectonism (Figure 4.2).

Figure 4.2: Schematic summary of possible origins for contorted limestones in the CHG. Refer to text for explanations.

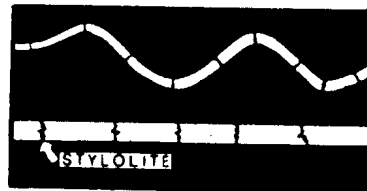
EXPANSIVE CRYSTALLIZATION



SLIDING



TECTONISM



4.4.2.1 Expansive Diagenesis

Expansive diagenesis, such as that responsible for "submarine anticlines" and overthrust "teepee" structures from the Holocene sea floor in the Persian Gulf (Shinn, 1969) as well as dolostone "megapolygons" in an Upper Jurassic shale sequence from southern England (Bellamy, 1977), results from the "force of crystallization" (see Weyl, 1959). There is abundant evidence for expansive crystallization in the CHG most obviously illustrated by fringes of displacive fibrous calcite (Chapter 9), but also illustrated on a much smaller scale by some neomorphic calcites (Chapter 8) and dolomites (Chapter 12). Most beds demonstrating expansive crystallization, however, are not contorted. Rare examples which provide no evidence, petrographic or otherwise, to indicate anything but a coincidental relationship. Due to the lack of evidence to suggest otherwise, expansive diagenesis is rejected as a viable mechanism to explain the origin of contorted limestones.

4.4.2.2 Submarine Sliding at the Sediment - Seawater Interface

Aspects of sea-floor instability in the CHG were discussed previously in Chapter 3. In light of this, limestones could have formed by sliding on the sea floor at the sediment - seawater interface, somewhat analogous to the crumpling of a rug on a slippery floor; or they could have formed within a subsurficial shear zone related to the downslope translation of overlying beds. If surficial sliding is the origin of contorted limestones, then there are a number of criteria with which this can be

tested. These include the following:

- (1) physical erosion (beveling) or other evidence to suggest exposure at the sediment-sea water interface (cf. Lindstrom, 1963);
- (2) lateral transformation to conglomerate;
- (3) intervals of missing sediment resulting from sliding away and accumulation elsewhere;
- (4) infiltration of younger, particulate sediment into the broken fold hinge areas (cf. Lindstrom, 1963);
- (5) ponding of sediments in depressions;
- (6) spatial association with definitive slides or related shear zones.

1. There is no unequivocal evidence of physical erosion (point 1), lateral transformation to conglomerate (point 2), or stratigraphic intervals which suggest sliding away of a thin sheet of limestone and its accumulation elsewhere (point 3). The mudstone intraclasts within cavities developed in some fold hinge areas (point 4) are identical to the contorted mudstones and are the result of in situ brecciation, with some mudstone fragments only slightly dislodged from their former positions. In light of this, associated peloids are considered to be small mudstone intraclasts. The geopetal fabric presumably could develop at any time. The nature of the ponded sediment at Green Point is also equivocal (point 5). This sediment consists of pseudospar which is identical in all respects to that forming concretions. There is no petrographic or field evidence to suggest that this sediment or a

precursor accumulated in a local depression on the sea floor. Contorted limestones are not spatially associated with the various sediment failure-related fabrics discussed in Chapter 3 (point 6). This is also an argument which is applicable in refuting a shallow subsurficial (shear zone) origin (discussed in next section).

Examples of surficial folding have been found in other sequences. Lindstrom (1963) described sedimentary folds from Lower Ordovician limestones in Sweden and concluded that they resulted from gliding down an "almost imperceptible slope". A sea floor origin was postulated based on the presence of corrosion, glauconite, and organism borings on fold crests and invasion of fold noses by younger sediments. Lindstrom's plate 1 demonstrates that flexures and buckling are always directed upwards, unlike those of the CHG.

The contorted limestones described by Fisher (1979) were interpreted to have resulted from submarine gravity sliding of the Giddings Brook - Van Buren allochthon into a westward-lying basin. This interpretation was based mainly on the confinement of the folds to a 2 m-thick stratigraphic interval, presumed erosive bevelling of folded limestones, and the relationship of age and attitude with the gravity slide suite. None of the possible criteria listed above to suggest a surficial origin for these folds are met in the Dolgeville sequence, however. The most critical relationship concerning the erosive bevelling is only mentioned in passing and not substantiated in any form. Furthermore, confinement of the folds to a limited stratigraphic interval indicates a maximum age for the deformation but it does not bracket the upper age as would be the case if the folding was a subsurficial shear zone or structural

decollement phenomenon (discussed below).

4.4.2.3 Synsedimentary Shear Zone Versus Tectonic Origin

The two remaining hypotheses which need be considered are a submarine sliding or synsedimentary shear zone origin versus a tectonic origin. From discussion in Chapter 3 it was seen that deformation resulting from sediment failure may extend from the sediment-water interface to depths of 3 m and possibly more. Because deformation in the shallow subsurface and during tectonism occurs within the sedimentary sequence, the problem of resolving synsedimentary versus tectonic deformation must be considered. This problem is particularly acute for these mudstones because they are lithified early in the sediment's history and are subject to elastic and plastic deformation in every way analogous to that of "hard rock" deformation.

Sliding on the southeastward-dipping paleoslope (James and Stevens, in prep.; Hiscott and James, in press) and dominant northwest-directed orogenic stress (Chapters 1 and 5) both could produce the observed northeast-southwest elongation of the dome-and-basin structures seen in bedding plane views of contorted limestones. Ideally these two origins could be differentiated based on asymmetry of the folds, but as described earlier, the folds are mostly symmetrical and therefore unsuitable for resolution using this criterion.

Criteria used to differentiate synsedimentary versus tectonic deformation are discussed in Hobbs et al. (1976, p. 156-159; also see Woodcock, 1976; Helwig, 1970), but these do not resolve the question.

Of the ten criteria listed in Hobbs et al. (1976), only the first three taken individually are unequivocal. These criteria are that in tectonically deformed sediments, deformed fossils (criteria 1) and foliation-controlled secondary mineral development (criteria 2) is expected. In soft-sediment deformation burrows which post-date deformation are undeformed (criteria 3). Unfortunately, these criteria are inapplicable to contorted limestones in the CHG.

More equivocal criteria which require a "safety-in-numbers" application to suggest synsedimentary deformation are the following: (1) chaotic or opposing structures, (2) absence of veins or joints, and (3) possibly the absence of axial plane cleavage. The regularity of these intrafolial folds relative to deformation observed within submarine sliding shear zones (see Chapter 3) suggests a tectonic origin more so than a synsedimentary origin. Veins and joints are abundant throughout the CHG and are therefore not reliable criteria. The development of cleavage is another dubious indicator of a tectonic rather than synsedimentary origin. Cleavage can form during soft-sediment deformation (Williams et al., 1969; Geiser, 1975; Woodcock, 1976; Davies and Cave, 1976) as well as during tectonism. There is also evidence to suggest that the early development of cleavage in tectonic folds may be suppressed by high fluid pressures which encourage grain boundary sliding rather than cleavage formation (Borradaile, 1978). In addition to cleavage, other soft-sediment structures which are typical for tectonic deformation include microfold lineations (Woodcock, 1976) and development of fold axial plane crenulation cleavage (Naylor, 1981).

The intrafolial folds characterized by chevron and box-like styles with

beds folded harmonically over thicknesses of 1 m or more are readily interpreted as tectonic. There is, however, not a sharp boundary demarcating these from contorted limestones and numerous outcrops demonstrate characteristics intermediate to both types of folds. This strongly suggests that contorted limestones are a tectonic phenomenon unrelated to syndimentary deformation.

The different fold styles seen, from contorted to chevron and box styles, may be explained in two ways. Firstly, the variety of fold styles may represent a spectrum of deformation responses where sinusoidal (contorted) folding ultimately proceeds to chevron style folds with increased shortening (Johnson, 1977; Hawkins and Jones, 1981). This, however, cannot be proven in the Cow Head Group due to the lack of strike sections which show the transition from contorted to chevron folding. Secondly, it is equally likely that contorted limestones and the chevron or box-style folds reflect mechanical differences in the sequences in which they are developed rather than differential shortening (see Hobbs *et al.*, 1976, chapter 4).

The predominant northeast-southwest elongation direction of the dome-and-basin structures is also parallel with other major and minor structural features which indicate major northwest-southeast directed compression. Large-scale regional structures are mainly northeast-southwest trending folds and reverse faults (Oxley, 1953). Tectonic stylolites which are oriented vertically or at high angle to bedding also trend northeast-southwest (discussed in Chapter 5). These stylolites are interpreted to have arisen from the same compressional regime and caused layer-parallel shortening. Although no measurements

are available for bedding overlaps, these, too, indicate horizontally-directed compression and layer-parallel shortening.

A tectonic origin for the contorted limestones also accounts for the enigmatic occurrence at Martin Point where a contorted mudstone is locally infolded into an overlying conglomerate. This is explained by the mudstones folding in response to layer parallel shortening whereas the conglomerate likely accommodated this stress by pressure solution throughout its mass, mostly along clast-matrix boundaries. A tectonic origin eliminates the necessity to invoke a mechanism which would allow a debris flow to override and come to rest on a contorted, irregular surface without fragmenting or otherwise effecting the thin underlying mudstone.

Within the contorted limestones of the New York State foreland the occurrence of (1) northeast-southwest oriented fold axes (Miller, 1908; Fisher, 1979), (2) northwest-trending bedding-parallel slickensides (Fisher, 1979), and (3) a homoaxial relationship between the contorted limestones and the regional structure (Miller, 1908) suggest that these contorted limestones, too, have a tectonic origin. There is no evidence presented in any of the cited papers to substantiate a synsedimentary origin.

4.5 CONCLUSIONS

Based on field and petrographic data, contorted limestones in the CHG are interpreted to reflect layer-parallel shortening generated by horizontal, tectonic compression. Additional work on the structural geology of the Cow Head area is required prior to more definitive resolution of the time of deformation, i.e. whether deformation is a Taconic, Acadian, or possibly, although unlikely, an Alleghanian event. Unequivocal evidence of a surficial or shallow subsurficial sliding origin is entirely lacking.

The above conclusions are based on a simplified geologic history which assumes that synsedimentary and tectonic deformations are removed from one another in time and space. Synsedimentary folds, however, could be the result of instabilities generated by tectonism (Hobbs et al., 1976). An example of this is an ocean closing episode where slide sheets developed at the active margin become involved in deformation associated with incorporation of the margin into an accretionary wedge (Woodcock, 1979). In addition, a soft-sediment deformed bed may have nucleated later tectonic folding because it formed a heterogeneity in the stratigraphic sequence. Finally, there may have been more than one regional deformation event which caused intrafolial folding. This could account for the variation in the cavity fills observed, for example variations in the nature of calcite as well as the presence and abundance of barite, sulphides, and megaquartz.

Chapter 5

COMPACTION IN THE COW HEAD GROUP

5.1 INTRODUCTION

Two types of compaction are recognized in this sequence: burial compaction, which is a response to increasing burial pressure from progressive sedimentation and perhaps loading of allochthonous terranes; and tectonic compaction, which is the result of horizontally-directed compression, interpreted to be due mainly to tectonic and possibly Acadian orogenesis. Burial compaction results in a vertical shortening of the sequence, either through mechanical and chemical processes (i.e. pressure solution), or both (see Bathurst, 1980b for review). Tectonic compaction, on the other hand, is evident as vertically-oriented zones of pressure solution resulting in horizontal shortening of the sequence.

To a first approximation, mechanical and chemical compaction are mutually exclusive and are relegated to the realms of shallow-burial and deep-burial diagenesis, respectively. Mechanical compaction is manifest as brittle fracture, collapse, or rearrangement of components whereas chemical compaction is characterized by solution seams ("non-sutured seams"; terminology of Wanless, 1979; 1983) and stylolites ("sutured

seams"). In addition, pervasive "non-seam solution" may occur where material loss is evenly distributed throughout the sediment without forming solution interfaces.

The purpose of this chapter is to describe and interpret the wide range of compactive phenomena in the CHG, based on an integrated approach of field observations and measurements, slab study, and petrography.

Answers to the following questions are sought: (1) How much compaction has occurred due to burial and due to tectonism? (2) With reference to burial compaction, can the effects of mechanical compaction and pressure solution be separated? (3) Is compaction homogeneously distributed throughout the sequence or is it restricted to specific "yielding" lithologies? (4) What is the relative timing of horizontal and vertical pressure solution?

5.2 BURIAL COMPACTION

5.2.1 Field Observations and Measurements

Clastic dikes along with several miscellaneous features [1] provide estimates of compaction (Plate 21a; data in Appendix E). Dikes were unfolded and restored to original inclination using the method outlined in Hiscott (1977). Based on clastic dikes, average compaction (i.e. stratigraphic thinning) in sequences of ribbon limestones, shales, and

1. The miscellaneous features comprise: (1) a rotated mudstone slab in a synsedimentary shear zone, (2) a nodule in silicified shale, and (3) vertical to sub-vertical mudstone nodules developed around grainstone dikes.

marls is 52% (8 measurements), with individual values ranging from 37-84%. Measurement of compaction of shale drapes around the miscellaneous features averages 64% (4 measurements), with individual values ranging from 55-81%. In ribbon limestone sequences, only the interbedded shales or marls are compacted.

5.2.2 Slab Study and Microscopy

In general, brittle-fractured components in limestones are extremely rare (Plate 21b). This, and the occurrence of unsquashed burrows (Plate 11b,c,d) and graptolites in both mudstones and grainstones, implies that early lithification prevented significant compaction. Most grainstones demonstrate normal, uncondensed packing fabrics and are devoid of intergranular microstylolites (Plate 22a-f). Some phosphate-rich granular sediments, however, were brittle fractured and compacted prior to cementation by chalcedony (Plate 21c). This relative timing is consistent with some silicification postdating the main phase of calcite cementation, which for unknown reasons, appears to have missed these particular sediments (see Chapter 13). Stylolites, solution seams, and accumulations of siliciclastics in the transition zone from continuous or nodular limestones to the surrounding argillaceous sediments occur but are not common (cf. Logan and Semeniuk, 1976; Wanless, 1979; 1983).

Shales and marls, on the other hand demonstrate: (1) squashed burrows and dikes (Plate 11b,c); (2) squashed graptolites; (3) squashed cracks of syneresis or synsedimentary shear origin (Plate 7d); and (4) convergent laminations at the margins of nodules (Plate 13g).

In contrast to the general absence of distinctive pressure solution features in the above-described sediments, some of the thicker grainstone beds exhibit prominent bedding-parallel, peaked stylolites outlined by accumulations of siliciclastic sand and silt (Plate 3c). More rarely, foreset bedding in mega-ripples is similarly outlined (Plate 3d; 4a). Conglomerates often display condensed clast-packing with prominent circumgranular stylolites and argillaceous seams. Insolubles, comprising mainly clays, organics, pyrite, dolomite, and siliciclastics, are often concentrated at stylolites or seams.

5.2.3 Interpretation and Discussion

Compaction measurements, in conjunction with qualitative evaluation of numerous unmeasureable dikes indicate that intervals with more shale or marl compact to a higher degree than those with a relatively greater proportion of limestone. This conclusion is consistent with information from slab and petrographic study which indicates that limestone compaction is usually minimal or nil and compaction of argillaceous sediments is mainly responsible for compaction in the succession. That limestones, particularly mudstones, show little or no evidence of compaction has also been noted in other studies and has been interpreted to indicate early lithification (e.g. Weller, 1959; Bathurst, 1975; Steinen, 1978; cf. Shinn et al., 1977; Bhattacharyya and Friedman, 1979; Shinn and Robbin, 1983).

The average compaction measurement is lower than that expected in pure terrigenous muds but the 2 highest compaction measurements from clastic dikes - 74 and 84% - are consistent with expected depositional

porosities in terrigenous muds, which often range from 70-85% (Raiswell, 1971a; Pettijohn, 1975, p. 263). This suggests that the observed compaction can be explained largely as the result of mechanical compaction of argillaceous sediments, with pressure solution being generally unimportant. The presence of stylolites, argillaceous seams, and accumulations of insolubles at the interface between some limestones and adjacent, argillaceous sediments does, however, indicate that pressure solution has occurred at these lithological transitions, but such occurrences are rare. Overall, obvious pressure solution effects are lacking. This topic is pursued further in Chapter 14.

The common occurrence of circumgranular stylolites and seams in conglomerates and stylolites in thicker grainstones is interpreted to be due to the greater thickness of these beds relative to more thinly-bedded sediments. Thicker-bedded conglomerate and grainstone sequences contain less easily-compactable shale per unit volume than thinly-bedded sediments. Consequently, some of the burial stress is accommodated by pressure solution within these thicker limestone beds, either along bedding-parallel (horizontal or foreset) stylolites in grainstones, or at clast-matrix transitions in conglomerates. Horizontal stylolites in grainstones imply that these are due to burial. Foreset-parallel stylolites in grainstones and chaotically-oriented stylolites and seams in conglomerates may be due either to burial or tectonic compaction or both.

5.3 TECTONIC COMPACTION

5.3.1 Description of Pressure Solution Effects

Included in the following discussion are the effects of regional horizontal compression and local structural perturbations; the former may be considered as the "background" against which local structural features are developed. Regional and local structures are likely related, as suggested in Suchecki's (1975) study, but for discussion purposes, their separate consideration is convenient.

Most outcrops of the CHG are relatively undeformed on an outcrop scale, although regional structures indicate northwest-directed compression (Oxley, 1953). Based on field and petrographic evidence, horizontal shortening caused by pressure solution is a common occurrence. These pressure solution zones are oriented perpendicular or at high angle to bedding and are dominated by peaked stylolites, thin argillaceous seams, and more rarely, diffuse horsetails and microstylolite swarms (Plate 21d,e; 48d; 53f; Wanless, 1979; 1983). In the following discussion these various pressure solution zones are included in the umbrella term "stylolite". The amount of lateral shortening these tectonic stylolites represent is unknown and must await further refinement of the structural geology.

Stylolite spacing is variable, typically ranging from 2-15 cm but may be as close as 5-10 mm apart. Within individual beds, however, spacing is

uniform. Tectonic stylolites are almost invariably restricted to limestones or their dolomitized equivalents, and only rarely extend into the interbedded argillaceous sediments. Insolubles accumulated at stylolites include clays, organics, pyrite, dolomite, and siliciclastics. These stylolites cross-cut all other diagenetic fabrics and components except for (1) fault-related dolomites (see Chapter 12) and (2) some late stage calcites in fractures (see Chapter 8). Orientations of vertical stylolites were measured from several major outcrops (Figure 5.1; data in Appendix E). Their orientations demonstrate a prominent northwest-southeast compressional regime, consistent with the orientation of larger-scale structures.

5.3.2 Local Structures

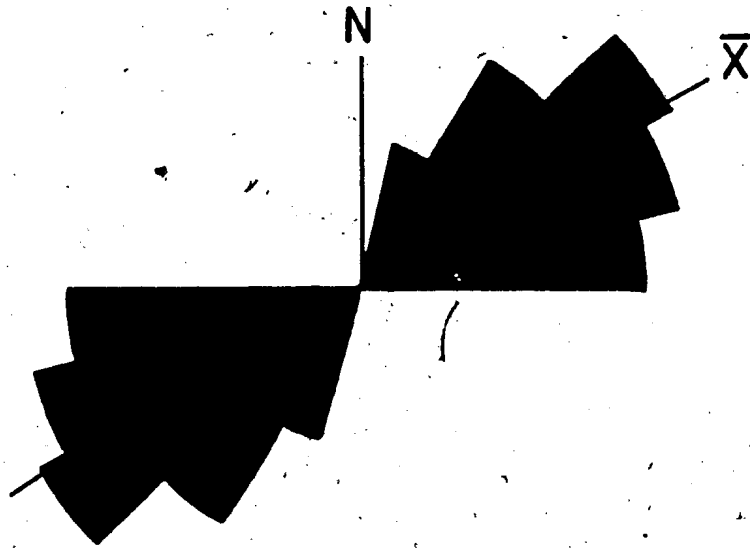
Localized folds, outcrop-size or larger, in an otherwise apparently undisturbed sequence of sediments commonly illustrate: (1) condensed grain-packing fabrics (Plate 21f); (2) intergranular microstylolites, including between quartz sand grains which have come into contact; (3) disturbed nodular horizons; (4) local drenulation cleavage developed in shales; (5) two or more sets of intersecting stylolites or joints or both; (6) increased extinction undulosity and twinning and formation of distinct subcrystals in calcite; and (7) occasionally strain, granularization, or fracturing of quartz sand grains which have been pressed together.

5.3.3 Interpretation and Discussion

Tectonic stylolites (also termed "solution cleavages" ¹ Geiser and

Figure 5.1: Orientation of vertical stylolites in the Cow Head Group (n=35). Field measurements are found in Table E.2 in Appendix E.

VERTICAL STYLOLITES



Sansone, 1981; "stylolitic joints" - Droxler and Schaer, 1979), both parallel and perpendicular to bedding, have been recognized by others and used in structural analysis of sedimentary sequences in the Appalachians (Geiser and Sansone, 1981), Rhone Valley (Baud and Masson, 1975), Jura Mountains (Droxler and Schaer, 1979), and Rhinegraben (Buchner, 1981). The above studies demonstrate that vertical stylolites more or less define the principal plane perpendicular to the axis of maximum shortening.

The orientation of vertical stylolites, along with reverse faults, thrusts, and folds in the CHG reflect horizontal shortening caused by the regional northwest-southeast stress system which characterizes the Appalachians (see Chapter 1). Timing of the formation of vertical stylolites is, however, ambiguous. The consistency of their orientation to bedding and their regional orientation both suggest that they formed in a homogeneous succession with similar stresses throughout. The most probable time for this condition to be met is during allochthon emplacement (i.e. Taconic orogeny) prior to complication of the structure and stress field which may have occurred during a later phase of Taconic orogeny or Acadian orogeny. In addition, the consistency of paleocurrent data (Hubert et al., 1977) and vertical stylolite orientation suggests that if the CHG consists of several structural slices, then no significant rotation of slices relative to one another, in a horizontal plane, has occurred.

5.3.4 Relative Timing of Burial and Tectonic Pressure

Solution

Although most burial compaction in the CHG can be explained as the result of mechanical rather than chemical processes, it is suggested that whatever burial pressure solution there is preceded pressure solution due to tectonism. This suggestion is based on qualitative arguments; field and petrographic cross-cutting relationships are rare and their interpretation equivocal. Assuming that the entire 300-500 m of the CHG was deposited, then overlain by 1000 m or more of Lower Head Sandstone (James, pers. comm., 1984) prior to significant Taconic horizontal compression, these burial depths were sufficient for burial pressure solution which, based on the available literature, starts at depths ranging from 300-900 m [2]. Depths would be expected to be variable, however, reflecting both mineralogical and fabric parameters (the "diagenetic potential" of Schlanger and Douglas, 1974) as well as solution chemistry (Neugebauer, 1974).

5.4 SUMMARY AND CONCLUSIONS

Integration of information from field, slab, and thin section study

2. The following are minimum depths suggested for the onset of pressure solution: (1) 600-900 m limestones in the Middle East (Dunnington, 1967), (2) 300 m in chalks (Neugebauer, 1974), and (3) 300 m depth in limestones of the Aquitaine Basin (Sellier, 1979 - cited in Bathurst, 1980b).

indicates that burial stresses have been accommodated mainly by compaction of argillaceous sediments whereas limestones are uncompacted, except for some thick grainstone beds and conglomerates which contain intrabed stylolites. The lack of compaction is consistent with evidence for early lithification such as flat pebble clasts and rafts in conglomerates; unsquashed burrows, graptolites, and other components; and general lack of microstylolites and other features suggestive of pressure solution.

Based on measurement of clastic dikes, the CHG has been compacted by approximately 50-60%. Sequences dominated by thick grainstones or conglomerates may have compacted less, depending on the importance of intrabed pressure solution. Sequences with greater amounts of argillaceous sediment may have compacted more, up to 80%, a value consistent with original depositional porosities of terrigenous muds. This implies that the observed compaction can be explained largely as the result of mechanical compaction of terrigenous mud-rich sediments, with pressure solution being relatively unimportant. Lateral compression from regional tectonism resulted in the formation of vertical stylolites throughout the CHG; however, the amount of horizontal shortening involved is not known. Pressure solution due to burial probably preceded that due to tectonism based on qualitative arguments. Their relative timing based on field and petrographic relationships is equivocal.

Chapter 6

SEDIMENTARY PARTICLES AND THE ROLE OF CALCIFIED ALGAE AS SEDIMENT PRODUCERS IN THE COW HEAD GROUP

6.1 INTRODUCTION

Grains in the CHG are divisible into 2 major groups: (1) grains of certain origin such as ooids, detrital siliciclastics, and bioclasts (including calcified algae), and (2) grains of uncertain origin, dominantly peloids [1] and larger, mostly microcrystalline grains which may be intraclasts [2].

Peloids are conspicuous particles in carbonate sediments of all ages, but especially Lower Paleozoic limestones, many of which are composed almost entirely of these particles (Beales, 1958; Folk, 1959). Whereas these particles are usually considered to be dominantly faecal pellets, petrographic study of these grains and associated intraclasts in the CHG

1. The term "peloid" was introduced by McKee and Gutschick (1969) to embrace all microcrystalline to cryptocrystalline grains regardless of their origin. Included in this umbrella term are faecal pellets, small intraclasts, micritized bioclasts and ooids, as well as precipitated micritic carbonate (Folk, 1959; Bathurst, 1975; Purser, 1980).

2. An intraclast is a fragment of penecontemporaneous, generally weakly consolidated sediment that has been eroded from the sea bottom and redeposited (Folk, 1962).

demonstrates an important algal contribution to sand- and silt-size sediments (Coniglio and James, 1984). This contribution is at least as important as that of faecal pellets.

6.2 GENERAL DESCRIPTION OF SEDIMENTS

Mudstones and the matrices of wackestones and packstones mainly consist of microspar and pseudospar [3] whereas micrite is restricted to allochems. Two mudstone microfacies are recognized: (1) homogeneous mudstone, characterized by uniformly crystalline microspar and pseudospar, and (2) marginally-aggraded mudstone in which crystal size progressively increases from the centre to the margin of the bed or nodule. These microfacies have already been described in Chapter 2. Wackestones are texturally similar, except for "pseudowackestones" which are actually spicule- and radiolarian-rich grainstones or packstones. This sediment type is discussed further in Chapter 13. The present chapter concentrates mainly on the grains which comprise grainstones and packstones, and which are dispersed in wackestones, mudstones, marls, and shales.

In addition to peloids and intraclasts, other locally important components include dispersed sand- and silt-size crystals of dolomite, ooids, argillaceous and dolomitic lithoclasts, and sand- and silt-size clasts of feldspar and quartz, the latter commonly being well-rounded.

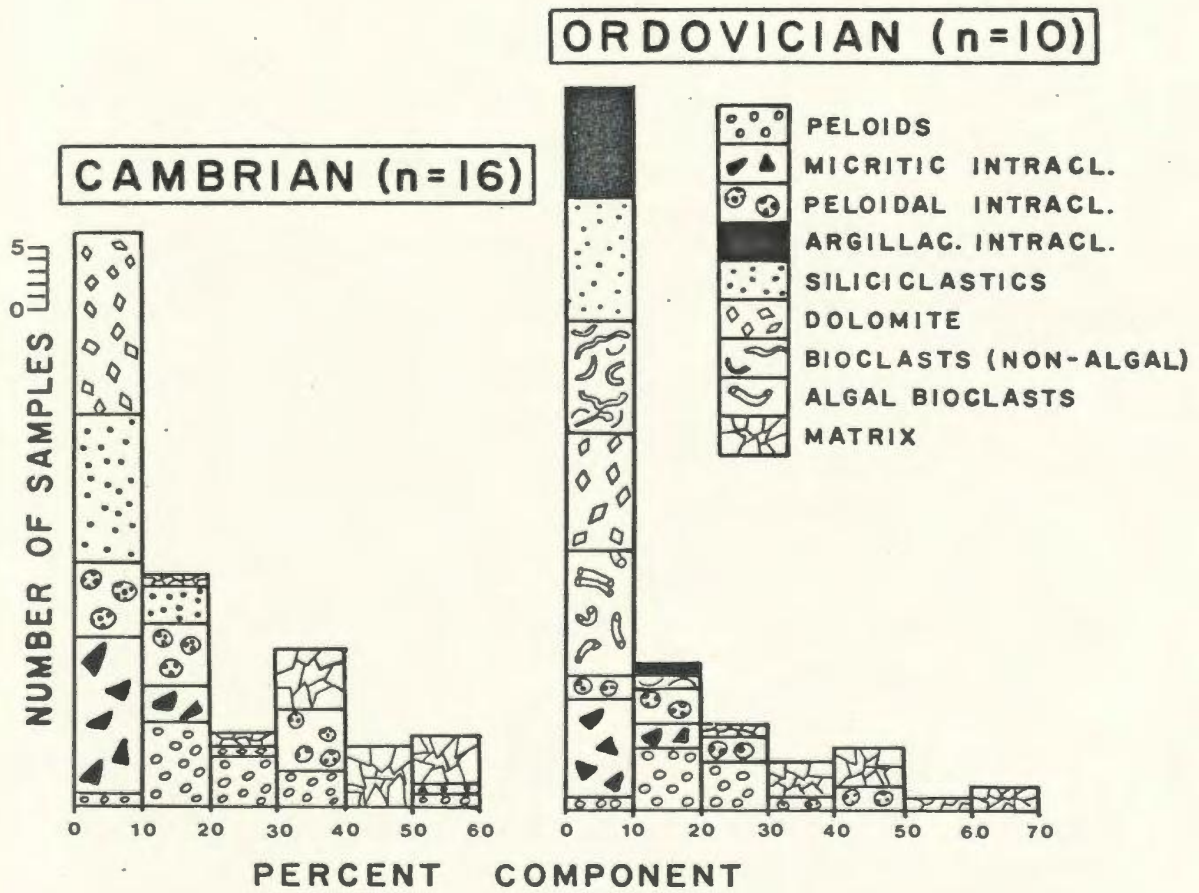
3. These terms are discussed in Appendix H.

Ubiquitous bioclasts include calcified algal clasts (discussed below), pelmatozoan debris, trilobite, brachiopod, and ostracod fragments, radiolarians, and sponge spicules. Sponges, bryozoan and gastropod clasts, graptolites, conodonts, chitinozoa, glauconitic peloids, unidentified heavy minerals, and mica flakes (white mica, biotite, and chlorite) are less abundant. Micrite envelopes, usually less than 10 μm in thickness, are developed on many ooids and bioclasts. Minor, sand-size, siliceous constituents include quartz arenite and chert rock fragments, silicified ooid grainstone fragments, and isolated, silicified ooids. Phosphate, as brachiopod fragments and as replaced allochems, shale and limestone intraclasts, and dolomite crystals, is locally important. Brief petrographic descriptions of ooids and siliciclastics and chemical analyses of feldspar and phosphate are found in Appendix F. Dolomitic and siliceous components are detailed in Chapters 12 and 13, respectively.

In general, sand-size siliciclastics are more abundant in Cambrian grainstones than in their Ordovician counterparts (Figure 6.1). Siliciclastics (sand and silt) usually constitute less than 20% of the sediment although an exceptional sample from the quartz sand-rich Bed 6 at Cow Head North contains 58% quartz. In contrast, Ordovician sediments are considerably more fossiliferous than their Cambrian counterparts (Figure 6.1). Bioclasts usually constitute less than 10% of the sediment volume. Cathode luminescence demonstrates that radiolarians and sponge spicules are significantly underrepresented in some sediments, especially "pseudowackestones" (see Chapter 13).

Using the visual comparison chart in Flugel (1982, p. 193, fig. 25)

Figure 6.1: Point-count histograms for representative Cambrian and Ordovician grainstones. Data from which these were drawn are found in Table F.1 in Appendix F.



sorting in both sand and silt-size grainstones ranges from poor to good. Grain packing varies according to (1) the importance of grain-to-grain pressure solution (usually negligible) and (2) the degree of authigenic overgrowth on dolomite and feldspar silt.

6.3 PELOIDS, MICRITIC INTRACLASTS, AND PELOIDAL

INTRACLASTS

What are commonly regarded as undifferentiated peloids and intraclasts are here subdivided into 3 separate, but intergradational categories - peloids, micritic intraclasts, and peloidal intraclasts (Figure 6.2). Collectively, these grains account for as much as 65% of the volume in grainstones, the remaining volume being largely calcite cement (see Table F.1 in Appendix F).

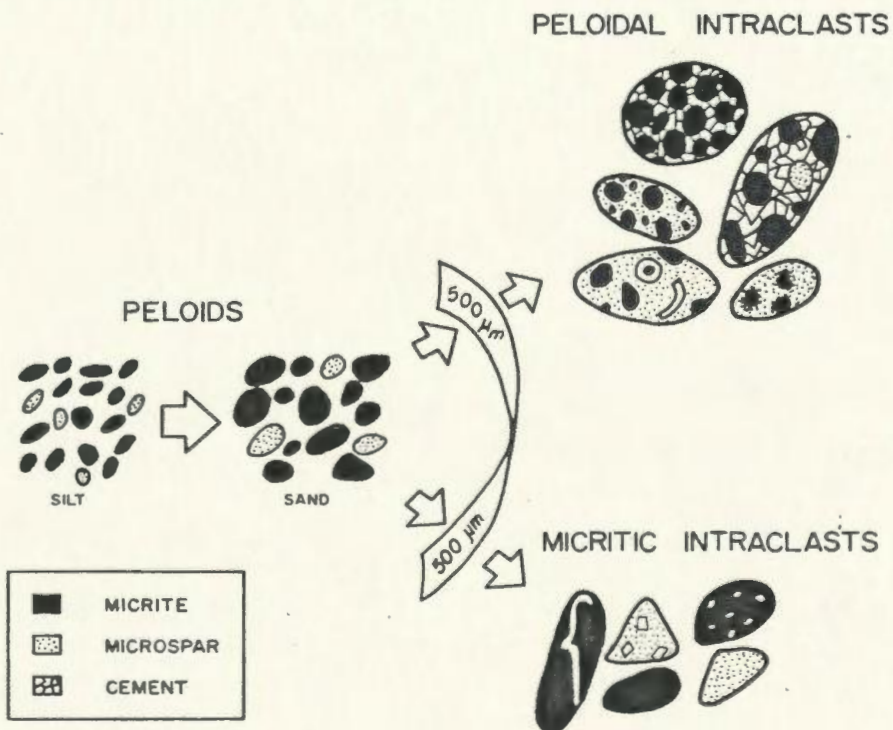
(1) Peloids: Up to 80% or more of the grains in medium sand-size and smaller grainstones are peloids (see Appendix F). Peloids are usually equant, ranging from 10-500 μm in size and commonly composed of dense, homogeneous micrite (Plate 22a, b, c). Less common are microspar peloids with crystals up to 10 μm in size. Some otherwise micritic peloids may have microspar centres.

(2) Micritic Intraclasts: The upper size limit [4] of 500 μm is arbitrary and serves to distinguish peloids from micritic intraclasts,

4. Flugel (1982) suggested that the boundary be placed at 200 μm but 500 μm appears to be a more suitable boundary for the Cow Head Group sediments.



Figure 6.2: Schematic diagram illustrating the relationship between peloids, micritic intraclasts, and peloidal intraclasts as discussed in text.



which have an identical microfabric to peloids but are larger and commonly more angular and may contain bioclasts along with dispersed dolomitic and siliciclastic silt (Plate 22d). Up to 28% of the grains in medium sand-size and coarser grainstones are micritic intraclasts, the remaining grains being peloids, dolomite, siliciclastics, and peloidal intraclasts (see Appendix F).

(3) Peloidal Intraclasts: This group includes grains illustrating a wide variety of microfabrics. At one end of the spectrum are intraclasts composed of peloids with subordinate ooids, siliciclastics, dolomite, or bioclasts and calcite cement (Plate 22d,e). Other peloidal intraclasts contain peloids in which the grain-matrix contact is gradational (Plate 22e,f). In these intraclasts, peloids are poorly-defined patches of micrite or microspar (10-15 μm crystal size) set in a matrix of slightly coarser calcite spar. At the other end of the spectrum are intraclasts in which the micrite patch-matrix boundaries are obscure and gradational and the overall microfabric is the familiar structure grumeleuse or "clotted" limestone (Cayeux, 1935) so common in Phanerozoic limestones. Peloidal intraclasts may be as small as 200-300 μm in size but the size range more commonly is 500-1000 μm , occasionally reaching granule- or small pebble-size. In sand-size grainstones, peloidal intraclasts account for up to 77% of the grains (see Appendix F).

Structure grumeleuse may be considered in a purely descriptive sense as a transitional fabric which bridges the spectrum of progressive change between a homogeneous micrite matrix with vague peloids (pelmicrite) and sediment in which peloids are sharply demarcated from interparticle matrix (Bathurst, 1975). The peloids or clots which are an integral part

of the microfabric usually vary in size from silt to fine sand [5].
Discussion on structure grumelense is provided in Appendix G.

6.4 PARTICLES OF CALCIFIED ALGAE

Algal particles are comparatively rare in Cambrian sediments relative to their Ordovician counterparts. Based on point counting of 10 Ordovician grainstones, the identifiable algal contribution varies from 3-9% of the total rock volume (Figure 6.1). In contrast, the visible contribution to Cambrian grainstones is typically less than 1%. The most common algal particles are Girvanella with lesser amounts of Epiphyton and Nuia.

Girvanella, Epiphyton, and Renalcis [6] are considered to be calcified cyanophytes (Wray, 1977) now generally regarded as cyanobacteria (Pratt, 1984). Recently, however, Pratt and James (1982a) and Pratt (1984) have suggested that both Epiphyton and Renalcis are related "diagenetic" taxa in which "genera" and "species" are a function of algal colony size and the nature of calcification. Nuia is a problematical microorganism of probable algal affinities (Toomey and Klement, 1966).

6.4.1 Girvanella

5. Size ranges of 20-150 μm , 20-100 μm , and 50-150 μm for peloids in structure grumelense are reported in Schwarzacher (1961), Fuchtbauer (1974), and Flugel (1982), respectively.

6. Renalcis is not seen in these fine grained limestones but is found in algal boundstone boulders - discussed later.

Girvanella is a uniform diameter, unbranching, and non-septate tubule 5-25 μm in external diameter and up to several hundred micrometres in length. Diameters from 10-15 μm are the most abundant (see Danielli, 1981). The tubule wall is less than 5 μm thick and is composed of micritic calcite.

Four types of Girvanella clasts can be differentiated in these sediments: single tubules, rafts, oncolites, and intraclasts. In clean, moderately-sorted grainstones, the most common algal particles are intraclasts. As sediments become more poorly-sorted and shell-rich, Girvanella rafts, single tubules and oncolites are more abundant.

6.4.1.1 Single Girvanella Tubules

Single Girvanella tubules are generally straight to slightly sinuous, and up to 75 μm in length (Plate 23a). The micrite walls and coarser microspar cores of these tubules suggest that scattered, equant, silt-size peloids with microspar centres and micritic margins may be either fragmented tubules or transverse views (Plate 23b). In the same sediment, numerous "rods" of dense micrite are found with exactly the same shapes and dimensions as the tubules (Plate 23c). In addition, there are large numbers of peloids which are identical to those described above as being derived from Girvanella tubules, except they are, like the rods, dense micrite throughout, without the coarser microspar core. Such peloids are dominant particles in many limestones in the CHG.

6.4.1.2 Girvanella Rafts

Rafts consist of loosely to tightly intertwined Girvanella tubules, equant to elongate in shape and up to 1 mm in length by 0.1-0.2 mm in width (Plate 23d). In elongate rafts, tubules are clearly sub-parallel to one another and the long dimension of the raft. Rafts are usually much larger than associated sand and silt-size particles suggesting that these algal clasts were deposited as brittle, porous particles which were hydraulically equivalent to the surrounding, smaller grains. The presence of former void space in the rafts is indicated by blocky inter- and intra-tubule cement identical to calcite spar between grains. The preservation of these porous, delicate rafts necessitates minimal reworking prior to transport into the slope environment.

6.4.1.3 Girvanella Oncolites

Girvanella oncolites range from fine to coarse sand-size and consist of a few layers of sinuously-disposed tubules arranged around spherical to elliptical nuclei which appear to be cement-filled molds (Plate 23e). These grains are uncommon relative to the other Girvanella particles.

6.4.1.4 Girvanella Intraclasts

Girvanella-bearing intraclasts are sub-rounded to rounded, equant to elongate in shape, and coarse sand- to pebble-size. The amount of Girvanella in any one intraclast varies; some consist entirely of tightly interwoven tubules whereas others are a few loosely intertwined tubules surrounded by micrite and microspar (structure grumeleuse; Plate

24a,b). These intraclasts were deposited as non-porous grains, unlike rafts (discussed above), because they are always the same size as surrounding grains, indicating hydraulic equivalence.

The sharpness of the boundary between Girvanella tubule and surrounding microspar is variable. In some intraclasts the transition is sharp and Girvanella preservation is perfect (Plate 24b, d) while in others Girvanella is represented by dense micritic filaments or threads in which the tubular structure is not apparent and the transition to interfilament microspar is gradational (Plate 24c). Except for the presence of Girvanella tubules or related dense micritic filaments, the range of microfabrics in Girvanella intraclasts is identical to that of peloidal intraclasts.

In larger intraclasts, radial fibrous cement and more finely crystalline cements are identical to those found in the algal boulders described by James (1981). Obvious algal intraclasts as well as peloidal intraclasts decrease in number with smaller particle size.

6.4.2 Epiphyton

Epiphyton intraclasts can be positively identified only where elongate portions of thalli can be seen (Plate 25a,b). Transverse views are, in most cases, not differentiable from well-sorted peloidal grainstone intraclasts. Epiphyton within intraclasts consists of dense micritic branches which vary from 35-60 μm in diameter.

6.4.3 Nuia

Nuia is usually spherical, rarely elongate, 200- 350 μm in diameter, and characterized by radial arrangement of elongate calcite crystals ("radial-hyaline wall structure" of Toomey and Klement, 1966) with a small, dark nucleus ("central canal"). These grains are scattered throughout the Ordovician and less commonly Cambrian grainstones (Plate 22c; 34b).

6.4.4 Summary

The most obvious algal contribution to limestones in the CHG (excluding conglomerates) is from Girvanella, in the form of pebble-sized intraclasts through to silt-sized single tubules. Silt-sized grains that have a clear, coarser microspar centre were derived from attrition of the tubules. More abundant, however, are micrite rods and peloids identical in size to the above, except that they lack the clear, coarser spar centres.

Girvanella can be obvious in intraclasts and constitute a large proportion of the grain, or it can occur as barely resolvable tubules or micritic filaments set in a matrix of structure grumeleuse. Peloidal intraclasts characterized by structure grumeleuse and without evidence of calcified algae are important components in many grainstones.

Epiphyton is present as identifiable fragments in intraclasts and Nuia occurs as single, sand-size particles.

6.5 ALGAL SEDIMENTS FROM THE PLATFORM MARGIN AND INTERIOR

6.5.1 Petrography of Platform Margin Boulders

Conglomerates in the Cow Head Group contain boulders of white to light gray limestone which are composed primarily of calcified algal boundstones (James, 1981). These boundstones, dominated by Girvanella, Epiphyton, and to a lesser extent Renalcis and cemented by submarine, radial fibrous calcite cement, were interpreted to represent mounds which grew within the photic zone at a platform margin characterized by agitated conditions and locally ooid-rich grainstones. Petrographic relationships indicate that the anhedral, finely crystalline calcite spar cementing Girvanella and Epiphyton, within Girvanella tubules, and forming part of the structure grumeleuse microfabric is cogenetic with the well-defined radial fibrous crystals. Pertinent details of the petrography of these boundstones are provided in the following paragraphs, based upon information in James (1981) and further work.

In the boulders Girvanella are loosely to tightly intertwined and define slightly curved to planar sheets or crusts up to 1.5 mm thick (Plate 26a). Sheets containing well-preserved Girvanella (Plate 26b) may grade laterally over a distance of several tens of micrometres into poorly preserved filaments ("micritic threads" of James, 1981) and to irregular peloidal micrite - microspar mosaics forming structure grumeleuse with no preserved filaments (Plate 26c). Sheets formed by dense micritic threads and structure grumeleuse are more common than sheets in which

well-preserved Girvanella tubules are abundant.

Epiphyton is well-preserved, and occurs as arborescent clusters ("bushes") up to 1 cm in size which consist of straight to slightly curved, branches 35-60 μm in diameter (Plate 25b). The common microfabric is one of dense, homogeneous micrite but in many samples the branches are chambered and following the taxonomy of Korde (1973) could be Gordonophyton. Some chambered branches grade in the same branch to dense micrite, suggesting that differences in the degree of calcification may result in the recognition of different algal "genera" and "species" (Pratt, 1984).

Renalcis typically occurs as a series of superposed lunate chambers with a poorly-defined micritic wall which grades into slightly larger and more transparent spar at the centre of the chamber.

Grainstones within the algal boundstone boulders contain numerous peloidal and Girvanella intraclasts and Girvanella rafts, commonly granule-size or larger, identical to those in fine-grained slope limestones. This, together with their occasional elongate shape and radial fibrous calcite cement, suggests that they came from Girvanella sheets on the nearby mounds.

Algal boundstone boulders have also been described from the Lower to Middle Cambrian Shady Dolomite of the southern Appalachian Valley and Ridge Province (Pfeil and Read, 1980; Read and Pfeil, 1983). As with the CHG boulders, some of the microfabrics in the southern Appalachian boulders illustrate variability in the preservation of Girvanella and possibly also Epiphyton. Girvanella was commonly recrystallized to a

gray microspar and some thrombolites contained a "wispy" fabric which suggested faintly preserved filaments of Girvanella.

6.5.2 Algae of the Platform Interior

In situ platform-margin equivalents to the CHG algal boundstones are not found in the western Newfoundland autochthonous platform succession due to erosion, metamorphism, or burial by allochthonous slices emplaced during Taconic Orogeny (James, 1981). Cryptalgal structures (Aitken, 1967), however, are important in the autochthonous, platform-interior sediments (Figure 6.3). Previous work on the Middle to Upper Cambrian Port au Port Group and the Lower Ordovician St. George Group indicate that stromatolites, thrombolites, and thrombolite-metazoa mounds are common (Swett and Smit, 1972; Levesque, 1977; Pratt and James, 1982b). In contrast to the Cow Head Group boulders, Renalcis is an important constituent of some of the Lower Ordovician mounds (Pratt and James, 1982b) whereas Epiphyton is absent (Pratt, 1979); this is consistent with its apparent preference for platform-edge lithofacies (James, 1981; Demicco et al., 1982; Read and Pfeil, 1983).

6.5.3 Summary

Algal boulders from conglomerates in the Cow Head Group indicate that calcified algae were major sediment producers at the shelf margin. Here, poorly preserved Girvanella sheets, characterized either by dense micritic filaments or structure grumeleuse, are volumetrically as important as sheets in which Girvanella tubules are clearly differentiable. Both Girvanella and Epiphyton are equally abundant in

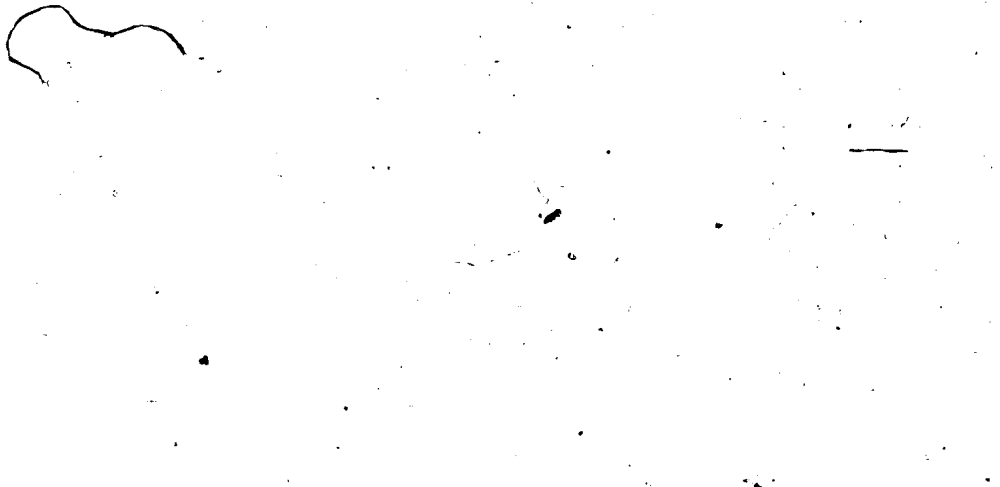
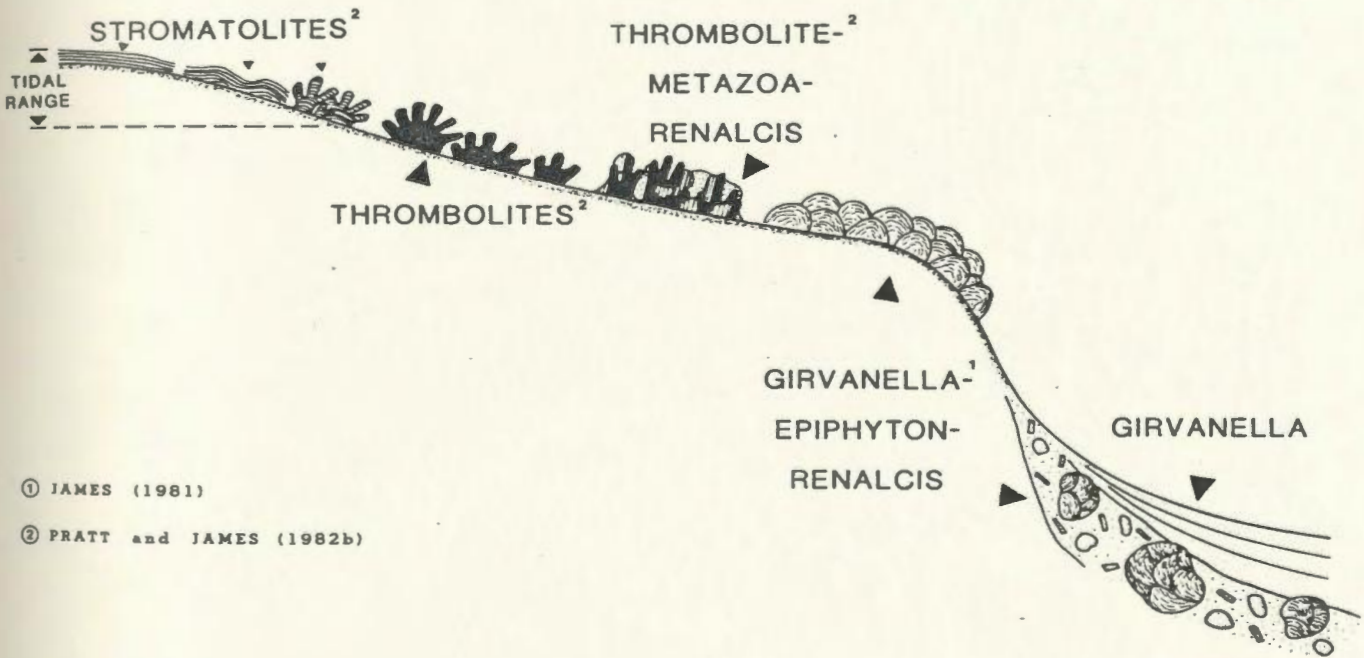


Figure 6.3: Schematic reconstruction of the distribution of Lower Paleozoic calcified and non-calcifying algae from western Newfoundland. The reconstruction of the platform interior setting is based on the synthesis of Lower Ordovician algal carbonates by Pratt and James (1982b). The Middle to Upper Cambrian distribution is assumed to be similar to the Lower Ordovician. Vertical and horizontal distances are not to scale.

- NW

- SE



① JAMES (1981)

② PRATT and JAMES (1982b)

the boundstone boulders but in the thinly-bedded slope limestones, only Girvanella is common and Epiphyton is rare. Sediments associated with the algal boulders contain particles identical to those found in the slope limestones. The presence of radial-fibrous calcite within these grains, and in some cases, their elongate shapes suggest that they are fragmented Girvanella sheets, probably derived locally from adjacent calcified algal mounds.

6.6 DISCUSSION

6.6.1 Girvanella

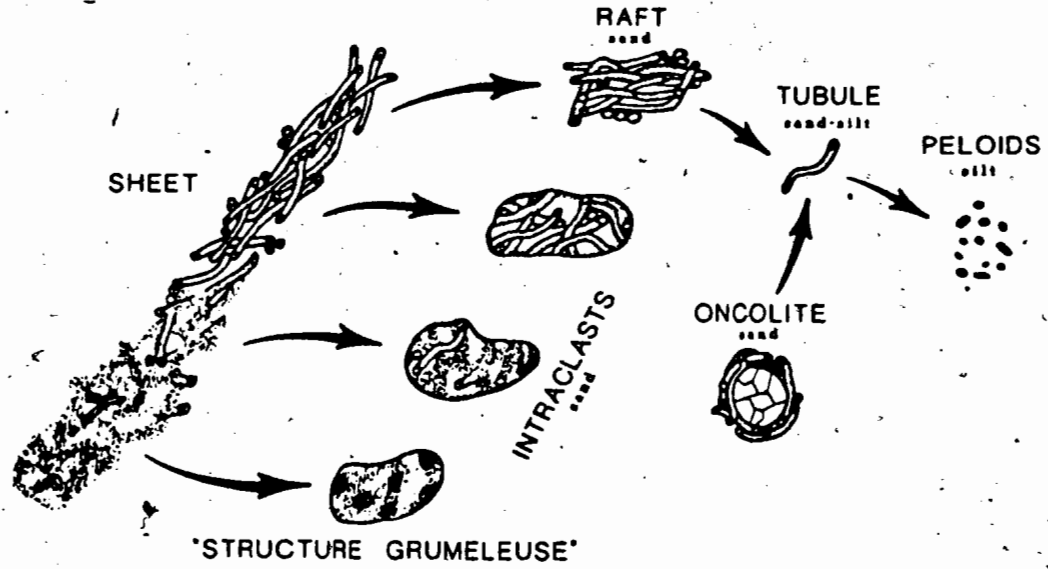
When observations on the distribution, relative abundance, and fabric of calcified algae in both limestone boulders and slope limestones are integrated, a clearer picture of the contribution of algal particles to the sediment emerges. Fragmentation of Girvanella sheets which comprise the algal boundstones produces intraclasts both with and without obvious Girvanella tubules, depending on the degree of Girvanella preservation in algal boundstones (Figure 6.4). With minor syndimentary cementation, porous rafts result instead, which in turn, fragment to yield single tubules and ultimately peloids with microspar centres and micritic margins. If the tubular structure is not preserved, dense micrite rods and the ubiquitous, dense, silt-size peloids result. It is not necessary to look further than the platform margin algal boundstone lithofacies to find a source for: (1) Girvanella clasts; (2) many peloidal intraclasts, especially those with structure grumeleuse; and

Figure 6.4: Summary diagram of break-down of calcified algae. Girvanella sheets from the platform edge lithofacies provide a potentially wide variety of algal clasts. Peloidal intraclasts characterized by structure grumeleuse abound in Cow Head Group sediments and also find a ready source in the platform edge lithofacies. Oncolites probably form in less energetic settings than the platform margin algal boundstones and are swept from the platform interior to locally contribute to slope sedimentation.

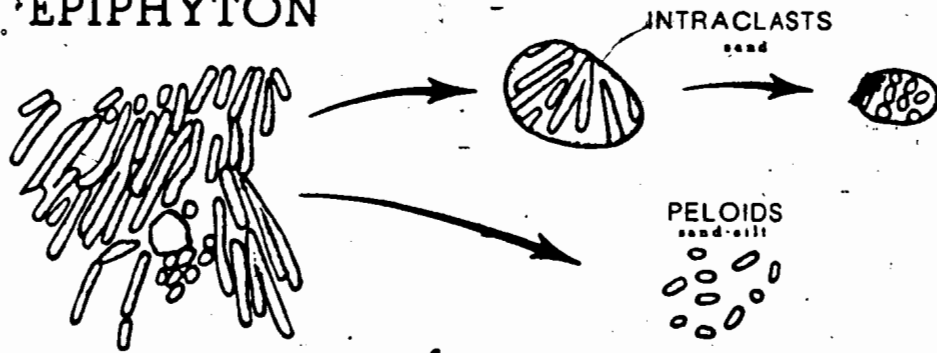
Break-down of Epiphyton is not as readily traceable as that for Girvanella. Destruction of the typically dense micritic branches will provide coarse silt- to very fine sand-size algal clasts which contain no distinguishing microstructure and are not differentiable from other similar-size peloids. Larger intraclasts are only differentiable from peloidal-grainstone intraclasts if elongate portions of the branches are seen.

The importance of the modern codiacean Halimeda as a contributor of granule- to mud-size carbonate provides a possible modern analogue for the ancient forms Girvanella and Epiphyton. This portion of the figure is adapted from Folk and Robles (1964).

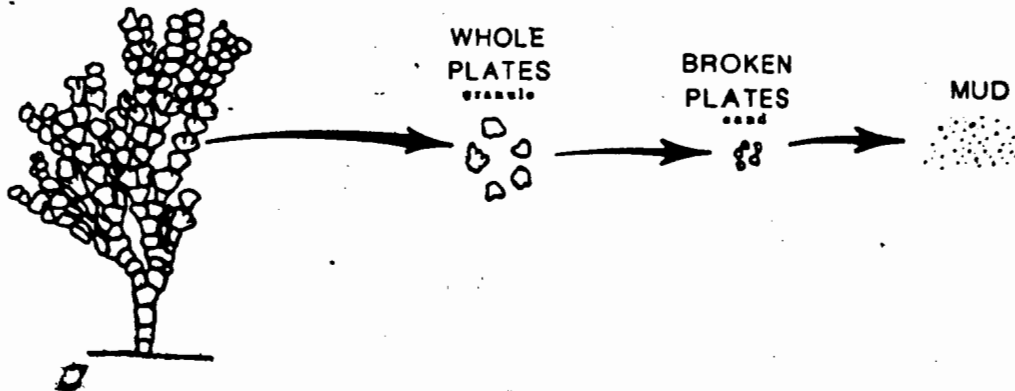
GIRVANELLA



EPIPHYTON



HALIMEDA



(3) micritic, silt-size peloids which characterize numerous limestones in this succession.

Although structure grumeleuse microfabric can form in numerous ways (see discussion in Appendix G), study of Girvanella sheets in algal boundstone boulders suggests that some structure grumeleuse may be due to syndimentary processes affecting living or dead filamentous and coccoid algae. This structure grumeleuse may be the result of either "overcalcification" with consequent loss of diagnostic microfabric, or insufficient calcification to define the Girvanella form.

6.6.2 Epiphyton

The importance of Epiphyton as a sediment producer is not as obvious as for Girvanella. The importance of Epiphyton in algal boundstones and the paucity of distinct Epiphyton clasts in fine-grained slope limestones implies that the Epiphyton contribution is extremely subtle. The diameter of the Epiphyton branch (35-60 μm) suggests that fragmentation will readily provide coarse silt- to very fine sand-size peloids. Due to the micritic composition of these branches, peloids produced in this way will provide no hint of their algal origin. Rees (in preparation) recently came to the same conclusion regarding the lack of obvious Epiphyton clasts in shallow-water, Epiphyton-rich lithofacies of the Middle Cambrian Wheeler Formation in western Utah.

Limestones of the CHG are not the only sediments in which an important algal contribution has been suggested. Wolf (1965) described the breakdown products from calcified algae in the Lower Devonian Nubrigyn

Formation of New South Wales. Aitken (1967) documented Girvanella in intraclasts in Cambrian and Ordovician limestones of southwestern Alberta. Other studies in which algal clasts have been reported include Ahr (1971), Toomey and Nitecki (1979), and Markello and Read (1981).

In addition to an algal origin for many of the peloids in the CHG, faecal pellets must also be important based on the amount of shelly debris found in the CHG as well as in the shallow-water equivalents of the platformal succession. The possibility that micritized bioclasts and ooids may be the parent grains of these peloids is discounted because micrite envelopes on bioclasts and ooids are never wider than 10 μ m and grains transitional between these and dense micritic peloids are never seen. An intraclastic origin is also a possibility but small, micritic intraclasts would not be readily differentiated from micritic peloids of other origins (see Fahraeus et al., 1974).

6.6.3 Comparison With Modern Calcified Algae

In modern tropical oceans, calcified algae, notably calcified chlorophytes and rhodophytes, are important sediment contributors on carbonate shelves (Wray, 1977). Although physiologically quite different, modern coralline and codiacean algae appear to have largely supplanted the Paleozoic calcified cyanobacteria in a major sediment-producing role. Articulated corallines, such as Amphiroa, readily disintegrate to produce sand-size particles. The codiacean Halimeda forms easily recognizable sand- to granule-size plates upon death and disaggregation and is regarded as the "single most abundant grain constituent in many sub-tropical lagoon and back-reef

environments" (Wray, 1977, p. 142; Figure 6.4). The role of Halimeda as an important sediment producer has been documented repeatedly in the literature on modern carbonate platforms (e.g. Purdy, 1963; Folk and Robles, 1964; Bathurst, 1975; Drew, 1983; Liebezeit et al., 1984). The destruction of Halimeda, Penicillus (also a codiacean), and other calcified green algae also results in the production of tiny aragonite needles to form lime muds (Folk and Robles, 1964; Stockman et al., 1967; Wray, 1977).

Recent work on deep-water sediments adjacent to shallow-water carbonate platforms in the modern ocean has shown that significant amounts of calcified algae, notably Halimeda, in addition to fragments of coralline algae and shallow water faunas (e.g. mollusks, benthic foraminifera, echinoids, corals), are transported to deep-water environments. Land and Moore (1977) reported Halimeda in sediments from water depths of 100-200 m on the island slope off Jamaica. James and Ginsburg (1979) also reported algal plates from the cliffed fore-reef off Glovers atoll at a depth of 310 m and from 2200 m depth from the Cayman Trough off Belize. Crevello and Schlager (1980) examined sandy turbidites from 1200 m and greater depths in Exuma Sound in the Bahamas and indicated an important Halimeda contribution. Halimeda plates also form an major part of the sand-size assemblage recovered from a modified grain flow deposited cored at 4000 m depth at the base of the Bahama Escarpment (Mullins and Van Buren, 1979). The large carbonate sediment drifts at depths up to 800 m in the northern Straits of Florida also contain Halimeda (Mullins et al., 1980b). Halimeda was found in sediments dredged from the deep waters (1400 m) surrounding the Bikini atoll (Emery et

al., 1954).

6.7 CONCLUSIONS

Clasts of the calcified algae Girvanella and Epiphyton were derived from algal mounds which grew at the shallow platform margin. These particles are volumetrically the most abundant bioclastic particles in fine-grained limestones of the CHG. Four types of Girvanella particles are differentiated - oncolites, rafts, single tubules, and intraclasts. Breakdown of Girvanella sheets in the platform-margin mounds provided intraclasts with obvious Girvanella as well as a variety of peloidal intraclasts lacking evidence of calcified algae but instead characterized by structure grumeleuse. In contrast to Girvanella, the petrographic evidence for Epiphyton in fine-grained limestones is rare, occurring only as intraclasts.

Micritic peloids and peloidal intraclasts, many characterized by structure grumeleuse, are the dominant particles in CHG limestones. Comparison of microfabrics in these particles with those in the algal boundstone boulders suggests that most peloids and peloidal intraclasts are cryptalgal.

Peloids and intraclasts such as those in the CHG also characterize many other Phanerozoic limestones and suggest that the role of calcified algae as sediment producers may be considerably underestimated. Testing of this hypothesis must await additional studies which seek to integrate data from known calcified algal accumulations with their surrounding

"peloidal" sediments.

PART B: DIAGENESIS

INTRODUCTION

The authigenic components in the CHG are, in order of volumetric importance, calcite, dolomite, silica, and barite. Pyrite and potassic feldspar overgrowths on detrital nuclei are also present and ubiquitous; but not abundant. Authigenic minerals of only minor and local importance include sphalerite, glauconite, chlorite, and fluorite (described in Appendix L). Authigenic clay minerals in shales presumably include illite and chlorite, in addition to the terrigenous fraction, and the mixed-layer clay, corrensite (discussed in Appendix B).

Chapters 7-11 deal mainly with calcite diagenesis, although dolomite (Chapter 12), silica, barite, and pyrite (Chapter 13) are also considered. Fine-grained as well as conglomeratic sediments are studied, and collectively they illustrate an extensive suite of diagenetic fabrics with which the diagenetic history of this succession can be deciphered. All diagenetic aspects discussed in the following chapters are the result of in situ processes. A notable exception, however, is radial fibrous cement found in some boulders in conglomerates. These cements, transported along with their host boulders from shallow-water, are examined in order to complete the inventory of fibrous calcites found in the CHG (see below). The

diagenesis of clasts in conglomerates are not detailed in this thesis, but reconnaissance observations of clasts presumed to be reworked slope sediments are considered.

Routine analysis of these sediments included thin section staining (calcite versus dolomite, ferroan versus non-ferroan [1]) and extensive use of cathode luminescence (abbreviated "CL") [2]. The degree of chemical heterogeneity resolvable with CL allows it to be used as a sensitive "fingerprint" of temporal and spatial chemical attributes of a carbonate-precipitating pore-water system, complimenting both staining and chemical analyses. The sensitivity of luminescence colour and intensity to slight changes in trace element composition allows the recognition of chemical heterogeneity in crystals which otherwise appear homogeneous by any other analytical method. In addition, CL plays an important role in the study of microfabrics. Such features as solution unconformities (corrosion surfaces), detrital calcite and dolomite particles, composite crystals, and morphologies of crystals at intermediate stages of growth can be seen.

TYPES OF CALCITE

Diagenetic or authigenic calcite is that which "has crystallized essentially in situ within the sediment..." (Folk, 1965, p.23).

1. The terms ferroan and non-ferroan simply refer to whether or not an iron stain is detectable in calcite or dolomite.

2. Procedures and instrumentation data are provided in Appendix I.

Diagenetic calcite forms in 4 ways: (1) direct precipitation as a cement into a void, (2) by neomorphism of previous calcite or aragonite, (3) by displacive precipitation, and (4) by replacement of other non-CaCO₃ minerals. All 4 types are found in the CHG, although only the first 3 are of any volumetric importance as well as informative in terms of providing useful data concerning the diagenetic history. The fourth type is represented by scattered occurrences of dedolomite and replacement of sphalerite, pyrite, and barite.

A brief discussion on terminology and definitions related to cementation and neomorphism is provided in Appendix H. In addition the criteria used to distinguish cements from neomorphic spar are also reviewed. In this thesis the term "neospar" is adopted to refer to both microspar and pseudospar, or either when their separate distinction is not important.

The spectrum of diagenetic calcites in the CHG is conveniently divided into 6 categories, some of which are intergradational. These are listed and briefly described below.

(1) Radiaxial Fibrous Calcite: ("RFC") cements are invariably restricted to the shallow-water boulders in conglomerates. These cements have the characteristic distally-convergent extinction of RFC. This distinguishes them from in situ fibrous calcites (see below). RFC is described in Chapter 7.

(2) Conglomerate Fibrous Calcite: ("CFC") cement crystals are elongate (i.e. fibrous), have unit extinction, and commonly develop scalenohedral terminations. They occur in conglomerate matrices and are therefore in situ precipitates. CFC is also associated with equant calcite cement,

dolomite cement, and internal sediment. These calcites are described in Chapter 8.

(3) Displacive Fibrous Calcite: ("DFC") is abundant throughout the CHG. These crystals have unit extinction or the characteristic sweeping extinction of radial fibrous aggregates. As with CFC, DFC may develop scalenohedral terminations, but unlike both RFC and CFC, DFC commonly contains a fibrous inclusion pattern. DFC is not a pore-filling, but instead occupies space resulting from its own displacive growth. DFC forms enigmatic "beef" and "cone-in-cone" fringes, as well as microscopic fringes developed around argillaceous intraclasts. These calcites are described in Chapter 9.

(4) Equant Cement: Intra- and interparticle equant cement is found in grainstones, grainstone matrices of conglomerates, and conglomerates with a sparry matrix. Most sand- and silt-sized, grain-supported sediments are grainstones. This cement, along with fracture cements, and neospar (see below), are described in Chapter 8.

(5) Fracture Cements: Vein and fracture cements are ubiquitous and generally composed of equant calcite crystals. The fractures and veins range from a shallow-burial origin to postdating tectonically-related dolomitization.

(6) Neospar: Equant to loaf-shaped crystals of intra- and interparticle neospar occur in packstones, wackestones, mudstones, and conglomerates with these matrices.

CL microfabrics of RFC, DFC, and some pseudospar suggests growth as

spherocrystals, similar to what Kendall (in press) recently proposed as a reinterpretation of RFC in general. Many CL microfabrics illustrated in these chapters have not, to my knowledge, been reported elsewhere in the literature. The exceptionally informative CL of RFC from the CHG provides the basis for a modification of Kendall's (in press) explanation of distally-convergent extinction in these crystals.

Trace element geochemistry of calcite as a function of progressive precipitation is discussed in Chapter 9. In Chapter 10 the stable isotopic geochemistry of a wide variety of authigenic calcites, as well as RFC from the shallow-water boulders, is examined.

OTHER DIAGENETIC MINERALS

Other important diagenetic processes in the CHG include dolomitization, silicification, replacement of siliceous components by calcite, and precipitation of barite and pyrite. Field, petrographic, and CL characteristics of dolomitization, along with trace elements and stable isotopes, are discussed in Chapter 12. Chapter 13 deals mainly with field relationships and petrography of silicification and replacement of siliceous components by calcite. This chapter also illustrates the power of CL as a microfacies tool and the importance of siliceous microfacies in the CHG. Barite and pyrite are also briefly examined in this chapter.

Chapter 7

RADIAXIAL FIBROUS CALCITE

7.1 INTRODUCTION

Radiaxial fibrous calcite ("RFC" [1]) and fascicular optic calcite ("FOC" [2]) are common constituents of ancient shallow-water and, to a lesser extent, deep-water limestones (e.g. Kendall and Tucker, 1971; Garrison, 1972; Kendall and Tucker, 1973; Tucker, 1973; Mountjoy and Walls, 1977; James and Klappa, 1983). Until recently, these fibrous calcites were interpreted as neomorphosed, fibrous, marine cements (Kendall and Tucker, 1973; Kendall, 1977). Their association with internal marine sediments in primary, often reefal, cavities provided the basis for a marine cement origin (however, see Ross *et al.*, 1975; Cross and Klosterman, 1981). That RFC were not primary, however, was based on the presence of distally convergent c-axes and apparent lattice strain; curved twins, cleavages, and glide plains; divergent

1. Radiaxial fibrous refers to a microfabric within single large crystals which is characterized by diverging subcrystals, distally convergent optic axes, and curved twins, cleavages, and glide lamellae (Bathurst, 1959; Kendall, in press).

2. The characteristics of FOC are similar to those of RFC except that the optic axes are distally divergent (Kendall, 1977; & in press).

sub-crystals; non-planar intercrystalline boundaries; inclusion patterns in calcites which appeared to not respect crystal boundaries and which formed irregular or rhombohedral growth fronts; lack of competitive growth fabrics; and occurrence of RFC and FOC in the same pores which suggested that they were diagenetic variants of one another (Bathurst, 1975; Kendall and Tucker, 1973; Kendall, 1977, in press). Kendall and Tucker's (1973) classic interpretation of RFC invoked the migration of a fluid film through the fibrous precursor, from base to top, dissolving the original cement crystals on one side and precipitating RFC on the other. Replacement was hypothesized to occur most rapidly between the original bundles of crystals thus leading to the centres of the neomorphic crystals being established here. A similar interpretation, though without the necessity of replacing preferentially along boundaries of the original acicular bundles, was proposed for FOC (Kendall, 1977).

Numerous papers published after that of Kendall and Tucker (1973) describe RFC, though provide little fresh insight into its interpretation beyond its probable original Mg-calcite mineralogy (Davies, 1977a; Lohmann and Meyers, 1977). Kendall's (in press) reevaluation of the origin of RFC dismisses most of the previous arguments demanding a neomorphic origin for these crystals and concludes that the fabric is indeed primary, and is the result of composite crystal growth.

RFC in the CHG, first recognized and described by Suchecki (1975), is found in various shallow-water boulders which were transported to the deep-water slope environment within debris flows. Although not part of

the in situ diagenetic assemblage, their petrographic, CL, and isotopic characteristics are important and relevant to the present study.

Firstly, the CL characteristics of RFC are similar to those of displacive fibrous calcite ("DFC" - discussed in Chapter 9) and together they provide a clearer picture of the kinds of microfabrics associated with spherocrystal growth. As with DFC and in agreement with Kendall (in press), the CL characteristics of RFC in the CHG are interpreted to be primary, not neomorphic. Based on these samples, a modification of Kendall's (in press) hypothesis for the origin of the distally-convergent extinction pattern is proposed. Secondly, the lack of significant alteration of these crystals, as shown by CL, adds impetus for their use as an internal standard with which other CHG calcites can be compared. This also lends support to the use of fibrous marine calcites as an index of the changing oxygen isotopic composition of the ocean through the Phanerozoic (James and Choquette, 1983).

7.2 FIELD RELATIONSHIPS

RFC is restricted to boulders of shallow-water derivation within conglomerates but is otherwise unrestricted stratigraphically or geographically. Host lithologies include fossiliferous wackestones to packstones as well as algal boundstones (see Chapter 6). RFC occurs mainly in fractures and vugs (Plate 27a,b) and less commonly it is associated with enigmatic, decimetre-size and larger, mound structures which occur in some of the large shallow-water boulders at Lower Head (Plate 27d,e). The nature of these mounds and the role of RFC in them }s

presently unclear and awaits further study.

Fractures are usually less than 2 cm in width, may extend for a metre or more through the boulder, and never continue beyond into the surrounding conglomerate matrix or into other clasts. This evidence indicates that fractures were filled with RFC and the boulder was subsequently transported into the slope environment. Both fractures and vugs are commonly lined by a prominent, rusty-weathering, millimetre-thick rind of chalcedonic chert at the base of the RFC fringe. Less commonly, thin, discontinuous crusts of glauconite up to 100 μm in width containing scattered pyrite crystals precede the earliest RFC. Later megaquartz cement or laminated internal sediments occlude remaining fracture or vug porosity. In and on the mound structures in the boulders, RFC forms fringes up to 5 cm in width, some of which consist of numerous, mutually-interfering botryoids up to 1 cm in size (Plate 28b).

Fractures and vugs are generally not fabric-controlled, however, "zebra-rock" boulders at Lower Head and Cow Head North demonstrate primary fabric control (Plate 27c). In these boulders, alternating, discontinuous, centimetre-thick beds of mudstones and wackestones and RFC layers resemble those from the Middle Ordovician Meiklejohn mound (see Ross et al., 1975).

7.3 PETROGRAPHY

7.3.1 General Description

RFC crystals are non-ferroan and vary from 500 μm to 3 cm in length with length to width ratios of approximately 10:1. In simple fringes composed of the larger crystals, each half-fringe is spanned by a single crystal and the two fringes meet along a medial suture (Plate 28a), or the half-fringes are overlain by equant, occasionally slightly ferroan, spar. In some cases, RFC crystals have rhombohedral terminations buried by the spar. More complex fringes are characterized by 2 or more superposed fringes of RFC. Smaller crystals are spindle-shaped and form aggregates which resemble the "coconut-meat" microfabric described from speleothems (Plate 28c; Folk and Assereto, 1976). Most of the following petrographic characteristics are based on examination of the easily studied, larger crystals.

Subcrystals typically vary from 30-250 μm in width and are defined by inclusion patterns, extinction domains, and CL (discussed later). Subcrystals are subparallel to one another within a major crystal, or they diverge radially from the base of the crystal. Crystals are length fast with the extinction pattern showing the characteristic, distally-convergent optic axes (see later discussion). A 20-25 degree rotation of the microscope stage is usually necessary to sweep the extinction band through the crystal. These calcites are commonly twinned but only rarely are curved twins seen. Intercrystalline

boundaries are irregular to concertal.

7.3.2 Inclusion Patterns

Most inclusions are micrometre-size and include irregular, opaque and translucent materials (possibly organics, clays, or pyrite), dolomite, microquartz, as well as rare two-phase, fluid inclusions. Three categories of inclusion patterns are recognized - Types A, B, and C. These are similar to those seen in DFC (Chapter 9). Type A is the most common inclusion pattern and is simply an homogeneous distribution of inclusions throughout the crystal. The Type B inclusion pattern is defined by thin to broad inclusion-rich domains parallel to the fringe. These may form convex-upward, botryoidal surfaces (Plate 28e,f) or more rarely define one or more rhombohedral surfaces within a crystal (cf. Kendall and Tucker, 1978; Kendall, in press). The density of inclusions within some of these bands may become reduced laterally. The Type C pattern is a sub-parallel to radiating array of inclusions which outlines the subcrystals within a major crystal (Plate 28e,f). A fine fibrous inclusion pattern similar to the Type D pattern in DFC is not found in RFC; this is consistent with observations of other RFC (Kendall, in press).

7.3.3 Microdolomite

Variable quantities of anhedral to euhedral dolomite crystals up to 50 μm in size, though usually 10 μm or less, are randomly scattered throughout many RFC crystals. Etching of polished thin sections is not required for their observation (cf. Lohmann and Meyers, 1977) and they

are easily viewed in stained thin sections under high power (Plate 28d) and are red-luminescent and zoned in CL. Where dolomite is particularly abundant, their alignment along the calcite cleavage directions indicates crystallographic control on their distribution as well as a replacement origin.

Microdolomite is not obvious in all the radiaxial calcite crystals examined but, in general, it is more abundant in RFC than in other fibrous calcites in the CHG. The ubiquity of similar microdolomites in the host sediments of DFC, other clasts in conglomerates, and in the in situ sediments precludes estimation of original $MgCO_3$ content of these calcites (cf. Lohmann and Meyers, 1977).

7.4 CATHODE LUMINESCENCE

In general, CL of RFC illustrates them to be mostly dark (non-luminescent), but often speckled with irregular, decimicrometre-size luminescent patches or streaks reminiscent of those commonly encountered in pelmatozoan debris. This "blotchy" luminescence appears to be typical for RFC (cf. Meyers, 1974; Lohmann and Meyers, 1977; James and Klappa, 1983). Some RFC are exceptional, however, in that they illustrate details of the microfabrics and growth histories of these crystals which have not been previously documented from luminescent specimens.

Bright-luminescent zones vary from 5-200 μm in width and the growth surfaces they define range from euhedral (Plate 29a,b) to anhedral

(Plate 30c,d), the latter often demonstrating irregularly-shaped projections convex toward the crystal termination. Many of the euhedral growth surfaces are flat or have the shape of obtuse rhombohedra (Plate 29a,b; 31a-d). The degree of "euhedralness" varies from one zone to the next and may gradually become higher or lower with progressive growth (Plate 30a,b; 31a-d). Some faces which appear to be planar are, upon closer inspection, actually non-planar "pseudofaces" (Plate 30 a,b). Similar growth surfaces are observed in DFC (see Chapter 9).

Within crystals, elongate domains characterized by either euhedral or anhedral growth zones can be correlated with the subcrystals seen in polarized light (Plate 31a,b). Other crystals contain non-luminescent rods with parallel, planar sides which vary from 30-180 μm in width and extend for short distances through the crystal. Several of these rods may be found splaying outward from a euhedral or anhedral growth surface within the crystal (Plate 30a-d). In other crystals, they dominate certain portions of the fringe (Plate 29c,d).

7.5 INTERPRETATION

7.5.1 Inclusion Patterns

The homogeneous Type A inclusion pattern is common in RFC of the CHG as well as in other RFC described in the literature (e.g. Kendall and Tucker, 1973). The Type B pattern which parallels the fringe and

substrate is interpreted to reflect changes in the physico-chemical conditions of precipitation during fringe growth. At certain times conditions were conducive for the creation and preservation of numerous inclusions and at other times conditions favoured the precipitation of more inclusion-free crystals. Their parallelism to the substrate reflects the morphology of the growth surface at any given time, and this is interpreted as a primary feature, not the former position of a neomorphic replacement front (Kendall, in press). The Type C inclusion pattern outlines subcrystals which, from CL, often appear as individual crystals (Plate 3la,b) or finger-like botryoids. The lack of a fibrous inclusion pattern similar to the Type D pattern in DFC, if one was ever present, may be due to masking by a younger generation of inclusions, or fluid-filled inclusions may become filled by calcite and thus be no longer visible (Kendall, in press).

7.5.2 Cathode Luminescence

7.5.2.1 Interpretation as Composite Crystals

The close association of euhedral or subhedral growth surfaces and more irregular or botryoidal surfaces suggests that RFC in the CHG are composite crystals, similar to those recently described by Kendall (in press). Obtuse rhombic and flat growth surfaces (zones) are here interpreted to indicate growth as a unit crystal, whereas anhedral (including botryoidal) growth surfaces suggest spherocrystal growth (Maleev, 1972; Kendall, in press - discussed below). A composite crystal origin for RFC in general has recently been suggested by Kendall

(in press) based on petrographic study of RFC from neptunian sills in Devonian forereef limestones from Australia. Unlike most RFC described in the literature, the Australian RFC exhibit a prominent radial fibrous inclusion pattern which provided Kendall (in press) with a basis for this revolutionary reinterpretation of these enigmatic calcites. The basic tenets of the composite crystal concept are also applicable to interpretation of DFC (discussed in Chapter 9).

Details concerning the nature of composite crystals are briefly reviewed in the following paragraphs (also see Kendall, in press).

Spherocrystals, as defined by Maleev (1972; p. 2) are spherulites that form by "a continuous splitting of the ends of one crystal and the deflection of its branches.". The splitting referred to is the split-growth process of Grigor'ev (1965) where a single, monocrystalline nucleus is laterally transformed into an aggregate of sub-parallel- to parallel-oriented crystallites to a fascicular bundle or a sheaf of weakly divergent crystallites [3]. With additional growth and divergence, a spherulite or botryoid ultimately results (Grigor'ev, 1965; Maleev, 1972; Spry, 1976; Kendall, in press) . Split-growth has been observed in synthetic and speleothem calcites as well as in numerous other minerals (e.g. chalcedony, tourmaline, barite, and augite - Grigor'ev, 1965; Maleev, 1972; Kendall and Broughton, 1978; Kendall, in press).

In order to maintain the small diameter of crystallites in the

3. The term "crystallite" is used in this thesis to refer to micrometre-wide or smaller fibrous or equant crystals. "Major" crystals consist of crystallites.

increasingly divergent bundle as well as the optical continuity, additional crystallites of near-identical lattice orientation fill spaces between the older crystallites (Kendall, in press). Crystallites in RFC from the CHG are too small to resolve using CL, but their existence is inferred based on the anhedral to subhedral shapes of growth surfaces. In addition, comparison with DFC, in which crystallites are commonly obvious, indicates by analogy that crystallites occur in RFC (see Chapter 9).

Crystallites growing at equal rates in all directions result in the formation of a spherulitic or botryoidal growth surface (Maleev, 1972). Crystallites growing at variable rates relative to one another produce more irregular growth surfaces. Planar crystal faces result when conditions are conducive to the development of monocrystalline surfaces which can grow layer by layer. Intermediate or transitional conditions form pseudofaces of varying shapes. Similar variations in shape of the growth surface also occur in DFC of this study (Chapter 9); in some Australian RFC (Kendall, in press); and in laminated, crystalline crusts formed in some Welsh streams (Braithwaite, 1979).

7.5.2.2 Controls on Growth Surface Morphology

Kendall (in press) interpreted the variations in RFC growth surfaces to be a function of the saturation state of the solution from which the calcite was precipitated. Higher saturation conditions, perhaps aided by a high crystallization rate, poisoning, or other causes (see Folk, 1974; Hartman, 1983) are thought to give rise to the growth of crystallites and consequently, anhedral growth surfaces, whereas smaller

levels of oversaturation may result in the growth of euhedral faces. Controls on crystal morphologies and original mineralogy also include the effects Mg, Na, and SO_4 (Folk, 1974), and possibly also the $[\text{Ca}]/[\text{CO}_3]$ concentration ratio (Lahann, 1978; Hartman, 1983).

7.5.2.3 Uncertainties

The identical petrographic characteristics of those segments of RFC crystals with flat or rhombic terminations and those segments containing anhedral zones suggest that unit crystal growth may be only apparent with the euhedral shapes resulting from perfectly aligned crystallites growing as a single crystal face. If this was not the case, continuity of the optical properties, such as sweeping extinction and subcrystal domains, through these crystals could not be reasonably explained. The existence of composite euhedral crystals does not dismiss Kendall's suggestion as to why euhedral versus anhedral growth surfaces form (see above discussion).

Another uncertainty regarding the growth mechanics of these composite crystals is how anhedral surfaces growing as spherocrystals become gradually more euhedral with progressive precipitation. This is especially common in DFC crystals (Chapter 9). Euhedral surfaces (zones) followed by progressively more anhedral growth surfaces are interpreted to reflect the transition from unit crystal growth to spherocrystal growth where crystallites grow at different rates depending on their orientations relative to the original monocrystalline nucleus as well as other possible controls. However, the opposite case where an uneven or botryoidal growth surface grows to become progressively more euhedral is

less straightforward to explain. To do this the crystallites may coalesce at their distal end and fill the resulting uneven surface to ultimately provide a flat crystal face which then can grow by even, face-wide increments.

7.5.2.4 Crystal Boundaries, Subcrystals

In the CHG, concertal and irregular, intercrystalline RFC boundaries are interpreted to result from the mutual interference of numerous crystallites or groups of crystallites. Such boundaries are predicted when composite crystals compete for space (Kendall, in press).

Composite crystals in which crystallites grew as groups or bundles of slightly varying orientation account for the origin of subcrystals as seen in polarized light as well as the Type C inclusion pattern. The cause of the initial grouping into separate, but approximately similarly-oriented bundles is uncertain, although slight misorientations could have occurred during the early stages of crystal-splitting, as recently suggested by Kendall (in press). Relationships between crystallites and the occurrence of subcrystals and concertal intercrystalline are discussed further in Chapter 9.

The non-luminescent rods which are differentiable with CL have also been noted in other studies of RFC (e.g. Lohmann and Meyers, 1977; Meyers and Lohmann, 1978). These rods in the CHG are interpreted to be primary precipitates based on their euhedral shapes and sharp zoning, when present. Each rod is further interpreted to consist of a bundle of crystallites which, for reasons unknown, differs in its trace element

composition (and therefore CL) relative to the surrounding synchronously-precipitated calcite. Within RFC crystals described by Lohmann and Meyers (1977), fibres of non-luminescing calcite were 10-20 μm in width and 100-300 μm in length. As with the RFC of this study, there is more highly-luminescent, syntaxial calcite between the fibres. In Lohmann and Meyers' (1977) study, the non-luminescent fibres were interpreted to represent the original cement fabric, and consequently the fibres were the site of Mg remobilization and microdolomite precipitation. The luminescent, interfibre calcite was interpreted to be a later, meteoric-water cement.

The "blotchy" luminescence in many RFC of this and other studies is at best confusing and usually not interpretable with any degree of confidence. Blotchy luminescence may represent domainal alteration, either in terms of dissolution with subsequent precipitation of calcite, or possibly neomorphism of the original cement.

7.5.3 Optic Axes Convergence: Kendall's Hypothesis

In the Devonian RFC examined by Kendall (in press), inclusion-defined fibres or crystallites were observed growing on unit crystal terminations. RFC in the CHG and in general lack such a radial inclusion pattern and the Australian examples are atypical in this respect. Other petrographic properties, however, are typical of RFC, suggesting that the Australian examples are simply better-preserved, not of a different origin. In these, crystallites, as determined by the

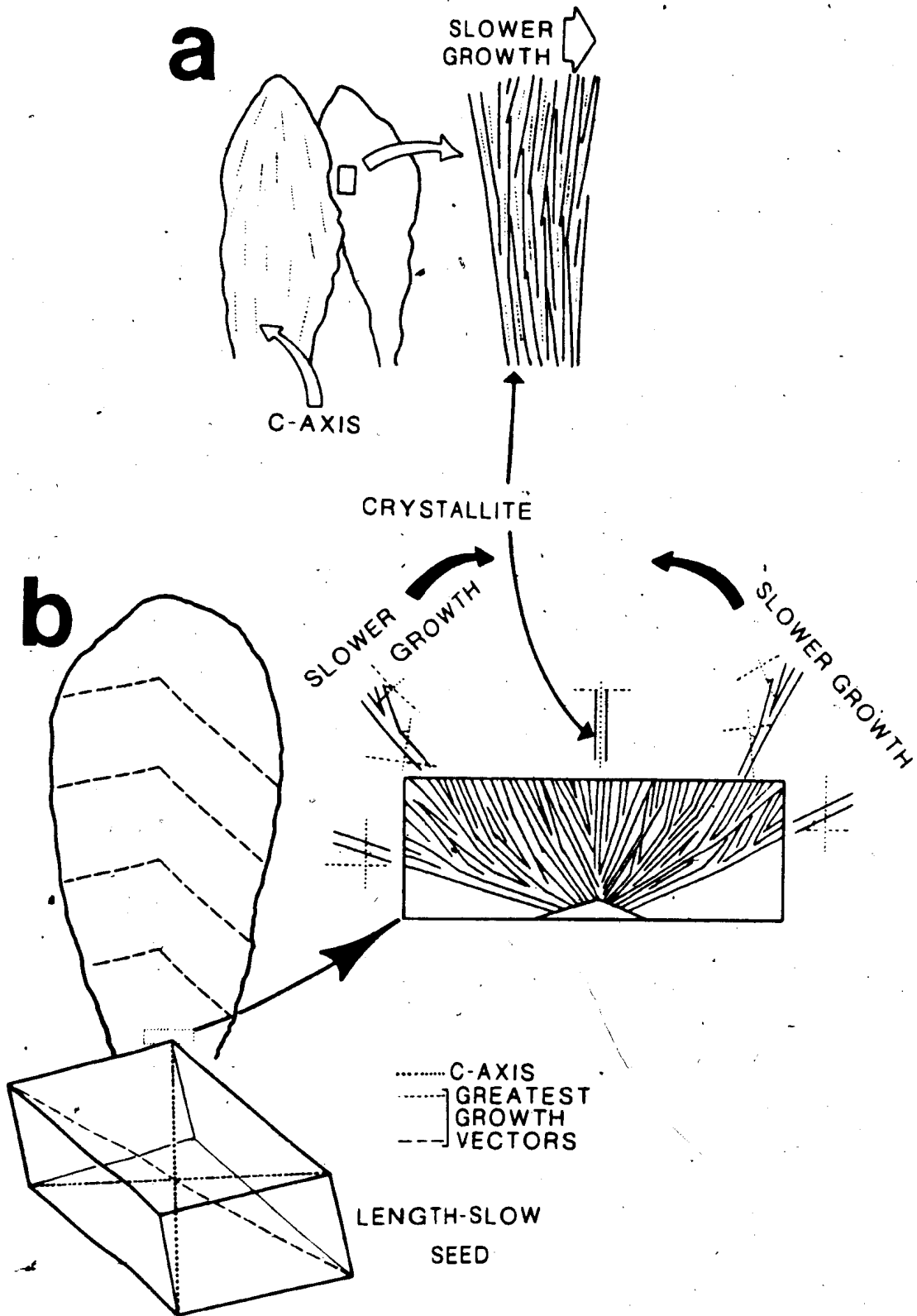
inclusion pattern, consistently curved toward the apex of the major crystal. To explain crystallite curvature and the characteristic RFC convergent extinction, Kendall (in press) concluded that these attributes are the product of a spherocrystal growth mechanism, but with the crystallites growing at different rates depending on their orientation relative to the underlying unit crystal substrate. The variation in growth rates of the crystallites leads to "asymmetric growth" (Maleev, 1972) in which the faster growing crystallites overtake their slower growing neighbours and they, in turn, are overtaken by even faster-growing crystallites. Competition for space in conjunction with split-growth causes crystallites to be deflected toward the slowest-growing part of the surface, assumed to be the apex of the crystal (Figure 7.1a). The convergent extinction pattern thus forms as the fast-vibration directions (optic or c-axes) in individual crystallites become more parallel with the growing surface by curving inward toward the centre of the crystal.

Kendall (in press) proposed two possible hypotheses to explain the more slowly-growing apical regions, "either the composite crystals (1) behaved more as spherocrystals and began to assume their most stable form - that of a spherulite, or (2) they behaved more as single crystals - crystals that were changing habit from length-fast to length-slow stable forms." The first possibility was dismissed based on the premise that a spherulitic growth form results when crystallites grow at equal rates, not the differential rates which are necessary to explain the slower-growing apical region.

Kendall's (in press) argument favouring the second possibility is based

Figure 7.1: (a) Radial fibrous calcite crystal at left illustrates distally-convergent c-axes. At right, asymmetric split-growth causes crystallites to deflect, along with their c-axes, toward the more slowly growing centre of the major crystal (adapted from Kendall, in press).

(b) Diagram schematically illustrates a modification to Kendall's (in press) hypothesis to explain distally-convergent extinction in radial fibrous calcite. Growth of crystallites from a length-slow seed crystal causes crystallites to deflect toward the more slowly growing central part of the major crystal, causing the characteristic distally-convergent extinction. Greatest growth vectors in the $\{10\bar{1}1\}$ unit rhombohedron are from Dixon (1978). See text for details.



upon: (1) interpretation of the acute rhombohedral or scalenohedral termination of the unit crystal substrate to be indicative of length-fast calcite, and (2) that the gradual flattening of the optic axis in individual crystallites implies the crystallites gradually evolved toward a length-slow character. The change from length-fast to length-slow growth results in faster growth rates on the sides of the former length-fast calcite substrate and slower growth rates in the apical region and, consequently, asymmetric growth. Therefore, convergent extinction is ultimately a function of whether or not split-growth is initiated. According to Kendall (in press), this arises from changes in the physical or chemical conditions of precipitation (previously discussed).

7.5.4 A Modification to Kendall's Hypothesis

Kendall's (in press) hypothesis explains all the characteristics seen in RFC. Kendall (in press) admits, however, there is little direct proof that length-slow crystal habits were favoured during RFC growth. More importantly, his hypothesis does not explain the occurrence of RFC and FOC within the same pores as described from other studies (e.g. Kendall, 1977; Chafetz, 1979; James and Klappa, 1983). It is difficult to imagine changes in physical or chemical conditions which would allow some cements to retain their length fast-character (FOC) and others (RFC) to change. An alternate hypothesis is outlined below.

It is suggested that an entire RFC crystal grows as a length-slow crystal, where c-axes are oriented approximately perpendicular to the substrate and parallel or approximately parallel to the crystallite

elongation (Figure 7.1b). The greatest growth vectors are approximately parallel to the substrate (see Dixon, 1978; 1983). The crystallites are elongate in the fast-direction or close to it, depending on their initial orientation relative to their substrate. The result of this is that they appear to be length-fast as does the composite crystal they form. What must be differentiated between is the length-character of the composite crystal, which is an apparent one caused by length-fast crystallites, and the true crystallographic length-character, which reflects the relationship between the c-axis and the fastest growth directions.

CL study of RFC from the CHG provides the basis for a modification of Kendall's (in press) hypothesis. The interior growth surfaces are commonly flat or have obtuse rhombohedral terminations (Plates 29b, 30a-b). These shapes are interpreted to reflect unit rhombohedra and not the acute rhombohedral (scalenohedral) habit, which is length fast. In length-slow forms, these flat or obtuse faces persist because of their relatively slow growth rates. In length-fast forms, where the angular separation of the c-axis and the greatest growth vectors is smaller, the fastest growing crystal faces are rapidly eliminated, thus producing acute rhombohedra or scalenohedra (the familiar dogtooth crystals), forms that are conspicuously dominated by relatively slowly-growing faces (see also explanation in Kendall, in press).

In light of the above, the distally-convergent optic axes in RFC are explained as follows (Figure 7.1b). Crystallites begin to grow on a unit crystal substrate, which could be any size. The length character of this substrate determines the subsequent growth and optical

characteristics of the resulting composite crystal. Assuming that the c-axis of this seed crystal is normal to the substrate, the most divergent crystallites will have the greatest angular relationship between the c-axis, which they inherit from the unit crystal substrate, and crystallite elongation. These crystallites will be approximately length-slow. As indicated by Kendall (in press), the c-axis is not necessarily parallel to crystallite elongation. Crystallites which are parallel to the c-axis will appear to be length-fast.

Because of the relationship between c-axes and crystallite orientation, the fastest-growing crystallites will be those whose orientation most nearly parallels the greatest growth vectors. In the length-slow major crystals, the greatest growth vectors are almost parallel to the substrate and perpendicular to the RFC crystal elongation. Therefore the most divergent crystallites grow fastest. This explains the slower-growing central portions of RFC crystals.

Because the most divergent crystallites have the most obtuse relationship between crystallite elongation and c-axis, their growth and curvature due to upward asymmetric, split-growth results in flattening of the c-axis, as described by Kendall (in press). This explains the distally-convergent optic axes which characterizes RFC.

7.5.5 Explanation of Fascicular-Optic Calcite

Kendall's (in press) hypothesis provides no explanation for the simultaneous precipitation of RFC and fascicular optic calcite (FOC). The hypothesis suggested here, however, provides a basis for explaining

the origin of FOC simply as a function of the length-character of the earliest precipitate upon which crystallite growth occurs. FOC is interpreted to be the result of asymmetric growth of crystallites from a length-fast form. Crystallites growing with their c-axis parallel to crystallite length in the apical region of the crystal grow more quickly than adjacent crystallites which have a more divergent relationship between crystallite elongation and c-axis. Consequently, the crystallites and c-axes splay-outward as a result of asymmetric, split-growth.

If the above suggestions are valid, how can the occurrence of RFC and FOC in the same fringe be explained? The most straightforward way to do this is to have the earliest precipitates, upon crystallites nucleate, vary from length-fast to length-slow. Thus, for length-slow nuclei, the resultant cement crystal will be RFC. For length-fast nuclei, FOC results. These two types of calcite could thus grow in the same pores at the same time from the same pore-waters.

Substrate control of length-character was also suggested by Kendall and Broughton (1977) in a discussion of Folk and Assereto's (1976) paper on elongate length-slow and length-fast speleothem calcites from the Carlsbad Cavern. Kendall and Broughton (1977; p. 1399) interpreted these calcites to have grown simultaneously on a speleothem surface where "fabric control by the chemistry of the depositing waters was minimal, whereas control by the substrate was of greater importance". The control of the length-character by Mg as proposed by Folk and Assereto (1976; or some other chemical variable (see Lindholm, 1972, 1974) could not occur if they were simultaneous precipitates,

7.6 SUMMARY AND CONCLUSIONS

RFC in the CHG is restricted to occurrences in fractures, vugs, and enigmatic mound structures in shallow-water boulders of conglomerates. Most RFC crystals have the typical "blotchy" luminescence described from other studies. Some, however, demonstrate exquisite CL zoning which supports Kendall's (in press) recent reinterpretation of these crystals as primary, not a neomorphosed fibrous cement.

Both RFC and FOC (not seen in CHG) are interpreted to have grown as spherocrystals which underwent asymmetric growth. The framework for the mechanics of their growth is essentially that described by Kendall (in press) but with some modification. In both RFC and FOC, c-axes are perpendicular to their substrate but their length-slow and length-fast nature, respectively, control the growth rates of the crystallites as well as the ultimate optical characteristics of the major crystal.

Chapter 8

AUTHIGENIC CALCITE CEMENT AND NEOSPAR

8.1 GENERAL INTRODUCTION

The following chapter describes authigenic calcites occurring both as neospar and cement. For clarity, this chapter is subdivided into 4 sections. The first describes equant calcite cement and neospar. This is followed by description of sparry calcite cement filling fractures which range in origin from shallow burial to tectonic. The third section examines the enigmatic fibrous calcites cementing some conglomerates. These particular calcites are especially important because they are interpreted as submarine cements, although isotopically, as will be discussed in Chapter 11, they were probably derived from modified seawater. Lastly, the foregoing eclectic assemblage of calcites, along with DFC (discussed in subsequent chapter) combine to generate a simple CL model, which, along with field and petrographic evidence, provide the basis for interpretation of most of these calcites as having formed during shallow burial on the sea floor.

8.2 EQUANT CEMENT AND NEOSPAR

In the CHG all grainstones and, to a lesser extent, conglomerates are cemented by blocky, sparry calcite. Mudstones, as well as the "muddy" matrix in packstones and in some conglomerates, consist of neospar. Such neospar is conventionally regarded as having been derived from the aggrading neomorphism of micrite, which in turn resulted from the alteration of lime mud (Folk, 1965). At first glance, these two types of calcite - cement and neospar - are unremarkable, resembling cements and neomorphic calcites described from countless other studies.

8.2.1 Equant Cement

The most easily-studied cement microfabrics are those in conglomerates and in medium sand-size and coarser grainstones. The larger interparticle spaces in these sediments permit a more advanced state "maturation" (sensu Dixon, 1983) to be reached prior to porosity occlusion. Cement crystals range from 25-150 μm in size and may reach 2 mm in the coarser sediments. Within a given sample, however, the size range is considerably more restricted. The largest cement crystals are often syntaxial, poikilotopic overgrowths of pelmatozoan debris. In place of equant crystals, fibrous, syntaxial fringes comprising crystals up to 125 μm in length and several tens of micrometres in width are found on many trilobite fragments and radial ooids.

A cement origin is suggested by the following:

- (1) Intercrystalline boundaries are sharp and there is no

"intercrystalline paste" (Plate 34a; cf. Plate 34d).

(2) Where calcite lines voids, crystal terminations are euhedral and remaining pore-space may be empty (rare) or filled with ferroan dolomite, megaquartz, or chalcedony (Plate 34b).

(3) In sediments with a bimodal grain size distribution of carbonate sand and siliciclastic silt, the silt is geopetal (perched on top of grains) or it is found between the sand-size framework grains (Plate 34c).

(4) The earliest CL zones clearly show euhedral outlines which are maintained until adjacent crystals impinge and subsequent growth zones are continuous across the compromise boundary (Plate 35a,d).

With a decrease in crystal size, the above characteristics become increasingly more difficult to observe and differentiation from neospar is less certain. Cements identified by the above criteria are more equicrystalline than neospar in packstones and are found in better sorted sediments. The dubious cement criteria of planar intercrystalline boundaries as well as enfacial junctions (see Dixon, 1983) are also more common in these mosaics relative to their neomorphic counterparts. Competitive growth fabric is rare and when it does occur it is crudely developed or immature (sensu Dixon, 1983). Solution unconformities are occasionally visible with CL in coarser crystals (Plate 35b).

Calcite cements contain few micrometre-size inclusions, are generally untwinned, and have straight extinction. Cements may be uniformly

non-ferroan or ferroan, or zoned, typically with a non-ferroan early stage and a late ferroan stage. Thin ferroan zones are rarely found in crystals that are otherwise non-ferroan.

The petrographic and luminescence characteristics of cement are generally constant within samples although some parallel- or cross-laminated grainstones demonstrate subtle variations in iron-content as well as zonation patterns between different laminations or in different parts of the same bed. These variations likely reflect permeability and porosity differences in the bed as a function of grain size and they imply the sediment was not cemented all at once.

8.2.2 Neospar

Neospar is differentiated from cement by the following characteristics:

(1) Intercrystalline "paste" is commonly prominent and crystals are easily differentiated from one another (Plate 34d).

(2) There is variability in facial development during the growth history of crystals, as revealed by CL. In the early stages of growth crystals tend to develop faces to a greater extent than later stages.

Development of anhedral shape during latter stages is commonly the result of discontinuous and unevenly distributed growth increments (zones) around the crystal, typically with preferential growth of crystals away from the centre of the bed or nodule (Plate 35e; 44a-b; 46f). Other neospar crystals demonstrate alternations of euhedral and subhedral faces during crystal growth (Plate 44a-d). Still other crystals are anhedral throughout their growth history.

(3) Neomorphic halos consisting of pseudospar up to 100 μm in size in a matrix of finer microspar occur around select grains. Folk (1965, p. 40) describes this microfabric as an "aureole of neomorphism".

(4) Crystal shape is generally anhedral for crystals smaller than 50 μm . In larger crystals, particularly those near the margins of beds or nodules, shape varies from euhedral, unit or acute rhombohedra to loaf-shaped crystals (Plate 35e, 46f) to crystals characterized by irregular, ameboid shapes, often in close proximity to one another.

In grain-supported sediments, neospar mosaics identified by the above characteristics are commonly less equicrystalline than cement mosaics. Neospar mosaics also tend to have obvious curved intercrystalline boundaries and lack enfacial junctions (Plate 34d).

The prominent intercrystalline paste which characterizes many neospar aggregates is interpreted to be the result of purging of impurities, such as clays and organics, from the growing crystals. Purging implies that the crystals are displacive on a microscopic scale; such occurrences, however, are conventionally regarded as neomorphic. Folk (1965) also considered purging of impurities to have been operative in the neospars of his study. With CL the intercrystalline paste contains numerous, blue-luminescent, micrometre-size specks which are interpreted to be detrital feldspar dust purged along with other impurities.

Poikilotopic enclosure of silt by neospar is uncommon.

In packstones, neospar spans the same range of crystal size as cement (25-150 μm). In wackestones and mudstones, however, the range is

considerably higher, from 10-300 μm , and mosaics often coarsen from the centres to the edges of beds or lateral margins of nodules (Plate 34e,f). As with cement, neospar contains few inclusions and may be uniformly non-ferroan, ferroan, or zoned from an early non-ferroan calcite to a late ferroan calcite. Extinction is generally sharp (cf. Bathurst, 1983b).

8.2.3 Timing: Evidence for Early Lithification

Equant calcite cement and neospar are interpreted to be the result of early, shallow-burial diagenesis based on the following evidence:

(1) Grainstone and mudstone clasts in conglomerates contain identical microfabrics and CL as their bedded counterparts. This implies that these sediments were lithified prior to incorporation into debris flows. In addition, mudstone clasts are commonly angular, and in rafts mudstone beds may develop a fracture cleavage, further suggesting early lithification (Chapter 2). Similarly, in synsedimentary shear zones, early-lithified beds fragment into slabs (Chapter 3).

(2) Although a rare occurrence, some nodular mudstones suggest exposure on the sea floor, thus indicating an early origin for these (Plate 53e,f). Details are provided in Appendix N.

(3) Mudstones to grainstones rarely demonstrate any evidence of mechanical compaction, implying early lithification (Chapter 5).

(4) CL zoning illustrates that mudstone substrates of DFC fringes were lithified prior to growth (e.g. Plate 43b). Similarly, the more ferroan Stage C luminescence of many DFC fringes on grainstone substrates cemented by less ferroan Stage B or C calcite indicates that porosity in

grainstones was entirely occluded prior to growth of the fringes. From field evidence, DFC fringes are interpreted as the product of shallow-burial diagenesis (Chapter 9).

8.2.4 Marginal Aggradation in Mudstones

Many mudstone beds and nodules are "marginally aggraded"; these mudstones are characterized by a coarsening of neospar crystal size toward the margins of the bed or nodule (Plate 34e,f; 35e; 37e,f). Some of these marginally aggraded beds grade further into fringes of displacive fibrous calcite (see Chapter 9); but the mudstone itself is identical regardless of whether or not subsequent DFC growth occurs. Marginally aggraded mudstones illustrate 2 fundamental relationships:

(1) Marginal aggradation is characterized by progressively fewer crystals separated from each other by increasingly greater amounts of intercrystalline paste. Some crystals are isolated.

(2) Accompanying the above change is a compositional change which almost invariably leads to progressively more ferroan calcite with later precipitation.

The first relationship is interpreted as the result of a decrease in nucleation density toward the bed margins. Marginal crystals grow to a large size simply as a function of available space prior to either impingement with neighbouring crystals or cessation of calcite precipitation.

Considering the second relationship, CL microstratigraphy illustrates that marginal crystals contain absolutely and proportionately more,

younger calcite than crystals at the centre of the bed or nodule. Many of these marginal crystals contain calcite at their centres with luminescence identical to that of crystals in the more finely crystalline parts of the bed. This critical observation indicates that the large marginal crystals do not develop at the expense of smaller ones.

Some mudstones contain continuous to discontinuous bedding-parallel laminations or millimetre-size patches of coarser neospar which differ from surrounding neospar by their larger crystal size, more prominent intercrystalline paste, and in some cases, later ferroan composition. These characteristics suggest they are the intra-bed equivalents of marginal aggradation. The laminations they form in otherwise monotonous mudstones is responsible for some of the vague bedding seen in some mudstones.

8.2.5 Discussion: Implications for Aggrading Neomorphism

8.2.5.1 Introduction

For Quaternary lime muds which are generally aragonite-dominated and contain smaller amounts of Mg-calcite and calcite, the range and variability of neomorphic processes [1] is relatively well-understood, having been observed by SEM in various degrees of completion (e.g. Steinen, 1978, 1982; Lasemi and Sandberg, 1984). Neomorphism in these

1. Definitions and related discussions are found in Appendix H.

sediments is controlled by the absolute and relative stabilities of the constituent particles in their ambient pore-waters. Recent studies have also shown that cementation in Quaternary lime muds is locally important (e.g. Steinen, 1978, 1979, 1982; Bhattacharyya, 1979; Lasemi and Sandberg, 1984).

As applied to most ancient carbonates, however, neomorphism, still appears to be truly a "term of ignorance" (Folk, 1965), a situation no doubt complicated by the wide variety of diagenetic environments in which it occurs, including: (1) meteoric-water diagenesis (e.g. Bathurst, 1975; Steinen, 1978); (2) while on the sea floor (e.g. Zankl, 1969); (3) during burial diagenesis (e.g. Longman, 1977; Bertrand et al., 1983); and (4) during re-exposure of limestones to surface weathering processes (e.g. Chafetz, 1972). Furthermore, interpretations based on Quaternary muds may not be applicable to some Paleozoic mudstones where calcite is suggested to have dominated organic as well as inorganic precipitation (see review in James and Choquette, 1983). Based on the presence of aragonite relics, Lasemi and Sandberg (1984) recently suggested that lime muds at least to the Ordovician may have been aragonite-dominated. Details concerning mineralogy and neomorphism of ancient lime muds, however, are still too meagre to safely generalize. Regardless of mineralogy, an even more fundamental uncertainty is whether smaller crystals were consumed to produce the resultant micrite, microspar, or pseudospar mosaic. The sequence of micrite to pseudospar is usually assumed to reflect increasing "maturity" of the sediment (e.g. Brand and Veizer, 1980).

8.2.5.2 Cathode Luminescence: Growth of Neospar

"Aggrading neomorphism" is defined as the process by which numerous, small carbonate crystals are recrystallized into fewer, coarser ones (Folk, 1965). This can occur along two possible pathways, either by porphyroid or coalescive neomorphism (refer to Appendix H). Although conceptually sound, definitive evidence of lime mud neomorphism having been arrested in intermediate stages is not found in ancient mudstones. The presence of micrite and microspar in the same sample does not necessarily imply microspar aggraded from micrite, although in many cases it is likely (e.g. Folk, 1965, figure 10c). All that is known with certainty is that some parts of the mosaic are now micritic, others consist of microspar (also see Lasemi and Sandberg, 1984).

Using CL would appear to be a reliable way to test whether coalescive or porphyroid neomorphic processes were operative by noting the critical relationships between an older, more finely crystalline mosaic and a coarser, younger one. If aggrading neomorphism is ever arrested in an intermediate stage, the replacement and corrosion relationships should be visible. For coalescive neomorphism, more finely crystalline (less evolved) and more coarsely crystalline (more evolved) mosaics could be characterized by calcites with differing luminescence. Porphyroid neomorphism should be especially straightforward to recognize.

CL data from the CHG strongly suggests that aggrading neomorphism, at least in the coarse microspar to pseudospar size-range, is not explained by either coalescive or porphyroid processes; but instead takes place by precipitation of progressively younger calcite on the margins of growing

beds and nodules. This is not aggrading neomorphism sensu stricto because there has not been any consumption of older, smaller crystals to form the coarser, younger crystals. This conclusion is based upon detailed and reconnaissance CL examination of more than 100 thin sections containing neospar, none of which revealed any evidence of a coarser neospar mosaic replacing a more finely crystalline one.

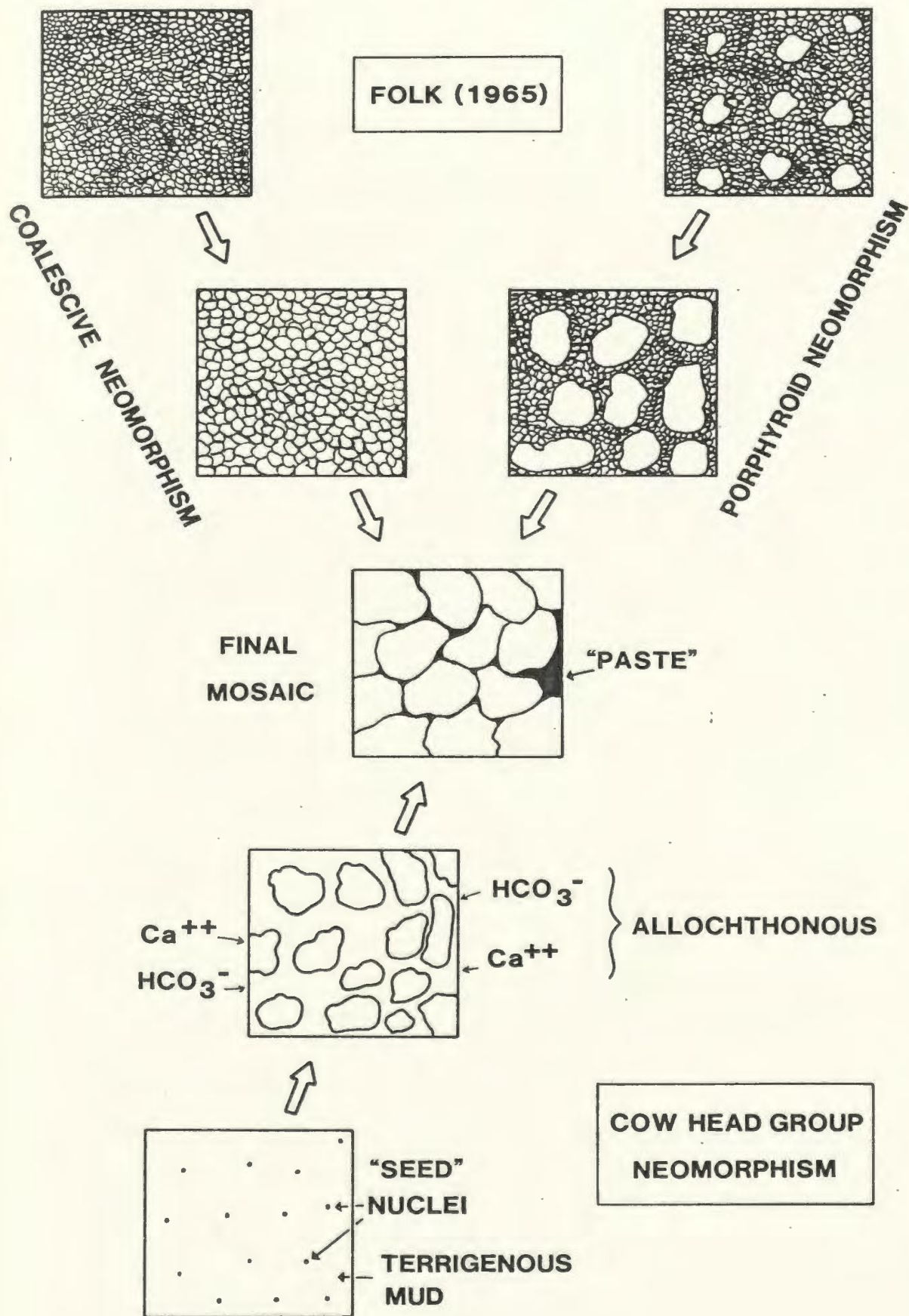
If the above observations are correctly interpreted, then it is apparent that calcium and bicarbonate ions must be allochthonous rather than derived from the gradual, in situ consumption of a more finely crystalline mosaic, as would be the case for neomorphic alteration (Figure 8.1). In Chapter 14 it is suggested that dispersed micrite-size crystals of calcite are dissolved and locally concentrated and reprecipitated to form calcite cement or neospar.

8.2.5.3 Other Ancient Examples of Aggrading Neomorphism

The lack of CL studies of other neospar precludes comparison with the CHG. The similarity of CHG microfabrics as revealed in transmitted light to those of other ancient mudstones, however, implies that relationships observed in the CHG are not unique. It is particularly relevant to note that some of the neomorphic microfabrics described by Folk (1965) are from mudstones, some of them nodular, associated either with interbedded shales or dispersed clays (Bathurst, 1975, p. 514). Many of Folk's (1965) illustrations of neomorphic microfabrics are strikingly similar to those of the CHG (e.g. fig. 12f in Folk, 1965).

Aggraded burrows and fossiliferous beds were noted by Tucker (1973) in

Figure 8.1: Schematic diagram of aggrading neomorphism by coalescive and porphyroid mechanisms according to Folk (1965) and aggrading neomorphism as it occurs in the Cow Head Group. Refer to text for details.



Devonian pelagic limestones of West Germany. Longman (1977) described coarsening of neospar crystal size around shale clasts and along contacts with interbedded shales in limestones from the Middle Ordovician Bromide Formation of south-central Oklahoma. Carozzi and Textoris (1967; their plate 48) illustrated "lenticular" calcite crystals which they interpreted as pseudomorphs after gypsum from the Devonian Jeffersonville Limestone of Indiana. Given the limited information available and the fact that these "pseudomorphs" are monocrystalline, these crystals could be original calcite pseudospar comparable to that found in the margins of some aggraded CHG mudstones. The SEM photographs of Fisher *et al.* (1967, figs. 85,87,88) clearly demonstrate irregularly-shaped neospar crystals with prominent scalloped margins within organic-rich, deep-water limestones of the Devonian Waterways Formation from Alberta. These and the equant to subrounded, loaf-shaped crystals up to 400 μm in diameter described by Tucker (1973) also resemble some of the coarser, more isolated marginal pseudospar in the CHG.

8.2.6 Conclusions

Equant calcite cement and neospar are both interpreted to be early, shallow-burial precipitates based on abundant evidence for early lithification of grainstones to mudstones as well as conglomerates. Using transmitted light microscopy in conjunction with CL, cement can be readily differentiated from neospar, but this becomes increasingly more uncertain with progressively smaller crystal size.

Marginal aggradation in mudstones, illustrating microfabrics

conventionally considered as those of aggrading neomorphism, is common and explained as the result of decreasing nucleation density toward bed margins in conjunction with precipitation of progressively younger calcite on the nuclei. Coalescive and porphyroid neomorphism as described by Folk (1965) cannot explain marginal aggradation in these mudstones and therefore aggrading neomorphism in the CHG, and possibly in other ancient sediments, is not neomorphism sensu stricto [2]. Precipitation of allochthonous calcite is responsible for crystal growth, not the in situ transformation of a more finely crystalline mosaic. It should be noted, however, that the above interpretations are based on neospar from argillaceous carbonates. This mechanism clearly does not apply to calcitization of aragonitic bivalve shells, for example, in which a more finely crystalline crystal mosaic (the original microfabric) is replaced by a coarser mosaic.

8.3 FRACTURE CALCITE

8.3.1 Introduction

Early lithification of limestones in the CHG implies that these sediments were brittle at the outset and fractures could have occurred and been filled with calcite at any time during the diagenetic history. Petrographic and CL study demonstrates this explicitly and samples with

2. For simplicity, the terms neomorphism, neospar, aggrading neomorphism, etc. will continue to be used, although these are not neomorphic sensu stricto processes or products.

two or more generations of fractures are not uncommon. Fracture calcite crystals are usually less than 500 μm in size; occasionally, some are as coarse as 1 cm. Intercrystalline boundaries are conspicuously planar. Ferroan and non-ferroan calcite are both equally common as well as zoned crystals characterized by later iron-enrichment. Most fracture calcites consist of dark, dull, or very weak orange-brown luminescent calcite.

Two end-member types of fracture calcite can be recognized, and to a first approximation, these correspond to early, shallow-burial diagenesis and later tectonism. Intermediate types are equally common, however.

8.3.2 Early Fracture Calcite

This type of calcite occurs in septarian cracks (Plate 12e), "ladder cracks" (Plate 11c,d; 46a), and V-shaped fractures on the margins of nodules (Plate 13e; 53a,e). Calcite cements in these fractures as well as in many of the ubiquitous millimetre-wide, penetrative fractures are similar to those in grainstones (discussed above) except for the larger crystal-size range and the more obvious planar intercrystalline boundaries. Crystals are usually unstrained, have minor or no twinning, contain few inclusions, and may be associated with scattered dolomite crystals which have nucleated upon dolomitic particles cut by the fracture.

8.3.3 Late Fracture Calcite

The best examples of late fracture calcites are found in tectonized

outcrops. This type of calcite does not occur in ladder cracks, septarian cracks, and V-shaped marginal fractures, but is found in many millimetre-wide, penetrative fractures. These calcites are often intensely twinned and have pronounced undulose extinction. These are interpreted as strain effects. Late fracture calcites are also inclusion-rich, occasionally form mosaics of lath-shaped crystals, and may truncate and displace vertical stylolites. CL characteristics are usually distinct from those of interparticle cement or neospar in the host sediment.

Fracture calcites having characteristics intermediate to those of the end members described above are common and their interpretation is usually equivocal. Some could also be early-diagenetic fracture fills which were enlarged or strained by subsequent tectonism or deeper burial.

8.3.4 Origin of Early Fractures

8.3.4.1 Septarian Cracks

The spindle-shaped fractures found in some mudstone nodules are interpreted to be septarian cracks (Plate 12e). The nodules resemble those described by Raiswell (1971a) but cracks from this study and Raiswell's (1971a) study have a simple fracture pattern which differs from the concentric and radial patterns which characterize more "classical" septaria (see illustrations in Richardson, 1919; Tarr and Twenhofel, 1932; Pettijohn, 1975). The ferroan calcite fill, and to a lesser extent, the pyrite fill, is typical of septaria. Previous

studies suggest that these fractures form in early-diagenetic concretions close to the sediment-water interface (e.g. Raiswell, 1971a; Lindholm, 1974; Baird, 1976). This early origin is also supported by their rare occurrence in CHG conglomerates and by stable isotope studies of this and other studies (see Chapter 11).

The origin of septarian nodules has been the focus of considerable attention, especially in the early 1900's; a concise review of the early theories of formation are given in Richardson (1919). The opposing views were shrinkage versus expansion, but most evidence appears to favour the former (Richardson, 1919; Lippman, 1955 - cited in Raiswell, 1971a).

Richardson (1919; p. 337) proposed that "cracking of the nodules is due to the dessication of a colloidal centre by chemical means." Raiswell (1971a) modified this basic idea and suggested the following origin (p. 156):

"The earliest growth stages of septarian concretions occurred in loose, uncompacted sediment and the growing concretion was hydroplastic, due to the lubrication of interparticle contacts by water films.... As the growth...proceeded, cementation occurred in compacted sediment with diminished hydroplastic properties and the outer concretionary layers were therefore more rigid than the preceding layers. The fissures then developed by water-loss and the subsequent contraction of the relatively hydroplastic concretion centre."

8.3.4.2 Ladder Cracks

The term "ladder cracks" is used in this study to refer to a series of evenly-spaced, parallel, spindle-shaped cracks whose distribution resembles the rungs on a ladder (Plate 11c,d; 53e). These cracks occur in thin grainstone dikes, burrow-fills, and laminations, and are always

encased in mudstone. Ladder cracks are also found in mudstone clasts within conglomerates and more rarely in mudstone-filled burrows. The cracks are typically 1-5 mm wide and are invariably oriented perpendicular to the dike, burrow, or lamination. The shape of these cracks resembles simple septarian cracks. They are widest within the dike, burrow, or lamination, and they wedge-out near the contact with surrounding mudstone. The crack is usually filled with equant calcite cement which may be predated by a thin crust of pyrite cement.

The origin of these cracks is uncertain. Based on petrographic and CL relationships, however, they are interpreted to be the result of minor displacive crystallization of the surrounding mudstone. CL microstratigraphy demonstrates that grainy laminations, burrows, or dikes are often cemented earlier than their associated mudstones. Later displacive growth in the surrounding mudstone results in the small tensional fractures in the earlier-lithified grainstone. An analogous situation is suggested for development in mudstone burrow-fills.

Ladder cracks strongly resemble tectonically-produced "microboudinage" described by Geiser (1974) in which rupturing of burrows perpendicular to length was attributed to horizontal compression. Such an origin for the ladder cracks of this study can be safely discounted for 2 reasons: (1) there are no other tectonic microstructures (e.g. stylolites) associated with ladder cracks, and (2) the calcite cement which fills these is smoothly transitional, in terms of staining and CL, from the host microspar.

8.3.4.3 V-Shaped Marginal Fractures

V-shaped, marginal fractures in nodules (Plate 53a,e) have been observed in other studies of nodular limestones and reflect "tension fracturing caused by preferential thinning between nodules and shear perpendicular to the fractures." (Wanless, 1983, p. 391). Presumably such fractures could arise at any time during the burial history of the sediments; from early (e.g. McCrossan, 1958; Fuzesy, 1980) to late burial (e.g. Hopkins, 1972, p. 82). Marginal fractures in the CHG nodules are interpreted to have been formed during shallow burial based on similarity of fracture cements to those which cement grainstones.

8.3.5 Conclusions

Early fracture calcite in septaria, ladder cracks, and V-shaped marginal cracks is commonly smoothly gradational in terms of staining and CL from grainstone cement or neospar of the host sediment. This suggests that the fractures and subsequent precipitate are also early, shallow burial features. Early fractures are formed in a number of ways: (1) septarian cracks arise by slight shrinkage of the centre of concretionary mudstone nodules; (2) ladder cracks arise by slight displacive crystallization of mudstone surrounding earlier-lithified laminations, burrows, or dikes; and (3) V-shaped marginal cracks arise by tensional fracturing of nodule margins during burial.

Late fracture calcites are multigenerational and usually distinct from cement or neospar in the host limestone. These crystals are commonly

strained and associated with tectonic folding and faulting. Fracture calcites with properties intermediate to those of early and late fracture calcite are common but their timing is not interpretable with any confidence.

8.4 CONGLOMERATE FIBROUS CALCITE

8.4.1 Introduction

The origin of matrix in most conglomerates is readily traced to the thinly-bedded slope limestones. These matrices consist of shale, marl, grainstone to mudstone including their dolomitized and silicified equivalents, equant cement, and neospar. In some conglomerates, however, the matrix consists in part of a fringe of conglomerate fibrous calcite ("CFC") apparently precipitated into an open framework of conglomerate clasts. Commonly associated with the fringe is dolomite, equant calcite cement, or internal sediment. These matrices have been found in only 3 beds at Cow Head North (Beds 2, 4, and 7); the most widespread occurrence is a 1 m-thick zone at the top of the Bed 2 conglomerate (Plate 32a,b).

These calcites are important because they are the only in situ fibrous calcite cements in the CHG. All other in situ cements are equant. RFC cements are transported into the slope environment within their host boulders, whereas DFC's are not cements. The relationship of CFC with internal sediments indicates a synsedimentary marine cement.

8.4.2 Petrography

8.4.2.1 Cement

CFC crystals vary from 5-10 mm in length and have length to width ratios of approximately 10:1. The crystals are length-fast, oriented normal to substrate, and form discontinuous to continuous fringes around pebbles and over earlier, internal geopetal sediments (Plate 32c; 33c,d).

Competitive growth fabric is obvious in many cases. Some fringes are isopachous, but more often they are not. One crystal usually spans the width of the fringe; however, some fringes are composite, being interrupted by thin, discontinuous layers of euhedral pyrite crystals, dolomite cement (Plate 33b), or internal sediment.

Intercrystalline boundaries are mostly jagged and characterized by micrometre-scale irregularities which appear to be controlled by cleavage (Plate 33b). Crystal terminations are commonly scalenohedral (Plate 33a-c), but where overlain by dolomite, are serrated due to local replacement by dolomite (Plate 33b). Extinction is typically sharp. The scalenohedral terminations along with sharp, unit extinction distinguishes these calcites from RFC.

Most inclusions are micrometre-size, have high relief relative to calcite, and appear to be solid. Twinning varies from absent to abundant (Plate 33a-d); in some fringes the latter is associated with stylolitization and suggests a deformational rather than growth origin. Inclusions are generally evenly scattered throughout the crystals, although in some samples, they are more concentrated in the latest

precipitates. CFC crystals do not demonstrate any evidence, such as fibrous inclusion patterns or internal, anhedral botryoidal growth surfaces, of having a more finely-fibrous microfabric (cf. RFC in Chapter 7 and DFC in Chapter 9).

These calcites are mostly non-ferroan; only rarely is there a thin, late, inclusion-rich, ferroan stage. With CL the earliest precipitates are dark or have dull luminescence and occasionally exhibit micrometre-scale zoning (Plate 27c). Later precipitates have weak to bright orange luminescence. The transition from the zoned, early precipitate to the outer, more luminescent calcite may be demarcated by an abrupt, irregular to scalloped boundary which suggests corrosion prior to renewed calcite growth. In other crystals, the transition is smooth and conformable.

8.4.2.2 Internal Sediments

Internal sediments which predate CFC comprise peloidal grainstones and packstones. These are either perched on top of pebbles in conglomerates (Plate 33c) or nested between the clasts (Plate 33d). Internal sediments postdating CFC are microspar mudstones and peloidal wackestones. These sediments may be replaced in part by isolated pseudospar crystals up to 1 mm in size or dolomite or both (Plate 33a; 35c). The pseudospar is anhedral to subhedral and tends to be ferroan when associated with the replacement dolomite. This dolomite is intensely zoned under CL, usually non-ferroan, and also replaces other types of limestone matrices besides internal sediments associated with CFC. This type of dolomite, including the cement, is the conglomerate matrix dolomite discussed in

Chapter 12.

8.4.3 Matrix Organization

Conglomerate matrices which include a stage of CFC precipitation have varying porosity-occlusion histories. The most complex matrix encountered in this study includes 6 stages of cementation and internal sedimentation: CFC (stage 1) encrusts conglomerate clasts and is overlain by a thin, discontinuous lamination of microspar internal sediment (stage 2) prior to renewed CFC growth (stage 3). The top of the fringe is overlain by more microspar internal sediment (stage 4) which is then followed by dolomite cement(?) with scattered pyrite crystals (stage 5). Remaining porosity is occluded by a coarse, blocky calcite (stage 6). A similar sequence but with a single CFC growth episode is illustrated in Plate 32c; 33c.

8.4.4 Interpretation and Discussion

The infiltration of marine internal sediments before and after precipitation of CFC suggests that the conglomerate was porous and in direct contact with the overlying seawater. Less compelling evidence of a submarine origin for CFC is based on a clast of conglomerate cemented by CFC within the Bed 2 conglomerate at Cow Head North. This clast clearly must have been lithified prior to its erosion and incorporation into the Bed 2 conglomerate (see figure 7 in James and Choquette, 1983). These sediments do appear to have undergone at least minor settling prior to cementation, however, as indicated by mudstone clasts with V-shaped fractures filled with CFC (Plate 32c).

Based on available literature, conglomerates with fibrous cement matrices are not common occurrences [3]. The most famous is the Scheck Limestone conglomerate of Austrian Jurassic. This 1-2 m thick conglomerate consists of reworked nodules cemented by RFC (Hudson and Jenkyns, 1969; Hudson and Coleman, 1978). As with CFC in the present study, the Scheck is clast-supported and contains internal geopetal sediments of marine origin. Isotopic analyses of the internal sediments and RFC support a marine origin for these components. Formation at depths of less than 150 m was suggested.

"Scheck"-type breccias also occur in Devonian stromatolitic and terrigenous marginal-slope deposits of the Canning Basin reef complexes (Kerans and Playford, 1984). These relatively thin (10-100 cm) breccias consist of clasts of mudstone and are clast-supported, inversely to normally graded, and contain perched and sheltered internal sediments of marine origin. These sediments are cemented by RFC and a fibrous calcite which petrographically resembles CFC from the present study [4]. Depositional depths were estimated at tens to hundreds of metres on slopes which range from 10-14 degrees.

3. Fibrous calcite-cemented conglomerates have been observed by the author in Cretaceous slope deposits in Oman as well as in Ordovician slope deposits from the St. Lawrence south shore in Quebec. The Quebec example exhibits microfabrics and dolomite identical to those of the CHG.

4. There is no mention of the latter fibrous calcite in the published abstract of Kerans and Playford (1984) - this information was made available at their poster session during the meeting for which the abstract was published.

8.4.5 Origin of "Scheck"-Type Conglomerates

The origin of the CFC-cemented conglomerates in the CHG is considered to result from dilation of the sediment during flow (Hiscott and James, in press). These authors hypothesize that dilation, which is due to intergranular friction, increases the volume of the debris flow, and matrix at the top of the flow is subsequently inhaled downward to fill the expanding intergranular spaces.

Another hypothesis to explain such deposits is that proposed by Kerans and Playford (1984) for the Devonian breccias - as bimodal density-modified grain flows. The breccias were deposited by frictional freezing and the residual, finer-grained flows continued to travel downslope leaving only minor perched sediments in their wake. Submarine cementation subsequently followed (Kerans and Playford, 1984).

In addition to the the above hypotheses, winnowing of an original matrix must also be considered. In Chapter 2 it was shown that density-driven currents have played a major role in sedimentation in the CHG. Presumably these currents could winnow finer matrix from debris flows as they passed over them (cf. Krause and Oldershaw, 1979; Mullins, 1983).

8.4.6 Conclusions

CFC is interpreted to be a synsedimentary (submarine) cement based on the presence of marine internal sediments which postdate and occasionally interrupt fringe growth. Internal sediments, as well as the precipitation of dolomite and pyrite, occasionally lead to pores with complex occlusion histories. CFC crystals are petrographically

distinct from RFC in the shallow-water boulders and, except for their elongate shape, these cements resemble more closely equant cements in grainstones and other conglomerates. The origin of the open framework conglomerates is uncertain but is most probably due to winnowing of the original fine-grained matrix by density-driven or other currents.

8.5 CATHODE LUMINESCENCE OF CALCITE

8.5.1 Luminescence Stages

Most calcite shows at least minor CL zoning, with colours typically ranging from orange-brown to orange to orange-yellow. Integration of data from cements and neospar defines 3 major CL stages which may be found in all sediment types (Plate 35a-e; Plate 46a-f).

Stage A is non-ferroan and non-luminescent or dull but may have micrometre-size, luminescent zones within. It is volumetrically minor and seldom dominates a cement or neospar mosaic.

Stage B calcite is the main luminescence stage of these calcites and ranges from weak orange-brown to bright orange or orange-yellow. Micrometre-scale zoning is common. Dull or dark zones are present but volumetrically minor. Stage B calcite may be non-ferroan or ferroan and there is no obvious correlation between stain-detectable iron content and luminescence intensity and colour.

Stage C calcite luminesces dull or weak orange-brown and is commonly ferroan. These may also show micrometre-scale zoning. Grain-supported

samples which are dominated by this type of calcite are especially difficult to study due to the similar luminescence of typical peloids and interparticle matrix.

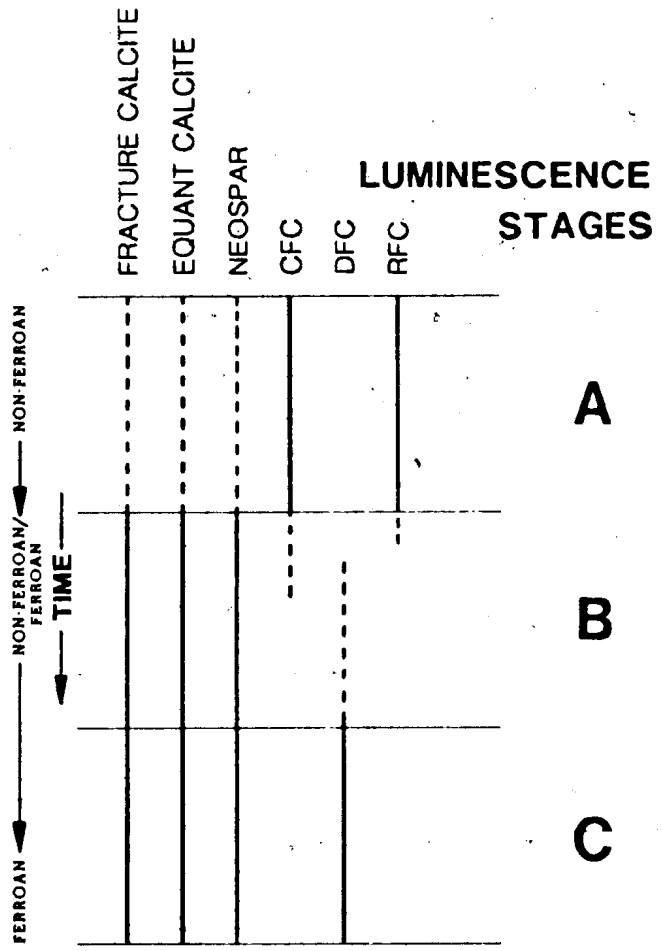
The transition between zones of contrasting luminescence may be characterized by (1) razor-sharp boundaries, (2) a gradual unidirectional change, or (3) a zone of micrometre-scale interbanding of the two adjacent luminescent zones.

Most cement and neospar mosaics consist largely of Stage B or Stage C calcite or both (Figure 8.2). Grainstones which show all 3 stages are typically dominated by Stages B and/or Stage C calcite with Stage A calcite relegated to thin rims around peloids (Plate 35a) and less commonly as syntaxial overgrowths on pelmatozoan and trilobite debris. The preferential overgrowth of these bioclasts has been termed "competitive cementation" [5]. These calcitic (Mg-calcite?) grains appear to have provided a convenient nucleus for precipitation prior to the attainment of conditions which allowed a more general cementation. These early-cemented grains fortuitously preserve the 3 luminescence stages of cementation history in a sediment that otherwise appears to be devoid of Stage A calcite. Similar competitive cementation by Stage B calcite occurs in mosaics dominated by Stage C calcite. Neospar crystals in which all three CL stages occur typically have a barely-resolvable Stage A calcite in the centres of crystals.

5. Competitive cementation was a term coined by L. C. Pray communicated to Bathurst (1975, p. 423) to account for the "observation that cements nucleated on different particles, and therefore on different substrates, occupy different volumes of the porosity."

7

Figure 8.2: Summary diagram of CL characteristics for various calcites encountered in the Cow Head Group.



The similarity of the CL properties of equant cements and neospar in the CHG clearly implies that they were precipitated from pore-waters of similar composition, and in samples which contain both cement and neospar, they are clearly synchronous precipitates.

The dark to weak-luminescence of the centres of CFC crystals and subsequent weak to bright orange-luminescence is considered to be equivalent to Stages A and B in equant cement and neospar. In the altered internal sediments associated with these crystals, the isolated, non-ferroan, pseudospar crystals are Stage B, and the ferroan crystals, including later, marginal ferroan zones, are Stage C.

CL of early fracture calcite may be identical to its host neospar or cement or more ferroan and less luminescent. In ladder cracks, for example, calcite may show luminescence Stages B and C whereas the associated grainstone cement and neospar is mainly Stage A (Plate 46a). Septarian nodules dominated by ferroan, dull-luminescent, Stage C calcite may have septarian cracks filled with more strongly ferroan, less luminescent Stage C calcite. The luminescence of calcite cement in V-shaped marginal fractures in nodules is often identical to the latest marginal pseudospar of the nodule, usually a ferroan Stage C calcite.

8.5.2 Cathode Luminescence and Trace Element Composition

The activating effect of Mn and the quenching effect of Fe on the CL of dolomite, and to a lesser extent calcite, is well established qualitatively (e.g. Sippel and Glover, 1965; Amieux, 1982; Frank *et al.*, 1982; Fairchild, 1983). The quantitative aspects of luminescence, however, are poorly known, especially for calcite. The complexity of

the variables involved and their mutual interaction likely accounts for variability in the empirically-determined luminescent fields (Figure 8.3; see recent discussion by Fairchild, 1983).

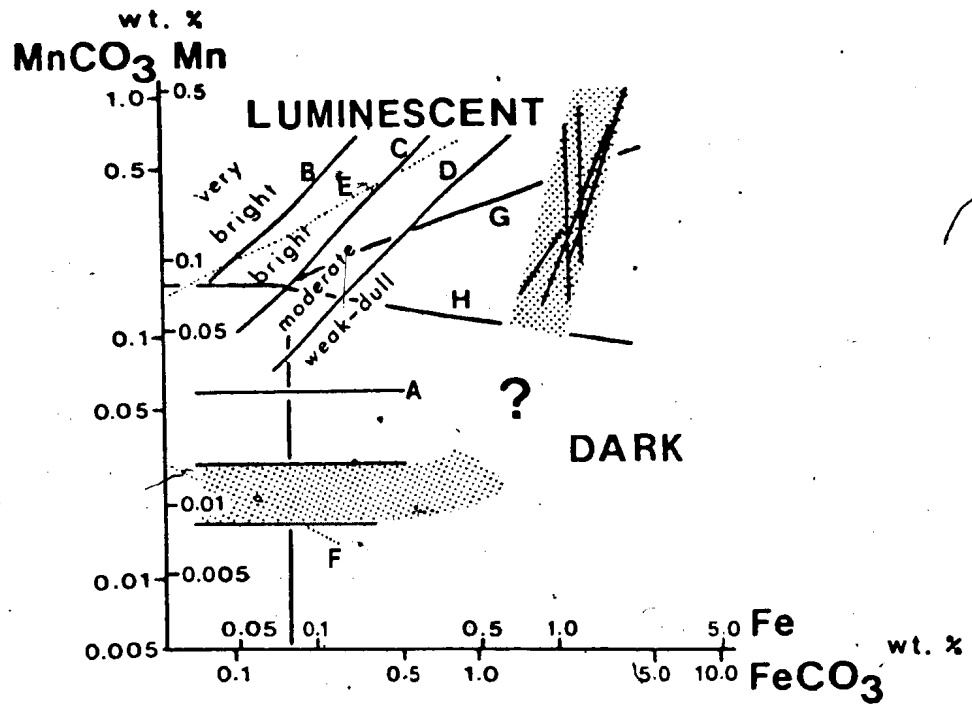
Semi-quantitative microprobe analysis (see Appendix I) for Fe and Mn in numerous calcite samples from the CHG suggests that the dominant controls on their CL are the relative concentrations of Mn and Fe (Figure 8.4). The role of sensitizers such as Ce and Pb (e.g. Machel, 1982) was not evaluated during this study. For concentrations of MnO less than 0.1 wt %, calcite is dull or dark, regardless of iron content. For concentrations greater than 0.1 wt % MnO and less than 0.3 wt % FeO, calcite is bright luminescent.

8.5.3 Discussion of Cathode Luminescence Trends

The sequence of CL stages observed in cements and neospar from the CHG is similar to that described from other studies of calcite cements (e.g. Meyers, 1974, 1978; Oglesby, 1976; Frank et al., 1982; Grover and Read, 1983). Comparable studies of neospar, however, are lacking and therefore the present study is unique in this respect.

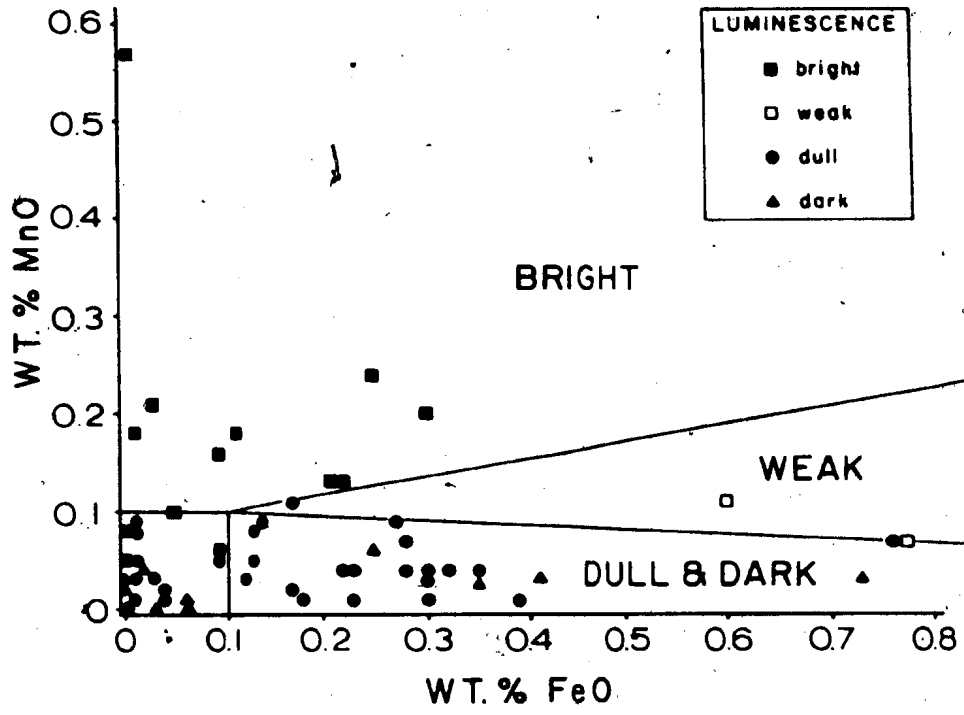
The transition from Stage A through C is most simply interpreted in terms of the evolution of pore-waters from initially oxidizing conditions to progressively more reducing with time. A model also incorporating the effects of dissolved sulphur content and to a lesser extent, pH, was proposed by Frank et al. (1982), based on the Upper

Figure 8.3: Summary of luminescence data for dolomite and calcite from literature survey. Dolomite: Stippled area denotes zone which separates luminescent from non-luminescent dolomite. Lines within and bounding stippled area are quench and luminescent lines from Pierson (1980), Fairchild (1983), and Frank (1981) as depicted in Fairchild (1983). Calcite: Line A is Mn activation line from Fairchild (1983). Below the line calcite is non-luminescent. Lines B, C, and D are approximations of boundary lines which separate luminescent fields in Frank *et al.* (1982). Fe/Mn (molar) ratios of lines B, C, and D are 0.5, 1.0, and 2.0, respectively. Line E is the approximate boundary which separates bright-luminescent calcite (above) from dull calcite (below) and line F separates dull calcite (above) from non-luminescent calcite (below) from Grover and Read (1983). Lines G and H are for calcites in the CHG; details are illustrated in Figure 6.4. Diagram is substantially modified from Fairchild (1983).



modified from Fairchild (1983)

Figure 8.4: Luminescence fields for calcite cement, neospar, and minor DFC from the CHG. This diagram outlines the positions of 3 luminescence fields - bright, weak, and dark and dull. The plot is based on 57 paired semi-quantitative microprobe analyses (see Appendix I), each of which is an average of at least 4 and as many as 10 individual spot analyses. Minimum detection limit for FeO and MnO is 0.1 wt %.



Cambrian Taum Sauk Limestone of southeast Missouri. In this model, bright-luminescent cements are precipitated from oxidizing or reducing solutions in which the Mn activator is incorporated into calcite but Fe forms either oxides/hydroxides or sulfides. In any case iron is not available for incorporation into calcite. In intermediate Eh conditions, both Mn and Fe are incorporated into calcite resulting in dull-luminescent cements. Extremely reducing (most evolved) fluids or extremely oxidizing (most pristine) fluids precipitate reduced or oxidized Mn and Fe compounds, respectively, with little or no Mn or Fe incorporated into calcite. Unfortunately, the difficulty in demonstrating co-precipitation of calcite with associated oxides or sulfides which act as sinks for Mn and Fe precludes rigorous practical testing of this model (Frank et al., 1982). Frank et al. (1982) also demonstrated that the Fe/Mn ratio affects luminescence and slight fluctuations in the relative amounts of Mn and Fe could account for the ubiquitous fine-scale zoning. Presumably similar fine-scale zoning might also reflect availability of Mn and Fe in pore-waters at constant Eh (see Meyers, 1978).

Variations of this model have been applied exclusively to diagenetic studies of shallow-water carbonate sequences (e.g. Meyers, 1974, 1978; Oglesby, 1976; Frank et al., 1982; Grover and Read, 1983). In these studies the sequence from oxidizing to reducing is interpreted to represent initial cementation in the oxidizing environment of the vadose zone - uppermost meteoric phreatic zone. With increased distance below the water table, ground waters become progressively more reducing and thus able to incorporate first divalent Mn and then both Mn and Fe into

the cements (also see Evamy, 1969; Champ et al., 1979). Phreatic ground waters may be of meteoric derivation (e.g. Grover and Read, 1983) or of meteoric-marine mixing zone origin (e.g. Oglesby, 1976; Meyers, 1978). Fine-scale zoning in the cements is usually interpreted in terms of the position of the paleoaquifer as controlled by sea level, or seasonal or other effects.

8.5.4 Conclusions

Based on CL examination of CHG calcites, the predictable sequence going from oxidizing at the outset to progressively more reducing also takes place during early diagenesis below the sea floor. Based solely on CL examination or staining, such sediments cannot be differentiated from those which have undergone meteoric to burial diagenesis or meteoric to mixed meteoric-marine phreatic diagenesis.

Chapter 9

DISPLACIVE FIBROUS CALCITE

9.1 INTRODUCTION

Displacive fibrous calcite ("DFC") fringes or veins commonly referred to as "beef" [1] and "cone-in-cone" [2] are common constituents of organic-rich shale sequences throughout the geologic column, from Precambrian to Tertiary, including marine and non-marine sequences (Woodland, 1964; Marshall, 1982). The association of DFC and organic material has been hypothesized for some time (Reis, 1962, cited in Richardson, 1923, p. 93; Brown, 1954; Mackenzie, 1972), and has been verified by stable isotopes (e.g. Hodgson, 1966; Campos and Hallam, 1979; Marshall, 1982; this study Chapter 11). Its tendency for widespread distribution in specific horizons has also made DFC an important stratigraphic marker in some outcrop and subsurface studies (e.g. Twenhofel and Tester, 1926; Mackenzie, 1972).

-
1. "Beef" was a term used by quarry workers in Dorset County to refer to fibrous calcite veins in strata of Purbeckian age (Chambre syndicale de la recherche, 1966, p. 229)
 2. The term is used to describe radiating or plumose aggregates of fibrous calcite crystals which form mutually interfering cones and in some cases are nested one inside the other.

Cone-in-cone was first described and illustrated in 1793 by Reverend Ure (Cayeux, 1935). The initial uncertainty regarding its inorganic or organic origin led Hildreth (1836) to consider it as a fossil columnar Madrepore and that "these fossils must have been among the first created animal productions of that ancient ocean..." (p. 100). With reference to the state of understanding of cone-in-cone by the middle 1800's, Sorby (1860, p. 124) stated that "no one appears to have...given any satisfactory explanation of its origin." Nearly 200 years after its formal introduction by Ure, Stoneley (1983), addressing the more fundamental origin of fibrous calcite in the first place, remarked "The difficulty in understanding the formation of these veins is knowing how the bedding planes were held or forced apart against the confining pressure of the overburden, to allow the mineralizing fluids to pass and the calcite to crystallize." (p. 1427).

The origin of DFC is neither simple nor straightforward, nor is there necessarily a unique origin [3]. An early or shallow-burial origin for DFC is suggested by most studies, based on association with pre-compactive or slightly compacted, occasionally septarian concretions and the demand for high plasticity in the surrounding shales to accommodate volume expansion (e.g. Richardson, 1923; Shaub, 1937; Woodland, 1974; Franks, 1969; Mackenzie, 1972). Other studies postulate a later diagenetic origin after the main phase of bacterial mediation of

3. In addition to calcite, other phases which demonstrate cone-in-cone structure include dolomite, gypsum, celestite (Cayeux, 1935), siderite (Hendricks, 1937), ankerite (Fuchtbauer, 1974), pyrite, and silica. The last two are generally thought to be replacements of calcite (Woodland, 1964; Love et al., 1983) although Hudson (1982) recently described pyrite with cone-in-cone structure which he interpreted to be original.

pore-waters, concretion formation, or even hydrocarbon emplacement (Fuchtbauer, 1974; Marshall, 1982; Stoneley, 1983).

Upon casual observation, DFC in the CHG appears to have only local significance, and is little more than an interesting diagenetic curio. Integration of field and petrographic observations, however, demonstrates DFC to be widespread both as: (1) "macro-fringes", which are macroscopically recognizable in most cases, and which are laterally continuous on thin section-scale, and (2) "micro-fringes" which surround granule- and sand-size argillaceous intraclasts in grainstones to mudstones. DFC is genetically linked to cementation and neomorphism in these sediments and it is therefore another important expression of early, post-depositional alteration in the CHG.

This chapter explores the nature of these intriguing calcites based on field and petrographic observations. Their CL, which has not been previously reported in the literature, provides additional insight into the mechanics of spherocrystal growth (see Chapter 7). Trace element and stable isotopic analyses are discussed elsewhere (Chapters 10 and 11). The following discussion is concerned primarily with the petrography of DFC in the macro-fringes. A brief discussion of DFC in micro-fringes is provided later.

9.2 FIELD RELATIONSHIPS

DFC fringes occur throughout the succession. Two localities were sampled intensively: (1) the Lower Ordovician sequence at Cow Head North, and (2) the Upper Cambrian and Lower Ordovician sequence at Green Point. Much of the following petrography relies heavily, though not exclusively, on information from these localities [4]. DFC is also found as scattered clasts in many conglomerates (see section 9.9.1).

DFC fringes vary from 1 mm to 5 cm in thickness and are attached to mudstone to grainstone "substrates" (on and/or under). Fringes which appear to lack an obvious substrate in the field often reveal in thin section the presence of millimetre-size or smaller silt laminations which have acted as substrate. As with the previously discussed nodular limestones, DFC fringes occur in discrete horizons, although individual fringes are rarely more continuous than 1 m in length. One particular fringe exposed along the wave-cut platform at Green Point was traced intermittently for 200 m.

Fringe - substrate relationships are variable and the spectrum of CHC occurrences is illustrated schematically in Figure 9.1. In planar and

4. The one single interval with the most abundant as well as variable fibrous calcite is from Bed 8.30 at Cow Head North. This 2 m thick sequence consists mainly of nodular mudstones up to 50 cm in length with subordinate grainstone beds. DFC is associated with many, but not all, mudstone and grainstone beds. Associated shales are black, fissile, slightly calcareous, and locally siliceous.

wavy beds, fringes over, under, or both over and under a substrate are equally common ("a" in Figure 9.1). In many outcrops, the cumulative thickness of substrate and fringe is often roughly maintained along strike. A typical example of this is a fringe on top of a bed which progressively thins with concomitant growth and increasing thickness of a fringe from the underside of the bed (a).

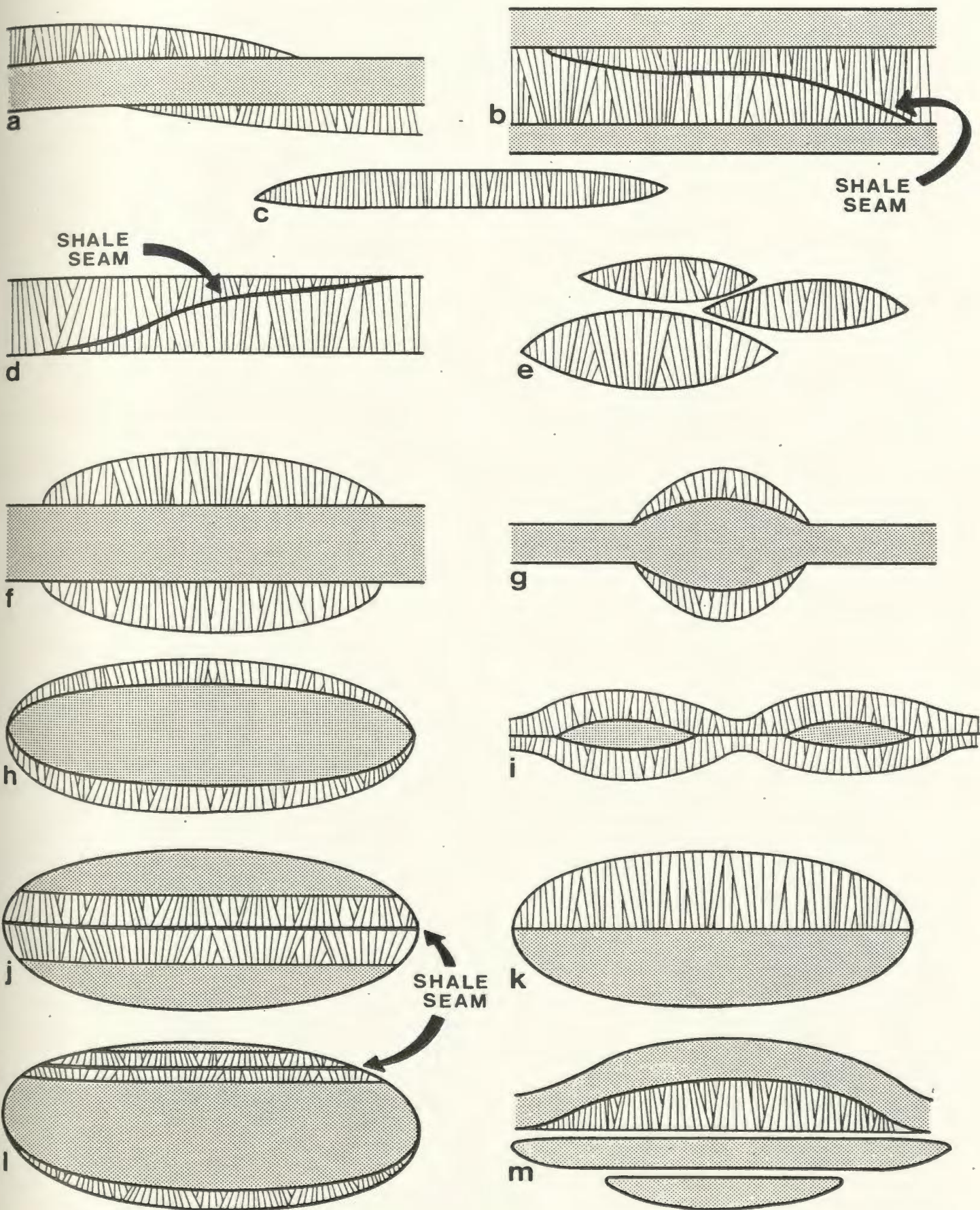
Conservation of fringe - substrate thickness is also exemplified by multiple fringes within parted limestones (b). In these, the multiple fringe is composed of a fringe nucleated on the underside of the upper bed and a fringe nucleated on the top of the lower bed. Fringes lacking (apparent or real) substrate are comparatively rare (c), and these, too may be multiple (d). In both of the above cases, the mutually interfering fringes meet along a medial shale seam. Occasionally, multiple fringes consist of fitted DFC lenticles separated from each other by shale seams (e). DFC may create relief in continuous beds which, otherwise, would be planar (f), and forms on and accentuates previous substrate swells in wavy beds (g).

Nodular beds demonstrate a comparable range of fringe - substrate relationships. Fringes commonly grow on and under a mudstone nodule and may be restricted to the nodule (h) whereas other fringes continue into the internodular areas (i) where they grow antitaxially (sensu Durney and Ramsay, 1973) from a medial shale or silty seam. Some nodules, like continuous parted limestones, contain an internal, multiple fringe of fibrous calcite with a prominent medial shale seam (j).

More complex fringe - substrate relationships are found but these are

Figure 9.1: Schematic summary of the various relationships observed between fringes of displacive fibrous calcite and its substrate. Letter labels are referred to in text. For scale, width of fringes is 5 cm.

DISPLACIVE FIBROUS CALCITE



comparatively rare. Three examples are illustrated in Figure 9.1. In the first (k), the upper half of a nodule consists of fibrous calcite whereas the lower half is mudstone. More complex relationships result where elements of the above variations are randomly combined (l, m).

9.3 PETROGRAPHY

9.3.1 Types of Displacive Fibrous Calcite

Two categories of DFC are differentiated based on their petrographic characteristics; for simplicity these are termed Types 1 and 2 ("DFC-1" and "DFC-2"). These calcites differ with respect to their crystal shapes, inclusion patterns, and extinction characteristics. DFC-1 is most apparent in the Lower Ordovician sequence at Cow Head North, whereas DFC-2 is found mainly, though not exclusively, at Green Point (Plate 36).

The most obvious difference between these calcites is the occasional presence of euhedral or subhedral terminations on DFC-1 crystals which contrasts with the typical anhedral terminations of DFC-2 (also see Tarr, 1932). DFC-1-type crystals have not been previously documented in the literature with the possible exception of the radial calcite aggregates described by Lindstrom (1979) from Lower Ordovician hardgrounds in Sweden. DFC-2, on the other hand, is the familiar "beef" which, in some instances, develops "cone-in-cone" structure. Fringes with characteristics intermediate to these two types are comparatively rare.

There is no difference in the mode of occurrence of either DFC-1 or DFC-2 fringes, except that DFC-1 clasts are more common than DFC-2 clasts in conglomerates and only DFC-2 fringes demonstrate curved crystals (discussed later). In the following discussion, DFC-1 and DFC-2 fringes are described together, noting separately any important differences.

9.3.2 General Characteristics

Size: DFC crystals may be as small as 150 μm in length and 25 μm in width to as large as 3 cm in length and 5 mm in width. They are typically narrowest at their bases and they progressively widen with progressive growth.

Crystal Terminations: The crystal terminations of both DFC-1 and DFC-2 are most commonly anhedral, and form: (1) one or several smooth, convex-upward, botryoidal surfaces (Plate 37a), (2) smooth or blunt surfaces (Plate 37b), or (3) several irregular, stubby projections (Plate 39e). DFC-1 crystals also may be characterized by rhombic or scalenohedral (steep rhombic) terminations or subhedral terminations (Plate 37a,c). Thin sections cut perpendicular to crystal elongation demonstrate that cross-sectional shapes are mostly anhedral.

Extinction: Extinction in DFC-1 and DFC-2 is usually sharp (unit extinction) or undulose with slightly divergent c-axes. In most cases the extinction sweep occurs within 10-15 degree rotation of the microscope stage. Similar extinction characteristics have been noted in other studies (e.g. Cayeux, 1935; Woodland, 1964). DFC calcites are

length-fast, although in some DFC-2 crystals, crystal length and c-axis are separated by an angle of up to 30 degrees.

Subcrystals: Many of the larger DFC crystals consist of several subcrystals up to 250 μm in width, each with its own slightly sweeping extinction. There is no correlation apparent between the positions of these subcrystals and inclusion patterns (discussed below).

Intercrystalline Boundaries: In both DFC-1 and DFC-2 fringes, intercrystalline boundaries may be planar (Plate 38d,e) to smoothly curved or wavy (Plate 37b,c,d; 39a; 40a), especially if they are surrounded by a prominent intercrystalline argillaceous paste. In other fringes, the lateral margins of the crystals are "stepped" or jagged due to groups of fibres with blunt terminations (see below) extending into the intercrystalline shale "paste" (Plate 39d,e; cf. "minor fractures" of Gilman and Metzger, 1967). Where stepped margins from one bundle impinge on another crystal, the shale is squeezed into "corrugated" patches (cf. Mackenzie, 1972, fig. 4). Other intercrystalline boundaries are concertal with mutual interpenetration up to 50 μm (Plate 38b). Within more obviously tectonized fringes of both DFC-1 and DFC-2 calcites, intercrystalline boundaries are microstylolitic.

Twinning: Both DFC-1 and DFC-2 calcites vary in their degree of twinning. Curved twins are rare and appear to be a strain feature related to tectonism. Twinning is not always pervasively developed within individual crystals but instead may be concentrated in the relatively inclusion-free centres of some crystals or may be patchily developed within crystals.

Iron Staining: DFC fringes are usually evenly ferroan, judging by iron stain and are considered to have late Stage C luminescence. In some cases, however, the fringe is non-ferroan at its base and grades upwards into more ferroan calcite. Non-ferroan fringes and fringes which grade from a ferroan base to a non-ferroan top are comparatively rare. Millimetre-wide non-ferroan zones are occasionally found in the last stages of growth in some otherwise predominantly ferroan fringes.

9.3.3 Inclusions

Inclusions in DFC appear to be identical to those found in calcite cements and neospar. Four types of inclusion patterns are recognized in these crystals, designated as Types A through D.

TYPE A: This inclusion pattern is characterized by a homogeneous distribution of inclusions throughout the crystal. However, their relative abundances vary in different samples.

TYPE B: In this pattern, inclusions are concentrated into bands parallel to the growth surface of the fringe. The surface morphology is typically irregular although occasionally there are smooth botryoidal surfaces (Plate 37a) and surfaces outlining former subhedral or euhedral terminations (Plate 38b). This type of inclusion pattern is also expressed in RFC (see Chapter 7). The Type B pattern is explained as the result of slight changes in physico-chemical conditions during precipitation of the fringe.

TYPE C: This inclusion pattern outlines elongate, relatively inclusion-free "cores" within DFC crystals, some of which extend for

most of their length. The cores vary in their abundance and size. Where only one or a few cores are present, their width typically varies from 200-400 μm . These cores may correspond to the subcrystals defined in polarized light. In crystals containing numerous cores, they are considerably smaller (25-100 μm wide) and are discontinuous in the two dimensional view of a thin section (Plate 38a). Regardless of their size, cores defined by the Type C pattern are usually less ferroan (and slightly more luminescent - discussed later) than the surrounding relatively inclusion- and iron-rich calcite.

These cores may be especially obvious in thin sections cut perpendicular to crystal elongation. Some DFC-1 crystals consist of 3 or 4 roughly circular cores joined together and surrounded by more inclusion-rich calcite (Plate 38c). Cross-sections of several DFC-2 samples demonstrate inclusion-rich trigonal-shaped centres which contain numerous small, circular to irregularly-shaped, inclusion-free cores outlined by inclusions (Plate 38e,f). The trigonal centres may be syntaxially enlarged by inclusion-free calcite until adjacent crystals meet along planar intercrystalline boundaries (Plate 38d,e) or enlarged further by inclusion-rich calcite (Plate 38f).

TYPE D: This inclusion pattern is the most common one and grades transitionally from the Type C pattern as the relatively clear cores diminish in size and become progressively less distinct. The Type D inclusion pattern consists of linearly-arranged inclusions which either splay from a medial inclusion trail which travels up the centre of the crystal, similar to the arrangement of the "hairs" on a feather, or the inclusions may radiate from a single point near the base of the crystal

(Plate 39a,d). In addition, at the tips of some DFC crystals, slivers of calcite project a short distance into adjacent shale and the thin inclusion-outlined fibres may be clearly seen (Plate 39b). The spacing of these fibrous inclusion trails typically ranges from 10-50 μm . As will be seen, this inclusion pattern indicates the presence of fine, fibrous crystallites only clearly visible with CL.

Distribution of Inclusion Types: DFC-1 may exhibit all 4 inclusion patterns whereas DFC-2 are mostly dominated by the Type D inclusion pattern and less commonly, the Type C pattern. In both types of calcite, crystals with the Type B inclusion pattern are rare.

9.4 CATHODE LUMINESCENCE

The common ferroan composition of these crystals renders many unsuitable for CL study (e.g. Plate 43a,b). CL zones which range in width from micrometre-size to millimetre-size are, however, detectable in some crystals, or certain parts of crystals. Growth surfaces delineated by fringe-wide changes in CL colour or intensity represent the surface morphology of a fringe at various times during its growth history.

As with crystal terminations, DFC-1 growth surfaces range from irregular, anhedral or botryoidal shapes to euhedral. Upon closer examination it is apparent that some of the euhedral faces are not truly planar but instead are slightly convex or gently undulating.

"pseudofaces" (Plate 46g). These "pseudofaces" are characterized by uneven, often sporadic, development of the youngest growth zones, a

situation similar to that described from neospar (discussed in Chapter 8). Some crystals demonstrate a tendency for the growth surface to become progressively more euhedral during subsequent growth, ultimately generating a crystal bearing a rhombic termination (Plate 41a-d; 46h). This relationship is not universal, however, and euhedral or subhedral growth surfaces may grade into progressively more anhedral surfaces, or euhedral and anhedral surfaces may alternate unsystematically (Plate 42a-d). In contrast to DFC-1, growth surfaces of DFC-2 are always anhedral, and occasionally botryoidal.

CL illustrates that portions of some DFC crystals consist of numerous, parallel-oriented to slightly diverging, fibrous crystallites 10 μm or less in width. Their orientation and size correspond to the Type D inclusion pattern. In many crystals, offsets of CL zones between adjacent crystallites or groups of crystallites result in the formation of pseudofaces or micrometre-scale irregularities on the growth surface (Plate 42c). Equant neospar within or transitional to a DFC fringe may also be characterized, either throughout or just on their margins, by a parallel or radiating Type D inclusion pattern (Plate 39c), micrometre-wide fibrous crystallites, and CL zone offsets (Plate 43c,d; 44a-d; 46e). In other DFC crystals as with most neospar and RFC (see Chapter 7), crystallites are not apparent and growth surfaces appear smooth.

9.5 FRINGE ORGANIZATION

Fringes may be simple, in which one calcite crystal spans the width, or they may be complex where numerous, parallel-oriented crystals nucleated continuously during growth of the fringe, with very few crystals, if any, spanning the width of the fringe (Plate 36d). Discontinuities within fringes marked by termination of crystal growth and renewed nucleation upon, but independent of the crystallographic orientation of, the older crystals are comparatively rare (Plate 36b,c; cf. Marshall, 1982).

Both DFC-1 and DFC-2 fringes may be composed either of pallasades of elongate crystals (mostly DFC-1; Plate 36a, 37b,c) or numerous, interfering bundles of crystals, which in shape and distribution, resemble the wool tufts in a hooked rug (Plate 36b,c,d). Radiating bundles are also found in fringes which are otherwise dominated by a pallasade of crystals. Although present in both DFC-1 and DFC-2 fringes, radiating bundles are only well-developed within DFC-2 fringes. The apices of the bundles or "cones" (see below) are invariably pointed toward their substrate and occasionally the bundles form raised circular areas on the surface of the fringe ("pustulate protuberances" of Kendall and Simpson, 1974).

Most fringes are characterized by competitive growth fabric where smaller, more equant, and more variably-oriented crystals progressively yield to fewer, more elongate, and larger crystals in a pallasade or

radial arrangement (Plate 36c; 37c). The degree to which the competitive growth fabric is developed varies and in some fringes it is absent.

The radiating bundles are comparable to the "cone-in-cone" structure described from numerous other localities (e.g. Woodland, 1964; Franks, 1969 and references therein) where bundles of crystals form mutually interfering cones and in some cases are nested one inside the other; the latter are truly cones inside of cones. Good examples of the nested cone-in-cone variety have not, however, been recovered from the CHG.

Not all fringes consist of well-organized pallasade or "coned" crystals. Other fringes contain only scattered rosettes of elongate crystals or isolated crystals oriented normal to bedding, both of these being surrounded by coarse, equant pseudospar (Plate 37f). Equant pseudospar ranging from 100-1000 μm in size also may: (1) overlie a DFC fringe (Plate 37e); (2) occur as irregularly-shaped, millimetre-size patches within fringes; or (3) form linear trails between DFC crystals (Plate 37d).

9.6 TRANSITION FROM SUBSTRATE TO FRINGE

Many samples exhibit a gradual transition from marginally-aggraded, coarse, equant pseudospar to DFC in terms of crystal size, shape and orientation; iron stain; CL (Plate 43a,b); and stable isotopes (Chapter 11). Equant pseudospar may evolve into elongate DFC crystals by further precipitation of calcite preferentially toward the margins of a bed or toward shale intraclasts. This leads to obvious asymmetric zoning

within individual crystals (Plate 44a-d). Iron stain and CL of DFC fringes nucleated on grainstones are commonly smoothly gradational from the interparticle cement.

In some samples, isolated rosettes and single elongate DFC crystals have identical staining and CL properties as their surrounding equant pseudospar matrix. In other samples, staining, CL, and stable isotopes of pseudospar and DFC are similar even though they occur on opposite sides of a bed (Plate 37e,f).

A peculiar microfabric seen in some mudstones which aggrade into DFC fringes do so via a transition zone of numerous bedding-parallel, calcite lenticles which are closely fitted to one another and are separated by a prominent, interlenticular paste (Plate 40b). These lenticles, which may be either monocrystalline or polycrystalline, reach up 1 mm in length and 250 μ m in width.

9.7 NATURE OF ASSOCIATED SHALE

Shales which overlie or underlie DFC fringes are identical to those described in Chapter 2. These shales are always black or green; DFC is never in contact with red shales. Millimetre-thick shale seams are also important components within DFC fringes. Horizontally-oriented shale seams occur at the junction of two inwardly-growing fringes (Plate 37b,c) or act as a common substrate for two oppositely-growing fringes (Figure 9.1b,d,j,l). U- or V-shaped seams outline and separate cones from one another. Vertical shale seams or patches of shale also form the intercrystalline paste between individual DFC crystals or associated pseudospar.

9.8 DISPLACIVE ORIGIN OF FRINGES

These fibrous calcites are displacive in origin, having pushed aside adjacent terrigenous muds and other insolubles during their growth in order to make room for themselves. This interpretation is based on the relative lack of siliciclastic silt within the fringes relative to the adjacent shales; shale paste caught between the elongate crystals of the fringe; and numerous other straightforward petrographic relationships, such as the occurrence of fringes surrounding mudstone nodules, which preclude a pore-filling origin. There is no evidence to suggest that the origin of the fringes is related to the filling of sheet-cracks (e.g. Kendall and Tucker, 1971; Tucker, 1973). Other studies have used other lines of evidence for a displacive origin, including the displaced upper and lower surfaces of trilobites, ammonites, and fossil fish (Brown, 1954; Woodland, 1964), and floating grains, suggesting an expanded detrital framework (Franks, 1969).

Some grains, however, were not pushed aside during fringe growth. Scattered grains of siliciclastic silt, up to 20 μm in size, are poikilotopically enclosed by some DFC crystals, but their abundance is considerably smaller than that in the adjacent shale or limestone. Non-ferroan, anhedral to subhedral dolomite crystals are also randomly scattered in DFC crystals although in some, dolomite is crystallographically controlled and therefore likely authigenic. One

fringe was observed to contain scattered, variably-preserved, calcite-replaced radiolaria in which the replacement crystals were syntaxial with the enclosing DFC crystals (Plate 40a; cf. Mackenzie, 1972 [5]).

9.9 EARLY ORIGIN OF DFC FRINGES: FIELD EVIDENCE

Several lines of evidence, used jointly, indicate that DFC is the product of early diagenesis, probably formed within 10 m of the sediment-water interface.

9.9.1 Fibrous Calcite Clasts

The strongest evidence for an early diagenetic origin is that DFC is found as clasts in conglomerates. These occurrences include: (1) nodular mudstone clasts with a peripheral fringe of DFC (Plate 45a); 10 cm-size or smaller pebbles, both with and without a substrate (Plate 45b); and parted mudstone rafts which contain DFC (Plate 45c). Only the pebble-size clasts are common, however. That the fringes are not in situ growths within conglomerates is suggested by the lack of fringes on adjacent pebbles as well as the improbability of DFC fringes having grown in conglomerates with grainy matrices.

9.9.2 Curved Crystals

Several DFC-2 fringes consist of crystals which are conspicuously curved

5. Mackenzie (1972) described unidentified thin-walled spherical bodies approximately 200 μ m in diameter within a DFC fringe which could also be radiolaria.

(Plate 45d,e). The curvature may begin at the base of the fringe or curvature may be apparent only near the upper portion of the fringe, the lower portion being straight and normal to its substrate. Curvature is usually not apparent in the field; it is most readily observed in slabs or thin sections.

Crystal curvature is interpreted to result from growth during synsedimentary shear related to submarine sliding (refer to Chapter 3). To test this hypothesis, two DFC fringes with obvious crystal curvature were measured in the field (Plate 45d). Assuming crystal curvature reflects relative movement of an upper pile of sediments over a lower stationary one, the upper sediment mass was translated eastward [6]. This sense of movement is consistent with an east to southeast dipping paleoslope as determined independently by other means (discussed previously).

Curved DFC have also been reported in other studies. Kendall and Simpson (1974) suggested the curved crystals from the Upper Cretaceous Medicine Hat Sandstone of the subsurface of southwestern Saskatchewan resulted from lateral shearing during expansive crystallization, which also caused micro-imbricate thrusting of the fringes. Marshall (1982) proposed a similar cause and suggested local stress conditions, possibly resulting from the crystallization itself, to have caused the curved crystals.

6. These fringes are from the Upper Cambrian strata at Green Point (units 7 and 8). Directions of 54 degrees NE and 110 degrees SE were measured.

9.9.3 Truncation Surface Deformation

The fragmented and rotated mudstone slabs which underlie the prominent truncation surface at Lower Head contain minor DFC-2 calcite (Plate 45f). These fringes are developed patchily on one or both sides of the mudstone fragments with crystals oriented normal to their substrates, regardless of slab orientation relative to bedding. The patchy distribution of the fringes is unlike those typically encountered in undisturbed sediments, and suggests a syndeformational origin.

Other evidence to suggest a syndeformational origin is based on a discontinuous DFC fringe which intersects the truncation surface southwest of the outcrop depicted in Figure 3.1a in Chapter 3. Within this otherwise unremarkable fringe is found a spherulite of DFC-2 calcite (Plate 45g). Such a radial arrangement of crystals is not recorded from any of the undisturbed fringes and suggests a syndeformational origin.

In both of the above examples, DFC growth is not considered to be post-deformational based on the assumption that properties of the strata return to their predeformed state afterwards and therefore only, undisturbed "normal" DFC growth could occur.

9.10 MICRO-FRINGS OF DISPLACIVE FIBROUS CALCITE

9.10.1 Introduction

Micro-fringes of DFC are developed around shale intraclasts, and together with the intraclast, they form a distinctive "grain" that is a common constituent of many limestones in the CHG (Plate 40c,d). The recognition and proper interpretation of these ubiquitous "grains" is important because they indicate that displacive crystallization is a common diagenetic process, to a much greater extent than would be inferred from the abundance of macro-fringes of DFC [7]. This microfabric does not appear to have been previously recorded in the literature, except possibly by Morawietz (1961, fig.2a) at the base of a cone-in-cone fringe. The poor quality of his published photograph, however, does not permit a more certain assessment. Based on reasoning analogous to that used to indicate a displacive origin for macro-fringe DFC, the shale intraclasts are interpreted to have been compressed during growth of the micro-fringe. Similar micro-fringes grow into discontinuous shale seams within some limestone beds. The origin of these shale seams is uncertain - they may be either shale flasers or large, squashed intraclasts.

7. Reconnaissance petrography of calcite-cemented sandstone concretions from the Tourelle Formation in Gaspe (see Hiscott, 1977) demonstrates that micro-fringes of DFC also occur here.

9.10.2 Petrography

Micro-fringes are usually spanned by only one crystal. Crystals composing micro-fringes vary from 35-125 μm in length and 10-35 μm in width; only rarely are they as large as 500 μm in length and 125 μm in width. Some micro-fringes lack obvious elongate crystals, consisting of equant 40-50 μm -size crystals instead. This, however, may be due to a thin section orientation effect. Fringes are seldom evenly distributed around the shale intraclast; more often crystals are perpendicular to the clay platelet foliation of the shale intraclast and only minor or no calcite grows parallel to the plane of the foliation. Crystal terminations and cross-sections through the fibrous crystals range from anhedral to euhedral, and in some cases irregular, skeletal extensions of the crystals branch into the shale intraclast. Some of the larger crystals demonstrate a fibrous inclusion pattern similar to the Type C pattern recognized in the macro-fringe DFC crystals.

9.10.3 Iron Content and Cathode Luminescence

Micro-fringe DFC consists mainly of non-ferroan calcite but many crystals have a latest stage iron enrichment. In this respect these are similar to or more "evolved" than their surrounding neospar or cement matrix, much in the same way as macro-fringe DFC relates to its substrates. These calcites are commonly bright-luminescent and become dull near their tips, indicating that most represent CL Stages B and C (Plate 51e,f). As with macro-fringe DFC, micro-fringe DFC commonly grades smoothly from the host neospar or cement crystals, both in terms of iron content and CL properties. In many instances, micro-fringe DFC

is syntaxially developed upon neospar or cement substrates, pelmatozoan debris, and trilobite fragments. Micro-fringe DFC demonstrates prominent CL zoning, variable facial development during growth of the crystal, and CL offsets. The similarity of DFC microfabrics in both the macro- and micro-fringes is due to their common displacive origin, which, in some cases, can be demonstrated with CL to be contemporaneous.

9.11 INTERPRETATION AND DISCUSSION

9.11.1 Interpretation of Microfabrics

The presence of fibrous crystallites in some parts of DFC crystals, especially near their terminations, and the variation in growth surface morphologies and crystal terminations indicates that these crystals have a complex origin. DFC crystals or portions of DFC crystals showing evidence of fibrous, micrometre-wide crystallites along with anhedral and occasionally botryoidal growth surfaces are readily interpreted to have grown as spherocrystals. This contrasts with "unit" crystal growth which lacks crystallite development but instead exhibits euhedral terminations or internal growth surfaces. These crystals appear to consist of one continuous, uninterrupted lattice. Crystals showing anhedral growth surfaces and planar zones or crystal boundaries imply that they grew as composite crystals - in part as spherocrystals and in part as unit crystals.

Discussion of composite crystals, spherocrystals, and split-growth has been presented in Chapter 7 and the reader is referred to this source

for background. The following interpretations are based mainly on information from DFC macro-fringes. These interpretations are also applicable to micro-fringe DFC as well as pseudospar exhibiting similar properties to DFC.

Extinction and Subcrystals: The sharp to slightly undulose extinction in most DFC crystals is readily explained by unit crystal growth or spherocrystal growth in which asymmetric growth has been relatively unimportant, otherwise the pronounced undulose extinction of RFC or FOC might be expected (see Chapter 7). As suggested for RFC, subcrystals are interpreted to be the result of crystallite bundles of slightly varying orientation. The cause of the initial grouping into separate, but approximately similarly-oriented bundles is uncertain, although slight misorientations could have occurred during the early stages of crystal-splitting, as Kendall (in press) suggested for RFC subcrystals. The origin of these subcrystals also explains the Type C inclusion pattern.

Intercrystalline Boundaries: Concertal and irregular, intercrystalline boundaries in DFC are, in most cases, attributable to the interference of individual crystallites or groups of crystallites from the juxtaposed major crystals. This effect is clearly seen in some samples in which DFC crystals are separated from one another by a shale paste and the jutting-out of groups of crystallites, as defined by the Type D inclusion pattern, creates a prominent step-like surface on the side of each major crystal (Plate 39d). Where crystallites are more or less parallel to major crystal elongation, as is commonly seen in some DFC-2 crystals, intercrystalline boundaries are correspondingly smoother. The

remarkably planar boundaries between some DFC crystals are interpreted as compromise boundaries between unit crystals.

Crystallites: The Type D inclusion pattern is the result of inclusions caught between the crystallites or small groups of crystallites. These crystallites are interpreted to be primary rather than relicts of some neomorphosed fibrous precursor. Their primary nature is suggested by the sharpness of CL zoning and the unlikely possibility that neomorphism could occur and still retain such exquisite zoning detail. In addition, the CL zoning is fringe-wide. Alteration of the DFC fringe by the migration of a neomorphic front starting at the base does not explain the same zoning sequence observed in associated pseudospar crystals in which zones are concentric, although commonly quite asymmetric.

9.11.2 Controls on Growth Surface Morphology and DFC Type

The shape of crystal terminations and internal growth surfaces as revealed by CL range from euhedral to anhedral. Crystals demonstrating anhedral or botryoidal surfaces which grow into more euhedral surfaces or terminations with progressive precipitation, or the opposite change, imply that the physico-chemical conditions of precipitation evolved unidirectionally. At times growth as spherocrystals was encouraged and, at other times, unit crystal growth occurred. Unsystematic fluctuations in these conditions are presumed to account for unsystematic changes in the nature of the growth surface. As for RFC, a major uncertainty in understanding this type of growth is how spherocrystal growth eventually transforms to unit crystal growth in which the major crystal is able to grow by discrete face-wide increments.

As for RFC, the transition from spherocrystal to unit crystal growth is likely regulated, in part, by the physico-chemical conditions of precipitation. Kendall (in press) suggested for RFC that the degree of solution saturation or the concentration of minor ions could control the type of crystal growth, whether spherocrystal or unit crystal. The fact that these calcites are displacive in origin suggests that the physical and chemical characteristics of the enveloping terrigenous muds, including lithostatic pressures, may also influence the growth surface morphology and perhaps other petrographic characteristics of DFC crystals. Theoretical determinations (Kamb, 1959) indicate that the c-axis in calcite grows preferentially in the direction of highest stress; DFC crystals are at least responding in orientation, if not also in habit, to lithostatic factors.

The almost total restriction of DFC-2 calcites to Green Point suggests that local, early diagenetic conditions are somewhat unique, at least with respect to the formation of DFC-2. Nucleation density may also be important as to whether precipitation of DFC-1 or DFC-2 occurs. If the nuclei are spaced far apart, the radiating aspect common to the DFC-2 and other cone-in-cone calcites will be encouraged (Fuchtbauer, 1971). Where nuclei are close together, a pallasade arrangement of crystals will be preferred.

In most samples examined in this study, staining and CL evidence indicates that growth of DFC postdates marginal aggradation of mudstones as well as cementation in grainstones. In some samples, however, it is evident that pseudospar and DFC growth was synchronous, occurring either together in the same fringe or on opposite sides of the same bed. A similar situation occurs for micro-fringe DFC and its enclosing

pseudospar or cement. The identical CL and staining of the pseudospar and DFC crystals indicate that they were precipitated by identical pore-waters but extremely local conditions must have determined whether the growth habit was to be the elongate DFC crystal or more equant pseudospar. The presence of compressible terrigenous muds next to limestone beds and clay intraclasts within beds appears to be a controlling factor as to why DFC precipitates where it does; but why DFC in some cases and coarse marginally-aggraded pseudospar, in others, is not certain.

9.11.3 Implications for Neospar as Composite Crystals

An uncertainty in the present understanding of DFC is whether the presence of non-planar growth surfaces implies spherocrystal growth, even though there is no fibrous inclusion pattern, nor are crystallites discernible with CL. Not only is this an important question for the origin of DFC, but it is also of fundamental importance for the understanding of more conventional neomorphism in general. From Chapter 7 it was concluded spherocrystal growth occurs in RFC although it characteristically does not show a fibrous inclusion pattern (see Kendall, in press) or CL-visible, micrometre-wide crystallites. By analogy, this must be considered as a likely possibility in DFC and neospar lacking evidence of spherocrystal growth, either by a fibrous inclusion pattern or CL-visible crystallites.

Except for coarsely crystalline neospar associated with DFC fringes,

neospar crystals in general have neither CL-visible crystallites nor spherulitic, radiating inclusion patterns. The fact that crystals which do show crystallites and a radiating inclusion pattern are intimately associated with pseudospar lacking these but which are otherwise identical in terms of shape, CL-zoning, and staining (e.g. Plate 44a), suggests that neospar, in general, also grew in part as spherocrystals. The lack of resolvable crystallites in many DFC and most neospar is explained as a result of the extremely small size of these crystallites in conjunction with even, crystallite growth-rates. The even growth rates discourage both the formation of CL zone offsets as well as the trapping of intercrystallite inclusions necessary to produce the inclusion patterns.

If the above suggestion that neospar grew in part as spherocrystals is true, other aspects of aggrading neomorphism in general are more readily explained. These are briefly discussed below.

(1) By analogy with DFC crystals, growth of neospar by the same mechanism may account for the displacement (i.e. "purging") of impurities, notably clays, in neospar mosaics of this as well as in numerous other studies (e.g. Folk, 1965, 1970; Chanda, 1967; Weider and Yaalon, 1974; Bathurst, 1975). Physical displacement of solids is also possible, however, with non-fibrous crystals (e.g. Steinen, 1982).

(2) The irregular, commonly scalloped, and embayed outlines of many neospar crystals and their irregular, uneven CL growth zones are also readily explained by a spherocrystal growth mechanism in which different bundles of crystallites within a major crystal grew at different rates.

This type of uneven spherulitic growth could account for complex interlocking boundaries and ameboid fabrics seen in other neospar mosaics (e.g. Fisher et al., 1967; Steinen, 1978, 1979; Bhattacharyya, 1979).

A fibrous crystallite microfabric in neospar was also noted by Folk (1971) in bladed, neomorphic calcite crystals formed in the clay-rich portions of a rock of unknown origin. These crystals were circular in cross-section, were patchily distributed in a more finely-crystalline, microspar matrix, had undulose extinction, and consisted of poorly-defined coalescing fibres. Some of these crystals tapered at their ends and others splayed out "like a worn toothbrush" (Folk, 1971, p. 163).

9.11.4 Origin of DFC and Cone-in-Cone Structure

It is not intended to review the numerous explanations for DFC and especially cone-in-cone structure that have been suggested during the last 200 years; there are several outstanding works which provide detailed and critical reviews of these hypotheses. Notable among these works are Cayeux (1935), the classic monograph of Woodland (1964), and Franks (1969). During the last decade or so there has been only a handful of studies on DFC (e.g. Mackenzie, 1972; Kendall and Simpson, 1974; Marshall, 1982).

A partial list of the various hypotheses concerning the origin of DFC and cone-in-cone structure and the authors which support or partially support them, though not necessarily are the originators of the

hypotheses, includes the following: organic origin (Hildreth, 1836); aragonite to calcite transition; result of gas rising through muds, or dewatering (Shaub 1937); dilational fracture fills (Twenhofel and Tester, 1926, Shearman et al., 1972; Stoneley, 1983); and displacive crystallization (Woodland, 1964; Mackenzie, 1972, Kendall and Simpson, 1974; Marshall, 1982). The fibrous nature of the calcite crystals prompted some authors to infer an aragonitic precursor (e.g. Brown, 1954; Mackenzie, 1972) and even aragonite with minor vaterite. The presence of vaterite was based on associated calcite crystals exhibiting radial or "spherulitic" extinction (Gilman and Metzger, 1967; also see Fong and Hesse, 1982).

The current model for the formation of DFC and more specifically cone-in-cone structure is summarized by Woodland (1964) and restated by Franks (1969). DFC and the cone-in-cone structure are interpreted to result from concretion growth in which stress produced by the overlying beds results in the displacive precipitation of the calcite [8], and accounts for its orientation, growth characteristics, and ultimately the cone-in-cone structure. The time of precipitation is considered to be during early diagenesis under a small sediment load, as confirmed in this study by field and geochemical relationships (discussed in Chapters 11 and 14). Whether or not cones form and their attributes, such as size and apical angle, are thought to be a function of the chemical

8. Durney (1976) defines such "pressure growth" as the "synkinematic additive overgrowth crystallization of a mineral at a grain contact subjected to 'pressure'". The term pressure growth replaces the ambiguous "force of crystallization" and is independent of idioblasticity.

conditions of precipitation as well as shale properties, especially plasticity. Based on Kamb's (1959) work illustrating preferential growth of the calcite c-axis in the predominant stress direction, and for successively younger crystals to lie at angles of up to 25-30 degrees to the original host crystal, displacive precipitation ultimately yields the conically-shaped tufts of DFC crystals. Lateral stresses induced by displacive precipitation crystallization probably also contribute to the formation of cone structures (Kendall and Simpson, 1974).

Woodland (1964) invoked the necessity of some compaction, although minor, to have already taken place in the shales because he thought that stratiform layers of DFC would not precipitate in a homogeneous, watery mud. This reasoning is far from convincing, however, as the CHG sediments and most other shales contain silt laminations or other bedding-parallel heterogeneities which could readily localize and control the precipitation of DFC layers parallel to bedding.

The early origin for DFC, based primarily on field relationships and geochemical evidence, is also supported by Reikes principle which states that the solubility of many minerals, including calcite, increases with increasing pressure. Therefore, DFC precipitation becomes increasingly more unlikely with increasing burial pressure. This pressure is transmitted to the crystal through a water layer only a few molecules thick (Weyl, 1959). For displacive crystallization to occur, the tendency for dissolution must be surmounted by a sufficiently high flux of solute ions toward the crystal (Weyl, 1959). An brief review of experimental and theoretical literature concerning displacive

crystallization is provided in Assereto and Kendall (1977) and the reader is directed to this source for further information.

Shallow burial ideally meets the necessary conditions for displacive growth of calcite. The overlying seawater column, anaerobic decay of organic matter, and possibly dissolution of dispersed CaCO_3 provide a ready source of solute ions. Shallow burial also implies that surrounding muds are largely uncompacted and therefore permeable, allowing solute ions to easily migrate through. These uncompacted muds also easily accommodate displacive crystal growth.

9.12 SUMMARY AND CONCLUSIONS

DFC growth is a significant diagenetic process in the CHG. Macroscopic fringes of DFC grow on both continuous and nodular beds, with crystals oriented in pallasade fashion or as a series of mutually interfering cones. Micro-fringes of DFC are ubiquitous and are identical, both genetically and in terms of microfabric (where assessable), to the macro-fringes of DFC. Based on staining and CL, DFC grew during the later stages, or as a continuation, of marginal aggradation in mudstones and cementation in grainstones. Why DFC grows on some beds and not on others is uncertain although the juxtaposition of DFC against easily-compressible terrigenous muds appears to be a necessity. Petrographic evidence indicates that DFC calcites are displacive, but minor poikilotopic enclosure of silt grains and scattered radiolaria also occur.

DFC are interpreted to have been precipitated during shallow burial. This is indicated by the incorporation of DFC clasts in conglomerates and by the distortion of DFC fringes by synsedimentary shearing. An early origin is also supported by stable isotopic data (see Chapter 11).

A fibrous, radiating inclusion pattern and the presence of crystallites visible with CL suggest that DFC grew as spherocrystals at times, and as unit crystals at other times, with both types of growth often occurring within the same crystal. The sharp CL zoning and presence of micrometre-size zoning offsets indicate that these crystallites are primary and not a relict of neomorphism. Growth surfaces on crystals vary from euhedral when growth occurred as a unit crystal to anhedral, and occasionally botryoidal, when spherocrystal growth occurred. The control of whether spherocrystal or unit crystal growth occurs is uncertain, although crystallization rate and the presence of impurities may be important.

Neospar associated with DFC occasionally also shows spherulitic inclusion patterns and crystallites. It is suggested that other neospar crystals also grew as spherocrystals only that the small size of their crystallites as well as their even growth rates precludes straightforward detection. It is suggested that fibrous microfabrics and spherocrystal growth are more widespread than is generally apparent.

Chapter 10

CALCITE TRACE ELEMENT GEOCHEMISTRY

10.1. INTRODUCTION

Authigenic calcites in the CHG are commonly non-ferroan in their early stages but become ferroan in later stages, ideally evolving through CL Stages A to C (Chapter 8). In context of the CL trends and the spectrum of previously discussed diagenetic calcites, the purpose of this chapter is to describe and interpret elemental oxide profiles as a function of progressive precipitation.

Microprobe analyses were carried out using a 10 second counting time, a 2 μm beam diameter, and for Fe and Mn, non-carbonate standards. Mg was standardized on dolomite. As such these analyses are considered to be semi-quantitative. Nevertheless, the overall relative increases or decreases of Fe, Mn, and Mg with progressive precipitation are considered to be real. Operating conditions for the microprobe analyses are discussed in Appendix I, reproducibility of analyses is demonstrated in Table I.8.

Intracrystalline trace element variations (Mg, Fe, Mn) were analysed in polished thin sections by automated microprobe traverses, usually from their centres (cores) or bases to their rims or tips (Figure 10.1a-i; step analysis paths and CL characteristics are shown in Plate 46.). The

selection of crystals for microprobe analysis and traverse paths followed CL examination. Individual traverses consist of 5-25 equidistant points, depending on crystal size. After microprobe analysis, samples were reexamined with CL to determine the exact position of analysis spots within CL zones.

Bulk samples of calcite were also analysed by atomic absorption spectrophotometry (AAS) of HCl acid leachates for all major elements (see Appendix I) but only the results for Fe, Mn, and Sr are reported. Mg concentrations as determined by this method are judged to be unreliable due to contamination by finely crystalline dolomite also dissolved in the leachate. The elements Na, K, and Al show strong positive correlations with Si, indicating a significant contribution of these elements by the leaching of clays and perhaps feldspars. On the other hand, the correlation of Fe and Mn with CL properties, staining, and microprobe analyses indicates that contamination of Fe and Mn by leached insolubles is not a problem, nor does original Sr appear to be significantly contaminated. These elements all show poor correlation with Si.

10.2 MAGNESIUM

Most calcites contain 0.5 wt % MgO or less; concentrations as high as 1 wt % MgO are relatively rare. In both pseudospar and equant cement, MgO content is highest in the centres of crystals and gradually decreases toward the edges to 0.1-0.2 wt % or below the detection limit (a,b,c,e in Figure 10.1). CFC calcites are uniformly low in MgO, generally less than 0.2 wt %. MgO depletion with progressive crystal growth is,

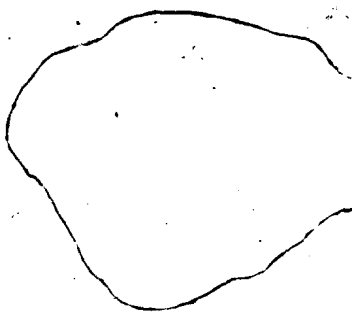


Figure 10.1: In this figure are plotted microprobe step-traverses across selected cements, neospar, and fibrous calcites. "i" is an exception however (see caption). The analyses points for each traverse are plotted on the X-axis. On the Y-axis is the wt % oxide for MgO, MnO, and FeO. Cathode luminescence descriptions are provided at the top of each plot - the abbreviation "M.Z." refers to "multi-zoned". All of the step-traverses as well as the CL characteristics of the crystals are shown in Plate 46. Sample location and age data are also provided in the caption to Plate 46.

(a) Cement in septarian ladder crack in parted mudstone dominated by CL Stage A microspar. The analysed cement crystal clearly demonstrates an MgO-rich, non-luminescent, CL Stage A calcite with low FeO and MnO and increases in these elements along with concomitant decrease of MgO in later (Stages B and C) precipitates. Traverse length is 91 μm .

(b) Intraparticle cement in intact brachiopod shell. MgO decreases with successive precipitation and FeO and, to a lesser extent MnO, increase. Traverse length is 304 μm and goes from CL Stages B to C.

(c) Pelmatozoan fragment and syntaxial cement overgrowth. The earliest cement is characterized by an increase in MgO over the levels present in the pelmatozoan, but these relatively high levels fall off with the latest precipitates. MnO and FeO are both low in the pelmatozoan and only MnO is present in any significant amount in the earliest cement. Traverse length is 195 μm and goes from CL Stages B to C.

continued on next page

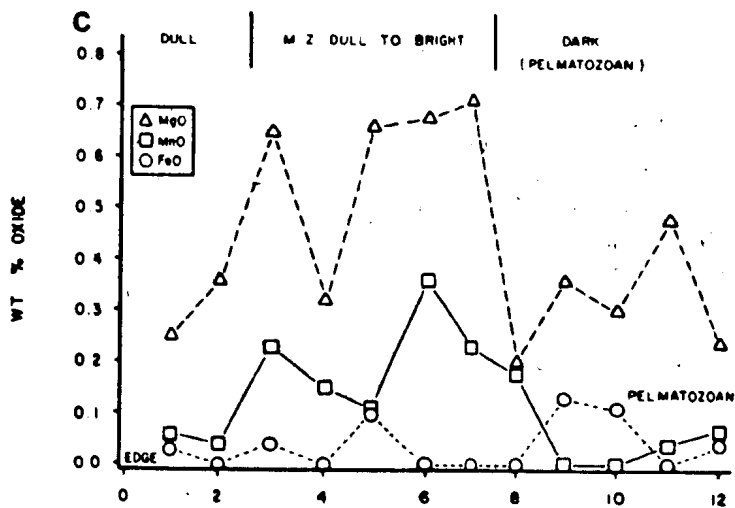
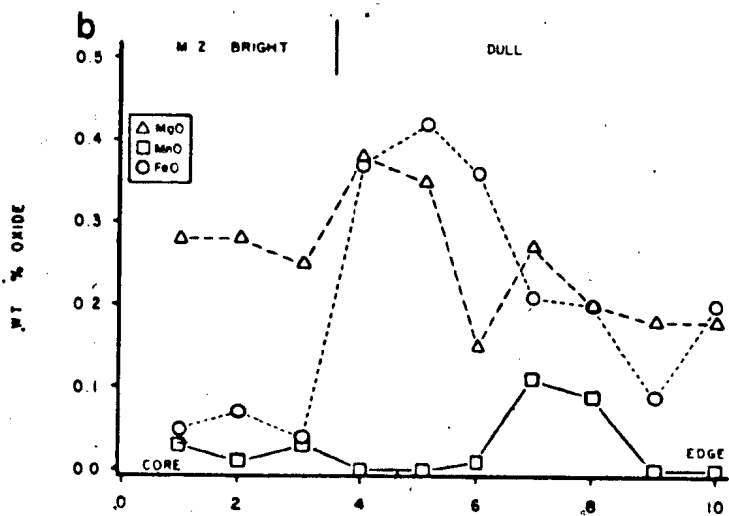
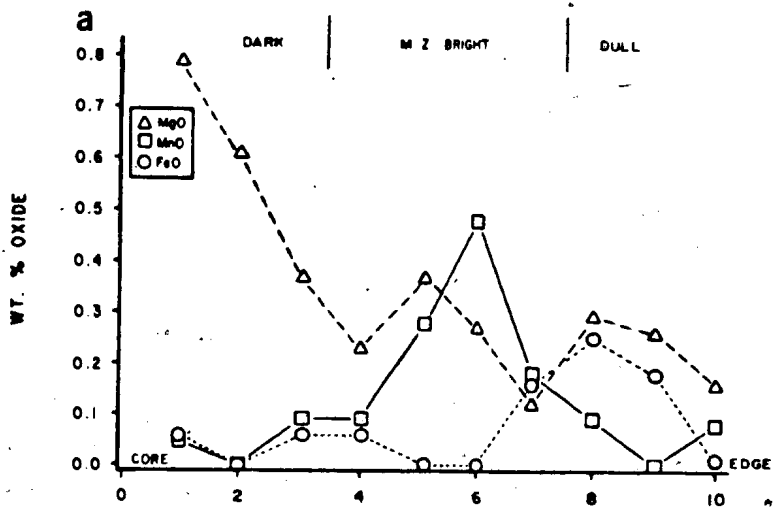


Figure 10.1 (continued)

(d) Cement in conglomerate matrix. This sample demonstrates that the earliest, non-luminescent precipitate is depleted in all the trace elements, but with later precipitation, MgO, and in the latest stages, FeO, are important. Traverse length is 341 μm and goes from CL Stages A to C.

(e) Coarse neospar at the base of DFC-1 demonstrates a general decrease in MgO with successive precipitation and a concomitant increase in FeO. The latest calcite also shows an increase in MgO. Traverse length is 271 μm and is mostly within CL Stage B calcite.

(f) Isolated, floating pseudospar crystal on lower margin of marginally-aggraded mudstone. This traverse demonstrates a slight increase in MgO with successive precipitation and decreases in MnO and FeO. FeO increases slightly near the margin of the crystal. Traverse length is 108 μm and goes from CL Stages B to C.

continued on next page

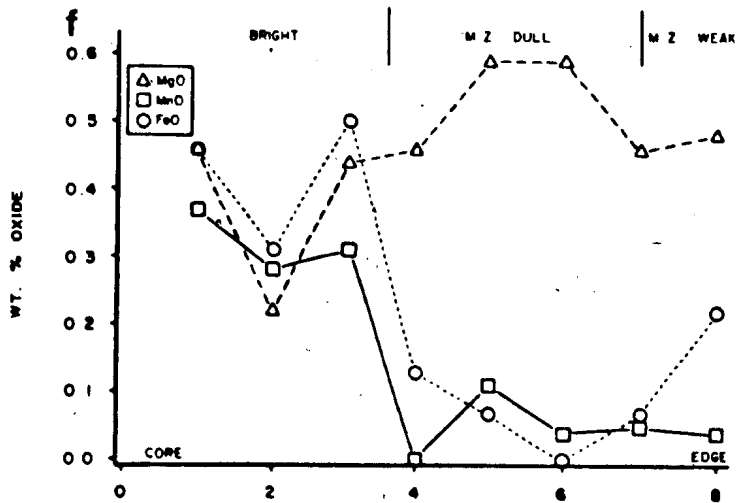
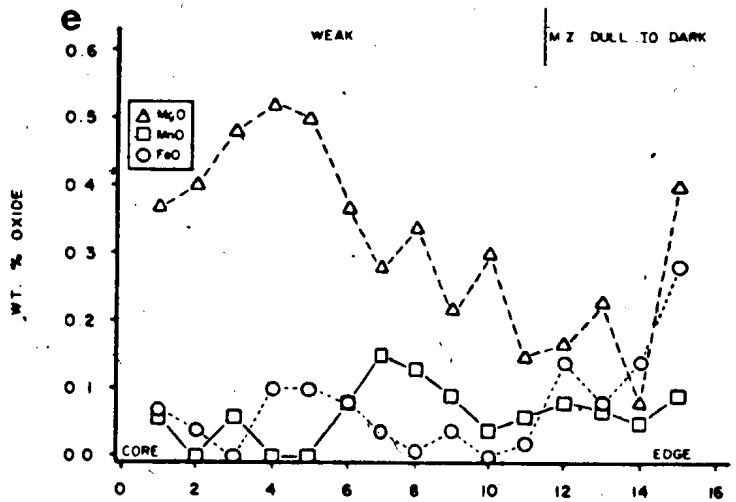
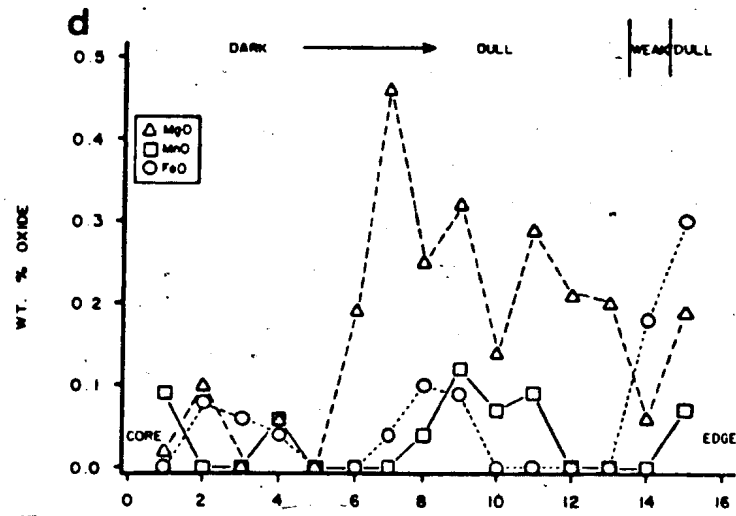
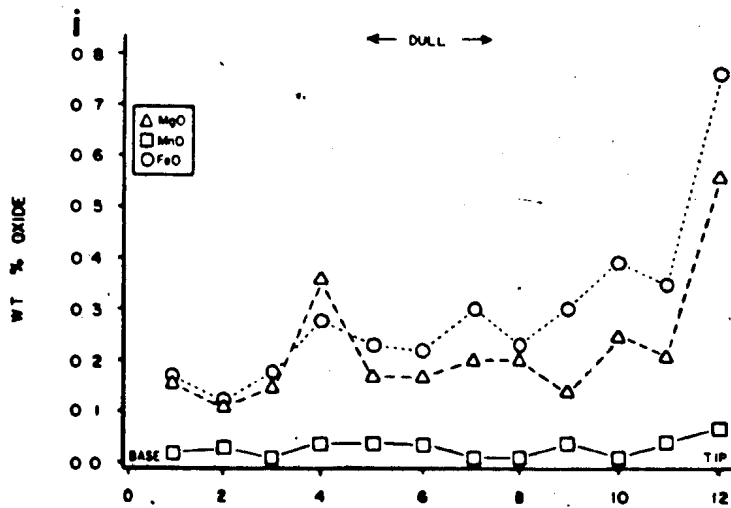
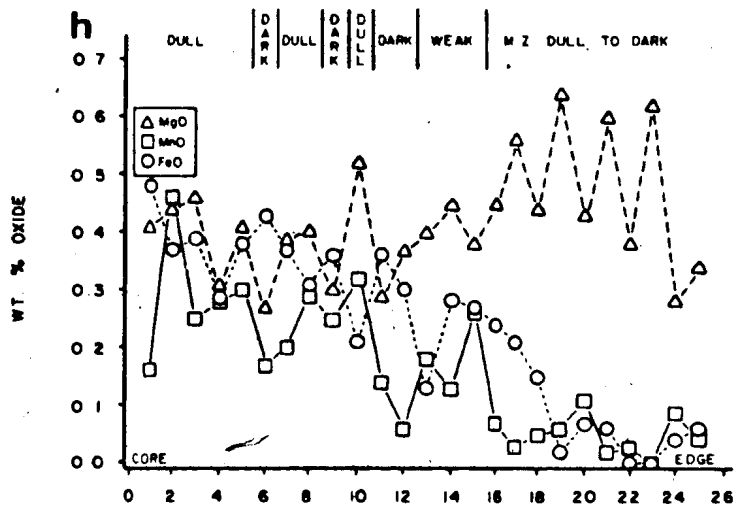
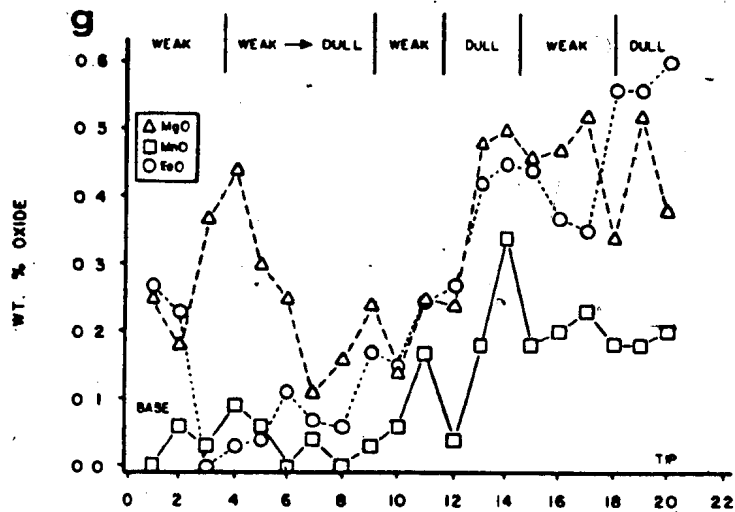


Figure 10.1 (continued)

(g) DFC-1 fringe at base of grainstone. With successive precipitation, MgO, FeO, and MnO all increase. Traverse length is 813 μm and goes from CL Stages B to C.

(h) Termination of DFC-1. MgO increases slightly toward margin whereas both FeO and MnO decrease. Traverse length is 1052 μm and is mostly within CL Stage C.

(i) DFC-2 (no complimentary CL microphotograph in Plate 46). Each point is an average of 3 closely-spaced analyses. Points are evenly-spaced over a distance of approximately 1 cm. MgO and FeO both increase in the latest precipitate. MnO remains below the detection limit. Traverse is mostly within CL Stage C calcite. Green Point, Upper Cambrian, unit 8, sample GP-3-A.



however, not universal. In the youngest zones of some coarse pseudospar crystals, the MgO depletion trend ceases and MgO contents gradually increase (Figure 10.1e,f). Other crystals of cement and pseudospar have approximately constant or irregularly varying MgO as well as FeO and MnO. Constant, irregularly varying, or increasing MgO content also characterizes DFC where concentrations of up to 0.7 wt % MgO occur (Figure 10.1g,h,i). As with other elemental oxides, MgO fluctuates considerably, especially so in samples with obvious fine scale CL zoning (e.g. Figure 10.1h).

10.3 IRON

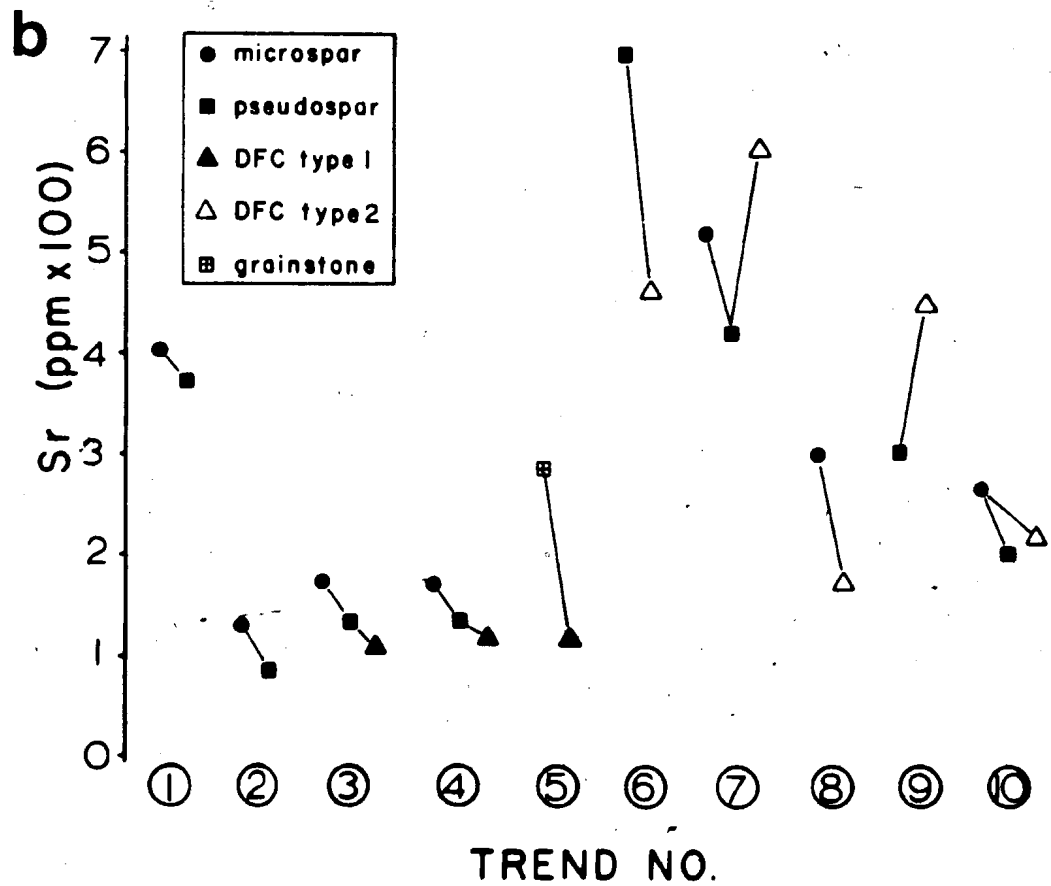
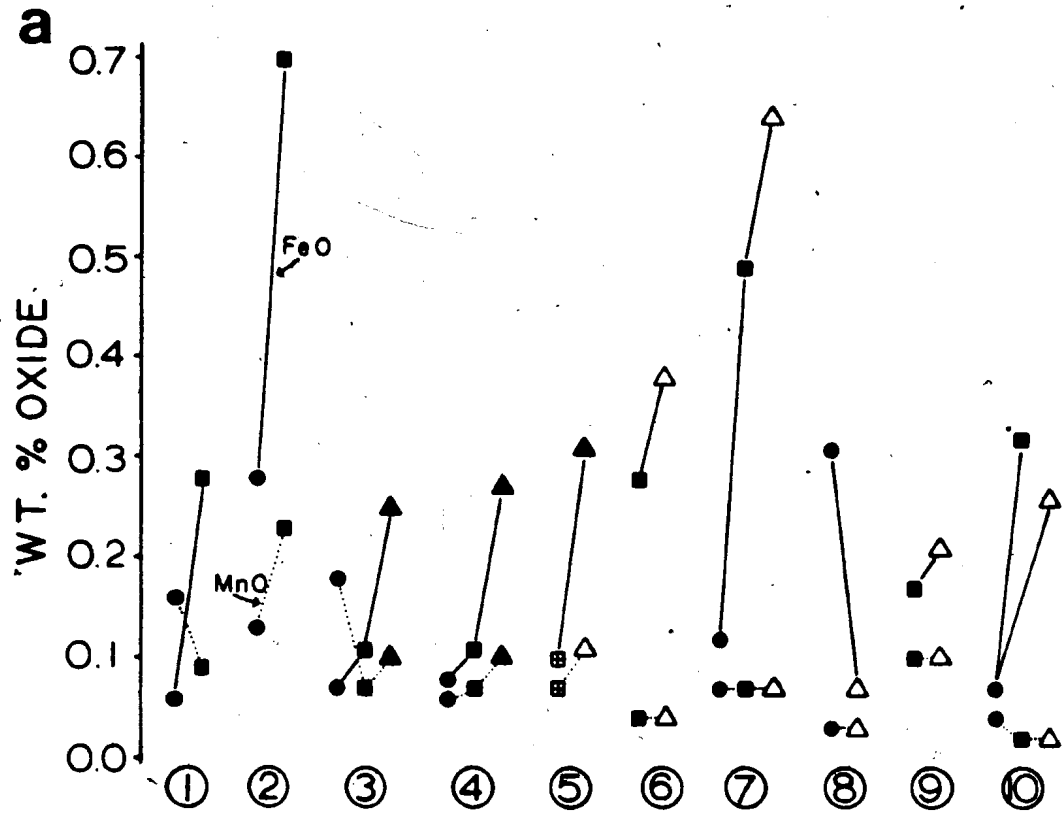
FeO contents typically range from below the detection limit to 0.5 wt % [1]. As indicated by staining, later growth stages in many cement, pseudospar, and DFC crystals are ferroan (Figure 10.1a,d,e,g) and coarse pseudospar and DFC are often completely ferroan (Figure 10.1i). Subsequent non-ferroan zones, if present, are relatively thin and infrequent.

The tendency for increasing FeO with progressive precipitation is lucidly shown in Figure 10.2a. Bulk serial samples of microspar (non-ferroan), pseudospar (ferroan mostly, but occasionally non-ferroan or zoned), and where present, DFC from continuous and nodular beds were analysed. These serial analyses are numbered as Trends 1-10. One

1. Comparison of stain with microprobe and AAS analyses indicates that calcite will slightly stain at FeO concentrations as low as 0.1-0.2 wt %. This contrasts with the higher minimum levels of FeO, approximately 0.5 wt %, necessary to slightly stain dolomite - refer to Chapter 12.

Figure 10.2: (a) FeO and MnO trends, as determined by atomic absorption spectrophotometry, of serial samples of microspar, pseudospar, and dispacive fibrous calcite. Circled numbers (horizontal axis) refer to the following serial samples (see Table I.1 in Appendix I): (1) GP-41, (2) SPN-66-D, (3) CHN-36-B, (4) CHN-101, (5) CHN-102, (6) GP-2, (7) GP-23, (8) GP-57, (9) GP(81-7), (10) LH-76-A.

(b) Sr trends, as determined by atomic absorption spectrophotometry, of serial samples of microspar, pseudospar, and dispacive fibrous calcite.



grainstone (Trend 5) is also included. In most cases, marginal aggradation from microspar to pseudospar and the subsequent development of fibrous calcite is characterized by an increase in bulk FeO content, confirming both stain and microprobe analysis. DFC-2 (Trends 6, 7, 9, 10) are more ferroan than DFC-1 (Trends 3, 4, 5).

Not all samples examined by AAS and microprobe analysis, however, demonstrate this progressive increase in FeO with progressive crystallization. In some crystals, FeO appears to fluctuate randomly, and in others, it decreases in later precipitates (Figure 10.1b,f,h; Trend 8 in Figure 10.2). In CFC, FeO is below detection limits.

10.4 MANGANESE

MnO content in neospar, equant cement, and DFC is usually less than 0.2 wt %, but occasionally reaches 0.5 wt % (Figure 10.1a). In CFC, concentrations are usually below the detection limit. MnO concentrations tend to be greatest where FeO levels are also high (Figure 10.1f, g, h). Few samples contain larger amounts of MnO than FeO (Figure 10.1c; Figure 10.2a).

In contrast to FeO, systematic changes in MnO concentration in the serial analyses are not apparent (Figure 10.2a). Some samples demonstrate an increase in MnO concentration accompanying an increase in crystal size and FeO content (Trends 2, 4, and 5). Others have approximately constant MnO (Trends 6, 7, 8, and 9), and still others demonstrate decreasing MnO (Trends 1 and 10).

10.5 STRONTIUM

Sr content, as determined by AAS, ranges from 60-700 ppm (Figure 10.2b; Figure 10.3). In most serial samples, the change from microspar to pseudospar to DFC, if present, is accompanied by a decrease in Sr concentration (except Trends 7 and 9), a tendency opposite to that seen with FeO. This decrease in Sr concentration is also apparent using average values for all microspar (average = 280 ppm, n = 13), pseudospar (average = 233 ppm, n = 8), and DFC-1 (average = 126 ppm, n = 4) analyses. The lack of correlation of Sr concentration with insoluble residue or Si (see Table I.1 in Appendix I) suggests that leaching of clays and feldspars is not responsible for these trends.

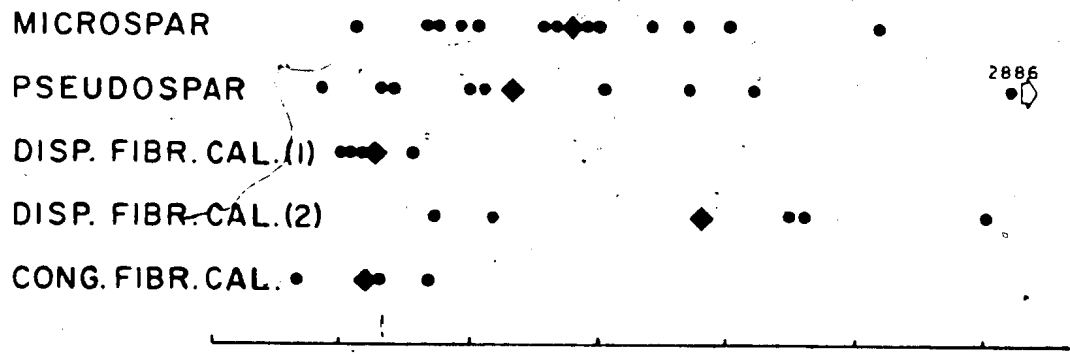
Three of the DFC-2 analyses in Trends 6, 7, and 9 (all from Green Point) are exceptional in that they contain relatively high Sr concentrations thus raising this group average to 381 ppm (n = 5). Microspar and pseudospar in these trends as well as in Trend 1 (also from Green Point) also demonstrate elevated Sr concentrations. An anomalous sample of pseudospar in Trend 6 contains 2900 ppm Sr, an amount 4 times higher than the next highest concentration analysed. Otherwise, there is nothing distinctive about this sample with respect to its petrographic or CL characteristics, or other trace element concentrations. Trends 8 and 10, also from Green Point, have levels of Sr comparable to other calcites analysed.

Sr content of CFC (average = 122 ppm, n = 3) is similar to that of DFC-1. Both of these groups' averages are considerably smaller than

Figure 10.3: Sr distribution in various diagenetic calcites, as determined by AAS. The squares are the average values for each individual group. In the pseudospar group, the anomalously high value of 2886 ppm Sr is not included in the average.

STRONTIUM (ppm)

0 100 200 300 400 500 600



2886

averages for the other groups.

10.6 INTERPRETATION AND DISCUSSION

Microprobe and AAS analyses of various types of calcite illustrate the following relationships:

(1) In many crystals, MgO concentration decreases with progressive precipitation. Other crystals, however, show a late stage increase in MgO content.

(2) In many crystals, FeO concentrations increase in later precipitates. This is also confirmed by bulk rock serial analysis and staining with potassium-ferricyanide solution.

(3) MnO concentrations increase, decrease, or are relatively constant within successive precipitates.

(4) Serial analyses illustrate a reduction of Sr concentration in successive precipitates. By analogy with FeO, individual crystals must also mirror this decrease with progressive precipitation.

More complex, often uninterpretable relationships may reflect local differences in pore-waters, as well as "aliasing" effects inherent in the microprobe step analysis method.

The later stage decreases in Mg and Sr and increases in Fe and occasionally Mn can be viewed in context of trace element partitioning behavior and degree of system closure, illustrated schematically in Figure 10.4a. In this figure pore-waters are assumed to be fresh, but

Figure 10.4: (a) This simplified model of trace element distribution illustrates the behavior of partitioning coefficients (k) greater and smaller than unity in diagenetic systems characterized by high ("open") and low ("closed") water-rock ratios. The model assumes solid phases of marine origin, mainly aragonite and Mg-calcite, and a typical, low-Mg meteoric pore-water. Calcite is the precipitated phase. The dissolution of aragonite and Mg-calcite is assumed to be the dominant control on the availability of Sr and Mg; both of these elements have k less than 1. Mn and Fe are both assumed to have k greater than 1. These elements are initially at "background" levels in the pore-water. Calcites precipitated in such a simplified open system ideally will show no concentration gradient of trace elements.

In a closed diagenetic system, concentrations of Mg and Sr will progressively increase in pore-waters and successive precipitates will contain higher concentrations (heavy stippling), the limiting concentrations being those of the source aragonite and Mg-calcite. For Fe and Mn, at constant Eh, the earliest precipitates will scavenge these elements (heavy stippling) and later precipitates will contain progressively less Fe and Mn. This model is explained more fully in Appendix K.

(b) Schematic distribution of Mg, Sr, Fe, and Mn in authigenic calcites of the CHG.

$\delta^{18}O$

-8

-6

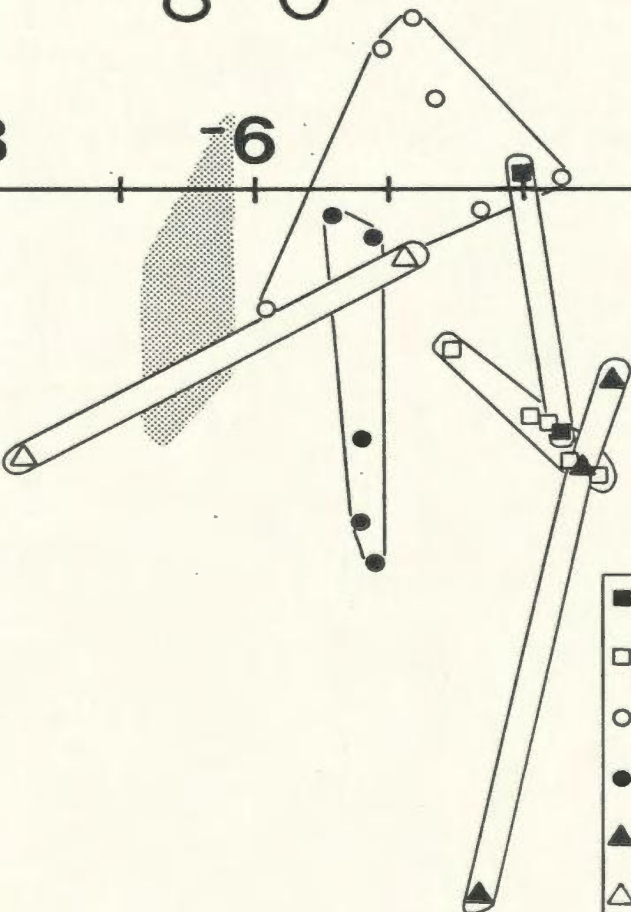
-2

-2

-4

-6

$\delta^{13}C$



- siltstone (bl. & gn. shale)
- " (red shale)
- matrix
- conglomerate matrix
- ▲ fault joint
- △ pervasive replacement

they need not be so. Marine or modified marine pore-waters do not change the fundamental enrichment-depletion relationships illustrated although the effects will be dampened somewhat relative to those of meteoric-water diagenesis (Veizer, 1983). The trace element distribution in authigenic calcites of the CHG is schematically illustrated in Figure 10.4b. Comparison of Figure 10.4b with Figure 10.4a suggests that the observed relationships are not explainable in terms of the relationship between a partitioning coefficient and the degree of system closure. In the following discussion it is assumed that deep-marine waters on the Cambro-Ordovician slope were similar in elemental composition to modern seawater (see discussion in Veizer, 1983) and pore-waters are derived from this marine water.

10.6.1 Magnesium and Strontium

The observed decreases in Mg and Sr concentrations with progressive precipitation are explained by the incorporation of these elements into other authigenic phases ("sinks"). This is a likely possibility based on interstitial water studies from DSDP cores of pelagic and hemipelagic sediments. Progressive Sr depletion with increasing sub-sea depth in deep-sea carbonates and increases in Sr concentrations in adjacent pore-waters have been explained as the result of recrystallization of carbonate minerals (e.g. Sayles and Manheim, 1975; Matter et al., 1975; Gieskes, 1981; Baker et al., 1982). The accumulated Sr in pore-waters may ultimately reach a maximum concentration plateau or steady state (Gieskes, 1981; Baker et al., 1982) balanced by incorporation of excess Sr into clays (e.g. Matter et al., 1975) or possibly by diffusion upward through the sediment pile to the surface or downward to some unknown sink. The question concerning removal of Sr from sedimentary pile,

however, is not satisfactorily answered.

Decreasing Mg concentrations in some CHG calcites may be explained by removal into sinks of quite diverse origin. These include: (1) dolomitization or Mg-calcite formation (e.g. Sayles and Manheim, 1975) and (2) silicate authigenesis (e.g. Harrison et al., 1982). Other potential (but unlikely for the CHG) sinks for Mg are discussed in Gieskes (1981). As will be shown in Chapter 12, dolomitization may be synchronous with or may postdate calcite authigenesis, and is therefore a likely sink for Mg. In addition, the domination of the clay mineral suite by illite and chlorite, and to a lesser extent corrensite (see Appendix B) also implies that clay mineral diagenetic reactions consumed Mg, but these probably occurred too late in the diagenetic history to effectively remove Mg from the shallow-burial pore-waters from which most, if not all, authigenic calcites were derived. As discussed previously, Mg-depletion with progressive precipitation is not ubiquitous, and local unknown factors may be important. Mg concentrations in some DSDP calcites have also been observed to increase with sub-sea depth (e.g. Baker et al., 1982) but information is too scarce to confidently interpret such changes.

Considering published partitioning coefficients of Mg and Sr as order-of-magnitude estimates only (see Appendix K), the concentrations of Mg and Sr in authigenic calcites of the CHG could be derived from unmodified seawater if the elemental composition of Lower Paleozoic seawater is identical to that of the modern ocean and the appropriate partitioning coefficient is assumed (Table 10.1). This is also consistent with other evidence indicating a near-surficial origin for many neospars and cements. The anomalously high analysis of 2900 ppm Sr

Table 10.1: This table compares pore-water chemistry calculated from chemical analysis of CHG calcites with the expected equilibrium precipitates from modern seawater for a wide range of possible partition coefficients (k). Calculations use the Berthelot-Nernst equation with the appropriate simplifying assumptions (see Appendix K). Diamond-shapes indicate calculated Cow Head Group pore-water Me/Ca ratios that are within an order-of-magnitude of ratios in modern seawater.

CHG and modern seawater concentrations of elements are assumed to be identical: Ca=411 mg/kg; Mg=1290 mg/kg; Sr=8 mg/kg; Fe=0.002 mg/kg; Mn=0.0002 mg/kg (source: Table 10.1 in Drever, 1982).

k values are obtained from the following sources: Ranges of k^{Fe} and k^{Mn} are for earth surface conditions (Veizer, 1983, table 3-1; Brand and Veizer, 1980). Range of k^{Sr} is for 0 degrees C (Baker et al., 1982, figure 1). k^{Mg} of 0.02 is extrapolated to below 5 degrees C (Fuchtbauer and Hardie, 1976). k^{Ca} of 8.1×10^{-4} is estimated at 5 degrees C (Baker et al., 1982).

		COW HEAD GROUP				MODERN SEAWATER	
	calcite analysis		pore-water chemistry		equilib. concent. in calcite (ppm)		$\left(\frac{m_{Me}}{m_{Ca}}\right)_{seaw.}$
	wt% ox.	ppm	$\left(\frac{m_{Me}}{m_{Ca}}\right)_{pore-water}$	concentration ppm			
Mg	0.1	600	$8.1 \times 10^{-4} \leftarrow k \rightarrow 2 \times 10^{-2}$	$8.1 \times 10^{-4} \leftarrow k \rightarrow 2 \times 10^{-2}$	$8.1 \times 10^{-4} \leftarrow k \rightarrow 2 \times 10^{-2}$		5.2×10^0
	0.5	3020	$3 \times 10^0 \blacklozenge 1 \times 10^{-1}$	$7 \times 10^2 3 \times 10^1$	$1 \times 10^3 3 \times 10^4$		
	1.0	6030	$1 \times 10^1 \blacklozenge \blacklozenge 6 \times 10^1$	$4 \times 10^3 2 \times 10^2$			
Fe	0.1	780	$3 \times 10^1 \blacklozenge \blacklozenge 1 \times 10^0$	$7 \times 10^3 3 \times 10^2$			3.5×10^8
	0.5	3890	$1 \times 10^0 \leftarrow k \rightarrow 2 \times 10^1$	$1 \times 10^0 \leftarrow k \rightarrow 2 \times 10^1$	$1 \times 10^0 \leftarrow k \rightarrow 2 \times 10^1$		
	1.0	7770	$1 \times 10^{-3} 7 \times 10^{-5}$	$8 \times 10^{-1} 4 \times 10^{-2}$	$2 \times 10^0 4 \times 10^1$		
Mn	0.1	770	$7 \times 10^{-3} 3 \times 10^{-4}$	$4 \times 10^0 2 \times 10^{-1}$			3.6×10^{-7}
	0.2	1550	$1 \times 10^{-2} 7 \times 10^{-4}$	$8 \times 10^0 4 \times 10^{-1}$			
	0.5	3870	$6 \times 10^0 \leftarrow k \rightarrow 3 \times 10^1$	$6 \times 10^0 \leftarrow k \rightarrow 3 \times 10^1$	$6 \times 10^0 \leftarrow k \rightarrow 3 \times 10^1$		
Sr	0.1	60	$2 \times 10^{-4} 5 \times 10^{-5}$	$1 \times 10^{-1} 3 \times 10^{-2}$			8.9×10^{-3}
	0.2	1550	$5 \times 10^{-4} 9 \times 10^{-5}$	$3 \times 10^{-1} 5 \times 10^{-2}$	$1 \times 10^0 6 \times 10^0$		
	0.5	3870	$1 \times 10^{-3} 2 \times 10^{-4}$	$6 \times 10^{-1} 1 \times 10^{-1}$			
Sr		60	$3 \times 10^{-2} \leftarrow k \rightarrow 1.7 \times 10^{-1}$	$3 \times 10^{-2} \leftarrow k \rightarrow 1.7 \times 10^{-1}$	$3 \times 10^{-2} \leftarrow k \rightarrow 1.7 \times 10^{-1}$		8.9×10^{-3}
		700	$2 \times 10^{-3} \blacklozenge 4 \times 10^{-4}$	$2 \times 10^0 4 \times 10^{-1}$			
		2900	$3 \times 10^{-2} \blacklozenge \blacklozenge 5 \times 10^{-3}$	$2 \times 10^1 4 \times 10^0$	$2 \times 10^2 1 \times 10^3$		
		2900	$1 \times 10^{-1} \blacklozenge 2 \times 10^{-2}$	$1 \times 10^2 2 \times 10^1$			

in a pseudospar sample is interpreted to represent precipitation from pore-waters with elevated Sr ratios which resulted from a local, more closed diagenetic system than for other calcites analysed.

These results do not imply that all calcites in the CHG and throughout the geologic column containing similar levels of Sr and Mg are also derived this way. Clearly, at this stage in our understanding of partitioning coefficients and ancient ocean chemistry, without the appropriate field and petrographic data (including CL), such a conclusion would at best be extremely suspect.

10.6.2 Iron and Manganese

The change from non-ferroan to ferroan calcite cements in limestones of diverse ages is unquestionably the most often-reported geochemical trend described in ancient limestones (e.g. Oldershaw and Scoffin, 1967; Evamy, 1969; Frank *et al.*, 1982; Grover and Read, 1983; James and Klappa, 1983). This trend, and a comparable one for Mn, are conventionally explained as the result of a decrease in Eh, thus mobilizing Fe and Mn contained in various oxides and hydroxides which form colloids or are adsorbed onto various types of particulate matter. Assuming comparable Fe, Mn, and Ca concentrations in the Lower Paleozoic and modern oceans, to reach 0.1 wt % FeO or MnO would involve an increase in the metal/Ca ratio of at least 20 times for Fe and over 100 times for Mn. The presence of reducing pore-waters within the uppermost metre, even few millimetres of the sediment-seawater interface in organic-rich sediments is well-established (see Chapter 11). Fe and Mn can also be released during later burial diagenesis from the alteration of clays or pressure solution (e.g. Oldershaw and Scoffin, 1967; Boles,

1978). DSDP interstitial pore-water profiles for Mn are often complex, but some show a close correlation between the concentration of dissolved Mn and dissolved silica. This may be explained by mobilization of adsorbed Mn-oxide phases on siliceous skeletons (Gieskes, 1981).

Based upon the relative stability fields of Fe and Mn and their compounds in Eh-pH space (Krauskopf, 1979; Berner, 1980; Maynard, 1983), upon depressing Eh, remobilization of Mn should occur first, followed by Fe as conditions become progressively more reducing. This earlier, preferential mobilization of Mn over Fe explains the sequence of CL stages discussed previously in Chapter 8. Stage A is dull or dark due to insufficient activator ion (Mn). Stage B reflects conditions characterized by Mn-activated luminescence. Stage C occurs when Fe levels rise above a critical concentration and quench Mn-activated luminescence.

10.7 SUMMARY AND CONCLUSIONS

Neospar, cements, and DFC commonly demonstrate decreasing Sr and Mg concentrations and increasing Fe concentrations with progressive precipitation. Mn concentration trends are not consistent although this may be in part a function of low concentrations. Extrapolation of CL data (discussed in Chapter 8) suggests that Mn concentrations do increase with progressive precipitation although its presence as an activator may be masked by the quenching effects of iron. The decrease in Sr and Mg is explained by incorporation into mineralogic sinks (e.g. Mg in dolomite) or possibly diffusion upward into the overlying water mass. Fe and Mn enrichment in the later stages of crystal growth

results from a lowering of Eh which remobilizes these elements from various dispersed oxides and hydroxides. The above trends are not without exceptions; for example some crystals demonstrate an enigmatic late stage increase in Mg concentration.

Trace element trends such as those from the CHG are also typical of meteorically-altered limestones where mineralogical stabilization proceeds by replacement of aragonite, incongruent dissolution of Mg-calcite, and precipitation of calcite with lower Sr and Mg concentrations (e.g. Bathurst, 1975; Pingitore, 1976; Brand and Veizer, 1980; James and Choquette, in press). An origin related to meteoric water diagenesis, such as might arise during eustatic sea level drop with resultant formation of major subaerial unconformities on the equivalent-age shallow-water platform, is not supported by field or petrographic evidence. Sedimentation on the equivalent-age shallow-water platform appears to have been relatively continuous for the duration of CHG deposition (see James and Stevens, 1982). Studies of sediments drilled from the modern ocean floor as well as sampled by submersible have also shown stabilization trends similar to those which occur during meteoric diagenesis (e.g. Schlager and James, 1978; Baker et al., 1982).

Using published partitioning coefficients for Mg and Sr extrapolated to below 5 degrees C, and assuming Lower Paleozoic seawater was identical to modern seawater with respect to Ca, Mg, Sr, and Mn concentrations, then the earliest precipitates in the CHG could have precipitated from unmodified or slightly modified seawater, a likely possibility given the abundance of field and petrographic evidence to suggest early, shallow-burial lithification.

Chapter 11

CALCITE STABLE ISOTOPE GEOCHEMISTRY

11.1 INTRODUCTION

Analysis of carbon and oxygen stable isotopes in carbonates has in recent years been a routine complement to studies of carbonate diagenesis (e.g. Bathurst, 1975; Hudson, 1977; Allan and Matthews, 1982; Anderson and Arthur, 1983). Isotopic analyses provide important information regarding pore-water chemistry and other parameters unassessable by any other method.

From previous discussions, it was shown that field and petrographic relationships indicate lithification within a few metres of the sediment-seawater interface. At such shallow burial depths the effects of marine as well as "evolved" pore-waters are expected. Pore-waters, particularly those associated with organic-rich sediments, undergo profound changes in their stable carbon isotope content as a function of several, important, bacterially-mediated reactions which oxidize organic matter (discussed below). The importance of these oxidation reactions in the early diagenesis of carbonate sediments has been illustrated repeatedly in the last decade or so by DSDP drilling (e.g. Sayles and Manheim, 1975; Claypool and Threlkeld, 1980; Garrison, 1981; Gieskes,

1981; Kelts and Mackenzie, 1982). As a result of these as well as numerous on-land studies particularly of Mesozoic, organic-rich sediments (e.g. Sass and Kolodny, 1972; Irwin *et al.* 1977; Hudson, 1978), the sequence of diagenetic changes which starts in the newly-deposited sediment and then evolves as a function of time, progressive burial, and alteration of pore-water chemistry are well known.

Samples for isotope analysis were analysed courtesy of Marathon Oil Company Denver Research Center in Littleton, Colorado, using standard procedures. Analyses are reported in parts permil (o/oo) $\delta^{13}\text{C}$ or $\delta^{18}\text{O}$ relative to the PDB-1 standard. Precision for both $\delta^{13}\text{C}$ and $\delta^{18}\text{O}$ is 0.1 - 0.2 o/oo based on selected replicate analyses (Appendix I). Technical and analytical data are provided in Appendix I.

The terms "enriched" and "heavy" refer to larger $\delta^{13}\text{C}$ or $\delta^{18}\text{O}$ values - such samples contain more of the heavier isotope. Likewise the terms "depleted" and "light" refer to smaller $\delta^{13}\text{C}$ or $\delta^{18}\text{O}$ values - these contain more of the lighter isotope.

11.2 BACKGROUND: FUNDAMENTALS OF ORGANIC MATTER OXIDATION

11.2.1 Oxidizing Reactions

Before proceeding to description and discussion of stable isotope analyses, a brief review of some fundamental aspects of the oxidation of organic matter is presented, emphasizing mainly the expected carbon

isotope fractionation.

On an oxidized sea floor, the earliest oxidation reaction is aerobic bacterial oxidation, occurring at and near the sediment-seawater interface (Table 11.1). Below the sediment surface, pore-waters become suboxic and eventually anaerobic at depths as shallow as a few millimetres (e.g. Fruth and Sherreiks, 1982) to a few 10's of centimetres (Berner, 1980). Oxidation of organic matter then continues by sulphate reduction followed by methane generation. Other inorganic oxidants are consumed; for example nitrate and manganese or iron oxides and hydroxides, but these are of relatively minor importance in terms of the amount of organic matter oxidized (Froelich *et al.*, 1979). With progressive burial and concomitant increase in temperature (greater than 50 degrees C) remaining reactive organics are eventually consumed during the thermogenic formation of methane and other hydrocarbons. Oxidation continues as long as there is a supply of metabolites or until suitably reactive organics are consumed.

The preponderance of black and green shales in the CHG suggests that bottom waters were generally dysaerobic or possibly anaerobic (refer to Chapter 2). In the younger, red shale-dominated part of the sequence, however, deep waters were obviously aerobic but pore-waters were eventually reduced so as to allow the formation of dolomite and thin reduction rims in the shale immediately underlying and overlying dolomitic siltstones (see Chapters 2 and 12). In the less oxygenated bottom waters associated with the deposition of dark-coloured shales, aerobic oxidation reactions may have not occurred; instead, suboxic or anoxic organic oxidation reactions such as nitrate reduction and

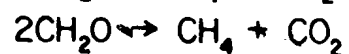
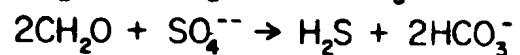
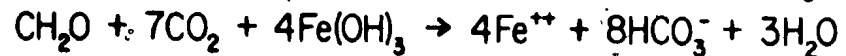
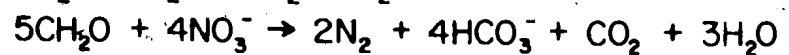
sulphate reduction could have occurred at the sediment-seawater interface.

The bacterial oxidation reactions (Table 11.1) all yield CO_2 which increases concentrations of bicarbonate as well as other carbon species. In aerobic oxidation, pore-water communication with the overlying sea water buffer maintains alkalinity but lowers pH thus forcing the carbonate equilibrium toward undersaturation (Gieskes, 1974). In contrast, and of great significance in anoxic pore fluids, the addition of bicarbonate leads to increased alkalinity and saturation with respect to various carbonate phases, the most important being calcite, Mg-calcite, aragonite, dolomite, siderite, ankerite, Mn-carbonates, and ankerite (Gieskes, 1981; Anderson and Arthur, 1983). The increase in alkalinity is controlled, to various degrees, by the production of ammonia, precipitation or dissolution of inorganic phosphate, pH buffering by proteolytic formation of hydrogen sulfide, effects of weak acids and bases, charge transfer between different ionic species, authigenic silicate formation, and sulphide precipitation (Berner et al., 1970; Sass and Kolodny, 1972; Ben-Yaakov, 1973; Gieskes, 1974; Suess, 1980). Whether or not precipitation ~~does~~ indeed occur also depends on the effects of organic and inorganic inhibitors and pre-existing carbonate nuclei (Berner et al., 1970; Baker and Kastner, 1981). Discussion of the above effects on the solution chemistry of interstitial fluids is beyond the scope of this study and the reader is referred to treatments in the above citations.

During shallow burial these reactions are controlled by a mutually exclusive succession of bacteria. At a given point in time, the

Table 11.1: Various bacterial reactions in order of decreasing free energy yield. CH_2O and MnO_2 are assumed to be sucrose and birnessite, respectively. Table is modified from Table 4-4 in Berner (1980).

REACTION



OXIDATION

DENITRIFICATION

Mn(IV) REDUCTION

Fe(III) REDUCTION

SULPHATE REDUCTION

FERMENTATION

FROM BERNER, 1980

sequence of reactions defines a depth-related diagenetic zonation ("spatial succession"); or, if viewed against a backdrop of progressive sedimentation, the reactions record the upward migration of several micro-ecological suites ("temporal succession"; Claypool and Kaplan, 1974; Mechalas, 1974). The sequence of reactions is characterized by a progressively diminished rate of CO₂ production as well as free energy yield (Claypool and Kaplan, 1974; Froelich et al., 1979; Irwin et al., 1977; Berner, 1980).

11.2.2 Isotopic Signatures

The various diagenetic reaction zones are characterized by isotopically distinct CO₂ (and therefore bicarbonate) $\delta^{13}\text{C}$ from that of seawater which, in the modern ocean, is approximately 0 o/oo. Bicarbonate resulting from bacterial oxidation (Zone I of Irwin et al., 1977) and sulphate reduction (Zone II) reflects the light, largely unfractionated carbon derived from precursor organic material, approximately -25 o/oo PDB (Irwin et al., 1977). In contrast, there is a large fractionation associated with bacterial methane generation (Zone III). The mechanism is less than perfectly understood although the strong carbon isotope fractionation that characterizes it is well-established (Irwin et al., 1977). Because methane concentrates the light isotope of carbon ($\delta^{13}\text{C}$ up to -50 to -100 o/oo; Anderson and Arthur, 1983), residual CO₂ is characterized by large $\delta^{13}\text{C}$, up to +10 to +15 o/oo (Irwin et al., 1980; Pisciotta, 1981). Upon further burial, abiotic reactions once again produce isotopically light CO₂ with $\delta^{13}\text{C}$ values of -10 to -25 o/oo. Carbonate precipitation associated with these reactions ideally will

reflect the isotopic composition of pore-water bicarbonate, the principal carbonate species in solution.

Stable isotopes are affected by a number of variables. The main influence on $\delta^{13}\text{C}$ is from oxidation of organic matter (Hudson, 1977; Irwin *et al.* 1977). The $\delta^{13}\text{C}$ of a carbonate will therefore reflect mixing of marine $\delta^{13}\text{C}$ with either very negative or positive bicarbonate derived from oxidation of organics. The small amount of dissolved carbon in pore-waters implies that pore-water $\delta^{13}\text{C}$ will be strongly moderated by any dissolution of the host sediment or by any other input. The resultant precipitate will also reflect this. In contrast, $\delta^{18}\text{O}$ is controlled by temperature, as well as the isotopic composition of the waters from which carbonate precipitates (Hudson, 1977). The $\delta^{18}\text{O}$ of pore-waters may be influenced by formation of diagenetic minerals or other water-mineral reactions, biological fractionation, isotopic composition of a precursor solid, salinity, secular changes, and water-rock ratios (Keith and Weber, 1964; Hudson, 1977; Brand and Veizer, 1981; Brand, 1982; Anderson and Arthur, 1983).

11.3 CALCITE STABLE ISOTOPES

The following section examines the distribution and relationships of various types of authigenic calcite in the CHG. RFC is not part of the in situ diagenetic suite; however, it does provide a convenient and conventional marine "base-line" to which other types of calcite may be compared isotopically. CFC is an in situ submarine cement, but as will

be shown below, its carbon isotopic composition demonstrates a variable organic influence. Microspar, pseudospar, and DFC are treated both separately and together, noting transitional relationships of one to the other. Grainstones and miscellaneous fracture-fill calcite cements are also examined, the cements in particular to characterize an early from a late, tectonic fracture calcite.

11.4 RADIAL FIBROUS CALCITE

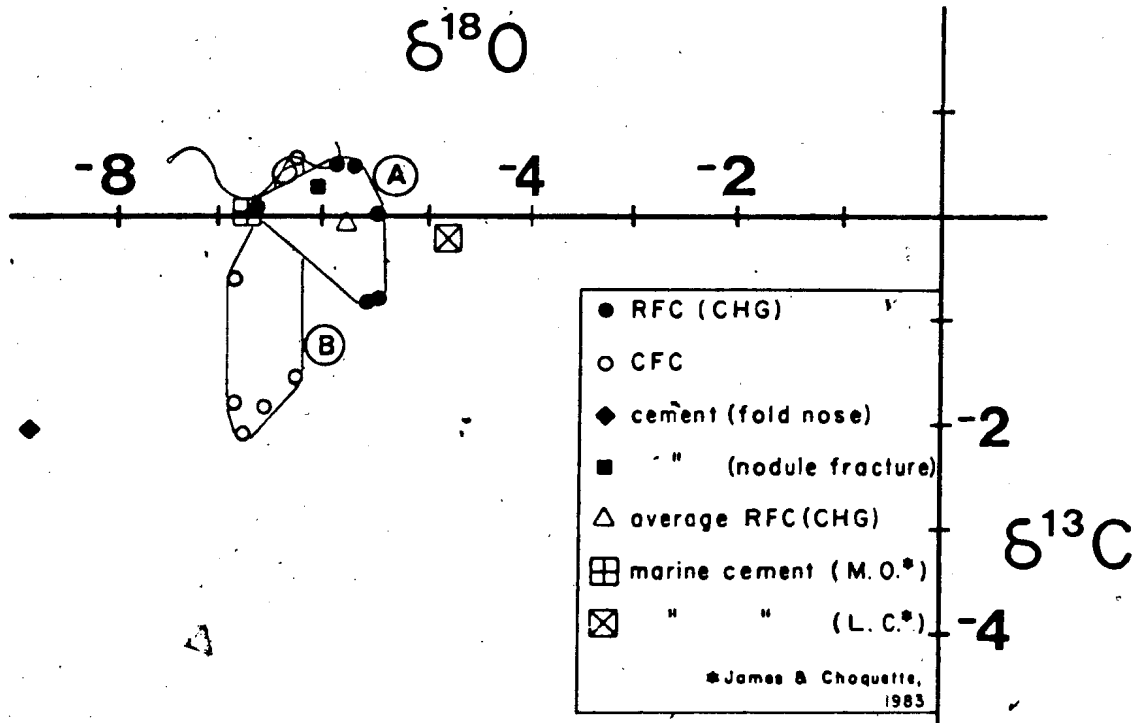
11.4.1 Samples and Data

Six samples of RFC were analysed from Lower and basal Middle Ordovician boulders at Cow Head North (Beds 10, 12, and 14) and from the enigmatic mounds in the large boulder at Lower Head (Group A in Figure 11.1). Their $\delta^{18}\text{O}$ range from -5.46 to -6.65 o/oo, averaging -5.78 o/oo. Their $\delta^{13}\text{C}$ range from +0.54 to -0.84 o/oo, averaging -0.07 o/oo.

11.4.2 Interpretation

The clustering of stable isotopic analyses, along with their sharp primary trace element distribution as indicated by CL (see Chapter 7), suggests that RFC are sufficiently unaltered to establish a "best estimate" of inorganically-precipitated calcite from Lower to Middle Ordovician seawater. Analyses of RFC from the CHG lie between James and Choquette's (1983, figs. 20, 21) best estimates of unaltered fibrous marine cements for the Lower Cambrian and Middle Ordovician. These estimates were obtained by using the "heaviest", an presumably most

Figure 11.1: $\delta^{13}\text{C}$ versus $\delta^{18}\text{O}$ of RFC, CFC, and miscellaneous calcite cements. Also plotted in this diagram are the "best estimates" of Middle Ordovician and Lower Cambrian fibrous marine cements from James and Choquette (1983). Circled letters are referred to in text. See text for discussion.



original, isotopic compositions of fibrous cements from a covariate data set. The validity of the marine isotopic "memory" in such fibrous calcites is supported by their significant and consistent temporal variations throughout the Phanerozoic (see compilation in James and Choquette, 1983).

Using the most positive RFC $\delta^{18}\text{O}$ of -5.46 o/oo and assuming a precipitation temperature of 23 degrees C, RFC were precipitated from sea water with $\delta^{18}\text{O}$ (SMOW) of -4 o/oo[1]. There is an uncertainty, however, in using RFC as an internal baseline. Although the RFC-bearing boulders are found in Lower and Middle Ordovician debris flows, the boulders may be older than their beds and some of the data scatter may reflect real temporal variations in the oceanic bicarbonate reservoir. The relatively small degree of data scatter, however, suggests that this effect, if it indeed occurs, is minor and can be safely ignored.

11.5 IN SITU AUTHIGENIC CALCITE: SAMPLES AND DATA

11.5.1 Conglomerate Fibrous Calcite

CFC's exhibit a narrow range of $\delta^{18}\text{O}$ from -6.26 to -6.85 o/oo (Group B in Figure 11.1). Their $\delta^{13}\text{C}$, however, are more variable, ranging from

1. These values were calculated using the modified paleotemperature equation of Shackleton and Kennett (1975):

$$T = 16.9 - 4.38(\delta^{18}\text{O} - W) + 0.10(\delta^{18}\text{O} - W)$$

where T is temperature in degrees C, $\delta^{18}\text{O}$ and W are the isotopic compositions of calcite and water, respectively.

+0.58 to -2.09 o/oo with 4 of the 6 analyses clustered toward more negative values.

11.5.2 Equant Calcite Cements

Also plotted in Figure 11.1 are analyses of an early and a late fracture-fill calcite cement, their timing being determined a priori by field relationships and petrography (previously discussed). The early cement has ferroan zones and occurs in a marginal fracture of a mudstone nodule ($\delta^{13}\text{C} = +0.28$ o/oo and $\delta^{18}\text{O} = -6.04$ o/oo; Plate 53e). The late cement is entirely ferroan and fills a void developed in the fold nose of a contorted mudstone (Plate 20). This calcite has the most negative $\delta^{18}\text{O}$ measured at -8.83 o/oo. The $\delta^{13}\text{C}$ is -2.05 o/oo.

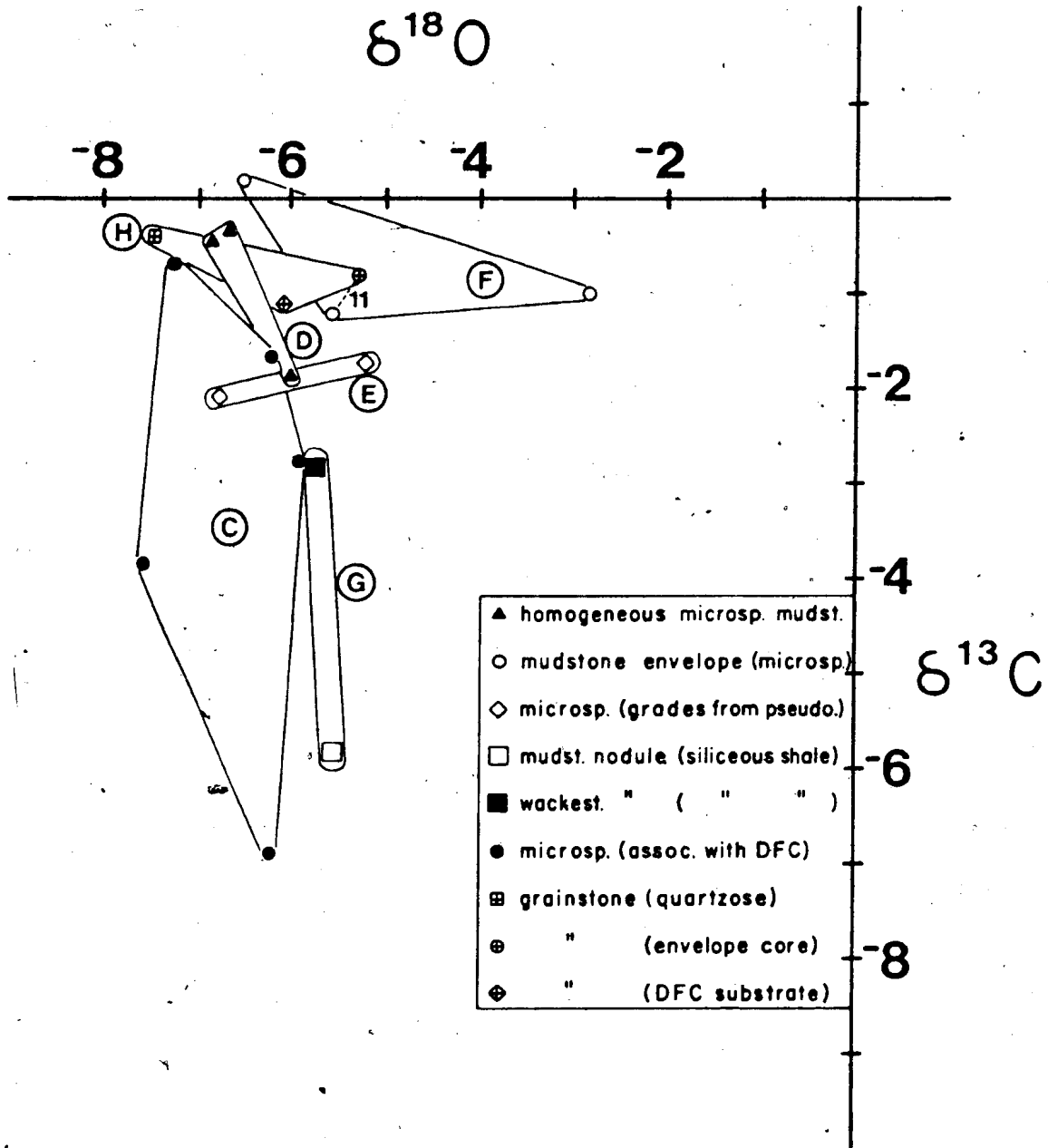
11.5.3 Grainstones

Whole-rock analysis of grainstones (Group H) plotted in Figure 11.2 include: (1) quartz-rich grainstone (non-ferroan cement); (2) grainstone substrate to DFC-1 (iron-zoned cement; also plotted in Figure 11.4); and (3) grainstone core to a mudstone envelope (non-ferroan cement). Grainstones vary little with respect to $\delta^{13}\text{C}$, all within 1 o/oo of each other (-0.39 to -1.12 o/oo). Their $\delta^{18}\text{O}$ range from -5.29 to -7.47 o/oo.

11.5.4 Microspar

Microspar analyses are plotted in Figure 11.2 in Groups C-G. These are petrographically similar, being all non-ferroan though some show CL

Figure 11.2: $\delta^{13}\text{C}$ versus $\delta^{18}\text{O}$ of various microspars, grainstones, and a wackestone nodule. Number 11 refers to a serial analysis of a rippled grainstone surrounded by a mudstone envelope. Circled letters are referred to in text. See text for discussion.



zoning. Included are: (1) microspar associated with DFC (Group C; also plotted in Figure 11.4); (2) homogeneous microspar mudstones (Group D); (3) microspar which marginally aggrades to pseudospar but which is not associated with DFC (Group E; also shown in Figure 11.3), (4) microspar envelopes in cored nodules (Group F), including one analysis of a grainstone core (Trend 11), and (5) microspar mudstone and wackestone nodules enclosed in silicified shale (Group G).

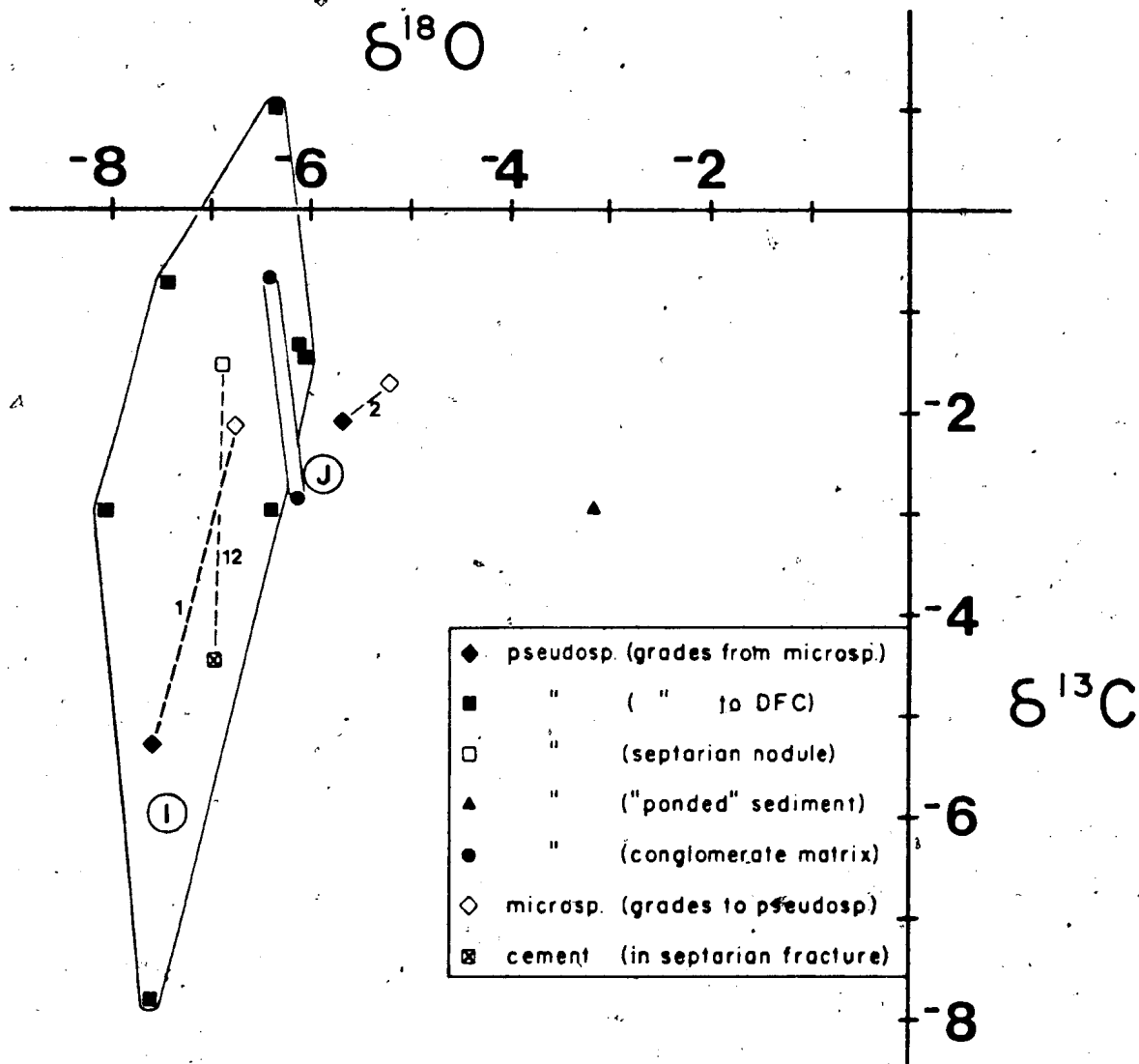
Their $\delta^{13}\text{C}$ range from slight positive values (+0.24 o/oo) to pronounced negative values (-6.87 o/oo). The most negative values are those of microspar associated with DFC (Group C) and the mudstone and wackestone nodules in silicified shale (Group G). The highest $\delta^{13}\text{C}$ microspars are homogeneous mudstones, including continuous beds and nodules (Group D), and mudstone envelopes (Group F). The grainstone and its mudstone envelope (Trend 11) contain similar $\delta^{13}\text{C}$ and $\delta^{18}\text{O}$. Microspar which aggrades to pseudospar, but which is not associated with DFC has intermediate values of $\delta^{13}\text{C}$ (Group E).

The $\delta^{18}\text{O}$, with one exception, range between -5.24 and -7.60 o/oo. The exceptional sample is a mudstone envelope developed around a peloidal silt grainstone (not analysed). This mudstone has the highest $\delta^{18}\text{O}$ encountered in this study ($\delta^{18}\text{O} = -2.81$ o/oo).

11.5.5 Pseudospar and Related Cement

The analyses plotted in Figure 11.3 include: (1) pseudospar associated with DFC (Group I; also plotted in Figure 11.4); (2) a septarian nodule

Figure 11.3: $\delta^{13}\text{C}$ versus $\delta^{18}\text{O}$ of various psuedospars, associated microspars, and a calcite cement filling a septarian crack. Trends 1 and 2 are the same serial analyses as in Figure 10.2. Circled letters are referred to in text. See text for discussion.



pseudospar with calcite cement filling crack (Trend 12); (3) marginally aggraded pseudospar which is transitional from microspar plotted in Figure 11.2 (shown as Trends 1 and 2 [2]); (4) pseudospar in conglomerate matrix (Group J); and (5) pseudospar from "ponded sediment" above a contorted limestone (see Chapter 4). Stable isotope analysis demonstrates the following:

(1) Pseudospar crystals in Group I may be ferroan, non-ferroan, or zoned and grade into DFC. They span a considerable range of $\delta^{13}\text{C}$, from +1.04 to -7.78 o/oo, with $\delta^{18}\text{O}$ ranging from -6.09 to -8.05 o/oo.

(2) The septarian nodule and its associated blocky calcite cement are both ferroan and contain similar $\delta^{18}\text{O}$ values (-6.87 and -6.91, o/oo, respectively). The cement, however, has considerably more negative $\delta^{13}\text{C}$ than its host pseudospar (-4.45 vs -1.54 o/oo, respectively).

(3) Pseudospar crystals in Trends 1 and 2 are ferroan and have more negative $\delta^{13}\text{C}$ (-2.06 and -5.27 o/oo) and $\delta^{18}\text{O}$ (-5.69 and -7.55 o/oo) than microspar to which they are transitional.

(4) Pseudospar in conglomerate matrices (Group J) is ferroan or non-ferroan and has $\delta^{13}\text{C}$ of -0.67 to -2.82 o/oo and $\delta^{18}\text{O}$ of -6.10 to -6.42 o/oo.

(5) The "ponded sediment" pseudospar is ferroan and contains the second heaviest oxygen ($\delta^{18}\text{O} = -3.11$) of all calcites analysed. Its carbon isotopes, however, are light ($\delta^{13}\text{C} = -2.92$ o/oo).

2. The trends numbered 1-10 are the same as those discussed in Chapter 10.

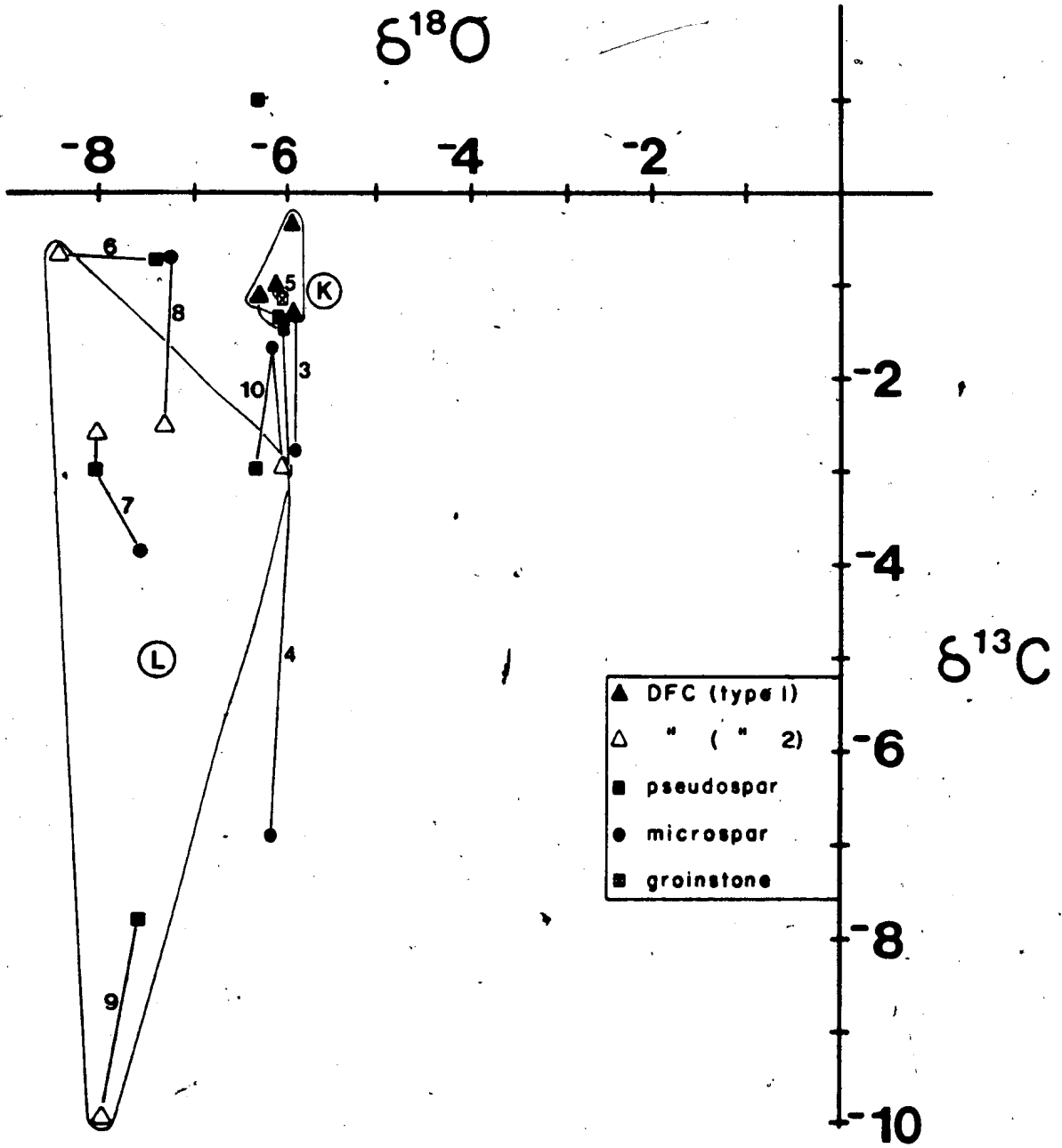
11.5.6 Displacive Fibrous Calcites and Associated Neospar

Seven serial analyses of neospar-to-DFC transitions are plotted in Figure 11.4. Also included are single analyses of: (1) DFC-1 without accompanying substrate analysis, (2) DFC-1 with grainstone substrate (also plotted in Figure 11.2), and (3) pseudospar substrate (also plotted in Figure 11.3) to DFC-1 (not analysed) in a conglomerate clast.

DFC-1 (Group K) and DFC-2 (Group L) are isotopically distinct. DFC-1 is clustered closely together with $\delta^{13}\text{C}$ ranging from -0.30 to -1.28 o/oo and $\delta^{18}\text{O}$ ranging from -5.96 to -6.31 o/oo. In contrast, DFC-2 vary widely with respect to both $\delta^{13}\text{C}$ and $\delta^{18}\text{O}$, and these calcites also have more negative $\delta^{13}\text{C}$ and $\delta^{18}\text{O}$ than DFC-1. In these, $\delta^{13}\text{C}$ ranges from -0.61 to -9.93 o/oo and $\delta^{18}\text{O}$ ranges from -6.09 to -8.41 o/oo.

Isotopic analysis of the serial trends previously examined in Chapter 10 demonstrates that the progressive precipitation of microspar, pseudospar, and DFC is accompanied by changes in isotopic compositions. Considering only DFC-1 trends, the transition from microspar to pseudospar to DFC in Trends 3 and 4 and from grainstone to DFC in Trend 5 is characterized by increasing $\delta^{13}\text{C}$ with minor, unsystematic fluctuations in $\delta^{18}\text{O}$. In contrast to the above, $\delta^{13}\text{C}$ of DFC-2 trends is more variable. Trends 8, 9, and 10 all show significant decreases in $\delta^{13}\text{C}$ from microspar or pseudospar to DFC, or from microspar to pseudospar. In Trend 10 microspar at the centre of the bed grades downward to pseudospar and upward into ferroan DFC (Plate 37e). The $\delta^{13}\text{C}$

Figure 11.4: $\delta^{13}\text{C}$ versus $\delta^{18}\text{O}$ (PDB) of serial analyses of microspar, pseudospar, and DFC. The solitary pseudospar analysis grades to DFC (not analysed). Trend numbers are the same serial analyses as in Figure 10.2. Circled letters are referred to in text. See text for discussion.



of the pseudospar and DFC is identical (-2.92 o/oo), a result congruous with the identical iron staining and CL. Trend 7 shows an increase in $\delta^{13}\text{C}$ in the transition from microspar to pseudospar to DFC, opposite to Trends 8, 9, and 10. Trend 6 shows little variation in $\delta^{13}\text{C}$.

In DFC-2 trends, $\delta^{18}\text{O}$ variations are more pronounced than in the DFC-1 trends, with a tendency for decreasing $\delta^{18}\text{O}$ with progressive precipitation. Trend 10 is an exception. In the transition from microspar to DFC, $\delta^{18}\text{O}$ increases slightly, but the change from microspar to pseudospar is characterized by a decrease, which resembles Trends 1 and 2 in Figure 11.3. Trend 6 shows the most dramatic decrease from pseudospar $\delta^{18}\text{O}$ of -7.44 o/oo to DFC $\delta^{18}\text{O}$ of -8.41, this value being the second smallest $\delta^{18}\text{O}$ measured in calcites of this study.

11.6 INTERPRETATION OF CALCITE STABLE ISOTOPES

11.6.1 Introduction

In situ calcite in the CHG demonstrates a wide range of $\delta^{18}\text{O}$ and $\delta^{13}\text{C}$ values but there is a cluster of $\delta^{18}\text{O}$ values between -5.5 and -7.0 o/oo and a cluster of $\delta^{13}\text{C}$ values between 0 and -2.0 o/oo. These values are "typical" for limestones of this age (see Keith and Weber, 1964; Veizer and Hoefs, 1976). A significant number of $\delta^{13}\text{C}$ analyses, however, fall below this range, indicating incorporation of isotopically-light bicarbonate derived from the oxidation of organics. Serial trends clearly demonstrate that many limestones with "typical" $\delta^{13}\text{C}$ values are genetically-related to limestones illustrating a much more obvious

organic carbon signature.

The greater variation in $\delta^{13}\text{C}$ relative to $\delta^{18}\text{O}$ of calcites in the CHG is similar to that expected during meteoric-water diagenesis.

Precipitation of carbonate in the vicinity of a subaerial surface commonly results in low but variable $\delta^{13}\text{C}$ values due to incorporation of carbon from isotopically light soil gases (e.g. Allan and Matthews, 1982; James and Choquette, in press). A meteoric origin for the in situ calcite in the CHG is dismissed, based on the previously-discussed field and petrographic evidence to indicate deposition and early lithification in a deep-water setting. A submarine, freshwater aquifer extending seaward under the shelf area to the slope is unlikely to have existed due to the high terrigenous mud content of these sediments and associated low permeabilities. Furthermore, such a freshwater aquifer would be expected to isotopically homogenize these sediments, not produce the small-scale isotopic variations observed within samples.

Using the previously-discussed paleotemperature equation and assuming a precipitation temperature of 4 or 5 degrees C, the average $\delta^{18}\text{O}$ of approximately -6 o/oo for in situ diagenetic calcites indicates that these calcites precipitated from pore solutions characterized by $\delta^{18}\text{O}$ of -9 o/oo. The highest $\delta^{18}\text{O}$ analysed (-2.81 o/oo from a mudstone envelope) indicates precipitation from pore solutions with $\delta^{18}\text{O}$ of approximately -6 o/oo. The equilibrium oxygen isotopic composition for calcite at these low temperatures, assuming an initial seawater $\delta^{18}\text{O}$ of -4 o/oo, is -1 o/oo.

To explain the observed, ^{18}O -depleted authigenic calcites, either: (1)

the original precipitation temperature estimate for shallow-burial on the sea floor is significantly in error; (2) late-diagenetic recrystallization occurred at elevated burial temperatures (26 degrees C assuming pore-water $\delta^{18}\text{O}$ equal to that of seawater); (3) meteoric waters were involved; or (4) shallow-burial pore-waters rapidly evolved toward a more ^{16}O -depleted state.

Geologic constraints requiring a shallow-subsurficial origin rule out the first possibility. The heaviest $\delta^{18}\text{O}$ of -2.81 o/oo indicates a temperature of 12 degrees C for precipitation from unmodified seawater. The more typical $\delta^{18}\text{O}$ of -6 o/oo indicates a precipitation temperature of 26 degrees C, an unrealistic figure for such a deep-water setting. Such a temperature might be attained at a burial depth of approximately 1 km, depending on the geothermal gradient, but this is inconsistent with a shallow-burial origin as deduced independently from field and petrographic data. The heterogeneity of trace element distributions and sharp CL zoning (discussed in Chapters 7-9) dismiss the second possibility, i.e. a late diagenetic, higher temperature recrystallization during deep burial. Regarding the third possibility, the improbability of meteoric water influences has already been discussed (Chapter 10). Furthermore, the near equatorial position of the Lower Paleozoic of western Newfoundland (Ziegler *et al.*, 1979) implies that the isotopic composition of meteoric waters may not have been very different from that of seawater (approximately -4 o/oo).

The remaining possibility is that early diagenetic pore-waters became rapidly depleted in the heavy isotope of oxygen. The concentration of the heavy isotope of oxygen in non-carbonate diagenetic minerals or in

altered pre-existing minerals could lead to a decrease in the $\delta^{18}\text{O}$ of the residual pore-water (e.g. Lawrence et al., 1976). There is no evidence of such reactions having been important in the CHG, however.

The introduction of isotopically light oxygen from the oxidation of organics or exchange with organics could conceivably also lead to ^{18}O depletion in early diagenetic pore-waters (e.g. Coleman and Raiswell, 1981). Carbon isotopes are variable and interpretable in terms of early diagenetic, bacterial oxidation processes (detailed in following section). Could not oxygen isotopes also undergo a pronounced disequilibrium fractionation? "Vital" effects are well-documented in isotopic studies of echinoderms, corals, foraminifera, and coccolithophorids (see discussion in Anderson and Arthur, 1983). The paucity of data in the literature, however, is insufficient to confidently generalize regarding the disequilibrium effects in oxygen isotopes from the bacterial oxidation of organic matter. Regardless of the above uncertainties, an early diagenetic lightening of pore-water $\delta^{18}\text{O}$ possibly related to the bacterial oxidation of organic matter appears to be the only viable explanation for in situ diagenetic calcites in the CHG.

11.6.2 Cements: CFC, Equant, Calcites, and Grainstones

CFC (Group B) are interpreted to be in situ submarine cements (see Chapter 8). The negative $\delta^{13}\text{C}$ and $\delta^{18}\text{O}$ values indicate incorporation of isotopically-light, organically-derived bicarbonate, probably from the decay of organics in the underlying strata. In the following discussion, CFC are used as a convenient reference point with which to

compare other in situ diagenetic calcites.

The single analysis of early calcite cement from a marginal fracture in a nodule lies close to the CFC field. An early origin for this cement is suggested by petrographic evidence which indicates the nodule was exposed at one time on the sea floor (see Appendix N; Plate 53e). The late calcite cement within a fold nose in a contorted limestone contains moderately negative $\delta^{13}\text{C}$ and strongly negative $\delta^{18}\text{O}$. This particular sample, the most ^{18}O -depleted of this study, may reflect either the influence of meteoric groundwaters circulated during tectonism, or precipitation from hydrothermal waters.

Grainstones (Group H) were previously interpreted to have been cemented during very shallow burial. The fact that they consist of 60-70% transported shallow-water allochems with the remaining volume being early cement accounts for their proximity to the CFC field. The cement-precipitating pore-waters are interpreted to be similar to those which precipitated CFC.

11.6.3 Microspar and Pseudospar (Omitting Groups C and I)

Homogeneous microspar which forms continuously-bedded mudstones (Group D) or mudstone envelopes around grainy sediments (Group F) have similar $\delta^{13}\text{C}$ and similar $\delta^{18}\text{O}$ values. Although their fields do not overlap, based on field and petrographic evidence, they are interpreted to be early diagenetic precipitates. An exceptional mudstone envelope (Group F) has an anomalously heavy $\delta^{18}\text{O}$, the highest analysed in this study. This particular sample is interpreted to have been precipitated from

pore-waters which had not "evolved" as highly as those which precipitated most other diagenetic calcites.

The pronounced negative $\delta^{13}\text{C}$ of microspar mudstone and wackestone nodules in silicified shale (Group G), and to a lesser extent microspar in Group E, are typical of many concretionary limestones which contain organically-derived carbon (discussed below). Group E microspar have higher $\delta^{13}\text{C}$ than their associated pseudospar in Trends 1 and 2 implying that with progressive calcite precipitation, the contribution of isotopically light bicarbonate, probably from sulphate reduction, became increasingly more important. A similar trend occurs in the septarian nodule between the host pseudospar and the later, more ^{13}C -depleted, calcite cement (Trend 12). Pseudospar in conglomerate matrices (Group J) also may show distinctly negative $\delta^{13}\text{C}$.

Trends 1 and 2 also demonstrate a decrease in $\delta^{18}\text{O}$ with progressive precipitation. This can be explained by either a slight temperature effect or precipitation from slightly more evolved ^{18}O -depleted pore-waters. A temperature increase of only a few degrees would be sufficient to cause the largest increase in $\delta^{18}\text{O}$ seen (Trend 1). In Trend 12, the $\delta^{18}\text{O}$ shift is negligible. Pseudospar comprising the "ponded sediment" has moderately negative $\delta^{13}\text{C}$, but more importantly, it has the second highest $\delta^{18}\text{O}$ measured in calcites of this study. This suggests precipitation from relatively unevolved pore-waters, similar to those which precipitated the ^{18}O -enriched mudstone envelope (discussed above).

7

11.6.4 Displacive Fibrous Calcite and Associated Neospar

Without the accompanying neospar analyses, it would be tempting to interpret the range of $\delta^{13}\text{C}$ and $\delta^{18}\text{O}$ and tight clustering of DFC-1 (Group K) analyses as being indicative of relatively early precipitation from modified, marine pore-waters, analogous to the interpretation proposed for CFC. Serial sampling, however, shows that this is not the case. The two serial analyses going from microspar to pseudospar and then to DFC (Trends 3 and 4) clearly demonstrate the youngest calcite, the DFC, to have been precipitated from pore-waters which had already reached a maximum light carbon stage due to sulphate reduction. The pore-water $\delta^{13}\text{C}$ trend then reversed due to the increasing importance of heavy carbon bicarbonate from fermentation reactions. The proximity of the $\delta^{13}\text{C}$ values in the grainstone substrate and DFC fringe in Trend 5 also suggests a similar trend, but the change in $\delta^{13}\text{C}$ is small, possibly due to relatively heavy marine carbon in the allochems which make up 60-70% of this sediment.

DFC-2 trends are characterized by constant, increasing, and decreasing $\delta^{13}\text{C}$ with progressive precipitation. Neospar in Trends 6, 8, and 10 are interpreted as early precipitates from modified seawater, as suggested for Groups D, F, and H. In Trends 8, 9, and 10, decreasing $\delta^{13}\text{C}$ of successive precipitates suggests incorporation of bicarbonate generated from sulphate reduction. The interpretation for the increasing $\delta^{13}\text{C}$ in Trend 7 is the same as that for DFC-1 trends. Little change in $\delta^{13}\text{C}$ is found in Trend 6.

The minor variations of $\delta^{18}\text{O}$ in DFC-1 trends indicates that thermal or other effects are negligible. The slight shift to more negative $\delta^{18}\text{O}$ in DFC-2 trends suggests a minor temperature increase (less than 5 degrees C) or a minor decrease in pore-water $\delta^{18}\text{O}$ with progressive precipitation.

11.7 DISCUSSION: COMPARISON WITH OTHER STUDIES

In the CHG, lithification occurs by the growth of neospar, cementation of granular sediments, and precipitation of DFC. The relatively low $\delta^{13}\text{C}$ values of continuously-bedded as well as nodular limestones suggests that these processes happen early, with carbonate precipitation driven by the anoxic decay of organic matter. Early lithification of these limestones (i.e. concretion formation) is thus substantiated isotopically as well as by a plethora of previously-discussed field and petrographic evidence. In an isotopic study of the limestone-shale rhythms in the Blue Lias of Dorset, Campos and Hallam (1979, p. 27) also concluded that "the limestone beds and obviously secondary concretions are no more distinguishable isotopically than they are in gross composition and texture."

Variable and low $\delta^{13}\text{C}$ reflecting incorporation of bacterially-generated bicarbonate also characterizes nodular concretions in numerous other studies (e.g. Keith and Weber, 1964; Hodgson, 1966; Galimov *et al.*, 1968; Sass and Kolodny, 1972; Hudson and Friedman, 1974; Dickson and Barber, 1976; Hudson, 1977, 1978; Campos and Hallam, 1979; Coleman and

Raiswell, 1981; Marshall, 1982). The $\delta^{18}\text{O}$ of concretions in some studies indicates that they may have formed in contact with normal marine water but in other studies, concretions with more negative $\delta^{18}\text{O}$, are interpreted as later precipitates from warmer or more evolved pore-waters (Hudson and Friedman, 1974; Hudson, 1977, 1978; Campos and Hallam, 1979; Dickson and Coleman, 1980; Marshall, 1982). Coleman and Raiswell (1981) demonstrated a significant difference (greater than 5 o/oo) in the $\delta^{18}\text{O}$ composition of 2 nodular concretions separated stratigraphically by 5 m and suggested that local, early diagenetic pore-water effects were responsible for these differences, rather than thermal or meteoric water influences.

As in the CHG, other studies have shown that concretion growth may start with extremely negative $\delta^{13}\text{C}$ which gradually increases with progressive growth, ultimately converging toward more "typical" limestone values (e.g. Hoefs, 1970; Hudson and Friedman, 1974; Hudson, 1977). These changes are interpreted to signify either: (1) the cessation of the contribution of organically-derived bicarbonate and dilution with normal marine bicarbonate (Hudson and Friedman, 1974; Hudson, 1977; Marshall, 1982); or (2) they may signify the onset of methanogenesis and the production of heavy carbon bicarbonate (Irwin et al., 1977; Irwin, 1980). These changes are often accompanied by a decrease of $\delta^{18}\text{O}$ for reasons discussed above.

Although they have received considerable attention in the literature, isotopic analyses of DFC are few in number (e.g. Hodgson, 1966; Campos and Hallam, 1979; Hudson, 1978; Marshall, 1982). Their wide-ranging $\delta^{13}\text{C}$ and $\delta^{18}\text{O}$ values are comparable to those of non-DFC concretions. For

example, the beef seams analysed by Campos and Hallam are characterized by slightly positive $\delta^{13}\text{C}$, ranging from -0.48 - $+1.17$ o/oo (5 analyses) whereas DFC analysed by Hodgson (1966) ranges from -29 o/oo to as high as $+2$ o/oo (18 analyses). The single analysis reported by Hudson (1978) has $\delta^{13}\text{C} = -0.90$ o/oo.

Notable among isotopic studies of DFC is the recent work of Marshall (1982) who examined DFC from various Mesozoic shales in England. His study was based on detailed serial analysis of several samples of DFC and in some, the mudstone or grainstone substrate. As many as 40 points were analysed for $\delta^{13}\text{C}$ and $\delta^{18}\text{O}$ in one particular sample. In contrast to the findings of this study, $\delta^{13}\text{C}$ of the British DFC is approximately 0 o/oo whereas $\delta^{18}\text{O}$ varies from -4 to -11 o/oo. These isotopic compositions were interpreted to indicate precipitation of DFC at burial depths of tens or hundreds of metres, after the termination of bacterial degradation of organics and after significant modification of the pore-water oxygen isotopic composition. The mudstone substrates were characterized by markedly negative $\delta^{13}\text{C}$ (as low as -14 o/oo), but $\delta^{13}\text{C}$ values progressively increased until the last stages of DFC growth were approximately 0 o/oo. Reversals in isotopic trends were noted in some samples and were correlated with sharp fabric discontinuities in the fringes.

11.8 SUMMARY AND CONCLUSIONS

Isotopic analysis of calcite demonstrates wide-ranging $\delta^{13}\text{C}$ values, reflecting derivation of bicarbonate from bacterial degradation of organic matter as well as the changing importance of different degradation reactions. Isotopic analyses are congruous with field and petrographic evidence which indicate early lithification of limestones, ranging from grainstones to parted, ribbon, and nodular mudstones.

RFC analyses, although not part of the in situ diagenetic suite, are clustered together and suggest, along with CL evidence, retention of their primary isotopic signature. Most authigenic, in situ calcites are characterized by more negative $\delta^{13}\text{C}$ than RFC, indicating a variable contribution of organically-derived carbon.

Serial analyses illustrate trends which are characterized by decreasing or increasing $\delta^{13}\text{C}$ with progressive precipitation. In the first case, precipitation is still largely driven by sulphate reduction, whereas in the second, rising $\delta^{13}\text{C}$ reflects the increasing importance of fermentation in controlling the $\delta^{13}\text{C}$ of pore-waters. Serial analyses also show that some microspar and pseudospar mudstones are lithified before $\delta^{13}\text{C}$ becomes obviously negative. Other mudstones contain prominently negative $\delta^{13}\text{C}$, suggesting relatively later lithification well within the zone of sulphate reduction.

Assuming a temperature of 23 degrees C for the precipitation of RFC in

the shallow waters of the platform margin, seawater $\delta^{18}\text{O}$ is estimated to be approximately -4 o/oo. Assuming a bottom temperature of approximately 5 degrees C, most in situ diagenetic calcites in the CHC suggest precipitation from pore-waters with $\delta^{18}\text{O}$ of -9 o/oo. This pore-water depletion of ^{18}O is suggested to be related to bacterial oxidation of organic matter during early diagenesis. Serial analyses show either approximately constant $\delta^{18}\text{O}$ during precipitation or a small decrease in $\delta^{18}\text{O}$ of the precipitates. The decrease may be due to either a small temperature increase (a few degrees C), or further bacterial modification of pore-water $\delta^{18}\text{O}$.

Chapter 12

DOLOMITIZATION IN THE COW HEAD GROUP

12.1 INTRODUCTION

Dolomite in the CHG is conveniently divided into two major groups - "Early" and "Late" - based on field and petrographic relationships. This simple dichotomy belies the complexity and variability within each of these groups. The Early dolomite group is the most important in terms of stratigraphic and geographic extent and volume. These dolomites are also significant petrogenetically because, in some instances, they can be related to calcite diagenesis. The group includes: (1) dolomitic siltstone, (2) matrix dolomite, (3) limestone-hosted dolomite, and (4) conglomerate matrix dolomite. Late dolomite, on the other hand, is geographically restricted although when it occurs it may be the dominant carbonate present. Included in this group are (5) joint dolomite and (6) pervasive replacement dolomite. Joint dolomite demonstrates structural control, namely faults and joints, although the controls of the more widespread pervasive replacement dolomite at the White Rock Islets, and a few smaller occurrences, is uncertain. Petrographically, pervasive replacement dolomite is similar to joint dolomite.

An additional occurrence of dolomite is in microveinlets. These are unrestricted geographically and stratigraphically and occur in all lithologies, truncate primary sedimentary structures, and may also include variable proportions of calcite, microquartz, and megaquartz. The petrographic, CL, and staining characteristics of these dolomites are similar to those of dolomite in the host sediment. Consequently, these likely have a similar origin, which could be either Early or Late. No further consideration is given to microveinlet dolomites.

12.2 EARLY DOLOMITES

12.2.1 Distribution

Early dolomites are distributed in the sediments in various ways, detailed below.

(1) Pervasive Dolomitic Siltstone: In outcrop these siltstones are tan-coloured and resistant-weathering. Interbedded shales may be any colour and are commonly also dolomitic (Plate 5b,d,e; 6a-e). In these sediments, primary sedimentary structures and burrows are well-preserved and undistorted (Plate 8c). Many of the outcrops of siltstone lithofacies described in Chapter 2 are dominated by these pervasive dolomitic siltstones.

(2) Matrix Dolomite: This dolomite occurs as the familiar tan-weathering, marl interbeds in ribbon limestone sequences, internodule matrix in nodular intervals, and as the paper-thin partings

in parted limestone sequences. Dolomitic shales (marls) may grade into shales containing few or no obvious dolomite crystals.

(3) Limestone-Hosted Dolomite: These dolomite crystals are dispersed in mudstones to grainstones. Also included in this group are polycrystalline clasts of dolostone. In sediments which have undergone tectonic pressure solution (see Chapters 5 and 13) dolomite crystals are concentrated as stylolites along with argillaceous material and siliciclastics (Plate 48d).

(4) Conglomerate Matrix Dolomite: Conglomerate matrix dolomite is restricted mainly to the matrices of Cambrian conglomerates at Cow Head North and at Martin Point. Where associated with CFC at Cow Head North, it occurs as a pore-filling which post-dates the calcite, either as a discontinuous crust or filling the remainder of the pore; or it selectively replaces internal mudstone and wackestones sediments which post-date the fibrous calcite (Plate 32b,c; 33a-c).

12.2.2 Petrography

Early dolomite crystals typically range from 10-75 μm in size, although within individual samples, there is usually only minor size variation. In dolomitic siltstones and limestones, the size of these crystals is commonly closely correlated with that of associated calcitic peloids and siliciclastics. Conglomerate matrix dolomite is generally more coarsely crystalline, and 50-100 μm -size crystals are common, and some reach 250 μm in size. Sand-size clasts of dolostone are well-rounded and consist of numerous tightly-intergrown crystals up to 80 μm in size.

Crystal shape varies from subhedral to euhedral, the latter commonly forming sucrosic mosaics in pervasive dolomitic siltstones, matrix dolomites, and conglomerate matrix dolomites. Undulose extinction is observable in most of the larger crystals and is also observed in silt-size crystals in high quality, doubly-polished, ultra-thin sections. Larger crystals also demonstrate gently curved crystal faces. ;

Most of these dolomite crystals are characterized by cloudy cores and relatively clear, inclusion-free rims ("CCCR"; Plate 48a). In some crystals, especially conglomerate matrix dolomites, inclusions are evenly distributed throughout. Core shape, as determined by the abundance of inclusions as well as CL (see below), varies from euhedral (rhombic) to anhedral; occasionally, some anhedral cores are spherical. The majority of inclusions are micrometre-size and generally unresolvable by methods used in this study. Pyrite cubes and Fe-free calcite inclusions up to 5 μm in size are differentiable and appear in some cases to replace portions of their host dolomite crystal.

Dolomitization occurs preferentially along selected laminations within some grainstones (Plate 47a). In other beds, bioclasts, peloids, and ooids are preferentially dolomitized over other allochems or calcite cement. Peloids and ooids are occasionally replaced by micrometre-size, anhedral dolomite crystals which faithfully retain original microfabrics. Where clast dolomitization is only partial, only the outer margins of grains are dolomitized. In some ooids the nuclei are preferentially dolomitized whereas in others the opposite is true. Dolomitization is also selective in some grainstone lithoclasts where peloids are dolomitized and interparticle calcite remains unaltered. Impingement (sensu Sibley, 1982) of peloids and bioclasts by dispersed

dolomite crystals occasionally preserves the original grain outline as "dust" inclusions in the dolomite crystal (Plate 34a; 48c).

12.2.3 Cathode Luminescence and Trace Elements

CL study demonstrates that most dispersed, matrix, and pervasive siltstone dolomite crystals consist of a central or innermost "core" and outer "rim". Later it will be shown that many cores are detrital grains, most are replaced calcitic peloids, and rims are diagenetic overgrowths which nucleated upon the cores or grew outward from the replaced peloids. Rims are distinguished from their cores by geometric or zoning discontinuities, or by the uniform crystal "microstratigraphy" of rims which contrasts with the variable zoning seen in cores. The common microstratigraphy of the rims reflects authigenesis under the same prevailing pore-water conditions.

12.2.3.1 Cores

The rhombic to spherical shape of many cores seen in CL corresponds to the inclusion-rich central regions seen in transmitted light. Most cores are dull-luminescent or dark and show little or no CL zoning (Plate 49d), except in some cases, by lengthy photographic exposures. Bright-luminescent red, orange, and yellow multi-zoned cores are locally common, and may be dominant in some dolomitic siltstones (Plate 49a,b,e). When abundant, it is clear that these bright cores comprise a heterogeneous group in terms of their CL zoning patterns and intensities. Zones within these bright cores are often discordant with subsequent overgrowth (Plate 49e). Sand-size, dolostone clasts are especially obvious with CL because of their larger size as well as variable luminescence characteristics (Plate 49e,f).

Most medium silt-size and smaller crystals are difficult to examine with CL because of their small size; this problem is especially acute in most siltstones associated with red shales (Plate 49c). Scattered bright orange, red, and yellow specks in limestone, matrix, and finely crystalline siltstones are logically interpreted to be more finely crystalline counterparts of the larger, easily-resolvable bright, zoned cores.

12.2.3.2 Rims

Rim size in crystals with cores is variable, typically 20-40 % of the crystal size (ca. 40-60 % volume; Plate 49a-e,f). Most matrix dolomites (Plate 49h,k) and conglomerate matrix dolomites (Plate 35c) do not have resolvable cores as described above, but instead all crystals within a given sample share the same CL microstratigraphy from the centre to the edge of the crystal. The CL microstratigraphy of these crystals as well as the rims in cored crystals is uniform within samples, but varies widely between samples. On the other hand, in some mudstones, dispersed dolomite crystals appear to lack rim growth altogether.

Many Early dolomite crystals with cores have rims which are totally, or just peripherally, ferroan [1]. Internal ferroan zones, crystals with more than one ferroan zone, and ferroan cores are comparatively rare.

1. As for calcites, the terms ferroan and non-ferroan simply reflect the presence or absence, respectively, of an iron-stain using potassium ferricyanide solution

Conglomerate matrix dolomite may be either non-ferroan or totally ferroan whereas many matrix dolomite crystals are mostly ferroan. Strongly ferroan (i.e. intensely stained) zones in rims (greater than 1.0 wt % FeO [2]) are dark whereas weakly ferroan (0.5-1.0 wt % FeO) or non-ferroan (less than 0.5 wt % FeO) zones have weak to bright, red-luminescent rims. These generalizations, however, are not applicable to cores, which are generally dull or dark, unstained, and contain less than 0.5 wt % FeO.

The peripheral increase in iron content is most pronounced in dolomite crystals within argillaceous sediments. This is clearly seen in the transition from limestone to argillaceous matrix where dolomite crystal rims become progressively more ferroan as they undergo additional growth. This relationship suggests that dolomite crystals in argillaceous sediments continue to grow after comparable crystals in limestone have ceased growing, a relationship also confirmed by CL.

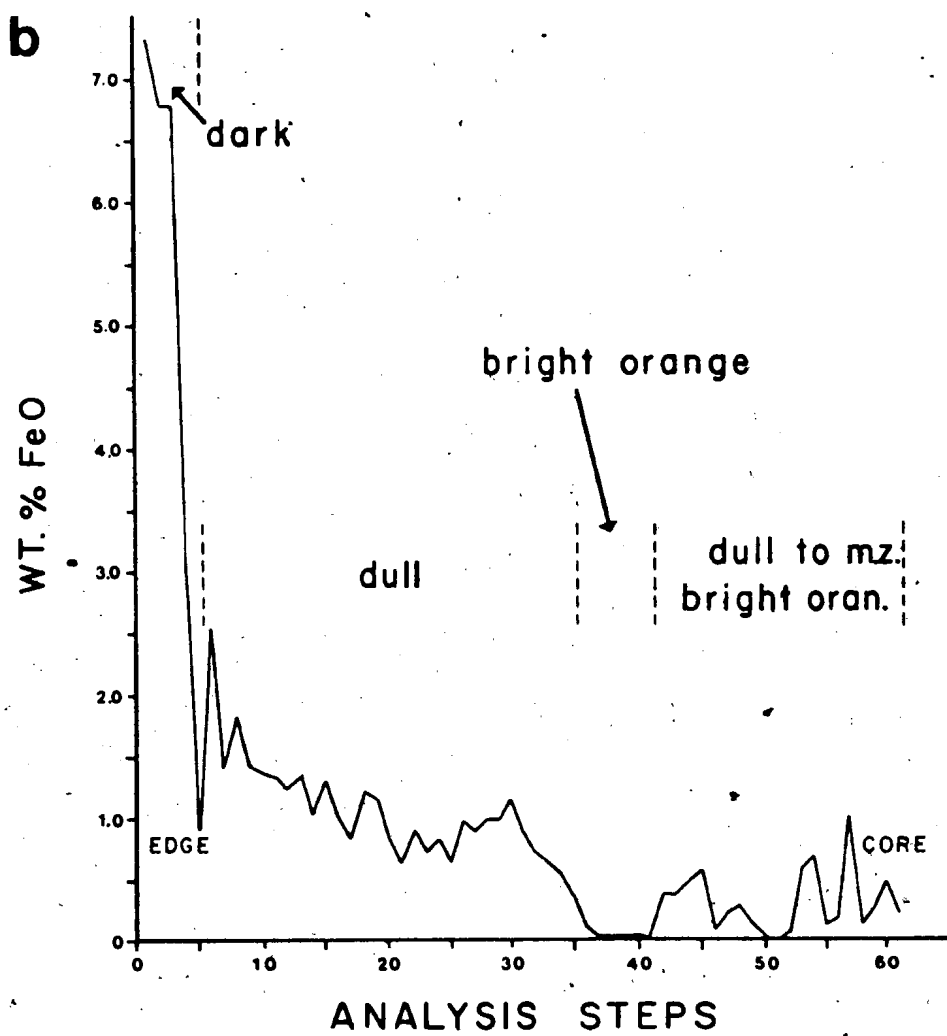
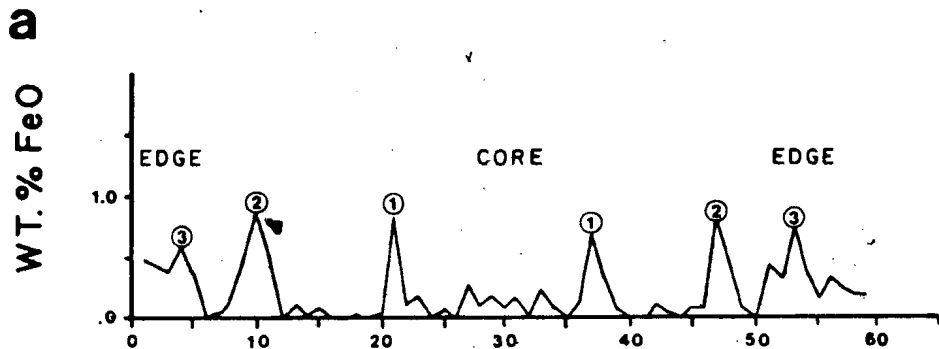
CL and microprobe analyses demonstrate that iron zoning occurs on a much finer scale than indicated by staining with zones typically ranging from 5-40 μm in width. These commonly can be further subdivided into numerous micrometre-wide, subtly-varying subzones.

In most dolomites iron content controls luminescence of this mineral (Figure 12.1a). This is not the case, however, in siltstones in red shales where elevated concentrations of MnO cause bright red luminescence (Plate 49c,d). In these crystals MnO contents commonly

2. FeO of 2 wt % is common in the outermost zones; the most ferroan zone analysed contains 7 wt % FeO.

Figure 12.1: (a) Microprobe step traverse (FeO wt % versus microprobe step number) across a replacive, conglomerate matrix dolomite crystal from the same thin section as shown in Plate 35c. Zones 1, 2, and 3 are all dark whereas the intervening areas are finely-zoned and moderately bright, orange-red luminescent. MnO is not detectable in this sample and CL appears to be exclusively controlled by FeO content. Distance between each step is 2 μ m. Cow Head North, Upper Cambrian, Bed 2, sample CHN-2.

(b) Microprobe step traverse (FeO wt % versus microprobe step number) from the centre to the edge of a fracture-filling joint dolomite cement from the same thin section as shown in Plate 49i. CL characteristics are indicated on diagram. MnO is not detectable in this sample and CL appears to be exclusively controlled by FeO content. Distance between each step is 5 μ m. Broom Point South, Upper Cambrian, unit 33, sample BPS-33-A.



reach 0.5 wt %; the most manganiferous zone analysed contains 2.6 wt % MnO. These dolomites are usually non-ferroan throughout. As with iron trends in other dolomite crystals, dolomite in red shales may show increasing MnO concentrations with progressive growth, with or without a complimentary increase in FeO.

12.2.4 Corrosion

Dissolution or corrosion occurred during growth of some dolomite crystals. This was usually followed by additional dolomite growth, calcite precipitation (dedolomitization), or silicification.

12.2.4.1 Corrosion Followed by More Dolomite Precipitation

With CL, corrosion and renewed growth of dolomite is suggested by embayed and jagged boundaries between core and rim or between successive zones within the rim (Plate 49g). These corrosion surfaces are not correlateable from sample to sample and most do not contain any evidence of corrosion. Peripheral corrosion of dolostone lithoclasts also occurs (Plate 49f).

12.2.4.2 Corrosion Followed by Calcite

Some dolomite crystals, especially those dispersed in limestone or forming pervasive dolomitic siltstones appear to have been corroded, with simultaneous or later precipitation of calcite. This calcite occurs in the following ways: (1) as irregular to crystallographically-controlled embayments into the dolomite crystal;

(2) within the core; (3) intermittently along the contact of core and rim; and (4) as dispersed, micrometre-size calcite inclusions. Rare dolomite cores are completely calcitic, have a rhombic shape, and are surrounded by a dolomite rim with which it is in optical continuity.

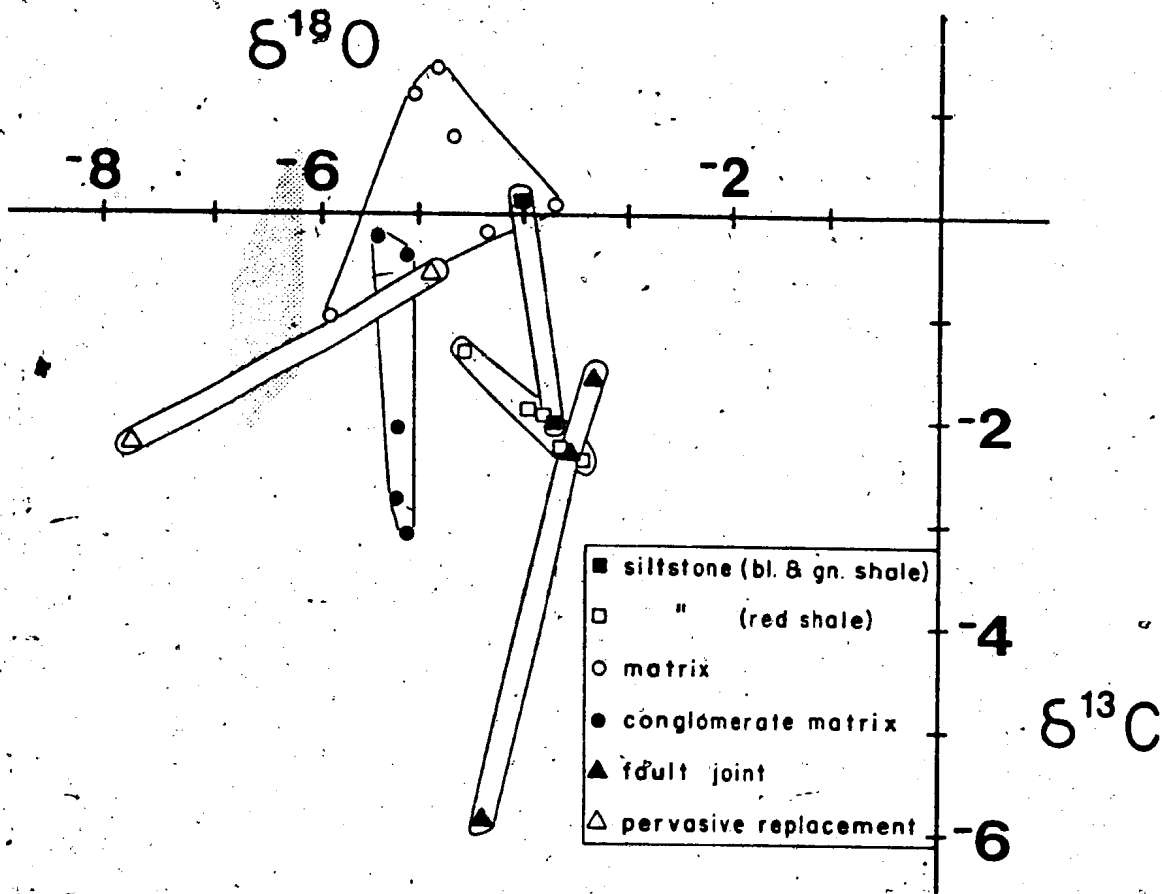
12.2.4.3 Corrosion Followed by Chert

Dolomite corrosion also occurs in some siltstones associated with red shales (Plate 48b). In these siltstones, the dolomite crystals often appear pitted and suspended within a chert matrix.

12.2.5 Stable Isotopes

Twenty-three bulk samples of Early and Late dolomite were analysed for their stable isotopes of carbon and oxygen; these are plotted in Figure 12.2, listed in Appendix I, and samples described in Appendix J. $\delta^{18}\text{O}$ values are uncorrected as recommended by Land (1980). The most serious drawback of using such averaged results is that characteristic isotopic fingerprints from diagenesis in one or more bacterial oxidation zones may be masked (see Chapter 11). For example, if dolomite commenced growth during sulphate reduction, the earliest dolomite might have $\delta^{13}\text{C}$ as low as -25 o/oo. Subsequent precipitates, perhaps in the zone of methane production, could produce dolomite with $\delta^{13}\text{C}$ as high as +15 o/oo (Irwin et al., 1977). Depending on the relative volumes of dolomite precipitated with these isotopic signatures, the resultant "averaged" $\delta^{13}\text{C}$ value may be quite unremarkable and indicate nothing of the importance of organic matter degradation in the generation of these dolomites.

Figure 12.2: $\delta^{13}\text{C}$ versus $\delta^{18}\text{O}$ plot of various types of dolomite recognized in the CHG. $\delta^{18}\text{O}$ values are uncorrected. Stippled area denotes the position of CFC from Figure 11.1. CFC and conglomerate matrix dolomite are the only calcite-dolomite pairs in which there are petrographic relationships to suggest possible co-precipitation or precipitation of one shortly after the other.



Three types of Early dolomite were analysed: (1) pervasive siltstones associated with green and black shales, and those associated with red shales, (2) matrix dolomite, and (3) conglomerate matrix dolomite (Figure 12.2). Only two samples of dolomitic siltstone associated with black and green shales were analysed. Their $\delta^{18}\text{O}$ are similar but their $\delta^{13}\text{C}$ differ by approximately 2 o/oo. Dolomitic siltstones in red shales cluster closely together, having 1 o/oo or less variation in both $\delta^{13}\text{C}$ and $\delta^{18}\text{O}$. Matrix dolomites vary widely with respect to both $\delta^{13}\text{C}$ and $\delta^{18}\text{O}$. They contain the highest $\delta^{13}\text{C}$ of the Early dolomites (+1.42 o/oo) as well as a greater than 2 o/oo variation in $\delta^{18}\text{O}$. Conglomerate matrix dolomites vary considerably in their $\delta^{13}\text{C}$ (-0.23 - -3.11 o/oo) but have minor variation in $\delta^{18}\text{O}$ (ca. 0.3 o/oo).

12.2.6 Timing

The lack of obvious compaction of primary sedimentary structures and burrows in pervasive dolomitic siltstones and their associated, dolomitized shales and the periodic interruption of CFC submarine cement fringes by conglomerate matrix dolomite suggests that these dolomites are of an early, precompaction origin (Plate 33 b; Figure 12.3). In contrast, matrix dolomite is interpreted to have fully lithified after limestone lithification and after some compaction, but prior to final compaction. This is indicated by the convergence of grainy laminations at the margins of early-lithified limestone nodules as well as relationships such as that illustrated in Plate 47b. This particular outcrop illustrates that matrix dolomitization preceded final compaction of the argillaceous sediments. Here, a 15 cm-thick, tan-weathering

Figure 12.3: Schematic summary of dolomitization in the Cow Head Group. In the field sketches, dolomite is lightly stippled, limestone is white and shale beds are black. In the thin section sketches, dolomite is represented by black rhombs, calcite is white.

Precompaction dolomitization is indicated by dolomitic marls containing uncompact burrows and dolomitic siltstones which have underformed primary sedimentary structures. Early-formed dolomite incorporated into conglomerates may act as plastic matrix or clast. In thin section, periodic interruption of CFC fringe growth indicates early dolomite precipitation.

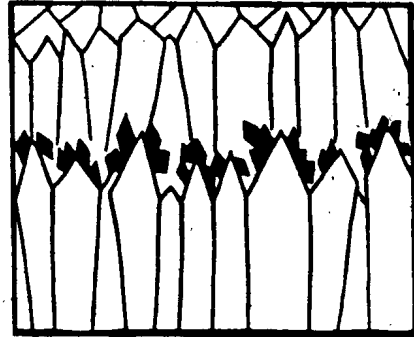
Syncompaction dolomitization is indicated by squashed burrows in dolomitic marl, convergent laminations at the margins of early-lithified limestone nodules, and dolomitic marl laterally grading to a more compacted shale.

Postcompaction dolomitization occurs along joints and faults overprinting both limestone and older dolomite. In thin section dolomite is found at stylolites. Comparison of these dolomites with those dispersed in limestone indicates that the stylolite has not been the focus of dolomitization but rather has simply mechanically gathered early-formed dolomite.

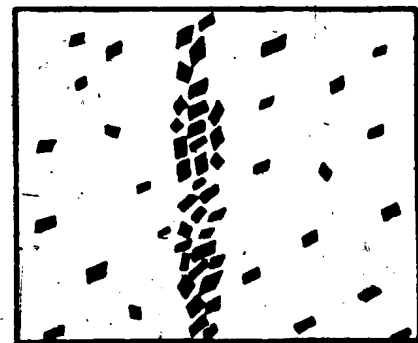
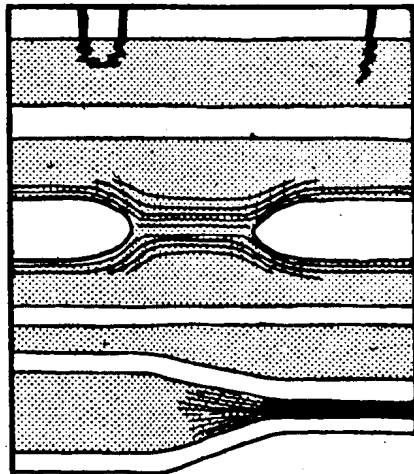
FIELD

THIN SECTION

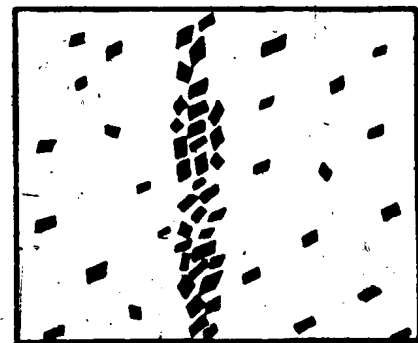
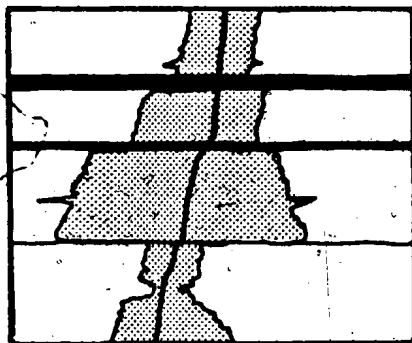
PRECOMPACTION



SYNCOMPACTION



POSTCOMPACTION



dolomitic marl is observed to grade laterally, over a distance of a few centimetres, into a 8 cm-thick black shale. Relative compaction is approximately 50 %. The petrographic characteristics of this marl and its laterally equivalent shale are identical to those of other marls and shales examined from the CHG.

That dolomitization is a shallow-burial phenomenon is also indicated by the incorporation of dolomite into conglomerates, either as discrete clasts or local, plastically-deformed matrix (Figure 12.3).

Dolomitization must have occurred within a few metres of the sediment-water interface so as to have dolomitic sediments available for incorporation into debris flows. The lower depth limit of dolomitization, however, is not known. Whereas lack of compactive relationships indicate lithification during shallow burial, the converse does not necessarily hold true. For example dolomitization may have occurred very early in a terrigenous mud but was not sufficiently widespread, perhaps due to lack of suitable nuclei, to develop a self-supporting framework and the terrigenous muds, therefore, were allowed to compact.

Additional uncertainties in estimating the timing of dolomitization are related to their complex and protracted diagenetic histories suggested in part by the extremely variable, fine-scale CL zoning. Dolomite may have started growing during very shallow burial and continued to grow until it was deeply buried (cf. Irwin, 1980; Kelts and McKenzie, 1982); or, sediments which were partially dolomitized early may have been eroded and incorporated into debris flows only to have acted as a template for later, deeper burial dolomitization.

Dolomite crystals gathered at stylolites in limestones are identical to those dispersed throughout the limestone host. This implies that precipitation of Early dolomite crystals predates pressure solution.

12.3 INTERPRETATION OF EARLY DOLOMITES

12.3.1 Cores

A detrital [3] or clastic origin for the bright, multi-zoned cores seen in CL accounts for the following: (1) variation in core shape and luminescence, (2) zoning discordance with subsequent overgrowth, and (3) the association with calcareous and siliciclastic grains of similar size. Variability of luminescence zoning patterns and colours is interpreted to reflect multiple sources, either geographic or stratigraphic, for these clastic dolomite grains. The discordance of core zoning with that of subsequent overgrowth and their often rounded shape is the result of mechanical abrasion during erosion and transport. Polycrystalline dolomite clasts, with their variably-zoned and tightly intergrown dolomite mosaic, are interpreted to have been

3. The term "detrital" has been used by different authors to mean different things. For example, Sabins (1962) used the term to refer to polycrystalline grains eroded from extrabasinal dolostones. These were distinguished from "primary" dolomite grains which were single crystals of dolomite formed, eroded, transported, and deposited intrabasinally. The present usage is consistent with that of Freeman *et al.* (1983) where "detrital" refers to grains which have been transported and sedimented. Detrital grains may be syndimentary and intrabasinally-derived or extrabasinally-derived from lithified dolostone. In the latter case such grains are also commonly referred to as terrigenous.

derived from the erosion of lithified dolostone.

In contrast to the relatively bright, multi-zoned cores, interpretation of the dark to weak-luminescent cores is less straightforward. Their correct interpretation is critical, however, as most pervasive dolomitic siltstones and dispersed dolomite crystals contain this type of core. In siltstones associated with red shales, dark to weak-luminescent cores are overwhelmingly dominant. The size and shape of the dark to weak-luminescent cores suggests that they are either detrital, as are the bright-luminescent, zoned cores, or a diagenetic alteration of calcitic peloids. A detrital origin for these cores implies that the primary sediment was a dolomitic siltstone containing no calcitic peloids. The existence of a primary sediment with such a composition, lacking calcitic peloids, is unlikely, given the ubiquity of peloids in all other sediments (including silicified and phosphatized equivalents). Based on this, the deposition of such pure detrital dolomite beds is considered to be highly unlikely.

The preferred explanation is that the dark to weak-luminescent cores result from the replacement of silt-size calcitic peloids by dolomite. Inclusions are interpreted to be peloid relics, either calcite that was subsequently dissolved (there are no calcite relics now), or possibly argillaceous, organic, or pyritic materials that were part of the peloids prior to dolomitization. A similar conclusion was reached by Sibley (1982) in a study of CCCR (cloudy-centered, clear-rimmed) Pliocene dolomites from the Netherlands Antilles. This explanation is also supported by dolomite crystals which impinge undolomitized peloids and bioclasts but preserve relic inclusions which outline the boundary

R

of the partially-replaced allochem (Plate 34a, 48c). Some of the dark and dull-luminescent cores must be detrital (why should detrital cores all be bright-luminescent?), but a peloid precursor for most of these is compositionally and texturally consistent with other sediments in the CHG.

Thus, dolomitization of these sediments occurs along two pathways: (1) diagenetic enlargement of detrital dolomite cores and (2) replacement of calcitic peloids and further enlargement by precipitation of relatively clear dolomite. CL microstratigraphy of authigenic overgrowths indicates that alteration along these two pathways occurs simultaneously. Together they account for the highly sorted nature of dolomitic siltstones, the CL characteristics, and the ubiquity of cloudy cores and clear rims.

Dolomite crystals with detrital cores have also been described in other sediments ranging in age from Middle Ordovician to Tertiary (Sabins, 1962; Amsbury, 1962; Reed, 1968; Lindholm, 1969; Freeman et al., 1983). Like CHG dolomites, these detrital dolomites are dominated by single crystal grains; polycrystalline dolomite grains are comparatively rare. Pitted, broken, and rounded rhombs occur and the abundance and size of detrital dolomite is positively correlated with their associated siliciclastics. In addition, these detrital crystals form the nuclei or cores for subsequent overgrowth (i.e. diagenetic enlargement) by relatively inclusion-free dolomite, thus forming the familiar crystals with cloudy cores and clear rims (e.g. Lindholm, 1969; Freeman et al., 1983).

12.3.1.1 Source

Two possible sources for detrital dolomite must be considered: (1) derivation from an older carbonate terrain (e.g. Amsbury, 1962; Sabins, 1962; Lindholm, 1969; Freeman et al., 1983), and (2) erosion of penecontemporaneous dolomite from tidal flats, the supratidal, or high intertidal zone (see Zenger, 1972). Considering the first possibility, the heterogeneity of luminescence characteristics in the bright-luminescent cores and polycrystalline dolomite grains is interpreted to reflect geographic and/or stratigraphic variation in the parental carbonates. Furthermore, the high degree of crystal intergrowth and grain rounding exhibited by polycrystalline clasts indicates that the source sediment must have been lithified. Subaerial or submarine highlands or fault scarps, for example, may have provided sufficient relief to expose a variety of dolostones to contribute both single crystals and polycrystalline clasts.

A brief study CL study of representative dololaminites which characterize much of the Middle to Lower Ordovician autochthonous, platformal succession in western Newfoundland was undertaken in order to assess the second possibility; i.e. the dull to dark cores could also be detrital [4]. A supratidal to shallow subtidal origin for these sediments is suggested by stratigraphic considerations as well as millimetre-scale laminations, mudcracks, prism cracks, tepees, and flat-pebble breccias (Haywick and James, 1984). Crystal size, cloudy cores, and clear rims are similar to those of the CHG and 4 out of the 5

4. Five dololaminites were examined, provided courtesy of D. Haywick.

samples examined are non-ferroan throughout. Luminescence is dull to weak orange-red and zoning is detectable in only one sample. The dull to weak luminescence of these crystals, their low iron content, and their size suggests that dololaminites, such as these Lower Ordovician ones, could also be a source for some of the dark to weak-luminescent dolomite cores in the CHG dolomites.

12.3.2 Cathode Luminescence and Trace Elements

The strong control of luminescence in the authigenic dolomites by iron is consistent with data in Pierson (1981). This may apply, however, only for low Mn concentrations (Fairchild, 1983). For the low MnO concentrations of this study, CHG dolomite is dark at FeO concentrations of 1 wt % or more. This limiting value corresponds closely with that determined in a number of other studies (compiled in Fairchild, 1983; see Figure 8.1).

The increase in iron content of many dolomites with progressive precipitation is consistent with progressively decreasing redox potential of the precipitating solutions and increasingly solubility (and availability?) of iron. Pertinent details have already been presented in Chapter 8 for calcite.

12.3.3 Interpretation of Stable Isotopes

$\delta^{18}\text{O}$: The variations in the trace element geochemistry as indicated by staining, microprobe, and more sensitively by CL, suggest that intracrystalline variations in isotopic composition are also probable.

Given this, it is surprising that the petrographically-defined fields are isotopically distinct (Figure 12.2). From petrographic and CL study, dolomitic siltstone analyses are a mixture of older isotopes derived from their detrital cores, as well as younger isotopes from the authigenic rims. Peloids which were dolomitized may have also influenced the composition of cores. Collectively these dolomites have the heaviest $\delta^{18}\text{O}$ values of the Early dolomites analysed (ca. -4 o/oo). In contrast, matrix dolomites and conglomerate matrix dolomites have slightly smaller $\delta^{18}\text{O}$ values (ca. -5 o/oo). These particular dolomites are almost totally authigenic; any detrital cores would contribute a volumetrically negligible amount of old isotopes to these analyses. Based on this simplistic approach, detrital cores have heavier $\delta^{18}\text{O}$ than authigenic dolomite. This conclusion is also consistent with a tidal flat origin for many of the cores (Haywick, pers. comm., 1984).

In his summary paper on dolomitization, Land (1980) indicated that the $\delta^{18}\text{O}$ of dolomite should be greater than that of coprecipitated calcite by a value of 2-4 o/oo at 25 degrees C, although values from 1-7 o/oo are possible depending on assumptions made. The $\delta^{18}\text{O}$ of -5 o/oo for dolomite and the clustering of $\delta^{18}\text{O}$ around -6 o/oo for the various calcites analysed roughly approximates the expected relationship for coprecipitates. From petrography, however, this is neither unequivocally established nor is it probable in many instances (discussed previously).

$\delta^{13}\text{C}$: Variation in $\delta^{13}\text{C}$ is considerably greater than that for $\delta^{18}\text{O}$. The siltstone and the conglomerate matrix dolomites both reach low $\delta^{13}\text{C}$ of

less than -2 o/oo and suggest incorporation of isotopically light carbon derived from the decomposition of organic matter, a situation analogous to that previously described for calcite. Matrix dolomites, which are collectively the most ferroan and latest(?) of all the Early dolomites, also have the highest $\delta^{13}\text{C}$. The relatively high iron content of matrix dolomite, either concentrated in peripheral zones or more evenly spread throughout the crystal, suggests that these dolomites were precipitated or continued to grow later than other Early dolomites analysed.

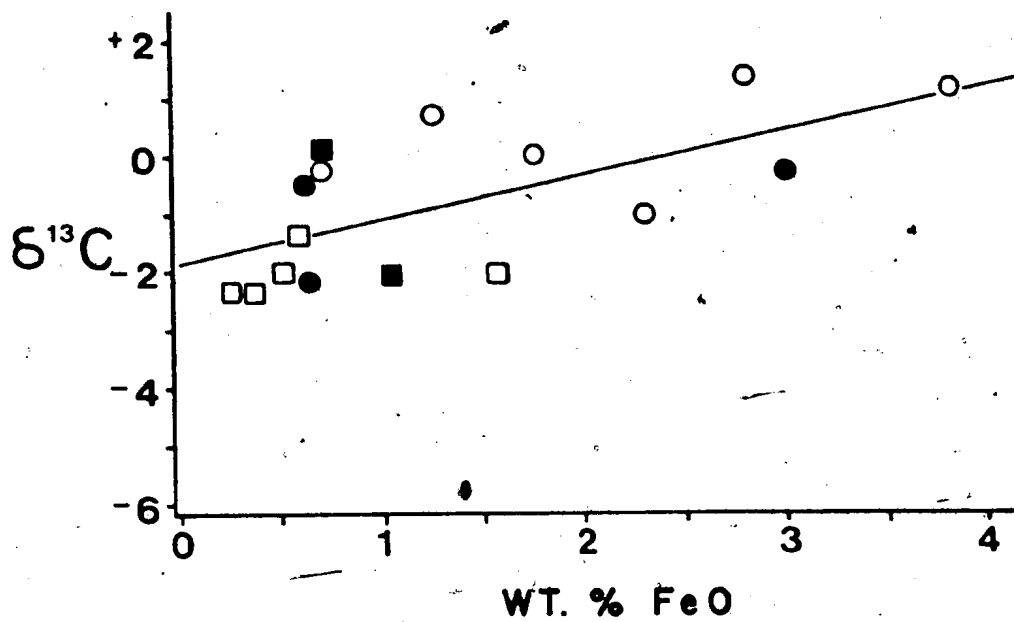
A plot of bulk FeO composition (determined by AAS [5]) versus $\delta^{13}\text{C}$ shows that they are positively correlated [6] (Figure 12.4). Assuming that most of the iron in dolomite is concentrated in the stained, ferroan rims, then with progressive precipitation, dolomite incorporates increasingly heavier $\delta^{13}\text{C}$. The most ferroan rim analysed contains approximately 7 wt % FeO, and the $\delta^{13}\text{C}$ of this precipitate is estimated to be approximately +3.5 o/oo.

The above approach is admittedly simplistic and necessarily ignores a host of potentially complicating factors, a most important one being that carbon in dolomite could be remobilized from a precursor calcite. If this was the case and the rock-water system was closed to carbon, then

5. Atomic absorption spectrophotometry (AAS) of dolomite leachates yielded high levels of Si and Al and suggest significant contamination by dissolution of clays and possibly other minerals (Appendix I). These analyses were also treated using R-mode factor analysis (SPSS) without yielding meaningful results other than confirming the contamination problem. Despite this, FeO concentrations are sufficiently high to be correlateable to staining trends, CL, and microprobe data.

6. A linear regression for FeO wt % versus $\delta^{13}\text{C}$ yields $r = 0.64$ for $n = 16$. This is significant at the 99% confidence level.

Figure 12.4: Plot of Early dolomite $\delta^{13}\text{C}$ versus bulk FeO concentration as determined by AAS. $\delta^{13}\text{C}$ is positively correlated with FeO concentration (at 99% confidence level; $r=0.64$). Filled squares - pervasive dolomitic siltstone associated with black and green shales; open squares - pervasive dolomitic siltstone associated with red shales; filled circles - conglomerate matrix dolomite; open circles - matrix dolomite.



dolomite would take on the carbon isotopic fingerprints of whatever calcite was replaced. In this manner even late burial or tectonically-related dolomite, well-beyond the stage of organic matter degradation, might have a carbon isotopic composition which was originally produced during much shallower burial.

12.4 DISCUSSION

The mechanism which best explains Early dolomites in the CHG is similar to that for calcite authigenesis, i.e. carbonate precipitation during the anoxic oxidation of organic matter. This mechanism is entirely consistent with the following observations:

- (1) Field and petrographic evidence indicates a shallow-burial origin.
- (2) The negative $\delta^{13}\text{C}$ of some of these dolomites (less than -2 o/oo) suggests incorporation of light, organically-derived carbon. These dolomites are not as isotopically light as the calcites analysed but a protracted growth history for the dolomites might account for this. The earliest precipitates could have been greatly depleted in ^{13}C due to sulphate reduction but the latest, ferroan precipitate is relatively enriched in this component, probably due to the domination of pore-waters by progressively greater amounts of methanogenic bicarbonate. The averaging inherent in bulk analysis fails to detect such a critical evolutionary trend.
- (3) Most dolomites are associated with organic-rich, often pyritiferous

black and green shales. Dolomitic siltstones found in red shale intervals are also interpreted to be the result of anoxic or sub-oxic (sensu Froelich et al., 1979) diagenesis. The presence of thin, green shale rims surrounding dolomitic siltstones enclosed in red shales, as well as the incorporation of Mn indicates reducing conditions, though not as reducing required to precipitate ferroan rims on dolomite crystals.

Shallow-burial, low temperature dolomitization has been recognized largely due to the Deep Sea Drilling Project which has shown repeatedly, that organic-rich sediments along continental margins and in small ocean basins are commonly the site of dolomitization (Pisciotta, 1981; Garrison, 1981 and references therein). Prominent among the various sediments in which this type of dolomitization has been described are the Neogene hemipelagic, diatomaceous muds of the continental margin of California, Baja California, and the Gulf of California (Pisciotta and Mahoney, 1981; Kelts and McKenzie, 1982) and the equivalent land outcrops of the Monterey Formation in California (Murata et al., 1969; Friedman and Murata, 1979). Other localities where early, authigenic dolomites have been studied include the continental margin of Peru (Kulm et al. (1981); the Red Sea (Supko et al., 1974), and the slope sediments north of Little Bahama Bank (Mullins et al., 1984). Ancient examples are considerably fewer in number and include dolomitic concretions in the Middle Ordovician flysch of Gaspe, Quebec (Islam, 1981), the well-known dolomitic layers in the Upper Jurassic Kimmeridge Clay of Dorset (Irwin et al., 1977; Irwin, 1980), and several other studies (Fruth and Sherreiks, 1982; Jorgensen, 1983).

In general, these dolomites are less than 10-15 μm in size and commonly euhedral but may be intergrown to form anhedral mosaics.

Compositionally they are Ca-rich (e.g. 49-56 % CaCO_3 in the Monterey Formation; Pisciotta, 1981), and are occasionally ferroan. Dolomite occurs as isolated crystals, or lenses and continuous layers which are generally less than a metre in thickness. Calcite may be an associated phase, either interspersed with dolomite or forming limestone layers. The crystals occur as cement or a replacement of calcareous bioclasts, commonly foraminifera. Primary bedding fabrics and sedimentary structures are commonly uncompacted relative to the host sediment, which is typically an organic-rich, pyritiferous, or siliceous shale (e.g. Monterey Formation). Depths of formation vary from near the sediment-water interface to greater than 500 m (Murata *et al.*, 1969; Davies and Supko, 1973; Friedman and Murata, 1979; Irwin, 1980; Islam, 1981; Pisciotta, 1981; Pisciotta and Mahoney, 1981; Kelts and McKenzie, 1982).

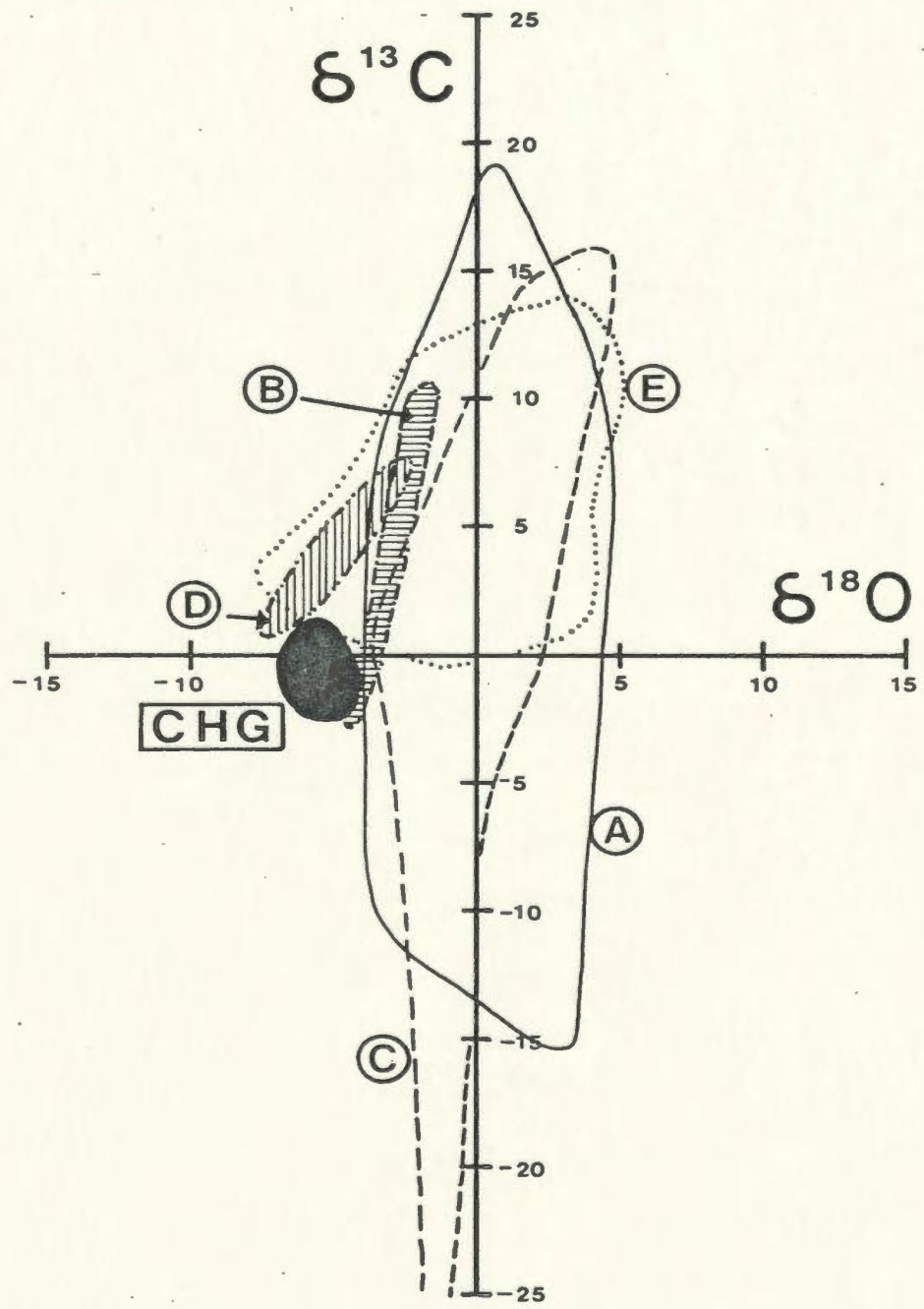
A listing and description, by no means comprehensive, of a number of occurrences of authigenic, organically-derived dolomite is presented in Table 12.1. All of these studies are characterized by highly variable $\delta^{13}\text{C}$, reflecting the changing importance of the various anaerobic CO_2 -producing reactions, namely sulphate reduction, methanogenesis, and abiotic reactions. The isotopic analyses from these studies are plotted in Figure 12.5.

Pore-waters which precipitate these dolomites are highly alkaline and are characterized by a high ammonia content and a low sulphate content. In addition, Mg/Ca ratios are commonly below the 5.3 value of

TABLE 12.1: SELECTED STUDIES OF ORGANICALLY-RELATED CONCRETIONARY DOLOMITES

<u>AUTHORS</u>	<u>LOCATION</u>	<u>AGE</u>	<u>DEPTH OF FORMATION</u>	<u>DOLOMITE CHARACTERISTICS</u>	<u>OTHER COMMENTS</u>
Pinciotto and Mahoney (1981)	DSDP Leg 63 S. California & Baja California	mostly Neogene	max. 881 m; calculated 86-658 m	occurs as decimetre-thick layers of dolomite cement, no repetitive fabrics, some disseminated crystals, size 5-10 μ m.	associated with authigenic limestones, dolomite is precipitated in zones with Mg/Ca smaller than 5 and under high alkalinity.
Murata et al. (1969); Friedman and Murata (1979)	California	Miocene Monterey Shale	less than 200 m	occurs as lenses and layers 0.1-1 m thick, 5-10 m apart stratigraphically, replaces fine grained calcite, forams. may be poikilotopic, crystals 5 μ m in size and euhedral.	in apparent isotopic equilibrium with seawater, associated with calcite concretions, derived from fermentation and methane oxidation reactions.
Keltu and McKenzie (1982)	DSDP Leg 64 Gulf of California	Neogene	40-440 m (total depth). 1st dolomite at 60 m (ooze); 1st hard dolomite at 90 m.	occurs as sporadic hard dolomite fragments and decimetre-thick beds within softer oozes to mudstones, replaces calcareous microfossils and occurs as cement crystals 1-2 μ m in soft samples, 10-30 μ m in harder samples, variable shape.	dolomite beds preserve sedimentary structures, precipitated in zones of high alkalinity and low sulphate, derived from fermentation and abiogenic reactions
Irwin (1980)	England	Jurassic Kimmeridge Clay	estimated 10-500 m or more	42 cm-thick bed, occurs as cement and replacement, crystals 8-40 μ m, ferroan composition.	vertical, systematic decrease in $\delta^{13}\text{C}$ and $\delta^{18}\text{O}$ signifies fermentation to abiogenic HCO_3^- - trend toward bed margins, bed grew marginal accretion focussed on a primary carbonate-rich bed.
Islam (1981)	Southern Quebec	M. Ordovician Chloridorme & Deslandes Fm.	started near surface, continued to unspecified depth	ellipsoidal concretions 50-200 cm in size in black shales, crystals less than 10 μ m (pers. observation) ferroan composition.	cores of concretions contain shrinkage cracks, derived from fermentation reactions.

Figure 12.5: $\delta^{13}\text{C}$ versus $\delta^{18}\text{O}$ plot of "methanogenic" dolomites from other studies and Early dolomites of this study. All $\delta^{18}\text{O}$ values are corrected downward by 0.8 o/oo (Sharma and Clayton, 1965). (A) Murata *et al.* (1969), n=36; (B) Irwin (1980), n=21; (C) Pisciotto and Mahoney (1981), n=22; (D) Islam (1981), n=19; (E) Kelts and McKenzie (1982), n=29; CHG, n=16.



present-day seawater (Kelts and McKenzie, 1982; Kastner, 1984). In Quaternary anoxic muds in the Gulf of California, for example, the Mg/Ca ratio may be as low as 1 (Kelts and McKenzie, 1982; also see Pisciotto and Mahoney, 1981). Until a few years ago, such low Mg/Ca ratios were thought to be incongruous with the precipitation of authigenic dolomite (e.g. Sass and Kolodny, 1972).

Present-day seawater is saturated with respect to dolomite yet dolomite is not precipitated in any significant quantity. Until recently, the prevailing dogma to explain the lack of dolomite precipitation in seawater was that kinetic obstacles hindered the process and the seawater Mg/Ca ratio had to be surpassed in order for dolomite to form (Baker and Kastner, 1981). Evaporative pumping, evaporative reflux, shale dewatering, and solution cannibalization models allowed the Mg/Ca ratio of pore-waters to increase to appropriately high values (Baker and Kastner, 1981; Morrow, 1982b). In an experimental study of the chemical controls on dolomitization, Baker and Kastner (1981) concluded that the absence or reduction of dissolved sulphate was the critical condition for dolomitization to occur, not the Mg/Ca ratio as had been previously proposed. Sulphate was found to be an effective inhibitor to dolomitization of calcite at concentrations as low as 5% of the seawater value; for aragonite the limiting value is higher, approximately 50% of the seawater value (Baker and Kastner, 1981; Kastner, 1984). In anoxic, deep sea sediments the appropriate conditions occur once sufficient sulphate is removed by bacterial reduction of sulphate, a process which also encourages carbonate precipitation by the consequent increase in alkalinity and the production of ammonia. Ammonia may exchange with Mg

in ion-exchange sites in clays, thus adding Mg to the solution (Baker and Kastner, 1981; also see McHargue and Price, 1982, for significance of clays in post-compactional dolomitization). Mg for dolomite could also be derived from ambient interstitial waters or solution cannibalization of Mg-calcites, or from chlorophyll in organic matter (Irwin, 1980).

12.5 LATE DOLOMITE

12.5.1 Introduction

Both joint and pervasive replacement dolomites are scattered throughout the CHG but pervasive replacement dolomite also replaces much of the conglomeratic sediment on the White Rock Islets. Similar dolomite is found at the "Arches", an isolated conglomeratic outcrop north of the study area (Plate 47e). The stratigraphic affinity of this particular conglomerate, however, is uncertain; it may be either CHG or part of the Cape Cormorant Formation of the Table Head Group (Middle Ordovician; N.P. James, pers. comm., 1983).

Joint dolomitization occurs as 10-20 cm thick "halos" or zones adjacent to joints or small faults with less than 50 cm stratigraphic throw (Plate 47c,d). Thin dolomitic stringers extend laterally from the halos into the host-limestone and either eventually dissipate or link up with another joint dolomitized zone. Dolomitized sediments include conglomerates, grainstones to mudstones, and their interbedded shales. These dolomitized sediments weather a tan colour and are more resistant

than laterally equivalent, undolomitized sediment. Primary sedimentary structures such as parallel and ripple laminations and graded bedding are usually thoroughly overprinted; their presence and the nature of the precursor sediment must be inferred from adjacent, relatively undolomitized sediment.

Pervasive replacement dolomite is characterized by preservation of primary fabrics due to differential dolomitization of clast and interparticle matrix. This results from the combined effects of: (1) crystal size, (2) degree of intergrowth (i.e. euhedral or anhedral mosaics), (3) iron content, (4) luminescence characteristics, and (5) abundance of relict calcite.

12.5.2 Petrography

Joint and pervasive replacement dolomite crystals are similar in many ways to Early dolomites. These similarities include the following: (1) variable inclusion content, (2) cloudy cores and clear rims, and (3) variation in the degree of crystal intergrowth resulting in euhedral to anhedral mosaics (Plate 48e). Other pervasive replacement crystals may be cloudy throughout and have thin (25-35 μm) clear rims. Crystal size varies from 5-75 μm in joint dolomites and is strongly controlled by the grain or crystal size of the precursor limestone. Consequently, replaced mudstones and marls are most finely crystalline. The largest crystals are fracture-filling cements (see below), attaining sizes up to 500 μm . Pervasive replacement dolomite crystals have the coarsest average size of all CHG dolomites, typically ranging from 150-500 μm in size. Both joint as well as the pervasive replacement dolomites have

pronounced undulose extinction and pleochroism and strongly resemble late-diagenetic "saddle" dolomites in the Lower Ordovician autochthonous succession (Haywick, pers. comm., 1984).

Joint dolomite may be replacive or may be cement. Replacive dolomite is typically more inclusion-rich and more commonly anhedral whereas dolomite cement varies from subhedral to euhedral with the occasional development of curved crystal faces (Plate 49i). In some thin sections dolomite cement extends from replacive mosaics without interruption.

Three types of secondary porosity are present: (1) intercrystalline (Plate 48f,g) which may grade into (2) vuggy, and (3) fracture (all sensu Choquette and Pray, 1970). Excluding fracture porosity, the largest pores are 0.5-1.0 mm-size vugs. Qualitative estimates suggest generally less than 2% porosity, but the most porous sample examined - a joint dolomitized grainstone - has 8% vuggy porosity [7].

In vuggy and intercrystalline pores distinct clay morphologies are not observed with SEM; most of the solids present are nondescript (Plate 48f). Some pores, however, do contain an opaque to translucent, yellow-brown, amorphous substance which is interpreted to be bitumen (Plate 48g). Authigenic microquartz and megaquartz prisms and possibly clays predate the emplacement of bitumen. A later calcite cement, which may be ferroan or non-ferroan, post-dates all other pore-filling phases.

7. This particular sample is from unit 25 at Broom Point South. Porosity estimate is based on thin section point count of 382 points.

12.5.3 Cathode Luminescence and Trace Elements

Luminescence colours in Late dolomites are usually red, pink-red, and orange-red, occurring in 5-20 μm -wide zones. Later growth stages are usually more luminescent than the central portions of crystals which are commonly dull or weak-luminescent. In joint dolomites, many of central portions are rounded or ellipsoidal and suggest, along with associated sand- and silt-size siliciclastics, replacement of peloids in a manner analogous to that which formed dolomitic siltstones. The central portions in other crystals consist of irregular, poorly-defined patches of weak luminescent and dark dolomite.

Most crystals are non-ferroan; however, some do have thin (10 μm or less) internal or marginal ferroan zones. Iron content is typically less than 1.0 wt % though locally may exceed 7.0 wt %. In both joint and pervasive replacement dolomites, MnO content rarely rises above the 0.1 wt % microprobe detection limit. An exceptional dolomitized conglomerate from Green Point (unit 44), however, contains approximately 7 wt % MnO. In this sample fluctuations in MnO concentration are detectable with microprobe but iron content is approximately constant (average of 22 point analyses is 0.30 wt %). As with the Early dolomites, iron content controls luminescence (Figure 12.1b).

Joint dolomite clearly post-dates rim growth in Early dolomites as well as vertical pressure solution. In limestones, for example, dolomite crystals with non-luminescent, ferroan rims are gathered at stylolites. The outer margins of these crystals are obviously corroded by joint dolomite (Plate 49j).

12.5.4 Stable Isotopes

Four stable isotope analyses of Late dolomites are plotted in Figure 12.2. These analyses vary widely with respect to both $\delta^{18}\text{O}$ and $\delta^{13}\text{C}$ and include the most negative $\delta^{18}\text{O}$ and $\delta^{13}\text{C}$ analysed (-7.73 o/oo and -5.89 o/oo, respectively).

12.6 INTERPRETATION

12.6.1 Field Relationships and Petrography

Dolomitization related to faults and joints has also been reported in other studies (e.g. Zenger, 1976; Jones, 1980; Dickson and Coleman, 1980; Haywick and James, 1984). Field and petrographic relationships indicate that the Late dolomitization event(s?) post-dates all other diagenetic modification of CHG carbonates, except perhaps for migration of hydrocarbons, some quartz authigenesis, and precipitation of latest calcite cement in fractures.

The occurrence of dull or weak-luminescent centres in many crystals, especially in mosaics which are interpreted to have replaced grainstone, is interpreted analogously to the cloudy cores in dolomitic siltstones, i.e. the central areas reflect the presence of precursor allochems, mostly peloids. In other mosaics the cause of the cloudy centres is not apparent.

12.6.2 Stable Isotopes

The variability in the petrographic and luminescence characteristics of Late dolomite and the occasional geochemical anomaly, such as the high Mn content in one particular sample, is further manifest in their stable isotopes. Due to the limited number of analyses and their wide scatter, little sense can be made of these. Their late diagenetic origin implies possible thermal fractionation effects on $\delta^{18}\text{O}$ but these are not be differentiable from those related to a high degree of pore-water evolution as discussed for in situ authigenic calcite (Chapter 11). The most negative $\delta^{13}\text{C}$ value could be due to either incorporation of isotopically light carbon from a precursor limestone, or meteoric groundwaters may have been circulated during the dolomitization process.

12.7 CONCLUSIONS

12.7.1 Early Dolomites

Bright-luminescent cores in many dolomite crystals characterized by cloudy cores and clear rims within pervasive dolomitic siltstones and dispersed in limestone and shale are interpreted to be detrital dolomite grains which were subsequently overgrown by authigenic dolomite. Most dolomite cores, however, are dark or dull-luminescent and are interpreted to be the result of dolomitization of silt-, and to a lesser extent, sand-size peloids. Based on comparison of CHG dolomite to Lower Ordovician dololaminites, dark and dull-cores may also be detrital,

having been derived from the shallow subtidal to supratidal environments on the carbonate platform to the west. Therefore, the most probable precursor of dolomitic siltstones is interpreted to have been a peloidal grainstone containing scattered clasts of detrital dolomite and siliciclastics.

Fe content of Early dolomites strongly controls their ^{57}Fe CL. Their cores, however, are usually non-ferroan and have little or no luminescence. Mn is rarely detectable with microprobe.

Field and petrographic relationships indicate that dolomitization was early, occurring in uncompactd and partially-compacted sediments.

Precipitation may have been contemporaneous with calcite authigenesis, but the latter stage of growth of dolomite postdated calcite growth.

The complexity and variability of the CL zoning in dolomite suggest that the growth history was protracted.

The light $\delta^{13}\text{C}$ values of some crystals suggests incorporation of isotopically light carbon derived from decomposition of organic matter. Linear regression of bulk $\delta^{13}\text{C}$ with FeO concentration indicates that with continued precipitation, methanogenically-produced bicarbonate became progressively more important.

A dolomitization model involving anoxic diagenesis, similar to what is described from numerous shallow-buried organic-rich sediments, is compatible with all characteristics of Early dolomites, especially the absence of or limited compaction, the petrographic relationships with early-formed calcite cement or neospar, and stable isotope data.

12.7.2 Late Dolomites

Late dolomites are spatially related to joints and small-displacement faults (joint dolomite), or they petrographically resemble these dolomites (pervasive replacement dolomite). Late dolomite may be either a replacement or a cement. Some samples are porous, though most contain less than 2% porosity. An amorphous substance, interpreted to be bitumen, is found in some intercrystalline areas. Late dolomites corrode Early dolomites and also postdate tectonic pressure solution.

Chapter 13

SILICIFICATION AND MINOR AUTHIGENIC PHASES

13.1 GENERAL INTRODUCTION

In this chapter the remaining authigenic components of volumetric or paragenetic significance - silica, barite, and pyrite - are described and interpreted. In addition to these minerals, traces of authigenic sphalerite, fluorite, and authigenic chlorite also occur. Petrographic descriptions of these minor components are found in Appendix L.

13.2 SILICIFICATION

13.2.1 Introduction

Chert, occurring as replaced limestone or shale, or cement, is a common diagenetic phase in the CHG, particularly in the Ordovician part of the succession. Silicified sediment weathers resistantly commonly with distinctive orange-brown to black-green colour. Exceptional silicified shales at Western Brook Pond North are characterized by vivid blue, green, yellow, and red colours arranged in irregular, convoluted patterns. Some of the green colouration is due to glauconite; other

colours may be due to oxidized iron compounds.

The importance of examining chert in this succession is two-fold.

First, silicified sediments are volumetrically important and therefore silicification is an integral part of the overall diagenetic history of the succession. Second, by studying siliceous sediments and their spatially-associated limestones and shales, the contribution of biogenic silica, predominantly from radiolaria and sponge spicules, can be evaluated.

13.2.2 Field Description

In outcrop chert occurs in a variety of ways. These are listed and briefly discussed below.

13.2.2.1 Conglomerate Crusts

The most striking chert, both in terms of appearance and utility as a stratigraphic marker, are hackly-weathering crusts, usually 5-20 cm thick, which cap many Ordovician conglomerates (Plate 50a). These crusts are generally continuous and penetrate downward, replacing conglomerate matrix. In other cases chert replaces the calcarenitic cap of the conglomerates, or overlying parted and ribbon limestones.

13.2.2.2 Marginal Crusts

In some parted mudstones and wackestones, the top and bottom centimetre or so of many beds is silicified to varying degrees (Plate 9c).

Incipient silicification is characterized by diffuse, tan-weathering

rinds whereas completely silicified margins weather prominently.

13.2.2.3 Completely Silicified Shale and Limestone

Completely silicified limestones and shales demonstrate evidence for both early as well as late, post-compactional, silicification. Because limestone is seldom compacted, field evidence alone cannot confirm whether limestone silicification is pre- or post-burial.

Early-silicified shales are indicated by unsquashed, vertical burrows (Plate 8e). Early silicification also accounts for chert clasts in conglomerates and erosion of silicified, parted mudstones by conglomerates (Plate 50b). The sharpness of the contact between the conglomerate and silicified parted mudstone suggests silicification preceded erosion. The drape of laminations in silicified shale surrounding limestone nodules indicates a later origin, after some compaction. In some cases the differentiation of silicified limestone from shale must rely on the presence of palimpsest structures.

13.2.2.4 Nodules

Chert nodules in mudstones to grainstones vary from regularly-shaped and spaced forms, usually less than 20 cm in length to irregular, "ropey" nodules which may cross-cut bedding (Plate 50c). The limestone-chert contact is typically razor-sharp. Incipient silicification appears as vague, tan-weathering, elliptically shaped domains in mudstones. Local silicification in shales also forms nodules.

13.2.2.5 Allochthonous(?) Chert

Chert is found as millimetre-thick crusts replacing the lower portions of RFC fringes in fractures and vugs in shallow-water boulders (see Chapter 7). Obvious megaquartz crystals may postdate these calcite fringes. In conglomerates, chert also occurs as flat pebble clasts up to 30 cm in length or as crusts on mudstone clasts.

13.2.3 Petrography

13.2.3.1 Components of Chert

The terminology used to describe authigenic quartz in this thesis follows that outlined by Folk and Pittman (1971). Microquartz refers to equant crystals less than 20 μm in size or chalcedonic fibres of unspecified length. Megaquartz is coarser than 20 μm in size.

Chert typically consists of microquartz which is equant and less than 5 μm in size or micrometre-wide chalcedony fibres commonly up to 100 μm , rarely up to 1 mm in length. Chalcedony may be either length-fast or length-slow and in some cases it demonstrates zebraic extinction. Megaquartz, occurring as limpid, anhedral to subhedral crystals up to 500 μm in size, is comparatively rare.

13.2.3.2 Replacive Chert

Chert is both replacive and pore-filling. Replacive chert is mostly equant microquartz, with crystal size variations preserving, to various

degrees, the microfabric of the precursor sediment. In slightly silicified limestones, bioclasts (mainly pelmatozoan and trilobite fragments) and ooids are preferentially silicified over other allochems. Although data are far from conclusive, some thin sections suggest preferential silicification of ferroan allochems (e.g. trilobite fragments) over non-ferroan ones. The razor-sharp limestone-chert boundary in outcrop is equally as sharp at the thin section scale, occurring over a distance of 250-500 μm and occasionally silicifying only portions of grains straddling the boundary. In some samples, silicification is spatially related to minor dolomitization. A dolomitic zone, up to 250 μm in width, containing anhedral to euhedral crystals up to 60 μm in size, may separate mudstone from its silicified counterpart. Anhedral dolomite crystals less than 5 μm in size are also seen in some silicified peloids and are largely responsible for their apparently high relief in plane light.

- 13.2.3.3 Pore-filling Chert

Microquartz cement is dominated by chalcedonic fringes up to 100 μm in width which isopachously coat substrate particles. Where pore spaces are sufficiently large, growth surfaces of cement fringes are botryoidal and some demonstrate internal, inclusion-defined growth bands.

Pore-space not completely filled by chalcedony may be further occluded by megaquartz or ferroan calcite. Based on the above relationships, including the lack of relict calcite cement, these chalcedonic fringes are interpreted to be original cement, not a replacement of an earlier calcitic cement.

Microquartz and, to a lesser extent, megaquartz are common in veinlets within chert-rich sequences. The intercrystalline matrix in sucrosic dolomitic siltstones in such sequences may also be mostly microquartz.

13.2.4 Diagenesis of Siliceous Bioclasts

13.2.4.1 Introduction

Silicification in the CHG is spatially associated with spicules and radiolaria, many of which are now calcitic. To explain the amount of silicification observed, however, many more radiolaria and spicules than are obvious must have been consumed without leaving a trace of their former presence. This suggestion has been made in innumerable other studies of both shallow- and deep-water sediments (e.g. Wilson, 1969; Wise and Weaver, 1974; Geeslin and Chafetz, 1982; Eley and Jull, 1982; Hein and Karl, 1983), but convincing petrographic evidence is seldom offered. In the present study, CL used as a primary microfacies tool demonstrates an unexpectedly high contribution of spicules and radiolaria to many limestones, particularly those with "pseudowackestone" depositional fabrics (discussed below).

13.2.4.2 Petrography of Radiolaria and Spicules

Radiolarians are most commonly 60-80 μm in diameter with exceptional tests reaching 250 μm in size. Circular cross-sections of spicules vary from 5-40 μm in diameter and rarely extend up to 100 μm . Spicules range from few hundred micrometres in length up to a maximum of 2 mm. Thin section examination illustrates a predominance of monaxon spicules with

relatively few polyaxon spicules (Plate 50d). Reconnaissance study of insoluble residues indicates that polyaxon spicules are significantly underrepresented in thin section views. In many radiolaria, the double-wall microstructure is preserved, and in spicules, axial canals are differentiable. CL often demonstrates excellent microfabric preservation in samples which appear, by conventional microscopy, to be poorly preserved.

Two microfacies "groups" are recognized based on the lithology of the host sediment: (1) a limestone group and (2) a shale group. Microfacies from these two groups commonly occur in close proximity, for example packstone or wackestone nodules in a silicified shale sequence.

13.2.4.3 Group 1: Limestone Microfacies

In this microfacies group, radiolaria usually consist of several non-ferroan, weak to bright orange-luminescent calcite crystals which range from 10-50 μm in size (Plate 51a,b). This calcite is usually identical to surrounding neospar or cement matrix. Radiolaria rarely consist of equant or chalcedonic microquartz. Spicules are generally composed of slightly ferroan calcite which has weak or dull-luminescence, and a higher abundance of inclusions than surrounding neospar or cement. In transverse sections, most spicules appear to be spanned by only one crystal, but in sections parallel to length, they are seen to consist of several calcite crystals. These calcitic spicules may have their axial canals filled with microquartz. The polycrystalline nature of most calcitic spicules suggests that these were originally siliceous. In the limestone microfacies, microquartz

spicules are more common than microquartz radiolaria, although such spicules are not as common as they are in the shale microfacies (discussed below).

In mudstones to grainstones, radiolaria and spicules usually occur together, are evenly dispersed within the host sediment, and seldomly exceed 2% of the sediment volume (visual estimate).

Radiolaria-dominated, grain-supported sediments (grainstone or packstone radiolarite) are comparatively rare (Plate 50e,f). Conventional petrographic examination of "pseudowackestones" shows that they are apparently dominated by peloids floating in a neospar matrix, thus giving these sediments a wackestone depositional fabric. Discernible radiolaria and spicules are minor or absent (Plate 5 a,c,e). This same sediment with CL examination, is commonly seen to be grain-supported (grainstone or packstone) with radiolaria and spicules composing up to half of the grains (Plate 5 b,d,f).

13.2.4.4 Group 2: Shale Microfacies

In contrast to the limestone microfacies, radiolaria and spicules consist of either ferroan calcite or more commonly, microquartz.

Radiolaria and spicules are occasionally preserved by finely crystalline pyrite (Plate 50d,g). As with the limestone microfacies, radiolaria and spicules are generally mixed together and evenly dispersed. Unlike the limestone microfacies, however, it is much more common to see sediments dominated by radiolaria (radiolarites) or spicules (spiculites) or mixtures of both. Shales are silicified to varying degrees and based on the presence of undeformed vertical burrows, many are uncompacted.

Millimetre-thick, size-graded laminations dominated by radiolaria or spicules are rare (Plate 50h).

13.2.4.5 Evidence for Vanished Radiolaria

The following example is discussed in order to illustrate that silicification is both an early and a late (post-compactional) process and that siliceous bioclasts can indeed vanish without a trace, adjacent to exceptionally well-preserved bioclasts.

Observations: A sample of silicified shale from Martin Point contains a centimetre-thick bed with abundant radiolaria, most of which consist entirely of microquartz. Dispersed among the silicified radiolaria are pyritized radiolaria in which the pores, ornamentation, and double wall of the test are remarkably well-preserved (Plate 50g). These radiolaria have their chambers filled with microquartz identical to that in the associated, unpyritized radiolaria. Other pyritized radiolaria in the shale surrounding the radiolaria-rich bed lack the internal microquartz fill, are compacted and broken, and in many cases, are almost unrecognizable as being radiolaria (Plate 50i).

Interpretation: Pyritization of the radiolaria, within and outside the band, was clearly the earliest alteration to this sediment and occurred prior to any significant compaction [1]. Preferential silicification of the radiolaria-rich bed, perhaps controlled by higher permeability in

1. Kelts (1976) also described pyritized radiolaria with excellent microfabric preservation from Miocene calcareous oozes drilled from the Central Pacific. Pyritization was suggested to be due to the effect of organic surface coatings.

this portion of the sediment, followed pyritization, filling the chambers of both pyritized and unpyritized radiolaria. Pyritized radiolaria outside the bed were not filled with microquartz and were subsequently compacted and broken and ultimately reduced to irregular patches of microcrystalline pyrite. Unpyritized radiolaria in this portion of the sediment were completely removed. Silicification of this part of the shale appears to have post-dated compaction which crushed the pyritized-only radiolaria.

If early pyritization of selected radiolaria had not occurred, the radiolaria-rich bed would contain silicified radiolaria only, and this bed would be surrounded by shale devoid of these microfossils. The fortuitous preservation of pyritized, but crushed radiolaria in the surrounding shale is clear proof that radiolaria did exist outside the bed. Unpyritized, unsilicified radiolaria in this portion of the shale vanished without a trace.

Similar relationships are found in other samples, though in many, interpretations are far more equivocal. For example, silicified radiolaria may be confined to burrow-fills and the surrounding, silicified shale is barren. Such an occurrence may be explained either by preferential dissolution of radiolaria in the host sediment, as proposed in the above example, or by the burrow-fill sediment having a different primary composition than the host sediment.

13.2.5 Interpretation

13.2.5.1 Origin of Replacement Minerals

Based on their common association with silicified sediments and analogy with extant forms (see Scholle *et al.*, 1983 for review), the original mineralogy of both radiolaria and sponge spicules is interpreted to have been opaline silica. In addition, the polycrystalline calcite composition of many spicules and the presence of axial canals further suggests an original, siliceous composition.

Calcite which replaces radiolaria and spicules is interpreted to be cement based on euhedral CL zones within calcite crystals (Plate 51b) and the occasional presence of rhombic faces buried by later microquartz cement (Plate 51e; cf. Faupl and Beran, 1983). Microquartz spicules and radiolaria typically lack internal microstructure and are also interpreted to be cement-filled molds, especially those containing geopetal pyrite crystals. Silica cement also occurs as interparticle chalcedonic rinds, microveinlet fills, and inter-dolomite microquartz.

The preservation of the double-wall structure in some radiolaria and the axial canal and inclusions in spicules implies that either complete dissolution of these components did not occur prior to cementation by calcite or microquartz or that organic templates helped preserve microstructure. Microquartz replacement of calcite without intervening porosity is suggested in some sediments by the high degree of fabric preservation associated with silicification of peloids and other

allochems. Changes in pH have the opposite effect on calcium carbonate and silica and it is therefore not surprising that one may replace the other, either with or without the creation of visible porosity (e.g. Geeslin and Chafetz, 1982; Eley and Jull, 1982). A decrease in pore water pH, for example, would cause calcite to dissolve and silica to precipitate. For discussion on the physico-chemical controls of silicification the reader is directed to Hein et al. (1978); Kastner (1979); Garrison et al. (1981); and Kastner and Gieskes (1983).

Silicification of terrigenous muds is common in the modern oceans, and along with silicified limestones and chalks, they constitute the principal protoliths of chert. However, the degree to which clay minerals are altered and importance of silica as a simple impregnation of the porous, uncompacted sediment is poorly known (e.g. Pisciotto, 1980; Hein and Karl, 1983).

13.2.5.2 Timing of Silicification: Relative and Absolute

The less luminescent, more ferroan calcite cement replacing spicules in limestones indicates that spicules were altered later than radiolaria, which are usually composed of non-ferroan calcite. With regards to the 3 luminescence stages defined earlier, radiolaria are composed mainly of Stage B calcite whereas spicules are Stage C. That calcite precipitation occurred shortly after silica dissolution is suggested by this difference in luminescence of radiolaria and spicules. The relative order of alteration of radiolaria and spicules is also predicted by studies of modern, biogenic, siliceous components. In the present-day ocean, resistance to dissolution increases from (1) silicoflagellates,

(2) diatoms, (3) delicate radiolaria, (4) robust radiolaria, and (5) sponge spicules (Scholle et al., 1983). This sequence is in part controlled by organic and inorganic protective coatings, surface areas, adsorbed ions, and crystallographic characteristics of the biogenic opal (Hein et al., 1978).

From petrographic relationships, alteration of radiolaria and spicules in the CHG may be contemporaneous with the main phase of calcite authigenesis, but may also extend beyond this. Early silicification is indicated by: (1) preservation of uncompact burrows in silicified shales; (2) compactive drape of unsilicified shale laminations around earlier-formed chert nodules; (3) uncompact graptolites in silicified shales; (4) silicified parted limestone scoured by overlying conglomerate; and (5) incorporation of chert clasts in conglomerate. Silicification postdating the main phase of calcite precipitation is indicated by: (1) the presence of nodules in and crusts on limestone beds; (2) evidence of grain compaction prior to cementation by chalcedony (Plate 21c); (3) compacted and silicified shales draping earlier-formed limestone nodules (cf. Baltuck, 1983); and (4) compacted, silicified shales containing crushed, pyritized radiolaria (previously discussed).

Precipitation of minor amounts of pyrite, occasionally as geopetal crystals within radiolaria and spicule molds and as total replacements of these, indicates pyritization prior to silicification in these cases, but usually no order of precipitation is apparent. Silicification of limestone also may be accompanied by minor dolomitization and also postdates dolomitization, as indicated by etched rhombs encased in chert

in some silicified siltstones (Plate 48b).

13.2.6 Discussion

Since the Cambrian, radiolarians and siliceous sponges have contributed to pelagic (i.e. open marine [2]) sedimentation. In the modern ocean, radiolaria are concentrated in the upper reaches of the water column (Scholle et al., 1983) whereas siliceous sponges range from shallow to deep waters (Rigby, 1983).

In grainy sediments, spicules occurring with shallow-water allochems such as algal clasts are either derived from shallow-water or they could have been incorporated during sediment gravity flow. In mudstones and shales, the ubiquity of sponge spicules and radiolaria suggests they are pelagic, derived by radiolaria settling out of the overlying water column and by dispersal of spicules from benthic, in situ(?) sponge communities. The occurrence of radiolaria and spicule grain-support fabrics may reflect turbidity current deposition of reworked pelagic debris or winnowing by bottom currents leaving these components behind as a lag (cf. Baltuck, 1983; Imoto, 1983). Such grain-supported beds, however, are rare. Although pressure solution also must be considered as a possible mechanism for the formation of grain-supported beds of radiolaria or spicules, there is no evidence to suggest this.

Radiolaria and sponge spicules were especially important in the Paleozoic as calcareous plankton (e.g. ammonites, tentaculitids,

2. see Scholle et al. (1983) for discussion of the term "pelagic".

styliolinids) were volumetrically minor as well as spatially restricted (Scholle *et al.*, 1983). This lack of a significant Paleozoic plankton is responsible for the abundance of "starved-basin" and condensed facies which are commonly characterized by abundant radiolaria and spicule cherts, and graptolitic shales. The presence of numerous spicules in many ancient deep-water sediments has led to their recognition as a potential indicator of basinal facies (e.g. Wilson, 1969 ; Rigby, 1983) although not necessarily representing abyssal depths (e.g. McBride and Folk, 1979).

13.2.7 Summary and Conclusions

Chert appears in a variety of ways in outcrop: as crusts on conglomerates and thinly-bedded limestones, as nodules in limestone and shale, as pervasively silicified limestone and shale, and within clasts in conglomerates. Chert occurs both as a replacement as well as a cement, although the latter is relatively uncommon. The silicification history of the CHG is protracted and there is evidence to indicate silicification prior to and after compaction. Chert occurrences in the CHG are remarkably similar to those in present-day oceans which occur mainly as millimetre- to centimetre-size nodules, lenses, or stringers in limestones, chalks, and shales (Hein and Karl, 1983). This similarity implies that modern processes can be confidently used to explain silica diagenesis in these ancient sediments.

Radiolaria and spicules are commonly found in the Ordovician part of the succession and this is where most siliceous sediments occur. CL study dramatically illustrates that calcite-replaced radiolaria and spicules

are much more common than is apparent using standard petrographic analysis. In addition, there is sound petrographic evidence to suggest that large quantities of radiolaria and spicules were dissolved without leaving a trace. Based on the above evidence, dissolution of radiolaria and spicules during shallow-burial diagenesis is interpreted to be responsible for most of the silicification in the CHG. Detrital siliciclastics, notably quartz sand grains, are uncorroded and therefore remobilized detrital silica is not a possible source of any importance. Hydrothermal emanations and volcanism are not considered to be plausible sources of silica.

13.3 BARITE

13.3.1 Occurrences and Petrography

Barite [3] is a minor phase present throughout the CHG but is only locally important at Green Point. Barite occurs as:

(1) equant to elongate, anhedral to euhedral crystals dispersed or concentrated into layers in mudstones, or as fringes under and over mudstones (common; Plate 52a,b);

(2) centimetre-size nodules of equant crystals or rosettes of subhedral to euhedral, elongate crystals in mudstone, shale, or dolomitic marl (rare; Plate 52c,d);

3. Barite mineralogy was confirmed by microprobe analysis and X-ray diffraction.

(3) large, anhedral crystals replacing neospar (rare); and

(4) anhedral to subhedral cements in grainstones and fractures, both early and late (rare; Plate 20a).

Barite crystals, especially elongate prisms, may reach 2 cm in size, but most crystals range from 100-1000 μm . They contain variable amounts of micrometre-size inclusions and only rarely are two-phase fluid-filled inclusions encountered. In some cases the former presence of barite is inferred from the presence of calcitic, polycrystalline pseudomorphs (Plate 52e). Other phases, such as hydrated carbonates, may have also been responsible for the now-filled crystal molds (cf. Boggs, 1972) but there is no evidence for this. Some crystal molds are only partially filled with either calcite or megaquartz (Plate 52f).

Paragenetic relationships between barite and calcite are variable. When barite is found within mudstone, either as bands or rosettes, and where it is replaced by calcite, either totally or partially, it is interpreted to predate calcite precipitation. When barite replaces microspar or pseudospar, occurs as fringes on and under mudstone beds, and poikilotopically encloses dispersed microspar crystals, it is interpreted to have postdated calcite. In some cases barite and pseudospar are intimately mixed together and replacive relationships are not seen, suggesting synchronous precipitation of barite and calcite (Plate 52g).

13.3.2 Interpretation and Discussion

The association of most barite occurrences with early-diagenetic neospar implies that barite is also an early diagenetic precipitate. Barite in veins interpreted to be tectonic in origin is precipitated much later in the diagenetic history. The history of barite precipitation is obviously protracted although late occurrences are comparatively rare and are ignored in the following discussion.

Authigenic barite is commonly formed during early diagenesis in many modern, deep-sea sediments, especially those from the eastern tropical Pacific, and it is also found in older sediments drilled from the sea floor (Dean and Schreiber, 1978). Most marine barite consists of euhedral crystals, 1-20 μm in size, which constitute up to 2% of the sediment (Cronan, 1974; Scholle *et al.*, 1983). Barite which is strikingly similar to that of the CHG occurs in Lower Cretaceous organic-rich sediments drilled from the continental margin of northwest Africa (Dean and Schreiber, 1978). Here, barite forms rosettes, displacive lenses, and laminations and is associated with relatively pure limestones. Some crystals are pseudomorphically-replaced by calcite, and elsewhere barite replaces calcite. Other relationships suggest simultaneous precipitation of barite and calcite.

Numerous organisms concentrate Ba and consequently their metabolic or degradational by-products are considered to be the primary source of this cation (Cronan, 1974; Dean and Schreiber, 1978). Sulphate is readily obtained from the overlying seawater column but in some

instances may also be derived intrastratally from dissolved evaporites as well as from the oxidation of earlier-formed pyrite (Dean and Schreiber, 1978). The first alternative, however, is clearly not applicable to the CHG. The amount of sulphate in pore-waters thus reflects the balance of input from seawater and elimination to due bacteriological sulphate reduction. Precipitation of barite is thought to occur under oxidizing or slightly reducing conditions (Church, 1970 - cited in Dean and Schreiber, 1978; Bjorlykke and Griffin, 1973).

The uppermost few centimetres to tens of centimetres of sediment is where the necessary conditions for barite authigenesis are most easily met; this is the meeting-place of oxidized, sulphate-bearing pore-waters derived from the overlying seawater column and substratal, anoxic or sub-oxic Ba-bearing pore-waters derived from oxidation of organic material within these sediments and from underlying sediments. The association of most barite occurrences with non-ferroan calcite implies that pore-waters were not sufficiently reduced to liberate Fe from various oxides and hydroxides, but some oxidation of organics must occur so as to increase pore-water alkalinity and precipitate non-ferroan calcite. Calcite replacing barite, barite replacing calcite, and simultaneous precipitation of calcite and barite may be explained by slight fluctuations of pore-water Eh-pH in this critical zone.

13.4 PYRITE

13.4.1 Occurrences and Petrography

Pyrite is a ubiquitous authigenic phase in the CHG and is particularly prominent in mudstones, and especially black and green shales. Pyrite is found as dispersed, single crystals or in small aggregates which range from less than 1 μm to 100 μm in size. Crystal shapes vary from anhedral (framboidal?) to euhedral, the latter ranging from equant to rod-shaped. Pyrite is occasionally concentrated and occurs in the following ways:

- (1) As pre-compaction nodules in shale up to 5 cm in size;
- (2) Replacing or outlining trace fossils (Plate 13b), beds (Plate 13b), allochems (Plate 34c), siliceous components (Plate 50d,g,i), or authigenic components;
- (3) As continuous to discontinuous crusts on the upper and/or lower surfaces of mudstones to grainstones;
- (4) It precipitates in various fractures from early-diagenetic (e.g. ladder, septarian, and V-shaped marginal) to tectonically-related (Plate 20b);
- (5) It forms the earliest cement in grainstones or leached radiolaria and spicules. Occasionally these crystals are geopetal. It may also occur as a cement overlying an earlier phase of calcite cementation

(Plate 32c; 33c).

13.4.2 Interpretation and Discussion

The ubiquity of pyrite in the CHG is typical of organic-rich sediments of all ages and it has been reported on almost all DSDP cruises (Kelts, 1976; Clark and Lutz, 1980). Pyrite is thought to be initially precipitated in the form of various fine-grained, poorly crystallized monosulphides; but with time, these metastable phases transform to pyrite, the stable end product (Berner, 1971). The rod-shaped crystals may be pseudomorphs after marcasite or some other iron sulphide (cf. Hudson, 1982).

In the CHG, interpretable paragenetic relationships with other phases are comparatively rare, considering the abundance of this mineral. In some samples, pyrite appears to be an early cement, preceding calcite or microquartz cement. In other samples, for example in pyrite-cored mudstone nodules, it precedes precipitation of neospar or may form pre-compaction nodules. More often than not, however, the interpretation of petrographic relationships is equivocal.

During early diagenesis, the depth limit of sulfide formation is controlled by numerous complexly-interwoven variables including availability of sulphate from the overlying water column, sediment permeability, bioturbation, rate of sedimentation, and availability of reactive organics (Hudson, 1982). The occurrence of pyrite in restricted areas, such as burrows or at the centres of dolomite crystals, implies that a reducing microenvironment is the major controlling factor on its

occurrence rather than the existence of widespread reducing pore-waters. Therefore, the utility of pyrite as an indicator of the general oxidation state of pore-waters is unreliable. During later diagenesis, however, a more widespread precipitation of pyrite is expected (Kelts, 1976; Hudson, 1982).

Sulphate reduction is usually considered to be responsible for the formation of pyrite by combining H_2S produced from the bacterial sulphate reduction reaction (Table 11.1) with Fe liberated by other microbiological processes (Hudson, 1978; Berner, 1980; see Chapter 11). The role of organic material is two-fold, causing sulphate reduction on one hand as well as reduction of various Fe-oxides and -hydroxides on the other. During later diagenesis, Fe may be derived from the alteration of clay minerals or pressure solution (e.g. Oldershaw and Scoffin, 1967; Boles, 1978; Hudson, 1982).

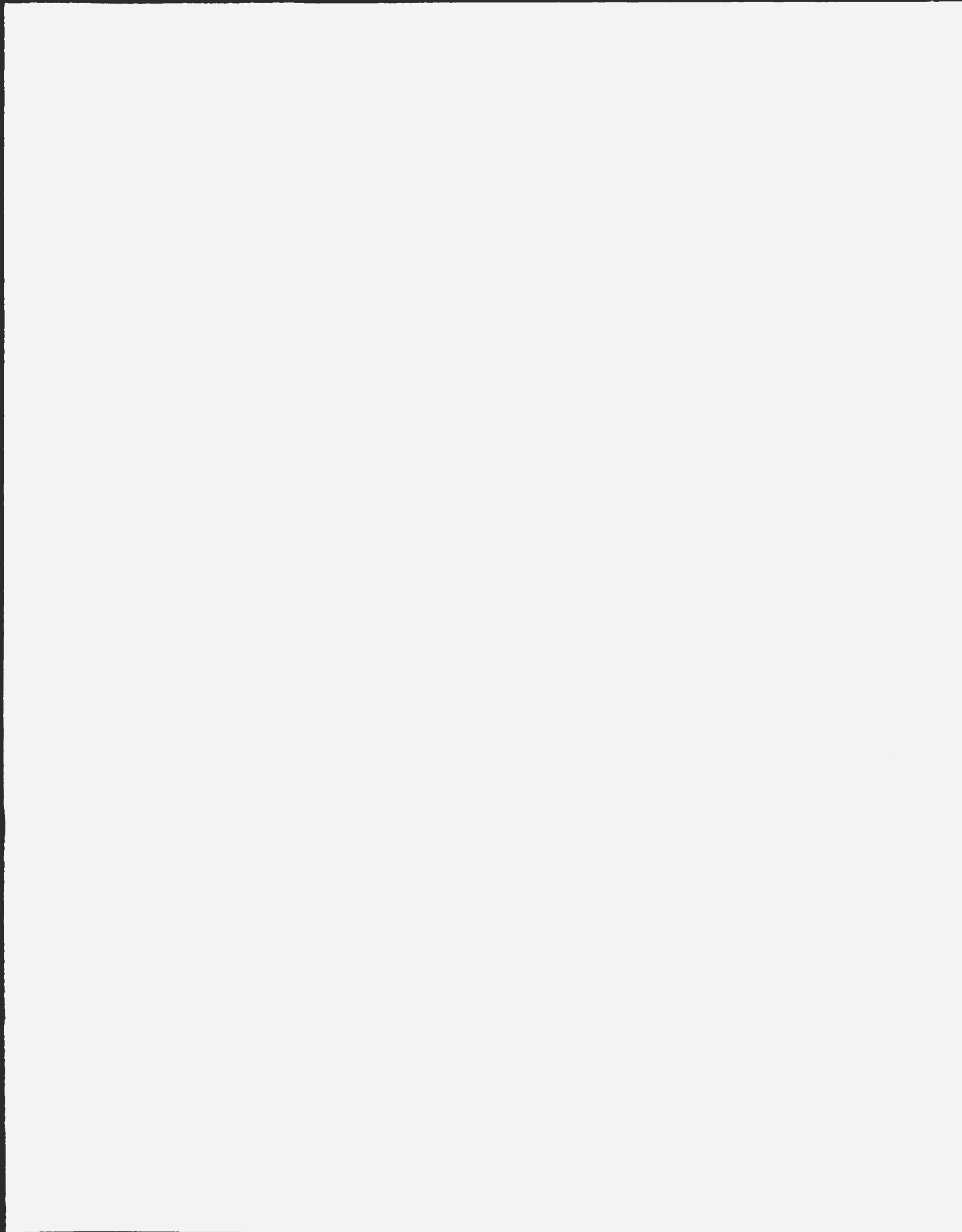
ORIGIN AND DIAGENESIS OF FINE-
GRAINED SLOPE SEDIMENTS: COW
HEAD GROUP (CAMBRO-ORDOVICIAN),
WESTERN NEWFOUNDLAND VOLUME 2

CENTRE FOR NEWFOUNDLAND STUDIES

**TOTAL OF 10 PAGES ONLY
MAY BE XEROXED**

(Without Author's Permission)

MARIO CONIGLIO



ORIGIN AND DIAGENESIS OF FINE-GRAINED SLOPE SEDIMENTS;
COW HEAD GROUP (CAMBRO-ORDOVICIAN), WESTERN NEWFOUNDLAND

VOLUME II

by

© Mario Coniglio, M.Sc.

A thesis submitted to the School of Graduate
Studies in partial fulfillment of the
requirements for the degree of
Doctor of Philosophy

Department of Earth Sciences
Memorial University of Newfoundland

January 1985

St. John's

Newfoundland

PART C

Chapter 14

ORIGIN OF PARTED, RIBBON, AND NODULAR LIMESTONES

14.1 INTRODUCTION

In Chapter 2 the rhythmite or "periodite" [1] character of parted and ribbon limestones was interpreted to be either a primary depositional or early diagenetic effect based on the contrasting rheologic behavior of interbedded mudstones and shales or marls in deformed rafts. The lateral continuity of parted and ribbon limestones, the intimate association of mudstones with parallel- and ripple-laminated grainstones, and compositional differences between burrows and host sediment collectively suggest that the mudstone-shale or -marl rhythmite is, in part, a reflection of primary sedimentation; either as fine grained turbidites or the result of settling of peri-platform ooze.

Integration of field, petrographic, CL, and geochemical data confirms and characterizes the nature of early lithification in grainstones to mudstones. The importance of early diagenesis in these sediments is

1. "Periodites" are cyclical sediments which consist of "periodically alternating beds which were deposited in a pelagic to hemipelagic environment below wave base. Sedimentation rate, texture, and fabric as well as composition changes gradually within one period while features of omission or erosion are atypical." (Einsele, 1982a, p. 4).

underlined by the inadequacy of the primary depositional models for mudstones to explain the relationships between continuously-bedded and nodular mudstones, as well as: (1) the striking rhythmicity of these sequences; (2) the generation of fitted fabrics; (3) the origin of composite beds and nodules with mudstone surrounding, on one or both sides, a more grainy sediment; and (4) marginal aggradation. The close association of primary and diagenetic attributes in these sequences is typical of parted, ribbon, and nodular limestones described from other, ancient, deep-water successions (see volume edited by Einsele and Seilacher, 1982).

The purpose of this chapter is to: (1) synthesize the previously discussed, relevant information on parted, ribbon, and nodular limestones; (2) develop a model which accounts for the intimate association of physical features suggestive of both primary deposition and diagenetic modification; and (3) develop a complimentary model emphasizing the temporal aspects of calcite authigenesis based on stable isotope $\delta^{13}\text{C}$ analyses.

14.2 DIAGENETIC MODELS FOR PERIODITES

The inadequacy of the primary depositional models to explain the generation of parted, ribbon, and nodular mudstones in conjunction with the early lithification of these sediments suggests that the mudstone-shale or -marl rhythmite is, at least in part, a product of diagenesis. In the following section, several diagenetic models for the

generation of periodites are considered. These models include: (1) rhythmic unmixing, (2) pressure solution, and (3) diagenetic overprint. The first two are purely diagenetic, the third involves a diagenetic modification of primary sediments.

14.2.1 Rhythmic Unmixing Model

In this model alternating limestone and marl beds are envisaged to result from the unmixing of an originally homogeneous sediment (Sujkowski, 1958; Hallam, 1960, 1964). Limestone beds and nodules are formed by the dissolution of carbonate from specific sites in the protolith and reprecipitation elsewhere as discrete beds or nodules. The homogeneity of the protolith demanded by this model is unlikely in most sedimentary successions. Furthermore, as nodules are usually found in discrete horizons and mudstone beds are often laterally continuous with little or no change in thickness, this implies some primary sedimentary control. The rhythmic unmixing model is therefore rejected as a working hypothesis.

14.2.2 Pressure Solution Model

The rhythmic character of these sediments is clearly established early in their history and therefore a purely pervasive, "non-seam" pressure solution origin is unlikely (see Wanless, 1979, 1983). In addition, rarity of stylolites, prominent argillaceous seams, microstylolite swarms, and accumulations of other insolubles in the transition zone between argillaceous sediment and continuously-bedded or nodular mudstones indicates that these limestones are not remnants of once

thicker beds; nor are nodules pressure solution relicts of once continuous beds (cf. Logan and Semeniuk, 1976; Wanless, 1979, 1983). This is also suggested by the common occurrence of marginally-aggraded mudstones. Coarsening of neospar crystals toward bed or nodule margins is not a microfabric expected from dissolution but instead from centrifugal precipitation on progressively more dispersed nuclei.

Near margins of nodules, grainy laminations often converge toward the horizontal axial plane of the nodule (Plate 13g; 53a-e). This could be interpreted to indicate pressure solution of a once-continuous limestone bed with one or several laminations, often siliciclastic-silt-rich, linking together the solution remnants (e.g. Wanless, 1983, fig. 11). In the CHG, however, nodules with draping laminations exhibiting marginal iron enrichment and aggrading crystal size suggest lithification during progressive compaction of the surrounding shales or marls. Furthermore, there is no evidence of pressure solution of the marginal crystals. Convergent laminations at nodule margins have been reported in numerous other studies of concretions (e.g. Raiswell 1971a; Oertel and Curtis, 1972; Henningsmoen, 1974).

That pressure solution features, such as argillaceous seams and microstylolite seams, do appear occasionally implies that some pressure solution does occur at the contact between mudstone and shale as well as within argillaceous sediments. A particularly informative example is illustrated in Plate 53a-d where a grainy lamination emerging from an early-formed limestone nodule can be traced for several centimetres into the adjacent, internodular matrix until it finally disappears. The lamination is initially subject to mechanical compaction, then pressure

solution. It remains to be shown, however, that this is other than a localized effect.

Pressure solution appears to only modify earlier-formed structures by enhancing continuous or nodular mudstone-shale or -marl boundaries and possibly dissolving dispersed calcite within argillaceous sediments. Both of these processes are catalysed by the presence of abundant clays which provide solvent for diffusion of ions away from the site of pressure solution (Weyl, 1959; Garrison and Kennedy, 1977; Wanless, 1979, 1983). In addition, pressure solution is enhanced at lithological transitions due to competency contrasts between adjacent units (Bathurst, 1980b; Buxton and Sibley, 1981). Enhancement of earlier-formed structures has been suggested in numerous studies, especially those concerned with the origin of nodular limestones (e.g. Bernoulli, 1972; Jenkyns, 1974; Jones et al., 1979; Fuzesy, 1980; Ricken and Hemleben, 1982; Schwarzacher and Fisher, 1982). Pressure solution has an analogous role in conglomerates in the CHG where "circum-idenic" stylolites or shale seams (Logan and Semeniuk, 1976) occur around pebbles. The role of clays in encouraging pressure solution is not proven, however, and experimental compaction of calcitic deep-sea oozes suggests that clays may actually retard the process (Baker et al., 1980).

14.2.3 Early Diagenetic Overprint Model

This model as outlined by Einsele (1982b) and Eder (1982) is similar to the rhythmic unmixing model as it assumes the sedimentary column is homogeneous with respect to the carbonate/clay ratio, but differs in

that the sedimentary column is inhomogeneous with respect to the nature of the carbonate, either compositionally or texturally. Consequently, more porous or permeable layers are cemented earlier, thus forming the limestone beds, and uncemented layers dissolve carbonate to generate the shale or marl layers.

A homogeneous protolith, as assumed by Einsele (1982b) and Eder (1982), was not present in the CHG where some characteristics of parted and ribbon limestones are interpreted to reflect primary deposition. Their model does, however, provide a conceptual framework for the development of a diagenetic overprint model applicable to the CHG (discussed below).

14.3 PHYSICAL MODEL

14.3.1 Introduction

In the sections which follow, a physical model which accounts for the origin of parted and ribbon limestones, their association with nodular mudstones, mudstone envelopes under and over grainy sediments, and fitted fabrics is outlined. Early diagenetic dolomitization, silicification, and the precipitation of barite also relate to this model but these phases are treated later in a separate section. Late authigenesis of calcite, dolomite, silica, barite, and pyrite is poorly constrained temporally and no further consideration is given to these late phases. A chemical model which compliments the physical model is presented in the following section.

14.3.2 Details

The physical model involves the following processes: (1) a climatically controlled carbonate rhythm which determines the basic periodicity of the mudstones; (2) formation of a primary sedimentary rhythm to provide fabric heterogeneity which allows carbonate to concentrate in specific horizons after remobilization; and (3) a remobilization process in which interaction of primary fabric heterogeneity and the carbonate rhythm produces a parted or ribbon limestone sequence.

Periodicity of periodites results from fluctuations in carbonate productivity, terrigenous mud content, or dissolution of carbonate (Einsele, 1982b). Based on measureable periodicity in numerous sequences, climate, as governed by astronomical factors, appears to be the principle control on periodicity (Einsele, 1982b) [2]. For simplicity in the following discussion, it is assumed climatic cycles control fluctuations in carbonate production.

In Chapter 2 the argillaceous "background" sediment in the CHG (shale lithofacies to siltstone lithofacies) was interpreted to comprise fine-grained turbidites interbedded with hemipelagites. These sediments

2. The duration of periods is generally thought to be controlled by the earth's orbital cycles of precession (21,000 years), obliquity (41,000 years), and eccentricity (100,000 years). These effects, often termed the Milankovitch parameters or hypothesis, affect climate which in turn regulates sea levels, current regimens, relative masses of the global carbon reservoirs, as well as the abundance and composition of sediments. Periods in many Quaternary and older sequences typically span 20,000-100,000 years and are interpreted to be climatically controlled (Fisher, 1980; see tables 1 and 2 in Einsele, 1982b).

were occasionally interrupted by coarser-grained, silt- and sand-size carbonate turbidites (siltstone lithofacies and calcarenite lithofacies), and sediments derived from high density flows (calcarenite lithofacies) and debris flows (conglomerate lithofacies).

During times of higher carbonate productivity in the shallow-water platform and possibly upper slope environments, these gravity flow deposits and hemipelagites were enriched in dispersed, silt- and clay-size carbonate mud. Hemipelagites may have also been enriched in dispersed carbonate mud, resulting either from storms washing out dense clouds of carbonate mud away from the platform, carbonate mud-rich gravity flows spreading out over pycnoclines and settling as a rain to the sea floor, or settling from nepheloid layers. During times of lower carbonate productivity, less carbonate fines were incorporated into the slope sediments.

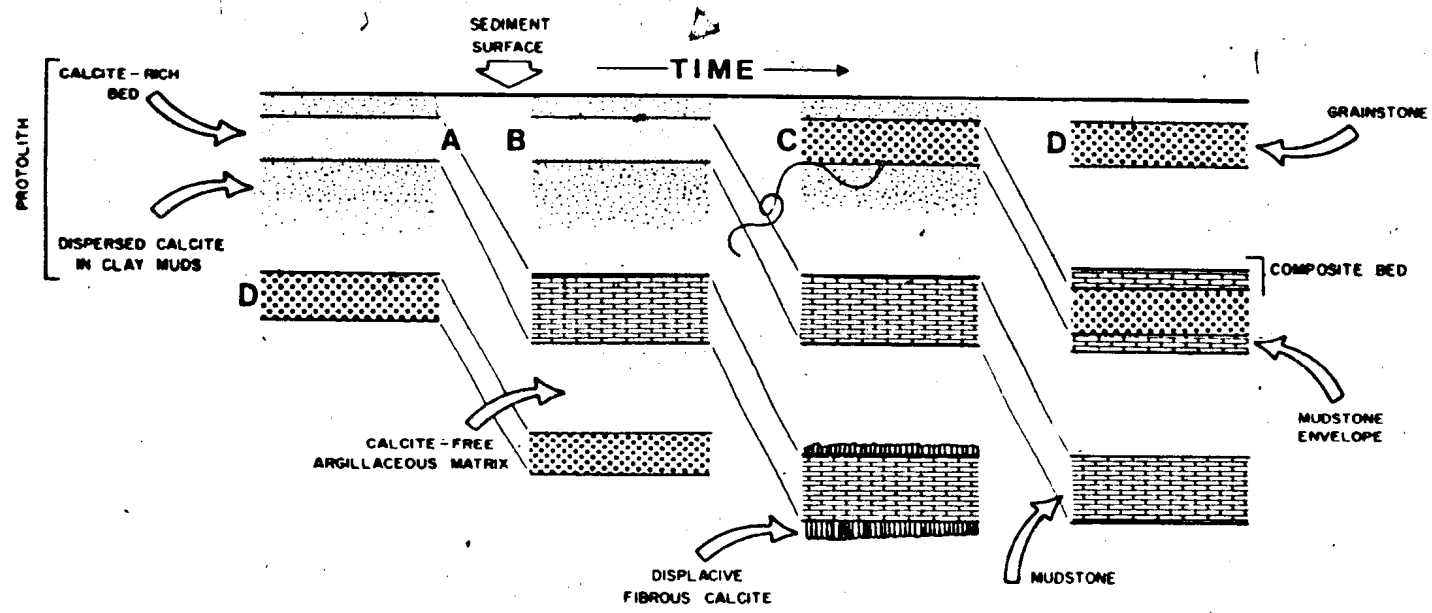
The spectrum of gravity flow deposits, ranging from fine-grained turbidite to conglomerate, are event deposits and interbedded with hemipelagites, form the framework of the physical model. The carbonate abundance cycles are superposed upon this framework to create a sequence of sediments that is notably rhythmic in character with respect to carbonate content, yet retains abundant evidence of gravity flow deposition. The rapid entombment of organic matter within turbidites results in further heterogeneity in the sediment. At deposition, therefore, the distribution of organics and carbonate is suggested to have been distinctly heterogeneous, although these two components were not necessarily correlated. Hand-in-hand with these compositional variations were porosity and permeability variations. Diagenetic

Figure 14.1: Schematic physical model for the generation of parted and ribbon limestones. From left to right across the diagram is a temporal/burial sequence showing the protolith and some of the common alterations which occur during early burial diagenesis. The model is simplified as it considers the calcite system only and ignores other possible effects such as early silicification and dolomitization.

The primary sediment of beds "A" and "B" are clay-rich carbonate muds which were deposited either as a fine-grained turbidites or as hemipelagites (fine stipple pattern). The terrigenous muds surrounding this layer are calcareous hemipelagites which reflect high carbonate productivity on the shallow-water platform. With burial, dispersed calcite in the hemipelagite is remobilized and reprecipitated in the adjacent, more calcite-rich bed which becomes the typical homogeneous or marginally-aggraded neospar mudstone (brick pattern). The dissolution-precipitation process has the effect of accentuating the primary depositional rhythm. With time and further calcite dissolution in the surrounding argillaceous sediment, DFC may be precipitated on bed "A", or as illustrated by bed "B", no more calcite is available for remobilization and therefore lithification ceases.

A similar situation is invoked for the early lithification of grainstones (coarse stipple pattern). Bed "C" is a turbidite deposited during a time of high carbonate productivity and, consequently, surrounding hemipelagite is calcite-rich. With burial, dispersed calcite in the hemipelagite is remobilized and reprecipitates as cement in the grainstone, and, if sufficient calcite is available and remobilized, additional calcite is reprecipitated to form a mudstone envelope around the grainstone, producing a composite bed.

At times of low carbonate productivity (bed "D"), grainstone turbidites remain unlithified for a longer period of time or are only partially lithified, and the remaining porosity is filled with other authigenic phases such as chert or dolomite. In these beds calcite cementation depends on allochthonous carbonate from beds below or above which were deposited during times of high carbonate productivity.



modification of these compositionally and texturally heterogeneous beds results in the limestone-shale or -marl rhythmite (also see Hallam, 1964; Campos and Hallam, 1979).

The heterogeneous distribution of organic material as well as variations in permeability suggest that carbonate (assumed to be calcite) dissolution will occur in some areas of the sediment from aerobic oxidation of organic matter, and in other areas where free molecular oxygen has been eliminated, oxidation continues by anaerobic processes and calcite precipitation occurs (cf. Sass and Kolodny, 1972). Calcite-rich horizons, occurring either as a primary grainy sediment (e.g. grainstone turbidite) or simply a carbonate-rich hemipelagite, are most likely to remain following dissolution caused by aerobic oxidation. Perhaps by initially providing a site for heterogeneous nucleation (Figure 14.1), these primary carbonate-rich beds become the locus of further calcite precipitation due to the establishment of a concentration gradient (Berner, 1980; Irwin, 1980). The calcite bed continues to lithify and grow until the supply of solute ions is eliminated, either by permeability decrease concomitant with further burial or by the cessation of anaerobic oxidation. In this model precipitation can occur above, below, or laterally within a bed, depending on the availability of calcite nuclei, a concentration gradient, suitably reactive organics, and basic sediment properties such as permeability.

14.3.3 Origin of Continuous Mudstone Beds

From previous discussion, early-lithified nodular mudstones or

concretions, are common in the CHG and except for their lateral discontinuity, many are identical to planar, continuously-bedded mudstones. The genetic relationship of the two is examined below.

It has already been argued on the basis of microfabric evidence that nodular mudstones are not the product of solution of a once continuous mudstone bed. The remaining possibilities to explain the relationship are: (1) nodular mudstones laterally coalesce to form a continuous mudstone bed (e.g. Shinn, 1969; Henningsmoen, 1974; Jenkyns, 1974; Kennedy and Garrison, 1975; Bromely, 1978; Jones et al., 1979), or (2) planar-bedded mudstones are lithified as "sheet concretions".

As discussed previously in Chapter 2, many mudstone nodules demonstrate marginal aggradation commonly concomitant with an increase in intercrystalline paste and iron content of calcite. If coalescence of these nodular concretions was responsible for the generation of continuous mudstone beds, internal concentric structures in the bed should be obvious, as illustrated in Plate 36a. Such structures are, however, rare. Homogeneous mudstone nodules would not leave such revealing evidence, but it can be argued in any case that lateral coalescence of nodular mudstones would be unlikely to produce such perfectly planar mudstone beds as is commonly found. Rather coalescence of homogeneously crystalline nodules would be expected to result in the formation of wavy beds. Chaotic nodules (see Chapter 2) and some "lumpy" mudstone beds are thought to result from bioturbation of the protolith to provide the irregular template which influences subsequent calcite precipitation (Plate 10d).

The overall lack of concentric structures in most continuous beds, in

concert with their remarkable planarity, is interpreted to indicate their origin as sheet concretions, formed by synchronous, widespread precipitation of calcite in the host strata. Precipitation may be focussed on obvious primary sedimentary laminations, or simply controlled by the permeability characteristics of the enclosing terrigenous muds.

14.3.4 Source of Calcium Carbonate

As discussed in Chapter 11, in organic-rich sediments, oxic bacterial decay of organics results in dissolution of carbonate whereas anoxic, decay causes carbonate to precipitate. Depending on the quantity of reactive organics and availability of free oxygen, within a few metres of the sediment-water interface the necessary conditions for wholesale redistribution of carbonate occur.

Because Ca and bicarbonate ions are also derived from other than dissolved CaCO_3 , the precipitation of early calcite cement and neospar is not necessarily a diagenetic remobilization of a precursor carbonate (e.g. Eder, 1982). Carbon isotopes suggest that bacterial decomposition of organic matter supplies significant bicarbonate to pore-waters.

Other sources of Ca besides a precursor CaCO_3 include trapped seawater, breakdown of feldspars, and clay mineral interactions (Irwin, 1980) although the latter two processes are only likely of any significance at greater depths. Upward expulsion of deeper pore-waters which do contain Ca from these sources, however, remains a possibility.

14.3.5 Origin of Mudstone Envelopes and Composite Bedding

The enhanced permeability of grainstone beds, dikes, and burrows allows pore-waters to readily travel through these sediments relative to the surrounding terrigenous muds and, consequently, their interparticle spaces are the sites of earliest cementation (also see Raiswell, 1971a). The concentration gradient thus established leads to precipitation of neospar on and/or under these beds to form composite beds (Figure 14.1), or around grainy nodules, dikes, or burrows to form cored nodules (see Chapter 2). The tendency for the precipitation of massive mudstone nodules to occur within certain horizons is interpreted to reflect a higher abundance of organic material, enhanced permeability, or both in these sediments.

Cored concretions are usually symmetrically developed around their nuclei. Nodules with asymmetric or incomplete development of the mudstone envelopes may reflect local permeability differences in the sediments surrounding the nucleus or the direction of greatest flux of Ca and bicarbonate to the site of precipitation.

3 Cored nodules are extremely common in other nodular limestones interpreted as early-formed concretions (e.g. Weeks, 1953; Waage, 1964; Baird, 1981). The association of organic cores, such as fish fossils, with the enveloping mudstone brought early attention to the role of organic matter in the development of concretions long before this was substantiated using stable isotope techniques (e.g. Tarr and Twenhofel, 1932, and references therein).

14.3.6 Origin of Fitted Fabrics

To explain fitted fabrics observed in many wavy, continuously-bedded, parted and nodular mudstones it is suggested that dispersed calcite is dissolved from the argillaceous interbeds and is locally reprecipitated onto nearby carbonate-rich beds. This results in conservation of CaCO_3 within a given stratigraphic thickness and accounts for the remarkably constant thickness of parted and ribbon limestone, even though individual beds may be wavy or discontinuous.

14.3.7 Origin of CFC and DFC

The precipitation of CFC, although strictly a submarine cement, incorporates bicarbonate derived by upward advection or diffusion from underlying or laterally equivalent, decaying organics. Their typical non-ferroan composition and dull to weak luminescence suggests they are synchronous with the earliest stages of precipitation in many equant cements and neospar calcites (also see Figure 8.2). Their elongate morphology is interpreted to result from the larger pore spaces in which they grew, allowing a higher degree of "maturity" (sensu Dixon, 1983) to the final mosaic than afforded by smaller pore spaces in grainstones.

Based on identical or gradational CL characteristics, precipitation of DFC is also controlled by the same or similar pore-waters which precipitate equant cements and neospar. Rheology of the immediately adjacent terrigenous muds, however, may dictate whether or not this peculiar type of displacive growth occurs (see Chapter 9). The

occurrence of DFC fringes above or below their substrate is attributed to the direction of greatest flux of solute ions, analogous to the development of asymmetric cored nodules or composite beds.

14.3.8 Original Mineralogy and Other Considerations

The calcitic mineralogy and ubiquitous pyrite in CHG mudstones and grainstones is typical of early-formed concretions described from most other ancient sequences (e.g. Noble and Howells, 1974; Dickson and Barber, 1976). From microprobe analyses, CHG calcites generally contain less than 1 mol % $MgCO_3$, levels which are low in comparison with Quaternary deep-water concretions and hardgrounds which usually have a few mol % to 10 mol % or more $MgCO_3$ (Fisher and Garrison, 1967; compilations in Milliman, 1974; Muller and Fabricius, 1974; Schlager and James, 1974; Mullins *et al.*, 1980). Submarine or slightly-modified submarine cements precipitated from cold, deep waters could, however, have such low Mg contents as are present in the CHG calcites, depending on the value assumed for the Mg partitioning coefficient (see Chapter 10). Based on their sharp CL zoning and microfabrics, trace element trends with progressive precipitation, and distinct isotopic signatures, authigenic calcites in the CHG are interpreted to be unaltered from their original low Mg-calcite compositions. This interpretation of original mineralogy and chemistry is consistent with conclusions reached in other studies of concretions (e.g. Galimov *et al.*, 1968; Hoefs, 1970; Raiswell, 1970b). Other aspects of the mineralogy, morphology, and geochemistry of authigenic calcites in the CHG are considered in Appendix O.

Although calcite cement and neospar are largely unaltered, the mineralogy of the presumed dispersed carbonate mud which is remobilized during shallow burial is uncertain. In addition, influence of the carbonate (calcite or aragonite) compensation depth may also be important in determining the primary distribution of carbonate in these sediments. There is, however, insufficient data on this aspect of the paleoceanography as well as mineralogy of Lower Paleozoic muds to determine whether deposition was above or below compensation levels (see review in James and Choquette, 1983).

14.4 CHEMICAL MODEL

14.4.1 Introduction

The relative ages of the various authigenic calcites is easily determined by staining, petrographic relationships, and especially CL when they occur within the same sample. Regional correlation based on a "cement stratigraphy" approach (Evamy, 1969; Meyers, 1974), however, is not possible in this succession. Intersample correlations based on CL is of little use due to the wide variety of reactions which liberate Fe and Mn into pore-waters, thus controlling calcite luminescence. A CL-based model is also inappropriate to temporally relate dolomite to calcite by their CL characteristics as Fe partitioning in each of these two phases is poorly-known (however, see Oglesby, 1976, p. 113-116).

In the previous section a "physical model" for the generation of parted, ribbon, and nodular limestones was discussed. The following section

outlines a complimentary "chemical model" which emphasizes the relative timing of calcite authigenesis based on $\delta^{13}\text{C}$, supported by petrographic and CL data. These serial trends previously detailed in Chapter 11 also provide information on the bacterial oxidation reactions governing pore-water composition at the time of calcite precipitation.

14.4.2 Features of the $\delta^{13}\text{C}$ Model

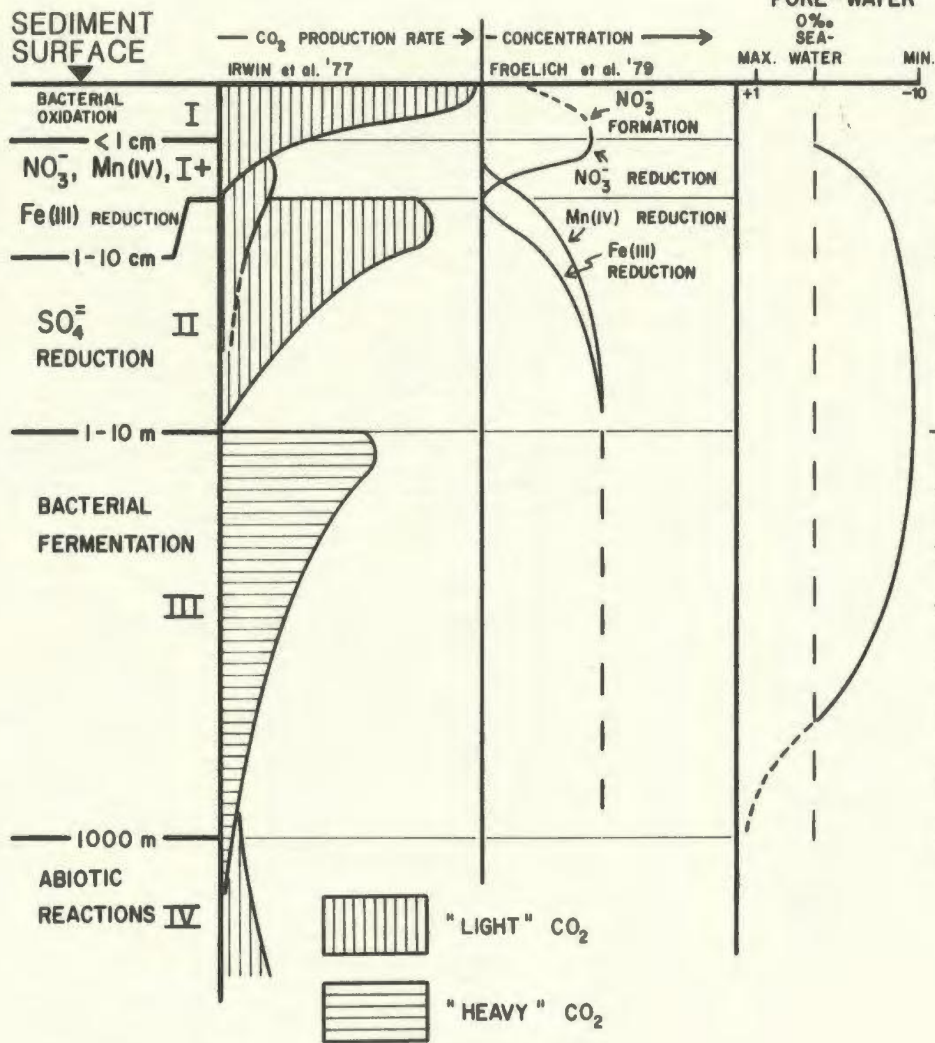
Irwin *et al.*'s (1977) idealized sequence of bacterially-controlled, diagenetic zones in organic-rich sediments provides the conceptual framework for this model (discussed in Chapter 11; Figure 14.2). Also included in Figure 14.2 are curves indicating the onset of other, relatively less important, "sub-oxic" reduction reactions, namely nitrate, Fe, and Mn reduction (Froelich *et al.*, 1979). Their order of occurrence is dependent on the nature of the Mn or Fe compound being oxidized.

The curve of pore-water $\delta^{13}\text{C}$ qualitatively demonstrates the importance of bicarbonate produced by sulphate reduction in Zone II and by methanogenesis in Zone III. The linear $\delta^{13}\text{C}$ scale is presented this way for simplicity, the minimum $\delta^{13}\text{C}$ value of -10 o/oo PDB being close to the most negative $\delta^{13}\text{C}$ analysed. Keeping all other sources and influences on bicarbonate $\delta^{13}\text{C}$ constant, changes in $\delta^{13}\text{C}$ with depth will be controlled mainly by sulphate reducing and methane-producing reactions. Obviously, the bicarbonate $\delta^{13}\text{C}$ curve as well as the linear $\delta^{13}\text{C}$ scale is a simplification of a potentially complex diagenetic system. The ultimate $\delta^{13}\text{C}$ of the pore-waters depends on several important factors:

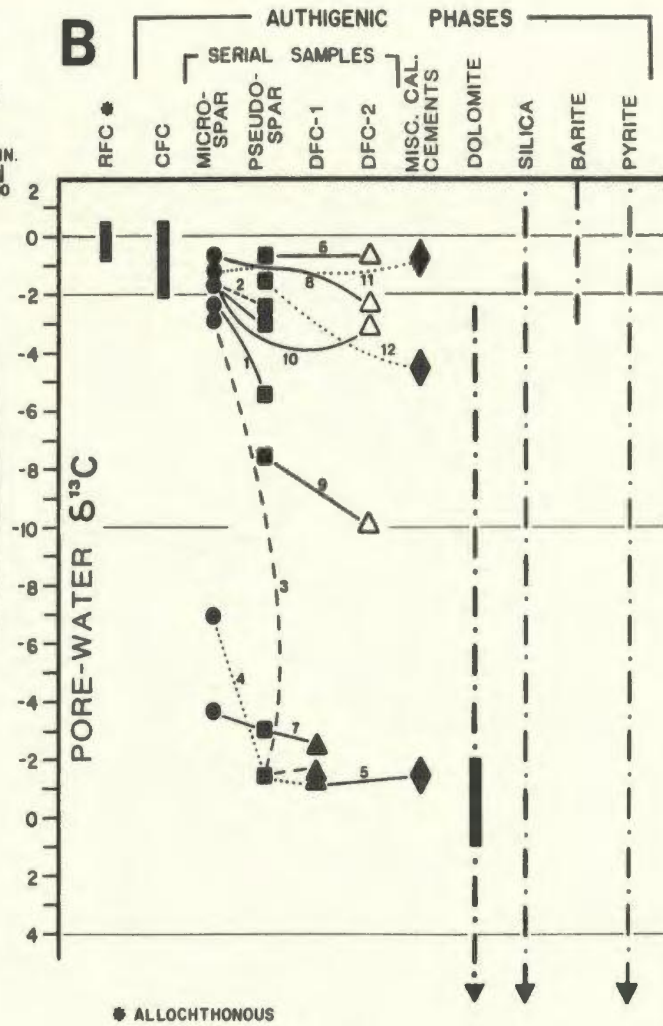
Figure 14.2: Chemical (isotopic) model for the evolution of parted and ribbon limestones. On the left side of the diagram ("A") are the various organic matter oxidation zones (I, II, III, IV from Irwin et al., 1977; I+ from Froelich et al., 1979). The " CO_2 PRODUCTION RATE" column is a qualitative representation of the rate as well as magnitude of CO_2 produced in the various oxidation zones. The "CONCENTRATION" column depicts the changes in concentration of nitrate and divalent Fe and Mn as a function of progressive burial and decrease in pore-water Eh. The " $\delta^{13}\text{C}$ PORE WATER" column is a representation of the $\delta^{13}\text{C}$ of pore-water bicarbonate as a function of the changing importance of the various bacterial oxidation reactions with depth. Maximum and minimum values are those analysed in this study.

In "B", the various authigenic phases encountered in the CHG are plotted against assumed depth and pore-water $\delta^{13}\text{C}$. The inflection point at $\delta^{13}\text{C} = -10$ o/oo is based on the most negative $\delta^{13}\text{C}$ analysed in this study. Solid bars for RFC and CFC are based on actual values of $\delta^{13}\text{C}$. The thick, solid portion of the dolomite line delineates the range of $\delta^{13}\text{C}$ determined by the regression analysis in Figure 12.4. The various serial trends discussed in Chapter 11 are shown as circles, squares, triangles, and diamonds. The broken lines showing the precipitation of dolomite, silica, barite, and pyrite are based on field and petrographic relationships. Opaline silica is considered to dissolve over an equally wide depth range as the silica line, and so is not indicated on this diagram. Late, tectonically-related calcite, dolomite, silica, barite, and pyrite are not considered in this model.

A



B



(1) production rate of bicarbonate generated by the various oxidation reactions balanced by removal by calcite precipitation or outward diffusion;

(2) $\delta^{13}\text{C}$ of the original organic carbon;

(3) degree of mixing of bacterially-derived bicarbonate with other bicarbonate. Mixing can occur when "end member" isotopic signatures are diluted by remobilized carbonate (e.g. bioclasts or peloids);

bicarbonate is a mixture of the products of two or more diagenetic zones; methane diffuses upward into Zone II and is oxidized during sulphate reduction thus contributing extremely light carbon to the dissolved carbon pool (less than -20 o/oo PDB); and there is "biological interference" and unaccounted for deviations in the source of organic carbon (Barnes and Goldberg, 1976; Savin and Yeh, 1981; Anderson and Arthur, 1983).

The order-of-magnitude depth limits shown in Figure 14.2 are compatible with the copious evidence for shallow-burial diagenesis in the CHG. The maximum depth limits for the zones are from Irwin et al. (1977). The boundaries between these diagenetic zones are transitional and their positions are a function of numerous variables including: amount and reactivity of the organic material, sedimentation rate, and geothermal gradient (Claypool, 1974). Sulphate reduction usually begins within 1 m of the sediment-water interface (Berner, 1980; Fruth and Sherreiks, 1982). Once sulphate is removed, oxidation of organic matter continues by the formation of methane which presumably continues until temperatures are too high (greater than 50 degrees C) or suitable

substrate is depleted (Claypool and Kaplan, 1974; Irwin et al., 1977). The recent study of peri-platform sediments cored from the northern slope of Little Bahama Bank at a seafloor depth of 600 m (Mullins et al. (1984) illustrates the shallow burial depth at which methane may form. These authors interpreted the relatively high $\delta^{13}\text{C}$ of authigenic dolomite at 1.2 m depth and below to reflect precipitation in the zone of methanogenesis after sulphate had been depleted by bacterial activity.

The use of this model depends on the following critical assumption - that with increasing burial, pore-water $\delta^{13}\text{C}$ trends do not fluctuate sufficiently to reverse the overall trend of reducing or increasing $\delta^{13}\text{C}$, except at the transition between Zones II and III.

14.4.3 Application of the Model: Implications for the Lithification of "Ordinary" CHG Mudstones

Using serial samples, the bacterial oxidation reactions which governed pore-water chemistry at the time of precipitation can be known by noting whether $\delta^{13}\text{C}$ increases or decreases with progressive precipitation. Most of the serial samples analysed are dominated by $\delta^{13}\text{C}$ trends which show decreasing $\delta^{13}\text{C}$ with progressive calcite precipitation (Figure 14.2). This can occur either during shallow burial (Zone II) where progressively more negative bicarbonate $\delta^{13}\text{C}$ is produced mainly by sulphate reduction, and possibly also nitrate, Fe, and Mn reduction; or during deeper burial as a result of abiotic reactions (Zone IV). All evidence points to the first alternative as being the only reasonable one and abiotic reactions are not considered further. By analogous

reasoning, some serial samples, mainly those related to DFC-1, demonstrate an increase in $\delta^{13}\text{C}$ with progressive precipitation and are interpreted to have been precipitated in the fermentation zone (Zone III).

Single analyses, however, are not easily interpreted and many provide no indication of an early, shallow-burial origin, for example Groups D, F, H, and E in Figure 11.2. Yet, (1) mudstone envelopes (Group F) are confidently interpreted as early-formed mudstone concretions; (2) microspar in Group E marginally aggrades to isotopically-lighter pseudospar, and these, too, were formed during shallow-burial; and one of the grainstones in Group H is a substrate to a DFC-1 fringe and was therefore lithified prior to the precipitation of DFC-1, which, from reasoning discussed in Chapter 9, was precipitated during shallow burial.

Isotopic analysis of 3 typical homogeneous, non-ferroan, microspar mudstones (Group D) provides no indication of their early lithification, yet these mudstones are identical in every respect to the ubiquitous mudstone clasts in most conglomerates in the CHG. Mudstones in Group D must have been lithified early, especially the one which shows evidence of having been exposed on the sea-floor (Plate 53f; discussed later). Their non-ferroan composition and identical petrographic and CL properties to obvious early-lithified mudstones [3] suggests that these

3. These would be obviously lithified early due to either: (1) distinctly negative $\delta^{13}\text{C}$ (e.g. Trend 7), or (2) association with later calcite having distinctly negative $\delta^{13}\text{C}$ (e.g. microspar in Trends 8 and 10).

typical and unremarkable mudstones must have been lithified close to the sediment-water interface, probably in Zone I+ or the upper part of Zone II, before pore-water bicarbonate became characterized by distinctively negative $\delta^{13}\text{C}$. Suboxic or anoxic bacterial oxidation of organic matter is, nevertheless, still required to increase pore-water alkalinity in order to precipitate carbonate.

The depth at which lithification is more or less completed by either growth of neospar or cementation is not known, but based on the: (1) ubiquity of mudstone clasts in conglomerates; (2) occasional evidence for seafloor exposure of exhumed nodular mudstones (see Plate 53e,f and Appendix N); and (3) comparison with studies which estimate depth using other criteria, lithification of CHG limestones is thought to occur within 5-10 m of the sediment-water interface. Depths as shallow as 1 m are compatible with all previously discussed evidence for shallow-burial lithification. Even if lithification occurred in Zone III rather than Zone I+ or II as is suggested above, limestones could still have been lithified within a few metres of the sediment-water interface otherwise their contribution to conglomerates would be considerably reduced.

The conclusion that not only are the ordinary parted and ribbon mudstones lithified close to the sediment-water interface, but that they are lithified before the formation of distinctly negative bicarbonate $\delta^{13}\text{C}$, emphasizes the importance of field and petrographic observation, and the supportive, not determinative role, of geochemical study.

14.5 OTHER DIAGENETIC COMPONENTS

14.5.1 Early Dolomite

14.5.1.1 Pervasive Dolomitic Siltstones

Field and petrographic evidence demonstrates that pervasive dolomitic siltstones and their associated shales were dolomitized early, prior to compaction (refer to Chapter 12). The apparently high degree of "sorting" of the dolomite crystals implies that the replaced peloidal grainstones were also highly sorted and therefore had high permeability. This, in conjunction with lateral continuity of the beds, suggests that the precursor grainstones would have been a preferred pathway for the lateral migration of dolomitizing fluids.

Dolomitization of the adjacent clay muds may have depended upon their permeabilities and possibly also on the presence of suitable nuclei. The high degree of microfabric preservation in these sediments strongly suggests that they were dolomitized at the outset without having been lithified to limestone first. If they were previously lithified limestones, they would not have been accessible pathways for lateral migration of pore-waters. The total lack of limestone relicts as well as the lack of variation in the degree of dolomitization within individual beds further suggests direct alteration of these sediments to dolomite.

The reasons for early dolomitization rather than limestone formation are

not known. Sulphate, which is considered to be a major inhibitor in the formation of sedimentary dolomite (Baker and Kastner, 1981), may have been eliminated or significantly reduced from pore-waters sooner than it normally would have been, either by an extensive barite sink (for which there is no evidence) or anaerobic bacterial oxidation. Dolomite might then have precipitated as a replacement of calcitic peloids and overgrowth of detrital dolomite cores. That dolomite precipitated before calcite possibly reflects the lower solubility of this mineral in slightly modified marine pore-waters. The relatively high sulphate concentrations in the more common calcite-precipitating pore-waters precluded such an early, wholesale dolomitization.

14.5.1.2 Conglomerate Matrix Dolomite

The occurrence of conglomerate matrix dolomite as a cement which periodically interrupts growth of CFC submarine cement fringes suggests that this dolomite precipitated from pore-waters which probably had a direct connection with seawater, but which must have also been influenced by alkaline, bacterially-modified pore-waters expelled upward from the underlying strata. The identical character of conglomerate matrix dolomite which postdates CFC either as a cement or a replacement of internal sediment indicates that all conglomerate matrix dolomites were precipitated from chemically-similar pore-waters. Gradual reduction of pore-water sulphate concentration may be responsible for the later dolomite which postdates CFC and replaces internal sediment, but a slight dip in sulphate concentration may be responsible for dolomite crystals which temporarily interrupt CFC growth.

14.5.1.3 Matrix Dolomite

Based on the common presence of ferroan rims on these crystals, they are thought to have completed their growth after the main phase of calcite authigenesis. These dolomite crystals probably started as small, scattered detrital(?) crystals dispersed in terrigenous muds early in the diagenetic history of these sediments and may have been an important sink for Mg throughout the period of calcite authigenesis. This readily available sink explains the progressive depletion of Mg concentration in various cement and neospar crystals.

The slightly- to moderately-compacted interbeds dominated by matrix dolomite are interpreted to result from their having not attained a crystal-support framework until later burial, past the main phase of calcite authigenesis. Consequently, they underwent some compaction before cessation of growth. Alternately, they may be explained by compaction of dolomite-rich, terrigenous muds to mechanically produce a crystal-support framework after they had ceased to grow. Regardless of which hypothesis is correct, the ferroan rims on most of these dolomite crystals suggests that they terminated their growth after calcite authigenesis, but they could have been growing along with calcite since the outset providing sulphate concentration was sufficiently reduced, at least locally.

14.5.1.4 Limestone-Hosted Dolomite

Limestone-hosted dolomite crystals may or may not have ferroan rims.

Crystals with ferroan rims suggest that they completed their growth after calcite authigenesis, as suggested for matrix dolomites. Non-ferroan dolomite may have been synchronous with calcite authigenesis.

14.5.1.5 Dolomite and the Chemical Model

The positive correlation of $\delta^{13}\text{C}$ with bulk FeO composition suggests that the outer, most ferroan zones in the dolomite crystals have positive $\delta^{13}\text{C}$ values. This implies precipitation in the fermentation zone (Zone III in Figure 14.2). The bulk of these crystals was probably precipitated at shallower depths in Zone III or in Zone II once sulphate levels were sufficiently depressed (dash-dot line in Figure 14.2). The solid bar in Figure 14.2 is the range of $\delta^{13}\text{C}$ derived from the linear regression of $\delta^{13}\text{C}$ and FeO in Figure 12.4 for compositions of 0-4 wt % FeO. The variability in the CL microstratigraphy underscores the importance of the local chemistry of pore solutions.

14.5.2 Silicification

As indicated in Chapter 13, silicification spans the entire diagenetic history of the CHG (Figure 14.2). Petrographic evidence in conjunction with field relationships indicate that radiolaria and siliceous sponge spicules are the principle contributors of silica to these sediments. Early silicification may be related to fluctuations in pore-water pH in sediments close to the sediment-water interface. Higher pH characterizes suboxic to anoxic pore-waters in Zones I+, II, III whereas lower pH is generated by aerobic oxidation in Zone I. Whether precipitation or dissolution of silica occurs depends on the net

influence of seawater and bacterial oxidation in the various zones. Higher and lower pH pore-waters encourage dissolution and precipitation, respectively. Intrinsic variations in the solubility of various species of radiolaria and siliceous sponges could conceivably provide dissolved silica over a wide depth interval. Silicification of some argillaceous interbeds in parted and ribbon limestone sequences appears to have post-dated dolomitization (and therefore calcite authigenesis), based on the presence of floating, corroded(?) dolomite rhombs in an argillaceous chert matrix. In other parted and ribbon limestone sequences, the presence of diffuse, slightly siliceous, tan-weathering crusts on the margins of some mudstones (Plate 9c) suggests that the later stages of mudstone lithification may have coincided with chert precipitation. Totally silicified sequences in which parted or ribbon limestones are not clearly differentiable are suggested to be the early-silicified protolith of these limestones. The lower portion of Bed 11 at Cow Head North is an example of this, where the only limestones encountered are isolated, widely-scattered nodules.

14.5.3 Barite Authigenesis

Most barite occurrences are interpreted to be early diagenetic (Figure 14.2; Chapter 13). Petrographic relationships involving barite and neospar in mudstones of parted, ribbon, and nodular sequences illustrate that barite predates, postdates, and is synchronous with calcite precipitation. These relationships are interpreted to represent slight fluctuations in Eh and pH within a few centimetres of the sediment-water interface.

14.5.4 Pyrite Authigenesis

Pyrite is found in all sediments; however, paragenetic relationships are seldom unequivocally interpreted. Within parted, ribbon, and nodular limestones pyrite occurs as both a replacement phase, a cement, and as nuclei for later neospar precipitation to form mudstone. As cement and nuclei pyrite predates calcite authigenesis, but such clearly defined relationships are exceptional.

14.6 MUDSTONE LITHOFACIES AND TIME

From previous discussion, the association of concretions and dark, organic-rich shales is a common one for reasons that have already been discussed at length. The conclusion that parted and ribbon mudstones and early lithification in general in the CHG are controlled in large part by suboxic and anoxic bacterial decay of organics indicates that this type of early lithification is widespread and probably also important in parted and ribbon limestones from numerous other localities that are associated with dark, finely laminated, presumably organic-rich shales (e.g. Wilson, 1969; Cook and Taylor, 1977; and other references in section 2.10 of Chapter 2).

It is generally recognized that the most spectacular development of black, organic-rich shales occurred in the early Paleozoic (Berry and Wilde, 1978; Jenkyns, 1980; Leggett, 1980). Mesozoic, especially upper Jurassic to middle Cretaceous, black shales are also widespread

(Jenkyns, 1980; Southam et al., 1980). Although there exist several models for the formation of black shales (refer to above citations), recent studies generally ascribe these to have been deposited during eustatic high-stands which had the effect of increasing the area of basin floor underlying highly fertile zones (Leggett, 1978; Berry and Wilde, 1978; Jenkyns, 1980).

Berry and Wilde (1978) considered the diminishing importance of the black shale facies from the early Paleozoic to the present to be due to progressive ventilation of the world ocean as a result of repeated, major glaciations. Consequently, widespread anoxic sedimentary facies are not found in the modern oceans, although organic-rich muds which could eventually form black shales do accumulate in certain physically restricted fjords as well as in some bays, estuaries, and in the Black Sea (Berry and Wilde, 1978):

The importance of organic-rich sediments for the generation of this distinctive style of slope sedimentation in many Lower Paleozoic and Mesozoic slope sequences is underscored by the observation that in the modern ocean, there are no ribbon and parted sequences, which, because of their shallow subsurface depth of formation, should be routinely encountered in deep-sampling of carbonate slopes such as in the Bahamas. Instead, what is found are micritic, commonly pelleted lumps and crusts and micrite-cemented grainstones (e.g. Mullins et al., 1980a) - sediments which are quite unlike those encountered in the fossil record.

Chapter 15

CONCLUSIONS

15.1 SEDIMENTATION

The Cow Head Group was deposited as a base-of-slope apron on the western continental margin of Iapetus. Five lithofacies are recognized in this succession.

Conglomerate Lithofacies: Most conglomerates are interpreted as debris flows based on the the following: (1) lack of or poor normal grading; (2) irregular tops with projecting boulders; (3) abrupt thinning at margins; (4) lack of stratification; (5) and incorporation of penecontemporaneously-deformed material. The lack of mud matrix (lime mud or terrigenous mud) in conjunction with occasional normal grading, coarse foreset beds, and local clast imbrication suggests that in some of these conglomerates, other particle-support mechanisms, such as dispersive pressure or turbulence, are important in addition to yield strength and bouyancy.

Calcarenite Lithofacies: The generally massive bedding of these grainstones and occasional normal grading and trough cross-lamination are inadequately accounted for by the classical turbidity current

model. These sediments do, however, resemble proximal siliciclastic turbidites described in other studies. The typical massive bedding with less common normal grading is interpreted to result from a direct suspension settling stage from these high density flows as they slowed and gradually became more dilute. The lack of dewatering structures is accounted for by an initial lack of fine, interstitial sediment. Thinly-bedded grainstones within parted and ribbon limestone sequences are probably turbidites.

Siltstone Lithofacies and Shale Lithofacies: Silt-shale couplets consisting of equal thicknesses of siltstone and shale (siltstone lithofacies), or isolated stringers of siltstone within shale (shale lithofacies) are interpreted as fine-grained turbidite-hemipelagite cycles. Turbidites are regarded as silt or terrigenous mud turbidites based on whether siltstone or shale is dominant. Silt turbidites exhibit the same sequence of sedimentary structures as the the Bouma (1962) sequence for sandy turbidites and were thus deposited by a waning, dilute turbidity current. Terrigenous mud turbidites are similar to those described by Stow (1982) from siliciclastic deep-water sediments and likewise demonstrate a predictable sequence of small-scale sedimentary structures. By analogy with terrigenous mud turbidites described from elsewhere, these sediments were deposited from thick, slow-moving, very dilute turbidity currents.

Millimetre-cycles of interlaminated black and green or red and green shales are interpreted to be a reflection of the different abundances as well as preservation potential of organic material in turbidite terrigenous muds versus hemipelagic terrigenous muds. The thicker

metre-cycles in shales are interpreted to result from climatically-controlled, periodic variations in the amount of organic matter delivered from the source regions of the terrigenous muds or oxygen levels of bottom waters.

Mudstone Lithofacies: The mudstone-shale or -marl rhythmite, although not perfectly understood on the basis of field work and petrography alone, is clearly an early feature. It has primary depositional characteristics, such as fine, parallel laminations and scattered allochems as well as those conventionally regarded as diagenetic in origin, such as nodules. Attempts to explain this complex lithofacies by deposition from carbonate mud-rich, dilute turbidity currents or settling of hemipelagic (peri-platform) fines fails to account for its most salient characteristics, such as the remarkable planarity of some beds; the association with nodular limestones; fitted fabrics; composite beds; and marginal aggradation on continuous and nodular mudstones. A contourite origin for both grainstones and mudstones, although a possibility, is not likely to be sufficiently distinct from turbidites to be recognizable. Except for their lenticular shape, many nodular mudstones are identical to their more continuously-bedded counterparts although, based on field work and petrography alone, the exact nature of their relationship is not clear.

As is typical for most modern and ancient carbonate slopes, packages of these lithofacies occur in an unpredictable, disorganized array, quite unlike submarine fan deposits where fan progradation creates a distinctive succession of fan environments. A base-of-slope apron depositional model, as suggested by James and Stevens (in prep.), is

also supported by the general lack of obvious channelling. The various gravity flows which do occur in the CHG are interpreted to have spread out as large sheet-flows from a semi-continuous line source at or near the platform margin.

15.2 INTRASTRATAL DEFORMATION

The occurrence of intraformational truncation surfaces, slide masses, and shear zones in the most distal outcrops of the CHG indicates that deposition occurred on a sloping surface. A simple model to relate the above features is outlined, based on several exceptionally informative outcrops. Practical recognition and differentiation of truncation surfaces, slide masses, and shear zones requires extensive strike exposure. Instead, what is most commonly encountered are numerous, minor bedding disruptions which are the result of shear zone deformation either (1) at the place of detachment of a slide mass (i.e. truncation surface); (2) at the base of the slide mass or at the surface of the overridden, in situ sediment; or (3) within a shallow, substratal shear zone along which minor creep of the overlying sediment has occurred, but there has been no detachment. These often subtly-expressed deformation fabrics include: (1) intrafolial folding, (2) brecciation, and (3) rotation of slabs of limestone. Phacoidal bedding (4) is produced in some mudstones and grainstones by the development of irregular, anastomosing, argillaceous seams. In addition, finely laminated shales and marls contain domains where laminations are (5) reoriented or (6) homogenized. Small-scale (7) isoclinal folding and (8) microfaulting

are also locally developed. Although the exact origin of the deformation may not be known due to outcrop limitations, their presence in strata is an important signpost that synsedimentary failure has occurred and that the depositional surface was not flat. The frequency of this type of intrastratal deformation in the CHG indicates that sediment failure was a common occurrence.

Association of the above shear-zone deformation fabrics with clearly defined slide masses and truncation surfaces, along with evidence to indicate a pre-compactive origin precludes a tectonic origin for this type of intrastratal deformation. In contrast, contorted limestones are interpreted to reflect layer-parallel shortening generated by horizontal, tectonic compression. Unequivocal evidence of a surficial or shallow subsurficial sliding origin for these enigmatic limestones is entirely lacking. The interpretation of contorted limestones as tectonic is compatible with the northeast-southwest trends of their fold hinges, similarly oriented vertical stylolites (see below), and regional structures. The amount of shortening accounted for by contorted limestones and vertical stylolites is not known.

15.3 MECHANICAL AND CHEMICAL COMPACTION

Based on measurement of clastic dikes, the CHG has been compacted by an estimated 50-60%. Sequences dominated by thick grainstones or conglomerates may have compacted less, depending on the importance of intrabed pressure solution. Sequences with greater amounts of

argillaceous sediment may have compacted more, up to 80%, a value consistent with original depositional porosities of terrigenous muds. This implies that the measured compaction can be explained largely as the result of mechanical compaction of terrigenous mud-rich sediments, with pressure solution generally being relatively unimportant. The role of pressure solution in the formation of nodular limestones as well as the parted and ribbon limestones has been mainly to modify earlier-formed structures. Pressure solution of grainstone laminations between nodules may be related to the original lack of cementation of the grainstone.

15.4 ORIGIN OF PELOIDS AND INTRACLASTS

Micritic peloids and peloidal intraclasts characterized by structure grumeleuse are dominant silt- and sand-size particles in CHG limestones. In this respect, these limestones are similar to many others described from Paleozoic sequences. Other primary components include detrital dolomite, siliciclastic sand and silt, shelly bioclasts and other fossils, and various types of Girvanella clasts - oncolites, rafts, single tubules, and intraclasts. Based on comparison of microfabrics in silt- and sand-size peloids and peloidal intraclasts with those of Girvanella sheets within algal boundstone boulders in conglomerates, it is concluded that this platform margin lithofacies could have been a major contributor of sand-size and smaller particles to CHG. Girvanella sheets in the boundstones often do not contain clear evidence of tubules. Instead the microfabric is most often

appropriately described as structure grumeleuse and thus Girvanella sheets are a likely progenitor of many intraclasts having this microfabric. Girvanella sheets which are less cemented could conceivably provide rafts and single tubules. Further destruction of these grains would yield silt-sized peloids, some of which may retain a vestige of their algal origin as a slightly more coarsely crystalline, microspar centre. Most peloids, however are devoid of tell-tale microfabrics which may be the result of intra-tubular micrite cementation.

In contrast to Girvanella, the petrographic evidence for Epiphyton in the fine grained limestones is comparatively rare, occurring only as intraclasts. The homogeneous micritic composition of many Epiphyton suggests that fragmentation of their branches will readily provide silt- to fine sand-size peloids but the lack of distinctive microstructure precludes the differentiation of such algally-derived peloids from those of other origins.

15.5 DIAGENETIC CALCITES

15.5.1 Field Data, Petrography, and Cathode Luminescence

Cements, neospar, and DFC are all significant authigenic components in the CHG, although the first two are volumetrically more important than the last. The following suggests individually, and especially collectively, that lithification, resulting from precipitation of calcite cement, neospar, or DFC occurred during shallow burial

diagenesis: (1) grainstones and mudstones have similar cement and neospar characteristics to those which occur as clasts in conglomerates; (2) there is no evidence for compaction of most limestones whereas interbedded argillaceous sediments are often obviously compacted; (3) microspar mudstone nodules may show evidence of exposure on the sea floor; (4) mudstone nodules, occasionally septarian, occur as clasts and in rafts in conglomerates; (5) mudstone rafts in conglomerates may develop fracture cleavage and fragmented clasts are often angular; (6) mudstones may be fragmented and rotated in synsedimentary shear zones; (7) DFC occurs as clasts in conglomerates; (8) curved DFC crystals suggest growth during shear; (9) displacive crystal growth would be easier if surrounding terrigenous muds were largely uncompactd and easily compressible; (10) CFC is associated with geopetal internal sediment and is interpreted as a submarine cement, although $\delta^{13}\text{C}$ values indicate an organic carbon influence.

Early lithification of these limestones is also supported by stable isotopic analyses in which negative $\delta^{13}\text{C}$ values indicate the incorporation of organically-derived bicarbonate. The general lack of evidence for submarine exposure suggests that these limestones be regarded as concretions (i.e. early lithification below sediment surface) rather than hardgrounds.

A generalized CL microstratigraphy is recognized for cements, neospar, and DFC which is identical to that described from shallow-water carbonates. The luminescence trend from dark to bright to dull is interpreted as a response to decreasing Eh conditions in which first Mn and then Fe is remobilized from various oxides and hydroxides and

incorporated into precipitated calcite. Intrasample correlation of CL characteristics of cements, neospar, and DFC indicates that these diagenetic calcites can all form from identical pore-waters, although DFC is usually later than the others. Detailed zoning correlation on a regional basis or even from outcrop to outcrop is not possible, underscoring the importance of local pore-water effects. This is also supported by variations in trace element geochemistry and stable isotope analyses. The sharp CL zoning in these calcites strongly suggests that they are largely unaltered and that their chemistry is primary.

15.5.2 Geochemistry of Calcite

Neospar, cements, and DFC commonly demonstrate decreasing Sr and MgO concentrations and increasing FeO concentrations with progressive precipitation. MnO concentration trends are not consistent although this may be in part a function of low concentrations. The decrease in Sr and MgO is explained by incorporation into mineralogic sinks (e.g. Mg in dolomite) or possibly diffusion upward into the overlying water mass. Fe and Mn enrichment in the later stages of crystal growth results from a lowering of Eh which remobilizes these elements from various dispersed oxides and hydroxides. The above trends are not, however, without exceptions. Trace element trends such as those from the CHG are also typical of meteorically-altered limestones where mineralogical stabilization proceeds by replacement of aragonite, incongruent dissolution of Mg-calcite, and precipitation of calcite with lower Sr and Mg concentrations.

Using published partitioning coefficients for Mg and Sr extrapolated to

below 5 degrees C, and assuming Lower Paleozoic seawater was identical to modern seawater with respect to Ca, Mg, Sr, and Mn concentrations, then the earliest precipitates could have precipitated from unmodified or slightly modified seawater, a likely possibility given the abundance of field and petrographic evidence to suggest early, shallow-burial lithification.

Stable isotope analysis of calcite demonstrates a considerable range of $\delta^{13}\text{C}$ and $\delta^{18}\text{O}$ values. Distinctly negative values of $\delta^{13}\text{C}$ indicate a variable contribution of organically-derived carbon. Serial analyses of successive precipitates within the same sample commonly illustrate decreasing or increasing $\delta^{13}\text{C}$ with progressive precipitation. In the first case, precipitation is interpreted to be driven by sulphate reduction. In the second case, rising $\delta^{13}\text{C}$ reflects the increasing importance of fermentation in controlling the $\delta^{13}\text{C}$ of pore-water bicarbonate. Serial $\delta^{13}\text{C}$ analyses in conjunction with staining and cathode luminescence data suggest that "ordinary" microspar and pseudospar mudstones may be lithified before $\delta^{13}\text{C}$ becomes distinctly negative. The negative $\delta^{18}\text{O}$ of most calcites in this study is also suggested to be related to bacterial oxidation of organic matter.

15.6 MODEL FOR GENERATION OF PARTED, RIBBON, AND NODULAR

LIMESTONES

A model which accounts for the origin of parted, ribbon, and nodular

limestones incorporates elements of both primary sedimentation as well as diagenetic features. The "background" sedimentation of shales consists mainly of millimetre- to centimetre-size terrigenous mud turbidite-hemipelagite cycles. During times of higher carbonate productivity in shallow-water platformal areas, terrigenous mud turbidites and their associated hemipelagites are carbonate-rich relative to times when carbonate is scarce. Based on analogy with Mesozoic and Cenozoic periodites, climatic cycles probably controlled the periodicity of carbonate abundance. Shortly after deposition aerobic bacterial oxidation of organic matter causes some of the calcite (assuming calcite mineralogy for simplicity) to dissolve. In other areas containing more organics, anaerobic reactions may continue to oxidize organics, increasing carbonate alkalinity, and inducing precipitation of calcite. With the establishment of concentration gradients, dissolved carbonate is driven toward already carbonate-rich areas to form: (1) sheet and nodular concretions, (2) cement grainstones, (3) precipitate mudstone on grainy sediments to form cored nodules and composite beds, and (4) precipitate DFC fringes. Some lumpy-bedded mudstones may result from the lateral coalescence of homogeneously crystalline concretions. Fitted fabrics in parted, wavy and nodular limestones imply a local redistribution of carbonate. Early dolomitization to form pervasive dolomitic siltstones and early silicification of the protolith may preclude the formation of parted and ribbon limestones.

In general, it appears that the most profound diagenetic alteration of these sediments occurs during shallow burial controlled by bacterial

oxidation of organic matter. Later diagenetic effects include more dolomitization, silicification, barite and pyrite precipitation, but these phases are relatively minor. The outcrop-wide late dolomitization which occurs in the White Rock Islets is clearly an exception. Many of these late phases also often appear to be related to tectonism.

15.7 DOLOMITIZATION

Three generations of dolomite are recognized in the CHG. The first is a transported, detrital phase; the second is "Early" diagenetic; and the last is related to tectonism ("Late" diagenetic). Early dolomite occurs mainly as a replacement of calcite allochems and overgrowth of detrital dolomite crystals. Field and petrographic relationships indicate that the Early dolomitization occurred in non-compacted or partially compacted sediments. Dolomite growth may have been synchronous with calcite authigenesis, but the presence of ferroan rims on many dolomite crystals suggests that the growth history of dolomite was protracted and continued past the main episode of calcite authigenesis. Pervasive dolomitic siltstones, however, are considered to have predated and therefore precluded calcite cementation of the precursor grainstones. The positive correlation of $\delta^{13}\text{C}$ and bulk FeO content suggests that the latest ferroan dolomite rims are characterized by progressively greater $\delta^{13}\text{C}$ values, implying that during the later stages of dolomite precipitation, bacterial fermentation was important. Anoxic dolomites described from numerous shallow-buried, organic-rich sediments are analogues for Early dolomites in the CHG.

15.8 SILICIFICATION

Chert occurs both as a replacement phase as well as a cement, although the latter is relatively uncommon. The silicification history of the CHG is protracted and there is abundant evidence for silicification which predates or postdates compaction. CL dramatically illustrates that calcite-replaced radiolaria and spicules are much more common than is apparent using standard petrographic analysis. In addition, there is sound petrographic evidence to suggest that vast quantities of radiolaria and spicules were dissolved without leaving a trace. Based on the above evidence, dissolution of radiolaria and spicules during shallow-burial diagenesis is interpreted to be responsible for most of the silicification in the CHG.

15.9 CALCITE MICROFABRICS

15.9.1 Radiaxial Fibrous Calcite

RFC is restricted to fractures, vugs, and enigmatic mound structures in shallow-water boulders of conglomerates. In all respects, except CL for which there is little comparative data available, RFC is typical of that described in most other studies. CL of some RFC from the CHG demonstrates their remarkable similarity to DFC (see below) with regards to the variability of internal growth surfaces. As recently described

by Kendall (in press), these crystals grew as spherocrystals at times and as unit crystals at other times. Although most of Kendall's (in press) reinterpretation of RFC as composite crystals is supported by CL data from the present study, an alternate hypothesis to that of Kendall (in press) is proposed to explain distally-convergent extinction. Microfabric evidence visible with CL suggests that RFC crystals are actually length-slow and not length-fast as perceived optically. If this is true, the distally-convergent extinction which characterizes RFC is explained simply as a function of asymmetric spherocrystal growth on a length-slow seed crystal. If both length fast and length-slow crystals precipitate initially, this leads to the cohabitation of RFC and FOC in the same pores, a phenomenon not explained by Kendall's (in press) hypothesis.

15.9.2 Neospar

CL study of neospar in marginally aggraded mudstones suggests that aggrading neomorphism in argillaceous sediments, for crystals of microspar-size and larger, does not occur by porphyroid or coalescive processes as hypothesized by Folk (1965). Rather marginal aggradation results from decreased nucleation density at the edges of the bed and precipitation of progressively younger calcite, not the cannibalization of microspar. CL clearly shows that neospar growth often occurs by asymmetric, irregular increments.

15.9.3 Displacive Fibrous Calcite

DFC is an important diagenetic constituent of the CHG both in terms of

its constraints on the timing of diagenesis as well as the microfabrics^m made visible by CL. Macroscopically-recognizable fringes of DFC grow on both continuous and nodular beds, with crystals oriented in pallasade fashion or as a series of mutually interfering cones. Micro-fringes of DFC are ubiquitous and are identical, both genetically and petrofabrically (where assessable), to the macro-fringes of DFC. A fibrous, radiating inclusion pattern and the presence of fibrous crystallites made visible with CL indicate that DFC grew as spherocrystals at times, and as unit crystals at other times, with both types of growth often occurring within the same crystal. Neospar associated with DFC occasionally also shows spherulitic inclusion patterns and crystallites. Based on staining and CL, DFC grew during the later stages, or as a continuation, of marginal aggradation in mudstones and cementation in grainstones.



REFERENCES CITED

- Abed, A.M. and Schneider, W., 1980: a general aspect in the genesis of nodular limestones documented by the Upper Cretaceous limestones of Jordan: *Sedimentary Geology*, v. 26, p. 329-335.
- Ahr, W.M., 1971: Paleoenvironment, algal structures, and fossil algae in the Upper Cambrian of central Texas: *Journal of Sedimentary Petrology*, v. 41, p. 205-216.
- Aitken, J.D., 1966: Middle Cambrian to Middle Ordovician cyclic sedimentation, southern Rocky Mountains of Alberta: *Bulletin of Canadian Petroleum Geology*, v. 14, p. 405-441.
- Aitken, J.D., 1967: Classification and environmental significance of cryptalgal limestones and dolomites with illustrations from the Cambrian and Ordovician of southwestern Alberta: *Journal of Sedimentary Petrology*, v. 37, p. 1163-1178.
- Allan, J.R. and Matthews, R.K., 1982: Isotope signatures associated with early meteoric diagenesis: *Sedimentology*, v. 29, p. 797-817.
- Amieux, P., 1982: La cathodoluminescence: methode d'etude sedimentologique des carbonates: *Bulletin de Centres Recherche Exploration-Production Elf-Aquitane*, v. 6, p. 437-483.
- Amsbury, D.C., 1962: Detrital dolomites in Central Texas: *Journal of Sedimentary Petrology*, v. 32, p. 5-14.
- Anderson, T.F. and Arthur, M.A., 1983: Stable isotopes of oxygen and carbon and their implication to sedimentologic and paleoenvironmental problems: In Arthur, M.A., Anderson, T.F., Kaplan, I.R., Veizer, J., and Land, L.S., *Stable isotopes in sedimentary geology*, Society of Economic Paleontologists and Mineralogists Short Course no. 10, p. 1-1 - 1-151.
- Anketell, J.M., 1976: Upper Llandoveryian Grogal sandstones and Aberystwyth grits in the New Quay area, Central Wales: a possible upwards transition from contourites to turbidites, *Geological Journal*, v. 11, p. 101-108.
- Assereto, R.L., and Kendall, C.G.St.C., 1971: Megapolygons in Ladinian Limestones of Triassic of southern Alps: evidence of deformation by penecontemporaneous dessication and cementation: *Journal of Sedimentary Petrology*, v. 41, p. 715-723.
- Assereto, R.L., and Kendall, C.G.St.C., 1977: Nature, origin and classification of peritidal tepee structures and related breccias: *Sedimentology*, v. 24, p. 153-210.

Baird, D.M., 1960: Observations on the nature and origin of the Cow Head breccias of Newfoundland: Geological Survey of Canada, Paper 60-3, 26p.

Baird, G.C., 1976: Coral encrusted concretions: a key to recognition of a "shale on shale" erosion surface: *Lethaia*, v. 9, p. 293-302.

Baird, G.C., 1981: Submarine erosion on a gentle paleoslope: a study of two discontinuities in the New York Devonian: *Lethaia*, v. 14, p. 105-122.

Baker, P.A. and Kastner, M., 1981: Constraints on the formation of sedimentary dolomite: *Science*, v. 213, p. 214-216.

Baker, P.A., Kastner, M., Byerlee, J.D., and Lockner, D.A., 1980: Pressure solution and hydrothermal recrystallization of carbonate sediments - an experimental study: *Marine Geology*, v. 38, p. 185-203.

Baker, P.A., Gieskes, J.M., and Elderfield, H., 1982: Diagenesis of carbonates in deep-sea sediments - evidence from Sr/Ca ratios and interstitial dissolved Sr²⁺ data, *Journal of Sedimentary Petrology*, v. 52, p. 71-82.

Baltuck, M., 1983: Some sedimentary and diagenetic signatures in the formation of bedded radiolarite: In Iijima, A., Hein, J.R., and Siever, R., eds., *Siliceous deposits of the Pacific Region*, Elsevier Scientific Publishing Company, Amsterdam, p. 299-316.

Barnes, R.O. and Goldberg, E.D., 1976: Methane production and consumption in anoxic marine sediments: *Geology*, v. 4, p. 297-300.

Bathurst, R.G.C., 1959: The cavernous structure of some Mississippian "stromatolites" reefs in Lancashire, England: *Journal of Geology*, v. 67, p. 506-521.

Bathurst, R.G.C., 1975: *Carbonate sediments and their diagenesis*: 2nd edition, Elsevier, Amsterdam, 658p.

Bathurst, R.G.C., 1977: Ordovician Meiklejohn bioherm, Nevada, *Geological Magazine*, v. 114, p. 308-311.

Bathurst, R.G.C., 1980a: Lithification of carbonate sediments: *Science Progress*, Oxford, v. 66, p. 451-471.

Bathurst, R.G.C., 1980b: Deep crustal diagenesis in limestones: *Revista del Instituto de Investigaciones Geologicas*, v. 34, p. 89-100.

- Bathurst, R.G.C., 1983a: Early diagenesis of carbonate sediments: In Parker, A. and Sellwood, eds., *Sediment diagenesis*, Reidel Publishing Company, Boston, p. 349-377.
- Bathurst, R.G.C., 1983b: Neomorphic spar versus cement in some Jurassic grainstones: significance for evaluation of porosity evolution and compaction: *Journal of the Geological Society of London*, v. 140, p. 229-237.
- Baud, A. and Masson, H., 1975: Preuves d'une tectonique liasique de distension dans le domaine brianconnais: failles conjugees et paleokarst a Saint-Triphon (Prealpes Medianes, Suisse): *Eclogae Geologica Helvetica*, v. 68, p. 131-145.
- Beales, F.W., 1958: Ancient sediments of Bahaman type: *American Association of Petroleum Geologists, Bull.*, v. 42, p. 1845-1880.
- Bein, A. and Weiler, Y., 1976: The Cretaceous Talme Yafe Formation: a contour current shaped sedimentary prism of calcareous detritus at the continental margin of the Arabian Craton: *Sedimentology*, v. 23, p. 511-532.
- Bellamy, J., 1977: Subsurface expansion megapolygons in Upper Jurassic Dolostone (Kimmeridge, UK): *Journal of Sedimentary Petrology*, v. 47, p. 973-978.
- Ben-Yaakov, S., 1973: pH buffering of pore water of recent anoxic marine sediments: *Limnology and Oceanography*, v. 18, p. 86-94.
- Berner, R.A., 1971: *Principles of chemical sedimentology*: McGraw-Hill, New York, 240p.
- Berner, R.A., 1980: *Early diagenesis, a theoretical approach*: Princeton University Press, Princeton, New Jersey, 241p.
- Berner, R.A., Scott, M.R., and Thomlinson, C., 1970: Carbonate alkalinity in the pore waters of anoxic marine sediments: *Limnology and Oceanography*, v. 15, p. 544-549.
- Bernoulli, D., 1972: North Atlantic and Mediterranean Mesozoic facies: a comparison: *Initial Reports of the Deep Sea Drilling Project*, v. 11, p. 801-871.
- Berry, W.B.N. and Wilde, P., 1978: Progressive ventilation of the oceans - an explanation for the distribution of Lower Paleozoic black shales: *American Journal of Science*, v. 278, p. 257-275.
- Bertrand, R., Humbert, L., Achab, A., Calise, G., Chagnon, A., Heroux, Y., Globensky, Y., 1983: Recristallisation des calcaires micritiques en fonction de la maturation thermique dans les Basses-Terres du Saint-Laurent du Québec: *Canadian Journal of Earth Sciences*, v. 20, p. 66-85.

- Bertrand-Sarfati, J. and Moussine-Pouchkine, A., 1983: Platform-to-basin facies evolution: the Late Proterozoic (Vendian) Gourma (West Africa): *Journal of Sedimentary Petrology*, v. 275-293.
- Bhattacharyya, A., 1979: Discussion - On the diagenesis of lime mud: scanning electron microscopic observations of subsurface material from Barbados, W.I.: *Journal of Sedimentary Petrology*, v. 49, p. 1353-1355.
- Bhattacharyya, A. and Friedman, G.M., 1979: Experimental compaction of ooids and lime mud and its implication for lithification during burial: *Journal of Sedimentary Petrology*, v. 49, p. 1279-1286.
- Bjorlykke, K., 1973: Origin of limestone nodules in the Lower Paleozoic of the Oslo Region: *Norsk Geologisk Tidsskrift*, v. 53, p. 419-431.
- Bjorlykke, K., 1974: A reply. Origin of limestone nodules in the Lower Palaeozoic of the Oslo Region: *Norsk Geologisk Tidsskrift*, v. 54, p. 397-399.
- Bjorlykke, K.O. and Griffin, W.L., 1973: Barium feldspars in Ordovician sediments, Oslo region, Norway: *Journal of Sedimentary Petrology*, v. 43, p. 461-465.
- Boles, J.R., 1978: Active ankerite cementation in the subsurface Eocene of southwest Texas: *Contributions to Mineralogy and Petrology*, v. 68, p. 13-22.
- Borradaile, G.J., 1978: Transected folds: a study illustrated with examples from Canada and Scotland: *Geological Society of America, Bull.*, v. 89, p. 481-493.
- Bouma, A.H., 1962: *Sedimentology of some flysch deposits*: Elsevier, New York, 168 p.
- Bouma, A.H., 1973: Contourites in Niesenflysch, Switzerland: *Eclogae Geologica Helvetica*, v. 66, p. 315-323.
- Bouma, A.H. and Hollister, C.D., 1973: Deep ocean basins and sedimentation: In Middleton, G.V. and Bouma, A.H., eds., *Turbidites and deep-water sedimentation*, Society of Economic Paleontologists and Mineralogists Mineralogists, Notes for a Short Course, p. 79-118.
- Braithwaite, C.J.R., 1979: Crystal textures of recent fluvial pisolites and laminated crystalline crusts in Dyfed, South Wales: *Journal of Sedimentary Petrology*, v. 49, p. 181-193.

- Brand, U., 1982: The oxygen and carbon isotope composition of Carboniferous fossil components: sea-water effects: *Sedimentology*, v. 29, p. 139-147.
- Brand, U. and Veizer, J., 1980: Chemical diagenesis of a multicomponent carbonate system - 1: Trace elements: *Journal of Sedimentary Petrology*, v. 50, p. 1219-1236.
- Brand, U. and Veizer, J., 1981: Chemical diagenesis of a multicomponent carbonate system - 2: stable isotopes: *Journal of Sedimentary Petrology*, v. 51, p. 987-997.
- Bromely, R.G., 1978: Hardground diagenesis: In Fairbridge, R.W. and Bourgeois, J., eds., *The encyclopedia of sedimentology*, Dowden, Hutchison and Ross, Stroudsburg, Pennsylvania, p. 397-400.
- Brown, R., 1954: How does cone-in-cone material become emplaced?: *American Journal of Science*, v. 252, p. 372-376.
- Buchner, F., 1981: Rhinegraben: horizontal stylolites indicating stress regimes of earlier stages of rifting: *Tectonophysics*, v. 73, p. 113-118.
- Bursnall and de Wit, M.J., 1975: Timing and development of the orthotectonic zone in the Appalachian orogen of northwest Newfoundland: *Canadian Journal of Earth Sciences*, v. 12, p. 1712-1722.
- Buxton, T.M. and Sibley, D.F., 1981: Pressure solution features in a shallow buried limestone: *Journal of Sedimentary Petrology*, v. 51, p. 19-26.
- Byers, C.W., 1977: Biofacies patterns in euxinic basins: a general model, In Cook, H.E. and Enos, P., eds., *Deep-water carbonate environments*, Society of Economic Paleontologists and Mineralogists, Special Publication no. 25, p. 5-17.
- Callahan, R.K.M., 1974: Stratigraphy, sedimentation, and petrology of the Cambro-Ordovician Cow Head Group at Broom Point and Martin Point, western Newfoundland: Unpublished M.Sc. thesis, University of Massachusetts, Amherst, Massachusetts, 119p.
- Calvert, S.E., 1974: Deposition and diagenesis of silica in marine sediments: In Hsu, K.J. and Jenkyns, H.C., eds., *Pelagic sediments: on land and under the sea*, International Association of Sedimentologists, Special Publication no. 1, p. 273-300.
- Campos, H.S. and Hallam, A., 1979: Diagenesis of English Lower Jurassic limestones as inferred from oxygen and carbon isotope analysis: *Earth and Planetary Science Letters*, v. 45, p. 23-31.

- Carozzi, A.V. and Textoris, D.A., 1967: Paleozoic carbonate microfabrics of the eastern stable interior (U.S.A): E.J. Brill, Leiden, 41p.
- Carter, R.M., 1975: A discussion and classification of subaqueous mass-transport with particular application to grain-flow, slurry-flow, and fluxoturbidites: *Earth-Science Reviews*, v. 11, p. 145-177.
- Cayeux, L., 1935, (translated by Carozzi, A.V., 1970): Carbonate rocks (limestones and dolomites): Hafner Publishing Company, Connecticut, 506p.
- Chafetz, H.S., 1972: Surface diagenesis of limestone: *Journal of Sedimentary Petrology*, v. 42, p. 325-329.
- Chafetz, H.S., 1979: Petrology of carbonate nodules from a Cambrian tidal inlet accumulation, Central Texas: *Journal of Sedimentary Petrology*, v. 49, p. 215-222.
- Chambers, R.L. and Eadie, B.J., 1981: Nepheloid and suspended particulate matter in south-eastern Lake Michigan: *Sedimentology*, v. 28, p. 439-447.
- Chambre syndicale de la recherche et de la production du petrole et du gaz naturel, 1966: *Essaie de nomenclature et caracterization des principales structures sedimentaires*, France, 291p.
- Champ, D.R., Gulens, J., and Jackson, R.E., 1979: Oxidation-reduction sequences in ground water flow systems: *Canadian Journal of Earth Sciences*, v. 16, p. 12-23.
- Chanda, S.K., 1967: Selective neomorphism and fabric discontinuities in limestones: *Journal of Sedimentary Petrology*, v. 37, p. 688-690.
- Choquette, P.W., 1968: Marine diagenesis of shallow marine lime-mud sediments: insights from $\delta^{18}O$ and $\delta^{13}C$ data: *Science*, v. 161, p. 1130-1132.
- Choquette, P.W. and Pray, L.C., 1970: Geologic nomenclature and classification of porosity in sedimentary carbonates: *American Association of Petroleum Geologists, Bulletin*, v.54, p. 207-250.
- Church, T.M., 1970: Marine barite: Unpublished Ph.D. thesis, University of California, San Diego, 133p.
- Church, T.M., 1979: Marine barite: In Burns, G., ed., *Marine minerals*, Mineralogical Society of America, Short Course Notes, v. 6, p. 175-209.

- Clari, P. and Ghuibaudo, G., 1979: Multiple slump scars in the Tortonian type area (Piedmont Basin, northwestern Italy): *Sedimentology*, v. 26, p. 719-730.
- Clark, G.R., II and Lutz, R.A., 1980: Pyritization in the shells of living bivalves: *Geology*, v. 8, p. 268-271.
- Claypool, G.E., 1974: Anoxic diagenesis and bacterial methane production in deep sea sediments: Unpublished Ph.D. thesis, UCLA, 276p.
- Claypool, G.E. and Kaplan, I.R., 1974: The origin and distribution of methane in marine sediments: In Kaplan, I.R., ed., *Natural gases in marine sediments*, Plenum Press, New York, p. 99-139.
- Claypool, G.E. and Threlkeld, C.N., 1980: Anoxic diagenesis and methane generation in sediments of the Blake Outer Ridge, Deep Sea Drilling Project Site 533, Leg 76: *Initial Reports of the Deep Sea Drilling Project*, v. 76, p. 391-402.
- Coleman, M.L. and Raiswell, R., 1981: Carbon, oxygen and sulphur isotope variations in concretions from the Upper Lias of N.E. England: *Geochimica et Cosmochimica Acta*, v. 45, p. 329-340.
- Colman-Sadd, S.P., 1982: Two stage continental collision and plate driving forces: *Tectonophysics*, v. 90, p. 263-282.
- Conaghan, P.J., Mountjoy, E.W., Edgecomb, D.R., Talent, J.A., and Owen, D.E., 1976: Nubrigyn algal reefs (Devonian), eastern Australia: allochthonous blocks and megabreccias: *Geological Society of America, Bull.*, v. 87, p. 515-530.
- Coniglio, M. and Harrison, R.S., 1983: Holocene and Pleistocene caliche from Big Pine Key, Florida: *Bulletin of Canadian Petroleum Geology*, v. 31, p. 3-13.
- Coniglio, M. and James, N.P., 1984: Algal origin of peloids, peloidal intraclasts, and structure grumeleuse in Paleozoic limestones: evidence from Cow Head Group, western Newfoundland: *American Association of Petroleum Geologists, Bull.*, v. 68, p. 464-465 (abstract).
- Cook, H.E., 1979: Ancient continental slope sequences and their value in understanding modern slope development: In Doyle, L.J. and Pilkey, O.H., eds., *Geology of continental slopes*, Society of Economic Paleontologists and Mineralogists, Special Publication no. 27, p. 287-305.

- Cook, H.E., 1983a: Introductory perspectives, basic carbonate principles, and stratigraphic and depositional models, In Cook, H.E., Hine, A.C., and Mullins, H.T., eds., Platform margin and deep water carbonates, Short Course no. 12, Society of Economic Paleontologists and Mineralogists, p. 1-1 - 1-89.
- Cook, H., 1983b: Ancient carbonate platform margins, slopes, and basins: In Cook, H.E., Hine, A.C., and Mullins, H.T., eds., Platform margin and deep water carbonates, Short Course no. 12, Society of Economic Paleontologists and Mineralogists, p. 5-1 - 5-189.
- Cook, H.E. and Egbert, R.M., 1981: Late Cambrian-Early Ordovician continental margin sedimentation, central Nevada: In Taylor, M.E., ed., 2nd International Symposium on the Cambrian system Proceedings, U.S. Geological Survey, Open File Report 81-743, p. 50-56.
- Cook, H.E. and Enos, P., eds., 1977: Deep-water carbonate environments: Society of Economic Paleontologists and Mineralogists, Special Publication no. 25, 336p.
- Cook, H.E. and Mullins, H.T., 1983: Basin margin environment: In Scholle, P.A., Bebout, D.G., and Moore, C.H., eds., Carbonate depositional environments, American Association of Petroleum Geologists, Memoir no. 33, p. 540-617.
- Cook, H.E. and Taylor, M.E., 1977: Comparison of continental and slope and shelf environments in the Upper Cambrian and Lowest Ordovician of Nevada: In Cook, H.E. and Enos, P., eds., Deep-water carbonate environments, Society of Economic Paleontologists and Mineralogists, Special Publication no. 25, p. 51-81.
- Cook, H.E., Field, M.E., and Gardner, J.V., 1982: Characteristics of sediments on modern and ancient continental slopes: In Scholle, P.A. and Spearing, D.R., eds., Sandstone depositional environments, American Association of Petroleum Geologists, Memoir no. 31, p. 329-364.
- Cook, H.E., McDaniel, P.W., Mountjoy, E.W., and Pray, L.C., 1972: Allochthonous carbonate debris flows at Devonian Bank ("reef") margins, Alberta: Bulletin of Canadian Petroleum Geology, v. 20, p. 439-497.
- Crevello, P.D. and Schlager, W., 1980: Carbonate debris sheets and turbidites, Exuma Sound, Bahamas: Journal of Sedimentary Petrology, v. 50, p. 1121-1148.
- Cronan, D.S., 1974: Authigenic minerals in deep-sea sediments: In Goldberg, E.D., ed., The Sea, John Wiley and Sons, New York, p. 491-525.

- Cross, T.A. and Klosterman, M.J., 1981: Primary submarine cements and neomorphic spar in a stromatolitic-bound phylloid algal bioherm, Laborcita Formation (Wolfcampian), Sacramento Mountains, New Mexico, U.S.A.: In Monty, C., ed., Phanerozoic stromatolites, Springer-Verlag, New York, p. 60-73.
- Cumming, L.M., 1973: Geology of Gros Morne National Park, western Newfoundland, Geological Survey of Canada, Regional and Economic Geology Division, open file report, 315p.
- Danielli, H.M.C., 1981: The fossil alga *Girvanella* Nicholson and Etheridge: Bulletin of the British Museum, Natural History, Geology Series, v.35, p. 79-107.
- Davies, G.R., 1977a: Former magnesian calcite and aragonite submarine cements in upper Paleozoic reefs of the Canadian Arctic: a summary: Geology, v. 5, p. 11-15.
- Davies, G.R., 1977b: Turbidites, debris sheets, and truncation structures in Upper Paleozoic deep-water carbonates of the Sverdrup Basin, Arctic archipelago: In Cook, H.E. and Enos, P., eds., Deep-water carbonate environments, Society of Economic Paleontologists and Mineralogists, Special Publication no. 25, p. 221-247.
- Davies, W. and Cave, R., 1976: Folding and cleavage determined during sedimentation: Sedimentary Geology, v. 15, p. 89-133.
- Dean, W.E. and Schreiber, B.C., 1978: Authigenic barite, Leg 41, Deep Sea Drilling Project: Initial Reports of the Deep Sea Drilling Project, v. 41, p. 915-932.
- Dean, W.E., Gardner, J.V., Jansa, L.F., Cepek, P., and Seibold, E., 1977: Cyclic sedimentation along the continental margin of northwest Africa: Initial Reports of the Deep Sea Drilling Project, v. 41, p. 965-990.
- Delgado, D.J., 1979: Submarine diagenesis (aragonite dissolution, cementation by calcite, and dolomitization) in Ordovician Galena Group, Upper Mississippi: American Association of Petroleum Geologists, Bull., v. 64, p. 697 (abstract).
- Demico, R.V., Hardie, L.A., and Haley, J.S., 1982: Algal mounds of Upper Cambrian carbonates of Appalachians, western Maryland: examples of early patch and marginal reefs: American Association of Petroleum Geologists, Bull., v. 66, p. 563 (abstract).
- Dickson, J.A.D., 1978: Length-slow and length-fast calcite: a tale of two elongations: Geology, v. 6, p. 560-561.
- Dickson, J.A.D., 1983: Graphical modelling of crystal aggregates and its relevance to cement diagnosis: Philosophical Transactions of the Royal Society of London, v. A 309, p. 465-502.

- Dickson, J.A.D. and Barber, C., 1976: Petrography, chemistry and origin of early diagenetic concretions in the Lower Carboniferous of the Isle of Man: *Sedimentology*, v. 23, p. 189-211.
- Dickson, J.A.D. and Coleman, M.L., 1980: Changes in carbon and oxygen isotope composition during limestone diagenesis: *Sedimentology*, v. 27, p. 107-118.
- Dixon, J. and Wright, V.P., 1983: Burial diagenesis and crystal diminution. The origin of crystal diminution in some limestones from South Wales: *Sedimentology*, v. 30, p. 537-546.
- Drever, J.I., 1982: *The geochemistry of natural waters*: Prentice-Hall, Englewood Cliffs, New Jersey, 388p.
- Drew, E.A., 1983: Halimeda biomass, growth rates and sediment generation on reefs in the central Great Barrier Reef Province: *Coral Reefs*, v.2, p. 101-110.
- Droxler, A. and Schaer, J.-P., 1979: Deformation cataclastique plastique lors du plissement, sous faible couverture, de strates calcaires: *Eclogae Geologica Helvetica*, v. 72, p. 551-570.
- Droxler, A.W., Schlager, W., and Whallon, C.C., 1983: Quaternary aragonite cycles and oxygen isotope record in Bahamian carbonate ooze: *Geology*, v. 11, p. 235-239.
- Dunham, R.J., 1962: Classification of carbonate rocks according to depositional texture: In: Ham, W.E., ed., *Classification of carbonate rocks*, American Association of Petroleum Geologists, Memoir no. 1, p. 108-121.
- Dunnington, H.V., 1967: Aspects of diagenesis and shape change in stylolitic limestone reservoirs: *World Petroleum Congress Proceedings, Mexico, 1967*, v. 2, p. 339-352.
- Dunoyer de Segonzac, G., 1970: The transformation of clay minerals during diagenesis and low-grade metamorphism: a review: *Sedimentology*, v. 15, p. 281-346.
- Durney, D.W., 1976: Pressure-solution and crystallization deformation: *Philosophical Transactions of the Royal Society of London*, v. 283A, p. 229-240.
- Durney, D.W. and Ramsay, J.G., 1973: Incremental strain measured by syntectonic crystal growths: In De Jong, K.A. and Scholten, R., eds., *Gravity and tectonics*, John Wiley and Sons, New York, p. 67-96.

- Eder, F.W., 1971: Riff-nahe detritische Kalke bei Balve im Rheinischen Schiefergebirge (Mittel-Devon, Garbecker Kalk): *Gottinger Arbeiten zur Geologie und Palaontologie.*, v. 10, 66p.
- Eder, W., 1982: Diagenetic redistribution of carbonate, a process in forming limestone-marl alternations (Devonian and Carboniferous, Rheinisches Schiefergebirge, W. Germany): *In* Einsele, G. and Seilacher, A., eds., *Cyclic and event stratification*, Springer-Verlag, New York, p. 98-112.
- Einsele, G., 1982a: General remarks about the nature, occurrence, and recognition of cyclic sequences (periodites): *In* Einsele, G. and Seilacher, A., eds., *Cyclic and event stratification*, Springer-Verlag, New York, p. 3-7.
- Einsele, G., 1982b: Limestone-marl cycles (periodites): diagnosis, significance, causes - a review: *In* Einsele, G. and Seilacher, A., eds., *Cyclic and event stratification*, Springer-Verlag, New York, p. 8-53.
- Einsele, G. and Kelts, K., 1982: Pliocene and Quaternary mud turbidites in the Gulf of California: sedimentology, mass physical properties and significance: *Initial Reports of the Deep Sea Drilling Project*, v. 64, p. 511-528.
- Einsele, G. and Seilacher, A., eds., 1982: *Cyclic and event stratification*, Springer-Verlag, New York, 536p.
- Eley, B.E. and Jull, R.K., 1983: Chert in the Middle Silurian Fossil Hill Formation of Manitoulin Island, Ontario: *Bulletin of Canadian Petroleum Geology*, v. 30, p. 208-215.
- Embley, R.W., 1982: Anatomy of some Atlantic margin sediment slides and some comments on ages and mechanisms: *In* Saxov, S. and Nieuwenhuis, J.K., eds., *Marine slides and other mass movements*, Nato Conference Series, Series IV, Marine Sciences, v. 6, p. 189-213.
- Embley, R.W. and Jacobi, R.D., 1978: Distribution and morphology of large submarine sediment slides and slumps on Atlantic continental margins: *Marine Geotechnology*, v. 2, p. 205-228.
- Emery, K.O, Tracey, J.I. Jr., and Ladd, H.S., 1954: *Geology of Bikini and nearby atolls: Part 1, Geology*, U.S. Geological Survey, Professional Paper 260-A, 265p.
- Enos, P., 1977: Tamabra Limestone of the Poza Rico Trend, Mexico, *In* Cook, H.E. and Enos, P., eds., *Deep-water carbonate environments*, Society of Economic Paleontologists and Mineralogists, Special Publication no. 25, p. 273-314.

- Enos, P. and Moore, C.H., 1983: Fore-reef slope environment: In Scholle, P.A., Bebout, D.G., and Moore, C.H., eds., Carbonate depositional environments, American Association of Petroleum Geologists, Memoir no. 33, p. 508-537.
- Evamy, B.D., 1969: The precipitational environment and correlation of some calcite cements deduced from artificial staining: Journal of Sedimentary Petrology, v. 37, p. 1204-1215.
- Evans, I. and Kendall, C.G.St.C., 1977: An interpretation of the depositional setting of some deep-water Jurassic carbonates of the central High Atlas Mountains, Morocco: Society of Economic Paleontologists and Mineralogists, Special Publication no. 25, p. 249-261.
- Ewing, M. and Thorndike, E., 1965: Suspended matter in deep-ocean water: Science, v. 147, p. 1291-1294.
- Fahraeus, L.E., 1970: Conodont-based correlations of Lower and Middle Ordovician strata in western Newfoundland: Geological Society of America, Bull., v. 81, p. 2061-2076.
- Fahraeus, L.E. and Nowlan, G.S., 1978: Franconian (Late Precambrian) to Early Champlainian (Middle Ordovician) conodonts from the Cow Head Group, western Newfoundland: Journal of Paleontology, v. 52, p. 444-471.
- Fahraeus, L.E., Slatt, R.M., and Nowlan, G.S., 1974: Origin of carbonate pseudopellets: Journal of Sedimentary Petrology, v. 44, p. 27-29.
- Fairbridge, R.W., 1946: Submarine slumping and location of oil bodies: American Association of Petroleum Geologists, Bull., v. 30, p. 84-92.
- Fairbridge, R.W. and Bourgeois, J., 1978: The encyclopedia of sedimentology: Dowden, Hutchison, and Ross, Stroudsburg, Pennsylvania, 901p.
- Fairchild, I.J., 1980: Stages in a Precambrian dolomitization: cementing versus replacement textures: Sedimentology, 27, p. 631-650.
- Fairchild, I.J., 1983: Chemical controls of cathodoluminescence of natural dolomites and calcites: new data and review: Sedimentology, v. 30, p. 579-583.
- Faupl, P. and Beran, A., 1983: Diagenetic alterations of radiolaria and sponge spicule-bearing rocks of the Strubberg Formation (Jurassic, Northern Calcareous Alps, Austria): Neues Jahrbuch für Geologie und Paläontologie, Monatsheft, v. 1983, p. 129-140.

- Fily, G. and Rioult, M., 1981: Discussion of - Development of relief on a Middle Jurassic cemented sea floor: origin of submarine pseudo-anticlines in the Bathonian of Normandy: *Sedimentology*, v. 28, p. 133-136.
- Fischer, A.G., 1980: Gilbert - bedding rhythms and geochronology: Geological Society of America, Special Paper 183, p. 93-104.
- Fischer, A.G. and Arthur, M.A., 1977: Secular variation in the pelagic realm: In Cook, H.E. and Enos, P., eds., *Deep-water carbonate environments*, Society of Economic Paleontologists and Mineralogists, Special Publication no. 25, p. 19-50.
- Fischer, A.G. and Garrison, R.E., 1967: Carbonate lithification on the sea floor, *Journal of Geology*, v.75, p. 488-496.
- Fischer, A.G., Honjo, S., and Garrison, R.E., 1967: *Electron micrographs of limestones and their nannofossils*: Princeton University Press, Princeton, New Jersey, 141p.
- Fisher, D.W., 1979: Folding in the foreland, Middle Ordovician Dolgeville facies, Mohawk Valley: *New York, Geology*, v. 7, p. 455-459.
- Flügel, E., 1982: *Microfacies analysis of limestones*: Springer-Verlag, New York, 633 p.
- Folk, R.L., 1959: Practical petrographic classification of limestones: *American Association of Petroleum Geologists, Bulletin*, v. 43, p. 1-38.
- Folk, R.L., 1962, Spectral subdivision of limestone types: In Ham, W.E., ed., *Classification of carbonate rocks*, American Association of Petroleum Geologists, Memoir no. 1, p. 62-84.
- Folk, R.L., 1965: Some aspects of recrystallization in ancient limestones: In Pray, L.C. and Murray, R.C., eds., *Dolomitization and limestone diagenesis: a symposium*, Society of Economic Paleontologists and Mineralogists, Special Publication no. 13, p. 14-48.
- Folk, R.L., 1971: Unusual neomorphism of micrite: In Bricker, O.P., ed., *Carbonate cements*, The Johns Hopkins Press, Baltimore, Maryland, p. 163-166.
- Folk, R.L., 1974a: The natural history of crystalline calcium carbonate: effect of magnesium content and salinity: *Journal of Sedimentary Petrology*, v. 44, p. 40-53.
- Folk, R.L., 1974b: *Petrology of sedimentary rocks*: Hemphill Publishing Company, Austin, Texas, 182p.

- Folk, R.L. and Assereto, R., 1976: Comparative fabrics of length-slow and length-fast calcite and calcitized aragonite in a Holocene speleothem, Carlsbad Caverns, New Mexico: *Journal of Sedimentary Petrology*, v. 46, p. 486-496.
- Folk, R.L. and Pittman, J.S., 1971: Length-slow chalcedony; a new testament for vanished evaporites: *Journal of Sedimentary Petrology*, v. 41, p. 1045-1058.
- Folk, R.L. and Robles, R., 1964: Carbonate sands of Isla Perez, Alacran reef complex, Yucatan: *Journal of Geology*, v. 72, p. 255-292.
- Fong, C. and Hesse, R., 1982: Relationship between spherulitic calcite-quartz intergrowth and cone-in-cone structure in carbonate nodules: Eleventh International Congress on Sedimentology, Hamilton, Ontario, p. 183 (abstract).
- Fortey, R.A. and Skevington, D., 1980: Correlation of Cambrian-Ordovician boundary between Europe and North America: *Canadian Journal of Earth Sciences*, v. 17, p. 382-388.
- Frank, J.R., Carpenter, A.B., and Oglesby, T.W., 1982: Cathodoluminescence and composition of calcite cement in the Taum Sauk Limestone (Upper Cambrian), southeast Missouri: *Journal of Sedimentary Petrology*, v. 52, p. 631-638.
- Franks, P.C., 1969: Nature, origin, and significance of cone-in-cone structures in the Kiowa Formation (Early Cretaceous), north-central Kansas: *Journal of Sedimentary Petrology*, v. 39, p. 1438-1454.
- Freeman, T., Rothbard, D., and Obrador, A., 1983: Terrigenous dolomite in the Miocene of Menorca (Spain): provenance and diagenesis: *Journal of Sedimentary Petrology*, v. 53, p. 543-548.
- Friedman, I. and Murata, K.J., 1979: Origin of dolomite in Miocene Monterey Shale and related formations in the Tremblor Range, California: *Geochimica et Cosmochimica Acta*, v. 43, p. 1357-1365.
- Froelich, P.N., Klinkhammer, G.P., Bender, M.L., et al., 1979: Early oxidation of organic matter in pelagic sediments of the eastern equatorial Atlantic: suboxic diagenesis: *Geochimica et Cosmochimica Acta*, v. 43, p. 1075-1090.
- Früth, I. and Sherreiks, R., 1982: Hauptdolomit (Norian) - stratigraphy, paleogeography and diagenesis: *Sedimentary Geology*, v. 32, p. 195-231.

- Fuchtbauer, H., 1971: Cone-in-cone, a low nucleation cement in marls: *In* Bricker, O.P., ed., Carbonate cements, The Johns Hopkins Press, Baltimore, Maryland, p. 193-195.
- Fuchtbauer, H., 1974: Sediments and sedimentary rocks - Sedimentary petrology. Part 1: John Wiley and Sons, New York, 464p.
- Fuchtbauer, H. and Hardie, L.A., 1976: Experimentally determined homogeneous distribution coefficients for precipitated magnesian calcites: Abstracts and Program Annual Meeting of the Geological Society of America, v. 8, p. 877 (abstract).
- Fürsich, F.T. and Palmer, T.J., 1979: Development of relief on a Middle Jurassic cemented sea floor: origin of submarine pseudo-anticlines in the Bathonian of Normandy: *Sedimentology*, v. 26, p. 441-452.
- Fuzesy, L.M., 1980: Origin of nodular limestones, calcium sulphates and dolomites in the Lower Magnesian Limestone in the neighbourhood of Selby, Yorkshire, England: *In* Fuchtbauer, H. and Peryt, T., eds., The Zechstein Basin with emphasis on carbonate sequences, *Contributions to Sedimentology*, v. 9, p. 35-44.
- Galimov, E.M., Girin, Yu.P., and Vernadskiy, V.I., 1968: Variation in the isotopic composition of carbon during the formation of carbonate concretions, *Geochemistry International*, v. 5, p. 178-182.
- Gardner, J.V., Dean, W.E., and Jansa, L., 1977: Sediments recovered from the northwest African continental margin, Leg 41, Deep Sea Drilling Project: Initial Reports of the Deep Sea Drilling Project, v. 41, p. 1121-1134.
- Garrison, R.E., 1972: Inter- and intrapillow limestones of the Olympic Peninsula, Washington: *Journal of Geology*, v. 80, p. 310-322.
- Garrison, R.E., 1981: Diagenesis of oceanic carbonate sediments: A review of the DSDP perspective: *In* Warne, J.E., Douglas, R.G., and Winterer, E.L., eds., *The Deep Sea Drilling Project: A decade of progress*, Society of Economic Paleontologists and Mineralogists, Special Publication no. 32, 181-207.
- Garrison, R.E. and Fischer, A.G., 1969: Deep-water limestones and radiolarites of the Alpine Jurassic: *In* Friedman, G.M., ed., *Depositional environments in carbonate rocks*, Society of Economic Paleontologists and Mineralogists, Special Publication no. 14, 29-55.
- Garrison, R.E. and Kennedy, W.J., 1977: Origin of solution seams and flaser structure in upper Cretaceous chalks of southern England: *Sedimentary Geology*, v. 19, p. 107-137.

- Garrison, R.E., Douglas, R.G., Pisciotto, K.E., Isaacs, C.M., and Ingle, J.C., eds., 1981: The Monterey Formation and related siliceous rocks of California: Pacific Section, Society of Economic Paleontologists and Mineralogists, Special Publication, 327p.
- Geeslin, J.H. and Chafetz, H.S., 1982: Ordovician Aleman ribbon cherts: an example of silicification prior to carbonate lithification: *Journal of Sedimentary Petrology*, v. 52, p. 1283-1293.
- Geiser, P.A., 1974: Cleavage in some sedimentary rocks of the central Valley and Ridge Province, Maryland: *Geological Society of America, Bull.*, v. 85, p. 1399-1412.
- Geiser, P.A., 1975: Slaty cleavage and the dewatering hypothesis - an examination of some critical evidence: *Geology*, v. 3, p. 717-720.
- Geiser, P.A. and Sansone, S., 1981: Joints, microfractures, and the formation of solution cleavage in limestone: *Geology*, v. 9, p. 280-285.
- Gieskes, J.M., 1974: Marine Chemistry: In Goldberg, E.D., ed., *The Sea*, v. 5, John Wiley and Sons, New York, p. 123-151.
- Gieskes, J.M., 1981: Deep-Sea Drilling interstitial water studies: implications for chemical alteration of the oceanic crust, layers I and II: In Warme, J.E., Douglas, R.G., and Winterer, E.L., eds., *The Deep Sea Drilling Project: A decade of progress*, Society of Economic Paleontologists and Mineralogists, Special Publication no. 32, 149-167.
- Gilman, R.A. and Metzger, W.J., 1967: Cone-in-cone concretions from western New York: *Journal of Sedimentary Petrology*, v. 37, p. 87-95.
- Ginsburg, R.N. and James, N.P., 1976: Submarine botryoidal aragonite in Holocene reef limestones, Belize: *Geology*, v. 4, p. 431-436.
- Girin, Yu.P., 1970: Geochemical stages during diagenesis of Middle Jurassic sediments of the High Caucasus: *Geochemistry International*, v. 4., p. 1146-1158.
- Grigor'ev, D.P., 1965: *Ontogeny of Minerals: Israel Program for Scientific Translations, Jerusalem, 250p.*

- Grover, G., Jr., and Read, J.F., 1983: Paleoquifer and deep burial related cements defined by regional cathodoluminescent patterns, Middle Ordovician carbonates, Virginia: American Association of Petroleum Geologists, Bull., v. 67, p. 1275-1303.
- Hallam, A., 1960: A sedimentary and faunal study of the Blue Lias of Dorset and Glamorgan: Philosophical Transactions of the Royal Society of London, Series B, v. 243, p. 1-44.
- Hallam, A., 1964: Origin of the limestone-shale rhythm in the Blue Lias of England: a composite theory: Journal of Geology, v. 72, p. 157-169.
- Harrison, R.S., 1977: Caliche profiles: indicators of near-surface subaerial diagenesis, Barbados, West Indies: Bulletin of Canadian Petroleum Geology, v. 25, p. 123-173.
- Harrison, W.E., Hesse, R., and Gieskes, J.M., 1982: Relationship between sedimentary facies and interstitial water chemistry of slope, trench, and Cocos plate sites from the Middle America trench transect, active margin off Guatemala, Deep Sea Drilling Project Leg 67: Initial Reports of the Deep Sea Drilling Project, v. 67, p. 603-614.
- Hartman, P., 1982: Crystal faces: structure and growth: Geologie en Mijnbouw, v. 61, p. 313-320.
- Hawkins, T.R.W. and Jones, F.G., 1981: Folds and cleavage development within Cambrian metasediments of the Vale of Ffestiniog, North Wales: Geological Journal, v. 16, p. 65-84.
- Haywick, D.W. and James, N.P., 1984: Dolomites and dolomitization of the Lower Ordovician St. George Group of western Newfoundland: Current Research, Part A, Geological Survey of Canada, Paper 84-1A, p. 531-536.
- Hecker, B., 1982: Possible benthic fauna and slope instability relationships: In Saxov, S. and Nieuwenhuis, J.K., eds., Marine slides and other mass movements, Nato Conference Series, Series IV, Marine Sciences, v. 6, p. 335-347.
- Heezen, B.C. and Ewing, M., 1952: Turbidity currents and submarine slumps, and the 1929 Grand Banks earthquake: American Journal of Science, v. 250, p. 849-873.
- Heezen, B.C. and Hollister, C.D., 1964: Deep-sea current evidence from abyssal sediments: Marine Geology, v. 1, p. 141-174.
- Hein, J.R. and Karl, S.M., 1983: Comparisons between open-ocean and continental margin chert sequences: In Iijima, A., Hein, J.R., and Siever, R., eds., Siliceous deposits of the Pacific Region, Elsevier Scientific Publishing Company, Amsterdam, p. 25-44.

- Hein, J.R., O'Neil, J.R., and Jones, M.J., 1979: Origin of authigenic carbonates in sediment from the deep Bering Sea: *Sedimentology*, v. 26, p. 681-705.
- Hein, J.R., Scholl, D.W., Barron, J.A., Jones, M.G., and Miller, J., 1978: Diagenesis of late Cenozoic diatomaceous deposits and formation of the bottom simulating reflector in the southern Bering Sea: *Sedimentology*, v. 25, p. 155-181.
- Helwig, J., 1970: Slump folds and early structures, northeastern Newfoundland Appalachians: *Journal of Geology*, v. 78, p. 172-187.
- Hemleben, C.F.D. and Reuther, C.D., 1980: Allodapic limestones of the Barcaliente Formation (Namurian A) between Luna and Cea Rivers (Southern Cantabrian Mountains, Spain): *Neues Jahrbuch für Geologie und Paläontologie, Abhandlungen*, v. 159, p. 225-255.
- Hendricks, T.A., 1937: Some unusual specimens of cone-in-cone in manganese siderite: *American Journal of Science*, series 5, v. 33, p. 458-461.
- Henkel, D.J., 1970: The rôle of waves in causing submarine landslides: *Geotechnique*, v. 20, p. 75-80.
- Henningsmoen, G., 1974: A comment. Origin of limestone nodules in the Lower Paleozoic of the Oslo Region: *Norsk Geologisk Tidsskrift*, v. 54, 401-412.
- Herzer, R.H., 1979: Submarine slides and submarine canyons on the continental slope off Canterbury, New Zealand: *New Zealand Journal of Geology and Geophysics*, v. 22, p. 391-406.
- Hesse, R., 1975: Turbiditic and non-turbiditic mudstone of Cretaceous flysch sections of the East Alps and other basins: *Sedimentology*, v. 22, p. 387-416.
- Hildreth, S.P., 1836: Observations on the bituminous coal deposits of the valley of the Ohio, and the accompanying rock strata; with notices of the fossil organic remains and the relics of vegetable and animal bodies, illustrated by a geological map, by numerous drawings of plants and shells, and by views of interesting scenery: *American Journal of Science*, v. 29, p. 1-154.
- Hill, P.R., Aksu, A.E., and Piper, D.J.W., 1982: The deposition of thin bedded subaqueous debris flow deposits: In Saxov, S. and Nieuwenhuis, J.K., eds., *Marine slides and other mass movements*, Nato Conference Series, Series IV, Marine Sciences, p. 273-287.

- Hiscott, R.N., 1977: Sedimentology and regional implications of deep-water sandstones of the Tourelle Formation, Ordovician, Quebec: Unpublished Ph.D. thesis, McMaster University, Hamilton, Ontario, 542p.
- Hiscott, R.N., 1982: Labrador Sea clay mineralogy: First Report, 12p.
- Hiscott, R.N. and James, N.P., in press: Carbonate debris flows, Cow Head Group, western Newfoundland: Journal of Sedimentary Petrology.
- Hiscott, R.N. and Middleton, G.V., 1979: Depositional mechanics of thick-bedded sandstones at the base of a submarine slope, Tourelle Formation (Lower Ordovician) Quebec: In Doyle, L.J. and Pilkey, O.H., eds., Geology of continental slopes, Society of Economic Paleontologists and Mineralogists, Special Publication no. 27, p. 307-326.
- Hiscott, R.N. and Middleton, G.V., 1980: Fabric of coarse deep-water sandstones, Tourelle Formation, Quebec: Journal of Sedimentary Petrology, v. 50, p. 703-722.
- Hobbs, B.E., Means, W.D., and Williams, P.F., 1976: An outline of structural geology: John Wiley and Sons, Toronto, 571p.
- Hodgson, W.A., 1966: Carbon and oxygen isotope ratios in diagenetic carbonates from marine sediments: Geochimica et Cosmochimica Acta, v. 33, p. 1223-1233.
- Hoefs, J., 1970: Kohlenstoff- und Sauerstoff-Isotopenuntersuchungen an Karbonatkonkretionen und umgebenden Gestein: Contributions to Mineralogy and Petrology, v. 27, p. 66-79.
- Hoffert, M., 1980: Les "argiles rouges des grands fonds" dans le Pacifique centre-est, authigenese, transport, diagenese: Sciences Geologiques, Memoire no. 61, 231p.
- Hollister, C.D. and Heezen, B.C., 1972: Geologic effects of ocean bottom currents: western North Atlantic: In Gordon, A.L., ed., Studies in physical oceanography, 2, Gordon and Breach, New York, p. 37-66.
- Holmann, R., 1962: Uber subsolution und die 'Knollenkalke' des Calcare Ammonitico Rosso Superiore im Monte Baldo (Malm), Norditalien: Neues Jahrbuch fur Geologie und Palaontologie, Monatsheft, v. 1962, p. 163-179.
- Holmann, R., 1964: Subsolutionsfragmente (zur biostratonomie der ammonoida im Malm des Monte Baldo/Norditalien): Neues Jahrbuch fur Geologie und Palaontologie, Monatsheft, v. 1964, p. 22-82.

- Hopkins, J.C., 1972: Petrography, distribution and diagenesis of foreslope, nearslope and basin sediments, Miette and Ancient Wall carbonate complexes (Devonian), Alberta: Unpublished Ph.D. thesis, McGill University, Montreal, 234p.
- Hopkins, J.C., 1977: Production of foreslope breccias by differential submarine cementation and downslope displacement of carbonate sands, Miette and Ancient Wall buildups, Devonian, Canada: In Cook, H.E. and Enos, P., eds., Deep-water carbonate environments, Society of Economic Paleontologists and Mineralogists, Special Publication no. 25, p. 155-170.
- Hower, J., 1981: X-ray diffraction identification of mixed-layer clay minerals: In Longstaffe, F.J., ed., Clays and the resource geologist, Mineralogical Association of Canada, Short Course Handbook, p. 39-59.
- Hubert, J.F., 1966: Modification of the model for internal structures in graded beds to include a dune division: *Nature*, v. 211, p. 614.
- Hubert, J.F., Suchecki, R.K., and Callahan, R.K.M., 1977: The Cow Head Breccia: sedimentology of the Cambro-Ordovician continental margin, Newfoundland: In Cook, H.E. and Enos, P., eds., Deep-water carbonate environments, Society of Economic Paleontologists and Mineralogists, Special Publication no. 25, p. 125-154.
- Hudson, J.D., 1977: Stable isotopes and limestone lithification: *Journal Geological Society of London*, v. 133, p. 637-660.
- Hudson, J.D., 1978: Concretions, isotopes and diagenetic history of the Oxford Clay (Jurassic) of Central England: *Sedimentology*, v. 25, p. 339-370.
- Hudson, J.D., 1982: Pyrite in ammonite-bearing shales from the Jurassic of England and Germany: *Sedimentology*, v. 29, p. 639-667.
- Hudson, J.D. and Coleman, M.L., 1978: Submarine cementation of the Scheck Limestone conglomerate (Jurassic, Austria): isotopic evidence: *Neues Jahrbuch fur Geologie und Palaontologie, Monatsheft*, v. 1978, p. 534-544.
- Hudson, J.D. and Friedman, I., 1974: Carbon and oxygen isotopes in concretions: relationship to pore-water changes during diagenesis: In Cadek, J. and Paces, T., eds., Proceedings International Symposium Water-Rock Interaction, Geological Survey, Prague, p. 332-339.
- Hudson, J.D. and Jenkyns, H.C., 1969: Conglomerates in the Adnet Limestones of Adnet (Austria) and the origin of the "Scheck": *Neues Jahrbuch fur Geologie und Palaontologie, Monatsheft*, v. 1969, p. 552-558.

- Hudson, J.H., 1983: Growth rate and carbonate production in *Halimeda opuntia*, Marquesas Keys, Florida: Third International Symposium on Fossil Algae, Program and Abstracts, p. 14 (abstract).
- Hurd, D.C., 1972: Factors affecting solution rate of biogenic opal in seawater: *Earth and Planetary Science Letters*, v. 15, p. 411-417.
- Hurst, J.M., 1981: Platform edge and slope relationships Silurian of Washington Land, north Greenland and comparison to Arctic Canada: *Bulletin of Canadian Petroleum Geology*, v. 29, p. 408-419.
- Hurst, J.M. and Surlyk, F., 1983: Depositional environments along a carbonate ramp to slope transition in the Silurian of Washington Land, north Greenland, *Canadian Journal of Earth Sciences*, v. 20, p. 473-499.
- Imoto, A., 1983: Sedimentary structures of Permian-Triassic cherts in the Tamba District, southwest Japan: In Iijima, A., Hein, J.R., and Siever, R., eds., *Siliceous deposits of the Pacific Region*, Elsevier Scientific Publishing Company, Amsterdam, p. 377-394.
- Irwin, H., 1980: Early diagenetic carbonate precipitation and pore fluid migration in the Kimmeridge Clay of Dorset, England: *Sedimentology*, v. 27, p. 577-591.
- Irwin, H., Curtis, C., and Coleman, M., 1977: Isotopic evidence for source of diagenetic carbonates formed during burial of organic-rich sediments: *Nature*, v. 269, p. 209-213.
- Islam, S., 1981: Thermal maturation patterns in Cambro-Ordovician flysch of the Taconic Belt, Gaspé Peninsula: Unpublished Ph.D. thesis, McGill University, Montreal, 191p.
- James, N.P., 1972: Holocene and Pleistocene calcareous crust (caliche) profiles: criteria for subaerial exposure: *Journal of Sedimentary Petrology*, v. 42, p. 817-836.
- James, N.P., 1981: Megablocks of calcified algae in the Cow Head Breccia, western Newfoundland: vestiges of a Cambro-Ordovician platform margin: *Geological Society of America, Bull.*, v. 92, p. 799-811.
- James, N.P. and Choquette, P.W., 1983: Limestones - the sea floor diagenetic environment: *Geoscience Canada*, v. 10, p. 162-179.
- James, N.P. and Choquette, P.W., in press: Limestones - the meteoric diagenetic environment: *Geoscience Canada*.

- James N.P. and Ginsburg, R.N., 1979: The seaward margin of the Belize barrier and atoll reefs: International Association of Sedimentologists, Special Publication no. 3, 191p.
- James, N.P. and Klappa, C.F., 1983: Petrogenesis of Early Cambrian reef limestones, Labrador, Canada: Journal of Sedimentary Petrology, v. 53, p. 1051-1096.
- James, N.P. and Stevens, R.K., 1982: Anatomy and evolution of a lower Paleozoic continental margin, western Newfoundland: Excursion 2B, International Association of Sedimentologists, Field Excursion Guide Book, 75p.
- James, N.P. and Stevens, R.K., in prep.: Stratigraphy and correlation of the Cow Head Group, western Newfoundland: Geological Survey of Canada, Paper.
- James, N.P., Ginsburg, R.N., Marszalek, D.S., and Choquette, P.W., 1976: Facies and facies specificity of early subsea cements in the shallow Belize (British Honduras) reefs: Journal of Sedimentary Petrology, v. 46, p. 523-544.
- James, N.P., Klappa, C.F., Skevington, D., and Stevens, R.K., 1980: Cambro-Ordovician of west Newfoundland - sediments and faunas: Geological Association of Canada Mineralogical Association of Canada Annual Meeting, Field Trip Guidebook, 88p.
- James, N.P., Knight, I., Levesque, R.J., and Stevens, R.K., in prep.: Cambro-Ordovician: a revised stratigraphy of western Newfoundland.
- James, N.P., Stevens, R.K., and Fortey, R.A., 1979: Correlation and timing of platform margin megabreccia deposition, Cow Head and related Groups, western Newfoundland: American Association of Petroleum Geologists, Bull., v. 63, p. 474 (abstract).
- Jansa, L.F., 1974: Trace fossils from the Cambro-Ordovician Cow Head Group, Newfoundland and their paleobathymetric implications: Palaeogeography, Palaeoclimatology, Palaeoecology, v. 15, p. 233-244.
- Jenkyns, H.C., 1974: Origin of red nodular limestones (Ammonitico Rosso, Knollenkalke) in the Mediterranean Jurassic: a diagenetic model: In Hsu, K.J. and Jenkyns, H.C., P., Pelagic sediments: on land and under the sea, International Association of Sedimentologists, Special Publication no. 1, p. 249-271.
- Jenkyns, H.C., 1980: Cretaceous anoxic events: from continents to oceans: Journal of the Geological Society of London, v. 137, p. 171-188.

- Johnson, A.M., 1977: Styles of folding - mechanics of folding of natural elastic materials: Developments in Geotectonics II, Elsevier, Amsterdam, 406p.
- Johnson, H., 1941: Paleozoic lowlands of northwestern Newfoundland, Transactions of the New York Academy of Science, series 2, v. 6, p. 141-145.
- Jones, B., Oldershaw, and Narbonne, G.M., 1979: Nature and origin of rubbly limestone in the Upper Silurian Read Bay Formation of Arctic Canada: Sedimentary Geology, v. 24, p. 227-252.
- Jones, R.M.P., 1980: Basinal isostatic adjustment faults and their petroleum significance: Bulletin of Canadian Petroleum Geology, v. 28, p. 211-251.
- Jopling, A.V. and Walker, R.G., 1968: Morphology and origin of ripple-drift cross-lamination, with examples from the Pleistocene of Massachusetts: Journal of Sedimentary Petrology, v. 38, p. 971-984.
- Jorgensen, N.O., 1983: Dolomitization in chalk from the North Sea Central Graben: Journal of Sedimentary Petrology, v. 53, p. 557-564. Kamb, W.B., 1959: Theory of preferred crystal orientation developed by crystallization under stress: Journal of Geology, v. 67, p. 153-170.
- Kastner, M., 1979: Silica polymorphs: In Burns, R.G., ed., Marine minerals, Mineralogical Society of America, v. 6, p. 99-109.
- Kastner, M., 1984: Origin of dolomite and its spatial and chronological distribution - a new insight: Reservoir (Canadian Society of Petroleum Geologists), v. 11, p. 1-3.
- Kastner, M. and Gieskes, J.M., 1983: Opal-A to Opal-CT transformation: a kinetic study; In Iijima, A., Hein, J.R., and Siever, R., eds., Siliceous deposits of the Pacific Region, Elsevier Scientific Publishing Company, Amsterdam, p. 211-228.
- Keith, B.D. and Friedman, G.M., 1977: A slope-fan-basin-plain model, Taconic sequence, New York and Vermont: Journal of Sedimentary Petrology, v. 77, p. 1220-1241.
- Keith, M.L. and Weber, J.N., 1964: Carbon and oxygen isotopic composition of selected limestones and fossils: Geochimica et Cosmochimica Acta, v. 28, p. 1787-1816.
- Kelts, K., 1976: Marcasite in Miocene calcareous sediments from Hole 315A: Initial Reports of the Deep Sea Drilling Project, v. 33, p. 867-870.

- Kelts, K. and Arthur, M.A., 1981: Turbidites after ten years of deep-sea drilling - wringing out the mop?: In Warne, J.E., Douglas, R.G. and Winterer, E.L., eds., Society of Economic Paleontologists and Mineralogists, Special Publication no.32, p.91-127.
- Kelts, K. and McKenzie, J.A., 1982: Diagenetic dolomite formation in Quaternary anoxic diatomaceous muds of Deep Sea Drilling Project Leg 64, Gulf of California: Initial Reports of the Deep Sea Drilling Project, v. 64, Part 2, p. 553-569.
- Kendall, A.C., in press: Radial fibrous calcite, a reappraisal: In Schneidermann, N. and Harris, P.M., eds., Carbonate Cements, Society of Economic Paleontologists and Mineralogists, Special Publication no. 37.
- Kendall, A.C., 1977: Fascicular-optic calcite: a replacement of bundled acicular carbonate cements: Journal of Sedimentary Petrology, v. 47, p. 1056-1062.
- Kendall, A.C. and Broughton, P.L., 1977: Discussion: calcite and aragonite fabrics, Carlsbad Caverns: Journal of Sedimentary Petrology, v. 47, p. 1397-1400.
- Kendall, A.C. and Broughton, P.L., 1978: Origin of fabrics in speleothems composed of columnar calcite crystals: Journal of Sedimentary Petrology, v. 48, p. 519-538.
- Kendall, A.C. and Simpson, F., 1974: Calcite layers in the uppermost Medicine Hat Sandstone (Upper Cretaceous) of southwestern Saskatchewan: Bulletin of Canadian Petroleum Geology, v. 22, p. 34-41.
- Kendall, A.C. and Tucker, M.E., 1971: Radial fibrous calcite as a replacement after syn-sedimentary cement: Nature Physical Science, v. 232, p. 62-63.
- Kendall, A.C. and Tucker, M.E., 1973: Radial fibrous cement: a replacement after acicular carbonate: Sedimentology, v. 20, p. 365-389.
- Kennedy, D.P.S., 1982: Geology of the Corner Brook Lake Area, western Newfoundland: Unpublished M.Sc. thesis, Memorial University, St. John's, Newfoundland, 370p.
- Kennedy, W.J. and Garrison, R.E., 1975: Morphology and genesis of nodular chalks and hardgrounds in the Upper Cretaceous of southern England: Sedimentology, v. 22, p. 311-386.
- Kerans, C. and Playford, P.E., 1984: Scheck breccias from Devonian reef complexes of Canning Basin, western Australia: American Association of Petroleum Geologists, Bull., v. 68, p. 495 (abstract).

- Kindle, C.H., 1982: The C.H. Kindle collection: Middle Cambrian to Lower Ordovician trilobites from the Cow Head Group, western Newfoundland: In Current Research, Part C, Geological Survey of Canada, Paper 82-1C, p. 1-17.
- Kindle, C.H. and Whittington, H.B., 1958: Stratigraphy of the Cow Head region, western Newfoundland: Geological Society of America, Bull., v. 69, p. 315-342.
- Kepper, J.C., 1981: Sedimentology of a Middle Cambrian outer shelf margin with evidence for syndepositional faulting, eastern California and western Nevada: Journal of Sedimentary Petrology, v. 51, p. 807-821.
- Klappa, C.F., 1979: Comment on - Displacive calcite: evidence from recent and ancient calcretes: Geology, v. 7, p. 420-421.
- Klappa, C.F., Opalinski, P.R., and James, N.P., 1980: Middle Ordovician Table Head Group of western Newfoundland: a revised stratigraphy: Canadian Journal of Earth Sciences, v. 17, p. 1007-1019.
- Kobluk, D.R and Risk, M.J., 1977: Micritization and carbonate-grain binding by endolithic algae: American Association of Petroleum Geologists, Bull. , v. 61, p. 1069-1082.
- Koning, H.L., 1982: On an explanation of marine flow slides in sand: In Saxov, S. and Nieuwenhuis, J.K., eds., Marine slides and other mass movements, Nato Conference Series, Series IV, Marine Sciences, v.6 , p. 83-94.
- Korde, K.B., 1973: Cambrian algae: U.S.S.R. Academy of Sciences, Paleontological Institute Trudy, v. 139, 349p.
- Krause, F.F. and Oldershaw, A.E., 1979: Submarine carbonate breccia beds - a depositional model for two-layer, sediment gravity-flows from the Sekwi Formation, (Lower Cambrian), Mackenzie Mountains, Northwest Territories, Canada: Canadian Journal of Earth Sciences, v. 16, p. 189-199.
- Krauskopf, K.B., 1979: Introduction to geochemistry: McGraw-Hill, New York, 617p.
- Kubler, B., 1973: La corrensite, indicateur possible de milieux de sedimentation et du degre de transformation d'un sediment: Bulletin Centre Recherche, Pau-SNPA, v. 7, p. 543-556.
- Kuenen, P.H., 1964: Deep-sea sands and ancient turbidites: In Bouma, A.H. and Brouwer, A., eds., Turbidites, Elsevier, Amsterdam, p. 3-33.

- Kulm, L.D., Schrader, H., Resig, J.M. et al., 1981: Late Cenozoic carbonates on the Peru continental margin: lithostratigraphy, biostratigraphy, and tectonic history: Geological Society of America, Memoir no. 154, p. 469-503.
- Lahanh, R.W., 1978: A chemical model for calcite crystal growth and morphology control: Journal of Sedimentary Petrology, v. 48, p. 337-344.
- Lancelot, Y., 1973: Chert and silica diagenesis in sediments from the central Pacific: Initial Reports of the Deep Sea Drilling Project, v. 17, p. 377-405.
- Land, L.S., 1979: The fate of reef-derived sediment on the North Jamaican island slope: Marine Geology, v. 29, p. 55-71.
- Land, L.S., 1980: The isotopic and trace element geochemistry of dolomite; state of the art: In Zenger, D.H., Dunham, J.B., and Ethington, R.L., eds., Concepts and models of dolomitization, Society of Economic Paleontologists and Mineralogists, Special Publication no. 28, p. 87-110.
- Land, L.S. and Moore, C.H., 1977: Deep foreereef and upper island slope, north Jamaica: Studies in Geology no. 4, p. 53-65.
- Land, L.S. and Moore, C.H., 1980: Lithification, micritization, and sydepositional diagenesis of biolithites on the Jamaican island slope: Journal of Sedimentary Petrology, v. 50, p. 357-370.
- Lang, W.D., Spath, L.F., and Richardson, W.A., 1923: Shales with "beef" a sequence in the Lower Lias of the Dorset Coast: Geological Society of London, Quarterly Journal, v. 79, p. 47-99.
- Lasemi, Z. and Sandberg, P.A., 1984: Transformation of aragonite-dominated lime muds to microcrystalline limestones: Geology, v. 12, p. 420-423.
- Lawrence, J.R., Gieskes, J., and Anderson, T.F., 1976: Oxygen isotope-material balance calculations, Leg 35: Initial Reports of the Deep Sea Drilling Project, v. 35, p. 507-512.
- Leggett, J.K., 1980: British Lower Paleozoic black shales and their paleo-oceanographic significance: Journal of the Geological Society of London, v. 137, p. 139-156.
- Levesque, R.J., 1977: Stratigraphy and sedimentology of Middle Cambrian to Lower Ordovician shallow water carbonate rocks, western Newfoundland: Unpublished M.Sc. thesis, Memorial University, St. John's, 267 p.
- Liebezeit, G., Bohm, L., Dawson, R., and Wefer, G., 1984: Estimation of algal carbonate input to marine aragonitic sediments on the basis of xylose content: Marine Geology, v. 54, p. 249-262.

Lindholm, R.C., 1969: Detrital dolomite in Onondaga Limestone (Middle Devonian) of New York: its implications to the "dolomite question": American Association of Petroleum Geologists, Bull., p. 1035-1042.

Lindholm, R.C., 1972: Magnesium content and crystal habits in ancient carbonates: Nature Physical Science, v. 237, p. 43-44.

Lindholm, R.C., 1974: Fabric and chemistry of pore filling calcite in septarian veins: models for limestone cementation: Journal of Sedimentary Petrology, v. 44, p. 428-440.

Lindstrom, M., 1963: Sedimentary folds and the development of limestone in an early Ordovician sea: Sedimentology, v. 2, p. 243-275.

Lindstrom, M., 1979: Diagenesis of Lower Ordovician hardgrounds in Sweden: Geologica et Paleontologica, v.13, p. 9-30.

Lippmann, F., 1955: Ton, geoden, und minerale des Barreme von Hoheneggelsen: Geol. Rundschau, v.43, p. 475-503.

Lock, B.E., 1972: Lower Paleozoic history of a critical area: eastern margin of the St. Lawrence Platform in White Bay, Newfoundland, Canada: 24th International Geological Congress, Section 6, p. 310-324.

Logan, B.W. and Semeniuk, V., 1976: Dynamic metamorphism; processes and products in Devonian carbonate rocks, Canning Basin, Western Australia: Geological Society of Australia, Special Publication no. 6, 138p.

Lohmann, K.C. and Meyers, W.J., 1977: Microdolomite inclusions in cloudy prismatic calcites: a proposed criterion for former high magnesium calcites: Journal of Sedimentary Petrology, v. 47, p. 1078-1088.

Longman, M.W., 1977: Factors controlling the formation of microspar in the Bromide Formation: Journal of Sedimentary Petrology, v. 47, p. 347-350.

Longman, M.W., 1980: Carbonate diagenetic textures from nearshore diagenetic environments: American Association of Petroleum Geologists, Bull., v. 64, p. 461-487.

Lorens, R.B., 1981: Sr, Cd, Mn and Co distribution coefficients in calcite as a function of calcite precipitation rate: Geochimica et Cosmochimica Acta, v. 45, p. 553-561.

- Love, L.G., Coleman, M.L., and Curtis, C.D., 1983: Diagenetic pyrite formation and sulphur isotope fractionation associated with a Westphalian marine incursion, northern England: Transactions of the Royal Society of Edinburgh: Earth Sciences, v. 74, p. 165-182.
- Lovell, J.P.B. and Stow, D.A.V., 1981: Identification of ancient sandy contourites: Geology, v. 9, p. 347-349.
- Lowe, D.R., 1976: Subaqueous liquified and fluidized sediment flows and their deposits: Sedimentology, v. 23, p. 285-308.
- Lowe, D.R., 1982: Sediment gravity flows: II. Depositional models with special reference to the deposits of high density turbidity currents: Journal of Sedimentary Petrology, v. 52, p. 279-297.
- Machel, H.-G., 1982: Cathodoluminescence of calcites: activator concentrations and environmental interpretations: Eleventh International Congress on Sedimentology, Hamilton, Ontario, p. 157 (abstract).
- MacIntyre, I.G., 1977: Distribution of submarine cements in a modern Caribbean fringing reef, Galeta Point, Panama: Journal of Sedimentary Petrology, v. 47, p. 503-516.
- Mackenzie, F.T. and Pigott, J.D., 1981: Tectonic controls of Phanerozoic sedimentary rock cycling: Journal of the Geological Society of London; v. 138, p. 183-196.
- Mackenzie, W.S., 1972: Fibrous calcite, a Middle Devonian geologic marker, with stratigraphic significance, District of Mackenzie, Northwest Territories: Canadian Journal of Earth Sciences, v. 9, p. 1431-1440.
- Maleev, M.N., 1972: Diagnostic features of spherulites formed by splitting of a single crystal nucleus. Growth mechanisms of chalcedony: Tschermaks Mineralogische und Petrographische Mitteilungen, v. 18, p. 1-16.
- Marcinowski, R., 1970: Turbidites in the Upper Oxfordian Limestones at Jaskrow in the Polish Jura chain: Bulletin de l'Academie Polonaise des Sciences, Serie de Sciences Geologique et Geographique, v. 18, p. 219-225.
- Markello, J.R. and Read, J.F., 1981: Carbonate ramp-to-deeper shale shelf transitions of an Upper Cambrian intrashelf basin, Nolichucky Formation, southwest Virginia Appalachians: Sedimentology, v. 28, p. 573-597.
- Marshal, D.J., 1975: The status of cathodoluminescence technique in the study of carbonates: talk given at the 9th International Congress of Sedimentology, Nice, (cited by Oglesby, 1976).

- Marshall, J.D., 1981: Zoned calcites in Jurassic ammonite chambers: trace elements, isotopes and neomorphic origin: *Sedimentology*, v. 28, p. 867-887.
- Marshall, J.D., 1982, Isotopic composition of displacive fibrous calcite veins: reversals in pore-water composition trends during burial diagenesis: *Journal of Sedimentary Petrology*, v. 52, p. 615-630.
- Marshall, J.D. and Ashton, M., 1980: Isotopic and trace element evidence for submarine lithification of hardgrounds in the Jurassic of eastern England: *Sedimentology*, v. 27, p. 271-289.
- Matter, A., Douglas, R. G., and Perch-Nielsen, K., 1975: Fossil preservation, geochemistry and diagenesis of pelagic carbonates from the Shatsky Rise, Northwest Pacific: *Initial Reports of the Deep Sea Drilling Project*, v. 32, p. 891-921.
- Maynard, J.B., 1983: *Geochemistry of sedimentary ore deposits*: Springer-Verlag, New York, 305p.
- McBride, E.F. and Folk, R.L., 1979: Features and origin of Italian Jurassic radiolarites deposited on continental crust: *Journal of Sedimentary Petrology*, v. 49, p. 837-868.
- McCorquodale, B.A., 1976: Concretions and some other sedimentary structures: *Saskatchewan Museum of Natural History, Popular Series no. 3*, 18p.
- McCrossan, R.G., 1958: Sedimentary boudinage structure in the Devonian Ireton Formation of Alberta: *Journal of Sedimentary Petrology*, v. 28, p. 316-320.
- McGregor, B.A., 1981: Smooth seaward-dipping horizons - an important factor in seafloor stability?: *Marine Geology*, v. 39, p. M89-M98.
- McGregor, B., Stubblefield, W.L., Ryan, W.B.F., and Twichell, D.C., 1982: Wilmington Submarine Canyon: a marine fluvial-like system: *Geology*, v. 10, p. 27-30.
- McHargue, T.R. and Price, R., 1982: Dolomite from clay in argillaceous or shale-associated marine carbonates: *Journal of Sedimentary Petrology*, v. 52, p. 873-886.
- McIlreath, I.A., 1977: Accumulation of a Middle Cambrian, deep-water limestone debris apron adjacent to a vertical, submarine carbonate escarpment, southern Rocky Mountains: In Cook, H.E. and Enos, P., eds, *Deep-water carbonate environments*, Society of Economic Paleontologists and Mineralogists, Special Publication no. 25, p. 113-124.

- McIlreath and James, N.P., 1984: Carbonate slopes: In Walker, R.G., ed., Facies Models, Geoscience Canada Reprint Series 1, p. 245-257.
- McIntire, W.L., 1963: Trace element partition coefficients - a review of theory with applications to geology: *Geochimica et Cosmochimica Acta*, v. 27, p. 1209-1264.
- McKee, E.D. and Gutschick, R.C., 1969: Analysis of lithology, Chapter 3: In McKee, E.D. and Gutschick, R.C., eds., History of the Redwall Limestone of northern Arizona, Geological Society of America, Memoir no. 114, p. 97-124.
- Mechalas, B.J., 1974: Pathways and environmental requirements for biogenic gas production in the ocean: In Kaplan, I.R., ed., Natural gases in marine sediments, Plenum Press, New York, p. 11-25.
- Meischner, K.D., 1964: Allodapische kalke, turbidite in riffnahen sedimentations-becken: In Bouma, A.H. and Brouwer, A., eds., Turbidites, Developments in Sedimentology 3, Elsevier, Amsterdam, p. 156-191.
- Meyers, W.J., 1974: Carbonate cement stratigraphy of the Lake Valley Formation (Mississippian) Sacramento Mountains, New Mexico: *Journal of Sedimentary Petrology*, v. 44, p. 837-861.
- Meyers, W.J., 1978: Carbonate cements: their regional distribution and interpretation in Mississippian limestones of southwestern New Mexico: *Sedimentology*, v. 25, p. 371-400.
- Meyers, W.J. and Lohmann, K.C., 1978: Microdolomite-rich syntaxial cements: proposed meteoric-marine mixing zone phreatic cements from Mississippian limestones, New Mexico: *Journal of Sedimentary Petrology*, v. 48, p. 475-488.
- Miall, A.D., 1982: Recent developments in facies models for siliciclastic sediments: *Journal of Geological Education*, v. 30, p. 222-240.
- Middleton, G.V. and Hampton, M.A., 1976: Subaqueous sediment transport and deposition by sediment gravity flows: In Stanley, D.J. and Swift, D.J.P., eds., Marine sediment transport and environmental management, John Wiley and Sons, New York, p. 197-217.
- Miller, W.J., 1908: Highly folded between non-folded strata at Trenton Falls, New York: *Journal of Geology*, v. 16, p. 428-433.
- Milliman, J.D., 1974: Marine carbonates: Springer-Verlag, New York, 375p.

- Milliman, J.D., 1977: Role of calcareous algae in Atlantic continental margin sedimentation: In Flugel, E., ed., Fossil algae, Springer-Verlag, New York, p. 232-247.
- Monroe, J.W., 1969: Slumping caused by organically derived gasses in sediments: *Science*, v. 164, p. 1394-1395.
- Monty, C.L., 1977: The origin and development of cryptalgal fabrics: In Walter, M.R., ed., *Stromatolites, Developments in Sedimentology* 20, Elsevier, Amsterdam, p. 193-249.
- Morawietz, F.-H., 1961: Zur genese des Nagelkalkes: *Neues Jahr. Geol. und Palaont.*, v. 112, p. 229-249.
- Morgenstern, R.N., 1967: Submarine slumping and the initiation of turbidity currents: In Richards, A., ed., *Marine geotechnique*, University of Illinois Press, Urbana, Illinois, p. 189-220.
- Morrow, D.W., 1982a: Dolomite - Part 1: the chemistry of dolomitization and dolomite precipitation: *Geoscience Canada*, v. 9, p. 5-13.
- Morrow, D.W., 1982b: Dolomite - Part 2: dolomitization models and ancient dolostones: *Geoscience Canada*, v. 9, p. 95-107.
- Morrow, D.W., 1982c: Descriptive field classification of sedimentary and diagenetic breccia fabrics in carbonate rocks: *Bulletin of Canadian Petroleum Geology*, v. 30, p. 227-229.
- Mountjoy, E.W. and Walls, R.A., 1977: Some examples of early submarine cements from Devonian buildups of Alberta: *Proceedings, third International Coral Reef Symposium*, p. 155-161.
- Mucci, A. and Morse, J.W., 1983: The incorporation of Mg^{2+} and Sr^{2+} into calcite overgrowths: influences of growth rate and solution composition: *Geochimica et Cosmochimica Acta*, v. 47, p. 217-233.
- Mullins, H.T., 1983: Modern carbonate slopes and basins of the Bahamas: In Cook, H.E., Hine, A.C., and Mullins, H.T., eds., *Platform margin and deep water carbonates*, Short Course no.12, Society of Economic Paleontologists and Mineralogists, p. 4-1 - 4-138.
- Mullins, H.T. and Van Buren, H.M., 1979: Modern modified carbonate grain flow deposit: *Journal of Sedimentary Petrology*, v. 49, p. 747-752.

- Mullins, H.T., Heath, K.C., Van Buren, H.M., and Newton, C.R., 1984: Anatomy of a modern open-ocean carbonate slope: northern Bahama Bank: *Sedimentology*, v. 31, p. 141-168.
- Mullins, H.T., Neumann, A.C., Wilber, R.J., and Boardman, M.R., 1980a: Nodular carbonate sediment on Bahamian slopes: possible precursors to nodular limestones: *Journal of Sedimentary Petrology*, v. 50, p. 117-131.
- Mullins, H.T., Neumann, A.C., Wilber, R.J., Hine, A.C., and Chinburg, S., 1980b: Carbonate sediment drifts in northern straits of Florida: *American Association of Petroleum Geologists, Bull.*, v. 64, p. 1701-1717.
- Murata, K.J., Friedman, I., and Madsen, B.M., 1969: Isotopic composition of diagenetic carbonates in marine Miocene formations of California and Oregon: U.S. Geological Survey, Professional Paper 614-B, 24p.
- Narbonne, G.M. and James, N.P., 1984: Ichnology of the Cow Head Group, western Newfoundland: Society of Economic Paleontologists and Mineralogists Mid-year meeting, San Diego, (abstract).
- Nardin, T.R., Hein, F.J., Gorsline, D.S., and Edwards, B.D., 1979a: A review of mass movement processes, sediment and acoustic characteristics, and contrasts in slope and base-of-slope systems versus canyon-fan-basin floor systems: *In* Doyle, L.J. and Pilkey, O.H., eds., *Geology of continental slopes*, Society of Economic Paleontologists and Mineralogists, Special Publication no. 27, p. 61-73.
- Nardin, T.R., Edwards, B.D., and Gorsline, D.S., 1979b: Santa Cruz Basin, California borderland: dominance of slope processes in basin sedimentation: *In* Doyle, L.J. and Pilkey, O.H., eds., *Geology of continental slopes*, Society of Economic Paleontologists and Mineralogists, Special Publication no. 27, p. 209-221.
- Natland, M.L. and Kuenen, P.H., 1951: Sedimentary history of the Ventura Basin and the action of turbidity currents: *Society of Economic Paleontologists and Mineralogists, Special Publication no.2*, p. 76-107.
- Naylor, M.A., 1980: The Kathikas melange, S.W. Cyprus: late Cretaceous submarine debris flows: *Sedimentology*, v. 27, p. 63-78.
- Naylor, M.A., 1981: Debris flow (olistostrome) and slumping on a distal passive continental margin: the Palombini limestone-shale sequence of the northern Apennines: *Sedimentology*, v. 28, p. 837-852.

- Nelson, S.J., 1955: Geology of the Portland Creek-Port Saunders area, west coast of Newfoundland: Newfoundland Department of Mines and Resources, Geological Survey Report 7, 58p.
- Nemec, W., Porebski, S.J., and Steel, R.J., 1980: Texture and structure of resedimented conglomerates: examples from Ksiaz Formation (Famennian-Tournaisian), southwestern Poland: *Sedimentology*, v. 27, p. 519-538.
- Neugebauer, J., 1974: Some aspects of cementation in chalk: In Hsu, K.J. and Jenkyns, H.C., eds., *Pelagic sediments: on land and under the sea*, International Association of Sedimentologists, Special Publication no.1, p. 149-176.
- Neumann, A.C. and Land, L.S., 1975: Lime mud deposition and calcareous algae in the Bight of Abaco, Bahamas: a budget: *Journal of Sedimentary Petrology*, v. 45, p. 763-786.
- Noble, J.P.A. and Howells, K.D.M., 1974: Early marine lithification of the nodular limestones in the Silurian of New Brunswick: *Sedimentology*, v. 21, p. 597-609.
- Normark, W.R., Piper, D.J.W., and Hess, G.R., 1979: Distributary channels, sand lobes, and mesotopography of Navy Submarine Fan, California borderland, with applications to ancient fan sediments: *Sedimentology*, v. 26, p. 749-774.
- Nowlan, G.S., 1974: Conodonts from the Cow Head Group, western Newfoundland, Unpublished M.Sc. thesis, Memorial University, St. John's, Newfoundland, 183p.
- O'Brien, N.R., Nakazawa, K., and Tokuhashi, S., 1980: Use of clay fabric to distinguish turbiditic and hemipelagic siltstones and silts: *Sedimentology*, v. 27, p. 47-61.
- Oertel, G. and Curtis, C.D., 1972: Clay-ironstone concretion preserving fabrics due to progressive compaction: *Geological Society of America, Bull.*, v. 83, p. 2597-2606.
- Oglesby, T.W., 1976: A model for the distribution of manganese, iron, and magnesium in authigenic calcite and dolomite cements in the upper Smackover Formation in eastern Mississippi: Unpublished M.Sc. thesis, University of Missouri-Columbia, 122p.
- Oldershaw, A.E. and Scoffin, T.P., 1967: The source of ferroan and non-ferroan calcite cements in the Halkin and Wenlock Limestones: *Geological Journal*, v. 5, p. 309-320.
- Oxley, F., 1953: Geology of the Parson's Pond - St. Paul's Area, west coast of Newfoundland: Newfoundland Department of Mines and Resources, Geological Survey Report 5, 53p.

- Palmer, T.J. and Fursich, F.T., 1981: Reply on - Development of relief on a Middle Jurassic cemented sea floor: origin of submarine pseudo-anticlines in the Bathonian of Normandy: *Sedimentology*, v. 28, p. 137-139.
- Pettijohn, F.J., 1975: *Sedimentary rocks*: Harper and Row Publishers, New York, 628p.
- Pfeil, R.W. and Read, J.F., 1980: Cambrian carbonate platform margin facies, Shady dolomite, southwestern Virginia, U.S.A.: *Journal of Sedimentary Petrology*, v. 50, p. 91-116.
- Pierson, B.J., 1981: The control of cathodoluminescence in dolomite by iron and manganese: *Sedimentology*, v. 28, p. 601-610.
- Pierson, T.C., 1981: Dominant particle support mechanisms in debris flows at Mt. Thomas, New Zealand, and implications for flow mobility: *Sedimentology*, v. 28, p. 49-60.
- Pigott, J.D. and Mackenzie, F.T., 1979: Phanerozoic ooid diagenesis: a signature of paleo-ocean and -atmospheric chemistry: *Geological Society of America, Abstracts with Programs*, v. 11, p. 495-496 (abstract).
- Pigott, J.D., Schoonmaker, J., and Mackenzie, F.T., 1980: Phanerozoic carbonate diagenesis - a new model: *American Association of Petroleum Geologists, Bull.*, v. 64, p. 764-765.
- Pingitore, N.E., Jr., 1976: Vadose and phreatic diagenesis: processes, products and their recognition in corals: *Journal of Sedimentary Petrology*, v. 46, p. 985-1006.
- Pingitore, N.E., Jr., 1978: The behavior of Zn^{2+} and Mn^{2+} during carbonate diagenesis: theory and applications: *Journal of Sedimentary Petrology*, v. 48, p. 799-814.
- Pingitore, N.E., Jr., 1982: The role of diffusion during carbonate diagenesis: *Journal of Sedimentary Petrology*, v. 52, p. 24-39.
- Piper, D.J.W., 1972: Turbidite origin of some laminated mudstones: *Geological Magazine*, v. 109, p. 115-126.
- Piper, D.J.W., 1978: Turbidite muds and silts on deep sea fans and abyssal plains: In Stanley, D.J. and Kelling, G., eds., *Sedimentation in submarine canyons, fans, and trenches*, Dowden, Hutchinson and Ross, Stroudsburg, Pennsylvania, p. 163-176.
- Pisciotta, K.A., 1980: Chert and porcellanite from Deep Sea Drilling Project Site 436, northwest Pacific: *Initial Reports of the Deep Sea Drilling Project*, v. 56, 57, p. 1133-1142.

- Pisciotta, K.A., 1981: Review of secondary carbonates in the Monterey Formation, California: In Garrison, R.E., Douglas, R.G., Pisciotta, K.E., et al., eds., The Monterey Formation and related siliceous rocks of California; Pacific Section, Society of Economic Paleontologists and Mineralogists, Special Publication, p. 273-283.
- Pisciotta, K.A. and Mahoney, J.J., 1981: Isotopic survey of diagenetic carbonates, Deep Sea Drilling Project Leg 63: Initial Reports of the Deep Sea Drilling Project, v. 63, p. 595-609.
- Plummer, P.S. and Gostin, V.A., 1981: Shrinkage cracks: dessication or syneresis: Journal of Sedimentary Petrology, v. 51, p. 1147-1156.
- Potter, P.E., Maynard, J.B., and Pryor, W.A., 1980: Sedimentology of shale: Springer-Verlag, New York, 303p.
- Pratt, B.R., 1979: The St. George Group (Lower Ordovician), western Newfoundland: sedimentology, diagenesis and cryptalgal structures: Unpublished M.Sc. thesis, Memorial University, St. John's, Newfoundland, 214p.
- Pratt, B.R., 1982: Stromatolitic framework of carbonate mud-mounds: Journal of Sedimentary Petrology, v. 52, p. 1203-1227.
- Pratt, B.R., 1984: Epiphyton and Renalcis - diagenetic microfossils from calcification of coccooid blue-green algae: Journal of Sedimentary Petrology, v. 54, p. 948-971.
- Pratt, B.R. and James, N.P., 1982a: Epiphyton and Renalcis - diagenetic microfossils from calcification of coccooid blue green algae: American Association of Petroleum Geologists, Bull., v. 66, p. 619 (abstract).
- Pratt, B.R. and James, N.P., 1982b: Cryptalgal-metazoan bioherms of early Ordovician age in the St. George Group, western Newfoundland: Sedimentology, v. 29, p. 543-569.
- Price, L.L. and Ball, N.L., 1971: Stratigraphy of the David Corporation Potash Shaft no. 1, Saskatoon, Saskatchewan: Geological Survey of Canada, Paper 70-71, 107p.
- Prior, D.B. and Coleman, J.M., 1982: Active slides and flows in underconsolidated marine sediments on the slopes of the Mississippi Delta: In Saxov, S. and Nieuwenhuis, J.K., eds., Marine slides and other mass movements, Nato Conference Series, Series IV, Marine Sciences, v. 6, p. 21-49.

- Prior, D.B., Bornhold, B.D., Coleman, J.M., and Bryant, W.R., 1982: Morphology of a submarine slide, Kitimat Arm, British Columbia: *Geology*, v. 10, p. 588-592.
- Prior, D.B., Wiseman, W.J., and Gilbert, R., 1981: Submarine processes on a fan delta, Howe Sound, British Columbia: *Geo-Marine Letters*, v. 1, p. 85-90.
- Purdy, E.G., 1963: Recent calcium carbonate facies of the Great Bahama Bank. 2. Sedimentary facies: *Journal of Geology*, v. 71, p. 472-497.
- Purser, B.H., 1980: *Sedimentation et diagenese des carbonates neritiques recents*, Editions Technip, Paris, 366p.
- Raiswell, R., 1971a: The growth of Cambrian and Liassic concretions: *Sedimentology*, v. 17, p. 147-171.
- Raiswell, R., 1971b: Cementation in some Cambrian concretions, South Wales: In Bricker, O.P., *Carbonate cements*, The Johns Hopkins Press, Baltimore, Maryland, p. 196-197.
- Raiswell, R., 1976: The microbiological formation of carbonate concretions in the Upper Lias of NE England: *Chemical Geology*, v. 18, p. 227-244.
- Ramsay, J.G., 1967: *Folding and fracturing of rocks*: McGraw-Hill, New York, 568p.
- Rao, C.P., 1981: Criteria for recognition of cold-water carbonate sedimentation: Berriedale limestone (Lower Permian), Tasmania, Australia: *Journal of Sedimentary Petrology*, v. 51, p. 491-506.
- Read, J.F., 1980: Carbonate ramp-to-basin transitions and foreland basin evolution, Middle Ordovician, Virginia Appalachians: *American Association of Petroleum Geologists, Bull.*, v. 64, p. 1575-1612.
- Read, J.F. and Pfeil, R.W., 1983: Fabrics of allochthonous reefal blocks, Shady Dolomite (Lower to Middle Cambrian), Virginia Appalachians: *Journal of Sedimentary Petrology*, v. 53, p. 761-779.
- Reed, B.E., Jr., 1968: *Petrology of the Dutchtown Formation, southeast Missouri*: M.A. thesis, University of Missouri, 36p.
- Rees, M.N., in prep: Cambrian calcified algal bioherms: Epiphyton and Renalcis in a lagoonal setting.
- Reineck, H.-E. and Singh, I.B., 1980: *Depositional sedimentary environments*: Springer-Verlag, New York, 549p.

- Reineck, H.-E. and Wunderlich, F., 1968: Classification and origin of flaser and lenticular bedding: *Sedimentology*, v. 11, p. 99-104.
- Reis, O.M., 1902: Ueber Stylolithen, Dutenmergel und Landschaftenkalk (Anthrakolith zum Theil), *Geognostische Jahreshefte*, v. 1902, p. 157-259.
- Rich, M., 1982: Ooid cortices composed of neomorphic pseudospar: Possible evidence for ancient originally aragonitic ooids: *Journal of Sedimentary Petrology*, v. 52, p. 843-847.
- Richardson, W.A., 1919: On the origin of septarian structure: *Mineralogical Magazine*, v. 18, p. 327-338.
- Richardson, W.A., 1923: Petrology of the Shales-with-"Beef": In Lang, W.D., Spath, L.F., and Richardson, W.A., *Shales-with-Beef, a sequence in the Lower Lias of the Dorset coast*, *Geological Society of London Quarterly Journal*, v. 79, p. 47-98.
- Ricken, W. and Hemleben, C., 1982: Origin of marl-limestone alternation (Oxford 2) in southwest Germany: In Einsele, G. and Seilacher, A., eds., *Cyclic and event stratification*, Springer-Verlag, New York, p. 63-71.
- Riding, R., 1977: Calcified Plectonema (blue-green algae), a recent example of Girvanella from Aldabra Atoll: *Palaeontology*, v. 20, p. 33-46.
- Riech, V. and von Rad, U., 1979: Silica diagenesis in the Atlantic Ocean; diagenetic potential and transformation: In Talwani, M., Hay, W.W., and Ryan, W.B.F., eds., *Results of deep drilling in the Atlantic Ocean; continental margins and paleoenvironments*, American Geophysical Union, Maurice Ewing Series No. 3, p. 315-340.
- Rigby, J.K., 1983: Introduction to the Porifera: In Rigby, J.K. and Stearn, C.W., eds., *Sponges and Spongiomorphs, Notes for a Short Course*, p. 1-11.
- Rodgers, J. and Neale, E.R.W., 1963: Possible "Taconic" klippen in western Newfoundland: *American Journal of Science*, v. 261, p. 713-730.
- Ross, R.J. Jr., Jaanusson, V., and Friedman, I., 1975: Lithology and origin of Middle Ordovician calcareous mudmound at Meiklejohn Peak, southern Nevada: U.S. Geological Survey Professional Paper 871, 48p.
- Ruiz-Ortiz, P.A., 1983: A carbonate submarine fan in a fault-controlled basin of the Upper Jurassic, Beltic Cordillera, southern Spain: *Sedimentology*, v. 30, p. 33-48.

- Rupke, N.A., 1975: Deposition of fine-grained sediments in the abyssal environment of the Algero-Balearic Basin, Western Mediterranean Sea: *Sedimentology*, v. 22, p. 95-109.
- Rupke, N.A., 1978: Deep clastic seas: *In* Reading, H.G., ed., *Sedimentary environments and facies*, p. 372-415.
- Ryan, W.B.F., 1982: Interrelationships between oceanographic events and mass wasting on the sea floor: *In* Saxov, S. and Nieuwenhuis, J.K., eds., *Marine slides and other mass movements*, Nato Conference Series, Series IV, Marine Sciences, v. 6, p. 263-272.
- Sabins, F.F., Jr., 1962: Grains of detrital, secondary, and primary dolomite from Cretaceous strata of the western interior: *Geological Society of America, Bull.*, v. 73, p. 1183-1196.
- Sandberg, P., in press: Aragonite cements and their occurrence in ancient limestones: *In* Schneidermann, N. and Harris, P.M., eds., *Carbonate Cements*, Society of Economic Paleontologists and Mineralogists, Special Publication no. 37.
- Sandberg, P.A., 1975: New interpretation of Great Salt Lake ooids and of ancient non-skeletal mineralogy: *Sedimentology*, v. 22, p. 497-537.
- Sandberg, P.A., 1983: An oscillating trend in Phanerozoic non-skeletal carbonate mineralogy: *Nature*, v. 305, p. 19-22.
- Sandberg, P.A. and Popp, B.N., 1981: Pennsylvanian aragonite from southeastern Kansas - environmental and diagenetic implications: *American Association of Petroleum Geologists, Bull.*, v. 65, p.985 (abstract).
- Sass, E. and Kolodny, Y., 1972: Stable isotopes, chemistry and petrology of carbonate concretions (Mishash Formation, Israel): *Chemical Geology*, v. 10, p. 261-286.
- Savin, S.M. and Yeh, H.W., 1981: Stable isotopes in ocean sediments: *In* Emiliani, C., ed., *The sea*, v. 7., *The oceanic lithosphere*, Wiley Interscience, p. 1521-1554.
- Savrda, C.E., Bottjer, D.J., Gorsline, D.S., 1984: Development of a comprehensive oxygen-deficient biofacies model: Evidence from Santa Monica, San Pedro, and Santa Barbara Basins, California Continental Borderland: *American Association of Petroleum Geologists, Bull.*, v. 68, p. 1179-1182.
- Saxov, S., 1982: Marine slides - some introductory remarks: *In* Saxov, S. and Nieuwenhuis, J.K., eds., *Marine slides and other mass movements*, Nato Conference Series, Series IV, Marine Sciences, v. 6, p. 1-7.

- Saxov, S. and Nieuwenhuis, J.K., eds., 1982: Marine slides and other mass movements, Nato Conference Series, Series IV; Marine Sciences, v. 6, 353 p.
- Sayles, F.L. and Manheim, F.T., 1975: Interstitial solution and diagenesis in deeply buried marine sediments: results from the Deep Sea Drilling Project: *Geochimica et Cosmochimica Acta*, v. 39, p. 103-127.
- Scheidegger, A.E., 1982: On the tectonic setting of submarine slides: In Saxov, S. and Nieuwenhuis, J.K., eds., Marine slides and other mass movements, Nato Conference Series, Series IV, Marine Sciences, v. 6, p. 11-20.
- Schlager, W. and Camber, O., 1982: Depositional, erosional and by-pass slopes on carbonate platforms: Eleventh International Congress on Sedimentology, Abstracts of Papers, p. 179 (abstract).
- Schlager, W. and Chermak, A., 1979: Sediment facies of platform-basin transition, Tongue of the Ocean, Bahamas: In Doyle, L.J. and Pilkey, O.H., eds., Geology of continental slopes, Society of Economic Paleontologists and Mineralogists, Special Publication no. 27, p. 193-208.
- Schlager, W. and James, N.P., 1978: Low-magnesian calcite limestones forming at the deep-sea floor, Tongue of the Ocean, Bahamas: *Sedimentology*, v. 25, p. 675-702.
- Schlager, S.O. and Douglas, R.G., 1974: Pelagic ooze-chalk-limestone transition and its implication for marine stratigraphy: In Hsu, K.J. and Jenkyns, H.C., P., Pelagic sediments: on land and under the sea, International Association of Sedimentologists, Special Publication no. 1, p. 117-148.
- Scholle, P.A., 1977: Deposition, diagenesis and hydrocarbon potential of "deeper-water" limestones: American Association of Petroleum Geologists, Continuing Education Course Notes, Series no. 7, 25p.
- Scholle, P.A., 1978: Carbonate rock constituents, textures, cements, and porosities: American Association of Petroleum Geologists, Memoir no. 27, 24p.
- Scholle, P.A., Arthur, M.A., and Ekdale, A.A., 1983: Pelagic environment: In Scholle, P.A., Bebout, D.G., and Moore, C.H., eds., Carbonate depositional environments, American Association of Petroleum Geologists, Memoir no. 33, p. 620-691.
- Schmitt, J.G. and Boyd, D.W., 1981: Patterns of silicification in Permian pelecypods and brachiopods from Wyoming: *Journal of Sedimentary Petrology*, v. 51, p. 1297-1308.

- Schuchert, C. and Dunbar, C.O., 1934: Stratigraphy of western Newfoundland: Geological Society of America, Memoir no. 1, 123p.
- Schwarz, H.-U., 1982: Subaqueous slope failures - experiments and modern occurrences: Contributions to Sedimentology, v. 11, 116p.
- Schwarzacher, W., 1961: Petrology and structure of some Lower Carboniferous reefs in northwestern Ireland: American Association of Petroleum Geologists, Bull., v. 45, p. 1481-1503.
- Schwarzacher, W. and Fischer, A.G., 1982: Limestone-shale bedding and perturbations of the Earth's orbit: In Einsele, G. and Seilacher, A., eds., Cyclic and event stratification, Springer-Verlag, New York, p. 72-95.
- Sellier, E., 1979: Contribution a l'etude petrologique experimentale de la genese des stylolithes dans les formations calcaires du bassin d'Aquitaine: Unpublished Ph.D. thesis, Universite de Bordeaux III, 300p.
- Shackleton, N.J. and Kennett, J.P., 1975: Palaeotemperature history of the Cenozoic and the initiation of the Antarctic glaciation: oxygen and carbon isotope analysis in DSDP sites 277, 279, and 281: Initial Reports of the Deep Sea Drilling Project, v. 29, p. 743-755.
- Shanmugam, G. and Walker, K., 1978: Tectonic significance of distal turbidites in the Middle Ordovician Blockhouse and lower Sevier Formations in east Tennessee: American Journal of Science, v. 278, p. 551-578.
- Sharma, T. and Clayton, R.N. 1965: Measurement of O^{18}/O^{16} ratios of total oxygen of carbonates: Geochimica et Cosmochimica Acta, v. 29, p. 1347-1353.
- Shaub, B.M., 1937: The origin of cone-in-cone and its bearing on the origin of concretions and septaria: American Journal of Science, series 5, v. 34, p. 331-344.
- Shearman, D.J., Mossop, G., Dunsmore, H., and Martin, M., 1972: Origin of gypsum veins by hydraulic fracture: Transactions of the Institute of Mining and Metallurgy, Section B, v. 181, p. 149-155.
- Shinn, E.A., 1969: Submarine lithification of Holocene carbonate sediments in the Persian Gulf: Sedimentology, v. 12, p. 109-144.
- Shinn, E.A. and Robbin, D.M., 1983: Mechanical and chemical compaction in fine-grained shallow-water limestones: Journal of Sedimentary Petrology, v. 53, p. 595-618.
- Shinn, E.A., Halley, R.B., Hudson, J.H., and Lidz, B.H., 1977: Limestone compaction - an enigma: Geology, v.5. p. 21-24.

- Sibley, D.F., 1982: The origin of common dolomite fabrics: clues from the Pliocene: *Journal of Sedimentary Petrology*, v. 52, p. 1087-1100.
- Sorby, H.C., 1860: On the origin of cone-in-cone: *British Association for the Advancement of Science, report of the 29th meeting, 1859, Transaction of Sections, Geology*, p. 124.
- Spry, A., 1976: *Metamorphic textures*: Pergamon Press, New York, 350p.
- Sramek, J., 1974: A comment. Origin of limestone nodules in the Lower Palaeozoic of the Oslo Region: *Norsk Geologisk Tidsskrift*, v. 54, p. 395-396.
- Srivastava, P., Stearn, C.W., and Mountjoy, E.W., A Devonian megabreccia at the margin of the Ancient Wall carbonate complex, Alberta: *Bulletin of Canadian Petroleum Geology*, v. 20, p. 412-438.
- Stanley, D.J., 1981: Unifites: structureless muds of gravity-flow origin in Mediterranean basins: *Geo-Marine Letters*, v. 1, p. 77-83.
- Stanley, D.J. and Maldonado, A., 1981: Depositional models for fine-grained sediment in the western Hellenic Trench, eastern Mediterranean: *Sedimentology*, v. 28, p. 273-290.
- Steinen, R.P., 1978: On the diagenesis of lime mud: scanning electron microscopic observations of subsurface material from Barbados, W.I.: *Journal of Sedimentary Petrology*, v. 48, p. 1139-1148.
- Steinen, R.P., 1979: Reply - On the diagenesis of lime mud: Scanning electron microscopic observations of subsurface material from Barbados, W.I.: *Journal of Sedimentary Petrology*, v. 49, p. 1355-1358.
- Steinen, R.P., 1982: SEM observations on the replacement of Bahamian aragonitic mud by calcite: *Geology*, v. 10, p. 471-475.
- Stevens, R.K., 1970: Cambro-Ordovician flysch sedimentation and tectonics in west Newfoundland and their bearing on a Proto-Atlantic Ocean: *Geological Association of Canada, Special Paper no. 7*, p. 165-176.
- Stockman, K.W., Ginsburg, R.N., and Shinn, E.A., 1967: The production of lime mud by algae in south Florida: *Journal of Sedimentary Petrology*, v. 37, p. 633-648.

- Stoneley, R., 1983: Fibrous calcite veins, overpressures, and primary oil migration: American Association of Petroleum Geologists, Bull., v. 67, p. 1427-1428.
- Stow, D.A.V., 1979: Distinguishing fine-grained turbidites and contourites on the Nova Scotian deep water margin: Sedimentology, v. 26, p. 371-387.
- Stow, D.A.V., 1982: Toward an anatomy of fine-grained sediments: Episodes, v. 1982, p. 3-4.
- Stow, D.A.V. and Bowen, A.J., 1978: Origination of lamination in deep sea, fine-grained sediments: Nature, v. 274, p. 324-328.
- Stow, D.A.V. and Bowen, A.J., 1980: A physical model for the transport and sorting of fine-grained sediment by turbidity currents: Sedimentology, v. 27, p. 31-46.
- Stow, D.A.V. and Lovell, J.P.B., 1979: Contourites: their recognition in modern and ancient sediments: Earth-Science Reviews, v. 14, p. 251-291.
- Stow, D.A.V. and Piper, D.J.W., in press: Deep-water fine-grained sediments: facies models: In Stow, D.A.V. and Piper, D.J.W., eds., Fine-grained sediments: deep water processes and facies, Blackwell Scientific Publications.
- Stow, D.A.V. and Shanmugam, G., 1980: Sequence of structures in fine-grained turbidites: comparison of recent deep-sea and ancient flysch sediments: Sedimentary Geology, v. 25, p. 23-42.
- Suchecki, R.K., 1975: Sedimentology, petrology, and structural geology of the Cow Head klippe: Broom Point, St. Paul's Inlet, and Black Brook, western Newfoundland: Unpublished M.Sc. thesis, University of Massachusetts, Amherst, Massachusetts, 180p.
- Suchecki, R.K., Perry, E.A., and Hubert, J.F., 1977: Clay petrology of Cambro-Ordovician continental margin, Cow Head Klippe, western Newfoundland: Clays and Clay Minerals, v. 25, p. 163-170.
- Suess, E., 1979: Mineral phases formed in anoxic sediments by microbial decomposition of organic matter: Geochimica et Cosmochimica Acta, v. 43, p. 339-352.
- Sujkowski, Z.L., 1958: Diagenesis: American Association of Petroleum Geologists, v. 42, p. 2692-2717.
- Supko, P.R., Stoffers, P., and Coplen, T.B., 1974: Petrography and geochemistry of Red Sea dolomite: Initial Reports of the Deep Sea Drilling Project, v. 23, p. 867-878.

- Surlyk, F., 1978: Submarine fan sedimentation along fault scarps on tilted fault blocks (Jurassic - Cretaceous boundary, East Greenland): *Gronlands Geologiske Undersogelse Bulletin*, no. 28, 108p.
- Swett, K. and Smit, D.E., 1972: Paleogeography and depositional environments of the Cambro-Ordovician shallow-marine facies of the North Atlantic: *Geological Society of America, Bull.*, v. 83, p. 3223-3248.
- Tarney, J. and Schreiber, B.C., 1976: Cone-in-cone and beef-in-shale textures from D.S.D.P. site 330, Falkland Plateau, South Atlantic: *Initial Reports of the Deep Sea Drilling Project*, v. 36, p. 865-870.
- Tarr, W.A., 1932: Cone-in-cone: *In* Twenhofel, W.H., *Treatise on Sedimentation*, (1961 edition), Dover Publications, New York, p. 716-733.
- Tarr, W.A. and Twenhofel, W.H., 1932: Concretions: *In* Twenhofel, W.H., *Treatise on sedimentation*, (1961 edition), Dover Publications, New York, p. 696-716.
- Thomson, A.F. and Thomasson, M.R., 1969: Shallow to deep water facies development in the Dimple Limestone (Lower Pennsylvanian), Marathon Region, Texas: *In* Friedman, G.M., ed., *Depositional environments in carbonate rocks*, Society of Economic Paleontologists and Mineralogists, Special Publication no. 4, p. 57-78.
- Toomey, D.F. and Klement, K.W., 1966: A problematical micro-organism from the El Paso Group (Lower Ordovician) of west Texas: *Journal of Paleontology*, v. 40, p. 1304-1311.
- Toomey, D.F. and Nitecki, M.H., 1979: Organic buildups in the Lower Ordovician (Canadian) of Texas and Oklahoma: *Fieldiana Geology*, New Series, 181p.
- Tucker, M.E., 1969: Crinoidal turbidites from the Devonian of Cornwall and their palaeogeographic significance: *Sedimentology*, v. 13, p. 282-290.
- Tucker, M.E., 1973: Sedimentology and diagenesis of Devonian pelagic limestones (Cephalopodenkalk) and associated sediments of the Rhenohercynian Geosyncline, West Germany: *Neues Jahrbuch fur Geologie und Palaontologie, Abhandlungen*, v. 142, p. 320-350.
- Tucker, M.E., 1974: Sedimentology of Palaeozoic pelagic limestones: the Devonian Griotte (southern France) and Cephalopodenkalk (Germany): *In* Hsu, K.J. and Jenkyns, H.C., *Pelagic sediments: on land and under the sea*, International Association of Sedimentologists, Special Publication no. 1, p. 71-92.

- Tucker, M.E., and Kendall, A.C., 1973: The diagenesis and low-grade metamorphism of Devonian styliolinid-rich pelagic carbonates from West Germany: Possible analogues of present pteropod oozes: *Journal of Sedimentary Petrology*, v. 43, p. 672-687.
- Twenhofel, W.A., 1950: Principles of sedimentation: McGraw-Hill Book Company, 673p.
- Twenhofel, W.A. and Tester, A.C., 1926: New data on the Commanchean strata of Central Kansas: *American Association of Petroleum Geologists, Bull.*, v. 10, p. 553-561.
- Van der Lingen, G.J., 1969: The turbidite problem: *New Zealand Journal of Geology and Geophysics*, v. 12, p. 7-50.
- Vanuxem, L., 1842: Geology of New York, Part 3, comprising the survey of the Third Geologic District, Albany, New York: 306p.
- Veizer, J., 1983: Chemical diagenesis of carbonates: theory and application of trace element technique: In Arthur, M.A., Anderson, T.F., Kaplan, I.R., Veizer, J., and Land, L.S., Stable isotopes in sedimentary geology, Society of Economic Paleontologists and Mineralogists, Short Course no. 10, p. 3-1 - 3-100.
- Veizer, J. and Hoefs, J., 1976: The nature of $^{18}\text{O}/^{16}\text{O}$ and $^{13}\text{C}/^{12}\text{C}$ secular trends in sedimentary carbonate rocks: *Geochimica et Cosmochimica Acta*, v. 40, p. 1387-1395.
- Waage, K.M., 1964: Origin of repeated fossiliferous concretion layers in the Fox Hills Formation: *Kansas Geological Survey Bulletin*, no. 169, p. 541-563.
- Walker, R.G., 1967: Turbidite sedimentary structures and their relationship to proximal and distal depositional environments: *Journal of Sedimentary Petrology*, v. 37, p. 25-43.
- Walker, R.G., 1975: Generalized models for resedimented conglomerates of turbidite association: *Geological Society of America, Bull.*, v. 86, p. 737-748.
- Walker, R.G., 1984: Turbidites and associated coarse clastic deposits: In Walker, R.G., ed., *Facies Models*, Geoscience Canada Reprint Series 1, p. 171-188.
- Walker, R.G. and Mutti, E., 1973: Turbidite facies and facies associations: In Middleton, G.V. and Bouma, A.H., eds., *Turbidites and deep-water sedimentation*, Society of Economic Paleontologists and Mineralogists, Notes for a Short Course, p. 119-157.

- Walls, R.A., Mountjoy, E.W., and Fritz, P., 1979: Isotopic composition and diagenetic history of carbonate cements in Devonian Golden Spike reef, Alberta, Canada: Geological Society of America, Bull., v. 90, p. 963-982.
- Wanless, H.R., 1979: Limestone response to stress: Pressure solution and dolomitization: Journal of Sedimentary Petrology, v. 49, 437-462.
- Wanless, H.R., 1983: Burial diagenesis in limestones: In Parker, A. and Sellwood, B.W., eds., Sediment diagenesis, Reidel Publishing Company, Boston, p. 379-417.
- Warne, J.E., Douglas, R.G., and Winterer, E.L., eds., 1981: The Deep Sea Drilling Project: A decade of progress: Society of Economic Paleontologists and Mineralogists, Special Publication no. 32, 564p.
- Watts, N.L., 1978: Displacive calcite: evidence from recent and ancient calcretes: Geology, v. 6, p. 699-703.
- Watts, N.L., 1979: Reply on - Displacive calcite: evidence from recent and ancient calcretes: Geology, v. 7, p. 421-422.
- Weaver, C.E., 1967: Potassium, Nitrate and the ocean: Geochimica et Cosmochimica Acta, v. 31, p. 2181-2196.
- Weeks, L.G., 1953: Environment and mode of origin and facies relationships of carbonate concretions in shales: Journal of Sedimentary Petrology, v. 23, p. 162-173.
- Weller, J.M., 1959: Compaction of sediments: American Association of Petroleum Geologists, Bull., v. 43, p. 273-310.
- Weyl, P.K., 1959: Pressure solution and the force of crystallization - a phenomenological theory: Journal of Geophysical Research, v. 64, p. 2001-2025.
- White, T.G., 1896: The faunas of the Upper Ordovician strata at Trenton Falls, Oneida County, New York: New York Academy of Sciences Transactions, v. 15, p. 71-96.
- Wieder, M. and Yaalon, D.H., 1974: Effect of matrix composition on carbonate nodule crystallization: Geoderma, v. 11, p. 95-121.
- Wilkinson, B.H., 1979: Biomineralization, paleoceanography, and the evolution of calcareous marine organisms: Geology, v. 90, p. 258-271.
- Wilkinson, B.H., 1982: Cyclic carbonates and Phanerozoic calcite seas: Journal of Geological Education, v. 30, p. 189-203.

- Wilkinson, B.H. and Landing, E., 1978: "Eggshell diagenesis" and primary radial fabric in calcite ooids: *Journal of Sedimentary Petrology*, v. 48, p. 1129-1138.
- Wilkinson, B.H., Janecke, S.U., and Brett, C.E., 1982: Low-magnesian calcite marine cements in Middle Ordovician hardgrounds from Kirkfield, Ontario: *Journal of Sedimentary Petrology*, v. 52, p. 47-57.
- Williams, H., 1975: Structural succession, nomenclature, and interpretation of transported rocks in western Newfoundland: *Canadian Journal of Earth Sciences*, v. 12, p. 1874-1894.
- Williams, H., 1979: Appalachian Orogen in Canada, *Canadian Journal of Earth Sciences*, v. 16, p. 792-807.
- Williams, H., 1980: Structural telescoping across the Appalachian Orogen and the minimum width of the Iapetus Ocean: *Geological Association of Canada, Special Paper no. 20*, p. 421-440.
- Williams, H., James, N.P., and Stevens, R.K., 1984: Humber Arm Allochthon and nearby Groups between Bonnie Bay and Portland Creek, western Newfoundland: *In Current Research, Part A, Geological Survey of Canada, Paper 85-1A*, p. 399-406.
- Williams, H., Kennedy, M.J., Neale, E.R.W., St. Julien, P., 1972: The Appalachian structural province: *In Variations in tectonic styles in Canada, Geological Association of Canada Special Paper no. 11*, p. 181-261.
- Williams, P.F., Collins, A.R., and Wiltshire, R.G., 1969: Cleavage and penecontemporaneous deformation structures in sedimentary rocks: *Journal of Geology*, v. 177, p. 415-425.
- Wilson, J.L., 1969: Microfacies and sedimentary structures in "deeper water" lime mudstones: *In Friedman, G.M., ed., Depositional environments in carbonate rocks, Society of Economic Paleontologists and Mineralogists, Special Publication no. 14*, p. 4-19.
- Wilson, J.L., 1975: Carbonate facies in geologic history: Springer-Verlag, New York, 471p.
- Wise, S.W. and Weaver, F.M., 1974: Chertification in ocean sediments: *In Hsu, K.J. and Jenkyns, H.C., Pelagic sediments: on land and under the sea, International Association of Sedimentologists, Special Publication no. 1*, p. 301-326.
- Wolf, K.H., 1965: Gradational sedimentary products of calcareous algae: *Sedimentology*, v. 5, p. 1-37.
- Wong, P.K. and Oldershaw, A., 1981: Burial cementation in the Devonian Kaybob reef complex, Alberta, Canada: *Journal of Sedimentary Petrology*, v. 51, p. 507-520.

- Wood, H.M., 1983: Clay mineralogy of Middle Cambrian to Lower Ordovician sediments, Port-au-Port, Newfoundland: Unpublished B.Sc. thesis, Memorial University, St. John's, Newfoundland, 49p.
- Woodcock, N.H., 1976: Structural style in slump sheets: Ludlow Series, Powys, Wales: Journal of the Geological Society of London, v. 132, p. 399-415.
- Woodcock, N.H., 1979: Sizes of submarine slides and their significance: Journal of Structural Geology, v. 1, p. 137-142.
- Woodland, B.G., 1964: The nature and origin of cone-in-cone structure: Fieldiana, Geology, Chicago Natural History Museum, v. 13, p. 185-305.
- Wray, J.L., 1977: Calcareous Algae: Elsevier, New York, 180p.
- Wright, V.P. and Wilson, R.C.L., 1984: A carbonate submarine-fan sequence from the Jurassic of Portugal: Journal of Sedimentary Petrology, v. 54, p. 394-412.
- Yurewicz, D.A., 1977: Sedimentology of Mississippian Basin carbonates, New Mexico and West Texas - the Rancheria Formation: In Cook, H.E. and Enos, P., eds., Deep-water carbonate environments, Society of Economic Paleontologists and Mineralogists, Special Publication no. 25, p. 203-209.
- Zankl, H., 1969: Structural and textural evidence of early lithification in fine-grained carbonate rocks: Sedimentology, v. 12, p. 241-256.
- Zenger, D.H., 1972: Significance of supratidal dolomitization in the geologic record: Geological Society of America, Bull., v. 83, p. 1-12.
- Zenger, D.H., 1976: Dolomitization and dolomite "dikes" in the Wyman Formation (Precambrian), northwestern Inyo Mountains, California: Journal of Sedimentary Petrology, v. 46, p. 457-462.
- Ziegler, A.M., Scotese, C.R., McKerrow, W.S., Johnson, M.E., and Bambach, R.K., 1979: Paleozoic paleogeography: Annual Review of the Earth and Planetary Sciences, v. 7, p. 473-502.

PLATES

All thin section microphotographs are taken in plane-polarized light unless otherwise indicated.

PLATE 1: CONGLOMERATE LITHOFACIES

- a: Massive polymictic conglomerate overlying thinly-bedded parted limestones with minor basal scour. The prominent white-weathering boulders are composed mainly of calcified algae and syndimentary cement (see James, 1981 and Chapter 5). The large boulder in the upper centre of the photograph is approximately 2 m across. Stratigraphic top is to upper right of photo. Cow Head North, Upper Cambrian, Bed 7.
- b: Conglomerate lens with gradually tapered margin laterally pinching out into a ribbon limestone sequence. Several broad, shallow scours occur on the sole of this conglomerate (not seen in photo), otherwise scour is not detectable. This suggests the conglomerate had depositional relief on the sea floor. Stratigraphic top is toward right. Broom Point South, Upper Cambrian, unit 43.
- c: Conglomerate with sandy matrix demonstrates exceptionally well-developed normal grading. Packing fabric varies from clast-supported to condensed. With decreasing clast size the tabular aspect also decreases. This 1.5 m thick conglomerate immediately overlies and is probably genetically related to the 1 m thick slide sheet shown in Plate 16b. Cow Head South, Middle Ordovician, Bed 13s.4.
- d: Soft-sediment folding in parted mudstone raft in conglomerate illustrates that the limestone is competent, though brittle, and controls folding style whereas interbedded marl flows into the fold hinge zone. This contrasting behaviour of mudstone and marl indicates that the rhythmite character is early and is either primary in origin or formed during shallow burial. As a result of interlayer shear generated during folding, an early-formed fracture cleavage allows offset of limestone microlithons. The high angle intersection of the fold hinge and the fracture cleavage is an uncommon relationship (T. Calon, pers. comm., 1982). Cow Head North, Middle Ordovician, Bed 14.
- e: Soft-sediment faulting and brecciation within a raft of parted mudstone produces numerous clasts with rectangular cross-sections. This reflects the existence of an early fracture cleavage. Cow Head North, Beachy Cove, Upper Cambrian, Bed 3.
- f: Bedding-plane view of shaly conglomerate matrix which preserves distorted, vestigial laminations, indicating minor transport or late stage incorporation of the precursor ribbon limestone into the conglomerate. Hammer head scale to right. Cow Head North, Beachy Cove, Upper Cambrian, Bed 3.



PLATE 2: CONGLOMERATE LITHOFACIES

- a: Flat-pebble imbrication in a 20 m-long lens resembles wave-forms described by Hubert et al. (1977). Stratigraphic top is up. Green Point, base of Upper Cambrian section on wave-cut platform.
- b: Coarse, tabular cross-bedding outlined by prominent fractures and alignment of flat mudstone clasts indicates current direction toward southeast (to left of photo). Stratigraphic top is up. Cow Head South, Shoal Cove Section, Lower Ordovician, Bed 9s.12-.13.
- c: This thin conglomerate with shaly matrix-supported fabric at its base grades upward into clast-supported fabric. Stratigraphic top is up. Martin Point, Upper Cambrian, unit 33.
- d: Draped, isolated boulder in a ribbon to parted limestone sequence has a thin veneer of pebbly conglomerate plastered against its base. This suggests the boulder was stranded by a debris flow which was eventually deposited further downslope. Refer to text for discussion. Stratigraphic top is up. Cow Head North, Upper Cambrian, Bed 6.37-.44.



PLATE 3: CALCARENITE LITHOFACIES

- a: Thick-bedded massive, pebbly grainstones are separated by recessive, thin beds of dolomitic and peloidal siltstones. The massive bed (arrow) immediately above the knapsack scale in foreground is approximately 40 cm thick. Stratigraphic top is to upper right of photo. Cow Head North, Upper Cambrian, Bed 6.
- b: Normally-graded grainstone with abundant flat mudstone pebbles grades upward to cross-laminated silt. Martin Point, Upper Cambrian, unit 33, sample MP-42.
- c: Graded grainstone with centimetre-long flat pebbles and abundant siliciclastic sand at its base (dark specks) demonstrates pronounced bedding-parallel stylolites which impart a false, thin-bedded aspect. Pocket-knife scale is 9 cm long. Stratigraphic top is up. Broom Point North, Upper Cambrian, units 20-23.
- d: Mega-rippled and rippled quartzose calcarenite shows flaggy partings in the mega-rippled units (arrowed) which are due to stylolitization parallel to foresets. Thinner interbeds are mudstones and peloidal packstones. Stratigraphic top is up. Martin Point, Upper Cambrian, unit 31c-e.

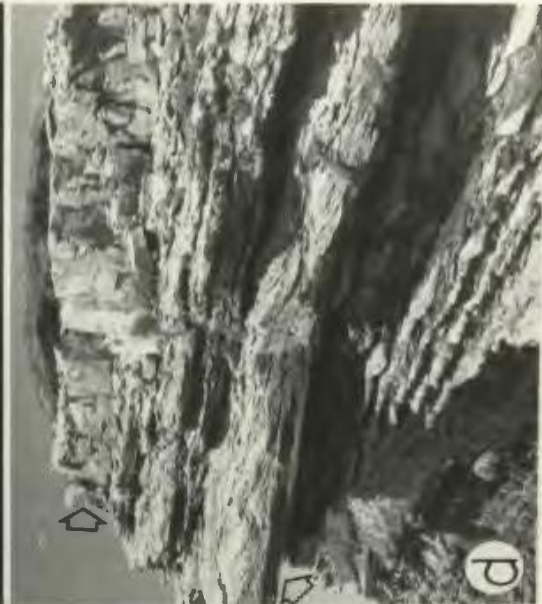
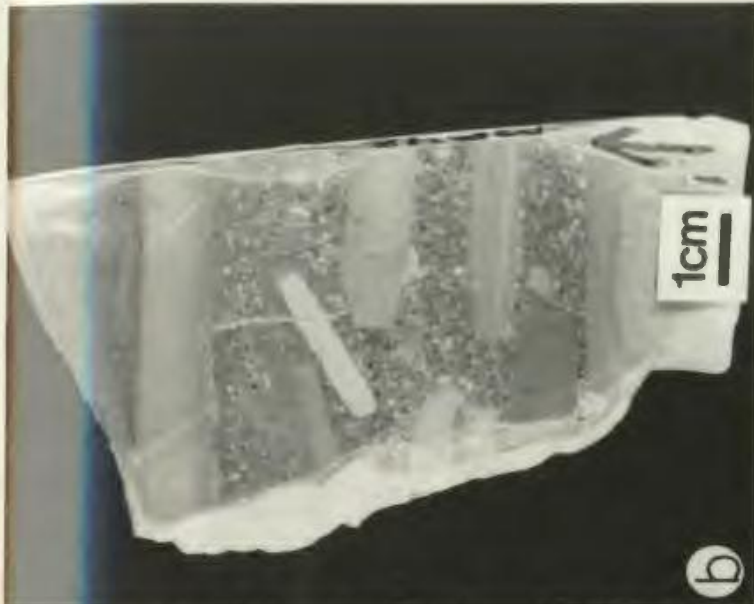


PLATE 4: CALCARENITE LITHOFACIES

- a: Bedding surface view of trough cross-lamination in quartzose grainstone. Paleocurrent is toward southeast (bottom right of photograph). Outline of troughs is enhanced by stylolites, which occasionally cross-cut each other, departing from the primary sedimentary lamination control. Cow Head North, Upper Cambrian, Bed 6.
- b: Arrow points to upside down T_{bc} sequence in peloidal siltstone (details not visible in photo) which is eroded and overturned by mega-rippled grainstone. Stratigraphic top is up. Broom Point North, Upper Cambrian, unit 22.
- c: Channelled pebbly grainstone scours and incorporates as pebble-size intraclasts underlying dolomitic siltstone and shale. Arrows point to base of channel. Scale card in 15 cm across. Stratigraphic top is up. Cow Head North, Upper Cambrian, Bed 6.20.
- d: This lenticular calcarenite is slightly graded and has parasitic ripples on its surface, some of which were subsequently scoured. Scale card in 15 cm across. Stratigraphic top is upper right of photo. Cow Head North, Upper Cambrian, Bed 6.20.



PLATE 5: SILTSTONE LITHOFACIES - SHALE LITHOFACIES

- a: A typical siltstone lithofacies interval in which sediments are mostly planar-bedded siltstones characterized by T_{oc} divisions, abundant sole marks and basal ichnofauna, and interbedded green shales. Scale card is 15 cm long. Stratigraphic top is toward left. Green Point, Upper Cambrian, unit 5.
- b: Resistant-weathering, parallel- and ripple-laminated dolomitic siltstones interbedded with recessive red shales. Stratigraphic top is up. St. Paul's North, Middle Ordovician, units 83-84.
- c: Interbedded green (light in photo) and black (dark) shales. Each of these broad 10-30 cm-thick bands is further subdivided into centimetre- to millimetre-scale alternating black and green laminations (arrows). Stratigraphic top is to lower left of photo (overturned section). Green Point, Lower Ordovician, unit 29.
- d: Numerous completely dolomitized siltstone-shale couplets (indicated in black ink) in which the dolomitized shales are as resistant as the dolomitic siltstones. Stratigraphic top is toward right of photo. Cow Head North, Upper Cambrian, Bed 6.
- e: Siltstone sole showing defect-initiated scours. These sediments occur within a red and green shale sequence. A few horizontal traces cross the scour trend. Scours indicate a southeastward paleocurrent (upper right of photo). Knife scale is 9 cm long. Green Point, Lower Ordovician, unit 35.

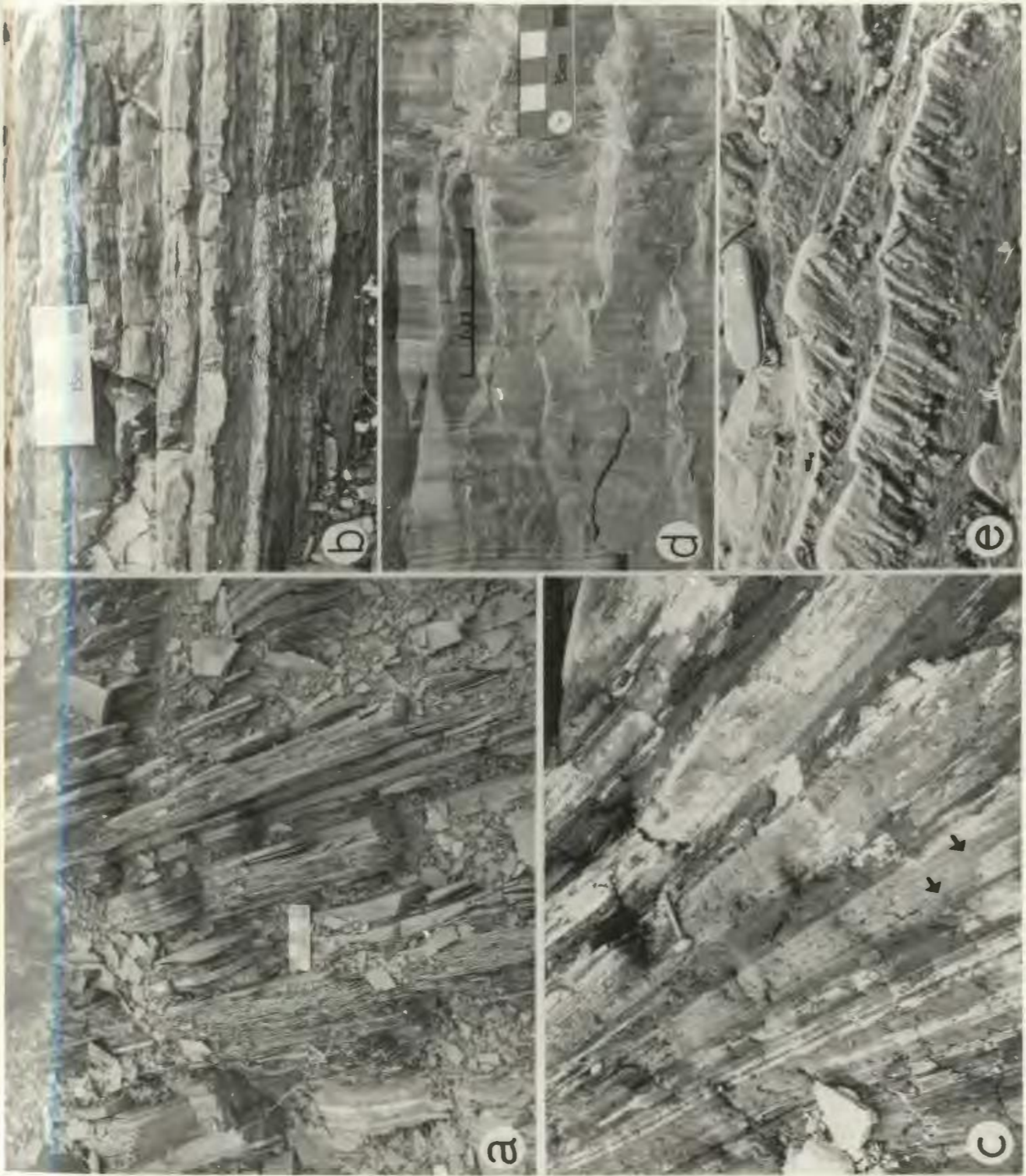


PLATE 6: SILTSTONE LITHOFACIES - SHALE LITHOFACIES

- a: Slab of dolomitic siltstone stringer in red shale sequence. Numerous coarse sand- to granule-size clasts of phosphate and chert are scattered throughout the bed. The dominantly massive lower portion of the bed is overlain by a division of graded laminations and a discontinuous siltstone stringer. Compacted burrows (arrows) are found in the upper portion of the sample. Stratigraphic top is up. Green Point, Lower Ordovician, units 47-49, sample GP-96-B.
- b: Slab of parallel-laminated siltstone overlain by convoluted laminations of siltstone and shale and finally capped by massive shale. The sediment is completely dolomitized. Stratigraphic top is up. St. Paul's North, Lower Ordovician, unit 12, sample SPN-30.
- c: Slab of dolomitic silt-shale couplets. Sequence A illustrates basal scour and upward gradation into fading ripples (arrows) which pass laterally into muddy (shale) troughs; this is overlain by shale. Sequence B shows a massive loaded basal division overlain by a division of graded laminations and then shale. Sequence C has a distorted massive basal division of fine sandstone which grades rapidly upward to siltstone with fading ripples (arrow). Sequence D shows parallel-laminated siltstone followed by graded laminations and then shale. Stratigraphic top is up. Cow Head North, Upper Cambrian, Bed 6, sample CHN-161.
- d: Slab of isolated, dolomitic siltstone ripples, graded laminations and grey-green shale. Stratigraphic top is up. Cow Head South, Shoal Cove, Lower Ordovician, Bed 11s.2, sample CHS-41.
- e: Thin section negative print of mud turbidite which demonstrates numerous graded dolomitic siltstone-shale couplets. In this negative print, as in all others which follow, the light and dark areas are opposite to the rock colours. Sequences A and F illustrate fading ripples which grade upward into a division of graded laminations, which in turn passes upward into massive shale. Sequence F also demonstrates basal loading. Sequences C and D show graded laminations which pass upward into massive shale. B and E consist of very finely laminated (100 μ m-scale) particle-foliated shale. Scale bar is 5 mm. Stratigraphic top is up. St. Paul's Quarry, Upper Cambrian, sample SPQ-2.

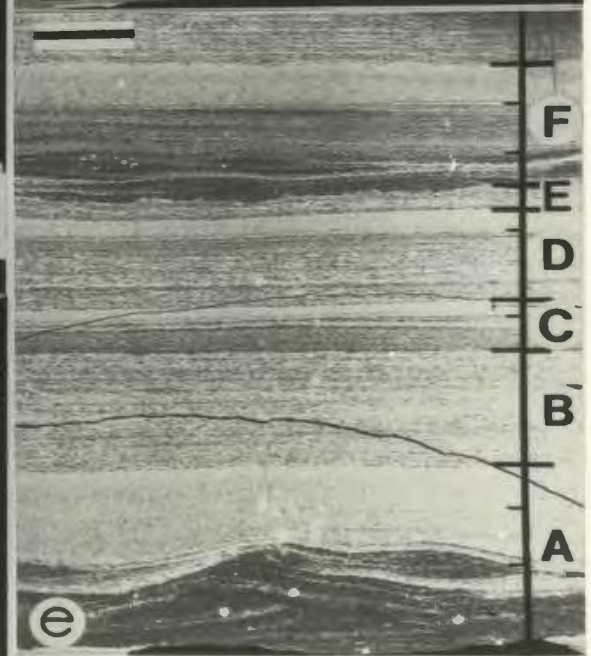
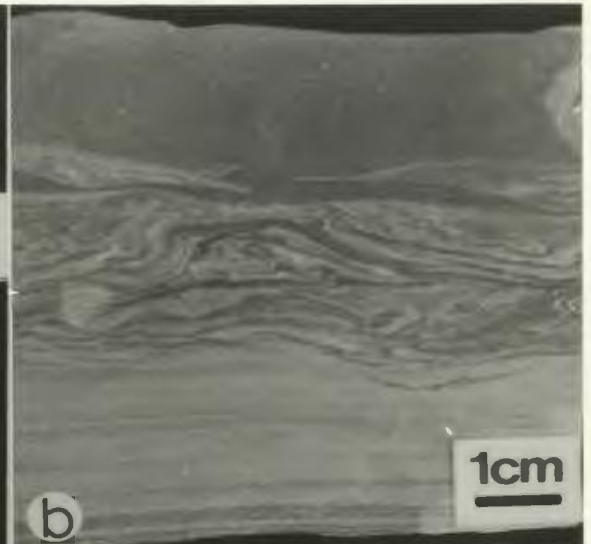
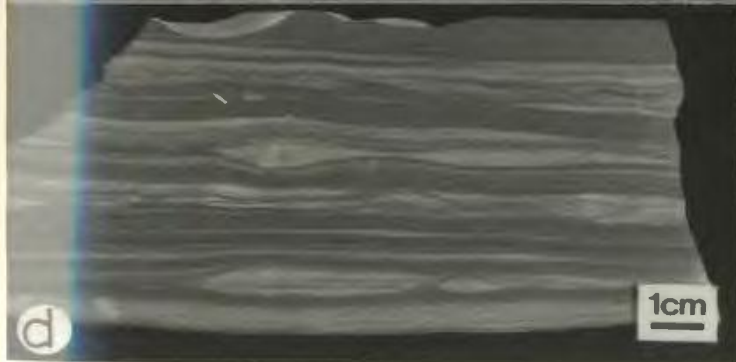
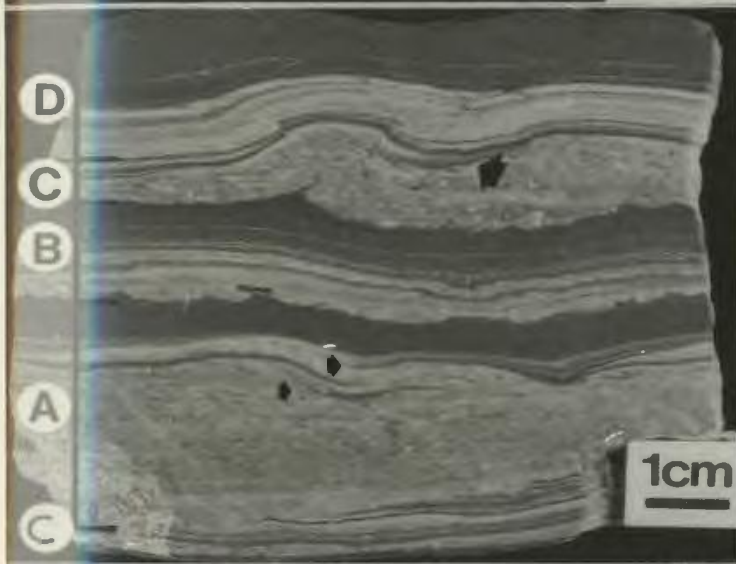
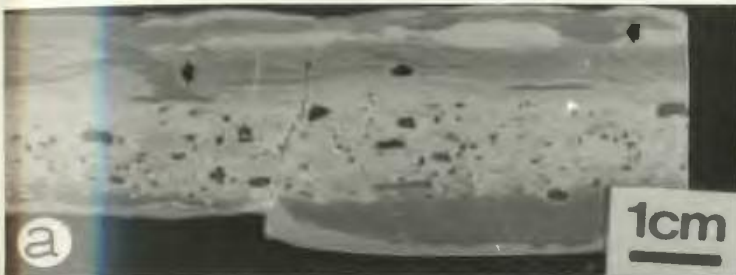
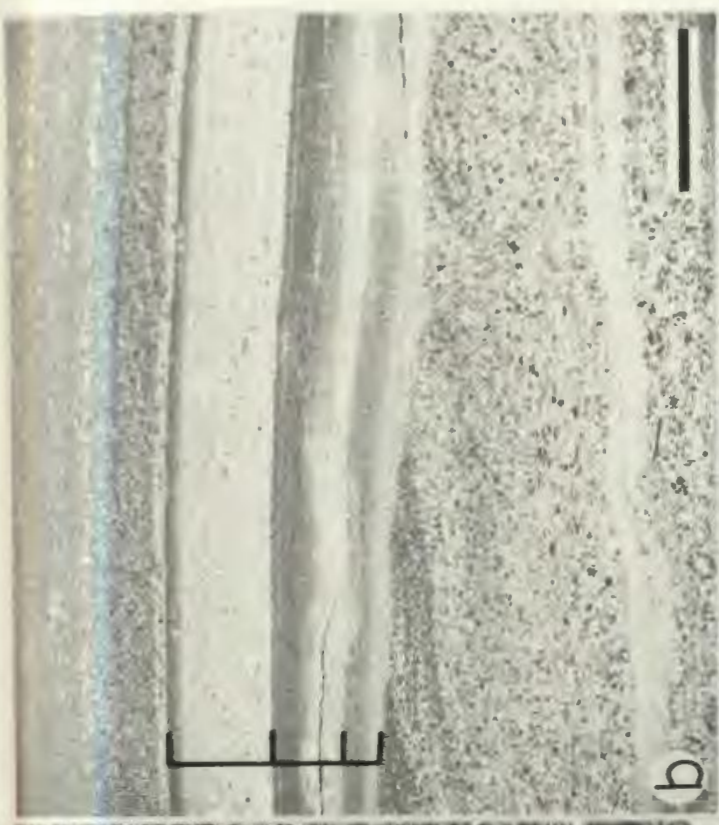


PLATE 7: SILTSTONE LITHOFACIES - SHALE LITHOFACIES

- a: Thin section microphotograph in plane light of particle-foliated shale showing numerous black, elongate particles, scattered compacted shale intraclasts (light-coloured spindle shapes) and radiolaria replaced by ferroan calcite (round light-coloured particles). Scale bar is 500 μ m. Stratigraphic top is up. Green Point, Lower Ordovician, unit 30, sample GP-78.
- b: Thin section negative print of 3 graded mud (shale) layers which abruptly overlie a very fine sand- to silt-size rippled peloidal and dolomitic grainstone. Each graded mud layer consists of a lower particle-foliated shale (light shade in photo) which passes transitionally upward, to massive shale (dark in photo). The graded layers are overlain by a faintly-laminated silty shale. Scale bar is 5 mm. Stratigraphic top is up. St. Paul's North, Lower Ordovician, unit 63, sample SPN-59.
- c: Thin section microphotograph of "shale" which consists dominantly of compacted shale intraclasts (light-coloured, irregular spindle shapes) and dispersed silt- and very fine sand-size peloids and dolomitic silt. Scale bar is 500 μ m. Stratigraphic top is up. Martin Point, Lower Ordovician, unit 42b, sample MP-98.
- d: Slab showing tension cracks in finely laminated green (dominant) and black shale. The cracks are compacted and are filled with ferroan calcite cement. These cracks could be the result of either synaeresis or down-slope creep. St. Paul's Quarry, Upper Cambrian, sample SPQ-8.



a

b

c

d

PLATE 8: SILTSTONE LITHOFACIES - SHALE LITHOFACIES

- a: Slab of burrowed dolomitic siltstone stringers (light-coloured) and red shale (dark). Branching burrow (arrow) is Chondrites. Scale bar is 2 cm. Stratigraphic top is up. Martin Point, Middle Ordovician, unit 58, sample MP-84.
- b: Thin section negative print of faecal pellet-filled Syncoprulus burrow (identified by G. Narbonne, 1984) in siltstone from red shale sequence. Sediment consists mostly of 5-15 μm -size dolomite crystals with intercrystalline microquartz. Scale bar is 5 mm. Stratigraphic top is up. St. Paul's North, Middle Ordovician, unit 82, sample SPN-2.
- c: Thin section negative print of faecal pellet-lined Cylindrichnus(?) burrow in siltstone from red shale sequence. Sediment consists of 10-25 μm -size dolomite crystals. Scale bar is 2.5 mm. Stratigraphic top is up. Western Brook Pond North, Lower Ordovician, unit 24, sample WN-11.
- d: Thin section negative print of highly disrupted siltstone stringers (dark) and shale (light grey). This sediment is entirely dolomite. Indeterminate bioturbation, such as illustrated in this photo, characterizes the prominent tan weathering dolomitic beds in Bed 11 at Cow Head North and South. Scale bar is 1 cm. Stratigraphic top is up. Cow Head South, Lower Ordovician, Bed 11s.16, sample 80-11s.16.
- e: Thin section negative print of silicified green shale with uncompact burrows. Most of this sediment consists of equant microquartz with minor chalcedony in burrows. Numerous radiolaria and sponge spicules are scattered throughout this sediment (arrows). Scale bar is 5 mm. Stratigraphic top is up. Western Brook Pond North, Lower Ordovician, unit 19, sample WN-10.

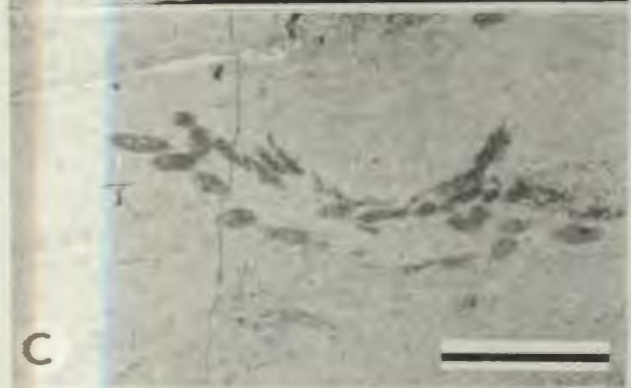
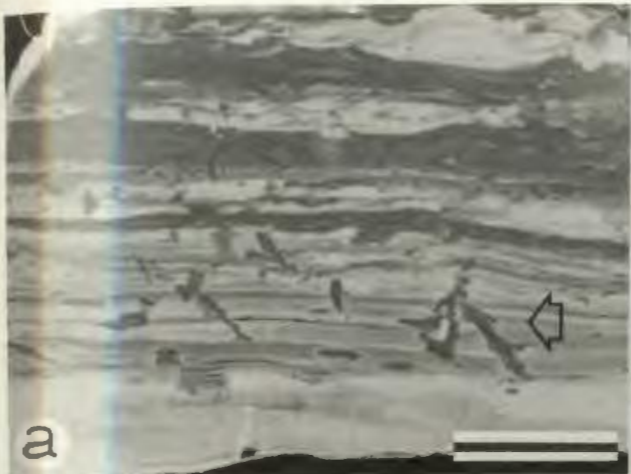


PLATE 9: MUDSTONE LITHOFACIES

- a: Ribbon limestone sequence (Type 1) consists mainly of continuously-bedded, planar mudstones. This outcrop is further described in Appendix A. Knapsack (arrow) for scale. Stratigraphic top is to upper right of photo. Cow Head North, Lower Ordovician, Bed 9.15-17.
- b: Ribbon limestone (Type 1) consisting of mudstone and minor grainstone passes gradationally upward into an overlying shale interval through an intermediate 1 m-thick nodular transition zone (located just above the 30-cm long metal clip-board scale). These nodules consist of rippled grainstone cores surrounded by mudstone envelopes. Stratigraphic top is to upper right of photo. Martin Point, Upper Cambrian, unit 36h-i.
- c: Planar-bedded parted mudstone (Type 2) has light-coloured, siliceous rinds on bed tops and bottoms. This outcrop is further described in Appendix A. Hammer head points to stratigraphic top. Cow Head North, Lower Ordovician, Bed 9.6.
- d: Thin ribbon mudstone packages (Type 3) up to 30 cm thick are interbedded with green and black shales of comparable thickness. Note continuity of bedding and slight tectonic flexure in the bedding (arrow). This outcrop is further described in Appendix A. Hammer head points to stratigraphic top. Green Point; Lower Ordovician, units 31-33.

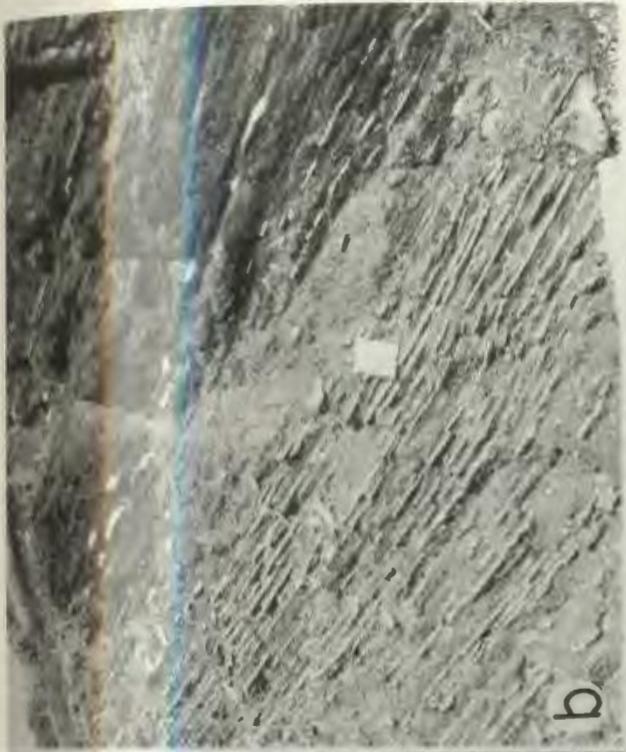


PLATE 10: MUDSTONE LITHOFACIES

- a: Planar and wavy mudstones (Type 2) with fitted fabric preserve overall sediment package thickness. Knife scale is 9 cm long. This outcrop is further described in Appendix A. Stratigraphic top is up. Green Point, Lower Ordovician, unit 28.
- b: Close-up of interbedded mudstones (M), grainstones (G), and calcareous marls (S) in a parted limestone sequence. Grainstones are considerably more lenticular and wavy-bedded than associated mudstones. Stratigraphic top is up. Cow Head North, Upper Cambrian, Bed 6.52-54.
- c: Bedding-plane view of sinuously-crested ripples which preserve steep lee (to left) and gentle stoss (to right) form. Paleocurrent direction is 152 degrees to the southeast. Martin Point, Upper Cambrian, unit 23d.
- d: Bedding-plane view of modified ripples. Paleocurrent direction is to the southeast and is pointed to by hammer handle. Cerebral weathering pattern is interpreted to be the result of bioturbation. St. Paul's South, Lower Ordovician, unit 1.
- e: Finely laminated mudstones (wide, light grey beds) grade into black marls (dark grey) which in turn grade into green (medium grey) marls. Repetition of black-green laminations within marl interbeds (arrow) demonstrates that the green to black transition is usually abrupt in contrast to the transitional black to green contact. This outcrop is further described in Appendix A. Knife scale is 9 cm long. Stratigraphic top is up. Green Point, Lower Ordovician, unit 30.

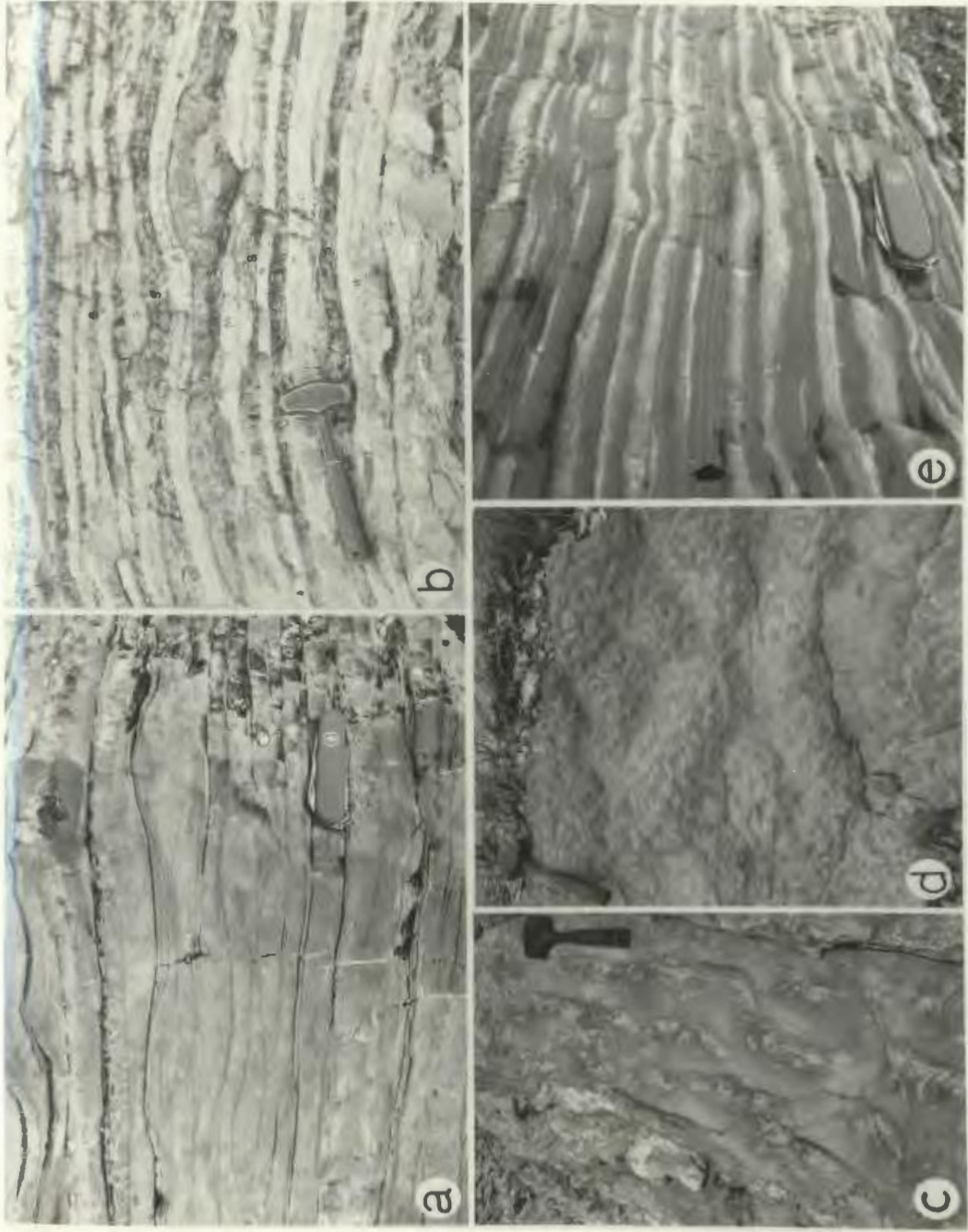


PLATE 11: TRACE FOSSILS IN MUDSTONE LITHOFACIES

- a: Planolites on the sole of a mudstone within large raft of parted limestone in conglomerate. Knife scale is 9 cm long. Cow Head North, Upper Cambrian, Bed 3.
- b: Slab of parted microspar mudstone showing grainstone-filled Skolithos burrows, one of which extends through the argillaceous parting. In mudstone portions of the slab, burrows are uncompacted. In the shaly parting, compaction is obvious. A close-up view of these relationships is shown in the next microphotograph. The scattered dark specks are loose aggregates of micrometre-size pyrite crystals. Stratigraphic top is up. Lower Head, Lower Ordovician, sample LH-53.
- c: Thin section negative print of burrowed mudstone and shaly parting shown in previous photograph. These are not Diplocraterion but instead are single Skolithos tubes which were filled at different times with different sediments comprising peloids, intraclasts, and bioclasts. In the shaly parting, most of the grains are squashed together and not clearly recognizable, except for a few thin trilobite shell fragments which have small syntaxial calcite fringes. Evenly-spaced "ladder cracks" (arrows) break up the burrow on the right. Scale bar is 5 mm. Stratigraphic top is up. Lower Head, Lower Ordovician, sample LH-53.
- d: Slab of microspar mudstone containing uncompacted, peloidal grainstone- and mudstone-filled Skolithos burrows. The largest one in this photograph shows prominent ladder cracks. The dark mottles are loose aggregates of micrometre-size pyrite crystals. Stratigraphic top is up. Broom Point North, Lower Ordovician, unit 100, sample BPN-35.
- e: Slab of mottled microspar mudstone shows one bed which pinches out into a finely-laminated, argillaceous parting. The pinch-out may be the result of syndimentary shear as this sample was collected from a shear zone. The mottled pattern is interpreted to be due to bioturbation. Stratigraphic top is up. Broom Point North, Lower Ordovician, unit 96, sample BPN-37.

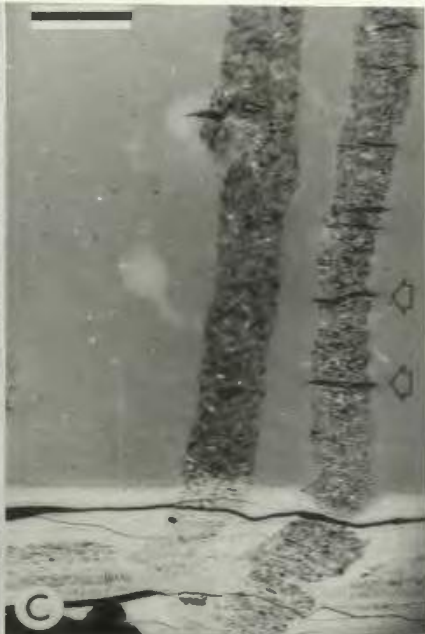


PLATE 12: NODULES IN MUDSTONE LITHOFACIES

- a: Thin section negative print of irregularly-shaped, centimetre-size mottles of peloidal grainstone to wackestone ("chaotic nodules"). The internodular matrix consists mainly of squashed peloids, indistinct micritic patches and varying amounts of argillaceous sediment. Scale bar is 1 cm. Stratigraphic top is up. Broom Point South, Lower Ordovician, unit 65, sample BPS-11-B.
- b: Detrital nodule in parted mudstone sequence demonstrates laminations oriented at high angle to bedding. This nodule consists of finely-laminated, siliciclastic-rich, silicified shale. Stratigraphic top is up. Lower Head, Lower Ordovician.
- c: Mudstone nodules extracted from grey and green shales demonstrate equant, rounded shapes. Black marker lines on each nodule indicate strike orientation. Nodules include both mudstone and cored types. These nodules were measured to evaluate the "syndimentary boudin" Hypothesis of Hubert *et al.* (1977). Further details are provided in Appendix M. Green Point, Upper Cambrian.
- d: Metre-length mudstone to peloidal packstone nodules in ribbon to parted limestone sequence are evenly spaced and surrounded by dolomitic marl. Stratigraphic top is to right. Green Point, Lower Ordovician, units 26-27.
- e: Septarian cracks in mudstone nodule are partially-filled with calcite cement. Knife scale is 9 cm long. Float from Green Point, Upper Cambrian.
- f: Nodular limestones separated by dolomitic marl consist of a core of rippled grainstone enveloped by homogeneous mudstone. The continuous, composite bed at the level of the hammer head shows mudstone "caked" both below and above the rippled grainstone. Both continuous and nodular beds are of comparable thickness. Stratigraphic top is up. Broom Point North, Upper Cambrian, unit 24.

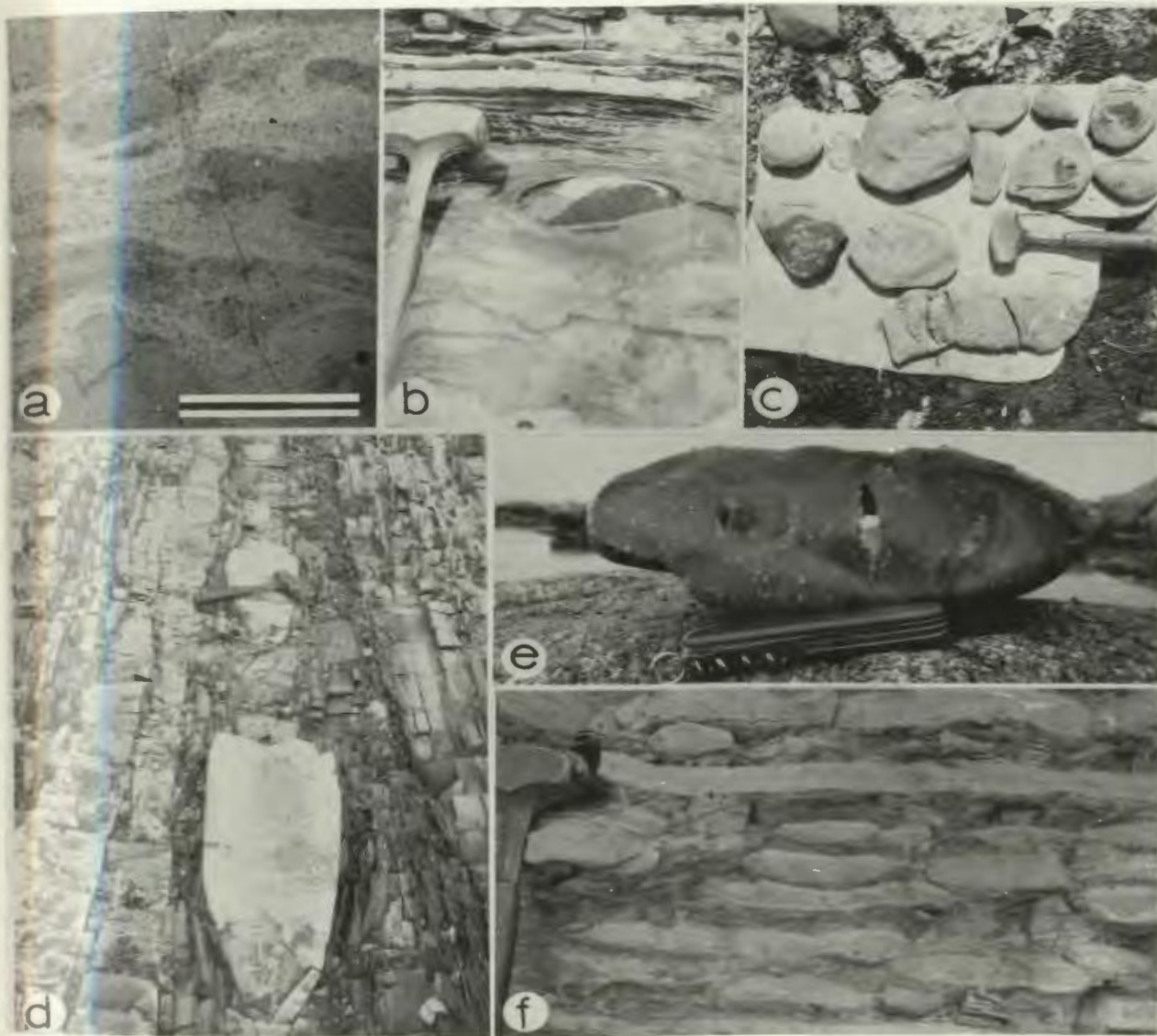


PLATE 13: NODULES IN MUDSTONE LITHOFACIES

- a: Slab of mudstone nodule demonstrates a rippled, peloidal grainstone core. The lower grainstone is deformed due to loading whereas the thinner, upper grainstone shows ripple forms. In the upper part of the nodule, the discontinuity pointed to by the large arrow marks an abrupt transition from microspar (below) to pseudospar (above). In the lower grainstone, the top of the bed is also characterized by faded ripples (small arrow). Stratigraphic top is up. Martin Point, Upper Cambrian, unit 36f, sample MP-12.
- b: Slab of nodular limestone shows mudstone envelopes (M) which surround discontinuous, horizontal laminations of pyrite (P), which may be replacement of horizontal burrows. Partial pyritization also occurs in parallel-laminated grainstone (G) and massive grainstone (H). Stratigraphic top is up. Western Brook Pond North, Lower Ordovician, unit 3, sample WN-3.
- c: Slab of nodular limestone bed consists of vertically-oriented mudstone nodules many of which are developed around grainstone-filled vertical burrows (arrows). This bed is slightly tectonized and some nodules are in stylolitic contact. Stratigraphic top is up. St. Paul's North, Lower Ordovician, unit 50, sample SPN-71.
- d: Thin section negative print of mudstone- and spar-filled (grey and black in photograph, respectively) burrows surrounded by mudstone (M) envelopes. The sub-vertical orientation of these nodules is clearly controlled by burrows. Internodular areas vary from carbonate-free shale (S) to slightly argillaceous mudstone which grades imperceptibly into the nodular mudstone (area around "X" in photograph). Scale bar is 1 cm. Stratigraphic top is up. St. Paul's South, Lower Ordovician, unit 1, sample SPS-10.
- e: This thin section negative print shows part of a cross-shaped mudstone nodule (M) developed around the intersection of a thin peloidal grainstone dike (D) and a thin peloidal-siliciclastic silt lamination (L). The surrounding shale (S) is mostly massive. A V-shaped fracture developed in the mudstone surrounding the lamination is partially filled with polycrystalline, non-ferroan, calcite pseudomorphs after barite(?) (arrow). The irregular white lines near the dike are clay accumulations of a vertical stylolite, cut obliquely in this thin section. Scale bar is 1 cm. Stratigraphic top is to top right of photograph. Broom Point South, Upper Cambrian, unit 42, sample BPS-25.
- f: Thin grainstone dike (arrow) encased in mudstone is found in a ~~nodular and continuously-bedded~~ ribbon mudstone sequence. Penny for scale. Stratigraphic top is up. Martin Point, Lower Ordovician, unit 36s-v.

continued on next page

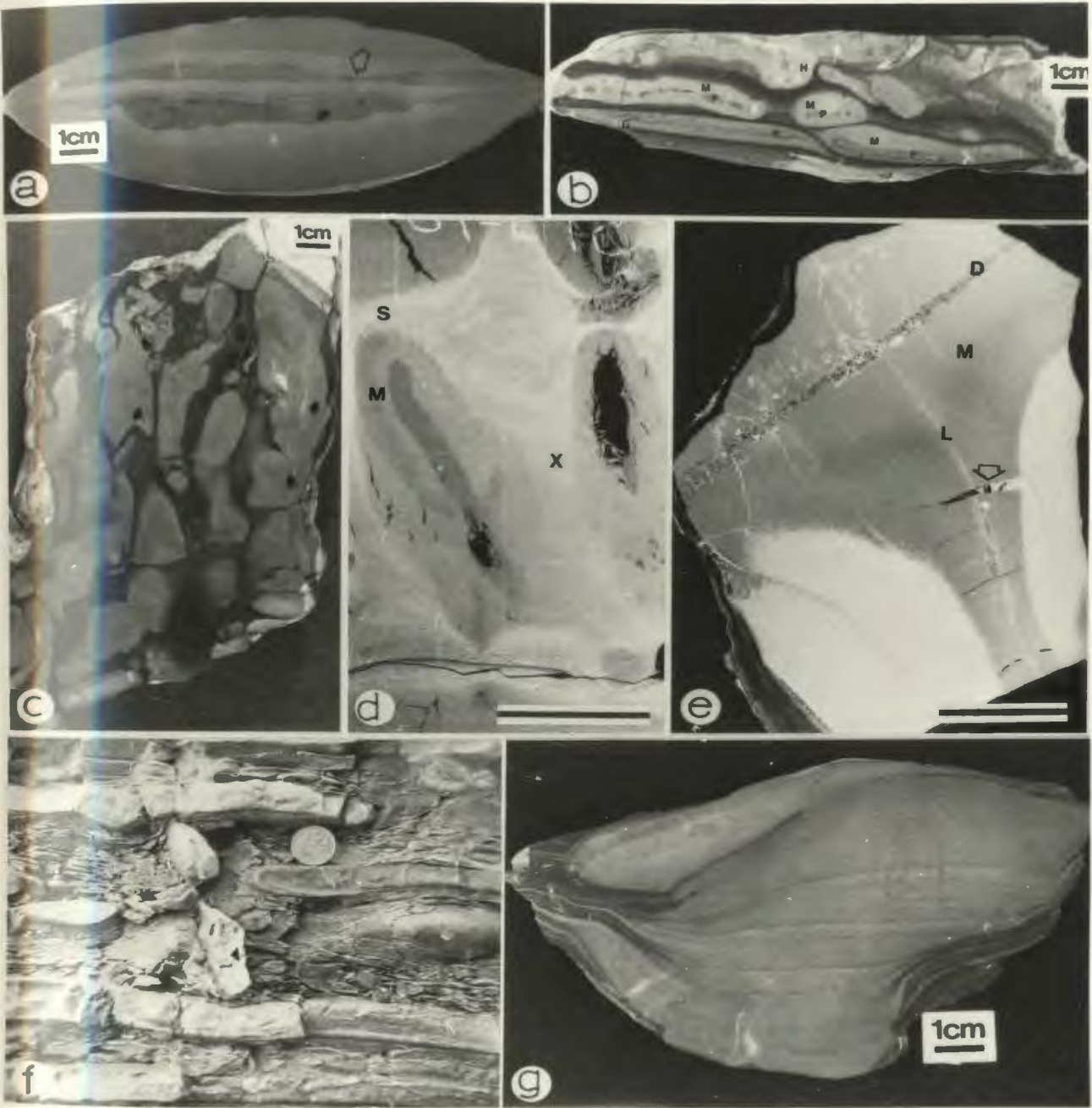


PLATE 13 (continued)

g: Slab of composite mudstone nodule from a ribbon limestone sequence demonstrates peloidal grainstone "tails" which extend into the surrounding argillaceous matrix. Stratigraphic top is up. Cow Head North, Lower Ordovician, Bed 9.15, sample CHN-47.

11

PLATE 14: LOWER HEAD TRUNCATION SURFACE

- a: Trace of the Lower Head truncation surface is outlined. A close up of the rotated mudstone slabs visible in centre of photograph is shown in "b". Stratigraphic top is to upper right.
- b: Fragmented, and sub-parallel aligned mudstone slabs are found in ribbon limestone bed 4 in Figure 3.1a. Stratigraphic top is up.
- c: A cluster of fragmented mudstone beds is found in ribbon limestone bed 6 in Figure 3.1a. Stratigraphic top is up.
- d: This vertically-oriented mudstone slab in the ribbon limestone of bed 6 in Figure 3.1a demonstrates drape of finely-laminated marls and mudstone beds. This illustrates that bed fragmentation and rotation of the slab occurred in uncompacted sediment - a syndimentary rather than tectonic disruption. Stratigraphic top is up.
- e: This small pod of mudstone clasts is located approximately 1 m below the truncation surface. The origin of the fragmentation and piling-up of the clasts is intrastratal shear associated with formation of the truncation surface. Pocket knife scale is 9 cm long. Stratigraphic top is up.
- f: Small domains of re-oriented laminations, often at high angle or vertical to bedding, are found in finely-laminated marl (bed 5) below the truncation surface. In other places in the marls other small domains appear to have been totally homogenized (not shown in photo). Pocket knife scale is 9 cm long. Stratigraphic top is up.



PLATE 15: TRUNCATION SURFACES

- a: Truncation surface (under hammer butt) in planar-bedded ribbon mudstones is overlain by parted and ribbon grainstones and mudstones. Stratigraphic top is to lower right (section is overturned). Green Point, Lower Ordovician, unit 28 (described in Appendix A).
- b: Prominent drag fold (between hammer and lower arrow) immediately underlies the truncation surface (pointed to by arrows). Stratigraphic top is to lower left (section is overturned). Green Point, Lower Ordovician, unit 28.
- c: Irregular, discontinuously bedded mudstone is particularly abundant in the immediate vicinity of the prominent drag fold illustrated in Figure 3.1b. Stratigraphic top is to left. Green Point, Lower Ordovician, unit 28.
- d: Truncation surface depression in parted mudstones is overlain by similar sediments. Shear zone deformation is apparently not developed in this case. The lack of discordance with overlying beds indicates that this is a truncation surface rather than a subsurficial shear. Scale card at centre of photograph is 15 cm long. Stratigraphic top is up. Outcrop is north of the Martin Point section.

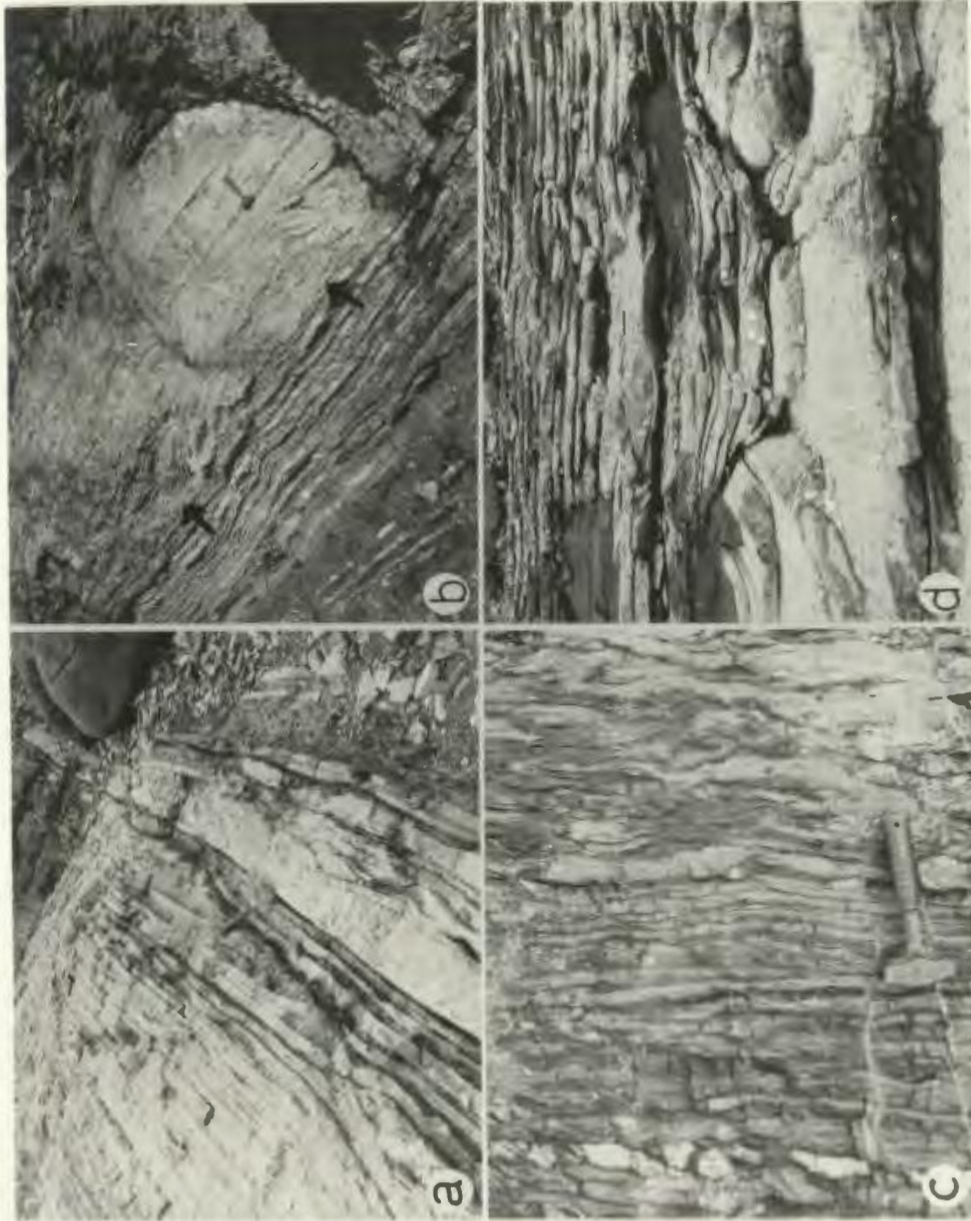


PLATE 16: SLIDE MASSES AND RELATED DEFORMATION

- a: This slide mass consists of burrowed mudstone with domains of both homogenized and chaotic bedding. Obvious basal scour of underlying argillaceous sediments and lateral pinch-out indicate that this is a slide mass. This particular slide mass was previously interpreted as a small massive algal mound by Cumming (1973, v.2, p. 50). Stratigraphic top is to left. Green Point, Lower Ordovician, unit 27.
- b: Slide mass is indicated by black lines. Both slide mass and underlying sediments are grainstones. Overlying conglomerate shows well-developed normal size-grading (see Plate 1c). Knapsack scale rests near top of slide mass. Stratigraphic top is up. Cow Head South, Middle Ordovician, Bed 13s.4.
- c: Detail of basal shear zone of slide mass in "b". Truncation surface is seen at the level of the "p" in the trade name "Evergrip" on hammer handle. In the overlying slide mass, anastomosing irregular partings diminish in intensity away from base of the slide mass and bedding becomes more regular. Stratigraphic top is up. Cow Head South, Middle Ordovician, Bed 13s.4.
- d: The mudstones in this outcrop are characterized by irregular, anastomosing partings which resemble those of "c". This outcrop is almost entirely contained within this photograph and this restricted exposure does not provide sufficient information to differentiate between a slide mass or subsurficial shear zone origin. The anastomosing partings indicate that the sediment is sheared and therefore a channel-fill origin is unlikely. Stratigraphic top is up. Western Brook Pond South, Lower Ordovician, unit 5.

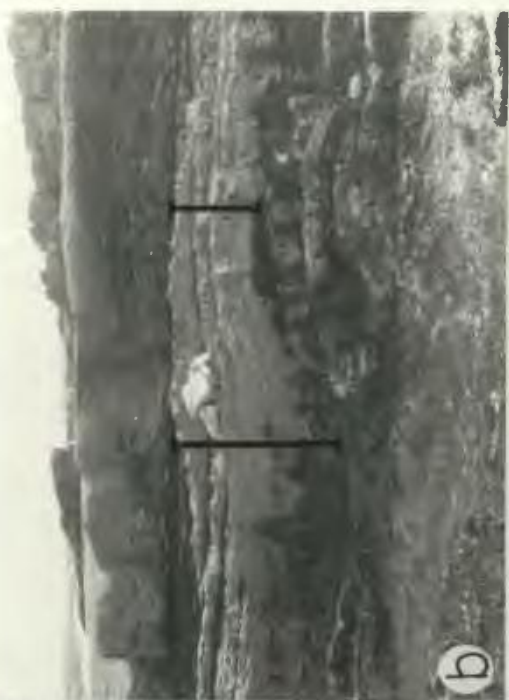
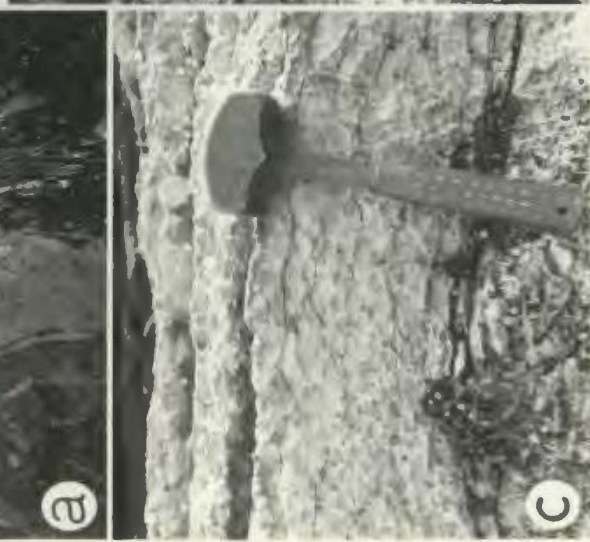


PLATE 17: SUBSURFICIAL SHEAR ZONES

- a: Thirty centimetre-thick shear zone contains fragmented, folded mudstones (light grey) in a marl matrix (dark grey). Apparent thinning and thickening of the mudstones is an artifact of the two dimensional outcrop. Planar bedded, undisturbed, mudstones occur on both sides of the shear zone. Stratigraphic top is up. Green Point, Lower Ordovician, unit 28.
- b: Folded and fragmented mudstones and grainstones are chaotically distributed and oriented in a subsurficial shear zone which is approximately 50 cm thick in the area photographed. Such rare three dimensional outcrops strongly suggest caution in attempting to derive quantitative results from measurements of two dimensional outcrops. Hammer butt rests on top of shear zone. Stratigraphic top is up. Cow Head North, Upper Cambrian, Bed 6.37-6.44.
- c: Recumbent drag fold in a subsurficial shear zone suggests transport of overlying sediment mass to the northeast (towards left) in this two dimensional outcrop. This photograph clearly illustrates that deformation may be extremely localized, and in much of the shear zone it is not possible to tell whether relative movement of sediment packages has occurred. Hammer butt rests on top of shear zone. Stratigraphic top is up. Cow Head North, Upper Cambrian, Bed 6.37-6.44.
- d: Subsurficial shear zone shows irregular pinching and swelling mudstones with discontinuous argillaceous partings (arrows). Stratigraphic top is up. Broom Point North, Lower Ordovician, unit 96.



PLATE 18: CONTORTED LIMESTONES

- a: Broken, disharmonic, anticlinal folds in ribbon mudstones affect overlying and underlying beds to a minor extent only. Compare these folds with those illustrated in figure 5 of Fisher (1979). Stratigraphic top is up. Cow Head North, Upper Cambrian, Bed 6.
- b: This discontinuously-bedded, 10-centimetre thick interval of contorted parted mudstones demonstrates abrupt upper and lower transitions to unfolded mudstones. A small cavity developed in the fold hinge area (arrow) is filled with blocky calcite. Stratigraphic top is up. Pocket knife scale is 9 cm long. Broom Point South, Upper Cambrian, unit 30.
- c: The most impressively folded and fractured contorted limestones in the CHG are shown in this photograph from Green Point. The view is at the undersurface of the beds. The bed to the right in the photograph has prominent fractures developed in the trough hinge areas (close-up in "d"). The hammer scale rests on a more gently folded and unfractured mudstone which also clearly demonstrate elongation of the dome-and-basin forms. Refer to text for additional details on this key outcrop. Green Point, Upper Cambrian, unit 18.
- d: Close-up of the contorted and fractured bed shown in "c". The fractures occur in the synclinal hinge areas of the bed and are most prominently developed in a trend going from the lower left to the upper right of the photograph. This northeast-southwest trend is parallel to several other major and minor structural features in the CHG. See text for details. Green Point, Upper Cambrian, unit 18.

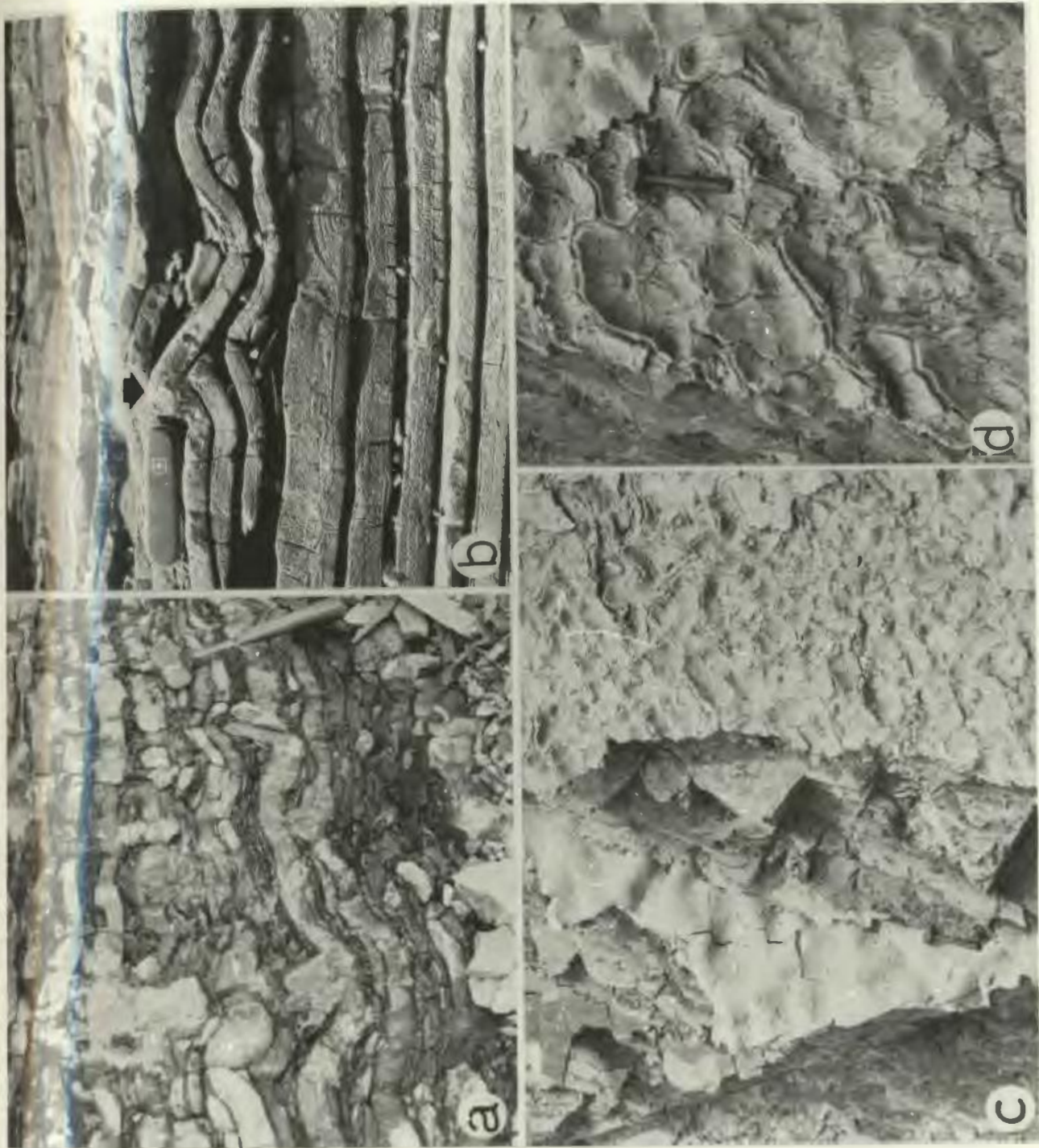


PLATE 19: CONTORTED LIMESTONES

- a: This 1-cm thick ribbon mudstone bed is undeformed over most of its length; it is only locally folded and fractured. Other beds in the photograph are undeformed. Stratigraphic top is up. Green Point, Upper Cambrian, wave-cut platform.
- b: A contorted mudstone which directly underlies a conglomerate is locally infolded into its base (arrow). See text for additional details. The folds gradually dissipate downward within a finely-laminated dolomitic marl. Stratigraphic top is up. Martin Point, Upper Cambrian, unit 8; overlying conglomerate is unit 9.
- c: This exceptional contorted mudstone demonstrates possible ponding of sediments in troughs (arrows) initially suggesting a surficial origin for at least some of the contorted limestones. Petrography does not bear this out, however. See text for additional details. Stratigraphic top is up. Green Point, Upper Cambrian, unit 18, wave-cut platform.
- d: Folds such as those shown in this photograph, which are harmonically folded and have chevron or box geometries and well-defined axial planes extending for a metre or more, are interpreted to be of tectonic origin. Folds intermediate in character to these and contorted limestones are common. Stratigraphic top is to lower right. Green Point, Lower Ordovician, units 31-33.

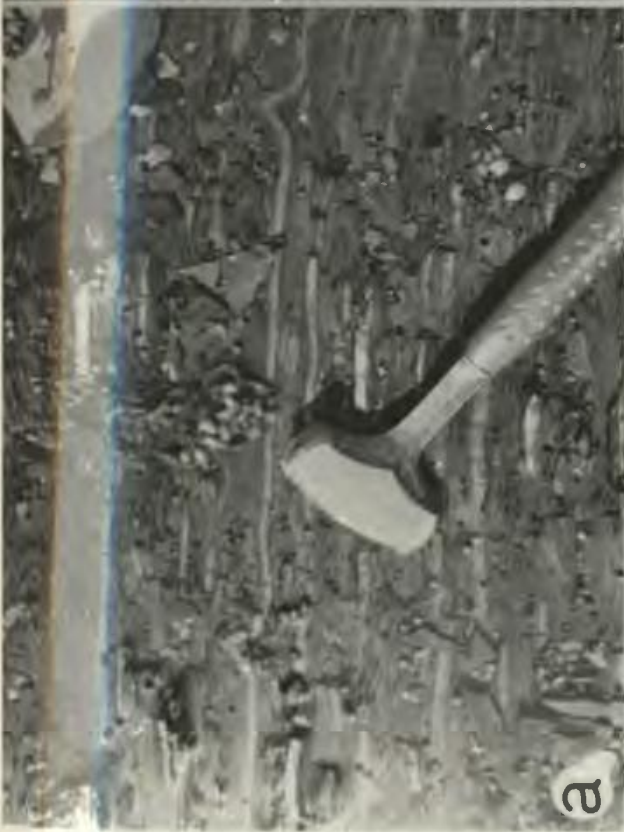


PLATE 20: VOIDS IN FOLD NOSES

- a: Thin section negative print of cavity developed in anticlinal fold nose which contains mostly ferroan, coarse calcite crystals (C) up to 1 cm in size. Endobreccia fragments (B) and surrounding silt-size peloids (not resolvable in this photograph) are found at the base of the cavity. Minor barite (black in photo) precedes calcite precipitation in associated veinlet (arrow). Scale bar is 1 cm. Stratigraphic top is up. Green Point, Upper Cambrian, unit 18, sample GP-9-A,B.
- b: Thin section negative print of cemented mosaic breccia ("B"; sensu Morrow, 1982c) overlies a geopetal accumulation of sand- and silt-size peloids (large arrow). Calcite cement (dark grey) is anhedral and iron-zoned. Numerous white specks (small arrow) are subhedral pyrite crystals. Scale bar is 1 cm. Stratigraphic top is up. Green Point, Cambro-Ordovician boundary, unit 23, sample GP-112.

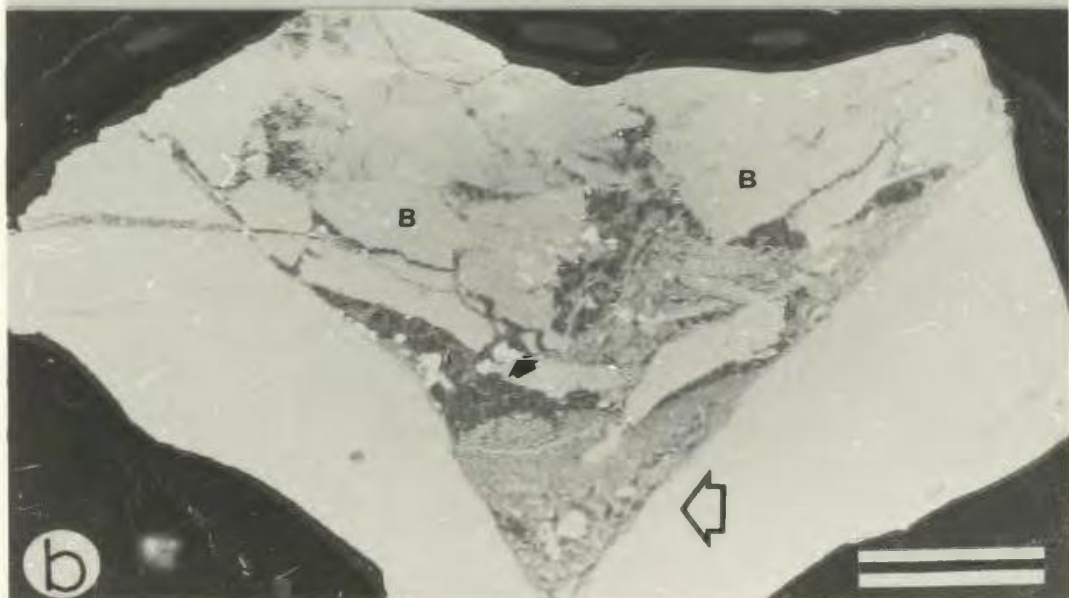
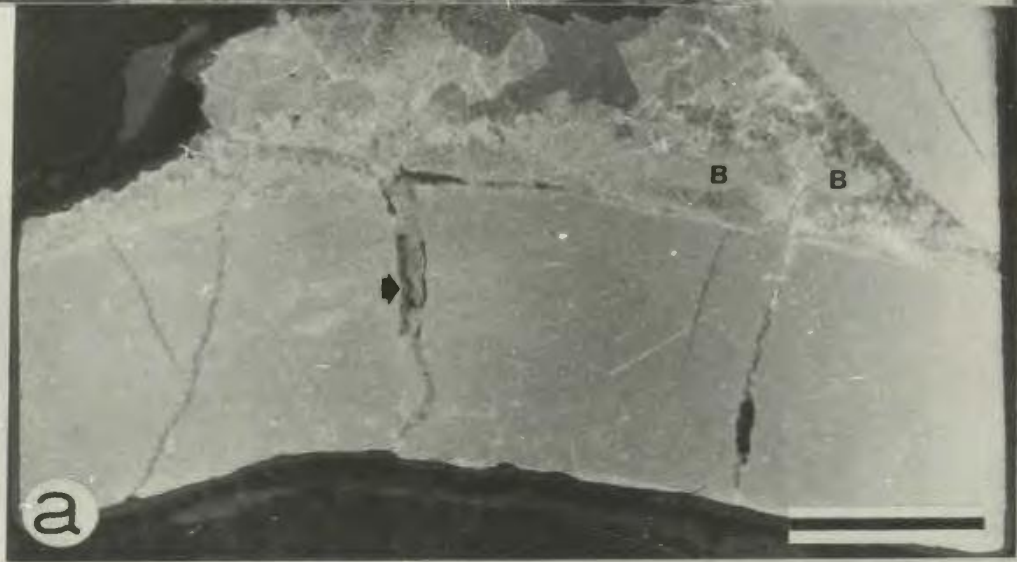


PLATE 21: COMPACTION

- a: Compacted, pebbly grainstone dike in blocky-weathering, slightly calcareous, green shale. Stratigraphic top is up. Martin Point, Lower Ordovician, unit 38a,b.
- b: Thin section microphotograph of a fractured trilobite shell in a peloidal grainstone. Fracturing clearly predates earliest cementation as shown by calcite overgrowing fracture surface (arrow). Scale bar is 500 μ m. Stratigraphic top is up. Green Point, Lower Ordovician, unit 28, sample GP-66.
- c: Thin section microphotograph of a mechanically-compacted, granule-size rudstone composed mainly of phosphatized mudstone(?) and shale(?) intraclasts, cemented by chalcedony. Fractures in grains (arrows) as well as incompletely filled interparticle spaces contain ferroan calcite. Scale bar is 1 mm. Cow Head North, Lower Ordovician, Bed 11.1, sample CHN-56.
- d: Vertical stylolites in parted mudstone sequence appear to be more closely spaced and insoluble-rich than they are actually due to oblique orientation of outcrop. Stylolites are not traceable through argillaceous interbeds. Stratigraphic top is up. Broom Point North, Lower Ordovician, unit 96.
- e: Thin section microphotograph of a vertical stylolite containing mainly siliciclastic silt. Host sediment is a siliciclastic and dolomite-rich peloidal siltstone. Scale bar is 1 mm. Stratigraphic top is up. Broom Point North, Upper Cambrian, unit 20, sample 80-70N-20.
- f: Thin section microphotograph of condensed packing of peloids in grainstone within an outcrop-size tectonic fold. Accumulation of dolomite crystals in upper right ("D") is along a stylolite. Scale bar is 500 μ m. Stratigraphic top is up. Martin Point, Upper Cambrian, units 16-20 (tectonized area), sample MP-31.

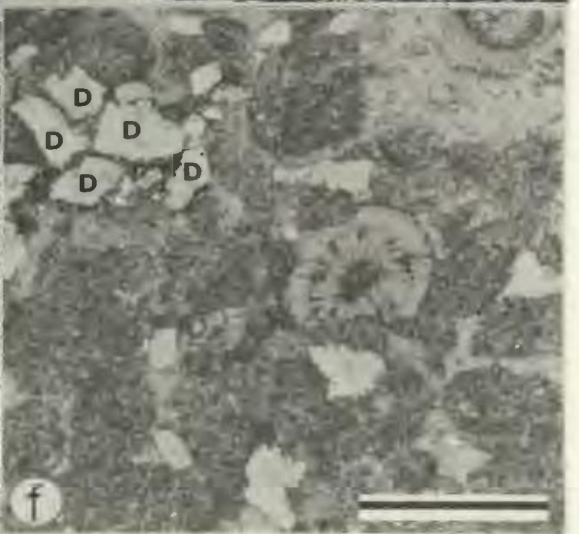
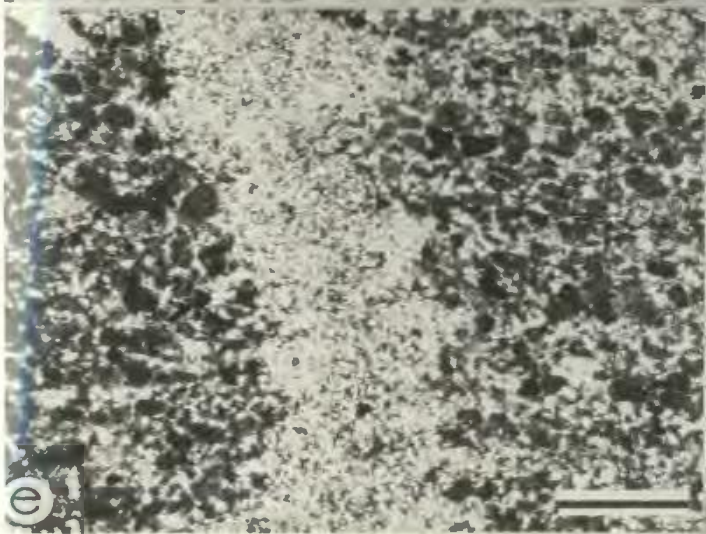
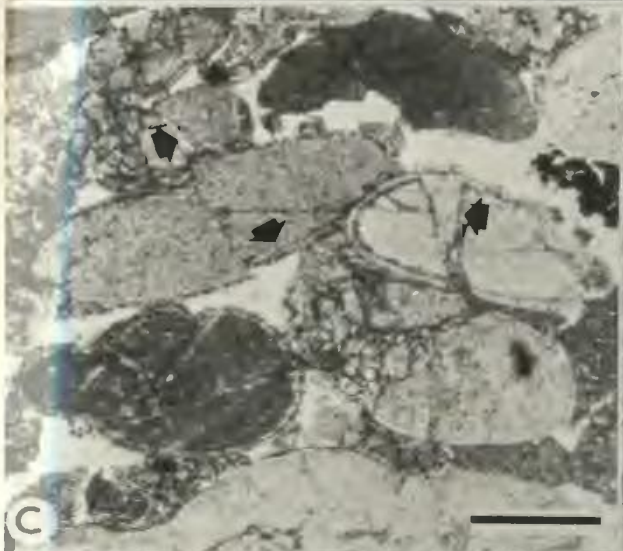


PLATE 22: PELOIDS AND INTRACLASTS

- a: Thin section microphotograph of fine sand-size peloidal grainstone containing minor dispersed dolomite and siliciclastics (quartz and feldspar). Scale bar is 500 μm . Cow Head Peninsula, Tuckers Cove, Upper Cambrian, sample CHN-69.
- b: Thin section microphotograph close-up of homogeneously microcrystalline peloids. Diagenetically-enlarged detrital dolomite (d) is seen in field of view. Sediment is from same thin section as "a" above. Scale bar is 200 μm . Cow Head Peninsula, Tuckers Cove, Upper Cambrian, sample CHN-69.
- c: Thin section microphotograph of grainstone characterized by a bimodal distribution of particles dominated by medium to coarse sand-size fragments of pelmatozoans (p), trilobites (t), Nuia (n), and numerous dense micritic peloids most of which are coarse silt-size. Scale bar is 500 μm . Broom Point, North, Lower Ordovician, units 103-105, sample BPN-22.
- d: Thin section microphotograph of peloidal intraclast - peloid grainstone containing micritic intraclasts ("m", very coarse sand-size), peloidal intraclasts (n), and numerous peloids (unmarked). Micritic intraclasts are differentiated from peloidal intraclasts by their relatively uniform crystal size in contrast to the marked heterogeneity which characterizes peloidal intraclasts. Micritic intraclasts are distinguished from peloids by an arbitrary boundary at 500 μm . Refer to text for discussion. Scale bar is 500 μm . Cow Head North, Cambro-Ordovician boundary, Bed 8, sample 80-8-7.
- e: Thin section microphotograph of peloidal intraclast - peloid grainstone. These peloidal intraclasts demonstrate part of the range of intraclast microfabrics. Intraclast (1) illustrates poorly defined micritic patches or "peloids". In intraclast (2) peloids are more sharply defined within the intraclast which also contains silt-size siliciclastics (white). Intraclasts (3) are unquestionably peloid grainstones. Scale bar is 500 μm . Martin Point, Upper Cambrian, unit 39, sample 80-39-31D.
- f: Thin section microphotograph close-up of faint micritic patches surrounded by microspar (structure grumeleuse) within a peloidal intraclast. Light grey areas are bioclasts ("p" pelmatozoan, "t" trilobite), white areas are siliciclastic silt. Sand-size quartz (q) and angular elongate feldspar (f) are also visible in this microphotograph. Sediment is from same thin section as "a" above. Scale bar is 200 μm . Martin Point, Upper Cambrian, unit 39, sample 80-39-31D.

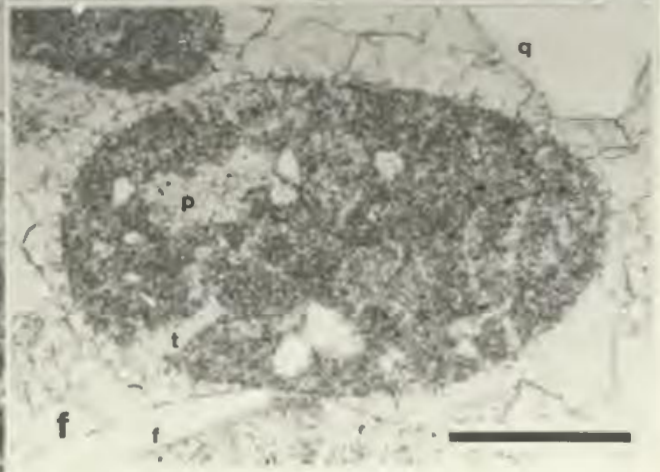
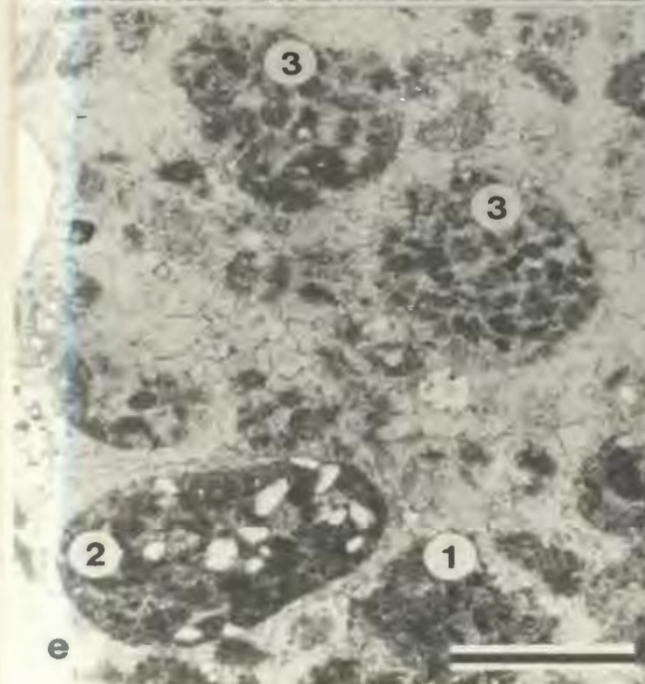
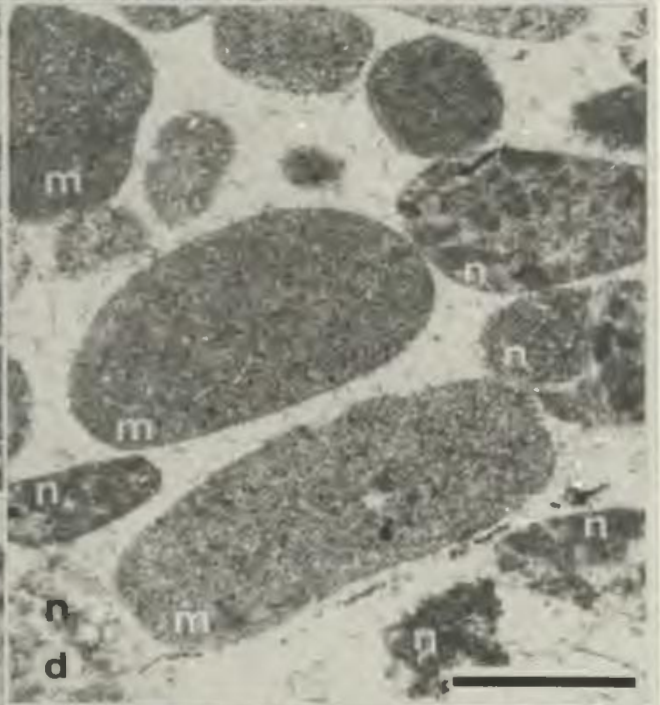
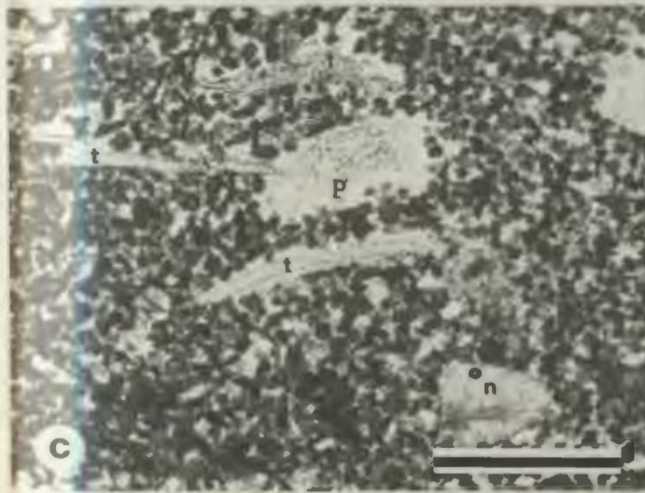
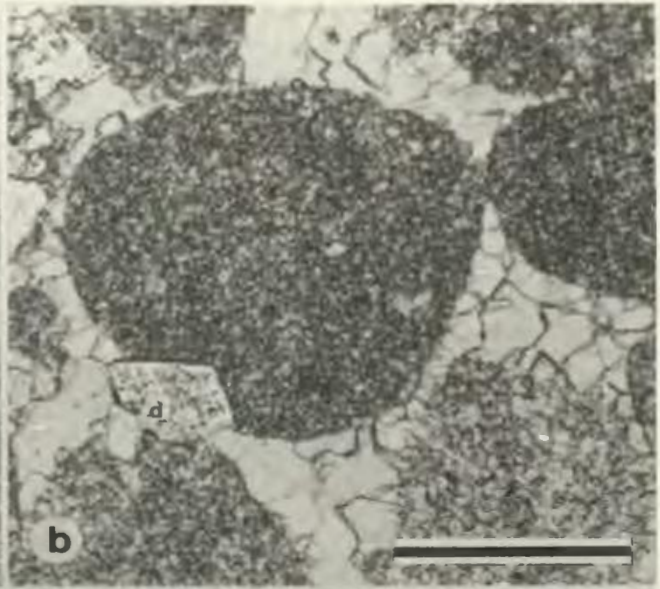
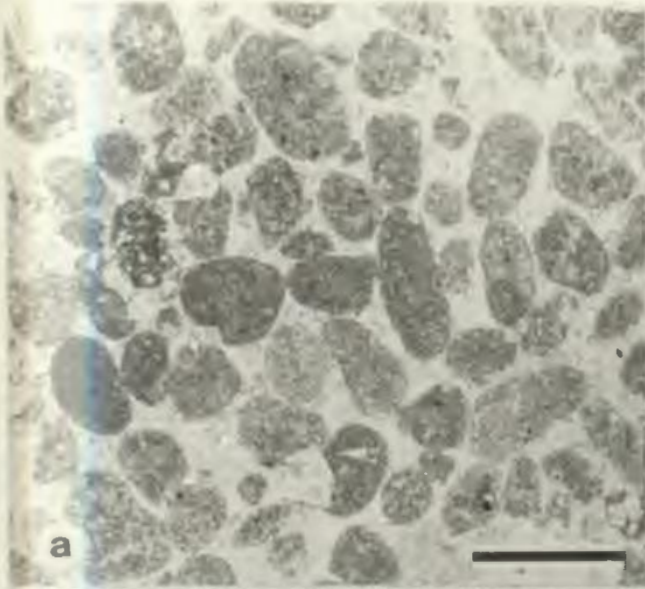


PLATE 23: GIRVANELLA CLASTS

- a: Thin section microphotograph of isolated Girvanella tubules (arrow) in a peloidal grainstone. Scale bar is 100 μm . Cow Head North, Middle Ordovician, Bed 13.6-.9, sample CHN-140.
- b: Thin section microphotograph of peloids with microspar centres (arrow) in peloidal grainstone. On top of the arrow is a transverse section through a calcitized sponge spicule (S). Scale bar is 100 μm . Cow Head North, Lower Ordovician, Bed 13, sample 80-13-0.
- c: Thin section microphotograph of silt-size peloidal grainstone with dense micritic rods (arrow) interpreted to be poorly preserved Girvanella. Scale bar is 200 μm . Long Point, Lower Ordovician, unit 1, sample LP-1-A.
- d: Thin section microphotograph of Girvanella rafts in bioclast-rich peloidal-intraclast grainstone. Rafts show parallelism of tubules; the raft in the upper portion of the microphotograph is mostly oriented perpendicular to the plane of the microphotograph. Interparticle and intra-raft cement is slightly ferroan, blocky calcite. Intraclast at lower right shows structure grumeleuse. Scale bar is 500 μm . St. Paul's North, Lower Ordovician, unit 75, sample SPN-51.
- e: Thin section microphotograph of an exceptionally large Girvanella oncolite in a peloidal-intraclastic grainstone. This oncolite has a nucleus which is replaced by an iron free, blocky calcite mosaic similar to that which forms the interparticle matrix. Scale bar is 500 μm . Cow Head South, Lower Ordovician, Bed 12s, sample 80-12s.

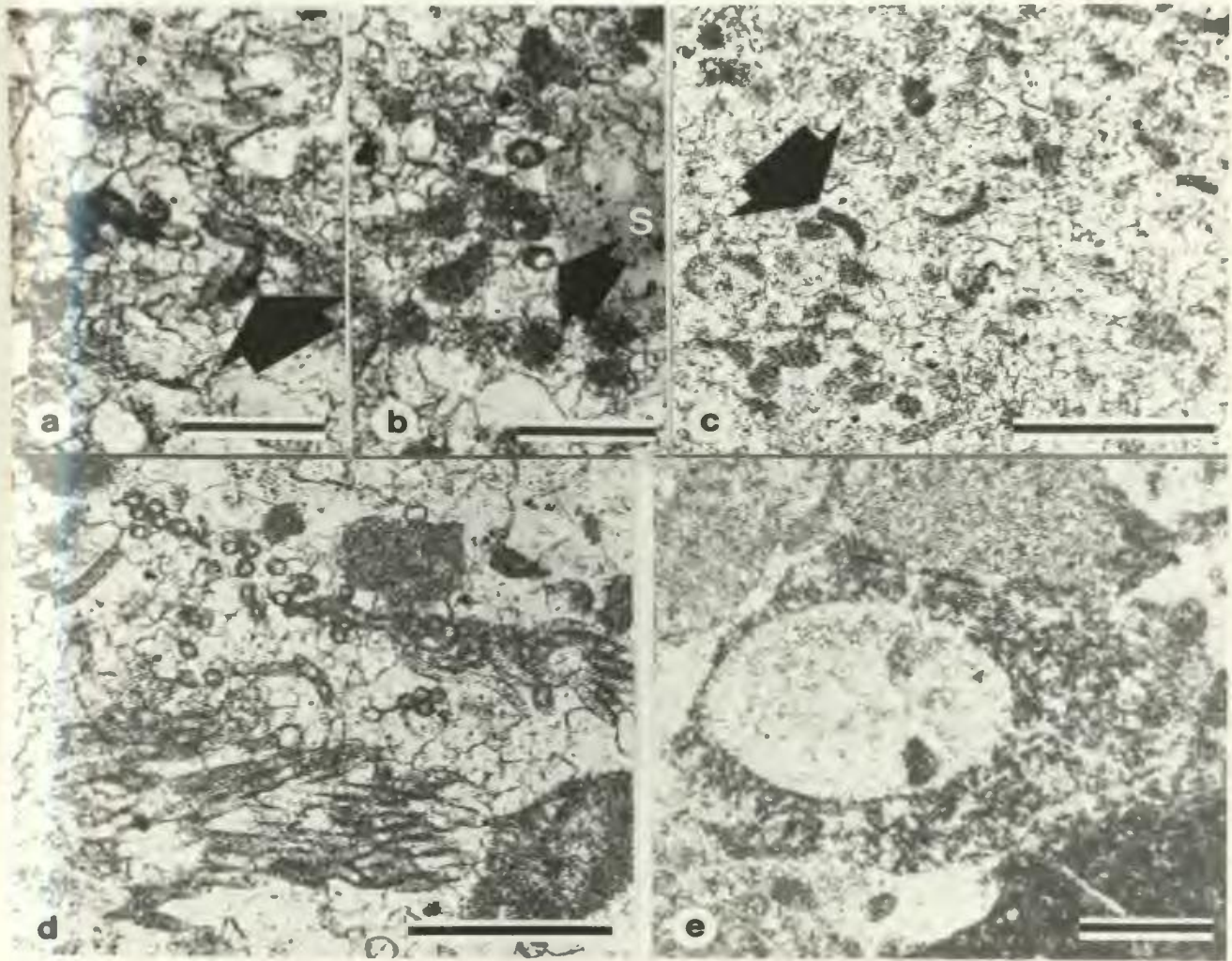
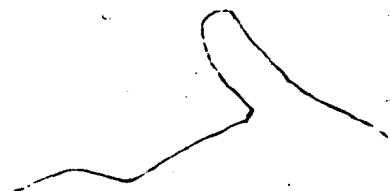


PLATE 24: GIRVANELLA INTRACLASTS

- a: This thin section microphotograph of an intraclast characterized by structure grumeleuse also contains Girvanella tubules and dense micritic filaments (rectangle is enlarged in "b" below). Host sediment is an ooid-peloid-intraclast grainstone. Intraparticle spar has undulose extinction and suggests equivalence with radiaxial fibrous calcite seen in algal boundstone boulders. Scale bar is 500 μm . Cow Head North, Upper Cambrian, Bed 6, sample 80-6N-3c.
- b: Thin section microphotograph of enlarged area from "a" above illustrates Girvanella tubules which are intimately associated with micritic patches and microspar (structure grumeleuse). Scale bar is 100 μm . Cow Head North, Upper Cambrian, Bed 6, sample 80-6N-3c.
- c: Thin section microphotograph of intraclast with vague, filamentous forms, interpreted as poorly preserved Girvanella. Sediment is a grainstone consisting of a bimodal mixture of coarse sand-size peloidal intraclasts and ooids, and coarse silt-size peloids. Scale bar is 100 μm . St. Paul's North, Lower Ordovician, unit 40, sample 80-70N-40.
- d: Thin section microphotograph of Girvanella intraclast rudstone (granule-size) within an algal boundstone boulder in conglomerate. Tubules are clearly visible in the two grains in the left half of the microphotograph. In contrast, Girvanella tubules can only be distinguished in the lower portion of the grain on the right, the rest of the clast consisting of structure grumeleuse to a uniformly crystalline micrite. Scale bar is 500 μm . Lower Head, Middle Ordovician, sample 78-368-F.



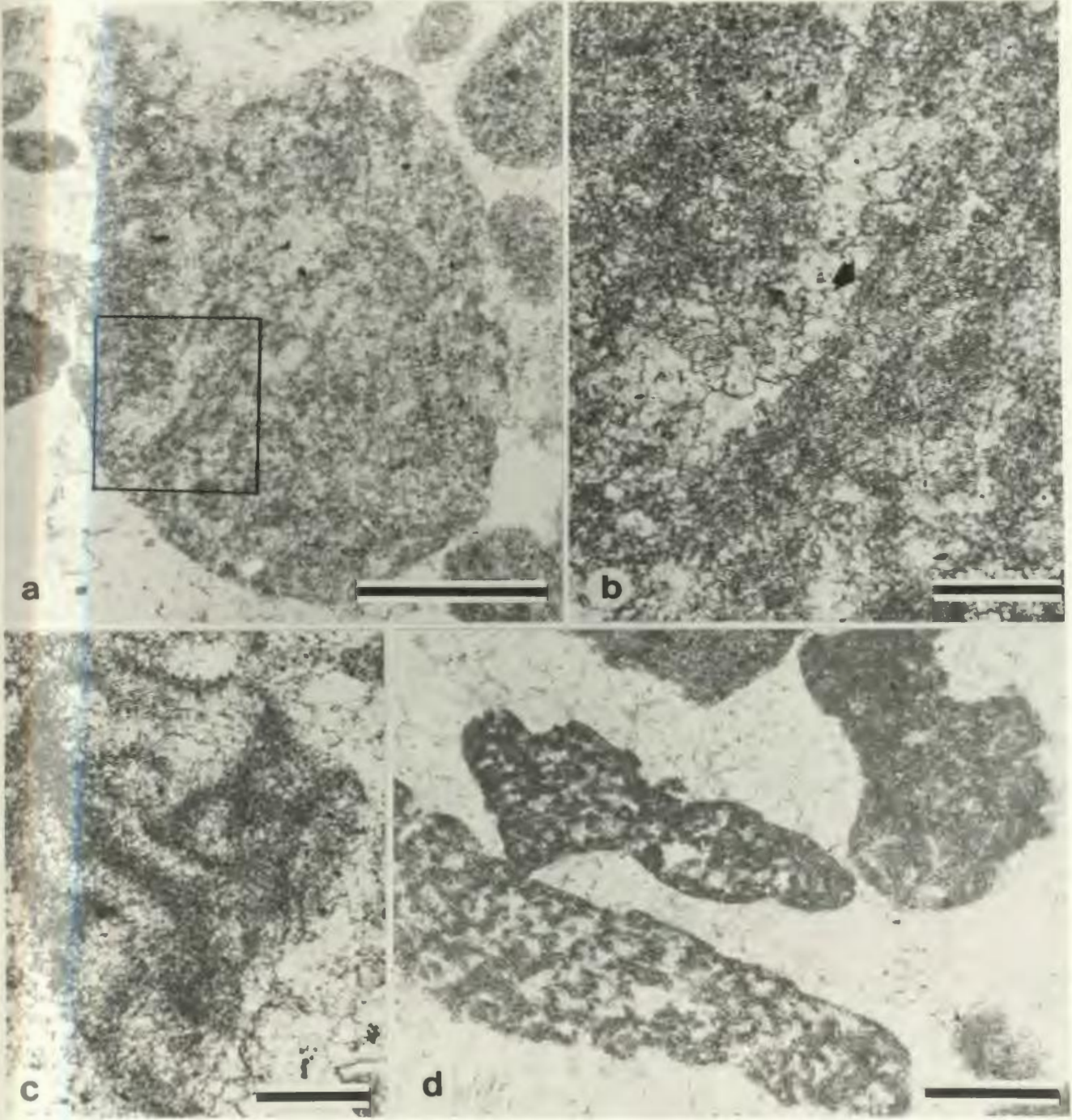


PLATE 25: EPIPHYTON

- a: Thin section microphotograph view of a tangential section through a small Epiphyton intraclast in an ooid-rich, peloidal intraclastic grainstone. Sediment is same as that illustrated in Plate 23c. Scale bar is 200 μm . St. Paul's North, Lower Ordovician, unit 40, sample 80-70N-40.
- b: Thin section microphotograph of Epiphyton clusters with variable thallus diameters suggest the ultimate production of dense micritic peloids of variable size, but still within the coarse silt- to fine sand-size range. Epiphyton is contained within an algal boundstone boulder. Scale bar is 500 μm . Lower Head, Middle Ordovician, sample 78-371-B.

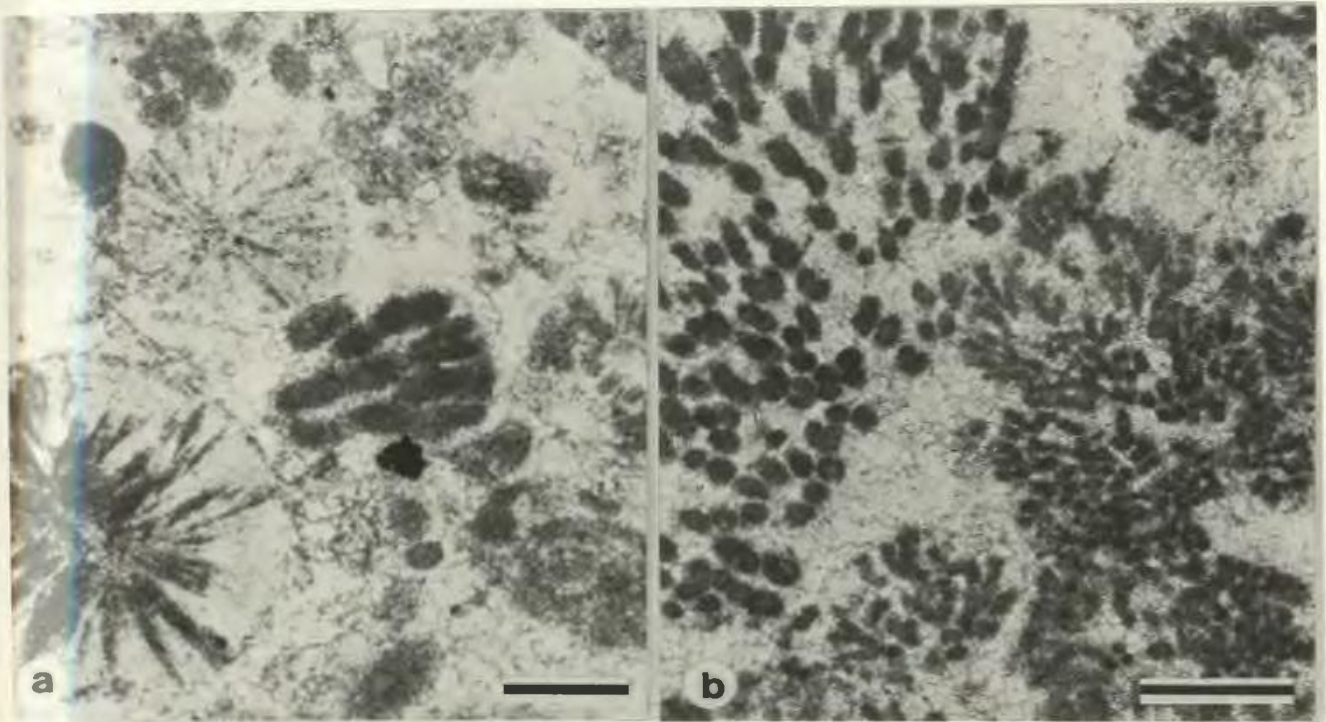


PLATE 26: BOUNDSTONE BOULDERS

- a: Thin section microphotograph of an algal boundstone boulder which consists of numerous Girvanella sheets and arborescent Epiphyton clusters cemented by radiaxial fibrous calcite. Geopetal sediments (pointed to by arrows) indicate that ~~depositional~~ way-up is to the upper left. Rectangular areas are shown in greater detail in "b" and "c" below. Scale bar is 3 mm. Cow Head North, Upper Cambrian, Bed 7, sample CHN-28.
- b: Thin section microphotograph of a thick Girvanella sheet which has well-preserved, loosely intertwined tubules. Inter-tubule spar demonstrates undulose extinction and suggests that it is co-genetic with larger, more easily studied radiaxial fibrous calcite. Position of microphotograph is indicated in "a" above. Scale bar is 500 μm .
- c: Thin section microphotograph illustrates (1) Girvanella tubules which laterally grade to structure grumeleuse and (2) microfabric within a Girvanella sheet. Position of microphotograph is indicated in "a" above. Scale bar is 200 μm .

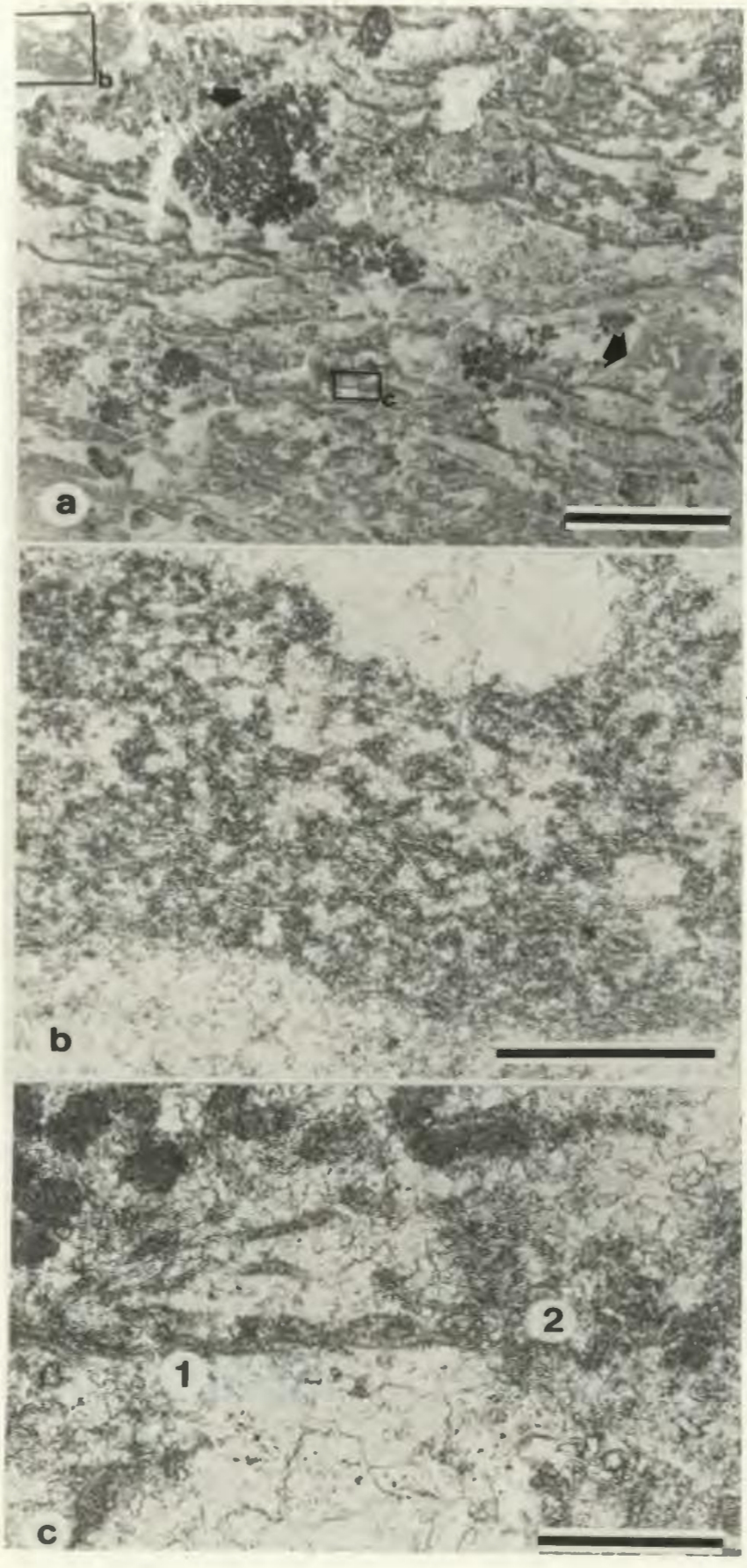


PLATE 27: RADIAL FIBROUS CALCITE: FIELD RELATIONSHIPS

- a: Shallow-water boulder in conglomerate has vugs lined with fringes of RFC (R) followed either by megaquartz cement (Q) or internal sediment (I). Bases of the RFC fringes are partially replaced by microquartz (M). Penny for scale. Cow Head North, Middle Ordovician, Bed 14.
- b: RFC fracture-fill (R) in shallow-water boulder. Prominent microquartz crust (Q) occurs at the base of the fringe. Knife scale is 9 cm long. Cow Head North, Lower Ordovician, Bed 10.
- c: "Zebra" rock consists of alternating bands of RFC and mudstone to packstone host sediment. Cow Head South, Lower Ordovician, Bed 10s.
- d: Shallow-water clast probably derived from a mound (see "e" below) contains a thick, inclusion-banded fringe of RFC. Cow Head North, Lower Ordovician, Bed 8.19.
- e: A prominent crust of RFC surrounds a mound (light grey beneath hammer) in the Large Boulder at Lower Head. Both the mound and the lighter-coloured intermound sediments contain abundant calcified algal clasts. Lower Head, Middle Ordovician.



PLATE 28: RADIAL FIBROUS CALCITE: PETROGRAPHY

- a: Thin section cross-polarized light microphotograph of two fringes of RFC meeting at a medial suture in a shallow-water boulder of "zebra" rock. The host lithology is peloidal grainstone. Scale bar is 2 mm. Cow Head North, Upper Cambrian, Bed 7, sample CHN-31.
- b: Thin section microphotograph of a botryoid of RFC. This sample comes from a fringe which surrounds one of the enigmatic mounds in the Large Boulder at Lower Head. Scale bar is 1 mm. Lower Head, Middle Ordovician, sample LH-8.
- c: Thin section cross-polarized light microphotograph of a RFC fringe in a fracture within a shallow-water boulder. Concertal intercrystalline boundaries are especially well-developed in this particular sample. Scale bar is 500 μ m. Cow Head North, Lower Ordovician, Bed 10, sample RAX-10.
- d: Thin section microphotograph of numerous anhedral dolomite inclusions (light shades) in a RFC crystal. This crystal forms part of a fringe precipitated in a fracture within a shallow-water boulder. Scale bar is 100 μ m. Cow Head North, Lower Ordovician, Bed 12, sample RAX-12-A.
- e, f: Thin section cross-polarized and plane light microphotographs of a RFC fringe which fills a fracture in a shallow-water boulder. This fringe demonstrates a botryoidal growth surface (large arrows) defined by the Type B inclusion pattern. Above this, the fringe is less inclusion-rich and subcrystals are clearly outlined by the Type C inclusion pattern (small arrows). In the crystal at the far left of the microphotographs, concave upward twins are visible. Scale bar is 1 mm. Cow Head North, Middle Ordovician, Bed 14, sample RAX-14-A.

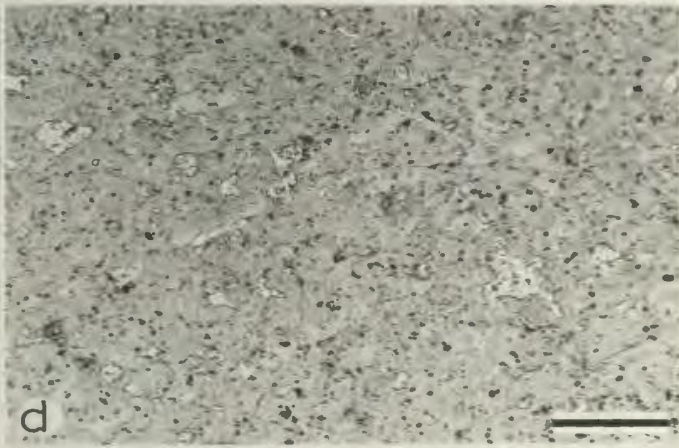
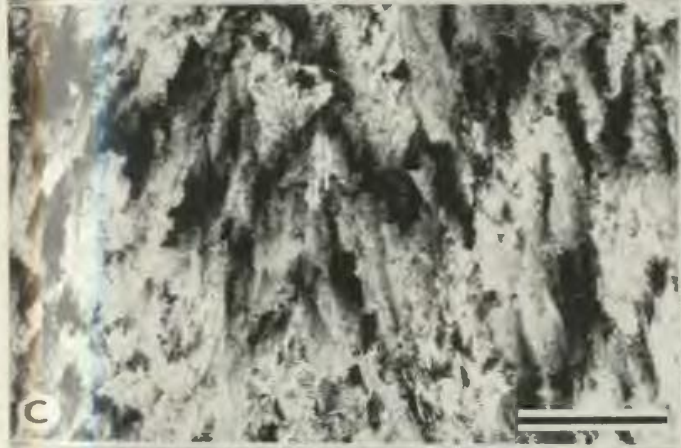


PLATE 29: RADIAL FIBROUS CALCITE:
CATHODE LUMINESCENCE

- a, b: Cross-polarized light and CL microphotographs of the base of a RFC fringe illustrating obtuse rhombohedral growth surfaces outlined by thin brightly-luminescent zones. Most of this fringe is non-luminescent. Sample is from a fracture in a shallow-water boulder. Scale bar is 250 μ m. Cow Head North, Lower Ordovician, Bed 12, sample RAX-12-A.
- c, d: Cross-polarized light and CL microphotographs of a RFC fringe showing a botryoidal surface in the non-luminescent, basal portion. This surface is also outlined by inclusions in microphotograph "c". This is overlain by dull to weak-luminescent rods, and finally weak-luminescent calcite showing little microfabric. Subcrystals consist of small groups of rods which dominate the middle portion of the microphotograph. Sample is from a fracture in a shallow-water boulder. Scale bar is 1 mm. Cow Head North, Middle Ordovician, Bed 14, sample RAX-14-A.



PLATE 30: RADIAL FIBROUS CALCITE:
CATHODE LUMINESCENCE

- a, b: Cross-polarized light and CL microphotographs of RFC from a vug in a shallow-water boulder. In the central third of the crystal in the middle of the microphotograph, the CL growth surface is approximately euhedral and suggests growth as a single crystal. Upward, however, the growth surface becomes more irregular and CL zones appear jagged. A few non-luminescent rod-like domains are seen (arrows). The transition to irregular growth zoning and presumably crystallite growth is accompanied by the development of obvious subcrystals, readily visible in cross-polarized light. The numerous black dots scattered in the lower half of these microphotographs are artifacts of thin section preparation. Scale bar is 2 mm. Cow Head North, Middle Ordovician, Bed 14, sample CHN-63.
- c, d: Cross-polarized light and CL microphotographs of RFC showing the upper part of the fringe seen in microphotographs "a" and "b", above. In microphotograph "c" the contact between the two inwardly-growing RFC fringes is outlined in black ink. The numerous black dots scattered in the lower half of these microphotographs are artifacts of thin section preparation. Scale bar is 2 mm.

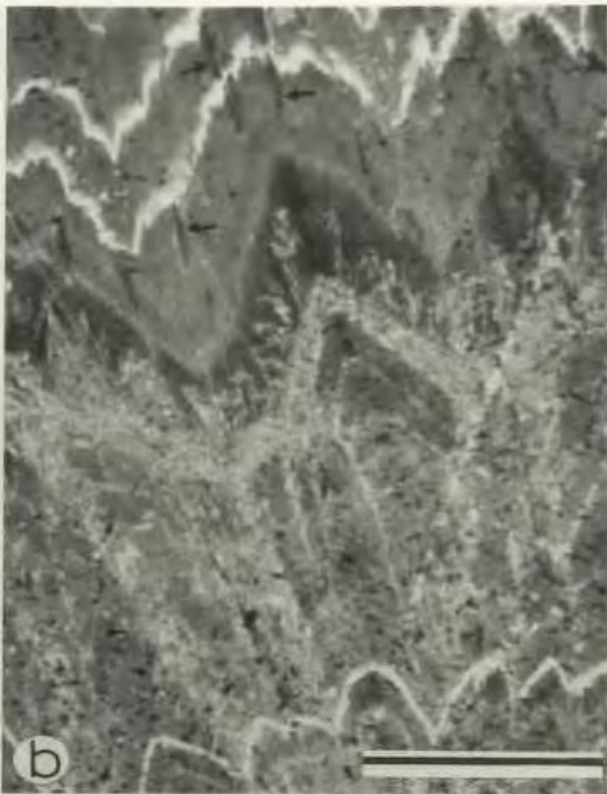


PLATE 31: RADIAL FIBROUS CALCITE:
CATHODE LUMINESCENCE

a, b: Cross-polarized light and CL microphotographs of an RFC fringe in a mound within the Large Boulder at Lower Head. In this fringe, flat-topped and obtuse rhombohedral growth surfaces are common. Subcrystals seen in cross-polarized light are correlated with the smaller, elongate domains visible with CL. Further along the fringe, zoning becomes more diffuse and irregular. Rectangle at bottom of microphotograph is enlarged in microphotographs "c" and "d". Scale bar is 2 mm. Lower Head, Middle Ordovician, sample LH-6.

c, d: Cross-polarized light and CL microphotographs of RFC from outlined area in microphotograph "b" above. Growth surfaces vary from euhedral, obtuse rhombohedra to anhedral. Scale bar is 500 μ m.



PLATE 32: CONGLOMERATE FIBROUS CALCITE

- a: Approximate bedding-plane view of conglomerate cemented by a rind of CFC overlain by coarse, equant spar. Shale matrix occurs in close proximity. Penny for scale (arrow). Cow Head North, Upper Cambrian, Bed 2.
- b: Approximate bedding-plane view of conglomerate cemented by rinds of CFC overlain by dolomite (D). Penny for scale (arrow). Cow Head North, Upper Cambrian, Bed 2.
- c: Thin section negative print illustrating complexity of pore-filling history. Internal sediments (I) directly overlies pebbly mudstone clasts and these are overlain by CFC (C). A sucrosic dolomite mosaic (D), commonly associated with dispersed pyrite, overlies the CFC. Coarsely crystalline pyrite (P) and equant calcite (E) postdate dolomite. V-shaped fracture in flat mudstone clast in centre of view indicates some mechanical compaction prior to precipitation of CFC. Boxed area is shown in detail in Plate 33c. Scale bar is 1 cm. Stratigraphic top to upper right. Cow Head North, Upper Cambrian, Bed 2, sample CHN-178-B.

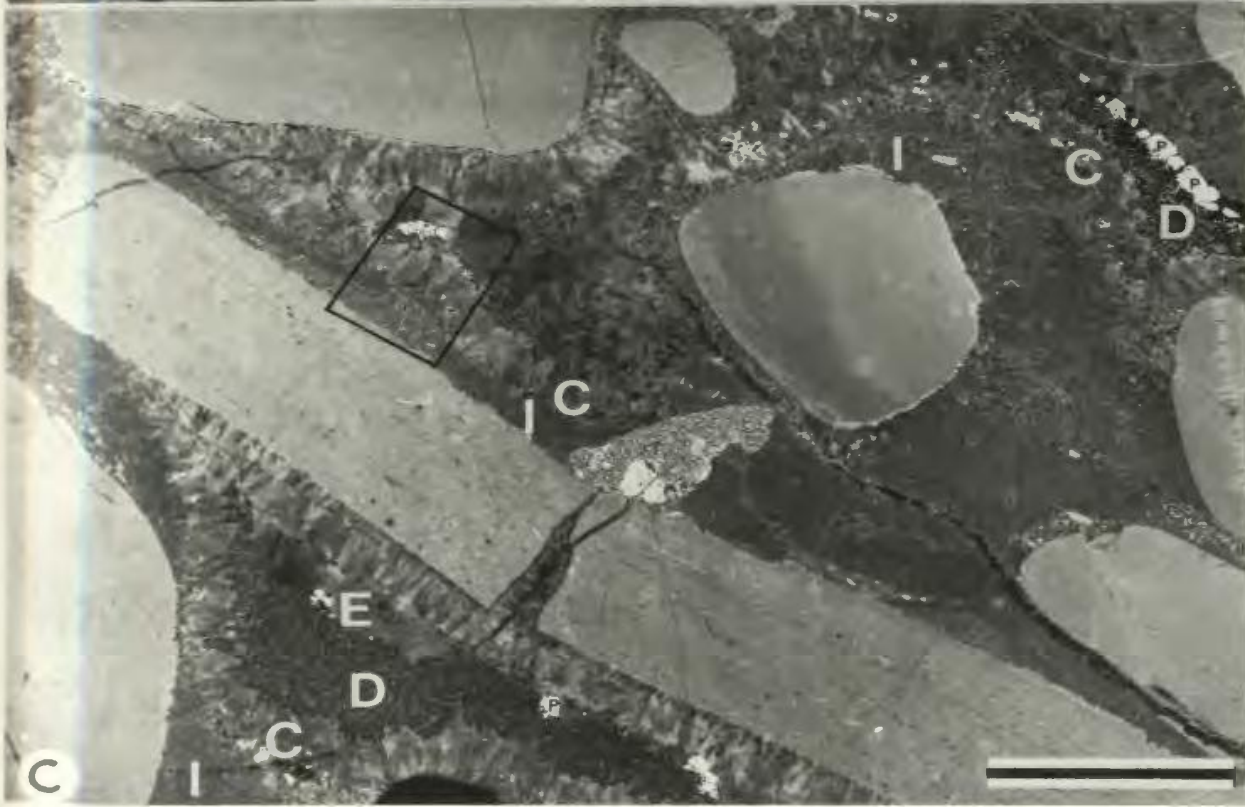
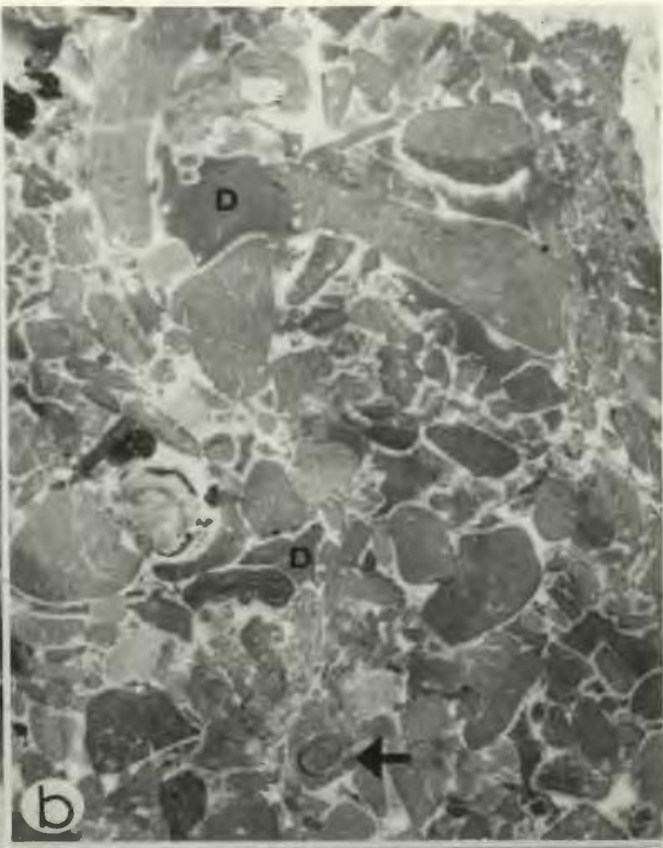
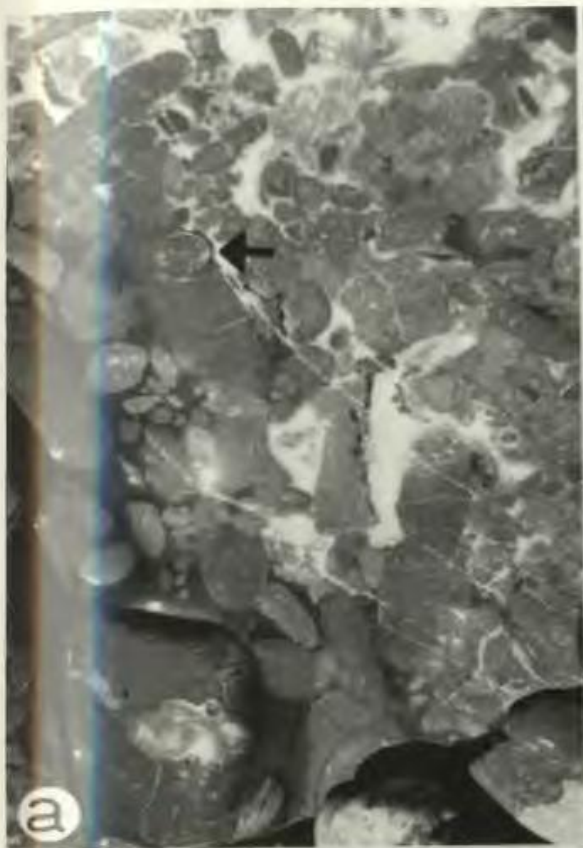
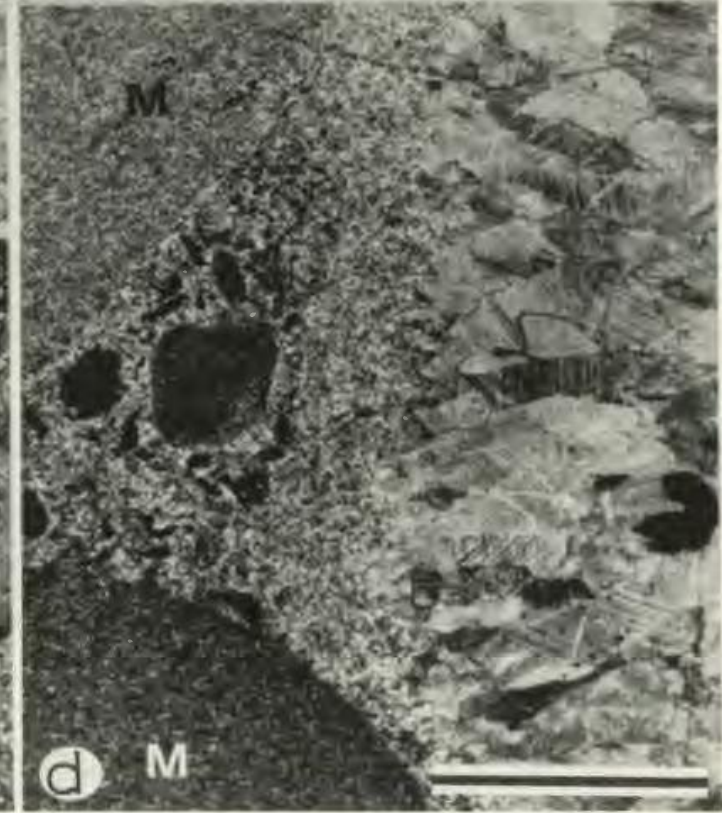


PLATE 33: CONGLOMERATE FIBROUS CALCITE

- a: Thin section microphotograph showing scalenohedral terminations of CFC crystals and the overlying sucrosic dolomite mosaic which replaces internal sediment. Faces of calcite crystals are serrated due to minor replacement by dolomite. Scale bar is 500 μ m. Stratigraphic top is to upper right. Cow Head North, Upper Cambrian, Bed 2, sample CHN-15-A.
- b: Close-up thin section microphotograph of scalenohedral termination on CFC crystal. Dolomite precipitation was only a minor interruption during growth of this fringe. Calcite crystal faces are serrated due to minor replacement by dolomite. Note highly irregular intercrystalline boundary (arrow). Scale bar is 500 μ m. Stratigraphic top is up. Cow Head North, Upper Cambrian, Bed 2, sample CHN-15-A.
- c: Close-up thin section microphotograph of boxed area shown in Plate 32c. Peloidal packstone/grainstone (I) directly overlies a mudstone pebble (M). The internal sediment is followed by a fringe of CFC (C) showing prominent scalenohedral terminations, and then a sucrosic dolomite mosaic (D) and pyrite (P). The upper equant calcite mosaic (E) appears to postdate precipitation of dolomite and possibly also pyrite. Scale bar is 2 mm. Stratigraphic top is up. Cow Head North, Upper Cambrian, Bed 2, sample CHN-178-B.
- d: Thin section microphotograph of peloidal and intraclastic grainstone perched between two mudstone pebbles (M). The internal sediment is overlain by CFC. Scale bar is 2 mm. Stratigraphic top is to right. Cow Head North, Upper Cambrian, Bed 2, sample CHN-178-AB.



• PLATE 34: CEMENT AND NEOSPAR

- a: Thin section microphotograph of peloidal grainstone illustrating calcite cement and replacive dolomite. The non-ferroan calcite cement shows numerous sharp, compromise boundaries (small arrows). These boundaries and the micrite to microspar composition of the sand-size peloids is clearly seen because this 10-15 μm thick thin section was polished prior to and after mounting on the glass slide. Inclusion-rich, dispersed dolomite crystals appear to replace both peloids and interparticle cement. The peloid-dolomite contact may be either a dolomite crystal face or very irregular. The euhedral, occasionally gently curved, dolomite crystal faces abutting interparticle calcite cement is typical. The cloudy central region of the dolomite crystal in the centre of the photograph is likely a detrital core. The relatively inclusion-free rim contains scattered relics of one peloid it has partially replaced (large arrow). Scale bar is 200 μm . Stratigraphic top is up. Cow Head North, Tucker's Cove, Upper Cambrian, Bed 6, sample CHN-69.
- b: Thin section microphotograph of a peloidal grainstone initially cemented by rhombic, non-ferroan calcite crystals (c) and then later by chalcedony (q). The grain labelled "N" is Nuia. Scale bar is 500 μm . Unoriented thin section. Martin Point, Middle Ordovician, unit 60, sample 80-39-60.
- c: Thin section microphotograph of perched siliciclastic silt grains (arrows) in a peloidal grainstone cemented by non-ferroan calcite. Dark spots within the grains are pyrite crystals. Scale bar is 500 μm . Stratigraphic top is up. Green Point, Upper Cambrian, unit 10, sample GP-42.
- d: Thin section microphotograph of a coarse pseudospar matrix in a conglomerate. Clasts are mainly peloidal grainstones. The pseudospar crystals are non-ferroan, anhedral, often show curved outlines, and exhibit a prominent intercrystalline argillaceous paste. Scale bar is 500 μm . Unoriented thin section. Cow Head North, Middle Ordovician, Bed 13.15, sample 80-13N-15.
- e: Thin section negative print of a planar-bedded mudstone showing central ferroan microspar (m) grading marginally to coarse, ferroan pseudospar (p). Burrows also contain loaf-shaped pseudospar crystals and a prominent argillaceous matrix. Scale bar is 1 cm. Stratigraphic top is up. St. Paul's North, Lower Ordovician, unit 43, sample SPN-66-C.
- f: Thin section negative print of a complex nodule from a ribbon limestone sequence which consists mainly of non-ferroan microspar (m) which grades to more dispersed and more ferroan pseudospar (p) both laterally and vertically (see Plate 13g). Peloidal silt laminations within the nodule are easily traced into the surrounding argillaceous matrix. CL of the boxed area is illustrated in Plate 35e. Scale bar is 1 cm. Stratigraphic top is up. Cow Head North, Lower Ordovician, Bed 9.15, sample CHN-47.

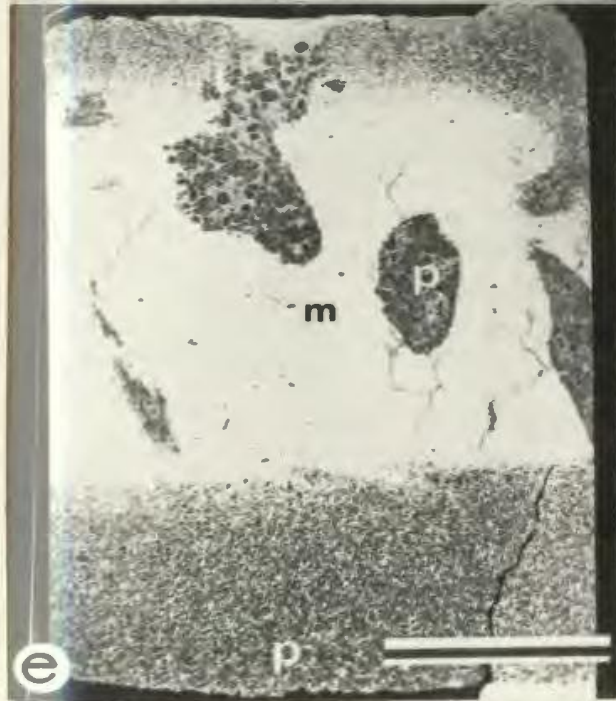
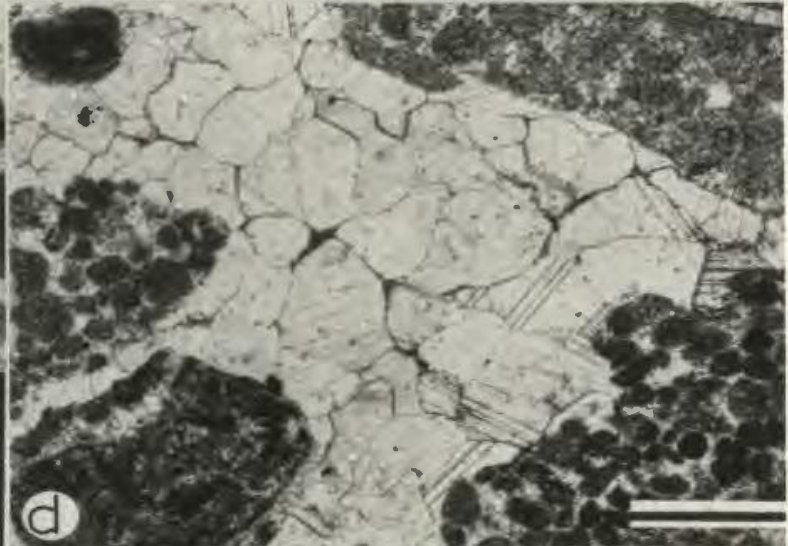
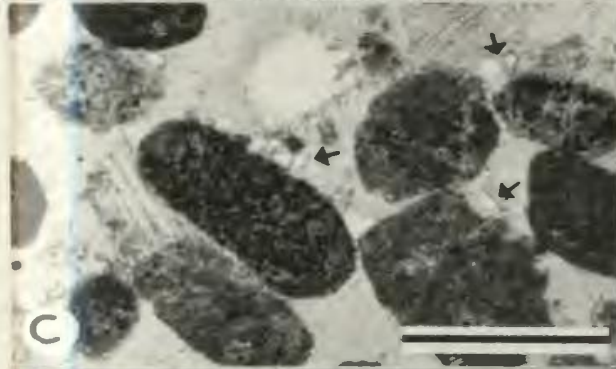
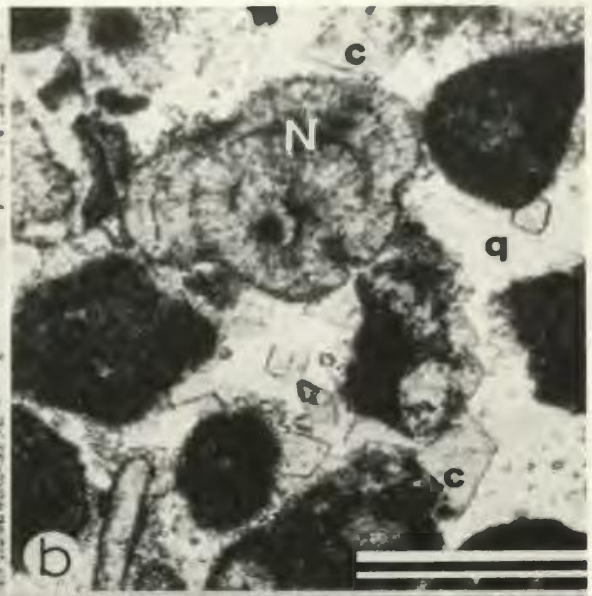
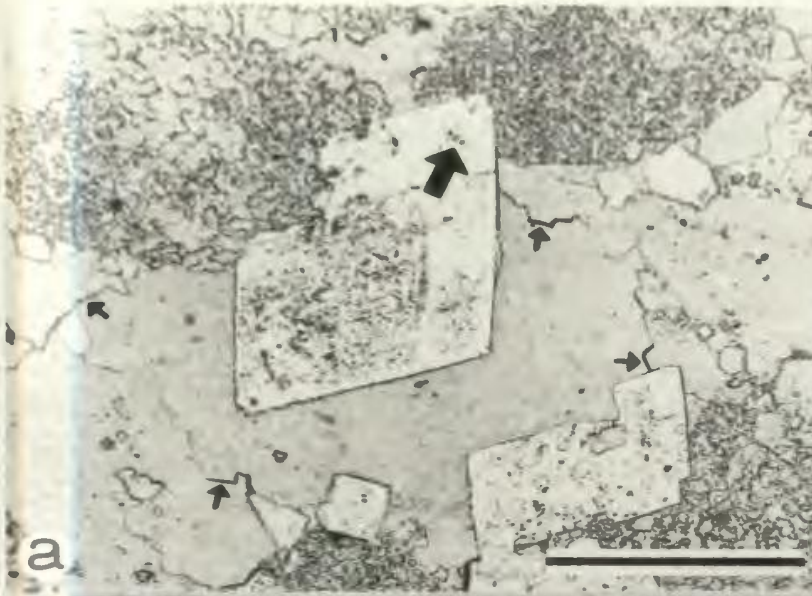


PLATE 35: CEMENT AND NEOSPAR: CATHODE LUMINESCENCE

- a: Peloidal grainstone with interparticle cement showing all 3 CL stages: A (dark), B (bright), and C (dull). Dull luminescence of peloids is typical. Scale bar is 250 μm . Stratigraphic top is up. Martin Point, Upper Cambrian, unit 23d, sample MP-105.
- b: Coarse, equant, non-ferroan calcite cement in conglomerate, probably contemporaneous with CFC. These crystals demonstrate a finely-zoned, Stage A CL which was corroded subsequent to precipitation of the weak-luminescent Stage B calcite which fills remaining porosity. Arrows point to zoning truncations and scalloped surfaces developed between these two stages of growth. Scale bar is 1 mm. Unoriented thin section. Cow Head North, Upper Cambrian, Bed 4, sample CHN-13.
- c: Dull-luminescent fringe of CFC is in stylolitic contact with mudstone pebble substrate. The early stage of growth is characterized by dull-luminescent Stage A calcite which is subsequently overgrown by dull- to weak-luminescent Stage B calcite exhibiting scalenohedral terminations. Finely-zoned rhombs of conglomerate matrix dolomite overlie the CFC fringe and replace internal sediment. A microprobe traverse across a dolomite crystal (arrow) is shown in Figure 12.1a. Light specks between the dolomite crystals are blue-luminescent feldspar silt. Scale bar is 200 μm . Unoriented thin section. Cow Head North, Upper Cambrian, Bed 2, sample CHN-2.
- d: Leached bioclast(?) preserved by a dull-luminescent micrite envelope (M) contains intramoldic cement which is identical to interparticle cement. The cement illustrates CL stages A (dark) and B (bright). The occurrence of leached bioclasts is rare in the CHG. Scale bar is 250 μm . Stratigraphic top is up. Lower Head, Lower Ordovician, sample LH-73.
- e: Close-up of marginally aggraded mudstone nodule previously illustrated in Plate 13g; 34f. From right to left, pseudospar has dominantly Stage B bright luminescence then Stage C dull luminescence. Minor zoning fluctuations occur near the contact with enclosing argillaceous matrix. Scale bar is 500 μm . Stratigraphic top is up. Cow Head North, Lower Ordovician, Bed 9.15, sample CHN-47.

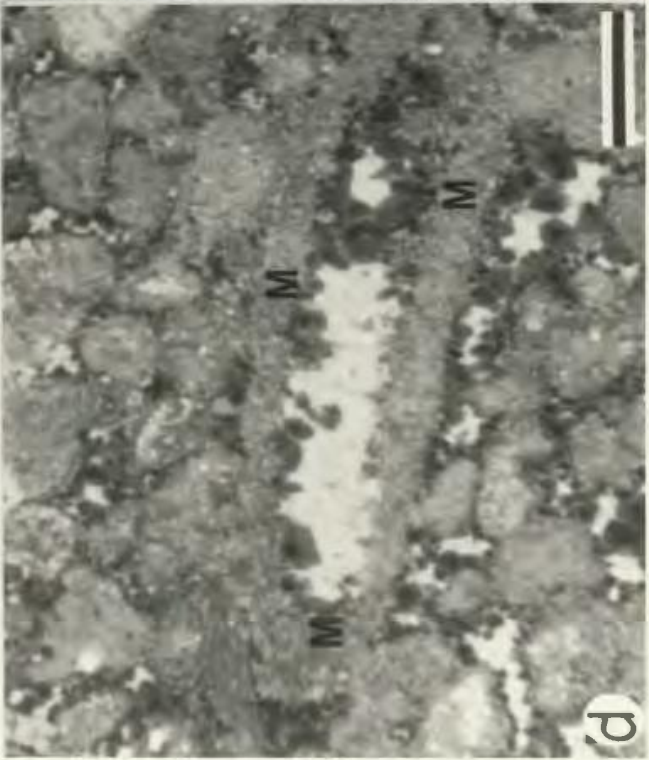
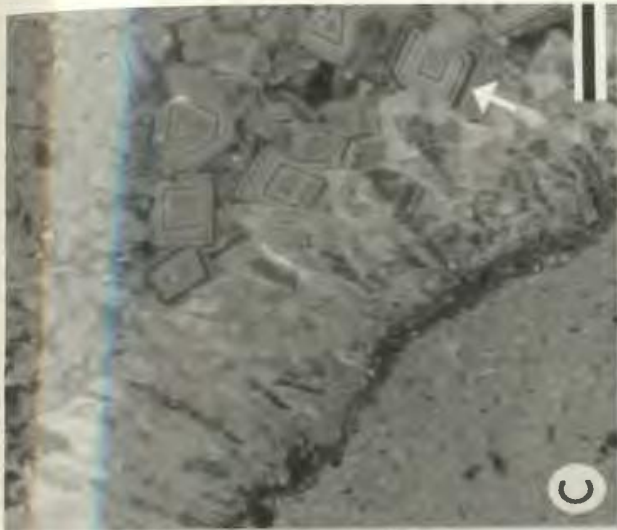


PLATE 36: DISPLACIVE FIBROUS CALCITE

- a: Slab of ferroan DFC-1 developed on both sides of a mudstone bed. This mudstone is slightly wavy-bedded and is obviously formed by the coalescence of concretionary nodules. Centres of the nodules are composed of non-ferroan microspar (M) which passes into non-ferroan pseudospar (P). The pseudospar links the nodules together into a continuous bed and grades upward and downward into the DFC fringes. Unoriented sample. Cow Head North, Lower Ordovician, Bed 8.30, sample CHN-36.
- b: Slab of non-ferroan to slightly ferroan DFC-2 overlying a substrate composed of non-ferroan to slightly ferroan microspar and pseudospar with scattered silt laminations. The interfering cones or "tufts" are clearly seen to the right in the photo, whereas 3 aberrant cone-like structures are seen in the left half, one of which is shown in detail in "c" below. This fringe is a multiple fringe where a discontinuity (arrows) separates lower and upper halves. Renewed fringe growth was independent of any control by the older substrate of DFC. The aberrant cone-like structures grew unimpeded through the discontinuity. Unoriented sample. Green Point, Upper Cambrian, sample GP-108.
- c: Thin section negative print of one of the aberrant cone-like structures seen in "b" above. The outer shell of the cone is characterized by numerous, closely-spaced argillaceous seams (white in photo). This cone-like structure grows through the discontinuity (arrow). Scale bar is 5 mm. Unoriented sample. Green Point, Upper Cambrian, sample GP-108.
- d: Thin section negative print of a ferroan DFC-2 fringe overlying a substrate of ferroan pseudospar. This fringe has well-developed cone structures in the upper half but the lower half is dominated by numerous, laterally and vertically interfering bundles of fibrous calcite. The U-shaped white and light grey seams are accumulations of clays. The numerous spindle-shaped medium grey areas in the top half of the fringe are the relatively inclusion-free "cores" illustrated in Plate 38a. Scale bar is 5 mm. Stratigraphic top is up. Green Point, Upper Cambrian, unit 1, sample GP-2.

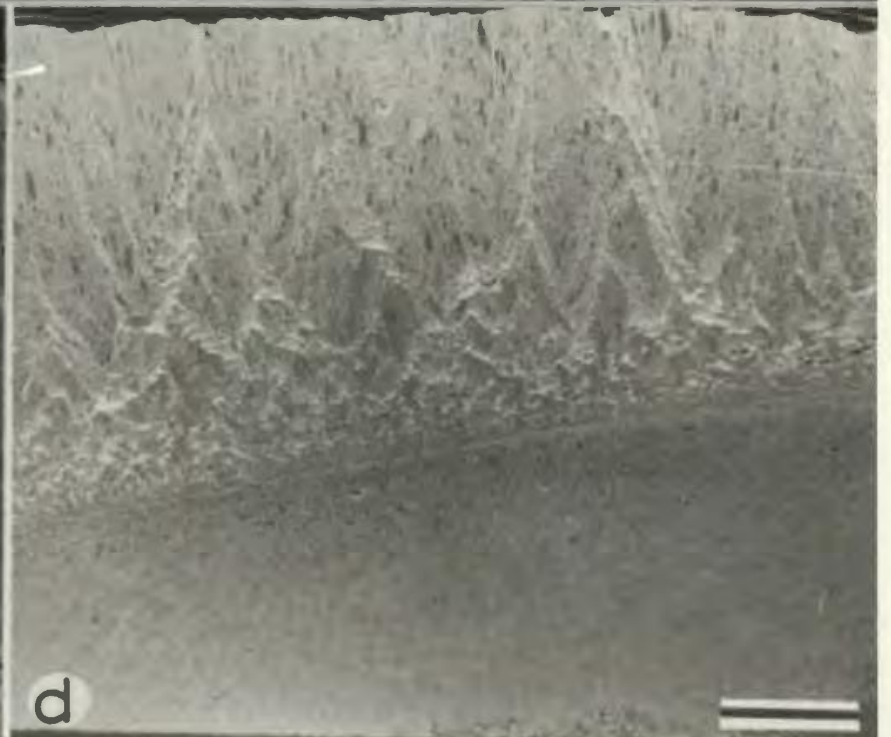
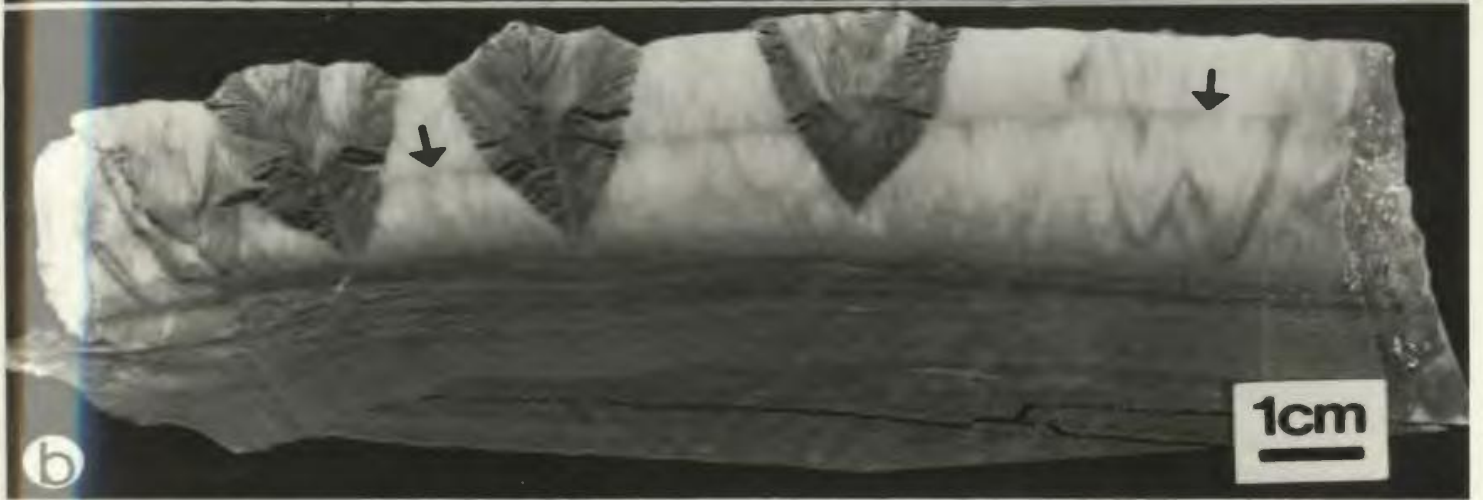
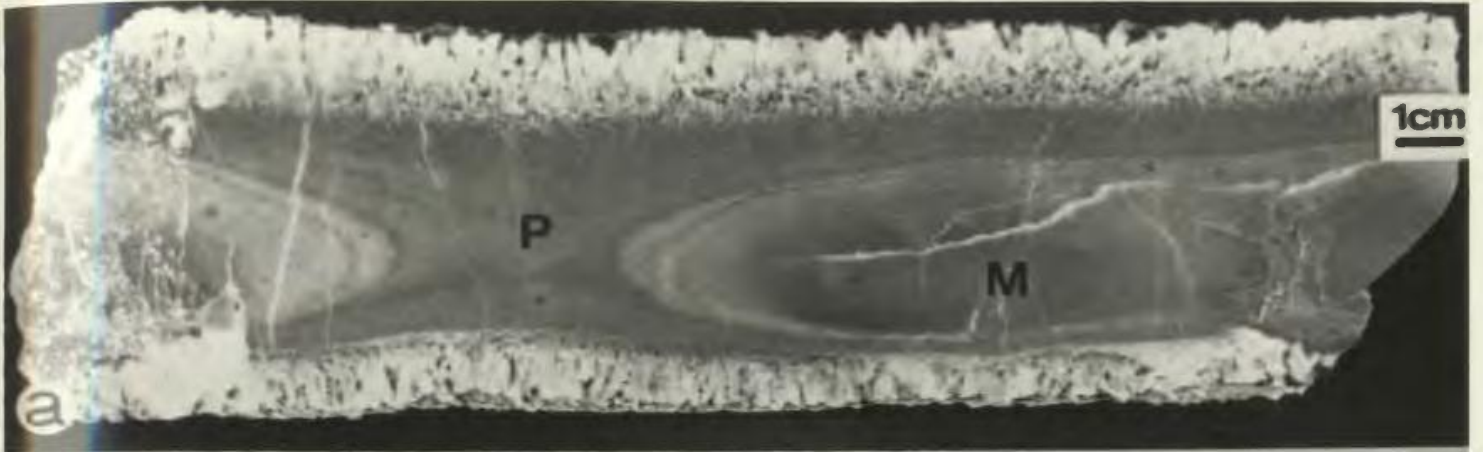


PLATE 37: DISPLACIVE FIBROUS CALCITE

- a: Thin section microphotograph of a ferroan DFC-1 fringe with a Type B inclusion pattern growing into a medial shale seam (black in photograph). Base and tips of crystals are non-ferroan. This fringe clearly illustrates convex-upward (botryoidal) growth increments except for a few crystals left of centre which demonstrate scalenohedral terminations. Scale bar is 1 mm. Stratigraphic top is up. Cow Head North, Lower Ordovician, Bed 8.30, sample CHN-104.
- b: Thin section negative print of a slightly ferroan to non-ferroan DFC-1 fringe composed of stubby crystals having anhedral, blunt terminations. Substrate grades from microspar (at base of photograph) to pseudospar (below lower fringe) to coarse fringe calcites. Black patches in shale (white) are artifacts of thin section preparation. Scale bar is 5 mm bar. Stratigraphic top is up. Black Brook, Lower Ordovician, unit 15, sample BB-5.
- c: Thin section negative print of ferroan DFC-1 fringes meeting at a medial shale seam (white). Several of the DFC crystals exhibit prominent, well-developed scalenohedral terminations. Scale bar is 1 mm. Stratigraphic top is up. Cow Head North, Lower Ordovician, Bed 8.30, sample CHN-37-B.
- d: Cross-polarized light microphotograph illustrating slightly ferroan, equant pseudospar mosaic between two DFC-2 crystals. The elongate crystals also demonstrate an obvious fibrous Type D inclusion pattern and sharp extinction. Scale bar is 500 μ m. Stratigraphic top is up. Green Point, Upper Cambrian, sample GP-47-B.
- e: Thin section negative print of planar-bedded mudstone with a poorly-developed, ferroan DFC-2 fringe overlying the bed and a ferroan, marginally aggraded lower portion. In some places, upper fringe growth is interrupted by pseudospar growth. The DFC fringe at the top of this bed and the aggrading pseudospar on the lower margin (boxed area enlarged in "f") are synchronous precipitates as indicated by iron stain, CL, and stable isotope analysis (Trend 10 in Figure 11.4). The mudstone substrate exhibits a slightly coarser microspar band running through the centre of the bed. The jagged white line traversing the mudstone left of centre is a vertical stylolite with accumulated argillaceous material. Scale bar is 1 cm. Stratigraphic top is up. Lower Head, Lower Ordovician, sample LH-76-A.
- f: Close-up, thin section microphotograph of boxed area from the marginally-aggraded lower mudstone surface shown in "e". The largest pseudospar crystals are elongate and tend to be oriented perpendicular to bedding. The increase in crystal size and shape and the amount of intercrystalline paste is clearly seen in this microphotograph. Scale bar is 1 mm. Stratigraphic top is up.

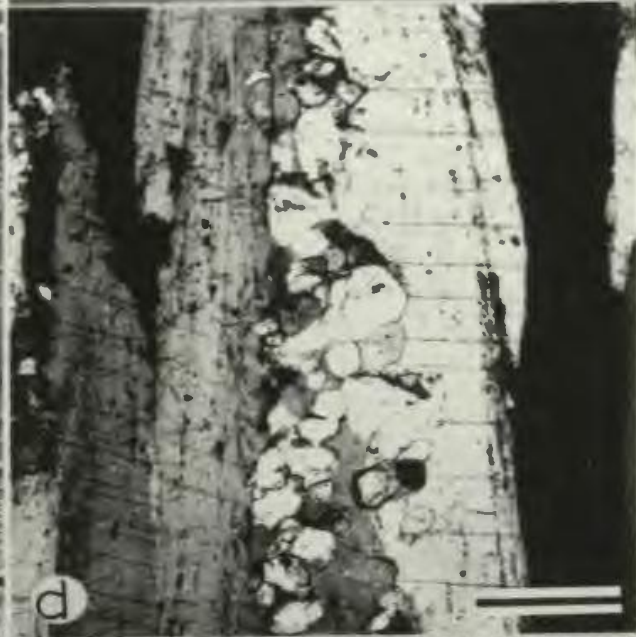
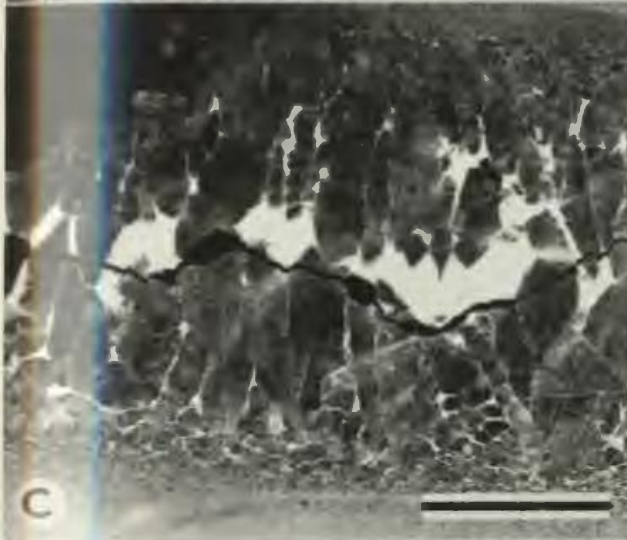
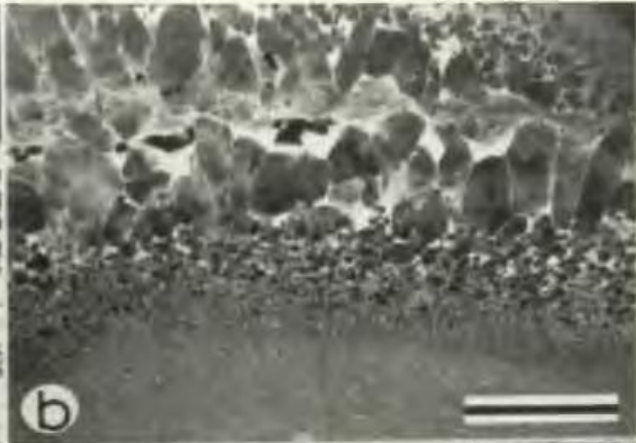


PLATE 38: DISPLACIVE FIBROUS CALCITE

- a: Thin section microphotograph of spindle-shaped, inclusion-free cores in a single crystal of ferroan DFC-2. This sample is the same as that shown in Plate 36d. These domains are up to 100 μm in width and appear to be discontinuous in 2-dimensional views. Most of the crystal is inclusion-rich and appears fibrous. The intercrystalline boundary to the right in the microphotograph (arrow) shows a smooth, planar boundary abutted by a jagged, stepped boundary. Scale bar is 500 μm . Stratigraphic top is up. Green Point, Upper Cambrian, unit 1, sample GP-2.
- b: Thin section microphotograph of DFC-1 crystal shows former subhedral terminations outlined by Type B inclusion pattern. Non-ferroan (N) and ferroan (F) zones are relatively inclusion-free and inclusion-rich, respectively. Note the concertal nature of the intercrystalline boundaries (arrows). Scale bar is 500 μm . Unoriented sample. Lower Head, Lower Ordovician, sample LH-73.
- c: Thin section microphotograph of ferroan DFC-1 crystals cut normal to crystal elongation. These crystals have anhedral outlines and usually consist of 3-5 relatively inclusion-free core areas (labelled "A" - "D" in one crystal) joined together to form one major crystal. The core areas are separated from each other by inclusion-rich calcite. Light areas surrounding crystals in right half of microphotograph are artifacts of sample preparation. Scale bar is 500 μm . Cow Head North, Lower Ordovician, Lower Ordovician, Bed 8.30, sample CHN-104.
- d: Thin section microphotograph near termination of a ferroan DFC-2 fringe shows inclusion-rich, fibrous crystals which are overgrown on their margins by inclusion-free calcite to form exceptionally planar intercrystalline boundaries (arrows). The fringe is growing downward from the base of its substrate. A view of this fringe cut normal to crystal elongation is shown in "e". Scale bar is 1 mm. Stratigraphic top is up. Green Point, Upper Cambrian, sample GP-25.
- e: Thin section microphotograph of the fringe shown in the "d" cut normal to crystal elongation. The inclusion-rich, main portion of the crystals are trigonal-shaped and these are surrounded by relatively inclusion-free overgrowths which meet one another along remarkably planar intercrystalline boundaries. Inclusions are particularly abundant at the contact of the overgrowth and the inclusion-rich trigonal core. Each trigonal centre consists of numerous, irregularly-shaped, inclusion-free micro-domains. Scale bar is 500 μm . Green Point, Upper Cambrian, sample GP-25.

continued on next page

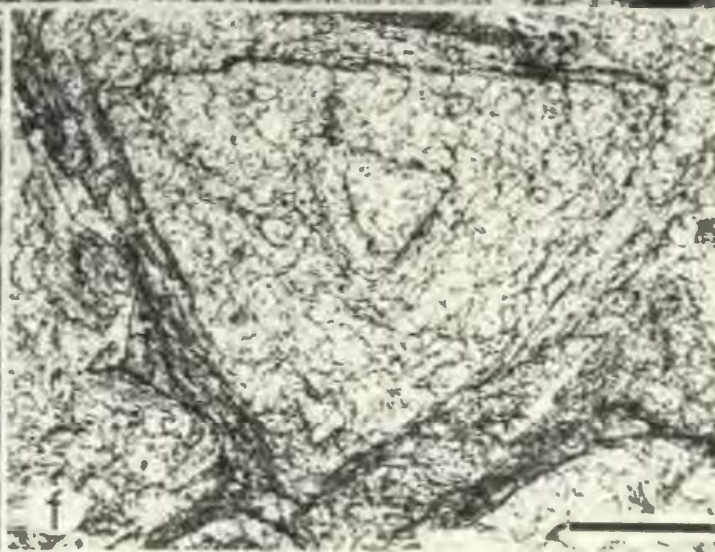
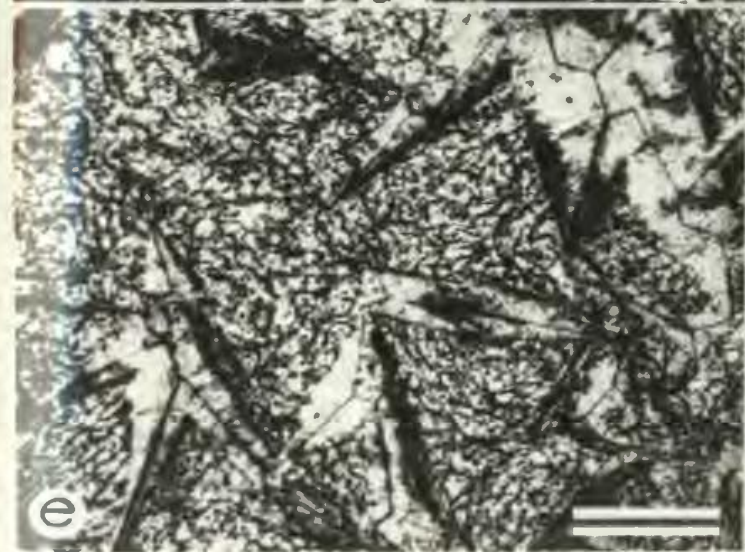
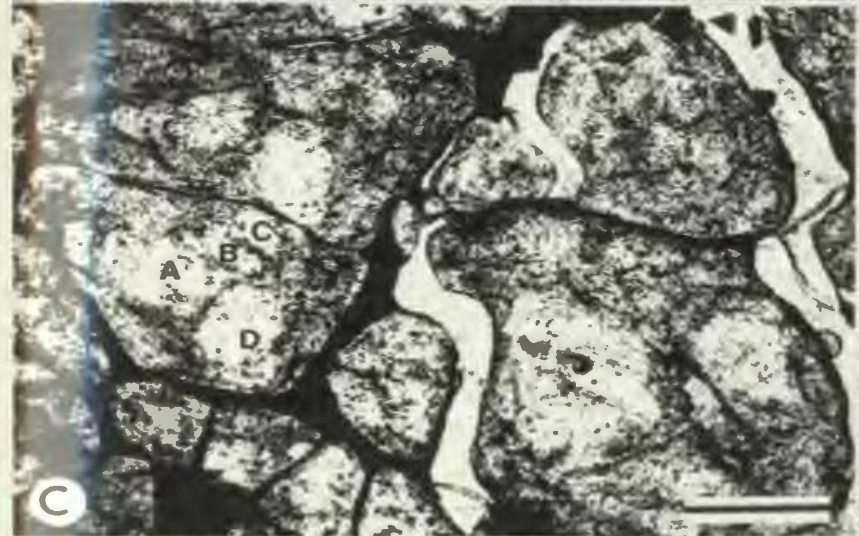
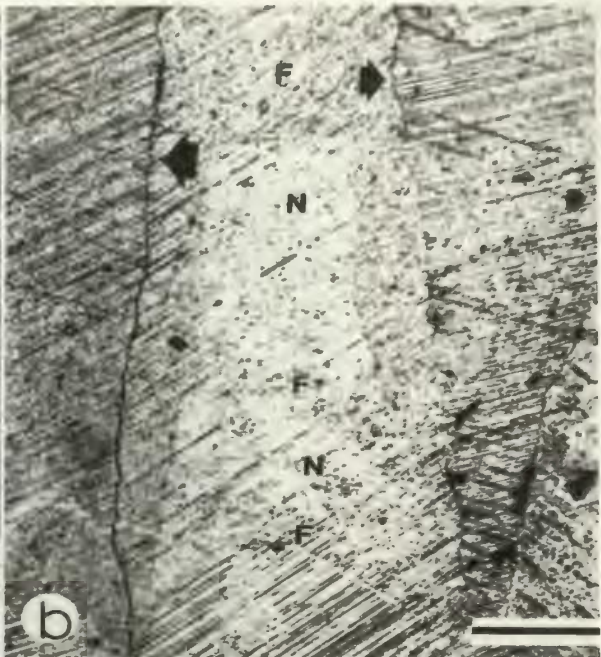
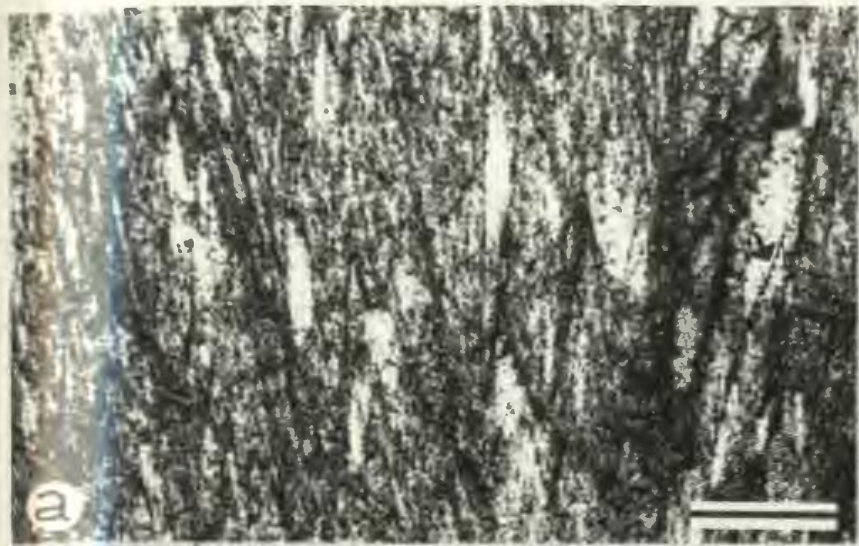


PLATE 38 (continued)

- f: Thin section microphotograph of a DFC-2 fringe viewed normal to crystal elongation. The prominent trigonal-shaped central area consists of numerous irregular to circular micro-domains which range from 25-60 μm across. These are separated from one another by inclusion-rich areas. These micro-domains are interpreted to represent small bundles of fibrous crystallites. The trigonal-shaped areas are overgrown by inclusion-rich calcite. Scale bar is 500 μm . Green Point, Upper Cambrian, sample GP(81-7).

PLATE 39: DISPLACIVE FIBROUS CALCITE

- a: Thin section microphotograph of a non-ferroan DFC-1 fringe which demonstrates a prominent radiating Type D inclusion pattern at the base of an elongate crystal. Twins traverse the crystal. A wavy intercrystalline boundary is seen at the right. Scale bar is 500 μ m. Stratigraphic top is up. Cow Head North, Lower Ordovician, Bed 8.30, sample CHN-37-B.
- b: Thin section microphotograph of the termination of an elongate calcite crystal with Type D inclusion pattern. Sample is from the same fringe as shown in the previous microphotograph. The termination of this crystal is characterized by pointed, inclusion-rich "tufts" which penetrate the overlying medial shale seam. The crystal to the upper right of the microphotograph is growing downward and is part of the overlying fringe. This crystal also shows a relatively planar crystal face. Scale bar is 500 μ m. Stratigraphic top is up. Cow Head North, Lower Ordovician, Bed 8.30, sample CHN-37-B.
- c: Thin section microphotograph of equant pseudospar at the base of a non-ferroan DFC-1 fringe. The crystal at the centre of the microphotograph demonstrates a spherulitic, fibrous inclusion pattern (Type D). The elongate crystal to the upper left also shows radiating fibrous inclusions, but from a medial zone along the length of the crystal. Scale bar is 500 μ m. Stratigraphic top is up. Cow Head North, Lower Ordovician, Bed 8.30, sample CHN-37-D.
- d: Thin section microphotograph of non-ferroan DFC-1 fringe showing the corrugated nature of the intercrystalline boundary by patches of trapped clays. With less clay "paste", intercrystalline boundaries become concertal in appearance. Scale bar is 500 μ m. Stratigraphic top is up. Another microphotograph of this fringe is shown in Plate 39a. Cow Head North, Lower Ordovician, Bed 9.6, sample CHN-115.
- e: Thin section microphotograph of a ferroan DFC-2 fringe showing an oblique section through a "tuft" of splayed calcite crystals. Tips of the various segments of the crystal are anhedral, consisting of stubby, finger-like projections. This sample is a clast within a conglomerate. Scale bar is 1 mm. Broom Point North, Upper Cambrian, unit 37, sample BPS-16.



PLATE 40: DISPLACIVE FIBROUS CALCITE

- a: Thin section microphotograph of a non-ferroan DFC-1 fringe containing calcified radiolaria (arrows) with calcite crystals optically continuous with those of the enclosing crystals. In each of the 3 radiolaria illustrated in this microphotograph, the double wall microstructure has been retained. Note wavy intercrystalline boundaries. Scale bar is 500 μm . Stratigraphic top is up. Another microphotograph of this fringe is shown in Plate 39d. Cow Head North, Lower Ordovician, Bed 9.6; sample CHN-115.
- b: Thin section microphotograph of non-ferroan pseudospar at the base of a DFC-2 fringe. This mosaic demonstrates (1) pronounced lenticularity of the crystals parallel to bedding, (2) a prominent intercrystalline paste, and (3) crystal size increase from the top to the bottom of the microphotograph, i.e. toward the DFC-2 fringe. Scale bar is 500 μm . Stratigraphic top is up. Martin Point, Upper Cambrian, unit 36m-n, sample MP-52.
- c: Thin section microphotograph of peloid-bioclastic grainstone/packstone containing several shale intraclasts surrounded by micro-fringes of DFC (labelled 1-4). The fibrous crystals as well as the interparticle matrix are non-ferroan, except near terminations of the fibrous crystals. This sample is from a limestone nodule enclosed within silicified shale. Scale bar is 500 μm . Stratigraphic top is up. Cow Head North, Lower Ordovician, Bed 11, sample CHN-183.
- d: Thin section microphotograph of a shale intraclast within a pebbly grainstone. This intraclast contains dispersed euhedral to subhedral calcite crystals and is surrounded by a microfringe of DFC many of which demonstrate scalenohedral terminations. The fibrous crystals as well as the interparticle matrix are non-ferroan, except near terminations of the fibrous crystals. Scale bar is 500 μm . Stratigraphic top is up. Broom Point North, Upper Cambrian, unit 33, sample 80-70N-33.

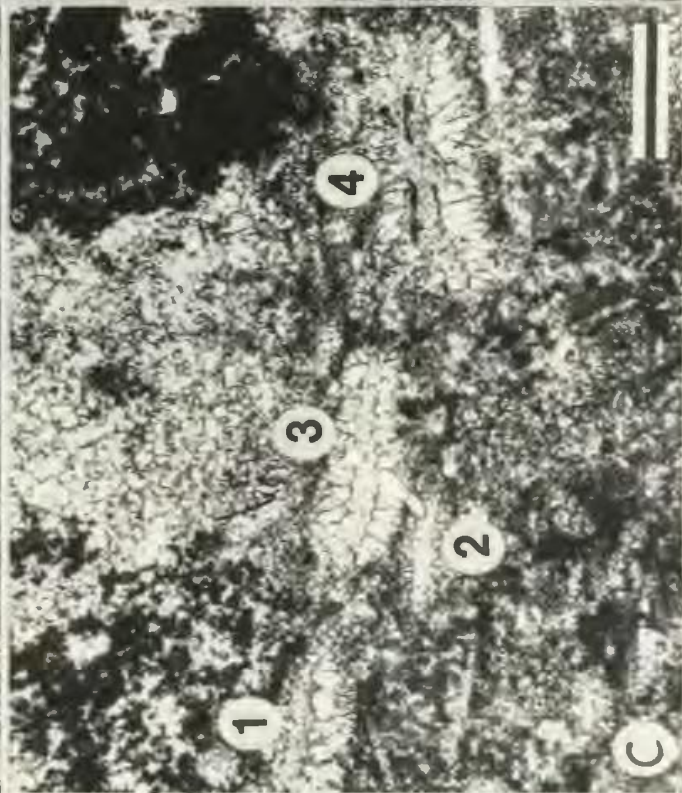
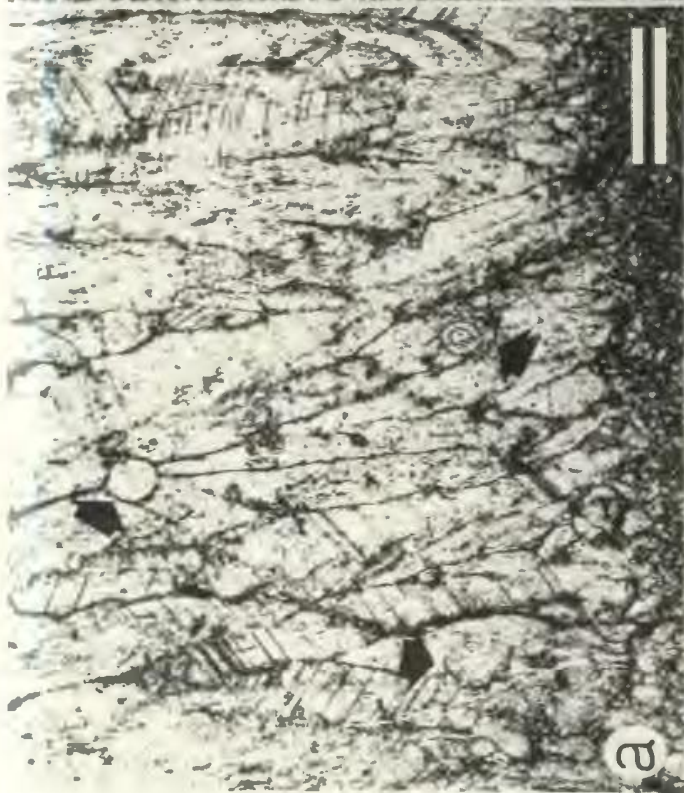


PLATE 41: DISPLACIVE FIBROUS CALCITE

- a, b: Thin section and CL microphotographs of the basal portion of a DFC-1 fringe which occurs as a clast in a conglomerate. Growth zones parallel to the substrate are defined by varying concentrations of inclusions as well as iron content in "a", and CL zones in "b". The inclusion-rich calcite is ferroan but there is little correlation between the CL intensities and the iron content (compare largest crystal on far left of each microphotograph). Most of these growth surfaces are anhedral, but some occasionally demonstrate planar crystals faces (arrows). The growth surfaces in the lower part of the fringe grade transitionally to more euhedral surfaces which characterize the upper part of the fringe ("c" and "d" below). Scale bar is 2 mm. Lower Head, Lower Ordovician, sample LH-73.
- c, d: Thin section and CL microphotographs of upper (distal) portion of the same DFC-1 fringe as shown in the above microphotographs. CL zones are sharp and euhedral. A latest dull-luminescent zone unconformably mantles the earlier zones and suggests possible corrosion of these crystals prior to renewed calcite precipitation. The contact between these two generations of calcite is delineated by arrows. The latest calcite is embayed and replaced by non-luminescent megaquartz (Q), which also fills the spaces between the DFC crystals as a cement. The latest calcite zone and megaquartz are interpreted to be effects related to local diagenesis in the conglomerate. Scale bar is 1 mm.

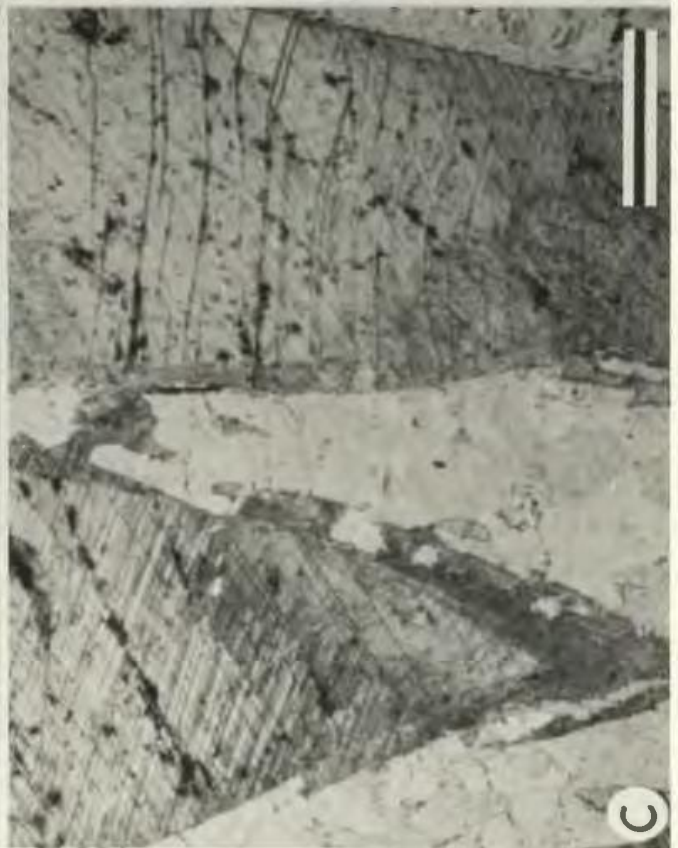


PLATE 42: DISPLACIVE FIBROUS CALCITE

- a: Thin section microphotograph of a DFC-1 fringe which occurs as a clast in a conglomerate. The upper and lower rectangles are the positions of CL microphotographs "c" and "d" below. Scale bar is 2 mm. Broom Point North, Upper Cambrian, sample BPN-14.
- b-d: "b" is a CL view of the same crystals at same scale as shown in "a". The part of the fringe seen in the microphotograph is non-ferroan. This grades into a ferroan upper part (not shown). The crystal in the centre of the field of view clearly demonstrates varying degrees of crystal face and crystallite development. The lower portion of the crystal (shown at greater magnification in "d" below with scale bar of 250 μm) exhibits a subhedral growth surface (faces indicated by arrows in "d") which quickly passes upward into an anhedral surface. With further crystal growth, crystallites and a very irregular growth surface are obvious (magnified in "c" with scale bar of 500 μm). Offsets of CL zones are easily seen in this part of the crystal. The anhedral surfaces progressively become more regular upward until they approximate acute rhombohedra (or scalenohedra - delineated by arrow in "b"). Beyond this the crystal is not sufficiently luminescent to observe zoning. The dull-luminescent, vertical to sub-vertical streaks through some of the crystals (shown in upper left hand portion of "c") are calcite-filled fractures, possibly tectonic in origin.

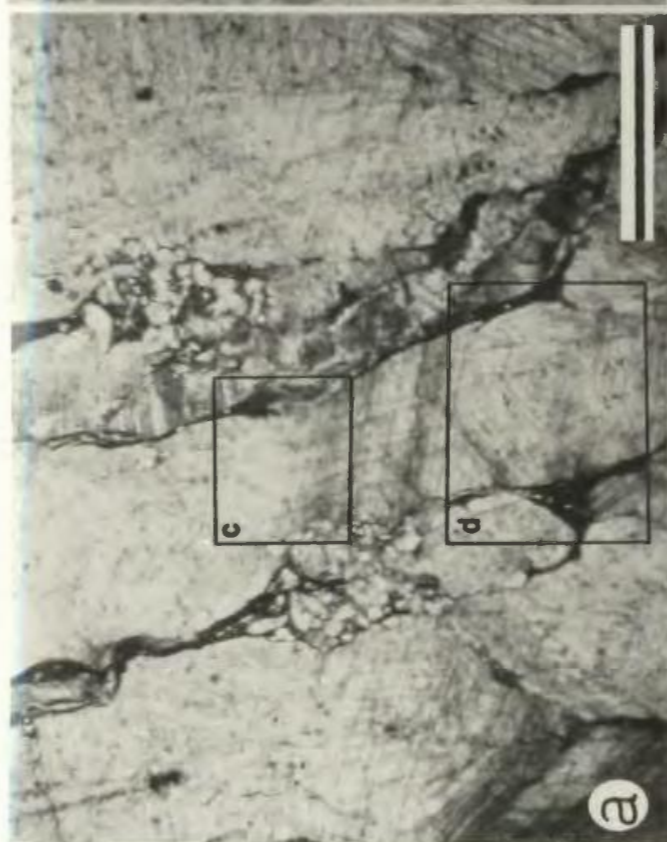


PLATE 43: DFC AND ASSOCIATED PSEUDOSPAR

- a, b: Plane light and CL microphotographs of the transition zone between pseudospar and the base of a DFC-2 fringe developed on a wavy to nodular bed. Most of the relief on this bed is due to the presence of the fringe. Both the underlying pseudospar as well as the base of the fringe are non-luminescent. Younger parts of the DFC crystals are dull. These basic relationships demonstrate that lithification of the mudstone substrate occurred prior to growth of DFC. All of the calcite in this sample is ferroan. Scale bar is 500 μm . Stratigraphic top is up. Green Point, Upper Cambrian, unit 8, sample GP-3-A.
- c: CL microphotograph of a conglomerate clast containing coarse pseudospar at the base of a DFC fringe (hybrid of DFC-1 and DFC-2 characteristics). Pseudospar is dull-luminescent and ferroan at the centre and has moderately bright-luminescent, non-ferroan rims. The prominent shale paste between the calcite crystals contains abundant zoned dolomite crystals and blue-luminescent detrital feldspar silt (seen as light specks). The pseudospar aggregate floating within the dolomitized shale consists of 3 crystals (intercrystalline boundaries traced in ink) with varying orientations. These crystals as well as those in the lower left of the microphotograph illustrate CL zone offsets and obvious crystallites. Scale bar is 250 μm . Stratigraphic top is up. Cow Head North, Lower Ordovician, Bed 8, sample CHN-30.
- d: CL microphotograph of 2 coarse ferroan pseudospar crystals overlying a DFC-1 fringe developed between mudstone nodules. In the crystal on the left, crystallites and CL zone offsets are conspicuous. Both crystals demonstrate asymmetrically-developed zoning. Scale bar is 250 μm . Cow Head North, Lower Ordovician, Bed 8.30, sample 6E.

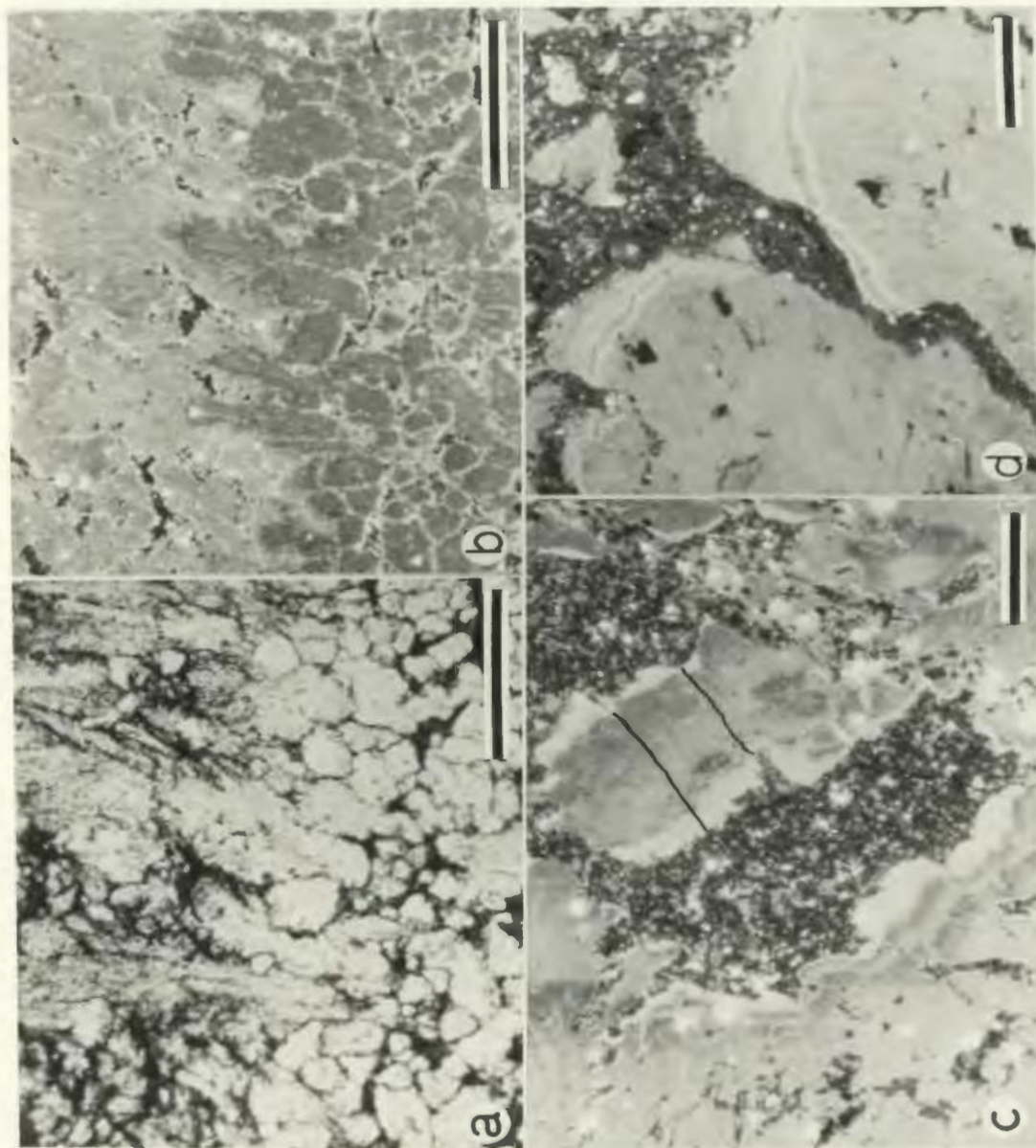


PLATE 44: EQUANT PSEUDOSPAR

- a, b: Plane light and CL microphotographs of dull- to weak-luminescent, non-ferroan, equant pseudospar at the base of a DFC-1 fringe (illustrated in Plate 42a). Crystal 2 demonstrates obvious crystallites as well as subhedral to anhedral growth surfaces (also crystals 1 and 3). In addition, this microphotograph shows that initially equant pseudospar may grow to elongate crystals by asymmetrical crystal growth preferentially toward the bed margin. Scale bar is 250 μm . Stratigraphic top is up. Broom Point North, Upper Cambrian, sample BPN-14.
- c, d: Plane light and cathode luminescence microphotographs of pseudospar in conglomerate matrix. The earliest precipitates are bright-luminescent. Later calcites have dull to weak luminescence. Ferroan zones occur but are not correlated with CL zones in this particular sample. Crystals adjacent to the shale (squashed intraclast?) develop obvious crystallites in the later stages of growth, making crystals elongate by asymmetrical growth (e.g. crystals 1, 2, and 3). Scale bar is 250 μm . Stratigraphic top is up. Cow Head South, Lower Ordovician, Bed 9s.21, sample CHS-23-A.

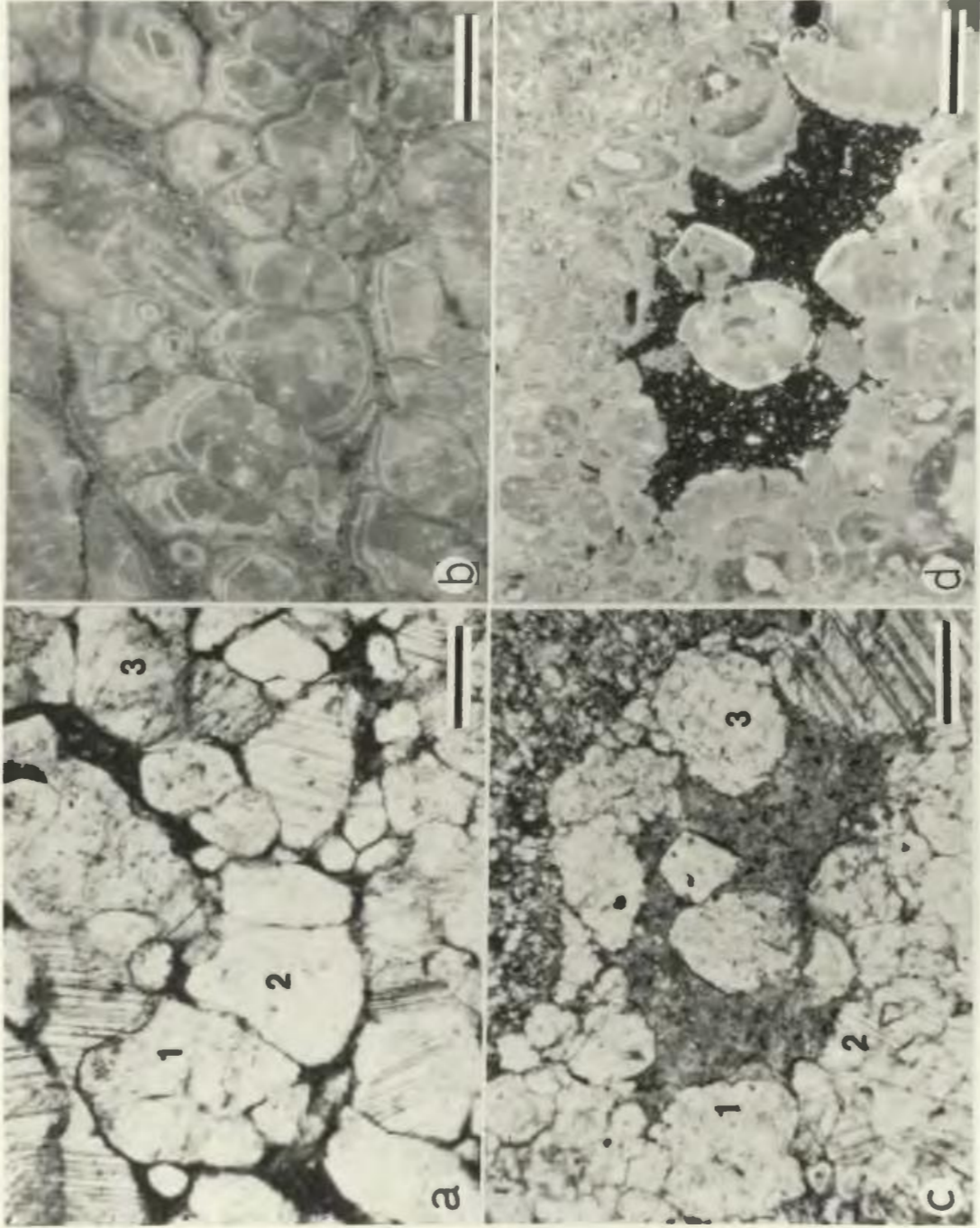


PLATE 45: DFC: EVIDENCE FOR EARLY ORIGIN

- a: DFC-1 fringe (arrow) developed on mudstone nodule clast in conglomerate. Stratigraphic top is up. Stearing Islands, Lower Ordovician, unit 6, sample SI-3.
- b: Clast of DFC-1 fringe and grainstone substrate in conglomerate. Knife scale is 9 cm long. Broom Point North, Upper Cambrian, sample BPN-12.
- c: Wide DFC-1 fringe developed on parted limestone raft in conglomerate within melange zone at Lower Head. Knife scale is 9 cm long. Sample LH-1.
- d: Thin section negative print of curved DFC-2 fringe which is interpreted to represent deformation related to submarine sliding. See text for details. Scale bar is 5 mm. Stratigraphic top is up. Green Point, Upper Cambrian, units 7-8, sample GP-109.
- e: Thin section negative print of curved DFC-2 fringe is interpreted to represent deformation related to submarine sliding. The fringes which overlie and underlie the seam thicken and thin out of phase with one another thus maintaining the multiple fringe thickness. This also indicates growth during shearing. Scale bar is 2 mm. Stratigraphic top is up. Green Point, Upper Cambrian, units 4-10, sample GP-23.
- f: Reoriented mudstone bed fragments underlie the major truncation surface at Lower Head (discussed in Chapter 3). Some of these fragments have DFC-2 fringes (arrows) whose patchy distribution suggests a syndeformational origin. Stratigraphic top is up. Lower Head, Lower Ordovician.
- g: Thin section negative print of DFC-2 fringe contains a spherulite of DFC-2. This fringe intersects the truncation surface at Lower Head. The anomalous development of a spherulite is interpreted to be a response to disturbance in the sediment pile related to the formation of the overlying truncation surface. Scale bar is 5 mm. Stratigraphic top is up. Lower Head, Lower Ordovician, sample LH-76-A.



PLATE 46: CATHODE LUMINESCENCE AND MICROPROBE TRAVERSES

N.B.: Black lines indicate positions of microprobe traverses used for the elemental oxide profiles plotted in Figure 10.1.

- a: Cement in septarian ladder crack in parted mudstone dominated by CL Stage A microspar. The analysed cement crystal clearly demonstrates an MgO-rich, non-luminescent, CL Stage A calcite with low FeO and MnO and increases in these elements along with concomitant decrease of MgO in later (Stages B and C) precipitates. Traverse length is 91 μm . Scale bar is 250 μm . Sample is from a raft in a conglomerate. St. Paul's South, Lower Ordovician, unit 2, sample SPS-13-B.
- b: Intraparticle cement within intact brachiopod shell. MgO decreases with successive precipitation and FeO and, to a lesser extent, MnO increase. Traverse length is 304 μm and goes from CL Stage B to C. Scale bar is 250 μm . Cow Head South, Lower Ordovician, Bed 9s.21, sample CHS-23-A.
- c: Pelmatozoan fragment and syntaxial cement overgrowth. The earliest cement is characterized by an increase in MgO over the levels present in the pelmatozoan, but these relatively high levels fall off with the latest precipitates. MnO and FeO are both low in the pelmatozoan and only MnO is present in any significant amount in the earliest cement. Scale bar is 250 μm . Traverse length is 195 μm and goes from CL Stage B to C. Scale bar is 250 μm . Cow Head North, Lower Ordovician, Bed 8.30, sample CHN-177.
- d: Cement in conglomerate matrix. This sample demonstrates that the earliest, non-luminescent precipitate is depleted in all the trace elements, but with later precipitation, MgO and FeO are important. This calcite is followed by megaquartz cement (black in microphotograph). Traverse length is 341 μm and goes from CL Stage A to C. Scale bar is 250 μm . Cow Head South, Lower Ordovician, Bed 9s.16, sample CHS-16.
- e: Coarse neospar at the base of DFC-1 fringe shows fibrous crystallites, CL zoning offsets, and an uneven growth surface. This sample demonstrates a general decrease in MgO with successive precipitation and a concomitant increase in FeO. The latest calcite also shows an increase in MgO. Traverse length is 271 μm and is mostly within CL Stage B calcite. Scale bar is 250 μm . Cow Head North, Lower Head, Bed 8.30, sample CHN-37-D.

continued on next page

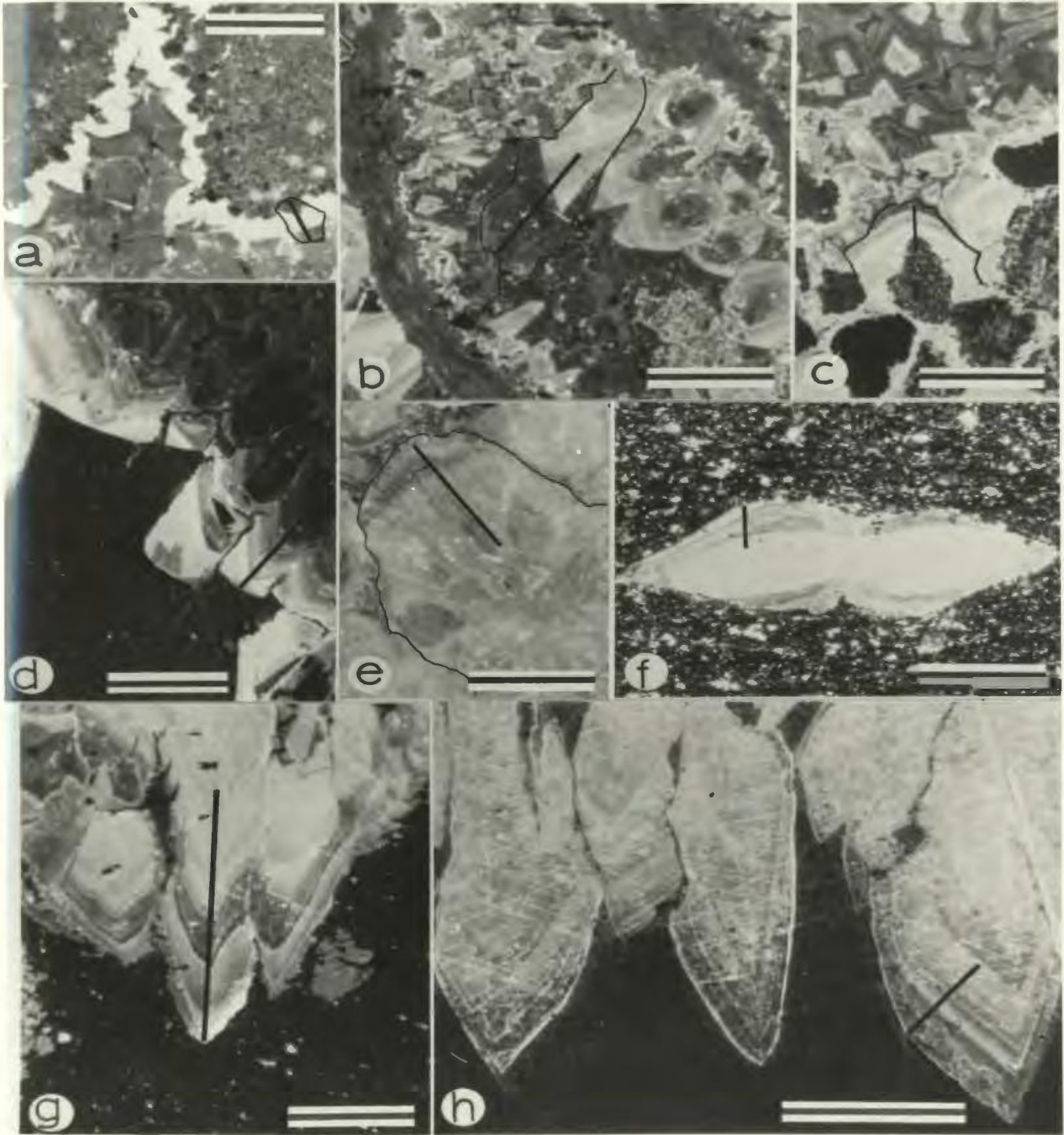


PLATE 46 (continued)

- f: Isolated, floating pseudospar crystal in lower part of marginally-aggraded mudstone. This traverse demonstrates a slight increase in MgO with successive precipitation and decreases in MnO and FeO. FeO increases slightly near the margin of the crystal. Note uneven growth surfaces. Small points visible in the microphoto are artifacts of various microprobe step analyses. Traverse length is 108 μm and goes from CL Stage B to C. Scale bar is 250 μm . Cow Head North, Lower Ordovician, Bed 8.30, sample CHN-37-C.
- g: DFC-1 fringe at base of grainstone. With successive precipitation, MgO, FeO, and MnO all increase. Prominent CL zoning allows distinction of obvious crystal pseudofaces. Traverse length is 813 μm and goes from CL Stages B to C. Scale bar is 350 μm . Cow Head North, Lower Ordovician, Bed 8.24, sample CHN-169.
- h: Termination of DFC-1. MgO increases slightly toward crystal termination whereas both FeO and MnO decrease. Traverse length is 1052 μm and is mostly within CL Stage C. Scale bar is 2 mm. Cow Head North, Lower Ordovician, Bed 8.30, sample CHN-104.

PLATE 47: DOLOMITIZATION: FIELD RELATIONSHIPS

- a: Cross-laminated grainstone contains a few resistant-weathering, selectively-dolomitized parallel and foreset laminations. Stratigraphic top is up. Western Brook Pond South, Lower Ordovician, unit 5.
- b: In an argillaceous interbed between a parted mustone interval and a massive grainstone is a 15 cm-thick, dolomitic marl (M) which extends for over 20 m until it is hidden by cover. This marl transforms laterally into an 8 cm-thick, relatively carbonate-free shale (S). Petrographic characteristics of the marl and shale are identical to those of other marls and shales in the CHG. This key outcrop provides unequivocal evidence that dolomitization precedes final compaction of the argillaceous sediments. Stratigraphic top is up. Cow Head North, Upper Cambrian, Bed 6.52-6.54.
- c: Massive and ripple-laminated grainstone (L) is in relatively sharp contact with a joint-dolomitized zone (D). Stratigraphic top is up. Broom Point South, Upper Cambrian, unit 34.
- d: Joint-dolomitized zone (D) in a parted mudstone sequence. Stratigraphic top is up. Broom Point South, Upper Cambrian, unit 33.
- e: Coarsely crystalline, pervasive replacement dolomite shows numerous, large vugs whose tabular shape suggests they are leached flat-pebbles. Stratigraphic top is up. Outcrop is the Arches, stratigraphic affinity is uncertain.

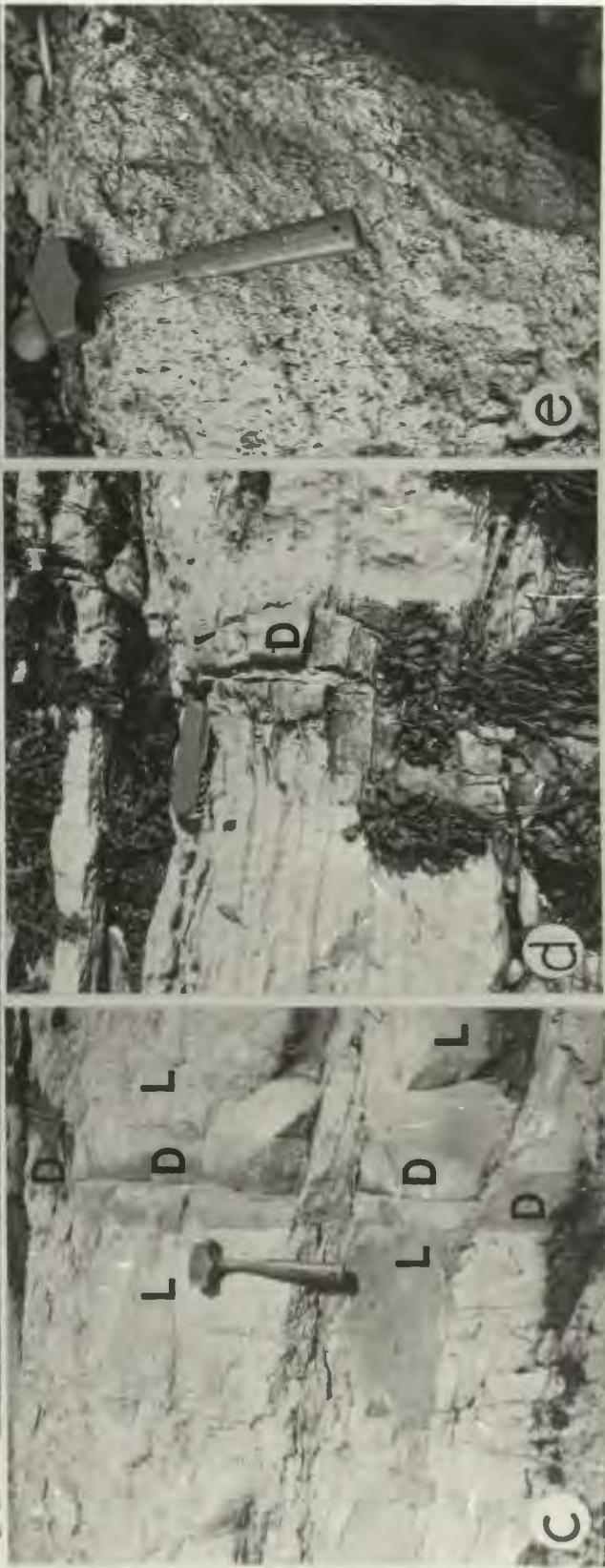


PLATE 48: DOLOMITIZATION: PETROGRAPHY

- a: Thin section microphotograph of dolomitic siltstone composed of cloudy-centered, clear-rimmed ("CCCR") crystals which have ferroan rims and non-ferroan centres. White patches are scattered siliciclastic silt grains. Arrow points to rounded, cloudy centre which is a detrital dolomite core. Scale bar is 200 μm . Stratigraphic top is up. Martin Point, Upper Cambrian, unit 32, sample MP-41.
- b: Thin section microphotograph of silicified dolomitic siltstone in red shale sequence illustrating etched dolomite crystals floating in a microquartz matrix. Scale bar is 100 μm . Stratigraphic top is up. St. Paul's North, Middle Ordovician, units 83-85, sample SPN-38.
- c: Thin section microphotograph of a dispersed dolomite crystal in peloidal grainstone which partially replaces a radial ooid cortex while retaining sufficient relics to outline the replaced portion. Scale bar is 200 μm . Unoriented thin section. Martin Point, Upper Cambrian, unit 23, sample 80-39-23.
- d: Thin section microphotograph of a vertical stylolite zone (bracketed) which consists of numerous dolomite crystals with CCCR and intercrystalline argillaceous material. Host sediment is a peloidal grainstone cap which overlies a conglomerate. Scale bar is 500 μm . Stratigraphic top is up. Cow Head North, Lower Ordovician, Bed 8.35, sample CHN-110.
- e: Thin section microphotograph of anhedral to locally sucrosic (see "f" and "g" below), joint dolomite mosaic which thoroughly overprints grainstone precursor. Microfabric preservation in rare clasts such as the radial ooid is due to replacement by dolomicrite. The cloudy patches surrounding the ooid are interpreted to be the inclusion relics of replaced peloids and other allochems. Scale bar is 500 μm . Stratigraphic top is up. Broom Point South, Upper Cambrian, unit 25, sample BPS-32.
- f: SEM view of fractured surface from same sample as in "e" and "g". The dolomite crystals show smooth rhombic forms and a nondescript intercrystalline substance (clays?) along with a microquartz prism (arrow). Scale bar is 10 μm .
- g: SEM view of fractured surface from same sample as in "e" and "f" above. Overlying the dolomite rhombs, possible clays, and authigenic quartz (Q) is a smooth, draping mantle interpreted to be bitumen (B). Scale bar is 20 μm .

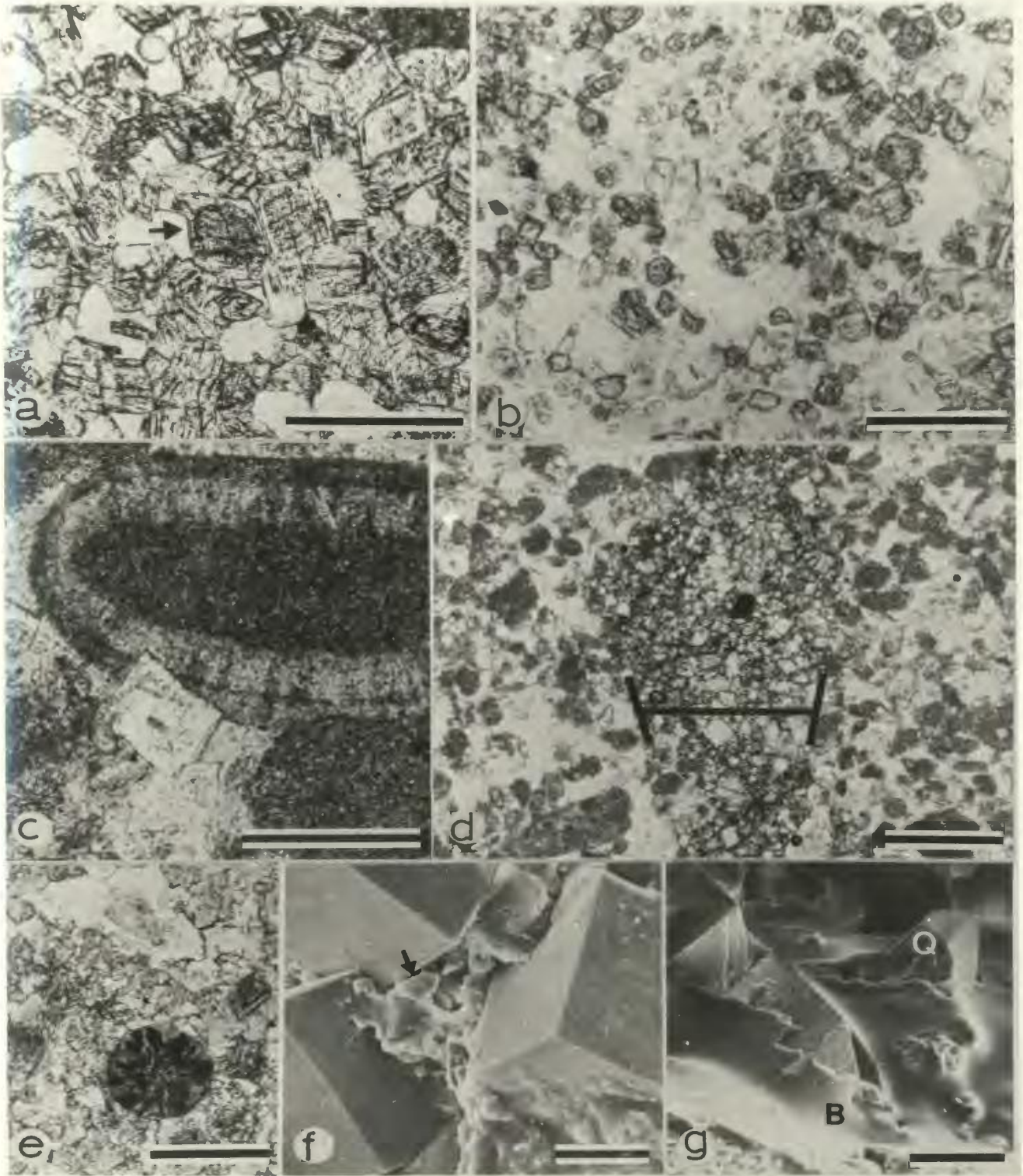
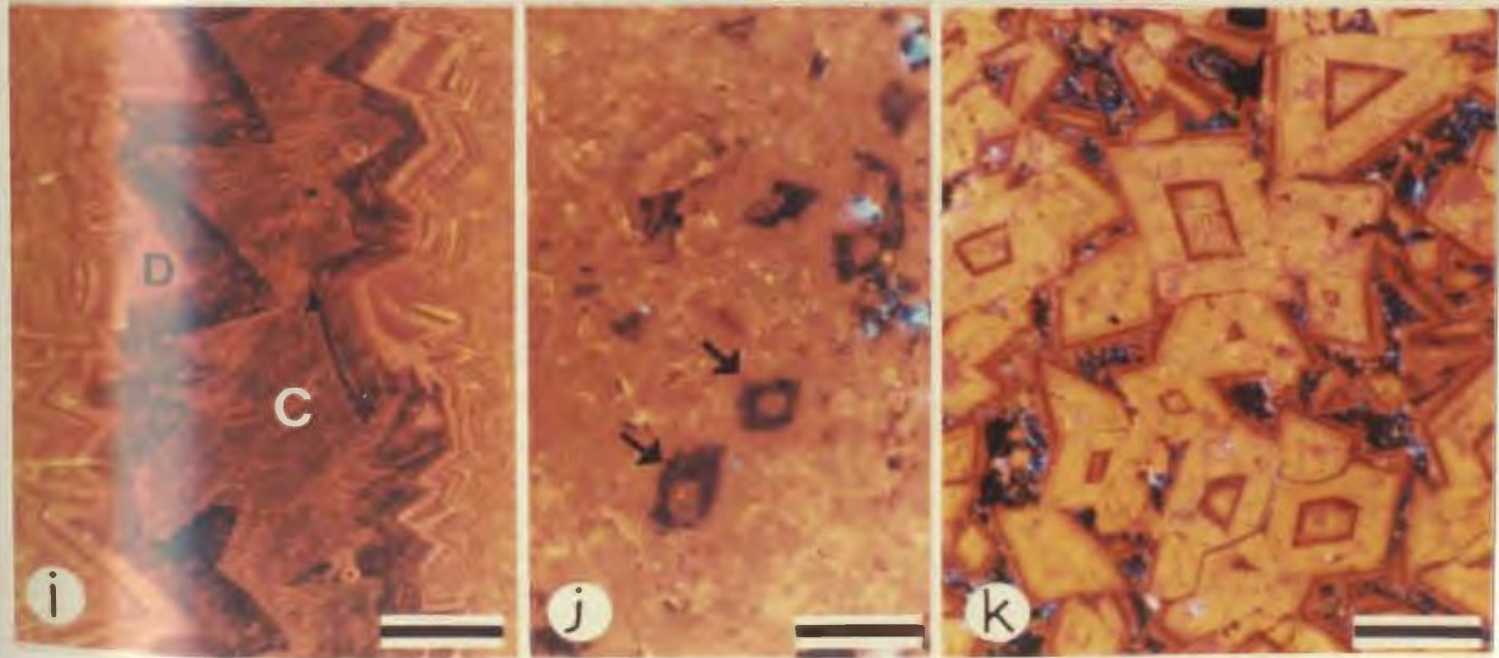
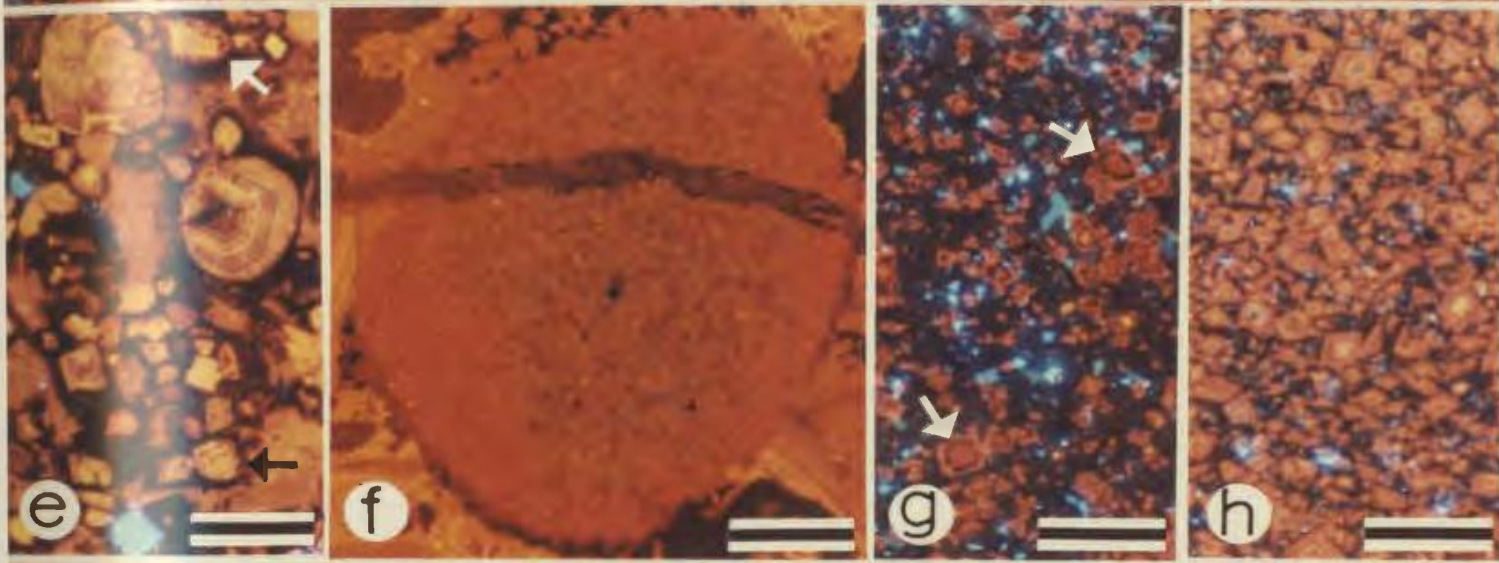
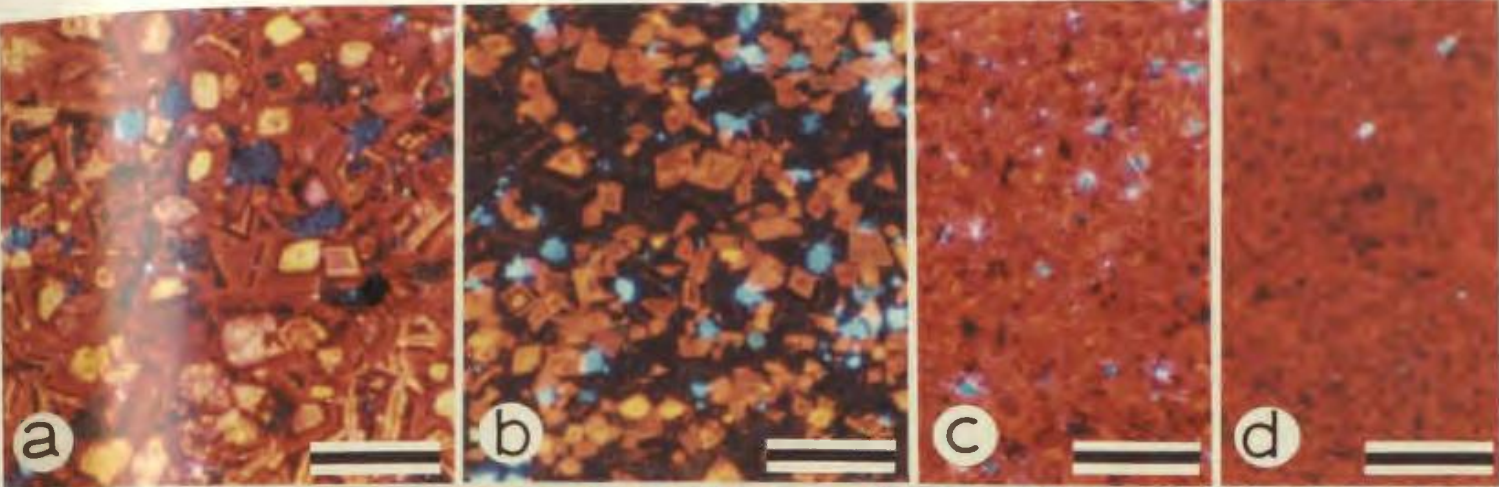


PLATE 49: DOLOMITIZATION: CATHODE LUMINESCENCE

- a: Dolomitic siltstone with numerous bright-luminescent detrital dolomite cores showing irregular, often angular, shapes and truncation of zoning. Finely-zoned authigenic overgrowths are weak red-luminescent. Weak blue luminescent grains are mostly quartz silt. Scale bar is 200 μm . Broom Point North, Upper Cambrian, unit 9, sample 80-70-9.
- b: Dolomitic siltstone with non-luminescent (ferroan) outer rims overgrowing an earlier stage of bright red-luminescent dolomite. Scattered yellow-orange centres are detrital dolomite. The dominant dull centres may be dolomitized peloids. Numerous bright blue specks are detrital feldspar silt grains. Scale bar is 200 μm . St. Paul's North, Upper Cambrian, unit 6, sample SPN-17.
- c: Dolomitic siltstone from red shale sequence is typically finely crystalline with thin bright red-luminescent rims and dull cores. Additional details are usually not resolvable with CL. Numerous bright blue specks are detrital feldspar silt grains. Scale bar is 200 μm . Martin Point, Middle Ordovician, unit 58, sample MP-84.
- d: Dolomitic siltstone from red shale sequence is seldom as coarsely crystalline as that shown in this microphotograph. The dull centres of the crystals may have rhombic or rounded shapes. These are overgrown by bright red-luminescent rims. Scale bar is 200 μm . St. Paul's North, Middle Ordovician, units 83-84, sample SPN-43-B.
- e: Dispersed dolomite crystals have detrital cores which show variable luminescence, angular to rounded shapes, and truncated zoning (black arrow). In the upper part of the microphotograph, a rounded polycrystalline dolostone clast is seen. Also near the top is a rounded, monocrystalline detrital core (white arrow) which appears to have been micritized prior to authigenic overgrowth by dark, ferroan dolomite. Evenly weak-luminescent material between dolomite crystals is the peloidal grainstone host sediment. Scale bar is 200 μm . Broom Point North, Upper Cambrian, units 20-23, sample BPN-42.
- f: Large polycrystalline dolostone clast is replaced on margins by bright red-luminescent (Early?) dolomite. Host sediment is a peloidal grainstone. A brown-luminescent calcite microveinlet which cut through the dolostone clast postdates all other diagenetic effects. Scale bar is 250 μm . Cow Head North, Lower Ordovician, Bed 8.30, sample CHN-177.

continued on next page



* PLATE 49 (continued)

- g: Detrital nodule consists of partially silicified shale and abundant siliciclastic silt (blue-luminescent feldspar and dark quartz). The latest red-luminescent zone in the dolomite crystals corrodes an earlier non-luminescent zone (arrows). Scale bar is 200 μ m. Lower Head, Lower Ordovician, sample LH-28.
- h: Matrix dolomite (marl interbed) within a ribbon mudstone raft in a conglomerate demonstrates that the dolomite crystals share a common microstratigraphy throughout and that detrital cores are apparently absent. The confinement of blue-luminescent feldspar silt to the intercrystalline areas indicates that dolomite crystal growth was displacive. Scale bar is 200 μ m. Cow Head South, Lower Ordovician, Bed 10s, sample CHS-55.
- i: Fracture-filling joint dolomite crystals (D) illustrate fine-scale zoning until the final broad, dark, ferroan precipitate. Remaining porosity is filled with brown-luminescent calcite (C). These dolomite crystals have curved crystal faces and pronounced undulosity. A traverse across a typical dolomite cement crystal from this sample is shown in Figure 10.1b. Scale bar is 500 μ m. Broom Point South, Upper Cambrian, unit 33, sample BPS-33-A.
- j: Joint dolomite replaces peloidal grainstone and engulfs earlier-formed, dark, authigenic rims which overgrow grains of detrital dolomite (arrows). Scale bar is 200 μ m. Broom Point South, Upper Cambrian, unit 34, sample BPS-29-A.
- k: These moderately bright-luminescent matrix dolomite crystals occur in a 5 mm thick band within a peloidal grainstone. The intercrystalline argillaceous(?) material contains abundant detrital feldspar dust and was displaced by the growing dolomite crystals. Scale bar is 200 μ m. Cow Head North, Lower Ordovician, Bed 8 in Tucker's Cove, sample CHN-73.

PLATE 50: SILICEOUS SEDIMENTS

- a: Chert cap (below hammer head) on conglomerate varies in composition from silicified grainstone to silicified shale. Stratigraphic top is to right (right half of field of view is bedding surface). Cow Head North, Lower Ordovician, Bed 10.
- b: Conglomerate eroded into silicified, dark-coloured parted mudstone. This suggests early diagenetic silicification of the mudstone. Stratigraphic top is up. Lower Head, Lower Ordovician.
- c: This photograph shows diffuse elongate, silicification zones developed in a massive mudstone (1) and more completely silicified zones in a parallel- and ripple-laminated silt-size grainstone/packstone (2). Stratigraphic top is up. Cow Head North, Lower Ordovician, Bed 9.6.
- d: Thin section microphotograph of pyritized sponge spicules (S) in a bright green-coloured, silicified shale. Arrow points to a pyritized radiolarian test. Scale bar is 250 μ m. Stratigraphic top is up. Western Brook Pond North, Lower Ordovician, unit 12, sample WN-9-C.
- e: Thin section negative print of completely silicified radiolaria packstone in a silicified shale sequence. Scale bar is 2 mm. Western Brook Pond South, Middle Ordovician, unit 52, sample WS-9.
- f: Thin section microphotograph of a limestone nodule (left half of photograph) consisting of radiolaria packstone surrounded by totally silicified equivalent, but with less microfabric preservation (right half of photograph). Scale bar is 1 mm. Stratigraphic top is up. Unmeasured section south of St. Paul's South, Lower Ordovician?, sample SPS-12-B.
- g: Thin section microphotograph of silicified (s) and partially pyritized (p) radiolaria in a silicified, dark green-coloured shale. In places, pyritization has clearly preserved microfabrics to a higher degree than when radiolaria are calcified or replaced by chalcedony. This view is from the same thin section as that in "i" below. Scale bar is 100 μ m. Martin Point, Lower Ordovician, unit 54, sample MP-82-A.

continued on next page

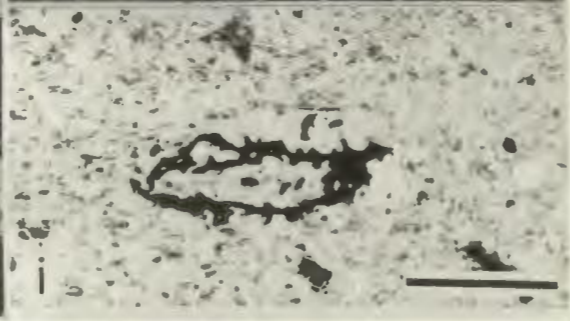
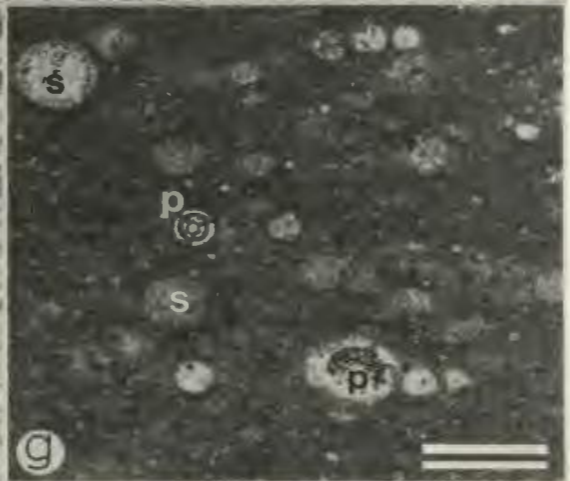
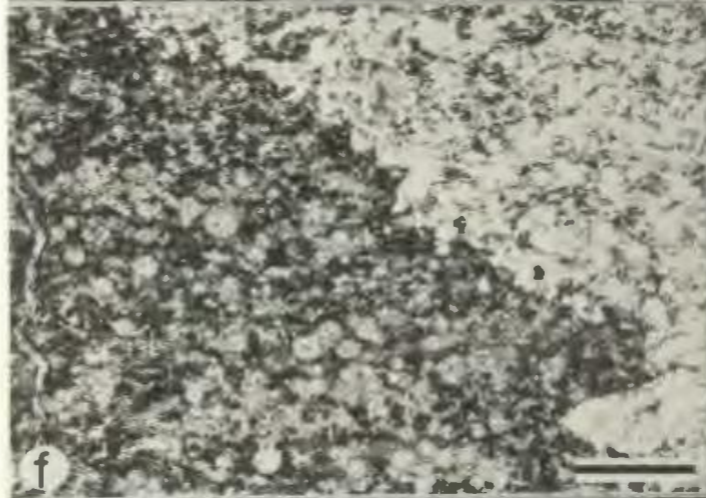
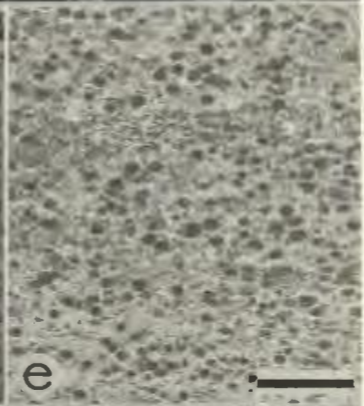


PLATE 50 (continued)

h: Thin section microphotograph of a graded, spicule-rich bed in a silicified, red shale. Scale bar is 250 μm . Stratigraphic top is up. Western Brook Pond South, Middle Ordovician, sample WS-1.

i: Thin section microphotograph of a collapsed, pyritized radiolarian in a silicified shale (same as that in "g" above). This radiolarian was initially pyritized but not silicified sufficiently quickly in order to prevent mechanical compaction. After compaction, a later stage of silicification occurred. Scale bar is 100 μm . Martin Point, Lower Ordovician, unit 54, sample MP-82-A.

PLATE 51: PSEUDO-WACKESTONES: CATHODE LUMINESCENCE

- a, b: Plane light and CL microphotographs of a limestone nodule from a silicified shale sequence. In plane light, the sediment appears to be a peloidal wackestone, containing numerous specks of pyrite (black) and the occasional calcified radiolarian and sponge spicule. With CL, however, both radiolaria and spicules are abundant and the depositional fabric is interpreted to be packstone. The matrix of the sediment as well as the earliest cement in the radiolaria is bright orange-luminescent (Stage B), non-ferroan calcite. The spicules were replaced at a later time and are dominantly dull-luminescent (Stage C), very slightly ferroan calcite. Scale bar is 250 μm . Stratigraphic top is up. Unmeasured outcrop in Saint Paul's Inlet, south of St. Paul's South section, Lower Ordovician, sample SPS-12.
- c, d: Plane light and CL microphotographs of a limestone nodule from a silicified shale sequence. As with the above microphotographs, only scattered spicules are differentiable in plane light, but CL illustrates calcified spicules are the volumetrically most important depositional components of this sediment. Their axial canals are filled with bright orange-luminescent (Stage B), non-ferroan calcite identical to the matrix neospar(?). Spicules are very slightly ferroan, dull-luminescent (Stage C) calcite. These spicules now consist of polycrystalline calcite and are interpreted to have originally been siliceous. Scale bar is 250 μm . Stratigraphic top is up. Cow Head North, Lower Ordovician, Bed 11.1, sample CHN-183.
- e, f: Plane light and CL microphotographs of a limestone nodule from a silicified shale sequence (same sample as "c" and "d" above). In the centre of the microphotographs a micro-fringe of DFC is dominated by Stage B calcite and has thin tips of Stage C calcite, identical to that which replaces the spicules. Fibrous crystallites in these DFC crystals are barely discernible. Arrow points to microquartz which has interrupted filling of the spicule mold by calcite cement, burying its rhombic termination. The shale intraclast (S) surrounded by the DFC fringe has been squashed and exhibits numerous blue luminescent detrital feldspar silt grains (light specks in microphotograph). Scale bar is 250 μm . Stratigraphic top is up. Cow Head North, Lower Ordovician, Bed 11.1, sample CHN-183.

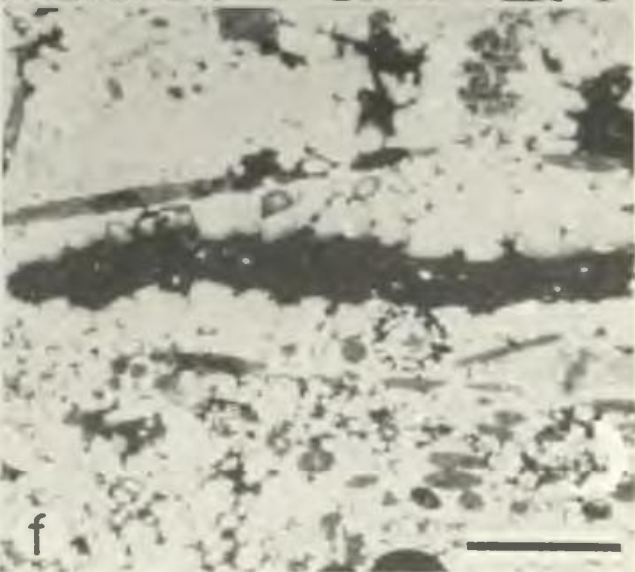
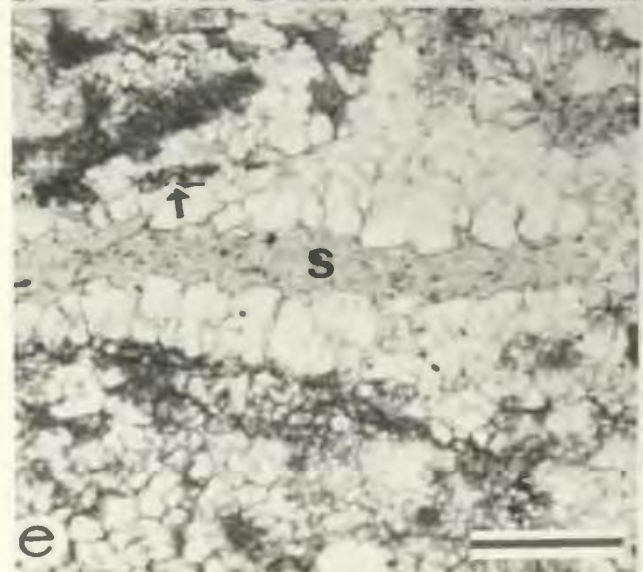
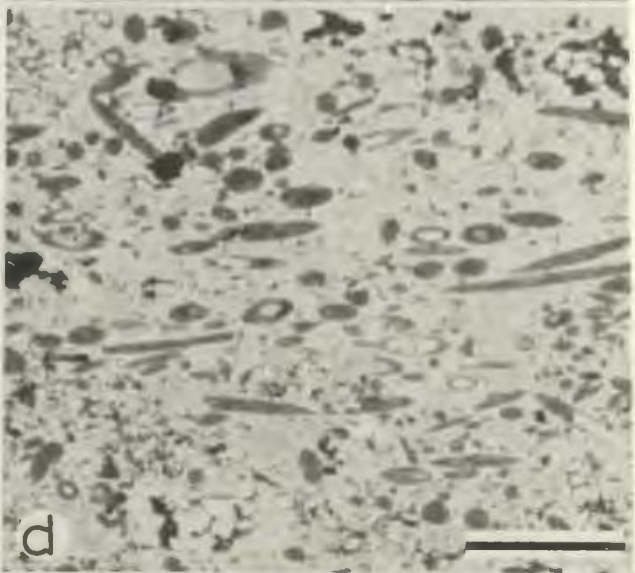
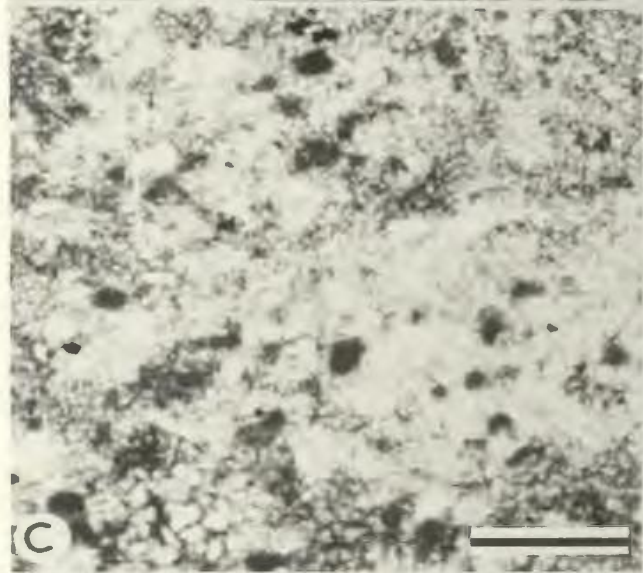
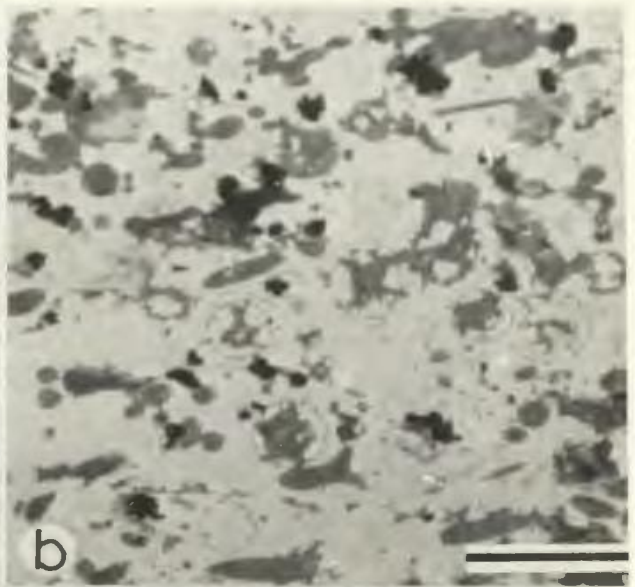
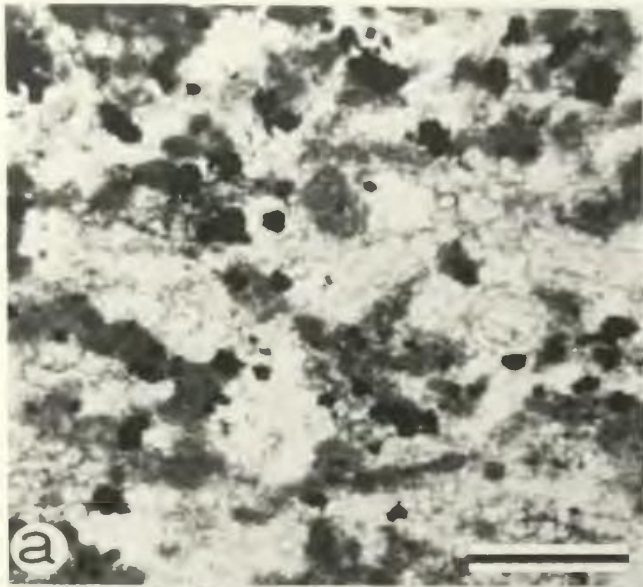


PLATE 52: BARITE

- a: Thin section negative print of a barite layer (b) within a nodular to wavy bed dominated by ferroan pseudospar (p). Barite increases in crystal size and becomes more elongate downward, and larger crystals also tend to be oriented at high angle to bedding. Inter-barite crystal matrix is argillaceous sediment. A fringe of ferroan, DFC-2 (f) underlies the bed. In the lower portion of the bed are faint ripple laminations outlined by silt-size siliciclastics and peloids (s). Slab photograph "d" below is also taken from this sample. Scale bar is 1 cm. Stratigraphic top is up. Green Point, Upper Cambrian, units 16-18, sample GP-47-D.
- b: Thin section negative print of a microspar mudstone-wackestone nodule with coarse barite crystals (dark) on the upper and lower margins. Scale bar is 1 cm. Stratigraphic top is up. Green Point, Upper Cambrian, sample GP-31.
- c: Thin section microphotograph of a barite nodule in which barite crystals (b) marginally aggrade and become progressively more replaced by non-ferroan calcite (c). Scale bar is 1 mm. Stratigraphic top is up. Black Brook, Lower Ordovician, unit 9, sample BB-3.
- d: Slab of a pseudospar nodule with a coarse barite rosette (b) locally developed near the centre of the bed. The lower portion of the nodule is underlain by DFC-2. Negative print "a" above is also taken from this sample. Stratigraphic top is up. Green Point, Upper Cambrian, units 16-18, sample GP-47-D.
- e: Thin section microphotograph of barite pseudomorphs in a non-ferroan microspar mudstone. The pseudomorphs are interpreted to be barite molds completely filled with non-ferroan calcite cement. This bed is also substrate to DFC-1 (not shown). Scale bar is 1 mm. Green Point, Upper Cambrian, sample GP(81-7).
- f: Cross-polarized light microphotograph of incompletely-filled barite molds. The calcite cement and surrounding microspar are non-ferroan. Scale bar is 1 mm. Stratigraphic top is up. Green Point, Upper Cambrian, units 16-17, sample GP-115.
- g: Thin section microphotograph of a barite (b) and ferroan pseudospar (c) mosaic in a mudstone. The lack of replacement microfabrics suggests that these phases grew simultaneously. Scale bar is 500 μm . Stratigraphic top is up. Green Point, Upper Cambrian, units 16-17, sample GP-116.

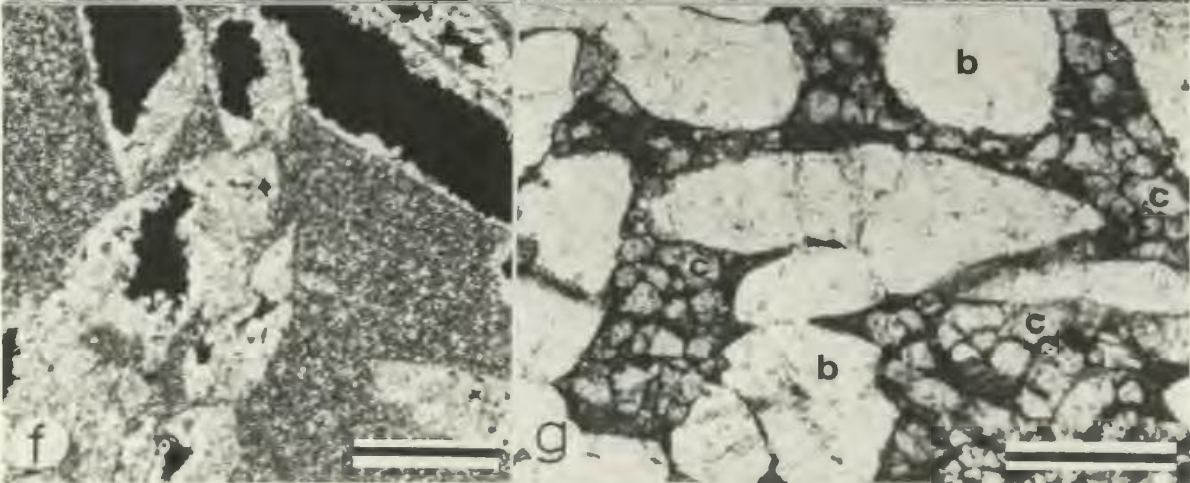
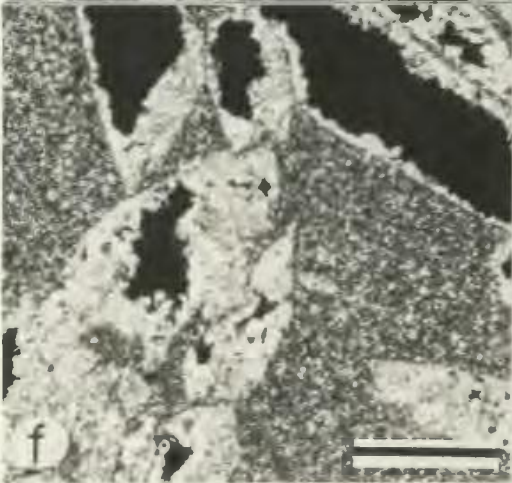
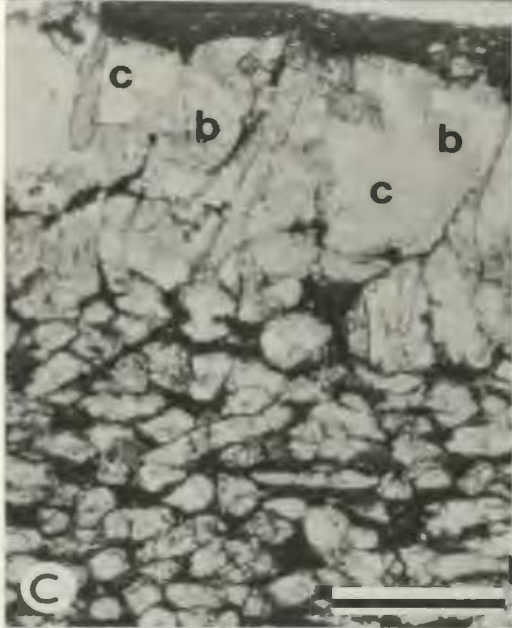
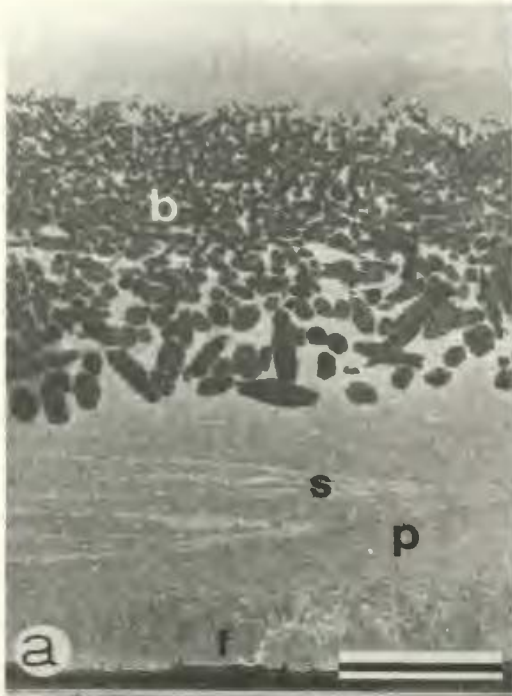
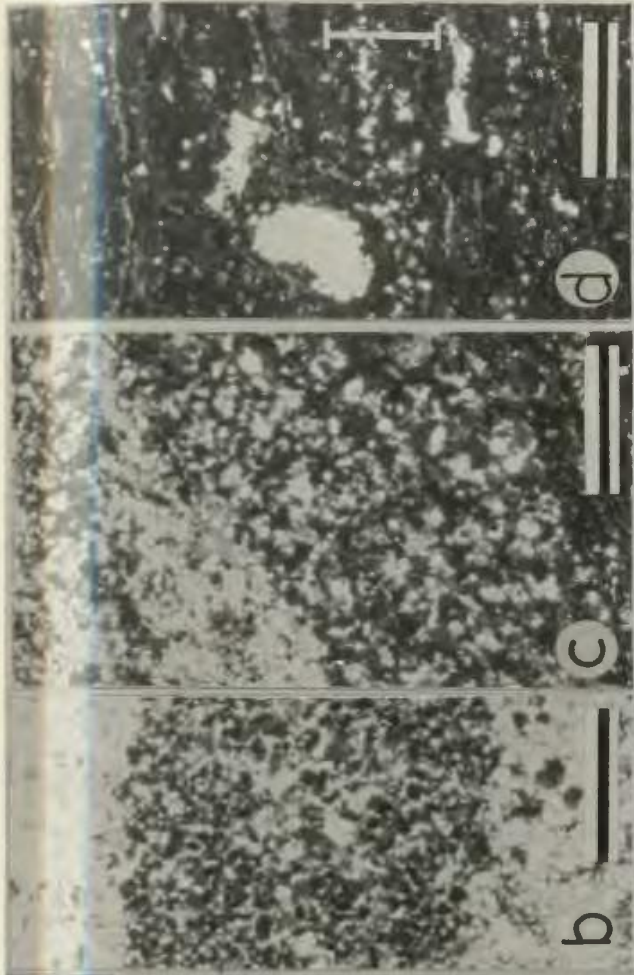


PLATE 53: NODULE-MATRIX RELATIONSHIPS

- a: Thin section negative print of nodule consisting of peloidal wackestone (W) overlain by peloidal grainstone (G). Thin peloidal grainstone laminations are found in the lower part of the nodule. A grainstone lamination which extends from the nodule into the internodular matrix is examined in the next 3 microphotographs, their locations shown by the arrows b, c, and d. Scale bar is 1 cm. Stratigraphic top is up. St. Paul's Quarry, Upper Cambrian, sample SPQ-6.
- b: Thin section microphotograph of peloidal grainstone lamination surrounded by pseudospar of nodule (white) which shows well-defined peloids cemented by non-ferroan calcite. Larger white specks in this lamination are bioclastic grains. Scale bar for this and the subsequent 2 microphotographs is 1 mm.
- c: Thin section microphotograph of the lamination (lower 3/4 of view) as it emerges from the nodule. The peloids rapidly lose their definition and are pressed one into the other. The white specks in this lamination are patches of cement and bioclastic grains.
- d: Thin section microphotograph of the lamination at a distance of a 2.5 cm from the edge of the nodule. The lamination (bracketed) consists of indistinct, clotted, argillaceous micrite with scattered dolomite crystals and siliciclastic silt (white specks). The large white patches are pelmatozoan debris. Beyond this the micrite fades out into the argillaceous matrix, probably due to pressure solution.
- e: Thin section negative print of a composite mudstone nodule illustrating evidence for exposure on the sea floor. Numbers and explanation are provided in Appendix N. Scale bar is 1 cm. Stratigraphic top is up. Cow Head North, Upper Cambrian, Bed 6, sample CHN-25.
- f: Slab of nodular mudstone (M) and grainstone between (G) and overlying (H) nodules. This sample suggests submarine exposure of the mudstone based on its relationship with the overlying grainstone lamination. This is further explained in Appendix N. The mudstone and the overlying planar-bedded, parallel-laminated grainstone above this contain vertical stylolites (S). The nodular bed near the top of the slab consists of isolated ripples. Stratigraphic top is up. St. Paul's Quarry, Upper Cambrian, sample SPQ-19.



Appendix A

OUTCROP LISTS AND DESCRIPTIONS OF LITHOFACIES

A.1 CALCARENITE AND SILTSTONE LITHOFACIES

The following tables list prominent outcrops of the calcarenite and siltstone lithofacies in the CHG. "*" indicates that variable proportions of other lithofacies are included in the interval.

TABLE A.1: CALCARENITE LITHOFACIES

- Broom Point North: units 9, 15-17, 20-23*, 73-76
- Broom Point South: units 34-38
- Cow Head North (Tucker's Cove): Bed 8
- Cow Head North: Beds 6*, 8*, 11*, 13.0-13.5
- Cow Head South: Bed 13s.2
- Martin Point: units 16, 22-23a*, 31, 33

TABLE A.2: SILTSTONE LITHOFACIES

- Broom Point North: units 9, 26*, 31-33, 35-38*, 44, 47, 68, 81
- Broom Point South: units 19, 25-31*, 47
- Cow Head North (Beachy Cove): Beds 6.16e-g
- Cow Head North (Point of Head): Beds 6.16, 6.20, 6.26, 6.31, 8.2, 9.1
- Green Point: units 1-9*, 20-24*
- St. Paul's North: units 4*, 5*, 9*, 12
- Martin Point: units 8, 10, 18, 20, 32, 36d

A.2 MUDSTONE LITHOFACIES: OUTCROP DESCRIPTIONS

The following outcrops of mudstone lithofacies contributed significantly to the generalized description in Chapter 2.

Cow Head North Bed 9.6: This 5 m thick interval is an excellent example of a parted limestone (Type 2) sequence which is dominated by planar-bedded mudstones and fine sand-size peloidal grainstones and packstones (Plate 9c). Mudstones vary from 2-20 cm in thickness, averaging approximately 10 cm. These are separated by centimetre-thick fissile marls.

Most beds consist of massive mudstone, but occasional parallel and ripple laminations also occur. Many beds have tan to buff weathering siliceous "rinds" on their tops and bottoms, and one 30 cm thick bed contains similarly-coloured nodular forms within, along with discontinuous lenses of black chert. Some bed surfaces have accumulations of sponge spicules, trilobite and brachiopod fragments, and horizontal traces.

Cow Head North Beds 9.15-9.17: This 11 m thick ribbon limestone (Type 1) interval is dominated by planar, massive- or parallel-laminated mudstones with minor wavy and lenticular, locally spicule-rich grainstone (Plate 9a). Grainstones are parallel-, wavy-, or ripple-laminated. Near the top of the sequence rippled grainstones are surrounded by massive mudstone "envelopes". Bedding thickness varies

from 5-15 cm with comparable thicknesses of black shale.

Local silicification occurs as orange-brown or tan to buff-weathering, resistant crusts on the upper and lower surfaces of beds. Minor fitted fabrics are also developed. The top of the sequence demonstrates approximately 1 m of scour by an overlying conglomerate (Bed 9.18).

Cow Head North Beds 6.37-6.44: This interval is 8 m thick and is exposed as a substantial strike section stretching over 200 m (Plate 17b,c). In addition to mudstone, this interval also contains abundant silt- and very fine sand-size grainstones. This is reflected in the presence of numerous wavy and lenticular beds. This interval also contains evidence of sediment failure and intrusion by clastic dikes.

The sequence is a hybrid of parted (Type 2) and ribbon (Type 3) limestones. Some portions are dominated by planar mudstones similar to those described from unit 28 at Green Point, whereas others contain subequal quantities of planar, wavy, and lenticular mudstones and grainstones. Bed thickness varies from 2-5 cm and interbedded marls vary from a few millimetres to 4 cm in thickness, rarely attaining 10 cm thickness. Composite bedding is common and includes rippled grainstones overlying parallel-laminated mudstones, and composite mudstones with faint colour banding. Size-graded T_{bc} grainstones also occur. Interbedded lenses of conglomerate up to 80 cm thick locally scour underlying beds.

Green Point Unit 28 - Southwest Outcrop: This parted (Type 2) to ribbon (Type 3) sequence can be followed along strike for approximately 700 m and is well-exposed on wave-cut platform and along shoreline outcrop

(Plate 15a,b). The interval is a maximum of 8 m thickness at the southwesternmost outcrop but diminishes to 2 m thickness along strike to the northeast. The southwestern end of the outcrop is also characterized by several 15-20 cm thick zones of disturbed bedding. The lateral change in thickness and the disturbed zones are the result of submarine sliding (see Chapter 3).

Sediments consist of planar- and wavy-bedded mudstones and minor grainstones interbedded with marls. Mudstones vary from 2-5 cm in thickness and are typically parallel-laminated but may also have minor wavy and ripple cross-lamination. Marl interbeds are massive or parallel-laminated and vary from 1 mm to 2 cm in thickness. The transition from mudstone to marl may be gradational or sharp. Grainstones occur in lenticular beds from less than 1 m to over 10 m in length. Fitted fabrics preserve the sediment package thickness.

Green Point Units 31-33: This 15 m thick interval is well-exposed on the wave-cut platform and clearly illustrates mudstone and shale lithofacies interrelationships and their occasionally arbitrary distinction (Plate 9d). This interval consists of several 0.3-3 m thick packages of ribbon limestones (Type 3) separated by green and minor black shale packages of comparable thickness.

Ribbon limestones are laterally persistent and consist of 1-2 cm thick mudstones and minor silt-size grainstones interbedded with 5-10 mm thick marls. Beds are massive or they may be parallel-, wavy-, or ripple-laminated. T_{bc} sequences are locally common. Some mudstone beds are irregular and lumpy; have thin vertical argillaceous seams; or are

contorted.

Green Point Unit 30: Several 1 m thick packages of ribbon limestone (Type 3) occur near the base of unit 30, a 15 m thick shale-dominated interval (Plate 10e). The ribbon limestones consist of laminated mudstones which are planar, wavy, and lenticular and which vary from 1-2 cm in thickness. These are interbedded with black and green marls of comparable thickness.

One of the exceptionally well-polished ribbon limestone sequences provides high resolution of the mudstone-marl relationships. The marl interbeds are characterized by 1-5 mm thick laminations. In this sequence mudstone typically grades upward into a black marl lamination which in turn grades into green. Where several black-green alternations occur, the green to black transition is abrupt relative to the black to green transition. Where green laminations are absent from the marl interbed, the black marl interbeds are identical to marls seen in most other parted and ribbon limestones. The only situation in which green marl directly overlies mudstone (i.e. without intervening black marl) is in the absence of black marl from the interbed. The laminations in the marls are interpreted to be mud turbidite-hemipelagite cycles and the mudstones appear to be localized by the darker, more organic-rich laminations or beds. The above relationships may be applicable to other, similar outcrops in the CHG. Most outcrops, however, are not sufficiently well-polished to demonstrate these small-scale relationships other than in slab or thin section.

Martin Point Unit 42a: This 2 m thick parted limestone (Type 2)

resembles the more heterogeneous portions of the above interval from Cow Head North. It differs, however, in that it contains a greater number of wavy and lenticular beds in a tightly fitted fabric. Bed thickness varies from 1-4 cm and sediments consist of parallel-, ripple-, and convolute-laminated grainstones. Marl partings are less than 1 cm thick. Locally, horizontal traces are found.

Appendix B

CLAY MINERALOGY OF SHALES

B.1 INTRODUCTION

Twenty-five shale samples were qualitatively analysed by X-ray diffraction to establish the nature of the dominant clay minerals; results are summarized in Table B.1. These samples span the CHG, include all colours and are taken from extensive shale intervals, interbeds between with ribbon limestones or dolomitic siltstones, and matrix separating limestone nodules. Clay mineralogy and geochemistry in the CHG [1] were previously examined by Suchecki (1975), and the results published in significantly revised form in Suchecki et al. (1977).

B.2 SAMPLE PREPARATION

The technique used for sample preparation is outlined in Hiscott's (1982) report on Labrador Sea Clay Mineralogy, omitting procedures

1. In their study, Suchecki et al. (1977) considered the "Red Shale" which characterizes the youngest parts of the CHG as separate from the the "Cow Head Breccia".

related to using the internal talc standard. The preparation uses the less than 2 μm fraction of the shales, removes amorphous iron and ultimately yields 3 oriented mounts per sample. Carbonates are not removed.

Oriented clay mounts are deposited on Gelman Metrical 0.45 μm filters using suction. The filters are then glued onto microscopic glass slides. One clay mount is left untreated. Another mount is exposed to ethylene glycol vapour overnight in a warm oven in order to expand the basal lattice spacing in smectite from 15 Å to 17 Å. A mount of acidified sediment (9 M HCl) eliminates the chlorite contribution to the combined chlorite-kaolinite peaks at approximately 12.5 and 25 degrees 2 theta.

All mounts are scanned one-way only from 2-32 degrees 2-theta at a rate of 1 degree 2-theta per minute. Results are outputted to a strip-chart recorder running at 1 cm/minute. Instrumentation used is a Philips diffractometer with Cu K-alpha radiation, operating at 40 kV and 20 mA.

B.3 OBSERVATIONS

The prominence of the 10 Å illite reflection and the 7.1 Å chlorite reflection indicates that these two clay minerals are by far the most important in all samples analysed. Kaolinite is found in most samples but is a minor phase judging by the relative size of the acidified reflections relative to the untreated ones. Corrensite is identified in 7 of the samples, occurring in minor amounts in Lower Ordovician

(Tremadoc and Arenig) shales. Corrensite, a mixed-layer clay consisting of variable proportions of chlorite and smectite (Hower, 1981), is recognized by the shift of the reflections at approximately 6.2 and 12.5 degrees 2-theta in untreated mounts to lower 2-theta positions in glycolated samples (as low as 5.6 and 11.2 degrees 2-theta, respectively). A residual reflection at the 12.5 degree 2-theta position suggests the presence of a discrete chlorite phase in addition to chlorite interstratified with smectite to form corrensite. In other cases, the 12.5 degree reflection transforms into a broad reflection upon glycolation without distinct maxima at either the chlorite or expanded corrensite positions. For unknown reasons, a discrete chlorite reflection at approximately the 6.2 degree 2-theta position does not occur.

Long-lattice reflections at 31 Å (glycolated) or 29 Å (untreated) are not found in any of the shale samples. These particular reflections characterize ordered corrensite within 10% of the ideal 1:1 chlorite to smectite ratio (Hower, 1981). It is uncertain whether the absence of these peaks is due to either disorder or compositional effects (see Hower, 1981, for details regarding these combined reflections). One exceptional grainstone, however, contains shale intraclasts, extracted by acid leaching, composed largely of ordered corrensite exhibiting the prominent 31 Å (glycolated) long-lattice reflection.

Using the positions of the shifted, glycolated peaks it is possible to make a rough estimate of the percentage chlorite layers in the corrensite phase based on theoretical calculations in Hower (1981).

Based on his table 3.6 which lists the positions of the $(001)_{14} / (001)_{17}$

and $(002)_{14} / (002)_{17}$ reflections in glycolated specimens as a function of percentage of chlorite layers and assuming random interstratification, glycolated corrensite peaks from the CHG indicate 42-80% chlorite layers (the previously mentioned reflections range from 5.6-5.9 and from 11.2-11.6 degrees 2-theta, respectively). If corrensite is ordered, the range diminishes to 44-74% chlorite layers. The exceptional ordered corrensite intraclasts within the grainstone sample indicate 52-58% chlorite layers.

One sample of "shale" underlying a grainstone and occurring locally as intraclasts is largely replaced by microcrystalline potassium feldspar (i.e. a feldspar "chert"), though it is not petrographically recognizable as such. X-ray diffraction verifies the feldspar mineralogy and both atomic absorption as well as microprobe analysis prove its high potassium content (Table B.2).

B.4 INTERPRETATION

The dominance of illite and chlorite in shales of the CHG is consistent with the general observation that with progressive increase in age, illite and chlorite become more important at the expense of kaolinite, montmorillonite, and mixed-layer clays (Weaver, 1967; Dunoyer de Segonzac, 1970). Domination of the clay minerals by illite and chlorite, the relative paucity of kaolinite, and the absence of a discrete smectite phase are also consistent with observations on clays from shallow water, Upper Cambrian sediments from the Port au Port Peninsula

in western Newfoundland (Wood, 1983). In these particular sediments it was concluded that both illite ($1M_4$ polytype) and chlorite are mainly detrital and were deposited in an outer shelf environment. These clays were ultimately derived from weathering of a granitic source terrain under arid to semi-arid equatorial conditions.

Corrensite, along with mixed illite-smectite are the most important mixed-layer clays (Hower, 1981). The elevated Mg concentrations necessary to form corrensite results in its association with evaporites (salts, sulphates), restricted-environment carbonates (limestone and dolomite), volcanics, and graywackes (Kubler, 1973). Formation of corrensite commences at temperatures as low as 90-100 degrees C and the phase is therefore indicative of intermediate and deeper diagenetic zones (Kubler, 1973). However, the corrensite referred to by Kubler (1973) is ordered and the quoted temperature range may be much higher than that necessary for randomly interstratified corrensite.

B.5 COMPARISON WITH SUCHECKI ET AL. (1977)

The present study confirms the main findings in Suchecki et al. (1977) [2] with regards to the importance of illite and chlorite. However, they also identified mixed-layer illite-smectite, 14 Å chlorite, corrensite (ordered), and expandable chlorite. Their description of

2. In addition to untreated, acidified, and glycolated treatments, their methodology also leached carbonate and used MgCl saturation in order to establish interlayer charge characteristics of the corrensite. Samples were also subjected to heat treatments (350 and 550 degrees C).

expandable chlorite suggests it is the disordered corrensite of the present study. Unfortunately, details concerning the recognition of illite-smectite mixed-layer clay are not given in Suhecki et al. (1977) and the present study does not confirm its presence.

These various clays are subdivided into 3 suites: (1) an illite-14 Å chlorite suite [middle Cambrian to early Lower Ordovician], (2) an illite-expandable chlorite suite [early to late Lower Ordovician], and (3) a corrensite-illite-smectite suite. This suite is Lower and Middle Ordovician in age and apparently also characterizes the 400 m thick overlying Green Sandstone [3] (now considered as the Lower Head Sandstone - Williams et al. 1984).

The oldest suite was interpreted to reflect slope deposition of continentally-derived clays. Later, the effects of increasing amounts of volcanic detritus, presumably transported westward from a volcanic arc terrain in what is now central Newfoundland, became important. Mg was interpreted to have been transported either as Mg-rich clays or ferromagnesian minerals which altered to Mg-smectites during early diagenesis at the depositional site. Further alteration during burial resulted in the formation of expandable chlorite and corrensite.

This interpretation is also supported by their geochemical analyses of the carbonate-free, less-than-1- μ m fraction of the clays. Suite 1 is characterized by high K₂O content which presumably reflects the continental provenance whereas younger clays are more Mg-rich indicating

3. This information is based on a single(!) analysis from Black Brook.

their volcanic derivation. It is suggested, however, that this trend may also be explained by the smaller amounts of detrital siliciclastic silt present in the younger shales, especially red shales. Potassium feldspar, both as detrital grains and syntaxial overgrowths, are locally important components of the non-carbonate silt-size fraction (Chapter 6) and glauconite is present in some shales as scattered, silt-size peloids scattered in some shales. In addition, a correlation coefficient calculated for K_2O and MgO analyses listed in Suhecki et al. (1977) indicates no negative correlation, a correlation which is expected to exist assuming their hypothesis to be correct ($r = -0.0523$ for $n = 32$).

TABLE B.1: CLAY MINERALOGY

LOCATION, SAMPLE	SHALE COLOUR	DOMINANT CLAYS	MINOR CLAYS	OTHER PHASES	AGE, STRATIGRAPHIC POSITION, COMMENTS
BPS-24	bl	ill, chl	kao*	q f d c	Tremp, unit 45, from ribbon-nodule lst.
BPS-28-A	bl-gy	ill, kao	---	q c d	Tremp, units 35-38 from ribbon lst.
BPS-35	gy	ill, chl	kao	q	Dres., unit 10, shale.
CHN-9	gn	ill	chl, kao	q f d c	Dres, Bed 3.1, shale.
CHN-80	bl	ill	chl	q f d c	Franc-Tremp, Bed 6 from ribbon lst.
CHN-106	bl	ill, chl	---	q f d c	Trem, Bed 8.30, from between nodules.
CHN-111	bl	ill, chl	kao	q f d	Aren, Bed 9.1, from dolomitic siltstone unit.
CHN-122	bl	ill, chl	kao	q c	Aren, Bed 9.17, from ribbon lst.
CHN-129	bl	ill	kao, chl	q d	Aren, Bed 11.1-11.4, silicified shale.
CHN-140	gn	ill, chl	corr	q	Aren, Bed 13.6-13.9, from between nodules.
GP-14	gn	chl, ill, kao	---	q d	Tremp, unit 1, shale interbedded with sample GP-15.
GP-15	bl	ill, chl	kao	q d c	Tremp, unit 1, shale interbedded with sample GP-14.
GP-44	gn	ill, chl	kao	q f d c	Tremp, unit 11, shale interbedded with sample GP-45.

continued on next page

TABLE B.1 (continued)

LOCATION, SAMPLE	SHALE COLOUR	DOMINANT CLAYS	MINOR CLAYS	OTHER PHASES	AGE, STRATIGRAPHIC POSITION, COMMENTS
GP-45	bl	ill, chl	kao	q	Trem, unit 11, shale interbedded with sample GP-44.
GP-50	bl	ill, chl	kao, corr	q	Trem, units 20-24, from ribbon lst.
GP-69	gn	chl, ill	kao, corr	q	Trem, units 30-33, shale to ribbon lst.
GP-85	bl	ill, chl	kao	q f c	Trem, unit 30, shale.
GP-94	rd	ill, chl	corr	q	Aren, unit 47, shale.
GP-99	pu	ill, chl kao	corr	q	Aren, units 43-49, from red shale unit.
MP-46	gy	ill, chl	---	q f d c	Trem, unit 36b, shale.
MP-53	gy	ill, chl	---	q f d c	Trem, unit 36o-r, shale.
MP-56	gn, bl	ill, chl, corr	kao	q d c	Trem, unit 36s-v, from ribbon lst.
MP-70	gn	ill, chl, kao	---	q f d c	Trem, unit 40a, siliceous shale assoc with dolomitic siltst.
SPN-42-B	rd	ill, chl, corr	kao	q d	Aren, unit 82, shale.
SPN-42-C	gy	ill, chl	kao, corr	q d	Aren, unit 82, reduced equiv to SPN-42-B.

*: uncertain due to lack of acidified sample.

Abbreviations used: bl-black, gn-green, gy-grey, rd-red, pu-purple, ill-illite, chl-chlorite, kao-kaolinite, q-quartz, f-feldspar, d-dolomite, c-calcite, corr-corrensite, Dres-Dresbachian, Franc-Franconian, Trem-Trempealeuian, Trem-Tremadoc, Aren-Arenig, lst-limestone.

TABLE B.2: POTASSIUM-METASOMATIZED SHALE

AAS ANALYSIS		MICROPROBE	
oxide	wt %	oxide	wt %
SiO ₂	62.4	SiO ₂	69.49
TiO ₂	0.43	TiO ₂	0.49
Al ₂ O ₃	14.8	Al ₂ O ₃	16.62
MnO	0.01	MnO	0.02
MgO	2.36	MgO	2.42
CaO	1.75	CaO	0.34
Na ₂ O	0.28	Na ₂ O	0.08
K ₂ O	8.02	K ₂ O	8.82
P ₂ O ₅	0.29	NiO ₂	0.00
Fe ₂ O ₃	2.05	FeO	1.97
LOI	5.96	Cr ₂ O ₃	0.01
TOTAL	98.35	Total	100.27

Sample CHN-169 from Cow Head North, Bed 8.24. Petrography and x-ray diffraction also indicate the presence of quartz, minor pyrite and dolomite, and possibly clay minerals. Microprobe analysis is the average of 5 spot analyses. These were conducted using a clinopyroxene standard and 30 second counts.

Appendix C

CAUSES OF SUBMARINE SEDIMENT FAILURE: AN OVERVIEW

C.1 INTRODUCTION

Sediment failure, which results in slides or mass flows, characterizes slope sedimentation on modern (active or relict) and ancient slopes (Cook et al., 1982; Prior and Coleman, 1982). In addition, both active and passive continental margins are subject to failure (Scheidegger, 1982). Sediment failures have also been reported from isolated oceanic ridges such as the Madeira Rise (Embley and Jacobi, 1978; Embley, 1982), ancient cratonic basins (McIlreath, 1977; Hopkins, 1977), modern deltas (Prior et al., 1981; Prior and Coleman, 1982), and modern fjords (Prior et al., 1982). The plethora of literature devoted to study of sediment failure from geological and geotechnical perspectives has recently been joined by studies emphasizing their biologic importance (e.g. Hecker, 1982).

Modern continental slope failures have been recorded on slopes of less than 1 degree (see Embley and Jacobi, 1978, table 1). Such small angles, which are insufficient to generate the required gravitational stress to cause failure in normally compacted sediment, emphasize the importance of the relationship between effective shear stress and pore pressures

(Prior and Coleman, 1982). Embley (1982) suggested that slope failure does not occur on slopes less than 20 degrees if there is no excessive pore pressure.

C.2 TECTONIC AND OCEANOGRAPHIC CAUSES

For purposes of this overview, it is convenient to consider two principle controls of sediment failure: tectonic and oceanographic causes both of which can gradually or catastrophically induce failure. Oceanographic causes are more directly related to elements of the hydrosphere such as sediment transport and sea level changes. Tectonism and oceanographic causes are certainly not unrelated, but for simplicity this initial dichotomy is established. The following discussion ignores artificial causes of sediment failure.

The most commonly cited cause of sediment failure for both modern and ancient situations is the earthquake (Table C.1). Volcanic eruptions can cause failure via their attendant explosions and ejection of rock material. Other less catastrophic tectonic causes include diapirism and gradual isostatic adjustments.

A major oceanographic control of sediment failure results from changes in sea level which, in siliciclastic systems, is a dominant control on the amount of sediment deposited on continental shelves and slopes.

Abundant sediment brought to the slope encourages overloading and failure. An increase in sea level causing rapid vertical growth of a carbonate platform may result in oversteepening and subsequent failure

of the slope (e.g. Schlager and Camber, 1982). Sea level and oceanic circulation also control the existence and strengths of bottom currents and the position of mineral compensation depths (see Fisher and Arthur, 1977). A change in calcite or aragonite compensation depth may cause patchy dissolution or cementation of sediments, decreasing or increasing sediment mass unevenly, and leading to failure (e.g. Hopkins, 1977). Other oceanographic effects include generation of surface and internal waves which affect sediment pore pressures.

Biological effects include production and sedimentation of organic matter which ultimately generate gas. Superimposed on this are changes in gas hydrate - free gas boundaries controlled partly by pressure and temperature, which are in turn sea level and climatically controlled (see Embley and Jacobi, 1978). Biologic effects also include bioerosion and bioturbation.

TABLE C.1: CAUSES OF SEDIMENT FAILURE

Tectonic

- Earthquakes [3,7,14,16]
- Volcanism [1]
- Diapirism [7]
- Isostatic adjustments

Oceanographic

Depositional factors

- oversteepening [5,6,7,15]
- rapid deposition [5]
- overloading [4,7,12,14]

Pore pressure effects

- change in pore pressure due to surface or internal waves [2,5,6,7,10]
- gas generation [5,13,14]
- ✓ shifting of gas hydrate - free gas boundary [7,8,14]
- artesian gas or water from deeper, buried sediments [5]
- migration of freshwater through aquifers to continental slope [7]

continued on next page

TABLE C.1 (continued)

Erosion

- undercutting by turbidity or geostrophic currents [4,6,7,14]
- bioerosion [8,9]
- bioturbation [9]

Changes in physico-chemical properties of the sediment

- dissolution
- quick clay effect due to pore water freshening [17]

Artificial causes

- explosions, vibrations, ship impacts [6]
- physical weakening

References for Table C.1:

- [1] Herzer (1979) in Saxov (1982); [2] Henkel (1970) in Saxov (1982); [3] Heezen and Ewing (1952) in Saxov (1982); [4] Scheidegger (1982); [5] Prior and Coleman (1982); [6] Koning (1982); [7] Embley (1982); [8] Ryan (1982); [9] Hecker (1982); [10] McGregor (1981); [11] Nardin et al. (1979a); [12] Hopkins (1977); [13] Monroe (1969); [14] Embley and Jacobi (1978); [15] Schlager and Camber (1982); [16] Morgenstern (1967); [17] Schwarz (1982)

TABLE C.2: SHEAR ZONE AND TRUNCATION
SURFACE LOCALITIES, COW HEAD GROUP

Broom Point North units 11, 53, 96

Broom Point South unit 62

Cow Head North beds 6.37-6.44, 8.30*, 13*

Cow Head South beds 11S.21*, 13S.4

Cow Head Peninsula Fish Plant

Green Point units 17-18**, 27, 28

Lower Head Bed 11 equivalent

Martin Point unit 40d

St. Paul's North units 71, 79

Western Brook Pond South units 5, 36

*:ambiguous field relationship with possible structural complications.

** :occurs within shale-dominated sequence.

Appendix D

CONTORTED LIMESTONE DATA

TABLE D.1: OUTCROP LOCATIONS

Contorted Limestones

Broom Point South: units 35-38, 40
Cow Head North: Bed 6
Green Point: units 11, 18, 21, 23, 31-35
Martin Point: units 8, 31, 33, 36
St. Paul's North: units 4, 9

Bedding Overlaps

Cow Head North: Bed 6
Cow Head South: Beds 9s.2-9s.4
Green Point: units 1-10, 26, 27, 28, 34
St. Paul's North: unit 24

TABLE D.2: ORIENTATION OF DOME-AND-BASIN ELONGATION

Location	Bedding Attitude (strike, dip) (degrees)	Horizontal Projection (degrees)
Green Point*:		Pitch
unit 23	52 NE, 65 SE	20 SW
unit 18	55 NE, 66 SE	20-30 SW
unit 18	55 NE, 66 SE	10 SW
Martin Point:		
unit 31b	121 SE, 22 SW	70 NE
unit 33	123 SE, 26 SW	77 NE
unit 36m	127 SE, 30 SW	40 NE
unit 36s-v	80 NE, 33 SE	96 SE

*: Green Point strata are overturned

Appendix E

TABLE E.1: COMPACTION ESTIMATION DATA

Clastic Dikes:	Calculated Compaction (%)	Intruded Lithology	Location
	42	rib.	BPN units 75-85
	84	rib.	BPN unit 91
	38	rib.)	BPS unit 40
	40	rib.)	BPS unit 42
	45	rib.	BPS unit 42
	37	rib.	BPS unit 42
	59	marl	Lower Head
	74	shale	MP unit 38a,b

Average: 52% (st. dev. = 15%)

Miscellaneous:	Calculated Compaction (%)	Comments and Location
	60	vertical mudstone nodule in rib. lst., BPN unit 65
	55	rotated mudstone slab, Lower Head
	61	sub-vertical mudstone nodule in rib. lst., MP unit 40d
	81	pre-compaction silicified shale, SPN unit 82

Average: 64% (st. dev. = 11%)

TABLE E.2: VERTICAL STYLOLITE DATA

Location	Bed, unit	Bedding strike, dip (degrees)	Horizontal Projection (degrees)
Broom Point North	9	58 NE, 42 SE	40 NE
	20	80 NE, 55 SE	68 NE
	20-23	58 NE, 45 SE	43 NE
	37-38	65 NE, 52 SE	66 NE
	41	86 NE, 36 SE	50 NE
		70 NE, 33 SE	44 NE
	55	61 NE, 68 SE	61 NE
	75-85	73 NE, 45 SE	58 NE
	91	86 NE, 41 SE	53 NE
	94	80 NE, 43 SE	60 NE
	96	80 NE, 42 SE	59 NE
		73 NE, 50 SE	60 NE
		87 NE, 44 SE	65 NE
	77 NE, 40 SE	65 NE	
	100	74 NE, 34 SE	51 NE
Cow Head East Fish Plant		57 NE, 40 SE	38 NE
Cow Head North	4	89 NE, 17 S	40 NE
	6	126 SE, 21 SW	52 NE
	6.1-.2	50 NE, 37 SE	*51 NE
	6.37-.44	56 NE, 42 SE	*52 NE
	6	50 NE, 51 SE	*51 NE
Cow Head South (Jim Cove)	9s.17	111 SE, 19 SW	42 NE
	11s.24	103 SE, 22 SW	23 NE

continued on next page

TABLE E.2 (continued)

Location	Bed, unit	Bedding strike, dip (degrees)	Horizontal Projection (degrees)
Martin Point	4	76 NE, 30 SE	81 NE
	5	94 SE, 28 SW	83 NE
	8	98 SE, 26 SW	65 NE
	10-15	145 SE, 28 SW	81 NE
	16	160 SE, 33 SW	85 NE
	23d	125 SE, 30 SW	70 NE
	35	108 SE, 33 SW	74 NE
	42a	98 SE, 29 SW	67 NE
Western Brook Pond South	5	30 NE, 50 SE	25 NE
Green Point**	28	58 NE, 70 SE	<u>Pitch</u> 30 SW
		54 NE, 63 SE	30 SW
		53 NE, 56 SE	32 SW

*: projection values after correction for plunging structure

** : overturned sequence

Appendix F

PETROGRAPHY OF OOIDS AND SILICICLASTICS

F.1 OOIDS

Ooids are mainly restricted to Cambrian grainstones where they constitute 4% or less of the sediment (Figure 6.1 and Table F.1). Their size typically ranges from 150-250 μm and the most common nuclei are coarse silt-size peloids. Small intraclasts, dolomitic lithoclasts or individual detrital dolomite crystals, and bioclast nuclei are comparatively rare. Cortices are mostly radial although concentric inclusion banding can usually also be differentiated. Broken ooids and micritic, concentrically-banded ooids are rare. Selectively dolomitized or silicified ooids occur; however, it is uncertain whether the alteration is transported or in situ.

F.2 QUARTZ SAND

The siliciclastic sand-size fraction is dominated by well-rounded quartz grains which typically range from 0.5-1.0 mm in size. Silt-size, angular quartz grains are ubiquitous and intimately mixed with feldspar

silt (discussed below). Extinction varies from straight to undulose and some grains are subdivided into subcrystals, each with its own undulose extinction. Quartz appears to be non-luminescent although the brighter luminescence of associated grains could easily mask a weak quartz luminescence. Authigenic overgrowths are rare and are only distinguishable under high magnification. These quartz sand grains possess all the attributes of "common" quartz typically derived from granites and granitic gneisses (see Folk, 1974b).

Both fluid and solid inclusions are abundant within quartz grains. Fluid inclusions are less than 5 μm in size and may be irregular or spherical in shape. Gas-liquid inclusions occasionally demonstrate Brownian movement, and some inclusions contain unidentified daughter crystals. Solid inclusions include aligned to randomly disposed needles up to 200 μm long and less than a micrometre in width and stubbier needles 20 μm long and 1 μm wide. These are probably rutile, apatite, or tourmaline. Cubic to anhedral opaque inclusions less than 5 μm in size may be pyrite. Other solid inclusions include subhedral zircons up to 130 μm in length and biotite flakes up to 75 μm in length.

These quartz grains were originally noted by Schuchert and Dunbar (1934, p. 76). Baird (1960) suggested an aeolian origin based on their excellent sorting, heavy frosting, and textural inversions. The bluish cast of these grains led Baird (1960) to suggest derivation from the Long Range gneisses. Although such a source is unlikely, the grains nevertheless reflect weathering and extensive reworking of terrigenous supracrustals.

F.3 FELDSPAR SILT AND SAND

Silt-size (15-75 μm) feldspar crystals are ubiquitous. Grains range from euhedral to subhedral, in part the result of syntaxial overgrowth of angular or rounded, slightly turbid, detrital cores to the rhombohedral habit of adularia. This is clearly demonstrated by CL and to a lesser degree by rare "dust" lines visible in transmitted light. With CL, most feldspar cores luminesce bright blue and less commonly yellow-green. In contrast, authigenic overgrowths are invariably non-luminescent. Based on a limited number of microprobe analyses, detrital cores consist of relatively pure potassium feldspar or oligoclase ($\text{Na}/\text{Na}+\text{Ca} = 0.754-0.808$; see Table F.2). Pure potassium feldspar syntaxially overgrows both of these detrital feldspar cores. Cores are typically untwinned but the rare albite and pericline twins that do occur rarely extend into the overgrowths.

Sand-size feldspar grains are usually syntaxially overgrown by authigenic feldspar and are often subhedral. The overgrowth is invariably unaltered whereas the detrital core is turbid and, in places, altered to calcite, white mica, and presumably clays. As with the silt-size feldspars, albite twins in plagioclase and Carlbud twins in alkali feldspar do not extend into the overgrowth. CL of these large grains is identical to that for feldspar silt. Some alkali feldspar sand grains are microperthitic or demonstrate braided perthite exsolution textures.

TABLE F.1: POINT-COUNT DATA OF SELECTED GRAINSTONES.

CAMBRIAN GRAINSTONES sample	% COMPONENT															
	1	2	3	4	5	6	7	8	9	10	11	12	13	14	15	16
CHN-24	319	26	4	1			2	2		8	3		1			53
80-6-3	331	36					1	3		5	8					46
80-6-5B	322	11		10			24	2		17	18		1			18
80-6-7	345	11	3					3		34	13			1		35
80-6N-19	311	16		1				1		38	1		1			42
80-6-21	307	3		58			4	2		6	1					25
80-6-38	319	21	2	2			1	2		31	5					35
80-6N-44	317	28	4	2			1	2		4	2			3		56
80-6N-47	337	12	3	9	1		3	3		31	3		1			32
80-8-5C	314	53					4	2		2						41
80-8-8A	331	18						2		36	11					33
80-8-8B	352	18		10		1	1	3		16	7	2		1		42
BPN-40	318	36		4			1	3				3				52
80-39-23	314	39	4	1			2	3		17	2	1				33
80-39-31D	326	19	2	19			1	2		12	1					44
80-39-33	417	23	2	5			3	1		12	1					53

ORDOVICIAN GRAINSTONES sample	% COMPONENT															
	1	2	3	4	5	6	7	8	9	10	11	12	13	14	15	16
80-9S-19	326	10						9	1	41	10	6				47
80-9-5	325	17						7	3	11	3	4	1	2		53
80-9S-12E	317	27			2			9	4	18	8	3				42
80-13S-4	317	18						9	3	18	8	3				42
80-10-0C	307	22		2		1		8	5	21	7					36
80-11S-1	335	25						3	3	3			1			64
80-61-33	328	7	1	9		3		11		11	11	16	1	1	24	7
80-61-23	315	19	1	1		6	5	3		40	2	1		3	18	
80-39-60	308	25				12	3	4	2	30	2					23
80-71-82	311	17						4	9	24	3	1				42

Column Headings: 1-number of points; columns 2-16 in volume %:
 2-peloids; 3-oids; 4-detrital quartz; 5-argillaceous seams;
 6-authigenic quartz; 7-dispersed dolomite; 8-bioclats (non-algal);
 9-algal clasts; 10-peloidal intraclasts; 11-micritic intraclasts;
 12-shale and phosphatic intraclasts; 13-dolostone lithoclasts;
 14-opaques; 15-calcite cement; 16- dolomite or barite cement.

TABLE F.2: FELDSPAR SILT MICROPROBE ANALYSES

Oxide	Wt %					
	grain 1 core (n=4)	grain 1 rim (n=2)	grain 2 core (n=1)	grain 2 rim (n=1)	grain 3 core (n=1)	grain 3 rim (n=1)
Na2O	8.43	0.06	8.82	0.04	0.46	0.03
MgO	0.01	0.04	0.01	0.02	0.00	0.00
Al2O3	22.29	18.36	22.43	18.08	17.81	17.69
SiO2	64.08	70.00	65.06	69.72	65.43	68.57
K2O	0.14	17.28	0.64	17.70	16.82	17.71
CaO	4.25	0.21	3.80	0.25	0.02	0.17
TiO2	0.01	0.02	---	---	0.00	0.00
Cr2O3	0.01	0.00	---	---	0.00	0.01
MnO	0.01	0.01	0.00	0.00	0.00	0.03
FeO	0.02	0.06	0.14	0.04	0.00	0.00
NiO2	0.01	0.00	0.00	0.01	0.05	0.03
Total:	99.26	106.04	100.91	105.87	100.59	104.23

Quartz and feldspar silt constitute approximately 5% of the sediment volume in this sample (MP-93-B). Analyses used a clinopyroxene standard and 30 second counts.

TABLE F.3: PHOSPHATE AAS ANALYSIS

Oxide	Wt %
Na2O	0.30
MgO	0.79
Al2O3	1.16
SiO2	15.45
K2O	0.11
CaO	43.30
MnO	0.01
Fe2O3	0.60
P2O5	25.75
L.O.I.	5.62
Total:	93.09

* Analysis also includes approximately 15 wt % ferroan calcite and minor quartz, pyrite, and dolomite (sample CHS-81).

Appendix G

STRUCTURE GRUMELEUSE AND CALCIFIED ALGAE

G.1 INTRODUCTION

The prominence of structure grumeleuse or clotted texture in the spectrum of limestone fabrics was first elucidated by Cayeux (1935) in describing Carboniferous limestones from France and Belgium. This fabric is common in many types of limestones throughout the geologic column (Bathurst, 1975) including stromatolites and thrombolites, and appears to be a standard microfabric in cryptalgal sediments (e.g. Wolf, 1965; Aitken, 1967; Monty, 1977; Pratt, 1982). Diffuse micrite patches separated by microspar occurs in sediments of diverse nature in terms of both depositional as well as diagenetic origins and structure grumeleuse is therefore poly-genetic. Structure grumeleuse has been described in sediments from submarine, intertidal, subaerial, shallow and deep burial regimes. The microfabric has been variously interpreted as the result of (1) merging of peloids due to compaction (Beales, 1958; also termed pseudomatrix by Flugel, 1982, p.119); (2) porphyroid neomorphism of an originally homogeneous micritic matrix, the micrite patches being residuals of the original texture (Cayeux, 1935); (3) alteration of pelletal limestone by aggradational neomorphism which begins in the

interparticle matrix and extend into pellets (Shinn, 1969; Bathurst, 1975); (4) precipitation of high Mg-calcite submarine cements (MacIntyre, 1977); (5) precipitation of micritic calcite in calcrete profiles (James, 1972; Harrison, 1977; Coniglio and Harrison, 1983); and (6) cryptalgal and bacterial influences, either by subsequent modification of trapped carbonate particles, or precipitation of micrite microspherulites as a direct or indirect response to metabolic processes (Bathurst, 1975; Monty, 1977).

G.2 ALTERATION OF GIRVANELLA SHEETS

The poor preservation of Girvanella and the abundance of structure grumeleuse within sheets in the algal boundstones and genetically-related Girvanella and peloidal intraclasts may be the result of several processes. If it is assumed that a monospecific flora (i.e. the Girvanella-forming precursor) forms the sheets in the platform margin mounds, the lack of calcified tubules and the prominence of structure grumeleuse may be explained as follows:

The Girvanella tubule as it is commonly preserved may represent an incipient stage of calcification related to algal metabolism or decay which, when entombed early by syndimentary cement, is well-preserved. Where calcification proceeds to a greater extent, obliteration of the fine-scale microfabric occurs due to precipitation of micritic cements within and upon the tubules. Precipitation within leads to the formation of dense micritic threads which eventually may be fragmented

to form short, micritic rods and, ultimately, peloids. If micritic cements are precipitated on the tubule, the process may be similar to that proposed for the generation of constructive micrite envelopes formed between grains in Quaternary sediments (Kobluk and Risk, 1977). In these sediments, calcified algal filaments underwent further calcification and infilling of the interfilament spaces by micrite and microspar with the eventual attainment of structure grumeleuse (see figure 9 in Kobluk and Risk, 1977; also Riding, 1977).

If Girvanella is considered as a diagenetic form of a number of biologically distinct taxa (Kobluk and Risk, 1977; Riding, 1977; Danielli, 1981; Pratt and James, 1982a; Pratt, 1984), it may have then been possible that some of the Girvanella-forming algae did not completely calcify, thus explaining the absence of tubules in many sheets of the boundstone boulders and their derivative intraclasts. These non-calcifying algae may have forced precipitation of micritic carbonate or may have trapped particles, processes analogous to those which occur in the common stromatolite-forming algae (Bathurst, 1975; Monty, 1977).

G.3 SUMMARY

Although structure grumeleuse microfabric can be derived in numerous ways, study of Girvanella sheets in the algal boundstone boulders suggests that structure grumeleuse may be due to synsedimentary processes affecting living or dead filamentous algae and probably also

coctoid algae. Structure grumeluse may be either the result of "overcalcification" with consequent loss of diagnostic microfabric, or the result of insufficient calcification to define the Girvanella form in conjunction with typical "stromatolite-forming" processes.

Appendix H

CEMENTATION AND NEOMORPHISM

H.1 TERMINOLOGY

Cement refers to "all passively precipitated, space-filling carbonate crystals which grow attached to free surface" (Bathurst, 1975, p. 416).

Neomorphism, in contrast, is "a comprehensive term of ignorance...for all transformations between one mineral and itself or a polymorph - whether inversion or recrystallization, whether the new crystals are larger or smaller or simply differ in shape from the previous ones"

(Folk, 1965, p.21). Inversion refers to polymorphic transformations without an intermediate stage of visible porosity creation, a typical example being the calcitization of aragonite. Recrystallization occurs when a mineral species remains unchanged, although allowing for trace element and isotopic changes to occur, for example the change from Mg-calcite to calcite. Aggrading and degrading neomorphism refer to an increase and decrease, respectively, of the resulting crystal aggregate.

Microspar is neospar which is 30 μm or less in size and larger than micrite (i.e. greater than 4 μm). It is generally characterized by uniformity of crystal size and equant shape (Folk, 1965). Neospar,

greater than 30 μm in size is pseudospar, the boundary in most cases being one of convenience rather than of genetic significance (Folk, 1965). This is the boundary used in this thesis. Bathurst (1975) uses a size boundary of 50 μm to separate microspar and pseudospar.

The above terminology of cement and neomorphic spar or neospar is clearly geared to the microfabric resolution possible with standard petrographic microscopy (Folk, 1965). As pore spaces progressively decrease beyond microscopic detection, the distinction between pore-filling precipitation and neomorphic solution-film or intercrystalline boundary processes diminishes (e.g. Bathurst, 1975; Pingitore, 1976; Brand and Veizer, 1980).

H.2 AGGRADING NEOMORPHISM ACCORDING TO FOLK (1965)

Aggrading neomorphism is the process in which numerous, small carbonate crystals are recrystallized into fewer, coarser ones (Folk, 1965). This transformation is considered to be "wet", i.e. solutions are involved in some capacity, either as thin films or pore fluids. Degrading neomorphism is considered to be insignificant under normal diagenetic conditions and is relegated to the relatively "dry" realm of metamorphism (Bathurst, 1975; however, see Dixon and Wright, 1983, for an exception).

According to Folk (1965), aggrading neomorphism occurs along one of two possible pathways, either by porphyroid or coalescive processes. During porphyroid neomorphism only a few crystals grow and a static matrix of

more finely-crystalline calcite is gradually consumed. If the process could be stopped at any point in time, the youngest and largest crystals would be enveloped by a matrix of older, smaller crystals. Termination of the process occurs when the larger crystals impinge and the finer matrix is finally consumed. The mosaic clearly went through a porphyroblastic stage. This type of aggrading neomorphism is typical of replacement of aragonitic fossils by calcite (Folk, 1965).

In contrast, coalescive neomorphism is characterized by a dynamic matrix wherein crystals enlarge by wet boundary migration at the expense of their neighbours (Bathurst, 1975, p. 500). Folk (1965, p. 22) described it as follows:

"a large proportion of the grains are growing at any given time, almost every grain is either consuming or being consumed, the process is continuous in time and in space without any static areas or natural stopping point, and at any given time the grain size is relatively uniform."

Folk (1965) suggested this process to be largely responsible for the generation of microspar from micrite.

The transition from micrite to microspar was hypothesized to result from removal of Mg from intercrystalline positions in the micrite mosaic either by freshwater flushing (Folk, 1974) or the action of clays such as chlorite and montmorillonite which act as "Mg ion sumps" (Longman, 1977). Removal of Mg from immediate contact with the crystals was thought to be a critical factor in hurdling micrite through Folk's (1974) "micrite curtain". Zankl (1969), based on his study of Triassic shallow- and deep-water fine-grained limestones, suggested that limestones with more than 2% clays inhibited aggrading neomorphism. In

a recent study of Ordovician platform carbonates from the St Lawrence Valley Lowlands, Bertrand et al. (1983) related increased crystal size and polyhedrality of the microcrystalline calcite to increasing thermal maturation.

The "maturity" concept of mud aggrading to micrite to microspar and finally to pseudospar was recently assaulted by Lasemi and Sandberg (1984). Based on SEM examination of Pleistocene micrite and microspar from Florida and the Bahamas, the transition from unaltered lime mud to micrite or microspar occurred as a one-step process, without the necessity for progressive aggrading neomorphism, as conventionally defined, to have taken place. Their conclusion was based on the similar abundances of aragonite relics in micrite- and microspar-size crystals they examined.

H.3 CEMENT AND NEOSPAR CRITERIA

Differentiating between cement and neospar is certainly not a contemporary problem (e.g. Rich, 1982; Bathurst, 1983b) but has been an ongoing concern for carbonate petrologists for more than the last two decades. As long ago as 1965 Folk saw the necessity for establishing guidelines, based on his own observations and drawing from those of earlier publications, that allowed reliable interpretation of diagenetic calcite using standard petrographic techniques. Much of Folk's (1965) study is critically reviewed in Bathurst (1975) which currently is the most comprehensive discussion of the cement-neospar problem and also

lists criteria for distinguishing between the two calcites. Most criteria are equivocal by themselves and the prevalent philosophy has been to use a "safety-in-numbers" approach.

Bathurst's (1975) criteria for the recognition of cement are divided into two groups: (1) criteria which depend on intuitive argument, and (2) criteria which characterize cements already established from the intuitive arguments. The first set of criteria establish a cement origin based on fabric relationships of calcite spar with other components of the sediment. Thus these fabric relationships are still suggestive of cement even when cement has been subsequently neomorphosed. Examples of this are (1) cement which lines a cavity, or (2) cements overlain by internal sediments (Bathurst's, 1975, criteria numbers 9 and 10). Both of these former cements would still be identifiable as cements due to their spatial arrangement within the sediment which makes other origins unlikely, for example aggrading neomorphism of lime mud.

The second set of criteria, i.e. those which characterized cements previously established using the intuitive arguments, has recently been critically reviewed by Dixon (1983). These criteria are that cements are characterized by: (1) planar intercrystalline boundaries, (2) crystal size increases away from the substrate, (3) preferred orientation of longest axes normal to substrate, (4) preferred orientation of optic axes normal to substrate, and (5) enfacial junctions.

The first 4 criteria are collectively referred to as the "competitive growth fabric" (Bathurst, 1975, p. 422). Such fabrics are not

restricted to cement aggregates as they also characterize neospar which begins recrystallization from a surface and extends outwards, yielding progressively larger and more preferentially-oriented crystals (Folk, 1965; Bathurst, 1975; Fairchild, 1980; Dixon, 1983). Such competitive growth fabrics also characterize displacive fibrous calcites (see Chapter 9). To complicate matters further, Dixon (1983) demonstrated that spar aggregates interpreted to be cement commonly are devoid of competitive growth fabrics!

The enfacial junction, the 5th cement criteria, is a triple junction where one of the 3 angles is 180 degrees. Bathurst (1975, p. 425) considered this to be one of the least equivocal of the cement criteria. Using graphical representation of crystal growth, Dixon (1983) focussed upon this problem and demonstrated that enfacial junctions were not present in modelled cement aggregates. In addition, his work on select examples which demonstrated enfacial junctions suggested that the occurrence of enfacial junctions may be caused by one of two factors: (1) cessation of growth of certain portions of crystals while other crystals continue to grow to eventually contact the halted crystals thus creating an intercrystalline boundary, or (2) modification of intercrystalline boundaries by dissolution. In light of the above, Dixon (1983) dismissed the list of textural criteria used to recognize cement.

Appendix I

GEOCHEMICAL ANALYSES: METHODOLOGY,
INSTRUMENTATION, AND DATA

I.1 ATOMIC ABSORPTION SPECTROPHOTOMETRY

Calcite and dolomite were analysed for major and minor elements (Ca, Mg, Fe, Mn, Sr, Na, K, Al, Si) by atomic absorption spectrophotometry (AAS).

Samples were washed with distilled water prior to powdering. Two methods were used to extract sample. A vibrating impact engraver was used for samples which required precise spot sampling. Where contamination was not a concern, slabs were cut into penny-size chips, washed with distilled water, and ground in a ball mill. During all stages of sample preparation after the distilled water wash, rubber gloves were worn in order to minimize contamination.

Approximately 1.0-1.5 grams of rock powder were dissolved in 25 ml of dilute HCl solution (8% volume/volume as suggested by Brand and Veizer, 1980). Calcite was leached for 30 minutes and dolomite for 90 minutes [1]. The leachate was then filtered, using pre-weighed filter papers,

1. These times are considerably less than those used by Brand and Veizer (1980) who suggested 5.5 hours

and brought to 50 ml of HCl solution by rinsing through the filter paper. Filter papers were allowed to air dry for 2-4 days prior to re-weighing in order to calculate insoluble residue and leachate concentrations. Analyses are listed in Table I.1 (calcite, n=37) and I.3 (dolomite, n=48). Duplicate analyses were run on 9 calcites (Table I.2) and 6 dolomites (Table I.4). Averages of these duplicate analyses were used in Tables I.1 and I.3. Samples are briefly described in Appendix J.

Artificial calcite and dolomite standards were prepared in identical HCl solutions using Spec-Pure chemicals. These standards were used to measure all elements except Ca and Mg, which were measured against natural dolomite (GFS-400) and calcite (GFS-401) standards. Prepared leachates were analysed by G. Andrews of Memorial University.

I.2 STABLE ISOTOPE ANALYSES

Samples for isotope analysis were extracted using the same methods as for AAS, minus the acid leach. Samples were submitted in 4 lots over the course of two years and analysed courtesy of Marathon Oil Company, Denver Research Center in Littleton, Colorado. Analyses were conducted by W. W. Walwey, supervised by P. W. Choquette.

Isotopic data are reported in per mil (o/oo) versus the PDB-1 carbonate standard. Samples were prepared by reaction in 100% anhydrous phosphoric acid at 25 degrees C (1 hour for calcite, 4 days for dolomite). Samples were not pretreated in any way, nor was dolomite

corrected downward by -0.8 o/oo for fractionation effects. Isotopes were measured on a 5 cm, 60 degree, sector-type ratio mass spectrometer with a double-collecting system and isotope ratio recording facilities; a substantially modified Nuclide instrument. Precision, based on selected replicate analyses, is $0.1 - 0.2$ o/oo for both $\delta^{13}\text{C}$ and $\delta^{18}\text{O}$.

Isotopic analyses of calcite ($n=55$) and dolomite ($n=23$) are listed in Tables I.5, I.6, and I.7. Samples are briefly described in Appendix J. The 2 sets of analyses for MP-4 (1 calcite and 1 dolomite) are from fractional preparations: for 1 hour to react calcite and then for 4 days for dolomite.

I.3 MICROPROBE ANALYSES

Microprobe analyses were made on polished thin sections, routinely analysing for Ca, Mg, Fe, and Mn in carbonates and also Na, K, Al, Si, Sr, Ba, Zn, and Cr for other miscellaneous phases. Analyses were performed on a JEOL JXA50A electron-probe x-ray microanalyser with KRISSEL automation. Data were acquired using ALPHA matrix corrections. Operating conditions were a beam current of 22 na at a potential of 15 kv, using a focussed beam of approximately $2 \mu\text{m}$ diameter. Counting times were 10 seconds. For carbonate analyses, Ca and Mg were standardized on dolomite; Mn and Fe were standardized on clinopyroxene (both "in-house" standards). Other elements used a variety of "in house" standards. The 10 second counting time, the small beam diameter, and the nature of the standards used suggest that the microprobe

analyses of calcite and dolomite be considered as semi-quantitative.

Examples of the reproducibility of microprobe analysis of a crystal of displacive fibrous calcite (sample GP-3-A) are found in Table I.8. A microprobe analysis of a coarse fracture-fill dolomite from Broom Point South (sample BPS-33-A) is also shown in Table I.8.

I.4 CATHODE LUMINESCENCE

Cathode luminescence was carried out on a Nuclide Corporation ELM-2A Luminoscope using ambient gas, a beam diameter of approximately 1 cm, beam current of 0.6 ma, and an accelerating voltage of 16 kv. The optical and photographic equipment was a Wild Photoautomat System mounted on a Leitz M-400 microscope. The luminescence chamber was positioned and levelled using a stage assembly designed by the author. Ektachrome 400 ASA daylight slide film and Kodacolor VR1000 daylight print film were used.

TABLE I.1: CALCITE AAS ANALYSES

SAMPLE	I.R. wt %	Al ppm	Si ppm	Na ppm	K ppm	Sr ppm
CHN-13	24	209	615	856	91	167
CHN-15-A	5	69	293	705	27	66
CHN-32	11	218	524	831	215	342
CHN-36-B-A*	9	253	423	632	166	174
CHN-36-B-B*	15	507	509	732	303	135
CHN-36-B-C*	11	305	558	731	156	110
CHN-42	16	60	792	2232	75	335
CHN-101-A	12	439	716	674	335	172
CHN-101-B	16	396	708	645	271	136
CHN-101-C	8	73	172	868	37	119
CHN-102-A	17	320	443	821	251	286
CHN-102-B	7	37	354	921	53	117
CHN-126	29	1048	848	972	669	207
CHN-168	18	43	288	832	51	132
CHN-169	15	134	590	1501	189	157
GP-2-A	32	656	843	773	379	2886
GP-2-B	17	361	643	715	217	462
GP-9-A	8	38	326	467	27	352
GP-23-A*	16	635	688	745	437	520
GP-23-B*	22	894	1624	865	579	422
GP-23-C*	17	441	1179	674	260	603
GP-41-A	34	408	616	876	307	404
GP-41-B	19	675	863	805	570	372
GP-57-A	30	994	1252	1036	1228	301
GP-57-B	10	99	410	644	80	173
GP-106*	17	787	1039	724	497	207
GP(81-7-AH*)	8	94	304	764	87	304
GP(81-7-BG*)	27	1027	1216	690	775	450
LH-76-A-A	12	404	648	540	307	268
LH-76-A-B	26	1548	1845	681	1323	202
LH-76-A-C	24	835	833	842	651	219
MP-3	9	407	549	908	386	195
MP-15	10	286	541	784	150	293
MP-57	20	869	842	737	311	256
SPN-66-D-A	11	298	526	538	162	130
SPN-66-D-B	26	857	1214	751	455	87
SPQ-9-F	11	138	373	584	93	372

continued on next page

TABLE I.1 (continued)

SAMPLE	FeO wt %	MnO wt %	MgO wt %	CaO wt %	CaO+MgO+ FeO+MnO
CHN-13	0.16	0.05	0.52	69.80	70.53
CHN-15-A	0.04	0.04	1.43	59.77	61.28
CHN-32	0.06	0.04	3.82	60.67	64.59
CHN-36-B-A*	0.07	0.18	0.45	60.92	61.62
CHN-36-B-B*	0.11	0.07	0.53	62.10	62.82
CHN-36-B-C*	0.25	0.10	0.40	61.08	61.82
CHN-42	0.34	0.02	2.04	67.42	69.82
CHN-101-A	0.08	0.06	0.49	61.76	62.39
CHN-101-B	0.11	0.07	0.57	63.10	63.85
CHN-101-C	0.27	0.10	2.62	60.56	63.55
CHN-102-A	0.10	0.07	0.93	61.19	62.28
CHN-102-B	0.31	0.11	3.18	61.43	65.03
CHN-126	0.07	0.12	0.84	67.20	68.23
CHN-168	0.10	0.11	0.48	68.61	69.30
CHN-169	0.14	0.10	3.37	65.60	69.22
GP-2-A	0.28	0.04	0.98	71.13	72.43
GP-2-B	0.38	0.04	0.42	61.93	62.77
GP-9-A	0.28	0.09	0.28	61.26	61.90
GP-23-A*	0.12	0.07	0.60	61.76	62.56
GP-23-B*	0.49	0.07	0.55	60.27	61.40
GP-23-C*	0.64	0.07	0.48	67.95	69.15
GP-41-A	0.06	0.16	0.70	82.75	83.67
GP-41-B	0.28	0.09	0.53	62.09	62.99
GP-57-A	0.31	0.03	1.46	60.60	62.40
GP-57-B	0.07	0.03	0.47	60.31	60.89
GP-106*	0.55	0.07	0.49	62.54	63.66
GP(81-7-AH*)	0.17	0.10	1.58	61.38	64.49
GP(81-7-BG*)	0.21	0.10	1.23	59.67	61.17
LH-76-A-A	0.07	0.04	0.45	61.33	61.89
LH-76-A-B	0.32	0.02	0.59	62.38	63.31
LH-76-A-C	0.26	0.02	0.52	61.35	62.15
MP-3	0.09	0.03	0.70	55.16	55.98
MP-13	0.05	0.05	5.26	59.70	65.06
MP-57	0.19	0.04	0.64	65.37	66.25
SPN-66-D-A	0.28	0.13	0.41	61.31	62.13
SPN-66-D-B	0.72	0.23	0.65	62.59	64.19
SPQ-9-F	0.07	0.04	0.50	60.18	60.78

 "*" analyses are averaged from those in Table I.2

TABLE I.2: REPLICATE CALCITE AAS ANALYSES

SAMPLE	I.R wt %	Al ppm	Si ppm	Na ppm	K ppm	Sr ppm
CHN-36-B-AX	10	257	485	548	167	177
CHN-36-B-Ay	8	249	362	717	165	171
CHN-36-B-Bx	16	569	597	691	307	141
CHN-36-B-By	13	446	421	773	299	129
CHN-36-B-Cx	12	281	493	670	145	112
CHN-36-B-Cy	9	330	623	791	167	108
GP-23-Ax	15	708	747	765	447	519
GP-23-Ay	16	562	629	726	427	522
GP-23-Bx	20	1069	2020	812	604	409
GP-23-By	24	720	1228	918	553	434
GP-23-Cx	22	430	1538	650	270	632
GP-23-Cy	11	453	819	699	250	573

SAMPLE	FeO wt %	MnO wt %	MgO wt %	CaO wt %	CaO+MgO+ FeO+MnO
CHN-36-B-AX	0.07	0.18	0.45	60.92	61.62
CHN-36-B-Ay	0.07	0.18	0.44	59.38	60.06
CHN-36-B-Bx	0.11	0.07	0.54	62.10	62.82
CHN-36-B-By	0.10	0.07	0.52	60.26	60.95
CHN-36-B-Cx	0.25	0.10	0.40	61.08	61.82
CHN-36-B-Cy	0.25	0.10	0.40	60.34	61.08
GP-23-Ax	0.12	0.07	0.61	61.76	62.56
GP-23-Ay	0.11	0.07	0.60	62.42	63.20
GP-23-Bx	0.49	0.07	0.56	60.27	61.40
GP-23-By	0.48	0.07	0.53	63.60	64.67
GP-23-Cx	0.64	0.07	0.50	67.95	69.15
GP-23-Cy	0.54	0.06	0.46	60.76	61.82

TABLE I.3: DOLOMITE AAS ANALYSES

SAMPLE	I.R. wt %	Al ppm	Si ppm	Na ppm	K ppm	Sr ppm
A-1	8	142	322	1280	58	122
BPS-20-A	57	4819	5338	2347	6288	279
BPS-22	64	3787	3804	2782	5113	299
BPS-23-A	29	1029	1850	1151	748	140
BPS-29-A	13	723	739	962	325	203
BPS-30	18	621	486	1090	279	89
BPS-32	15	613	919	1028	411	88
BPS-33-B	12	347	734	885	295	180
CHN-0	44	1423	1434	1507	1522	535
CHN-12	15	895	730	835	370	205
CHN-15-A	12	403	831	1613	362	176
CHN-19	26	2777	1141	917	970	123
CHN-57	38	4043	5235	2469	599	253
CHN-87	24	855	1167	1122	782	133
CHN-166	44	4104	3565	2724	2782	196
CHN-167	66	3159	2740	2366	4549	265
CHN(80-4-0)	14	371	583	1324	232	168
CHS-55*	42	4462	4817	1868	1429	524
CHS-69	65	12780	14583	3632	5582	480
GP-63-B*	51	2853	6316	2406	4112	676
GP-67*	49	2705	5454	2106	3157	495
GP-88-A	29	734	1195	1280	421	53
GP-89*	33	815	1266	1672	638	57
GP-95*	43	2428	4645	2948	1371	118
GP-96-B*	74	4103	6992	6149	2482	234
GP(80-61-34)	29	1642	2609	2218	404	221
GP(80-61-44B)	25	954	1402	2149	133	192
LC-3	41	2213	3157	2469	1402	238
LC-4	39	1965	2805	2375	1377	300
LC-5	41	2826	3814	2295	1484	229
MP-4	21	886	1241	1477	948	147
MP-8	21	201	695	1294	215	160
MP-30	69	5138	4531	8439	7173	301
MP-41	21	948	583	1131	284	166
MP-69-B	38	2334	1819	2176	563	89
MP-84	58	1829	2412	2976	1441	136
SPN-1	42	2532	2506	2319	1938	154
SPN-3	48	1856	2208	2423	2264	154
SPN-32	42	1900	3506	2242	2197	565
SPN-38	70	3964	4846	3366	3648	158
SPN-41	38	1315	1744	1980	983	228
SPN-43-B	28	731	1013	1274	203	132
WI-1	16	242	457	960	131	113
WN-4-A	43	4777	6413	1581	3303	121
WN-11	35	2729	4134	1490	1857	197
WS-8	61	3240	4847	2485	1609	137
WS-11	37	2426	3635	1368	2056	116
WS-19	22	812	1737	1258	496	222

continued on next page

TABLE I.3 (continued)

SAMPLE	FeO wt %	MnO wt %	MgO wt %	CaO wt %	CaO+MgO+ FeO+MnO
A-1	0.11	0.03	22.67	34.73	57.53
BPS-20-A	1.91	0.07	21.98	39.25	63.20
BPS-22	2.71	0.06	17.30	47.64	67.72
BPS-23-A	0.92	0.05	12.48	23.29	36.74
BPS-29-A	0.26	0.04	18.43	32.61	51.33
BPS-30	0.98	0.05	22.11	32.23	55.37
BPS-32	0.93	0.06	21.37	32.07	54.42
BPS-33-B	0.41	0.06	19.88	35.14	55.49
CHN-0	1.15	0.10	22.04	43.01	66.31
CHN-12	0.84	0.07	16.53	38.78	56.21
CHN-15-A	0.64	0.11	19.81	37.67	58.23
CHN-19	0.59	0.06	20.21	33.94	54.80
CHN-57	1.06	0.04	23.72	38.14	62.97
CHN-87	0.71	0.07	20.83	34.87	56.47
CHN-166	0.71	0.06	18.45	53.03	72.25
CHN-167	1.38	0.07	19.47	49.02	69.94
CHN(80-4-0)	0.64	0.10	18.73	38.39	57.85
CHS-55*	1.77	0.11	20.53	40.07	62.49
CHS-69	1.91	0.07	27.37	56.63	85.98
GP-63-B*	2.83	0.06	18.50	44.09	65.48
GP-67*	3.85	0.06	17.89	41.60	63.41
GP-88-A	0.60	0.12	22.75	33.80	57.27
GP-89*	0.40	0.16	23.64	34.90	59.11
GP-95*	0.43	1.38	23.49	34.94	60.25
GP-96-B*	0.53	1.23	23.84	45.90	71.50
GP(80-61-34)	1.24	0.21	20.66	37.24	59.35
GP(80-61-44B)	0.44	7.01	15.75	36.85	60.05
LC-3	2.34	0.09	23.38	38.40	64.21
LC-4	2.30	0.08	22.85	37.13	62.37
LC-5	1.24	0.18	23.47	34.58	59.46
MP-4	3.01	0.08	16.81	40.20	60.10
MP-8	2.60	0.08	20.10	35.90	58.69
MP-30	2.32	0.06	10.19	36.89	49.46
MP-41	2.43	0.08	19.42	33.88	55.80
MP-69-B	2.05	0.15	24.81	37.98	64.99
MP-84	0.22	0.41	24.52	37.30	62.45
SPN-1	0.24	0.16	24.66	36.22	61.28
SPN-3	0.27	0.19	24.61	37.14	62.21
SPN-32	1.26	0.09	15.78	34.89	52.02
SPN-38	0.38	0.14	27.53	42.40	70.45
SPN-41	0.17	0.14	22.89	36.42	59.61
SPN-43-B	0.14	0.14	22.47	36.69	59.44
WI-1	0.21	0.04	17.30	36.22	53.77
WN-4-A	3.30	0.29	22.15	35.63	61.36
WN-11	1.58	1.36	20.53	35.17	58.65
WS-8	0.58	0.47	16.07	25.77	42.89
WS-11	0.26	0.45	22.34	32.35	55.40
WS-19	1.14	0.10	20.80	34.89	56.93

* analyses are averaged from those in Table I.4

TABLE I.4: REPLICATE DOLOMITE AAS ANALYSES

SAMPLE	I.R. wt %	Al ppm	Si ppm	Na ppm	K ppm	Sr ppm
CHS-55x	42	4462	4977	1868	1395	505
CHS-55y	15	4462	4658	1868	1464	543
GP-63-Bx	50	1916	8806	2512	4240	629
GP-63-By	52	3791	3825	2301	3983	723
GP-67x	48	3163	7875	2203	3662	449
GP-67y	51	2247	3032	2010	2652	541
GP-89x	32	855	1322	1885	640	50
GP-89y	33	774	1211	1460	637	64
GP-95x	40	2896	6882	3125	1466	105
GP-95y	46	1960	2407	2770	1276	130
GP-96-Bx	73	3960	7299	6376	2333	231
GP-96-By	75	4245	6684	5921	2630	237

SAMPLE	FeO wt %	MnO wt %	MgO wt %	CaO wt %	CaO+MgO+ FeO+MnO
CHS-55x	1.76	0.11	20.55	39.93	62.35
CHS-55y	1.78	0.11	20.52	50.21	72.62
GP-63-Bx	2.92	0.06	18.30	44.03	65.37
GP-63-By	2.73	0.06	18.71	44.16	65.65
GP-67x	3.97	0.06	17.46	40.42	61.91
GP-67y	3.73	0.06	18.33	42.79	64.91
GP-89x	0.40	0.16	23.72	35.10	59.38
GP-89y	0.40	0.16	23.56	34.71	58.83
GP-95x	0.45	1.33	22.47	33.33	57.58
GP-95y	0.42	1.43	24.51	36.54	62.90
GP-96-Bx	0.51	1.17	22.81	43.80	68.29
GP-96-By	0.55	1.30	24.87	47.99	74.71

TABLE I.5: CALCITE STABLE ISOTOPE ANALYSES

<u>SERIAL SAMPLES</u> SAMPLE	$\delta^{13}\text{C}$	$\delta^{18}\text{O}$	LOT NO.
CHN-36-D	-1.30	-6.62	[1]
CHN-36-E	-1.31	-6.44	[1]
CHN-36-B-A	-2.74	-5.91	[2]
CHN-36-B-B	-1.29	-6.12	[2]
CHN-36-B-C	-1.28	-5.99	[2]
CHN-101-A	-6.87	-6.22	[2]
CHN-101-B	-1.43	-6.09	[2]
CHN-101-C	-1.09	-6.31	[2]
CHN-102-A	-1.12	-6.07	[3]
CHN-102-B	-0.96	-6.17	[3]
GP-2-A	-0.68	-7.44	[2]
GP-2-B	-0.61	-8.41	[2]
GP-23-A	-3.81	-7.60	[2]
GP-23-B	-2.93	-8.05	[2]
GP-23-C	-2.57	-8.01	[2]
GP-41-A	-2.10	-6.78	[3]
GP-41-B	-5.27	-7.55	[3]
GP-52-BA	-1.54	-6.87	[4]
GP-52-BB	-4.45	-6.91	[4]
GP-57-A	-0.65	-7.26	[3]
GP-57-B	-2.46	-7.33	[3]
GP(81-7-A)	-15.09	-8.38	[1]
GP(81-7-B)	-6.78	-7.90	[1]
GP(81-7-G)	-7.78	-7.60	[3]
GP(81-7-H)	-9.93	-7.93	[3]
LH-76-A-A	-1.62	-6.21	[3]
LH-76-A-B	-2.92	-6.40	[3]
LH-76-A-C	-2.92	-6.09	[3]
SPN-66-D-A	-1.71	-5.24	[3]
SPN-66-D-B	-2.06	-5.69	[3]
SPN-76-A	-0.78	-5.29	[4]
SPN-76-B	-1.20	-5.55	[4]

TABLE I.6: CALCITE STABLE ISOTOPE ANALYSES

<u>SINGLE SAMPLES</u>	$\delta^{13}\text{C}$	$\delta^{18}\text{O}$	LOT NO.
BPN-12	+1.04	-6.59	[4]
CHN-13	-0.58	-6.85	[2]
CHN-15-A	-1.54	-6.26	[2]
CHN-25	+0.28	-6.04	[2]
CHN-32	-1.84	-5.98	[1]
CHN-53-B	-0.76	-5.46	[4]
CHN-126	-5.81	-5.43	[2]
CHN-168-B	+0.58	-6.29	[2]
CHN-169	-0.30	-5.96	[3]
CHN-178-AB	-2.09	-6.73	[4]
CHN-178-B	-1.81	-6.55	[4]
CHN-178-F	-1.79	-6.81	[4]
CHN-178-G	-2.85	-6.10	[4]
CHN-183	-2.82	-5.71	[4]
GP-9-A	-2.05	-8.83	[2]
GP-106	-2.92	-3.11	[3]
LH-4	+0.50	-5.70	[4]
LH-8	+0.54	-5.87	[4]
MP-3	-0.97	-2.81	[3]
MP-4	-0.67	-6.42	[2]
MP-15	-0.41	-6.88	[1]
MP-57	+0.24	-6.53	[2]
MP(80-39-31D)	-0.39	-7.47	[4]
RAX-12-A	+0.04	-5.46	[4]
RAX-12-B	-0.84	-5.53	[4]
RAX-14-A	+0.08	-6.65	[4]
SPQ-9-F	-0.28	-6.68	[2]

REPLICATE ANALYSES

CHN-101-B	-1.49	-6.05
	-1.38	-6.06
	-1.41	-6.17

TABLE I.7: DOLOMITE STABLE ISOTOPE ANALYSES

SAMPLE	$\delta^{13}\text{C}$	$\delta^{18}\text{O}$	LOT NO:
BPS-29-A	-5.89	-4.30	[2]
BPS-32	-1.60	-3.34	[2]
BPS-33-B	-2.33	-3.53	[3]
CHN-15-A	-2.09	-5.17	[2]
CHN-57	-2.02	-3.71	[2]
CHN-87	+0.11	-4.01	[2]
CHN-166	-0.16	-4.33	[3]
CHN-178-B	-3.11	-5.09	[4]
CHN-178-F	-2.78	-5.20	[4]
CHN(80-4-0)	-0.40	-5.11	[2]
CHS-55	+0.08	-3.73	[3]
GP-63-B	+1.42	-4.83	[3]
GP-67	+1.18	-5.09	[2]
GP-88-A	-1.34	-4.51	[2]
GP-96-B	-1.96	-3.89	[3]
GP(80-61-44B)	-2.24	-7.73	[3]
MP-4	-0.23	-5.43	[2]
MP-30	-1.00	-5.92	[3]
SPN-32	+0.76	-4.68	[2]
SPN-38	-2.34	-3.48	[3]
WI-1	-0.59	-4.90	[2]
WN-11	-1.96	-3.81	[3]
WS-11	-2.28	-3.62	[3]

REPLICATE ANALYSES

CHN-178-B	-3.16	-5.06
	-3.05	-5.12
GP-67	+1.14	-5.03
	+1.21	-5.07
	+1.20	-5.18

TABLE I.8: PRECISION OF MICROPROBE ANALYSES

CALCITE GP-3-A

	NO. OF POINTS	OXIDE	WT %	ST. DEV.
1:	n=3	MgO	0.17	0.02
		CaO	53.48	0.24
		MnO	0.02	0.02
		FeO	0.17	0.05
2:	n=3	MgO	0.11	0.01
		CaO	55.84	1.88
		MnO	0.03	0.06
		FeO	0.12	0.04
3:	n=3	MgO	0.15	0.06
		CaO	55.19	0.87
		MnO	0.02	0.03
		FeO	0.20	0.05
4:	n=3	MgO	0.40	0.17
		CaO	53.40	1.11
		MnO	0.04	0.02
		FeO	0.30	0.09

DOLOMITE BPS-33-A

	NO. OF POINTS	OXIDE	WT %	ST. DEV.
	n=10	FeO	7.02	0.30
		MnO	0.36	0.08
		CaO	32.74	0.40
		MgO	16.06	0.33

Appendix J

SAMPLE DESCRIPTIONS

J.1 INTRODUCTION

All calcite and dolomite samples analysed for stable isotopes and by AAS are listed and briefly described below. All calcite samples except CHN-42 were analysed for isotopes. Most calcite samples except radialial fibrous calcites and sample MP-4 were analysed by AAS. All dolomite samples were analysed by AAS except samples CHN-178-B and CHN-178-F.

The term "ferroan" refers to detectable iron content using potassium ferricyanide solution.

The following conventions apply to the dolomite sample descriptions: "ISOTOPE" indicates the sample was analysed for stable carbon and oxygen isotopes. CCCR refers to cloudy core with clear rim. Clear refers to relatively inclusion-free crystals in which cores and rims are not differentiable in transmitted light. Fe-rims refer to crystals in which the outermost or near outermost zones are ferroan.

J.2 CALCITE SAMPLES

BPN-12: Non-ferroan pseudospar (25-125 μm) which grades into DFC-1. Clast in conglomerate. [Broom Point North, units 1-26].

CHN-13, 15-A: Non-ferroan CFC. [Cow Head North, Bed 2].

CHN-25: Zoned equant cement which fills crack in mudstone nodule. [Cow Head North, Bed 6].

CHN-32: Non-ferroan microspar mudstone. [Cow Head North, Bed 8.21].

CHN-36-B-A,B,C; CHN-36-D,E: Non-ferroan microspar (B-A,D) to pseudospar (B-B,E) to ferroan DFC-1 (B-C) transition. [Cow Head North, Bed 8.30].

CHN-42: Ferroan calcite vein in wackestone. [Cow Head North, Bed 9.6].

- CHN-53-B: RFC. [Cow Head North, Bed 10].
- CHN-101-A,B,C: Non-ferroan microspar (A) to pseudospar (B) to ferroan DFC-1 (C) transition. [Cow Head North, Bed 8.30].
- CHN-102-A,B: Grainstone and coarse (100-500 μm size) zoned, equant cement (A) from centre of bed abruptly overlies ferroan DFC-1 (B). [Cow Head North, Bed 8.30].
- CHN-126: Non-ferroan microspar nodule in chert interval. [Cow Head North, Bed 11.1-11.4].
- CHN-168-B: Non-ferroan CFC. [Cow Head North, Bed 7].
- CHN-169: Ferroan DFC-1 at base of grainstone. [Cow Head North, Bed 8.24].
- CHN-178-AB,B,F: Non-ferroan CFC. [Cow Head North, Bed 2].
- CHN-178-G: Non-ferroan pseudospar in conglomerate matrix [Cow Head North, Bed 2].
- CHN-183: Non-ferroan peloidal wackestone nodule in chert interval. [Cow Head North, Bed 11.1].
- GP-2-A,B: Ferroan pseudospar (A) grades to ferroan DFC-2 (B). [Green Point, unit 1].
- GP-9-A: Coarse ferroan, sparry cement in fold nose cavity of contorted limestone. [Green Point, unit 18].
- GP-23-A,B,C: Non-ferroan microspar (A) and ferroan pseudospar (B) both grade to DFC-2 (C). [Green Point, units 2-9].
- GP-41-A,B: Non-ferroan microspar (25-50 μm size; A) at centre of bed grades to ferroan pseudospar (250-500 μm size; B) at top of bed. [Green Point, unit 9-10].
- GP-52-B-A,B: Ferroan pseudospar (25-50 μm ; A) nodule has spindle-shaped septarian crack filled with ferroan, zoned, equant to bladed cement (B). [Green Point, units 16-18].
- GP-57-A,B: Non-ferroan microspar (15-35 μm size) wackestone (A) at centre of bed grades to non-ferroan DFC-2 at base of bed. [Green Point, unit 26].
- GP-106: Ferroan pseudospar (35-120 μm size) is "ponded" sediment in depression of contorted limestone. [Green Point, Upper Cambrian section of wave-cut platform].
- GP(81-7-A,B,G,H): Non-ferroan pseudospar (35-200 μm size; B,G) near centre of bed grades upwards to ferroan DFC-2 (A,H). [Green Point, Upper Cambrian section].

- LH-4,8: RFC from mound. [Lower Head, Lower Head Boulder].
- LH-76-A-A,B,C: Non-ferroan microspar (10-15 μm size; A) at centre of bed grades into slightly ferroan pseudospar (50-500 μm size; B) at base of bed and slightly ferroan DFC-2 at top of bed (C). [Lower Head, strata cut by major truncation surface].
- MP-3: Non-ferroan microspar (15-25 μm) nodule surrounding rippled grainstone core. [Martin Point, unit 8].
- MP-4: Ferroan pseudospar dispersed in conglomerate matrix dolomite (decanted from dolomite analysis). [Martin Point, unit 15].
- MP-15: Non-ferroan microspar of contorted limestone. [Martin Point, unit 36p,q].
- MP-57: Non-ferroan microspar "jacket" around grainstone dike. [Martin Point, unit 36s-v].
- MP(80-39-31-D): Quartz-rich grainstone and non-ferroan, equant cement. [Martin Point, unit 31].
- RAX-12-A,B: RFC. [Cow Head North, Bed 12].
- RAX-14-A: RFC. [Cow Head North, Bed 14].
- SPN-66-D-A,B: Non-ferroan microspar (10-15 μm ; A) at centre of bed grades to ferroan pseudospar (150-250 μm ; B) at base of bed. [St. Paul's North, unit 43].
- SPN-76-A,B: Rippled grainstone (A) surrounded by radiolaria and spicule-rich wackestone envelope (B). [St. Paul's North, unit 75].
- SPQ-9-F: Discontinuous non-ferroan microspar bed. [St. Paul's Quarry, Cambrian section].

J.3 DOLOMITE SAMPLES

- A-1: Porous pervasive replacement breccia with minor bitumen in vuggy pores. Crystal size varies from 150-250 μm . CCCR. No Fe-stain. Analysis contamination from calcite in secondary pores, estimated less than 2%. [Arches, stratigraphic affinity uncertain].
- BPS-20-A: Joint-dolomitized parted mudstone. Crystal size varies from 10-20 μm . Clear. Fe-rim. [Broom Point South, unit 50].
- BPS-22: Finely laminated matrix dolomite. Crystal size varies from 10-25 μm . CCCR. Fe-rim. Analysis contamination from finely dispersed Fe-calcite, estimated less than 1%. [Broom Point South, unit 46].

BPS-23-A: Joint-dolomitized mudstone. Crystal size varies from 5-25 μm . CCCR in larger crystals. Internal Fe-zones. [Broom Point South, unit 46].

BPS-29-A: ISOTOPE. Joint-dolomitized calcarenite. Crystal size varies from 25-50 μm . CCCR. Fe-rim and internal zone. Analysis contamination from Fe-calcite in fracture, estimated less than 5 percent. [Broom Point South, unit 34].

BPS-30: Probable joint-dolomitized calcsiltite. Crystal size varies from 60-120 μm . CCCR. Slight Fe-rim. [Broom Point South, unit 25?].

BPS-32: ISOTOPE. Probable joint-dolomitized calcarenite. Crystal size varies from 100-250 μm . CCCR. Slight Fe-stain overall, minor Fe-rim. Analysis contamination from calcite in secondary pores, estimated less than 2%. [Broom Point South, unit 25].

BPS-33-B: ISOTOPE. Joint-dolomitized calcarenite. Crystal size varies from 60-250 μm . CCCR. Fe-rim and internal zone. Analysis contamination from Fe-calcite in secondary pores, estimated less than 5%. [Broom Point South, unit 33].

CHN-0: Armoured dolomitic siltstone clast in breccia. Crystal size varies from 10-50 μm . CCCR. No stain evaluation. [Cow Head North, Bed 12].

CHN-12: Dolomitized calcarenite(?). Crystal size varies from 25-175 μm . Clear. Slight Fe-rim and internal zone. Analysis contamination from Fe-zoned calcite in intercrystalline spaces, estimated 10%. [Cow Head North, Bed 3].

CHN-15-A: ISOTOPE. Conglomerate matrix dolomite associated with CFC. Crystal size varies from 60-120 μm . Clear. No iron stain. Possible analysis contamination from CFC. [Cow Head North, Bed 2].

CHN-19: Parallel- and ripple-laminated pervasive dolomitic siltstone. Crystal size varies from 25-75 μm . CCCR. No Fe-stain. [Cow Head North, Bed 6].

CHN-57: ISOTOPE. Pervasive parallel-laminated and bioturbated dolomitic siltstone. Crystal size varies from 10-25 μm . CCCR. No Fe-stain. [Cow Head North, Bed 11.7].

CHN-87: ISOTOPE. Quartz-silt-rich, parallel- and ripple-laminated dolomitic siltstone. Crystal size varies from 60-120 μm . Local Fe-rim. [Cow Head North, Bed-6].

CHN-166: ISOTOPE. Massive and parallel-laminated matrix dolomite between mudstone and calcsiltite beds. Crystal size varies from 10-25 μm . CCCR. Local Fe-rims. Analysis contamination from dispersed calcite, estimated less than 5%. [Cow Head North, Bed 6.37-.44].

CHN-167: Massive matrix dolomite. Crystal size varies from 5-25 μm .

- CCCR. Fe-rim. [Cow Head North, Bed 6.37-.44].
- CHN-178-B: ISOTOPE. Conglomerate matrix dolomite associated with bladed calcite. Crystal size varies from 35-85 μm . Slight internal Fe-zones. Clear. Analysis contamination from CFC and cross-cutting Fe-calcite veinlets, calculated 17.5%. [Cow Head North, Bed 2].
- CHN-178-F: ISOTOPE. Conglomerate matrix dolomite associated with bladed calcite. Crystal size varies from 35-85 μm . Slight internal Fe-zones. Clear. Analysis contamination from CFC and cross-cutting Fe-calcite veinlets, calculated 21.2%. [Cow Head North, Bed 2].
- CHN(80-4-0): ISOTOPE. Conglomerate matrix dolomite associated with bladed calcite. Crystal size varies from 60-125 μm . Clear with minor core cloudiness in some crystals. Minor Fe-rim. Possible analysis contamination from proximal CFC. [CHN, Bed 4].
- CHS-55: ISOTOPE. Massive matrix dolomite between mudstone beds. Crystal size varies from 25-50 μm . CCCR. Fe-rim. Analysis contamination from calcite veinlets, estimated less than 2%. [Cow Head South, Shoal Cove section, Bed 10s].
- CHS-69: Massive matrix dolomite between mudstone beds. Crystal size varies from 3-10 μm . Cannot evaluate core cloudiness. No Fe-stain. [Cow Head South, Jim Cove section, Bed 11s.22].
- GP-63-B: ISOTOPE. Parallel-laminated matrix dolomite between mudstone beds. Crystal size varies from 10-25 μm . CCCR. Fe-rim and internal zone. Analysis contamination from Fe-calcite veinlet, estimated less than 2%. [Green Point, unit 28].
- GP-67: ISOTOPE. Massive matrix dolomite between mudstone beds. Crystal size varies from 10-25 μm . Fe-rim and internal zone. Analysis contamination from dispersed Fe-calcite, estimated 5-10%. [Green Point, unit 28].
- GP-88-A: ISOTOPE. Parallel- and ripple-laminated dolomitic siltstone stringer associated with red shale. Crystal size varies from 30-60 μm . CCCR. No Fe-stain. [Green Point, unit 35].
- GP-89: Parallel- and ripple-laminated dolomitic siltstone stringer associated with red shale. Crystal size varies from 30-60 μm . CCCR. No Fe-stain. [Green Point, unit 35].
- GP-95: Parallel- and ripple-laminated dolomitic siltstone stringer associated with red shale. Not examined by thin section. [Green Point, unit 47].
- GP-96-B: ISOTOPE. Granule- and coarse sand-size clasts of chert and phosphate which grade upwards into dolomitic siltstone. Associated with red shale. Crystal size varies from 5-35 μm , CCCR. No Fe-stain. [Green Point, units 47-49].
- GP(80-61-34): Pervasively dolomitized calcarenite similar to alteration

- seen in conglomerate GP(80-61-44B). Crystal size varies from 25-125 μm . CCCR. Slight Fe-rim. Analysis contamination from Fe-calcite veinlet, estimated less than 2%. [Green Point, unit 34].
- GP(80-61-44B): ISOTOPE. Pervasively dolomitized conglomerate. Crystal size is variable according to clast and matrix, range is from 25-250 μm . CCCR. No Fe-stain. Analysis contamination from Fe-calcite veinlet, estimated less than 2%. [Green Point, unit 44].
- LC-3: Massive, parallel- and ripple-laminated pervasive dolomitic siltstone. Crystal size varies from 10-50 μm . CCCR. Fe-rim. [Lobster Cove].
- LC-4: Massive- and parallel-laminated, bioturbated, pervasive dolomitic siltstone. Crystal size varies from 10-20 μm . CCCR. Fe-rim. [Lobster Cove].
- EC-5: Massive and rippled, pervasive dolomitic siltstone. Crystal size varies from 15-40 μm . CCCR. Fe-rim. [Lobster Cove].
- MP-4: ISOTOPE. Conglomerate matrix dolomite. Crystal size varies from 25-125 μm . Clear. Fe-stained throughout. Analysis contamination from peloids, estimated 10%. [Martin Point, unit 15].
- MP-8: Parallel- and ripple-laminated pervasive dolomitic siltstone. Crystal size varies from 35-85 μm . CCCR. Fe-rim. [Martin Point, unit 32].
- MP-30: ISOTOPE. Matrix (internodule) dolomite between discontinuous mudstone beds. Crystal size varies from 35-85 μm . CCCR. Fe-rim to Fe-stained throughout. Analysis contamination from dispersed Fe-calcite, estimated 15-20%. [Martin Point, units 16-20].
- MP-41: Parallel- and convolute-laminated, pervasive dolomitic siltstone. Crystal size varies from 35-85 μm . CCCR. Fe-rim. [Martin Point, unit 32].
- MP-69-B: Parallel- and ripple-laminated, pervasive dolomitic siltstone. Crystal size varies from 25-60 μm . CCCR. Fe-rim. [Martin Point, unit 40a].
- MP-84: Burrowed, parallel-laminated, dolomitic siltstone stringer associated with red shale. Crystal size varies from 15-75 μm . Clear mostly. No Fe-stain. [Martin Point, unit 58].
- SPN-1: Burrowed, parallel-laminated dolomitic siltstone stringer associated with red shale. Crystal size varies from 25-50 μm . Clear mostly. No Fe-stain. [St. Paul's North, units 84-85].
- SPN-3: Massive dolomitic siltstone stringer associated with red shale. Crystal size varies from 10-25 μm . Clear and CCCR. No Fe-stain. [St. Paul's North, unit 83].
- SPN-32: ISOTOPE. Massive matrix dolomite between mudstone beds. Crystal

size varies from 10-25 μm . CCCR. Fe-rim. Possible analysis contamination from adjacent mudstones, estimated less than 2%. [St. Paul's North, unit 24].

SPN-38: ISOTOPE. Burrowed and parallel-laminated dolomitic siltstone stringer associated with red shale. Crystal size varies from 10-25 μm . Clear. No Fe-stain. [St. Paul's North, units 83-85].

SPN-41: Dolomitic siltstone associated with silicified beds and red shale. Crystal size varies from 25-50 μm . CCCR. No Fe-stain. [St. Paul's North, units 83-84].

SPN-43-B: Graded dolomitic siltstone (loose boulder) associated with red shale. Crystal size varies from 15-100 μm . CCCR. No Fe-stain. [St. Paul's North, units 83-84].

WI-1: ISOTOPE. Pervasively dolomitized conglomerate. Crystal size varies from 60-600 μm . Very cloudy crystals, some thin clear rims. No Fe-stain. Analysis contamination from calcite in secondary pores, estimated less than 10%. [White Rock Islets].

WN-4-A: Burrowed, parallel-laminated dolomitic siltstone stringer associated with red shale. Crystal size varies from 15-35 μm . CCCR. Fe-rim. [Western Brook Pond North, unit 5].

WN-11: ISOTOPE. Burrowed, parallel- and ripple-laminated dolomitic siltstone stringer associated with red shale. Crystal size varies from 10-25 μm . CCCR. Minor Fe-rim. [Western Brook Pond North, unit 24].

WS-8: Ripple-laminated dolomitic siltstone stringer associated with red shale. Crystal size varies from 25-35 μm . Variably cloudy throughout. No Fe-stain. [Western Brook Pond South, unit 56].

WS-11: ISOTOPE. Burrowed, parallel- and ripple-laminated dolomitic siltstone stringer associated with red shale. Crystal size varies from 25-35 μm . Variably cloudy throughout. No Fe-stain. [Western Brook Pond South, units 49-50].

WS-19: Ripple-laminated dolomitic siltstone stringer associated with red shale. Crystal size varies from 25-50 μm . CCCR. Minor Fe-rim. [Western Brook Pond South, unit 6].

Appendix K

TRACE ELEMENTS AND WATER-ROCK RATIOS: BACKGROUND

The cornerstone of trace element study is based on partitioning theory. In its simplest form, considering only inorganically-precipitated, homogeneous crystals, the critical relationship is the Berthelot-Nernst equation:

$$\left(\frac{mT}{mC}\right)_{\text{MINERAL}} = k_{\text{MINERAL}} \times \left(\frac{mT}{mC}\right)_{\text{SOLUTION}}$$

where "m" refers to molar concentrations of trace element ("T") and carrier or major element ("C" - Ca in this case) in the mineral (calcite) and solution. "k" is the partitioning coefficient for the trace element in the mineral, at a specific temperature. The above relationships assume equilibrium as well as the lack of concentration gradients of the trace element within the mineral. In addition the solution must be sufficiently dilute to allow molar concentrations to equal activity. In crystals where more than one trace element is incorporated into the lattice, the relationship between a particular trace and major element is independent of other trace-major element relationships (McIntire, 1963; Pingitore, 1978; Brand and Veizer, 1980; Oglseby 1976 p. 7; Veizer, 1983). The partitioning coefficients of various metals in carbonates at surface and diagenetic conditions are poorly known; consequently, partition coefficients are most practically used as

order-of-magnitude estimates (Veizer, 1983). Partitioning coefficients are subject to numerous controls among them being temperature (e.g. k^{Mg} - Fuchtbauer and Hardie, 1976), precipitation rate (e.g. k^{Sr} - Lorens, 1981), influence of other solid solutions in host crystals (e.g. k^{Sr} is influenced by $MgCO_3$ content of calcite - Mucci and Morse, 1983), as well as trace element concentrations (e.g. k^{Sr} - Baker et al., 1982).

Informative reviews of the earlier work on Sr, Mg, Fe, and Mn as trace elements are found in most of the above references. Veizer (1983) also discusses the use of trace elements in carbonates in general.

With reference to the common situation of marine sediments undergoing subaerial diagenesis, and assuming that conditions are conducive to the precipitation of calcite, the fate of tracers is determined by the interaction of 3 factors: (1) the partitioning coefficient of the element being considered; (2) the water-rock ratio; and (3) the magnitude of the difference in mMe/mCa of freshwater and seawater (Veizer, 1983) where Me is the substituting trace cation. Diagenetic systems characterized by high water-rock ratios are considered to be open. In such systems the dissolving and precipitating phase(s) have little effect on the chemistry of pore solutions. In contrast, systems with low water-rock ratios are closed, and a relatively small amount of pore fluid is strongly controlled or "buffered" by the partitioning characteristics of associated minerals (Veizer, 1983). Systems with intermediate degrees of closure (partially open or partially closed) more closely approximate natural diagenetic systems in which there is at least minor loss of some component.

Figure 10.4a summarizes the expected trace element trends in greatly

simplified open and closed diagenetic system composed of aragonite, Mg-calcite, and a typical fresh pore-water. The dissolution of aragonite and Mg-calcite is assumed to be the dominant control on the availability of Sr and Mg. Mn and Fe are initially at "background" levels in the pore-water. Under more reducing conditions, Mn and Fe can be released from a wide variety of dispersed oxide and hydroxide phases thus greatly increasing their concentration in solution. Situations are considered for tracers having k less than unity (e.g. Sr and Mg) and k greater than unity (e.g. Mn and Fe [1]).

In an open diagenetic system, released Sr and Mg are removed from the system. Any calcite that does precipitate will be depleted in both Sr and Mg, incorporating only "background" levels of these elements, distributed according to their k values. No build-up of Sr and Mg occurs in the pore-water despite k less than unity. Considering these same elements in a closed diagenetic system, k 's less than unity imply that Mg and Sr levels will progressively increase in the pore-waters and successive precipitates will contain greater amounts of Sr and Mg, the limiting concentrations being those of the source aragonite and Mg-calcite.

Trace elements having k 's greater than unity (e.g. Fe and Mn) in an open diagenetic system at constant Eh will result in calcite with a homogeneous distribution of these elements, regardless of whether Fe and

1. The range of values for k^* is estimated between 1 and 20 in Veizer (1983, table 3-1) but for purposes of the following discussion, it is assumed that k is greater than unity, a likelihood based on the similar size and charge to Mn (also see Oglesby, 1976).

Mn is scarce or abundant in pore-waters. In closed systems at constant Eh, however, any Fe and Mn in pore-waters will be scavenged by the earliest precipitates, and successive precipitates will contain progressively less of these elements.

Appendix L

MINOR AUTHIGENIC MINERALS

L.1 SPHALERITE

Subhedral to euhedral sphalerite [1] crystals usually range from 40-400 μm in size and reach a maximum of 1 mm. These crystals are associated with both early and late diagenetic features, occurring in the following ways:

- (1) dispersed in shales and limestones;
- (2) in contorted limestones and their associated shales or other tectonized sediments; and
- (3) in pressure-shadow zones in nodular limestones and with calcite in fractures in nodules.

Most sphalerite crystals are radially zoned and exhibit a prominent "Maltese Cross"-type pattern of dark, inclusion-rich sectors (the cross) and translucent, inclusion-poor sectors which are occasionally replaced

1. X-ray diffraction demonstrates the presence of the 9.12 Å peak which indicates sphalerite rather than the wurtzite polymorph. However, only one sample was analysed using a one-way scan.

by calcite. Microprobe analyses demonstrate iron enrichment in the translucent sectors of the crystal relative to the dark sectors (0.45 versus 0.17 metal wt %; data in Table L.1). CL examination shows some translucent zones to have a bright yellow luminescence with micrometre-scale growth zoning. The inclusion-rich sectors and most sphalerite crystals in general, however, are non-luminescent.

L.2 FLOURITE

Flourite is extremely rare and has been identified, following initial verification by X-ray diffraction, in only a few thin sections from Green Point and Martin Point. It forms 50-250 μm -size cubes or mosaics of anhedral crystals which occur in veins along with dolomite or calcite, fills moldic(?) pores, and partially replaces shale intraclasts.

L.3 CHLORITE

A minor amount of chlorite occurs in veins within dolomitic siltstones in red shale. These fibrous crystals range up to 750 μm in length and exhibit strong green pleochroism and anomalous blue birefringence. Chlorite, identified by its light green colour, also locally forms the intercrystalline matrix between dolomite crystals. One sample examined contains sponge spicules replaced by chlorite.

TABLE L.1: SPHALERITE MICROPROBE ANALYSIS

Sphalerite from Green Point (sample GP-7-C) was analysed using a sphalerite standard and 30-second counting time.

Dark, Inclusion-rich Sectors: n = 5

	<u>S</u>	<u>Fe</u>	<u>Zn</u>	<u>Total</u>
Metal %	33.36	0.17	67.40	100.93
St. Dev.	0.50	0.04	1.34	
Stoich.	1.006	0.002	0.991	1.999

Translucent Sectors: n = 5

	<u>S</u>	<u>Fe</u>	<u>Zn</u>	<u>Total</u>
Metal %	33.20	0.45	68.03	101.68
St. Dev.	0.67	0.07	0.92	
Stoich.	0.997	0.007	0.996	1.999

Appendix M

SYNSEDIMENTARY BOUDINS

M.1 INTRODUCTION

Synsedimentary or sedimentary boudinage was invoked to explain the origin of nodules in the Ireton Formation of western Alberta (McCrossan, 1958). These structures were interpreted to have formed in the shallow subsurface of the sea floor from penecontemporaneous sliding on a slope or from turbidity current drag (McCrossan, 1958). The resultant nodules are analogous to "pull-apart" structures of Natland and Kuenen (1951). The contrasting rheology between carbonate layers and interbedded argillaceous sediments resulted in plastic flowage of the surrounding, incompetent shales or marls and stretching or necking of the more competent limestones to ultimately produce isolated nodules. The process also accounts for brittle fracturing of the nodules and the formation of V-shaped cracks on the margins of nodules. These structures were subsequently modified by burial.

Synsedimentary boudinage was invoked by Hubert et al. (1977; also see Suchecki, 1975) to account for the origin of nodular limestones or "boudins" in the CHG. These boudins were reported to have length to width ratios of 2-4:1 with the long axis parallel to their reconstructed

paleoslope contours. Boudin orientations were used to substantiate their complex paleogeographic reconstruction.

M.2 FIELD TEST

To assess the reliability of the above interpretation, two localities were selected where nodules (boudins) could be easily extracted from enclosing green and gray shales (Upper Cambrian at Green Point and St. Paul's North). The nodules comprise the "mudstone" and "cored" types (refer to Chapter 2), the latter having cores of grainstone or pebble conglomerate. A total of 21 nodules were oriented, extracted, and then measured (Plate 12c; Table M.1).

According to Hubert et al. (1977), the paleoslopes at Green Point and St. Paul's North are oppositely-dipping (northeast and southwest, respectively - see their figure 20), however, both depositional slopes strike northwest-southeast. For both localities maximum boudin elongation should then occur parallel to this strike. At both localities, outcrops strike approximately northeast-southwest and therefore, maximum elongation of the nodules should be approximately perpendicular to outcrop strike.

The measurements in Table M.1 indicate that no preferred orientation exists parallel to Hubert et al.'s (1977) paleoslope contours. Furthermore, the reported 2 to 4:1 axial ratio also does not occur; rather, the long axes are only 30-40% longer than the short axes at right angles to them. The round to subrounded shapes in plan view are

consistent with concretionary growth shapes reflecting homogeneous permeability along bedding planes (Raiswell, 1971a). The similarity of McCrossan's (1958) boudins from the Ireton Formation to other nodular limestones interpreted to be mainly the result of early lithification on or just below the sea floor (e.g. Raiswell, 1971a) suggests that the "type" boudins are probably also isolated, discrete concretions.

TABLE M.1: NODULE MEASUREMENTS

At Green Point, strike is 50 degrees NE with strata overturned and steeply dipping. At St. Paul's North, strike is 43 degrees NE, dip is 40 degrees SE. All measurements are in centimetres.

GREEN POINT (UPPER CAMBRIAN)

perpend. strike X	para. strike Y	ratio X/Y	max. axis A	min. axis B	ratio A/B
8.0	10.5	0.8	10.5	8.0	1.3
7+	4.5	---	7+	4.5	---
18.5	19.0	1.0	21.0	17.8	1.2
8.8	13.4	0.7	13.5	9.2	1.5
13.5	7.2*	1.9	13.5	7.2*	1.9
7.0	7.0	1.0	8.5	5.5	1.5
14.0	14.0	1.0	17.4	13.4	1.3
8.8	11.8	0.7	11.8	8.8	1.3
13.2	12.0*	1.1	13.2	12.0*	1.1
14.5	17.0*	0.9	17.0*	14.5	1.2
16.0	18.5	0.9	18.5	16.0	1.2
17.0	34+	---	34+	17.0	---
Average (1 sigma):		1.0 (0.3)			1.3 (0.2)

ST. PAUL'S NORTH (UPPER CAMBRIAN)

perpend. strike X	para. strike Y	ratio X/Y	max. axis A	min. axis B	ratio A/B
11.5	16.5	0.7	16.5	11.5	1.4
6.0	8.5	0.7	8.5	6.0	1.4
13.0	21.0	0.6	21.0	13.0	1.6
11.0	15.5	0.7	18.0	10.5	1.7
7.5	5.0	1.5	7.5	5.0	1.5
11.5	11.0	1.0	11.5	11.0	1.0
8.0	7.0	1.1	8.0	7.0	1.1
12.0	9.0	1.3	12.0	9.0	1.3
9.5	8.5	1.1	9.5	8.5	1.1
Average (1 sigma):		1.0 (0.3)			1.4 (0.2)

*:complete nodule form is extrapolated, +:minimum estimate (extrapolation was uncertain). Both * and + data are excluded from averages.

Appendix N

EVIDENCE FOR SUBMARINE EXPOSURE OF NODULAR MUDSTONES

N.1 INTRODUCTION

During this investigation, evidence for submarine exposure of nodular limestones was observed only twice (see Plate 53e,f): Two interpretations are offered for each occurrence. The first interpretation appeals to submarine exposure, whereas the second does not require exposure, but is instead explained by selective calcite precipitation.

N.2 EXAMPLE 1: NODULE FROM COW HEAD NORTH

Description: A compound nodule from Cow Head North consists of non-ferroan microspar with dispersed, fine to medium silt-size siliciclastics (Plate 53e). The upper (1) and lower (2) nodules are separated by an argillaceous seam which is locally stylolitic (3). V-shaped marginal cracks (9) are found in the upper nodule, and septarian ladders (4) fracture a peloidal silt lamination (5) which can be followed into the adjacent internodule matrix (6). The internodule

matrix which is laterally equivalent to the lower nodule (2) contains abundant 25-35 μm siliciclastics (7). A key observation is that no comparable-size siliciclastics are found in the laterally equivalent nodule (2).

Interpretation 1: The lower nodule (2) formed either at the surface or slightly below the sediment surface and was subsequently exhumed. The laterally equivalent silty sediments (7) were deposited next to this obstacle and also lapped onto its top (8). This explains the lack of 25-35 μm siliciclastics in the lower nodule and their presence in the lower internodular matrix (7). Deposition of clay muds (6) containing a thin lamination of peloidal siltstone (5) followed and buried the lower nodule. Subsequent calcite precipitation (1) was initiated around the lamination above the lower nodule, thus forming the compound nodule.

Interpretation 2: Deposition of internodular matrix sediment (7) may have taken place in a shallow scour within uncompactd clay muds (laterally equivalent to insoluble component of lower nodule). Additional clay muds (6) and the peloidal silt lamination (5) were subsequently deposited. Calcite precipitation in the clay muds adjacent to the lower matrix (7) as well as around the overlying peloidal silt lamination (5) followed thus forming the lower (2) and upper (1) nodules, respectively.

N.3 EXAMPLE 2: NODULE FROM ST. PAUL'S QUARRY

Description: The second example is taken from a quasi-autochthonous

block of ribbon limestone exposed in the quarry wall in St. Paul's Quarry (Plate 53f). Blasting dislodged this block from its original position which is presently covered. Bedding could not be traced laterally for more than 1 m.

This outcrop contains a non-ferroan, microspar, nodular mudstone (M) with a conspicuous sand-size pebbly grainstone (G) lodged between the nodules. The pebbles consist of mudstone identical to that of the nodules. A 1 mm-thick lamination of shale covers both the nodules as well as the grainy internodular fill, and this is subsequently overlain by a 1 mm-thick continuous grainstone lamination (H). As with the first example, there are two possible explanations.

Interpretation 1: The first interpretation is that a mudstone bed was formed either at the surface or was exhumed from the shallow subsurface. This mudstone bed may have been continuous and then eroded (dissolved?) into nodules or it may have originally been nodular. Subsequent sedimentation of the grainstone (G) occurred, incorporating some of the smaller exhumed mudstone nodules or pieces of nodules. Clay mud and then grainstone (H) deposition followed.

Interpretation 2: The second explanation is identical to that in the first example calling upon fortuitous calcite precipitation to postdate a grainstone-filled scour within clay muds.

N.4 CONCLUSION

It is concluded that the nodules in both examples 1 and 2 were exposed on the sea-floor at some during their early history. This conclusion is based on the improbability of second interpretation being correct in each case. The siliciclastic-rich internodule matrix in the first example and the pebbly grainstone in the second example both would have been the preferred sites of early cementation due to their high depositional porosities and permeabilities. Any subsequent calcite precipitation in these sediments would have occurred as mudstone envelopes on these grainy cores, based on this extremely common and consistent relationship seen elsewhere in the Cow Head Group.

Appendix 0

MINERALOGY OF CONCRETIONS AND HARDGROUNDS

0.1 INTRODUCTION

Concretions are continuous to discontinuous crusts; which, if exhumed, form hardgrounds (Bathurst, 1983a; "hiatus concretions" of Baird, 1976). The classical hardground develops at the sediment surface but it is now well established that many hardgrounds are exhumed concretions which begin to form slightly below the sediment-seawater interface, usually within the first 50 cm (Bathurst, 1983a). Evidence for exposure of submarine-hardened crusts on the sea-floor implies that the crusts are hardgrounds, but the opposite case, the lack of evidence for exposure, cannot be used to preclude such an origin. In light of this, the mineralogy as well as morphology of submarine cements and concretionary cements cannot be divorced from one another.

0.2 DISCUSSION

The calcitic mineralogy and ubiquitous pyrite in CHG mudstones and grainstones is typical of early-formed concretions described from most

other ancient sequences. Based on their sharp CL zoning and microfabrics, trace element trends with progressive precipitation, and distinct isotopic signatures, authigenic calcites in the CHG are interpreted to be unaltered from their original low Mg-calcite compositions. This interpretation of original mineralogy and chemistry is consistent with conclusions reached in other studies of concretions (e.g. Galimov et al., 1968; Hoefs, 1970; Raiswell, 1971b).

In contrast, cements in Quaternary hardgrounds and concretions are commonly Mg-calcite and micritic [1] and often appear "pelleted" (Mullins et al., 1980a), quite unlike the equant calcite cements in grainstones and CFC in conglomerates. Two hypotheses are proposed to explain this: (1) precipitation from modified seawater, assuming a composition identical to modern seawater; or (2) seawater chemistry was different.

Considering the first possibility, if Mg-poisoning does determine the composition and morphology of calcite as suggested by Folk (1974), then depletion of pore-water Mg/Ca below the ratio in seawater may explain the sparry calcite crystals. If, however, Lahann's (1978) surface-charge model more realistically explains morphological and chemical variations in submarine precipitates, increases in Ca and bicarbonate concentrations in shallow-burial pore-waters could,

1. Sparry intermediate Mg-calcites do exist, however, but these are rare. Al-Hashimi (1977) described intermediate Mg-calcites up to 750 μm in size with 2-9 mol % MgCO_3 . These calcites were found in secondary pores developed within Carboniferous dolostones exposed in the modern intertidal zone on the North Sea Coast of northeast England. Purser (1980, p. 82) described sparry Mg-calcites with 7-8 mol % MgCO_3 dredged from depths of 250-500 m in the Mediterranean.

depending on their relative abundances, have the opposite effect and encourage micritic or fibrous morphologies instead. It remains unclear as to which factors govern the precipitation of sparry versus micritic or fibrous calcites.

The remaining hypothesis is that these calcites were precipitated from seawater or slightly-modified seawater characterized by physico-chemical conditions different from those of the modern ocean. These conditions may have favoured calcite or aragonite or perhaps lower levels of Mg in Mg-calcite. Examination of fossils (Pigott and Mackenzie, 1979; Wilkinson, 1979), carbonate mud (Folk, 1974; Sandberg, 1975), marine ooids (Sandberg, 1975; Wilkinson and Landing, 1978), cements (Folk, 1974; Wilkinson, 1982; Sandberg, 1983), and stable isotopes (James and Choquette, 1983) suggests that the Phanerozoic has been characterized by major oscillations in oceanic chemistry. The causes for these changes are not obvious. Mg/Ca ratio of marine waters (Folk, 1974), atmospheric pCO₂ levels (Pigott and MacKenzie, 1979; Pigott *et al.*, 1980), or some other as yet unknown variable affecting carbonate equilibria may have been a major control (Wilkinson *et al.*, 1982). Further discussion on the above can be found in James and Choquette (1983) and numerous references therein.

Whereas sparry calcite cements are unknown from modern tropical marine environments they have been recently reported from several Paleozoic and Mesozoic shallow-water carbonate environments (e.g. Delgado, 1979; Wilkinson *et al.*, 1982). These studies demonstrate unequivocal evidence of submarine exposure in the form of organic borings and encrustations. This does not imply, however, that the sparry calcites were precipitated

at the sediment-seawater interface and a shallow burial origin is at least likely for the cements described by Wilkinson et al. (1982). This suggestion is based on the reported bright orange luminescence of these sparry calcites which Wilkinson et al. (1982) attributed to Mn-activation and therefore precipitation in a reducing, anoxic microenvironment close to, perhaps millimetres away from, the sediment-seawater interface. These cemented grainstones could alternately be explained as exhumed concretions (early-cemented grainstones) which had relatively little to do with true marine cementation.

